

© 2013

DAN SU

ALL RIGHTS RESERVED

**RELIABILITY-BASED SERVICEABILITY LIMIT STATES FOR
CONCRETE GIRDER BRIDGES**

by

Dan Su

A Dissertation submitted to the
Graduate School-New Brunswick
Rutgers, The State University of New Jersey

In partial fulfillment of the requirements

For the degree of

Doctor of Philosophy

Graduate Program in Civil and Environmental Engineering

Written under the direction of

Dr. Hani H. Nassif, Ph.D.

And approved by

New Brunswick, New Jersey

OCTOBER, 2013

ABSTRACT OF THE DISSERTATION

Reliability-Based Serviceability Limit States For Concrete Girder Bridges

by DAN SU

Dissertation Director:

Dr. Hani H. Nassif, Ph.D.

Although ultimate limit state, such as flexural capacity, shear, or stability, governs the overall safety of the structure, the accumulated damage due to cracking, excessive deflections, and vibrations also would lead to limitation of structural performance, abbreviation of service life, as well as extensive maintenance cost. Regarding the bridge structure, current AASHTO LRFD Bridge Design Specification (LRFD) was developed based on structural reliability approach and provided a uniform reliability at strength limit state. However, only strength limit states were considered and calibrated during the development and calibration of LRFD. Unlike strength limit state, exceedance of serviceability limit state in bridge structures might not result in catastrophic consequences directly. However, Serviceability limit states related to stress, deformation, and cracks under regular service conditions are essential to the performance, human experience, and durability of structure. To ensure consistent and rational reliability level

to be achieved for all limit states, rational serviceability limit states need to be developed and investigated for bridge structures.

In this study, various serviceability limit states were developed and investigated, including Service I limit state for crack control of reinforced concrete decks and Service III limit state for tension in prestressed concrete superstructures. The resistances of various serviceability limit states were derived and the statistical models were developed based on statistics of various random variables and using different methods including Monte Carlo simulation method. The live load model was developed based on national as well as local Weigh-in-Motion (WIM) data using various extrapolation techniques. Based on current practice, consequence of failure, and experience from previous research, target reliability indices were proposed for each serviceability limit state. Moreover, the reliability analysis was performed for various serviceability limit states and new design criteria were proposed to achieve the target reliability levels consistently for various design scenarios. In addition, the deterioration of structural resistance was investigated and the reliability level of various serviceability limit states with and without consideration of deterioration was compared.

DEDICATION

To My Parents, I love you.

ACKNOWLEDGEMENTS

I would like to start by acknowledging my advisor, Dr. Hani Nassif, for his continuous support throughout my academic career in Rutgers University. This work would not have been possible without his guidance, continual support, and wisdom in this area. It is a blessing to have him as my advisor.

It has been an honor and a privilege to have Dr. Kaan Ozbay, Dr. Husam Najm and Dr. David Coit serve on my committee. Their encouragement and continual support goes beyond the completion of this dissertation.

A special acknowledgement is made to National Cooperative Highway Research Program (NCHRP) for providing the financial support of this study. I also would like to thank the invaluable guidance and inspiration from other members of NCHRP 12-83 team, Dr. John Kulicki, Dr. Wagdy Wassef, Dr. Andrzej Nowak, and Dr. Dennis Mertz.

My appreciation is extended to the departmental staff: Gina Cullari and Linda Szary. I also would like to extend my appreciation to Judy Pellicane and Ufuk Ates for their help and assistance at early year of my study in Rutgers University. Special thanks to Gonca Unal for her tremendous contribution to develop hundreds of bridges as well as encouragement and friendship. Special thanks also go to my friends and colleagues for their help in this study and many other projects: Peng Lou, Dr. Ye Xia, Dr. Yingjie Wang, Dr. Suhail Albhasi, Dr. Chaekuk Na, Etkin Kara, Tim Walkowich, Opeoluwa Adediji, Zeeshan Ghanchi, Malek Shadidi, Miguel Beltran, and Khalid Machich.

I also would like to thank my friends Hougui Zhang, Jingming Zhang, Xiao Zhang, Xiaodao Ye, Yipeng Zhao, Qingnan Sun, Jianchang Li, Lihe Sun, Weizhi Shi, Hong Lin, and Yixing Qi, you made my journey in Rutgers University full of sunshine.

Deep appreciation and gratitude is expressed to my family for their support and encouragement during my academic pursuits.

Finally, I would like to thank my wife, Wei Li, and my sons, Christopher and Jonathan, for their love, support, and patience without which none of this would be possible.

TABLE OF CONTENTS

ABSTRACT OF THE DISSERTATION	ii
DEDICATION	iv
ACKNOWLEDGEMENTS	v
LIST OF FIGURES	xi
LIST OF TABLES	xxvii
1 INTRODUCTION	1
1.1 Motivation.....	3
1.2 Research Significance	5
1.3 Objectives and Scope	6
1.4 Organization of the Thesis	7
2 LITERATURE REVIEW	9
2.1 Bridge Design Specifications.....	9
2.1.1 Allowable Stress Design (ASD)	10
2.1.2 Load and Resistance Factor Design (LRFD)	10
2.1.3 Eurocode	11
2.1.4 Canadian Code	13
2.1.5 ISO 2394 Document (General Principles on Reliability for Structures)	13
2.2 Serviceability Limit States	15
2.3 Structural Reliability Analysis	16
2.4 Target Reliability Index	18
2.5 Random Variables	19
2.6 Crack Control Reinforcement	21
2.6.1 Bottom Face of Concrete Member	21
2.6.2 Side Face of Concrete Member	28
2.6.3 Summary	35
2.7 Control of Cracks in Current AASHTO LRFD Specifications Provisions.....	35
2.8 Concrete Tension Stresses	39
2.8.1 Historical Development of Tensile Strength Limit Provisions	39
2.8.2 Research Related to the Tensile Stress Limits	42
2.8.3 Summary	49
2.9 Deflection of Concrete Members	50
3 MODELS FOR STRUCTURAL RESISTANCE AND DEAD LOAD	61
3.1 Service I Limit State (Traditional)	62
3.1.1 Derivation of Resistance Prediction Equation	62
3.1.2 Comparison of Predication Equation for Maximum Crack Width of Reinforced Concrete Members	63
3.1.3 Statistical Model for Structural Resistance	67
3.2 Service I Limit State (Empirical)	70
3.2.1 Investigation of Arching Action of Concrete Deck	71
3.2.2 Derivation of Resistance Prediction Equation	78
3.2.3 Statistical Model for Structural Resistance	79
3.3 Service III Limit State	79

3.3.1	Derivation of Resistance Prediction Equation	80
3.3.2	Comparison of Predication Equation for Maximum Crack Width at bottom fiber of Prestressed Concrete Girders	89
3.3.3	Statistical Model for Structural Resistance.....	101
3.4	Deflection Limit State	102
3.4.1	Derivation of Resistance Prediction Equation	102
3.4.2	Statistical Model for Structural Resistance	103
4	MODELS FOR LIVE LOAD	105
4.1	Analysis of Live Load Data	107
4.1.1	WIM Data Processing	107
4.1.2	Statistics of WIM data	110
4.1.3	Multiple Presence Probabilities	115
4.2	Prediction of Long Term Live Load Effects.....	120
4.2.1	Rate of Increase in Vehicle Weight	121
4.2.2	Probabilistic Based Extrapolation Methods.....	122
4.2.3	Long Term Load Effects from Various Sites.....	124
4.2.3.1	Site-Specific Bias Factors for Various WIM Sites	125
4.2.3.2	Comparison between Different WIM Sites.....	130
4.2.3.3	Effects of Extrapolation Methods	139
4.2.3.3.1	NY Site 0580.....	140
4.2.3.3.2	NY Site 2680.....	141
4.2.3.3.3	NY Site 8382.....	142
4.2.3.3.4	NY Site 9631.....	143
4.3	Proposed Live Load Models	144
4.3.1	Proposed Live Load Model for Service I Limit State.....	144
4.3.2	Proposed Live Load Model for Regular Truck Load for Service III Limit State	148
4.3.3	Proposed Live Load Model for Permit Vehicle Load for Service III Limit State	151
5	DETERIORATION MODEL OF BRIDGE ELEMENTS	155
5.1	Deterioration Model for Prestressed Concrete Girders for Service III Limit State	156
5.2	Deterioration Model for Reinforced Concrete Decks at Service I Limit State.....	162
6	STRUCTURAL RELIABILTY ANALYSIS	164
6.1	Reinforced Concrete Decks Designed using Traditional Method (Service I Limit State)	166
6.1.1	Reinforced Concrete Deck Database	166
6.1.2	Limit State Function for Reinforced Concrete Decks Designed using Traditional Method	167
6.1.3	Target Reliability Index for Service I Limit State (Traditional Deck)	170
6.1.4	Reliability analysis results for Service I Limit State	172
6.1.4.1	Class 1 Exposure Condition (Maximum Crack Width of 0.017 in) ...	172
6.1.4.2	Class 2 Exposure Condition (Maximum Crack Width of 0.01275 in)	176

6.1.5	Effects of Structural Deterioration on Reliability of Service I Limit State (Traditional Deck).....	182
6.2	Reinforced Concrete Decks Designed using Empirical Method (Service I Limit State) 184	
6.2.1	Reinforced Concrete Deck Database	184
6.2.2	Limit State Function for Reinforced Concrete Decks Designed using Empirical Method	185
6.2.3	Target Reliability Index for Service I Limit State (Empirical Deck)	186
6.2.4	Reliability analysis results for Service I Limit State	186
6.2.4.1	Class 1 Exposure Condition (Maximum Crack Width of 0.017 in) ...	186
6.2.4.2	Class 2 Exposure Condition (Maximum Crack Width of 0.01275 in)	191
6.2.5	Effects of Structural Deterioration on Reliability of Service I Limit State (Empirical Deck).....	196
6.3	Prestressed Concrete Girders (Service III Limit State).....	197
6.3.1	Prestressed Concrete Girder Database	198
6.3.2	Limit State Function for Service III Limit State	199
6.3.3	Target Reliability Index for Service III Limit State.....	200
6.3.4	Reliability analysis results for Service III Limit State.....	207
6.3.4.1	Maximum Allowable Tensile Stress Limit of $f_t = 0.0948\sqrt{f'_c}$	207
6.3.4.2	Maximum Allowable Tensile Stress Limit of $f_t = 0.19\sqrt{f'_c}$	213
6.3.4.3	Maximum Allowable Tensile Stress Limit of $f_t = 0.253\sqrt{f'_c}$	217
6.3.5	Effects of Structural Deterioration on Reliability of Service III Limit State 223	
6.4	Prestressed Concrete Girders (Deflection Limit State).....	224
6.4.1	Prestressed Concrete Girder Database	224
6.4.2	Limit State Function for Deflection Limit State	225
6.4.3	Target Reliability Index for Deflection Limit State.....	225
6.4.4	Reliability analysis results for Deflection Limit State	227
6.4.4.1	Uncracked Section	227
6.4.4.2	Cracked Section	229
7	SUMMARY AND CONCLUSIONS	232
7.1	SUMMARY	232
7.2	PROPOSED REVISION IN AASHTO LRFD SPECIFICATION	233
7.2.1	Service I Limit State	233
7.2.2	Service III Limit State.....	233
7.3	CONCLUSIONS.....	234
	REFERENCES	237
	APPENDIX A. BRIDGE DATABASES	245
A.1	I Girder Bridges	246
A.2	Adjacent Box Girder Bridges.....	270
A.3	Spread Box Girder Bridges	278
A.4	PCI ASBI Box Girder Bridge	290
A.5	Existing Bridges from NCHRP 12-78	292

APPENDIX B. RELIABILITY ANALYSIS RESULTS.....	295
B.1 I Girder Bridges.....	295
B.2 Adjacent Box Girder Bridges.....	343
B.3 Spread Box Girder Bridges	355
B.3 ASBI Box Girder Bridges	367

LIST OF FIGURES

Figure 1.1 Reliability Indices for Bridges Designed According to (a) LFD and (b) LRFD (Kulicki (2006))	4
Figure 1.2 Excessive Cracks at the Bottom of Reinforced Concrete Structure	5
Figure 2.1 irreversible (a) and reversible (b) limit states (Gulvanessian and Holicky, 1996)	16
Figure 2.2 PDF of Load and Resistance	17
Figure 2.3 Illustration of Probability of Failure.....	17
Figure 2.4 Flexural tensile strength vs. compressive strength (Raphael, 1984)	45
Figure 2.5 Static Deflection vs. First Flexural Frequency (Ministry, 1991; CSA International, 2000).....	57
Figure 2.6 Static Deflection vs. First Mode Flexural Frequency (AUSTROADS, 1992; AUSTRALIAN, 1996).....	57
Figure 2.7 Human Response to Particle Velocity (Oriard, 1972).....	58
Figure 2.8 Criterion for Human Response to Acceleration (Ministry, 1995).....	59
Figure 3.1 Comparison of the measured and predicted maximum crack width using equation developed by Clark (1956).....	65
Figure 3.2 Comparison between the measured and predicted maximum crack width using equation developed by Karr and Mattock (1963).	65
Figure 3.3 Comparison of the measured and predicted maximum crack widths using equation developed by Gergeley and Lutz (1968).	66
Figure 3.4 Comparison between the measured and predicted maximum crack width using equation developed by Frosch (1999).....	66
Figure 3.5 Compressive Membrane Action in Cross Section of Reinforced Concrete Beam-and-Slab Bridge Deck (Hon et al., 2005)	70
Figure 3.6 Correlation of Predictions with test results (Rankin and Long, 1997)	75
Figure 3.7 Comparison between peak loads for flexural failure tests (Hon et al., 2005) .	77
Figure 3.8 Stress Distribution Diagrams for a Typical Prestressed Concrete Bridge Girder at Various Stages of Loading	81
Figure 3.9 Strain distribution at service loads.	86
Figure 3.10 Cross section and loading arrangement of testing beams (Bennett and Veerasubramanian, 1972)	92
Figure 3.11 Comparison of the measured and predicted maximum crack widths using equations developed by Nawy and Huang (1977) and Nawy and Potyondy (1971).	99
Figure 3.12 Comparison of the measured and predicted maximum crack widths using equations developed by Nawy and Huang (1977) and Bennett and Veerasubramanian (1972).....	99
Figure 3.13 Comparison between the measured and predicted maximum crack widths using equations developed by Nawy and Huang (1977) and CEB-FIP (1970).	100
Figure 3.14 Comparison between the measured and predicted maximum crack widths using equations developed by Nawy and Huang (1977) and Rao and Dilger (1992).	100

Figure 4.1 HL-93 Design Live Load Model (Nowak 1999).....	105
Figure 4.2 NJDOT Design Permit Vehicle (NJDOT, 2010).....	106
Figure 4.3 Histogram of Site 0199-South Bound	110
Figure 4.4 Histogram of Site 0199-North Bound	110
Figure 4.5 Histogram of Site 0580-East Bound.....	111
Figure 4.6 Histogram of Site 0580-West Bound	111
Figure 4.7 Histogram of Site 2680.....	112
Figure 4.8 Histogram of Site 8280.....	112
Figure 4.9 Histogram of Site 8382.....	113
Figure 4.10 Histogram of Site 9121.....	113
Figure 4.11 Histogram of Site 9631.....	114
Figure 4.12 Histogram of Florida Site 9919	114
Figure 4.13 Histogram of Florida Site 9927	115
Figure 4.14 Multiple Presence Categories	116
Figure 4.15 Time variation of total weight statistics for site 195, 1993-2009, (without filtering permits)	121
Figure 4.16 Time variation of total weight statistics for site 195, 1993-2009, (with filtering permits)	122
Figure 4.17 Typical Extrapolation of 75-Year Moment Ratio using Various Approaches	124
Figure 4.18 Comparison of Moment Ratio for Various WIM Sites (1 day period).....	130
Figure 4.19 Comparison of Difference for Various WIM Sites (1 day period).....	131
Figure 4.20 Comparison of Moment Ratio for Various WIM Sites (2 weeks period) ..	131
Figure 4.21 Comparison of Difference for Various WIM Sites (2 weeks period)	132
Figure 4.22 Comparison of Moment Ratio for Various WIM Sites (1 month period) ..	132
Figure 4.23 Comparison of Difference for Various WIM Sites (1 month period)	133
Figure 4.24 Comparison of Moment Ratio for Various WIM Sites (2 months period). 133	
Figure 4.25 Comparison of Difference for Various WIM Sites (2 months period).....	134
Figure 4.26 Comparison of Moment Ratio for Various WIM Sites (6 months period). 134	
Figure 4.27 Comparison of Difference for Various WIM Sites (6 months period).....	135
Figure 4.28 Comparison of Moment Ratio for Various WIM Sites (1 year period)	135
Figure 4.29 Comparison of Difference for Various WIM Sites (1 year period).....	136
Figure 4.30 Comparison of Moment Ratio for Various WIM Sites (5 years period)....	136
Figure 4.31 Comparison of Difference for Various WIM Sites (5 years period)	137
Figure 4.32 Comparison of Moment Ratio for Various WIM Sites (50 years period) ..	137
Figure 4.33 Comparison of Difference for Various WIM Sites (50 years period)	138
Figure 4.34 Comparison of Moment Ratio for Various WIM Sites (75 years period) ..	138
Figure 4.35 Comparison of Difference for Various WIM Sites (75 years period)	139
Figure 4.36 Extrapolation of Long Term Load Effects for Site 0580	140
Figure 4.37 Extrapolation of Long Term Load Effects for Site 2680	141
Figure 4.38 Extrapolation of Long Term Load Effects for Site 8382	142
Figure 4.39 Extrapolation of Long Term Load Effects for Site 9631	143
Figure 4.40 Extrapolation Levels for Different Return Periods (Nowak, 1999)	146
Figure 4.41 Ratio of GVW and Permitted GVW for Permit Vehicles	152

Figure 5.1 Variation of ultimate tensile strength for selected degrees of uniform corrosion of a 6 mm diameter steel bar, from Almusallam (2001).....	161
Figure 6.1 Reliability Indices of Various Bridge Decks Designed Using 1.0 Live Load Factor over 1 Year Returning Period (ADTT=1000), Positive Moment Region. ..	173
Figure 6.2 Reliability Indices of Various Bridge Decks Designed Using 1.0 Live Load Factor over 1 Year Returning Period (ADTT=1000), Negative Moment Region..	173
Figure 6.3 Reliability Indices of Various Bridge Decks Designed Using 1.0 Live Load Factor over 1 Year Returning Period (ADTT=2500), Positive Moment Region. ..	174
Figure 6.4 Reliability Indices of Various Bridge Decks Designed Using 1.0 Live Load Factor over 1 Year Returning Period (ADTT=2500), Negative Moment Region..	174
Figure 6.5 Reliability Indices of Various Bridge Decks Designed Using 1.0 Live Load Factor over 1 Year Returning Period (ADTT=5000), Positive Moment Region. ..	175
Figure 6.6 Reliability Indices of Various Bridge Decks Designed Using 1.0 Live Load Factor over 1 Year Returning Period (ADTT=5000), Negative Moment Region..	175
Figure 6.7 Reliability Indices of Various Bridge Decks Designed Using 1.0 Live Load Factor over 1 Year Returning Period (ADTT=10000), Positive Moment Region.	176
Figure 6.8 Reliability Indices of Various Bridge Decks Designed Using 1.0 Live Load Factor over 1 Year Returning Period (ADTT=10000), Negative Moment Region.	176
Figure 6.9 Reliability Indices of Various Bridge Decks Designed Using 1.0 Live Load Factor over 1 Year Returning Period (ADTT=1000), Positive Moment Region ...	177
Figure 6.10 Reliability Indices of Various Bridge Decks Designed Using 1.0 Live Load Factor over 1 Year Returning Period (ADTT=1000), Negative Moment Region..	177
Figure 6.11 Reliability Indices of Various Bridge Decks Designed Using 1.0 Live Load Factor over 1 Year Returning Period (ADTT=2500), Positive Moment Region. ..	178
Figure 6.12 Reliability Indices of Various Bridge Decks Designed Using 1.0 Live Load Factor over 1 Year Returning Period (ADTT=2500), Negative Moment Region..	178
Figure 6.13 Reliability Indices of Various Bridge Decks Designed Using 1.0 Live Load Factor over 1 Year Returning Period (ADTT=5000), Positive Moment Region. ..	179
Figure 6.14 Reliability Indices of Various Bridge Decks Designed Using 1.0 Live Load Factor over 1 Year Returning Period (ADTT=5000), Negative Moment Region..	179
Figure 6.15 Reliability Indices of Various Bridge Decks Designed Using 1.2 Live Load Factor over 1 Year Return Period (ADTT=5000), Class II Exposure Condition, Positive Moment Region.....	180
Figure 6.16 Reliability Indices of Various Bridge Decks Designed Using 1.2 Live Load Factor over 1 Year Return Period (ADTT=5000), Class II Exposure Condition, Negative Moment Region.	180
Figure 6.17 Reliability Indices of Various Bridge Decks Designed Using 1.0 Live Load Factor over 1 Year Returning Period (ADTT=10000), Positive Moment Region.	181
Figure 6.18 Reliability Indices of Various Bridge Decks Designed Using 1.0 Live Load Factor over 1 Year Returning Period (ADTT=10000), Negative Moment Region.	181
Figure 6.19 reliability index for reinforced concrete deck designed by traditional method (with and w/o deterioration).....	183
Figure 6.20 Reliability Indices of Various Bridge Decks Designed Using 1.0 Live Load Factor over 1 Year Returning Period (ADTT=1000), Positive Moment Region. ..	187

Figure 6.21 Reliability Indices of Various Bridge Decks Designed Using 1.0 Live Load Factor over 1 Year Returning Period (ADTT=1000), Negative Moment Region..	187
Figure 6.22 Reliability Indices of Various Bridge Decks Designed Using 1.0 Live Load Factor over 1 Year Returning Period (ADTT=2500), Positive Moment Region. ..	188
Figure 6.23 Reliability Indices of Various Bridge Decks Designed Using 1.0 Live Load Factor over 1 Year Returning Period (ADTT=2500), Negative Moment Region..	188
Figure 6.24 Reliability Indices of Various Bridge Decks Designed Using 1.0 Live Load Factor over 1 Year Returning Period (ADTT=5000), Positive Moment Region. ..	189
Figure 6.25 Reliability Indices of Various Bridge Decks Designed Using 1.0 Live Load Factor over 1 Year Returning Period (ADTT=5000), Negative Moment Region..	189
Figure 6.26 Reliability Indices of Various Bridge Decks Designed Using 1.0 Live Load Factor over 1 Year Returning Period (ADTT=10000), Positive Moment Region.	190
Figure 6.27 Reliability Indices of Various Bridge Decks Designed Using 1.0 Live Load Factor over 1 Year Returning Period (ADTT=10000), Negative Moment Region.	190
Figure 6.28 Reliability Indices of Various Bridge Decks Designed Using 1.0 Live Load Factor over 1 Year Returning Period (ADTT=1000), Positive Moment Region ...	191
Figure 6.29 Reliability Indices of Various Bridge Decks Designed Using 1.0 Live Load Factor over 1 Year Returning Period (ADTT=1000), Negative Moment Region..	191
Figure 6.30 Reliability Indices of Various Bridge Decks Designed Using 1.0 Live Load Factor over 1 Year Returning Period (ADTT=2500), Positive Moment Region. ..	192
Figure 6.31 Reliability Indices of Various Bridge Decks Designed Using 1.0 Live Load Factor over 1 Year Returning Period (ADTT=2500), Negative Moment Region..	192
Figure 6.32 Reliability Indices of Various Bridge Decks Designed Using 1.0 Live Load Factor over 1 Year Returning Period (ADTT=5000), Positive Moment Region. ..	193
Figure 6.33 Reliability Indices of Various Bridge Decks Designed Using 1.0 Live Load Factor over 1 Year Returning Period (ADTT=5000), Negative Moment Region..	193
Figure 6.34 Reliability Indices of Various Bridge Decks Designed Using 1.0 Live Load Factor over 1 Year Returning Period (ADTT=10000), Positive Moment Region.	194
Figure 6.35 Reliability Indices of Various Bridge Decks Designed Using 1.0 Live Load Factor over 1 Year Returning Period (ADTT=10000), Negative Moment Region.	194
Figure 6.36 reliability index for reinforced concrete deck designed by empirical method (with and w/o deterioration).....	197
Figure 6.37 Composition of Simulated Bridge Database	199
Figure 6.38 Reliability indices for bridges at decompression limit state (ADTT=5000), $\gamma_{LL}=0.8, (f_t = 0.0948\sqrt{f'_c})$	210
Figure 6.39 Reliability indices for bridges at maximum allowable tensile stress limit state (ADTT=5000), $\gamma_{LL}=0.8, (f_t = 0.0948\sqrt{f'_c})$	210
Figure 6.40 Reliability Indices for bridges at maximum allowable crack width limit state (ADTT=5000), $\gamma_{LL}=0.8, (f_t = 0.0948\sqrt{f'_c})$	211
Figure 6.41 Reliability indices for bridges at decompression limit state (ADTT=5000), $\gamma_{LL}=1.0 (f_t = 0.0948\sqrt{f'_c})$	211

Figure 6.42 Reliability indices for bridges at maximum allowable tensile stress limit state (ADTT=5000), $\gamma_{LL}=1.0$ ($f_t = 0.0948\sqrt{f'_c}$).....	213
Figure 6.43 Reliability indices for bridges at maximum allowable crack width limit state (ADTT=1000), $\gamma_{LL}=1.0$ ($f_t = 0.0948\sqrt{f'_c}$).....	213
Figure 6.44 Reliability indices for bridges at decompression limit state (ADTT=5000), $\gamma_{LL}=0.8$ ($f_t = 0.19\sqrt{f'_c}$).....	215
Figure 6.45 Reliability indices for bridges at maximum allowable tensile stress limit state (ADTT=5000), $\gamma_{LL}=0.8$ ($f_t = 0.19\sqrt{f'_c}$).....	215
Figure 6.46 Reliability indices for bridges at maximum allowable crack width limit state (ADTT=5000), $\gamma_{LL}=0.8$ ($f_t = 0.19\sqrt{f'_c}$).....	216
Figure 6.47 Reliability indices for bridges at decompression limit state (ADTT=5000), $\gamma_{LL}=1.0$ ($f_t = 0.19\sqrt{f'_c}$).....	216
Figure 6.48 Reliability indices for bridges at maximum tensile stress limit state (ADTT=5000), $\gamma_{LL}=1.0$ ($f_t = 0.19\sqrt{f'_c}$).....	217
Figure 6.49 Reliability indices for bridges at maximum crack width limit state (ADTT=5000), $\gamma_{LL}=1.0$ ($f_t = 0.19\sqrt{f'_c}$).....	217
Figure 6.50 Reliability indices for bridges at decompression limit state (ADTT=5000), $\gamma_{LL}=0.8$ ($f_t = 0.25\sqrt{f'_c}$).....	218
Figure 6.51 Reliability indices for bridges at maximum allowable tensile stress limit state (ADTT=5000), $\gamma_{LL}=0.8$ ($f_t = 0.25\sqrt{f'_c}$).....	219
Figure 6.52 Reliability indices for bridges at maximum allowable crack width limit state (ADTT=5000), $\gamma_{LL}=0.8$ ($f_t = 0.25\sqrt{f'_c}$).....	219
Figure 6.53 Reliability indices for bridges at decompression limit state (ADTT=5000), $\gamma_{LL}=1.0$ ($f_t = 0.25\sqrt{f'_c}$).....	220
Figure 6.54 Reliability indices for bridges at maximum tensile stress limit state (ADTT=5000), $\gamma_{LL}=1.0$ ($f_t = 0.25\sqrt{f'_c}$).....	220
Figure 6.55 Reliability indices for bridges at maximum crack width limit state (ADTT=5000), $\gamma_{LL}=1.0$ ($f_t = 0.25\sqrt{f'_c}$).....	221
Figure 6.56 reliability index for prestressed concrete girder (Bridge A) at decompression level (with and w/o deterioration).....	223
Figure 6.57 reliability index for prestressed concrete girder (Bridge B) at decompression level (with and w/o deterioration).....	224
Figure 6.58 Reliability indices for Uncracked Section at Deflection Limit State (ADTT=1000), $\gamma_{LL}=0.8$, ($f_t = 0.19\sqrt{f'_c}$).....	227

Figure 6.59 Reliability indices for Uncracked Section at Deflection Limit State (ADTT=2500), $\gamma_{LL}=0.8$, ($f_t = 0.19\sqrt{f'_c}$).....	228
Figure 6.60 Reliability Indices for Uncracked Section at Deflection Limit State (ADTT=5000), $\gamma_{LL}=0.8$, ($f_t = 0.19\sqrt{f'_c}$).....	228
Figure 6.61 Reliability Indices for Uncracked Section at Deflection Limit State (ADTT=10,000), $\gamma_{LL}=0.8$, ($f_t = 0.19\sqrt{f'_c}$).....	229
Figure 6.62 Reliability Indices for Cracked Section at Deflection Limit State (ADTT=1000), $\gamma_{LL}=0.8$, ($f_t = 0.19\sqrt{f'_c}$).....	230
Figure 6.63 Reliability Indices for Cracked Section at Deflection Limit State (ADTT=2500), $\gamma_{LL}=0.8$, ($f_t = 0.19\sqrt{f'_c}$).....	230
Figure 6.64 Reliability Indices for Cracked Section at Deflection Limit State (ADTT=5000), $\gamma_{LL}=0.8$, ($f_t = 0.19\sqrt{f'_c}$).....	231
Figure 6.65 Reliability Indices for Cracked Section at Deflection Limit State (ADTT=10,000), $\gamma_{LL}=0.8$, ($f_t = 0.19\sqrt{f'_c}$).....	231
Figure B.1 Reliability Indices for AASHTO I Girder Bridges at Decompression Limit State (ADTT=1000), $\gamma_{LL}=0.8$ ($f_t = 0.0948\sqrt{f'_c}$)	295
Figure B.2 Reliability Indices for AASHTO I Girder Bridges at Maximum Allowable Tensile Stress Limit State (ADTT=1000), $\gamma_{LL}=0.8$ ($f_t = 0.0948\sqrt{f'_c}$)	296
Figure B.3 Reliability Indices for AASHTO I Girder Bridges at Maximum Allowable Crack Width Limit State (ADTT=1000), $\gamma_{LL}=0.8$ ($f_t = 0.0948\sqrt{f'_c}$)	296
Figure B.4 Reliability Indices for AASHTO I Girder Bridges at Decompression Limit State (ADTT=1000), $\gamma_{LL}=1.0$ ($f_t = 0.0948\sqrt{f'_c}$)	297
Figure B.5 Reliability Indices for AASHTO I Girder Bridges at Maximum Tensile Stress Limit State (ADTT=1000), $\gamma_{LL}=1.0$ ($f_t = 0.0948\sqrt{f'_c}$)	297
Figure B.6 Reliability Indices for AASHTO I Girder Bridges at Maximum Crack Width Limit State (ADTT=1000), $\gamma_{LL}=1.0$ ($f_t = 0.0948\sqrt{f'_c}$)	298
Figure B.7 Reliability Indices for AASHTO I Girder Bridges at Decompression Limit State (ADTT=1000), $\gamma_{LL}=0.8$ ($f_t = 0.158\sqrt{f'_c}$)	298
Figure B.8 Reliability Indices for AASHTO I Girder Bridges at Maximum Allowable Tensile Stress Limit State (ADTT=1000), $\gamma_{LL}=0.8$ ($f_t = 0.158\sqrt{f'_c}$)	299
Figure B.9 Reliability Indices for AASHTO I Girder Bridges at Maximum Allowable Crack Width Limit State (ADTT=1000), $\gamma_{LL}=0.8$ ($f_t = 0.158\sqrt{f'_c}$)	299
Figure B.10 Reliability Indices for AASHTO I Girder Bridges at Decompression Limit State (ADTT=1000) , $\gamma_{LL}=1.0$ ($f_t = 0.158\sqrt{f'_c}$)	300

Figure B.11 Reliability Indices for AASHTO I Girder Bridges at Maximum Tensile Stress Limit State (ADTT=1000), $\gamma_{LL}=1.0$ ($f_t = 0.158\sqrt{f'_c}$).....	300
Figure B.12 Reliability Indices for AASHTO I Girder Bridges at Maximum Crack Width Limit State (ADTT=1000), $\gamma_{LL}=1.0$ ($f_t = 0.158\sqrt{f'_c}$)	301
Figure B.13 Reliability Indices for AASHTO I Girder Bridges at Decompression Limit State (ADTT=1000), $\gamma_{LL}=0.8$ ($f_t = 0.19\sqrt{f'_c}$)	301
Figure B.14 Reliability Indices for AASHTO I Girder Bridges at Maximum Allowable Tensile Stress Limit State (ADTT=1000), $\gamma_{LL}=0.8$ ($f_t = 0.19\sqrt{f'_c}$)	302
Figure B.15 Reliability Indices for AASHTO I Girder Bridges at Maximum Allowable Crack Width Limit State (ADTT=1000), $\gamma_{LL}=0.8$ ($f_t = 0.19\sqrt{f'_c}$)	302
Figure B.16 Reliability Indices for AASHTO I Girder Bridges at Decompression Limit State (ADTT=1000) , $\gamma_{LL}=1.0$ ($f_t = 0.19\sqrt{f'_c}$)	303
Figure B.17 Reliability Indices for AASHTO I Girder Bridges at Maximum Tensile Stress Limit State (ADTT=1000), $\gamma_{LL}=1.0$ ($f_t = 0.19\sqrt{f'_c}$).....	303
Figure B.18 Reliability Indices for AASHTO I Girder Bridges at Maximum Crack Width Limit State (ADTT=1000), $\gamma_{LL}=1.0$ ($f_t = 0.19\sqrt{f'_c}$)	304
Figure B.19 Reliability Indices for AASHTO I Girder Bridges at Decompression Limit State (ADTT=1000), $\gamma_{LL}=0.8$ ($f_t = 0.253\sqrt{f'_c}$)	304
Figure B.20 Reliability Indices for AASHTO I Girder Bridges at Maximum Allowable Tensile Stress Limit State (ADTT=1000), $\gamma_{LL}=0.8$ ($f_t = 0.253\sqrt{f'_c}$).....	305
Figure B.21 Reliability Indices for AASHTO I Girder Bridges at Maximum Allowable Crack Width Limit State (ADTT=1000), $\gamma_{LL}=0.8$ ($f_t = 0.253\sqrt{f'_c}$).....	305
Figure B.22 Reliability Indices for AASHTO I Girder Bridges at Decompression Limit State (ADTT=1000), $\gamma_{LL}=1.0$ ($f_t = 0.253\sqrt{f'_c}$)	306
Figure B.23 Reliability Indices for AASHTO I Girder Bridges at Maximum Allowable Tensile Stress Limit State (ADTT=1000), $\gamma_{LL}=1.0$ ($f_t = 0.253\sqrt{f'_c}$).....	306
Figure B.24 Reliability Indices for AASHTO I Girder Bridges at Maximum Allowable Crack Width Limit State (ADTT=1000), $\gamma_{LL}=1.0$ ($f_t = 0.253\sqrt{f'_c}$).....	307
Figure B.25 Reliability Indices for AASHTO I Girder Bridges at Decompression Limit State (ADTT=2500), $\gamma_{LL}=0.8$ ($f_t = 0.0948\sqrt{f'_c}$)	307
Figure B.26 Reliability Indices for AASHTO I Girder Bridges at Maximum Allowable Tensile Stress Limit State (ADTT=2500), $\gamma_{LL}=0.8$ ($f_t = 0.0948\sqrt{f'_c}$)	308
Figure B.27 Reliability Indices for AASHTO I Girder Bridges at Maximum Allowable Crack Width Limit State (ADTT=2500), $\gamma_{LL}=0.8$ ($f_t = 0.0948\sqrt{f'_c}$)	308

Figure B.28 Reliability Indices for AASHTO I Girder Bridges at Decompression Limit State (ADTT=2500), $\gamma_{LL}=1.0$ ($f_t = 0.0948\sqrt{f'_c}$)	309
Figure B.29 Reliability Indices for AASHTO I Girder Bridges at Maximum Tensile Stress Limit State (ADTT=2500), $\gamma_{LL}=1.0$ ($f_t = 0.0948\sqrt{f'_c}$)	309
Figure B.30 Reliability Indices for AASHTO I Girder Bridges at Maximum Crack Width Limit State (ADTT=2500), $\gamma_{LL}=1.0$ ($f_t = 0.0948\sqrt{f'_c}$)	310
Figure B.31 Reliability Indices for AASHTO I Girder Bridges at Decompression Limit State (ADTT=2500), $\gamma_{LL}=0.8$ ($f_t = 0.158\sqrt{f'_c}$)	310
Figure B.32 Reliability Indices for AASHTO I Girder Bridges at Maximum Allowable Tensile Stress Limit State (ADTT=2500), $\gamma_{LL}=0.8$ ($f_t = 0.158\sqrt{f'_c}$)	311
Figure B.33 Reliability Indices for AASHTO I Girder Bridges at Maximum Allowable Crack Width Limit State (ADTT=2500), $\gamma_{LL}=0.8$ ($f_t = 0.158\sqrt{f'_c}$)	311
Figure B.34 Reliability Indices for AASHTO I Girder Bridges at Decompression Limit State (ADTT=2500), $\gamma_{LL}=1.0$ ($f_t = 0.158\sqrt{f'_c}$)	312
Figure B.35 Reliability Indices for AASHTO I Girder Bridges at Maximum Tensile Stress Limit State (ADTT=2500), $\gamma_{LL}=1.0$ ($f_t = 0.158\sqrt{f'_c}$)	312
Figure B.36 Reliability Indices for AASHTO I Girder Bridges at Maximum Crack Width Limit State (ADTT=2500), $\gamma_{LL}=1.0$ ($f_t = 0.158\sqrt{f'_c}$)	313
Figure B.37 Reliability Indices for AASHTO I Girder Bridges at Decompression Limit State (ADTT=2500), $\gamma_{LL}=0.8$ ($f_t = 0.19\sqrt{f'_c}$)	313
Figure B.38 Reliability Indices for AASHTO I Girder Bridges at Maximum Allowable Tensile Stress Limit State (ADTT=2500), $\gamma_{LL}=0.8$ ($f_t = 0.19\sqrt{f'_c}$)	314
Figure B.39 Reliability Indices for AASHTO I Girder Bridges at Maximum Allowable Crack Width Limit State (ADTT=2500), $\gamma_{LL}=0.8$ ($f_t = 0.19\sqrt{f'_c}$)	314
Figure B.40 Reliability Indices for AASHTO I Girder Bridges at Decompression Limit State (ADTT=2500), $\gamma_{LL}=1.0$ ($f_t = 0.19\sqrt{f'_c}$)	315
Figure B.41 Reliability Indices for AASHTO I Girder Bridges at Maximum Tensile Stress Limit State (ADTT=2500), $\gamma_{LL}=1.0$ ($f_t = 0.19\sqrt{f'_c}$)	315
Figure B.42 Reliability Indices for AASHTO I Girder Bridges at Maximum Crack Width Limit State (ADTT=2500), $\gamma_{LL}=1.0$ ($f_t = 0.19\sqrt{f'_c}$)	316
Figure B.43 Reliability Indices for AASHTO I Girder Bridges at Decompression Limit State (ADTT=2500), $\gamma_{LL}=0.8$ ($f_t = 0.253\sqrt{f'_c}$)	316
Figure B.44 Reliability Indices for AASHTO I Girder Bridges at Maximum Allowable Tensile Stress Limit State (ADTT=2500), $\gamma_{LL}=0.8$ ($f_t = 0.253\sqrt{f'_c}$)	317

Figure B.45 Reliability Indices for AASHTO I Girder Bridges at Maximum Allowable Crack Width Limit State (ADTT=2500), $\gamma_{LL}=0.8$ ($f_t = 0.253\sqrt{f'_c}$).....	317
Figure B.46 Reliability Indices for AASHTO I Girder Bridges at Decompression Limit State (ADTT=2500) , $\gamma_{LL}=1.0$ ($f_t = 0.253\sqrt{f'_c}$)	318
Figure B.47 Reliability Indices for AASHTO I Girder Bridges at Maximum Tensile Stress Limit State (ADTT=2500), $\gamma_{LL}=1.0$ ($f_t = 0.253\sqrt{f'_c}$).....	318
Figure B.48 Reliability Indices for AASHTO I Girder Bridges at Maximum Crack Width Limit State (ADTT=2500), $\gamma_{LL}=1.0$ ($f_t = 0.253\sqrt{f'_c}$)	319
Figure B.49 Reliability Indices for AASHTO I Girder Bridges at Decompression Limit State (ADTT=5000), $\gamma_{LL}=0.8$ ($f_t = 0.0948\sqrt{f'_c}$)	319
Figure B.50 Reliability Indices for AASHTO I Girder Bridges at Maximum Allowable Tensile Stress Limit State (ADTT=5000), $\gamma_{LL}=0.8$ ($f_t = 0.0948\sqrt{f'_c}$)	320
Figure B.51 Reliability Indices for AASHTO I Girder Bridges at Maximum Allowable Crack Width Limit State (ADTT=5000), $\gamma_{LL}=0.8$ ($f_t = 0.0948\sqrt{f'_c}$).....	320
Figure B.52 Reliability Indices for AASHTO I Girder Bridges at Decompression Limit State (ADTT=5000), $\gamma_{LL}=1.0$ ($f_t = 0.0948\sqrt{f'_c}$)	321
Figure B.53 Reliability Indices for AASHTO I Girder Bridges at Maximum Tensile Stress Limit State (ADTT=5000), $\gamma_{LL}=1.0$ ($f_t = 0.0948\sqrt{f'_c}$).....	321
Figure B.54 Reliability Indices for AASHTO I Girder Bridges at Maximum Crack Width Limit State (ADTT=5000), $\gamma_{LL}=1.0$ ($f_t = 0.0948\sqrt{f'_c}$)	322
Figure B.55 Reliability Indices for AASHTO I Girder Bridges at Decompression Limit State (ADTT=5000), $\gamma_{LL}=0.8$ ($f_t = 0.158\sqrt{f'_c}$)	322
Figure B.56 Reliability Indices for AASHTO I Girder Bridges at Maximum Allowable Tensile Stress Limit State (ADTT=5000), $\gamma_{LL}=0.8$ ($f_t = 0.158\sqrt{f'_c}$).....	323
Figure B.57 Reliability Indices for AASHTO I Girder Bridges at Maximum Allowable Crack Width Limit State (ADTT=5000), $\gamma_{LL}=0.8$ ($f_t = 0.158\sqrt{f'_c}$).....	323
Figure B.58 Reliability Indices for AASHTO I Girder Bridges at Decompression Limit State (ADTT=5000), $\gamma_{LL}=1.0$ ($f_t = 0.158\sqrt{f'_c}$)	324
Figure B.59 Reliability Indices for AASHTO I Girder Bridges at Maximum Tensile Stress Limit State (ADTT=5000), $\gamma_{LL}=1.0$ ($f_t = 0.158\sqrt{f'_c}$).....	324
Figure B.60 Reliability Indices for AASHTO I Girder Bridges at Maximum Crack Width Limit State (ADTT=5000), $\gamma_{LL}=1.0$ ($f_t = 0.158\sqrt{f'_c}$)	325
Figure B.61 Reliability Indices for AASHTO I Girder Bridges at Decompression Limit State (ADTT=5000), $\gamma_{LL}=0.8$ ($f_t = 0.19\sqrt{f'_c}$)	325

Figure B.62 Reliability Indices for AASHTO I Girder Bridges at Maximum Allowable Tensile Stress Limit State (ADTT=5000), $\gamma_{LL}=0.8$ ($f_t = 0.19\sqrt{f'_c}$)	326
Figure B.63 Reliability Indices for AASHTO I Girder Bridges at Maximum Allowable Crack Width Limit State (ADTT=5000), $\gamma_{LL}=0.8$ ($f_t = 0.19\sqrt{f'_c}$)	326
Figure B.64 Reliability Indices for AASHTO I Girder Bridges at Decompression Limit State (ADTT=5000), $\gamma_{LL}=1.0$ ($f_t = 0.19\sqrt{f'_c}$)	327
Figure B.65 Reliability Indices for AASHTO I Girder Bridges at Maximum Tensile Stress Limit State (ADTT=5000), $\gamma_{LL}=1.0$ ($f_t = 0.19\sqrt{f'_c}$)	327
Figure B.66 Reliability Indices for AASHTO I Girder Bridges at Maximum Crack Width Limit State (ADTT=5000), $\gamma_{LL}=1.0$ ($f_t = 0.19\sqrt{f'_c}$)	328
Figure B.67 Reliability Indices for AASHTO I Girder Bridges at Decompression Limit State (ADTT=5000), $\gamma_{LL}=0.8$ ($f_t = 0.253\sqrt{f'_c}$)	328
Figure B.68 Reliability Indices for AASHTO I Girder Bridges at Maximum Allowable Tensile Stress Limit State (ADTT=5000), $\gamma_{LL}=0.8$ ($f_t = 0.253\sqrt{f'_c}$)	329
Figure B.69 Reliability Indices for AASHTO I Girder Bridges at Maximum Allowable Crack Width Limit State (ADTT=5000), $\gamma_{LL}=0.8$ ($f_t = 0.253\sqrt{f'_c}$)	329
Figure B.70 Reliability Indices for AASHTO I Girder Bridges at Decompression Limit State (ADTT=5000), $\gamma_{LL}=1.0$ ($f_t = 0.253\sqrt{f'_c}$)	330
Figure B.71 Reliability Indices for AASHTO I Girder Bridges at Maximum Tensile Stress Limit State (ADTT=5000), $\gamma_{LL}=1.0$ ($f_t = 0.253\sqrt{f'_c}$)	330
Figure B.72 Reliability Indices for AASHTO I Girder Bridges at Maximum Crack Width Limit State (ADTT=5000), $\gamma_{LL}=1.0$ ($f_t = 0.253\sqrt{f'_c}$)	331
Figure B.73 Reliability Indices for AASHTO I Girder Bridges at Decompression Limit State (ADTT=10000), $\gamma_{LL}=0.8$ ($f_t = 0.0948\sqrt{f'_c}$)	331
Figure B.74 Reliability Indices for AASHTO I Girder Bridges at Maximum Allowable Tensile Stress Limit State (ADTT=10000), $\gamma_{LL}=0.8$ ($f_t = 0.0948\sqrt{f'_c}$)	332
Figure B.75 Reliability Indices for AASHTO I Girder Bridges at Maximum Allowable Crack Width Limit State (ADTT=10000), $\gamma_{LL}=0.8$ ($f_t = 0.0948\sqrt{f'_c}$)	332
Figure B.76 Reliability Indices for AASHTO I Girder Bridges at Decompression Limit State (ADTT=10000), $\gamma_{LL}=1.0$ ($f_t = 0.0948\sqrt{f'_c}$)	333
Figure B.77 Reliability Indices for AASHTO I Girder Bridges at Maximum Tensile Stress Limit State (ADTT=10000), $\gamma_{LL}=1.0$ ($f_t = 0.0948\sqrt{f'_c}$)	333
Figure B.78 Reliability Indices for AASHTO I Girder Bridges at Maximum Crack Width Limit State (ADTT=10000), $\gamma_{LL}=1.0$ ($f_t = 0.0948\sqrt{f'_c}$)	334

Figure B.79 Reliability Indices for AASHTO I Girder Bridges at Decompression Limit State (ADTT=10000), $\gamma_{LL}=0.8$ ($f_t = 0.158\sqrt{f'_c}$)	334
Figure B.80 Reliability Indices for AASHTO I Girder Bridges at Maximum Allowable Tensile Stress Limit State (ADTT=10000), $\gamma_{LL}=0.8$ ($f_t = 0.158\sqrt{f'_c}$)	335
Figure B.81 Reliability Indices for AASHTO I Girder Bridges at Maximum Allowable Crack Width Limit State (ADTT=10000), $\gamma_{LL}=0.8$ ($f_t = 0.158\sqrt{f'_c}$)	335
Figure B.82 Reliability Indices for AASHTO I Girder Bridges at Decompression Limit State (ADTT=10000), $\gamma_{LL}=1.0$ ($f_t = 0.158\sqrt{f'_c}$)	336
Figure B.83 Reliability Indices for AASHTO I Girder Bridges at Maximum Tensile Stress Limit State (ADTT=10000), $\gamma_{LL}=1.0$ ($f_t = 0.158\sqrt{f'_c}$)	336
Figure B.84 Reliability Indices for AASHTO I Girder Bridges at Maximum Crack Width Limit State (ADTT=10000), $\gamma_{LL}=1.0$ ($f_t = 0.158\sqrt{f'_c}$)	337
Figure B.85 Reliability Indices for AASHTO I Girder Bridges at Decompression Limit State (ADTT=10000), $\gamma_{LL}=0.8$ ($f_t = 0.19\sqrt{f'_c}$)	337
Figure B.86 Reliability Indices for AASHTO I Girder Bridges at Maximum Allowable Tensile Stress Limit State (ADTT=10000), $\gamma_{LL}=0.8$ ($f_t = 0.19\sqrt{f'_c}$)	338
Figure B.87 Reliability Indices for AASHTO I Girder Bridges at Maximum Allowable Crack Width Limit State (ADTT=10000), $\gamma_{LL}=0.8$ ($f_t = 0.19\sqrt{f'_c}$)	338
Figure B.88 Reliability Indices for AASHTO I Girder Bridges at Decompression Limit State (ADTT=10000), $\gamma_{LL}=1.0$ ($f_t = 0.19\sqrt{f'_c}$)	339
Figure B.89 Reliability Indices for AASHTO I Girder Bridges at Maximum Tensile Stress Limit State (ADTT=10000), $\gamma_{LL}=1.0$ ($f_t = 0.19\sqrt{f'_c}$)	339
Figure B.90 Reliability Indices for AASHTO I Girder Bridges at Maximum Crack Width Limit State (ADTT=10000), $\gamma_{LL}=1.0$ ($f_t = 0.19\sqrt{f'_c}$)	340
Figure B.91 Reliability Indices for AASHTO I Girder Bridges at Decompression Limit State (ADTT=10000), $\gamma_{LL}=0.8$ ($f_t = 0.253\sqrt{f'_c}$)	340
Figure B.92 Reliability Indices for AASHTO I Girder Bridges at Maximum Allowable Tensile Stress Limit State (ADTT=10000), $\gamma_{LL}=0.8$ ($f_t = 0.253\sqrt{f'_c}$)	341
Figure B.93 Reliability Indices for AASHTO I Girder Bridges at Maximum Allowable Crack Width Limit State (ADTT=10000), $\gamma_{LL}=0.8$ ($f_t = 0.253\sqrt{f'_c}$)	341
Figure B.94 Reliability Indices for AASHTO I Girder Bridges at Decompression Limit State (ADTT=10000), $\gamma_{LL}=1.0$ ($f_t = 0.253\sqrt{f'_c}$)	342
Figure B.95 Reliability Indices for AASHTO I Girder Bridges at Maximum Tensile Stress Limit State (ADTT=10000), $\gamma_{LL}=1.0$ ($f_t = 0.253\sqrt{f'_c}$)	342

Figure B.96 Reliability Indices for AASHTO I Girder Bridges at Maximum Crack Width Limit State (ADTT=10000), $\gamma_{LL}=1.0$ ($f_t = 0.253\sqrt{f'_c}$)	343
Figure B.97 Reliability Indices for AASHTO Adjacent Box Girder Bridges at Decompression Limit State (ADTT=5000), $\gamma_{LL}=0.8$ ($f_t = 0.0948\sqrt{f'_c}$).....	343
Figure B.98 Reliability Indices for AASHTO Adjacent Box Girder Bridges at Maximum Allowable Tensile Stress Limit State (ADTT=5000), $\gamma_{LL}=0.8$ ($f_t = 0.0948\sqrt{f'_c}$)	344
Figure B.99 Reliability Indices for AASHTO Adjacent Box Girder Bridges at Maximum Allowable Crack Width Limit State (ADTT=5000), $\gamma_{LL}=0.8$ ($f_t = 0.0948\sqrt{f'_c}$) .	344
Figure B.100 Reliability Indices for AASHTO Adjacent Box Girder Bridges at Decompression Limit State (ADTT=5000), $\gamma_{LL}=1.0$ ($f_t = 0.0948\sqrt{f'_c}$).....	345
Figure B.101 Reliability Indices for AASHTO Adjacent Box Girder Bridges at Maximum Tensile Stress Limit State (ADTT=5000), $\gamma_{LL}=1.0$ ($f_t = 0.0948\sqrt{f'_c}$)	345
Figure B.102 Reliability Indices for AASHTO Adjacent Box Girder Bridges at Maximum Crack Width Limit State (ADTT=5000), $\gamma_{LL}=1.0$ ($f_t = 0.0948\sqrt{f'_c}$)	346
Figure B.103 Reliability Indices for AASHTO Adjacent Box Girder Bridges at Decompression Limit State (ADTT=5000), $\gamma_{LL}=0.8$ ($f_t = 0.158\sqrt{f'_c}$)	346
Figure B.104 Reliability Indices for AASHTO Adjacent Box Girder Bridges at Maximum Allowable Tensile Stress Limit State (ADTT=5000), $\gamma_{LL}=0.8$ ($f_t = 0.158\sqrt{f'_c}$) .	347
Figure B.105 Reliability Indices for AASHTO Adjacent Box Girder Bridges at Maximum Allowable Crack Width Limit State (ADTT=5000), $\gamma_{LL}=0.8$ ($f_t = 0.158\sqrt{f'_c}$) ...	347
Figure B.106 Reliability Indices for AASHTO Adjacent Box Girder Bridges at Decompression Limit State (ADTT=5000), $\gamma_{LL}=1.0$ ($f_t = 0.158\sqrt{f'_c}$)	348
Figure B.107 Reliability Indices for AASHTO Adjacent Box Girder Bridges at Maximum Tensile Stress Limit State (ADTT=5000), $\gamma_{LL}=1.0$ ($f_t = 0.158\sqrt{f'_c}$)	348
Figure B.108 Reliability Indices for AASHTO Adjacent Box Girder Bridges at Maximum Crack Width Limit State (ADTT=5000), $\gamma_{LL}=1.0$ ($f_t = 0.158\sqrt{f'_c}$)	349
Figure B.109 Reliability Indices for AASHTO Adjacent Box Girder Bridges at Decompression Limit State (ADTT=5000), $\gamma_{LL}=0.8$ ($f_t = 0.19\sqrt{f'_c}$).....	349
Figure B.110 Reliability Indices for AASHTO Adjacent Box Girder Bridges at Maximum Allowable Tensile Stress Limit State (ADTT=5000), $\gamma_{LL}=0.8$ ($f_t = 0.19\sqrt{f'_c}$) ...	350
Figure B.111 Reliability Indices for AASHTO Adjacent Box Girder Bridges at Maximum Allowable Crack Width Limit State (ADTT=5000), $\gamma_{LL}=0.8$ ($f_t = 0.19\sqrt{f'_c}$)	350
Figure B.112 Reliability Indices for AASHTO Adjacent Box Girder Bridges at Decompression Limit State (ADTT=5000), $\gamma_{LL}=1.0$ ($f_t = 0.19\sqrt{f'_c}$).....	351

Figure B.113 Reliability Indices for AASHTO Adjacent Box Girder Bridges at Maximum Tensile Stress Limit State (ADTT=5000), $\gamma_{LL}=1.0$ ($f_t = 0.19\sqrt{f'_c}$)	351
Figure B.114 Reliability Indices for AASHTO Adjacent Box Girder Bridges at Maximum Crack Width Limit State (ADTT=5000), $\gamma_{LL}=1.0$ ($f_t = 0.19\sqrt{f'_c}$)	352
Figure B.115 Reliability Indices for AASHTO Adjacent Box Girder Bridges at Decompression Limit State (ADTT=5000), $\gamma_{LL}=0.8$ ($f_t = 0.253\sqrt{f'_c}$)	352
Figure B.116 Reliability Indices for AASHTO Adjacent Box Girder Bridges at Maximum Allowable Tensile Stress Limit State (ADTT=5000), $\gamma_{LL}=0.8$ ($f_t = 0.253\sqrt{f'_c}$) .	353
Figure B.117 Reliability Indices for AASHTO Adjacent Box Girder Bridges at Maximum Allowable Crack Width Limit State (ADTT=5000), $\gamma_{LL}=0.8$ ($f_t = 0.253\sqrt{f'_c}$) ...	353
Figure B.118 Reliability Indices for AASHTO Adjacent Box Girder Bridges at Decompression Limit State (ADTT=5000), $\gamma_{LL}=1.0$ ($f_t = 0.253\sqrt{f'_c}$)	354
Figure B.119 Reliability Indices for AASHTO Adjacent Box Girder Bridges at Maximum Allowable Tensile Stress Limit State (ADTT=5000), $\gamma_{LL}=1.0$ ($f_t = 0.253\sqrt{f'_c}$) .	354
Figure B.120 Reliability Indices for AASHTO Adjacent Box Girder Bridges at Maximum Allowable Crack Width Limit State (ADTT=5000), $\gamma_{LL}=1.0$ ($f_t = 0.253\sqrt{f'_c}$) ...	355
Figure B.121 Reliability Indices for AASHTO Spread Box Girder Bridges at Decompression Limit State (ADTT=5000), $\gamma_{LL}=0.8$ ($f_t = 0.0948\sqrt{f'_c}$)	355
Figure B.122 Reliability Indices for AASHTO Spread Box Girder Bridges at Maximum Allowable Tensile Stress Limit State (ADTT=5000), $\gamma_{LL}=0.8$ ($f_t = 0.0948\sqrt{f'_c}$)	356
Figure B.123 Reliability Indices for AASHTO Spread Box Girder Bridges at Maximum Allowable Crack Width Limit State (ADTT=5000), $\gamma_{LL}=0.8$ ($f_t = 0.0948\sqrt{f'_c}$) .	356
Figure B.124 Reliability Indices for AASHTO Spread Box Girder Bridges at Decompression Limit State (ADTT=5000), $\gamma_{LL}=1.0$ ($f_t = 0.0948\sqrt{f'_c}$)	357
Figure B.125 Reliability Indices for AASHTO Spread Box Girder Bridges at Maximum Tensile Stress Limit State (ADTT=5000), $\gamma_{LL}=1.0$ ($f_t = 0.0948\sqrt{f'_c}$)	357
Figure B.126 Reliability Indices for AASHTO Spread Box Girder Bridges at Maximum Crack Width Limit State (ADTT=5000), $\gamma_{LL}=1.0$ ($f_t = 0.0948\sqrt{f'_c}$)	358
Figure B.127 Reliability Indices for AASHTO Spread Box Girder Bridges at Decompression Limit State (ADTT=5000), $\gamma_{LL}=0.8$ ($f_t = 0.158\sqrt{f'_c}$)	358
Figure B.128 Reliability Indices for AASHTO Spread Box Girder Bridges at Maximum Allowable Tensile Stress Limit State (ADTT=5000), $\gamma_{LL}=0.8$ ($f_t = 0.158\sqrt{f'_c}$) .	359
Figure B.129 Reliability Indices for AASHTO Spread Box Girder Bridges at Maximum Allowable Crack Width Limit State (ADTT=5000), $\gamma_{LL}=0.8$ ($f_t = 0.158\sqrt{f'_c}$) ...	359

Figure B.130 Reliability Indices for AASHTO Spread Box Girder Bridges at Decompression Limit State (ADTT=5000), $\gamma_{LL}=1.0$ ($f_t = 0.158\sqrt{f'_c}$)	360
Figure B.131 Reliability Indices for AASHTO Spread Box Girder Bridges at Maximum Tensile Stress Limit State (ADTT=5000), $\gamma_{LL}=1.0$ ($f_t = 0.158\sqrt{f'_c}$)	360
Figure B.132 Reliability Indices for AASHTO Spread Box Girder Bridges at Maximum Crack Width Limit State (ADTT=5000), $\gamma_{LL}=1.0$ ($f_t = 0.158\sqrt{f'_c}$)	361
Figure B.133 Reliability Indices for AASHTO Spread Box Girder Bridges at Decompression Limit State (ADTT=5000), $\gamma_{LL}=0.8$ ($f_t = 0.19\sqrt{f'_c}$)	361
Figure B.134 Reliability Indices for AASHTO Spread Box Girder Bridges at Maximum Allowable Tensile Stress Limit State (ADTT=5000), $\gamma_{LL}=0.8$ ($f_t = 0.19\sqrt{f'_c}$) ...	362
Figure B.135 Reliability Indices for AASHTO Spread Box Girder Bridges at Maximum Allowable Crack Width Limit State (ADTT=5000), $\gamma_{LL}=0.8$ ($f_t = 0.19\sqrt{f'_c}$)	362
Figure B.136 Reliability Indices for AASHTO Spread Box Girder Bridges at Decompression Limit State (ADTT=5000) $\gamma_{LL}=1.0$ ($f_t = 0.19\sqrt{f'_c}$)	363
Figure B.137 Reliability Indices for AASHTO Spread Box Girder Bridges at Maximum Tensile Stress Limit State (ADTT=5000), $\gamma_{LL}=1.0$ ($f_t = 0.19\sqrt{f'_c}$)	363
Figure B.138 Reliability Indices for AASHTO Spread Box Girder Bridges at Maximum Crack Width Limit State (ADTT=5000), $\gamma_{LL}=1.0$ ($f_t = 0.19\sqrt{f'_c}$)	364
Figure B.139 Reliability Indices for AASHTO Spread Box Girder Bridges at Decompression Limit State (ADTT=5000), $\gamma_{LL}=0.8$ ($f_t = 0.253\sqrt{f'_c}$)	364
Figure B.140 Reliability Indices for AASHTO Spread Box Girder Bridges at Maximum Allowable Tensile Stress Limit State (ADTT=5000), $\gamma_{LL}=0.8$ ($f_t = 0.253\sqrt{f'_c}$) .	365
Figure B.141 Reliability Indices for AASHTO Spread Box Girder Bridges at Maximum Allowable Crack Width Limit State (ADTT=5000), $\gamma_{LL}=0.8$ ($f_t = 0.253\sqrt{f'_c}$) ...	365
Figure B.142 Reliability Indices for AASHTO Spread Box Girder Bridges at Decompression Limit State (ADTT=5000), $\gamma_{LL}=1.0$ ($f_t = 0.253\sqrt{f'_c}$)	366
Figure B.143 Reliability Indices for AASHTO Spread Box Girder Bridges at Maximum Allowable Tensile Stress Limit State (ADTT=5000), $\gamma_{LL}=1.0$ ($f_t = 0.253\sqrt{f'_c}$) .	366
Figure B.144 Reliability Indices for AASHTO Spread Box Girder Bridges at Maximum Allowable Crack Width Limit State (ADTT=5000), $\gamma_{LL}=1.0$ ($f_t = 0.253\sqrt{f'_c}$) ...	367
Figure B.145 Reliability Indices for ASBI Box Girder Bridges at Decompression Limit State (ADTT=5000), $\gamma_{LL}=0.8$ ($f_t = 0.0948\sqrt{f'_c}$)	367
Figure B.146 Reliability Indices for ASBI Box Girder Bridges at Maximum Allowable Tensile Stress Limit State (ADTT=5000), $\gamma_{LL}=0.8$ ($f_t = 0.0948\sqrt{f'_c}$)	368

Figure B.147 Reliability Indices for ASBI Box Girder Bridges at Maximum Allowable Crack Width Limit State (ADTT=5000), $\gamma_{LL}=0.8$ ($f_t = 0.0948\sqrt{f'_c}$)	368
Figure B.148 Reliability Indices for ASBI Box Girder Bridges at Decompression Limit State (ADTT=5000), $\gamma_{LL}=1.0$ ($f_t = 0.0948\sqrt{f'_c}$)	369
Figure B.149 Reliability Indices for ASBI Box Girder Bridges at Maximum Tensile Stress Limit State (ADTT=5000), $\gamma_{LL}=1.0$ ($f_t = 0.0948\sqrt{f'_c}$)	369
Figure B.150 Reliability Indices for ASBI Box Girder Bridges at Maximum Crack Width Limit State (ADTT=5000), $\gamma_{LL}=1.0$ ($f_t = 0.0948\sqrt{f'_c}$)	370
Figure B.151 Reliability Indices for ASBI Box Girder Bridges at Decompression Limit State (ADTT=5000), $\gamma_{LL}=0.8$ ($f_t = 0.158\sqrt{f'_c}$)	370
Figure B.152 Reliability Indices for ASBI Box Girder Bridges at Maximum Allowable Tensile Stress Limit State (ADTT=5000), $\gamma_{LL}=0.8$ ($f_t = 0.158\sqrt{f'_c}$)	371
Figure B.153 Reliability Indices for ASBI Box Girder Bridges at Maximum Allowable Crack Width Limit State (ADTT=5000), $\gamma_{LL}=0.8$ ($f_t = 0.158\sqrt{f'_c}$)	371
Figure B.154 Reliability Indices for ASBI Box Girder Bridges at Decompression Limit State (ADTT=5000), $\gamma_{LL}=1.0$ ($f_t = 0.158\sqrt{f'_c}$)	372
Figure B.155 Reliability Indices for ASBI Box Girder Bridges at Maximum Tensile Stress Limit State (ADTT=5000), $\gamma_{LL}=1.0$ ($f_t = 0.158\sqrt{f'_c}$)	372
Figure B.156 Reliability Indices for ASBI Box Girder Bridges at Maximum Crack Width Limit State (ADTT=5000), $\gamma_{LL}=1.0$ ($f_t = 0.158\sqrt{f'_c}$)	373
Figure B.157 Reliability Indices for ASBI Box Girder Bridges at Decompression Limit State (ADTT=5000), $\gamma_{LL}=0.8$ ($f_t = 0.19\sqrt{f'_c}$)	373
Figure B.158 Reliability Indices for ASBI Box Girder Bridges at Maximum Allowable Tensile Stress Limit State (ADTT=5000), $\gamma_{LL}=0.8$ ($f_t = 0.19\sqrt{f'_c}$)	374
Figure B.159 Reliability Indices for ASBI Box Girder Bridges at Maximum Allowable Crack Width Limit State (ADTT=5000), $\gamma_{LL}=0.8$ ($f_t = 0.19\sqrt{f'_c}$)	374
Figure B.160 Reliability Indices for ASBI Box Girder Bridges at Decompression Limit State (ADTT=5000), $\gamma_{LL}=1.0$ ($f_t = 0.19\sqrt{f'_c}$)	375
Figure B.161 Reliability Indices for ASBI Box Girder Bridges at Maximum Tensile Stress Limit State (ADTT=5000), $\gamma_{LL}=1.0$ ($f_t = 0.19\sqrt{f'_c}$)	375
Figure B.162 Reliability Indices for ASBI Box Girder Bridges at Maximum Crack Width Limit State (ADTT=5000), $\gamma_{LL}=1.0$ ($f_t = 0.19\sqrt{f'_c}$)	376
Figure B.163 Reliability Indices for ASBI Box Girder Bridges at Decompression Limit State (ADTT=5000), $\gamma_{LL}=0.8$ ($f_t = 0.253\sqrt{f'_c}$)	376

Figure B.164 Reliability Indices for ASBI Box Girder Bridges at Maximum Allowable Tensile Stress Limit State (ADTT=5000), $\gamma_{LL}=0.8$ ($f_t = 0.253\sqrt{f'_c}$).....	377
Figure B.165 Reliability Indices for ASBI Box Girder Bridges at Maximum Allowable Crack Width Limit State (ADTT=5000), $\gamma_{LL}=0.8$ ($f_t = 0.253\sqrt{f'_c}$).....	377
Figure B.166 Reliability Indices for ASBI Box Girder Bridges at Decompression Limit State (ADTT=5000), $\gamma_{LL}=1.0$ ($f_t = 0.253\sqrt{f'_c}$)	378
Figure B.167 Reliability Indices for ASBI Box Girder Bridges at Maximum Allowable Tensile Stress Limit State (ADTT=5000), $\gamma_{LL}=1.0$ ($f_t = 0.253\sqrt{f'_c}$).....	378
Figure B.168 Reliability Indices for ASBI Box Girder Bridges at Maximum Allowable Crack Width Limit State (ADTT=5000), $\gamma_{LL}=1.0$ ($f_t = 0.253\sqrt{f'_c}$).....	379

LIST OF TABLES

Table 2.1 Design Working Lives (adapted from Table (2.1) – EN1990)	12
Table 2.2 <i>Eurocode</i> Consequence Classes (adapted from Table (B1) – EN1990)	12
Table 2.3. Design life for different types of structures (Adapted from Table 1 of ISO 2394-1998)	14
Table 2.4. Target β –values (Adapted from Table E-.2 of ISO 2394-1998)	14
Table 2.5. Relationship between β and Pf (Adapted from Table E.1 of ISO 2394-1998)	15
Table 2.6 Irreversible Service Limit States Reliability Indices (Adapted from Table (C2)-EN1990)	19
Table 2.7 Target Reliability Indices (Adapted from Table E-2 of ISO 2394-1998)	19
Table 2.8 Summary of typical statistical information for various variables from previous research	20
Table 2.9- Tensile Stress Limits in Prestressed Concrete at Service Limit State After Losses, Fully Prestressed Components (AASHTO 2008 Table 5.9.4.2.2-1)	41
Table 2.10 Summary of 28-day bias factors (Hueste et. al, 2004)	46
Table 2.11 AASHTO LRFD Table 2.5.2.6.3-1 Traditional Minimum Depths for Constant Depth Superstructures (AASHTO LRFD (2008))	53
Table 2.12 Evolution of Deformation Requirements in Bridge Design	56
Table 2.13 Peak Acceleration for Human Response to Harmonic Vertical Vibration (Wright and Walker, 1971)	56
Table 3.1 Equations of Maximum Crack Width	64
Table 3.2 Summary of Statistical Information for Random Variables for Service I Limit State	69
Table 3.3 Geometrical Properties of the Prestressed Beams (Nawy and Potyondy, 1971)	90
Table 3.4 Observed vs. theoretical max. crack width at tensile face of beam (Nawy and Huang, 1977)	94
Table 3.5 Random variables and the value their statistical parameters	101
Table 4.1 Mean Maximum Moments for Simple Spans Divided by Corresponding HL-93 Moments (Nowak 1999)	107
Table 4.2 Percentage of Filtered Data for Various WIM Sites	109
Table 4.3 Summary of Multiple Presence Statistics (Newark Bay Bridge WIM Site)	117
Table 4.4 Summary of Multiple Presence Statistics (NY WIM Site 2680)	117
Table 4.5 Summary of Multiple Presence Statistics (NY WIM Site 0199-I95)	117
Table 4.6 Summary of Multiple Presence Statistics (NY WIM Site 0199-Bronx)	118
Table 4.7 Summary of Multiple Presence Statistics (NY WIM Site 0580-EB)	118
Table 4.8 Summary of Multiple Presence Statistics (NY WIM Site 0580-WB)	118
Table 4.9 Summary of Multiple Presence Statistics (NY WIM Site 8280)	119
Table 4.10 Summary of Multiple Presence Statistics (NY WIM Site 8382)	119
Table 4.11 Summary of Multiple Presence Statistics (NY WIM Site 9291)	119
Table 4.12 Summary of Multiple Presence Statistics (NY WIM Site 9631)	120

Table 4.13 Mean Maximum Moments for Simple Spans Divided by Corresponding HL-93 Moment for site NY0199-NB	125
Table 4.14 Mean Maximum Moments for Simple Spans Divided by Corresponding HL-93 Moment for Site NY0199-SB	126
Table 4.15 Mean Maximum Moments for Simple Spans Divided by Corresponding HL-93 Moment for Site NY0580	126
Table 4.16 Mean Maximum Moments for Simple Spans Divided by Corresponding HL-93 Moment for Site NY2680	127
Table 4.17 Mean Maximum Moments for Simple Spans Divided by Corresponding HL-93 Moment for Site NY8280	127
Table 4.18 Mean Maximum Moments for Simple Spans Divided by Corresponding HL-93 Moment for Site NY8382	128
Table 4.19 Mean Maximum Moments for Simple Spans Divided by Corresponding HL-93 Moment for Site NY9121	128
Table 4.20 Mean Maximum Moments for Simple Spans Divided by Corresponding HL-93 Moment for Site NY9631	129
Table 4.21 Mean Maximum Moments for Simple Spans Divided by Corresponding HL-93 Moment Based on NJ data	129
Table 4.22 Extrapolation Summary for Site 0580 with respect to HL-93 Moment	140
Table 4.23 Extrapolation Summary for Site 2680 with respect to HL-93 Moment	141
Table 4.24 Extrapolation Summary for Site 8382 with respect to HL-93 Moment	142
Table 4.25 Extrapolation Summary for Site 9631 with respect to HL-93 Moment	143
Table 4.26 Time Period and Corresponding Inverse Normal Coordinate (ADTT= 5,000)	145
Table 4.27 Statistics for Various ADTTs at Various Return Periods	147
Table 4.28 Live Load Bias Factors for Various ADTTs (Service I)	147
Table 4.29 Coefficient of Variation (COV) for Various ADTTs (Service I)	147
Table 4.30 Live Load Bias Factors for Various Span Lengths (ADTT=1000)	148
Table 4.31 Coefficient of Variation (COV) for Various Span Lengths (ADTT=1000) ..	148
Table 4.32 Live Load Bias Factors for Various Span Lengths (ADTT=2500)	149
Table 4.33 Coefficient of Variation (COV) for Various Span Lengths (ADTT=2500) ..	149
Table 4.34 Live Load Bias Factors for Various Span Lengths (ADTT=5000)	149
Table 4.35 Coefficient of Variation (COV) for Various Span Lengths (ADTT=5000) ..	150
Table 4.36 Live Load Bias Factors for Various Span Lengths (ADTT=10000)	150
Table 4.37 Coefficient of Variation (COV) for Various Span Lengths (ADTT=10000) ..	150
Table 4.38 Live Load Bias Factors for Various Span Lengths (ADTT=1000)	151
Table 4.39 Live Load Bias Factors for Various Span Lengths (ADTT=2500)	152
Table 4.40 Live Load Bias Factors for Various Span Lengths (ADTT=5000)	153
Table 4.41 Live Load Bias Factors for Various Span Lengths (ADTT=10000)	153
Table 4.2. Summary of Crack Width information for Various Span Lengths	154
Table 6.1 Information of 15 Bridge Decks that Designed using AASHTO Traditional Deck Design Method	167
Table 6.2 Summary of Reliability Indices for Concrete Decks Designed according to AASHTO LRFD Design Specification 2012.....	170

Table 6.3 Reliability Indices of Existing Bridges based on 1-year return period.....	172
Table 6.4 Summary of Reliability Indices for Concrete Decks Designed with Different Live Load Factors	182
Table 6.5 Information of 15 Bridge Decks that Designed using AASHTO Empirical Deck Design Method.....	185
Table 6.6 Summary of Reliability Indices for Concrete Decks Designed using Empirical Design Method.....	195
Table 6.7 Summary of Reliability Indices for Concrete Decks Designed using Modified Empirical Design Method	196
Table 6.8 Summary of Matrix of Designed Parameters	198
Table 6.9 Summary of Reliability Indices for Existing Bridges with One Lane Loaded and Return Period of 1 Year	201
Table 6.10 Summary of the Reliability Indices of Bridges Designed Using AASHTO Girders with ADTT 5000 and $f_t = 0.0948\sqrt{f'_c}$	204
Table 6.11 Summary of the Reliability Indices of Bridges Designed Using AASHTO Girders with ADTT 5000 and $f_t = 0.19\sqrt{f'_c}$	205
Table 6.12 Reliability Indices for Existing and Simulated Bridges (Return Period of 1 Year and ADTT 5000)	207
Table 6.13 Summary Information of Bridges Designed with $\gamma_{LL}=0.8$, ($f_t = 0.0948\sqrt{f'_c}$)	209
Table 6.14 Summary Information of Bridges Designed with $\gamma_{LL}=1.0$, ($f_t = 0.0948\sqrt{f'_c}$)	212
Table 6.15 Summary of Reliability Indices for Simulated Bridges Designed for $f_t = 0.0948\sqrt{f'_c}$	221
Table 6.16 Summary of Reliability Indices for Simulated Bridges Designed for $f_t = 0.158\sqrt{f'_c}$	222
Table 6.17 Summary of Reliability Indices for Simulated Bridges Designed for $f_t = 0.19\sqrt{f'_c}$	222
Table 6.18 Summary of Reliability Indices for Simulated Bridges Designed for $f_t = 0.253\sqrt{f'_c}$	222
Table 6.19 Summary of Reliability Indices for Existing Bridges with One Lane Loaded and Return Period of 1 Year at Deflection Limit State.....	226
Table 6.20 Reliability Indices for Existing and Simulated Bridges at Deflection Limit State (Return Period of 1 Year and ADTT 5000)	226
Table A.1- Design Outcomes of I Girder Bridges Designed with Compressive Strength of 6ksi, Live Load Factor of 0.8 and Tensile Stress Limit of $0.0948\sqrt{f'_c}$	246
Table A.2- Design Outcomes of I Girder Bridges Designed with Compressive Strength of 6ksi, Live Load Factor of 0.8 and Tensile Stress Limit of $0.158\sqrt{f'_c}$	247
Table A.3- Design Outcomes of I Girder Bridges Designed with Compressive Strength of 6ksi, Live Load Factor of 0.8 and Tensile Stress Limit of $0.19\sqrt{f'_c}$	248

Table A.4- Design Outcomes of I Girder Bridges Designed with Compressive Strength of 6ksi, Live Load Factor of 0.8 and Tensile Stress Limit of $0.253\sqrt{f'c}$	249
Table A.5- Design Outcomes of I Girder Bridges Designed with Compressive Strength of 6ksi, Live Load Factor of 1.0 and Tensile Stress Limit of $0.0948\sqrt{f'c}$	250
Table A.6- Design Outcomes of I Girder Bridges Designed with Compressive Strength of 6ksi, Live Load Factor of 1.0 and Tensile Stress Limit of $0.158\sqrt{f'c}$	251
Table A.7- Design Outcomes of I Girder Bridges Designed with Compressive Strength of 6ksi, Live Load Factor of 1.0 and Tensile Stress Limit of $0.19\sqrt{f'c}$	252
Table A.8- Design Outcomes of I Girder Bridges Designed with Compressive Strength of 6ksi, Live Load Factor of 1.0 and Tensile Stress Limit of $0.253\sqrt{f'c}$	253
Table A.9- Design Outcomes of I Girder Bridges Designed with Compressive Strength of 8ksi, Live Load Factor of 0.8 and Tensile Stress Limit of $0.0948\sqrt{f'c}$	254
Table A.10- Design Outcomes of I Girder Bridges Designed with Compressive Strength of 8ksi, Live Load Factor of 0.8 and Tensile Stress Limit of $0.158\sqrt{f'c}$	255
Table A.11- Design Outcomes of I Girder Bridges Designed with Compressive Strength of 8ksi, Live Load Factor of 0.8 and Tensile Stress Limit of $0.19\sqrt{f'c}$	256
Table A.12- Design Outcomes of I Girder Bridges Designed with Compressive Strength of 8ksi, Live Load Factor of 0.8 and Tensile Stress Limit of $0.253\sqrt{f'c}$	257
Table A.13- Design Outcomes of I Girder Bridges Designed with Compressive Strength of 8ksi, Live Load Factor of 1.0 and Tensile Stress Limit of $0.0948\sqrt{f'c}$	258
Table A.14- Design Outcomes of I Girder Bridges Designed with Compressive Strength of 8ksi, Live Load Factor of 1.0 and Tensile Stress Limit of $0.158\sqrt{f'c}$	259
Table A.15- Design Outcomes of I Girder Bridges Designed with Compressive Strength of 8ksi, Live Load Factor of 1.0 and Tensile Stress Limit of $0.19\sqrt{f'c}$	260
Table A.16- Design Outcomes of I Girder Bridges Designed with Compressive Strength of 8ksi, Live Load Factor of 1.0 and Tensile Stress Limit of $0.253\sqrt{f'c}$	261
Table A.17- Design Outcomes of I Girder Bridges Designed with Compressive Strength of 10 ksi, Live Load Factor of 0.8 and Tensile Stress Limit of $0.0948\sqrt{f'c}$	262
Table A.18- Design Outcomes of I Girder Bridges Designed with Compressive Strength of 10 ksi, Live Load Factor of 0.8 and Tensile Stress Limit of $0.158\sqrt{f'c}$	263
Table A.19- Design Outcomes of I Girder Bridges Designed with Compressive Strength of 10 ksi, Live Load Factor of 0.8 and Tensile Stress Limit of $0.19\sqrt{f'c}$	264
Table A.20- Design Outcomes of I Girder Bridges Designed with Compressive Strength of 10 ksi, Live Load Factor of 0.8 and Tensile Stress Limit of $0.253\sqrt{f'c}$	265
Table A.21- Design Outcomes of I Girder Bridges Designed with Compressive Strength of 10 ksi, Live Load Factor of 1.0 and Tensile Stress Limit of $0.0948\sqrt{f'c}$	266
Table A.22- Design Outcomes of I Girder Bridges Designed with Compressive Strength of 10 ksi, Live Load Factor of 1.0 and Tensile Stress Limit of $0.158\sqrt{f'c}$	267
Table A.23- Design Outcomes of I Girder Bridges Designed with Compressive Strength of 10 ksi, Live Load Factor of 1.0 and Tensile Stress Limit of $0.19\sqrt{f'c}$	268
Table A.24- Design Outcomes of I Girder Bridges Designed with Compressive Strength of 10 ksi, Live Load Factor of 1.0 and Tensile Stress Limit of $0.253\sqrt{f'c}$	269

Table A.25- Design Outcomes of Adjacent Box Girder Bridges Designed with Compressive Strength of 6 ksi, Live Load Factor of 0.8 and Tensile Stress Limit of $0.0948\sqrt{f' c}$	270
Table A.26- Design Outcomes of Adjacent Box Girder Bridges Designed with Compressive Strength of 6 ksi, Live Load Factor of 0.8 and Tensile Stress Limit of $0.158\sqrt{f' c}$	270
Table A.27- Design Outcomes of Adjacent Box Girder Bridges Designed with Compressive Strength of 6 ksi, Live Load Factor of 0.8 and Tensile Stress Limit of $0.19\sqrt{f' c}$	271
Table A.28- Design Outcomes of Adjacent Box Girder Bridges Designed with Compressive Strength of 6 ksi, Live Load Factor of 0.8 and Tensile Stress Limit of $0.253\sqrt{f' c}$	271
Table A.29- Design Outcomes of Adjacent Box Girder Bridges Designed with Compressive Strength of 6 ksi, Live Load Factor of 1.0 and Tensile Stress Limit of $0.0948\sqrt{f' c}$	272
Table A.30- Design Outcomes of Adjacent Box Girder Bridges Designed with Compressive Strength of 6 ksi, Live Load Factor of 1.0 and Tensile Stress Limit of $0.158\sqrt{f' c}$	272
Table A.31- Design Outcomes of Adjacent Box Girder Bridges Designed with Compressive Strength of 6 ksi, Live Load Factor of 1.0 and Tensile Stress Limit of $0.19\sqrt{f' c}$	273
Table A.32- Design Outcomes of Adjacent Box Girder Bridges Designed with Compressive Strength of 6 ksi, Live Load Factor of 1.0 and Tensile Stress Limit of $0.253\sqrt{f' c}$	273
Table A.33- Design Outcomes of Adjacent Box Girder Bridges Designed with Compressive Strength of 8 ksi, Live Load Factor of 0.8 and Tensile Stress Limit of $0.0948\sqrt{f' c}$	274
Table A.34- Design Outcomes of Adjacent Box Girder Bridges Designed with Compressive Strength of 8 ksi, Live Load Factor of 0.8 and Tensile Stress Limit of $0.158\sqrt{f' c}$	274
Table A.35- Design Outcomes of Adjacent Box Girder Bridges Designed with Compressive Strength of 8 ksi, Live Load Factor of 0.8 and Tensile Stress Limit of $0.19\sqrt{f' c}$	275
Table A.36- Design Outcomes of Adjacent Box Girder Bridges Designed with Compressive Strength of 8 ksi, Live Load Factor of 0.8 and Tensile Stress Limit of $0.253\sqrt{f' c}$	275
Table A.37- Design Outcomes of Adjacent Box Girder Bridges Designed with Compressive Strength of 8 ksi, Live Load Factor of 1.0 and Tensile Stress Limit of $0.0948\sqrt{f' c}$	276
Table A.38- Design Outcomes of Adjacent Box Girder Bridges Designed with Compressive Strength of 8 ksi, Live Load Factor of 1.0 and Tensile Stress Limit of $0.158\sqrt{f' c}$	276

Table A.39- Design Outcomes of Adjacent Box Girder Bridges Designed with Compressive Strength of 8 ksi, Live Load Factor of 1.0 and Tensile Stress Limit of $0.19\sqrt{f' c}$	277
Table A.40- Design Outcomes of Adjacent Box Girder Bridges Designed with Compressive Strength of 8 ksi, Live Load Factor of 1.0 and Tensile Stress Limit of $0.253\sqrt{f' c}$	277
Table A.41- Design Outcomes of Spread Box Girder Bridges Designed with Compressive Strength of 6ksi, Live Load Factor of 0.8 and Tensile Stress Limit of $0.0948\sqrt{f' c}$	278
Table A.42- Design Outcomes of Spread Box Girder Bridges Designed with Compressive Strength of 6ksi, Live Load Factor of 0.8 and Tensile Stress Limit of $0.158\sqrt{f' c}$	278
Table A.43- Design Outcomes of Spread Box Girder Bridges Designed with Compressive Strength of 6ksi, Live Load Factor of 0.8 and Tensile Stress Limit of $0.19\sqrt{f' c}$	279
Table A.44- Design Outcomes of Spread Box Girder Bridges Designed with Compressive Strength of 6ksi, Live Load Factor of 0.8 and Tensile Stress Limit of $0.253\sqrt{f' c}$	279
Table A.45- Design Outcomes of Spread Box Girder Bridges Designed with Compressive Strength of 6ksi, Live Load Factor of 1.0 and Tensile Stress Limit of $0.0948\sqrt{f' c}$	280
Table A.46- Design Outcomes of Spread Box Girder Bridges Designed with Compressive Strength of 6ksi, Live Load Factor of 1.0 and Tensile Stress Limit of $0.158\sqrt{f' c}$	280
Table A.47- Design Outcomes of Spread Box Girder Bridges Designed with Compressive Strength of 6ksi, Live Load Factor of 1.0 and Tensile Stress Limit of $0.19\sqrt{f' c}$	281
Table A.48- Design Outcomes of Spread Box Girder Bridges Designed with Compressive Strength of 6ksi, Live Load Factor of 1.0 and Tensile Stress Limit of $0.253\sqrt{f' c}$	281
Table A.49- Design Outcomes of Spread Box Girder Bridges Designed with Compressive Strength of 8ksi, Live Load Factor of 0.8 and Tensile Stress Limit of $0.0948\sqrt{f' c}$	282
Table A.50- Design Outcomes of Spread Box Girder Bridges Designed with Compressive Strength of 8ksi, Live Load Factor of 0.8 and Tensile Stress Limit of $0.158\sqrt{f' c}$	282
Table A.51- Design Outcomes of Spread Box Girder Bridges Designed with Compressive Strength of 8ksi, Live Load Factor of 0.8 and Tensile Stress Limit of $0.19\sqrt{f' c}$	283
Table A.52- Design Outcomes of Spread Box Girder Bridges Designed with Compressive Strength of 8ksi, Live Load Factor of 0.8 and Tensile Stress Limit of $0.253\sqrt{f' c}$	283
Table A.53- Design Outcomes of Spread Box Girder Bridges Designed with Compressive Strength of 8ksi, Live Load Factor of 1.0 and Tensile Stress Limit of $0.0948\sqrt{f' c}$	284

Table A.54- Design Outcomes of Spread Box Girder Bridges Designed with Compressive Strength of 8ksi, Live Load Factor of 1.0 and Tensile Stress Limit of $0.158\sqrt{f' c}$.	284
Table A.55- Design Outcomes of Spread Box Girder Bridges Designed with Compressive Strength of 8ksi, Live Load Factor of 1.0 and Tensile Stress Limit of $0.19\sqrt{f' c}$.	285
Table A.56- Design Outcomes of Spread Box Girder Bridges Designed with Compressive Strength of 8ksi, Live Load Factor of 1.0 and Tensile Stress Limit of $0.253\sqrt{f' c}$.	285
Table A.57- Design Outcomes of Spread Box Girder Bridges Designed with Compressive Strength of 10ksi, Live Load Factor of 0.8 and Tensile Stress Limit of $0.0948\sqrt{f' c}$.	286
Table A.58- Design Outcomes of Spread Box Girder Bridges Designed with Compressive Strength of 10ksi, Live Load Factor of 0.8 and Tensile Stress Limit of $0.158\sqrt{f' c}$.	286
Table A.59- Design Outcomes of Spread Box Girder Bridges Designed with Compressive Strength of 10ksi, Live Load Factor of 0.8 and Tensile Stress Limit of $0.19\sqrt{f' c}$.	287
Table A.60- Design Outcomes of Spread Box Girder Bridges Designed with Compressive Strength of 10ksi, Live Load Factor of 0.8 and Tensile Stress Limit of $0.253\sqrt{f' c}$.	287
Table A.61- Design Outcomes of Spread Box Girder Bridges Designed with Compressive Strength of 10ksi, Live Load Factor of 1.0 and Tensile Stress Limit of $0.0948\sqrt{f' c}$.	288
Table A.62- Design Outcomes of Spread Box Girder Bridges Designed with Compressive Strength of 10ksi, Live Load Factor of 1.0 and Tensile Stress Limit of $0.158\sqrt{f' c}$.	288
Table A.63- Design Outcomes of Spread Box Girder Bridges Designed with Compressive Strength of 10ksi, Live Load Factor of 1.0 and Tensile Stress Limit of $0.19\sqrt{f' c}$.	289
Table A.64- Design Outcomes of Spread Box Girder Bridges Designed with Compressive Strength of 10ksi, Live Load Factor of 1.0 and Tensile Stress Limit of $0.253\sqrt{f' c}$.	289
Table A.65- Design Outcomes of Spread Box Girder Bridges Designed with Compressive Strength of 8ksi, Live Load Factor of 0.8 and Tensile Stress Limit of $0.0948\sqrt{f' c}$.	290
Table A.66- Design Outcomes of Spread Box Girder Bridges Designed with Compressive Strength of 8ksi, Live Load Factor of 0.8 and Tensile Stress Limit of $0.158\sqrt{f' c}$.	290
Table A.67- Design Outcomes of Spread Box Girder Bridges Designed with Compressive Strength of 8ksi, Live Load Factor of 0.8 and Tensile Stress Limit of $0.19\sqrt{f' c}$.	290
Table A.68- Design Outcomes of Spread Box Girder Bridges Designed with Compressive Strength of 8ksi, Live Load Factor of 0.8 and Tensile Stress Limit of $0.253\sqrt{f' c}$.	291

Table A.69- Summary of NCHRP 12-78 I-Girder Bridge.....	292
Table A.70- Summary of NCHRP 12-78 Spread Box Girder Bridge.....	293
Table A.71- Summary of NCHRP 12-78 Adjacent Box Girder Bridge	294

CHAPTER 1

INTRODUCTION

Although ultimate limit state, such as flexural capacity, shear, or stability, governs the overall safety of the structure, the accumulated damage due to cracking, excessive deflections, and vibrations also would lead to limitation of structural performance, abbreviation of service life, as well as extensive maintenance cost. Regarding the bridge structure, current AASHTO LRFD Bridge Design Specification (LRFD) was developed based on structural reliability approach and provided a uniform reliability at strength limit state. However, only strength limit states were considered and calibrated during the development and calibration of LRFD. Unlike strength limit state, exceedance of serviceability limit state in bridge structure might not result in catastrophic consequences directly. However, Serviceability limit states related to stress, deformation, and crack under regular service conditions are essential to the performance, human experience, and durability of structure. To ensure consistent and rational reliability level to be achieved for all limit states, rational serviceability limit states need to be developed and investigated for bridge structures.

In this study, various serviceability limit states were developed and investigated, including Service I limit state for crack control of reinforced concrete decks and Service III limit state for tension in prestressed concrete superstructures. The resistances of various serviceability limit states were derived and the statistical models were developed

based on statistics of various random variables and using different methods including Monte Carlo simulation method. The live load model was developed based on national as well as local Weigh-in-Motion (WIM) data using various extrapolation techniques. Based on current practice, consequence of failure, and experience from previous research, target reliability indices were proposed for each serviceability limit states. Moreover, The reliability analysis were performed for various serviceability limit states and new design criteria were proposed to achieve the target reliability levels consistently for various design scenarios. In addition, the deterioration of structural resistance was investigated and the reliability levels of various serviceability limit states with and without consideration of deterioration were compared.

1.1 Motivation

Although we anticipate certain desired strengths when we produce concrete or steel rebars, we observe large fluctuations when we test for the strength of the materials. This is one example of inherent uncertainty in structural design. Despite what we often think and use during the design, the parameters of the loading and resistance capacity of structural members are random variables rather than deterministic quantities (e.g. dimensions of the members, material properties, live load etc.). Consequently, no absolute safety (probability of failure of zero) can be achieved. However, the structures must be designed with acceptable probability of failure to assure the structure can function properly at a desired safety level (Nowak and Collins, 2000). Please note that the term “failure” here does not necessarily mean the collapse of the structure but is used to describe the violation of certain design criteria.

Before the application of AASHTO LRFD Bridge Design Specifications, the girder bridges were designed according to Allowable Stress Design method (ASD) (1930s-1970s) and Load Factor Design method (LFD) (1970s-1999). Both ASD and LFD method were developed based on engineering judgment rather than a rational state-of-the-art analysis. These design methodologies result in large fluctuations of safety level (Figure 1.1 (a)). Therefore, in order to consider the variability of applied loads and material properties and ensure a uniform level of safety, new LRFD Bridge Design Specifications, which stands for Load and Resistance Factor Bridge Design Specifications, have been developed and calibrated from actual bridge statistics for strength limit states. As shown in Figure 1.1 (b), a more uniform reliability level around

3.5 was achieved after the calibration. Eq. (1) presents a general form of a design equation in AASHTO LRFD Bridge Design Specifications.

$$\sum \gamma_i Q_i \leq \phi R \quad \text{Eq. 1.1}$$

Where,

γ_i = load factor,

Q_i = load effect,

ϕ = strength reduction factor,

R = resistance.

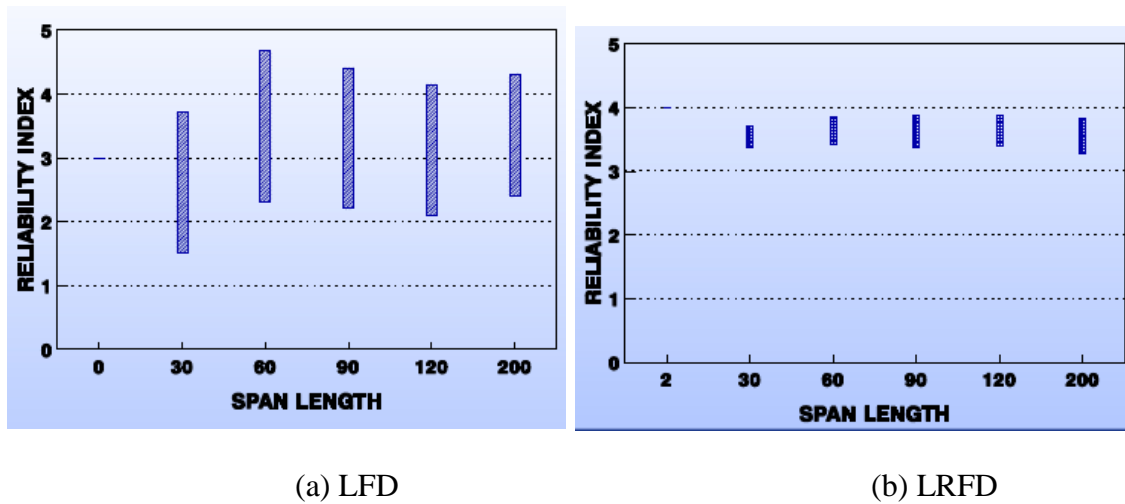


Figure 1.1 Reliability Indices for Bridges Designed According to (a) LFD and (b) LRFD (Kulicki (2006))

However, the LRFD specifications have only been calibrated for strength limit states. To ensure that consistent and rational reliability level is achieved for all limit states, the reliability-based serviceability limit states need to be developed and calibrated.

As specified in AASHTO LRFD Bridge Design Specifications, the service limit states are the limit states to control the stress, deformation, and crack width under regular service conditions (AASHTO (2010)). Figure 1.2 demonstrates the service limit state regarding the cracking at the bottom of the reinforced concrete structure. Unlike the strength limit states, the violation of service limit states will not result in collapse of structures, but will affect the service life and the maintenance costs of the structure.

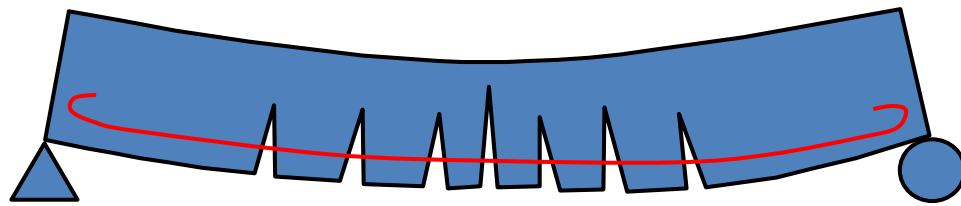


Figure 1.2 Excessive Cracks at the Bottom of Reinforced Concrete Structure

In addition, the deterioration of structural resistance has significant impact on the long term reliability of the structure. The deterioration of the structural resistance can be attributed to deterioration of section properties and material properties. Therefore, it is important to investigate the effect of deterioration of the structural resistance.

1.2 Research Significance

The demand for reliability based serviceability limit states was initialized after and even during the development and calibration of strength limit states for bridge design. NCHRP has adopted and approved a research statement (Project 12-83) titled “Calibration of LRFD Concrete Bridge Design Specification for Serviceability”. As an associated study with NCHRP project 12-83, part of this study will be included in NCHRP 12-83 and some of the conclusions will be proposed to be adopted in AASHTO LRFD Bridge Design Specification.

Although exceedance of serviceability limits state in bridge structures might not result in catastrophic consequences directly, frequent violation of serviceability limit states would cause accumulated damages over period of time, which would induce significant influences or reduction of structural performance, human experience, durability of structure, and would also increase the cost of maintenance. Reliability based serviceability limit states would provide a rational approach to evaluate the performance of the structure at serviceability limit state. Furthermore, Calibration of serviceability limit state would enable the design for various scenarios to achieve a target reliability level consistently. In addition, deterioration of structural resistance is also an important factor that would affect the performance of the structure at long term. Therefore, incorporating the deterioration of structural resistance into structural reliability analysis would provide a more insightful understanding of structural reliability long term.

1.3 Objectives and Scope

The primary objective of this research is to develop and calibrate various serviceability limit states for concrete girder bridges using a reliability-based approach. Based on the research, new design criteria or parameters such as new live load and resistance factors or design provisions are proposed for various serviceability limit states.

In this research, databases for prestressed concrete girder bridges and reinforced concrete decks were assembled. The comprehensive live load study was performed using the WIM data collected over different states, and statistical parameters of live load effect were summarized for regular truck load as well as permit vehicle load. The characterization of truck load at long term was investigated based on 10 years of WIM

data collected in New Jersey. Also, the resistance of structure was derived for various limit states and the statistical model was developed based on statistical information of various random variables. Based on developed load and resistance models, the structural reliability analysis was performed. Various design parameters such as live load and resistance factors and various design provisions were modified until a consistent, rational safety level was achieved for each serviceability limit state. Furthermore, the deterioration models for structural resistances were developed for various serviceability limit states. The reliability analysis was performed incorporating deterioration model and the analysis results were compared with the ones without considering the deterioration of the structure.

1.4 Organization of the Thesis

The thesis contains seven chapters. This chapter serves as an introduction of the thesis outlining the problem statement and statement of objectives.

Chapter two presents a comprehensive literature review of various issues and available research experiences in various related topics, including a brief introduction on past and current design code methodologies and calibration procedures, serviceability limit states in various design codes, techniques for structural reliability analysis, target reliability index, statistics for various random variables, crack control reinforcement and provisions regarding control of crack in AASHTO Specification, and concrete tension stresses.

Chapter three provides the derivation of structural resistance for various serviceability limit states and also provides the development of statistical models for

resistance and dead load. The resistance models developed in this chapter will be applied in structural analysis in Chapter six.

Chapter four describes development of live load models for reliability analysis. The techniques utilized for analyzing and processing WIM data were described. The live load effects from various data sources were summarized and discussed. The characterization of truck load at long term was investigated based on 10 years of WIM data collected in New Jersey. Finally, the live load models were developed for both regular truck load and permit vehicle load.

Chapter five presents the deterioration models for different bridge elements. The deterioration of structural section properties as well as material properties was discussed. The deterioration model for different bridge elements were developed for various serviceability limit states.

Chapter six presents the results from structural reliability analysis and calibration of various serviceability limit states. Based on reliability analysis and calibration results, new design parameters or design provisions were proposed to be included in AASHTO LRFD Design Specification. Furthermore, the reliability analysis results that were incorporated with a deterioration model were discussed and compared with the results not considering a deterioration model of the structural resistance.

Chapter seven contains the summary and conclusions of this thesis.

CHAPTER 2

LITERATURE REVIEW

2.1 Bridge Design Specifications

Over the decades, bridge engineers strived to improve the design of bridges by updating the design specifications followed over different states. Load and Resistance Factor Designed (LRFD) was introduced by AASHTO in 1994 (AASHTO 1994) to replace the allowable stress method (ASD) and load factor design (LFD) given in the AASHTO 1992 code (AASHTO 1992). As a product of code calibration performed during NCHRP Project 12-33, the AASHTO LRFD Design Specification was developed based on a rational reliability based approach. It is approved that more uniform reliability level could be achieved by designing using AASHTO LRFD Design Specification. In contrast, the previous AASHTO 1992 code has been continuously updated during its more than fifty years of service and was proven to result in inconsistencies in safety levels for different spans and bridge materials (Nowak 1995). The present code methodology utilizes reliability theory to achieve uniform safety levels for different materials and span lengths and considers statistical variability of various parameters for both loads and resistance.

2.1.1 Allowable Stress Design (ASD)

The Allowable Stress Design (ASD) specification which was used before the adoption of the AASHTO LRFD Specification was based on basic principles that the resistance should be greater than the loads applied. The design requirements were designated in terms of a fraction of yield strength of the material, which was named as allowable stress. However, although ASD design specification is efficient in many earlier designs such as truss and arch structures, it was found that ASD is not appropriate in many design scenarios such as dealing residual stresses for thin walled sections. Thus, adjustments were added to ASD to compensate the residual stresses.

Furthermore, since ASD was based on yield stress of materials rather than stress interactions, it does not consider different load combinations for different scenarios. Also since ASD was developed based on steel material, it might not be appropriate for other materials especially non-linear materials such as concrete in which properties vary with the load and the time.

As practitioners realized the inherent complexity of material and applied loads, along with the development of the reliability based approach, a new, reliability based bridge design specification was required.

2.1.2 Load and Resistance Factor Design (LRFD)

A new, reliability based design specification, Load and Resistance Factor Design, LRFD was adopted by AASHTO in 1994. In comparison with previous specification, the LRFD approach incorporated the variability of loads into the design and provides similar reliability levels for different designs. The LRFD design specification was developed

based on reliability analysis considering the uncertainties of loads and resistances. In the reliability analysis, the structural performance was measured by probability of failure or reliability index. Various materials, section types and span lengths were considered during the development of LRFD. Eq. 2.1 shows a basic form of the LRFD design equation (Nowak, 1995). In this equation, the resistance factor, ϕ , with a value less than or equal to 1.0 is applied to the resistance, Q . on the other hand, the load factor, γ , is applied to each load component. Both resistance factors and load factors were selected and calibrated through reliability analysis in order to achieve uniform reliability level for different designs.

$$\phi R_n \geq \sum \gamma_i Q_i \quad \text{Eq. 2.1}$$

Where,

ϕ = resistance factor,

R_n = nominal (design) resistance,

γ_i = load factor for given load type, and

Q_i = nominal (design) load component.

2.1.3 Eurocode

Eurocode is a set of specifications developed by European Committee for Standardization for structural design of construction works in European Union. There are ten sections which have been developed and published as of 2002 as listed below:

EN 1990 Eurocode 0: Basis of Structural Design

EN 1991 Eurocode 1: Actions on structures

EN 1992 Eurocode 2: Design of concrete structures

EN 1993 Eurocode 3: Design of steel structures

EN 1994 Eurocode 4: Design of composite steel and concrete structures

EN 1995 Eurocode 5: Design of timber structures

EN 1996 Eurocode 6: Design of masonry structures

EN 1997 Eurocode 7: Geotechnical design

EN 1998 Eurocode 8: Design of structures for earthquake resistance

EN 1999 Eurocode 9: Design of aluminum structures

The concept of design working life is adopted in the *Eurocode*. The design working life is the period of time that a structure can be used for its intended design purpose without major repair but with anticipated maintenance. The design working life of various categories is summarized in Table 2.1.

Table 2.1 Design Working Lives (adapted from Table (2.1) – EN1990)

design working life category	design working life (years)	examples
1	10	temporary structures
2	10 to 25	replaceable structural parts, e.g. gantry girders, bearings
3	15 to 30	agricultural and similar structures
4	50	building structures and other common structures
5	100	monumental building structures, bridges and other civil engineering structures

Eurocode also considers three different levels of reliability, RC1, RC2, RC3 that relate to strength and service limit states. These levels of reliability correspond to three different levels of consequences classes, CC1, CC2 and CC3, as defined in Table 2.2.

Table 2.2 *Eurocode* Consequence Classes (adapted from Table (B1) – EN1990)

consequence class	description related to consequences	reliability class
CC1	low consequence for loss of human life; economic, social or environmental consequences small or negligible	RC1
CC2	moderate consequence for loss of human life; economic, social or environmental consequences considerable	RC2
CC3	serious consequences for loss of human life, or for economic, social or environmental concerns	RC3

2.1.4 Canadian Code

Both ultimate limit states (ULS) and serviceability limit states (SLS) were included in Canadian Highway Bridge Design Code (CHBDC), and earlier Ontario Highway Bridge Design Code (OHBDC). The calibration of ULS in Canadian Code followed a similar procedure as calibration of the strength limit states in the AASHTO LRFD Bridge Design Specifications. Thus, the outcomes of calibration such as load and resistance factors are also similar to ones that are used in AASHTO LRFD Bridge Design Specification. Also similar to AASHTO LRFD Specification, the serviceability limit states have not been calibrated using a reliability based approach.

2.1.5 ISO 2394 Document (General Principles on Reliability for Structures)

The International Organization for Standardization (ISO) has published a document “ISO 2394 Document (General Principles on Reliability for Structures)” which provides general principles for reliability evaluation and the verification for structures.

The general principles presented in this document are applicable to various types of structures such as buildings, bridges, industrial structures, etc. In addition, the general

principles are also applicable to the structural elements during their construction as well as normal use. In order to incorporate different practices in different countries, this document provides the option of revising the items to fit the specific needs of different countries. Based on cause, mode, and consequences of failure, the expense of effort to reduce the risk of failure and structure type, different reliability levels and design life were considered. Table 2.3 shows the design life based on the type of structure and Table 2.5 shows the target reliability indices for different cases.

Table 2.3. Design life for different types of structures (Adapted from Table 1 of ISO 2394-1998)

Class	Working life (years)	Examples
1	1-5	Temporary structures
2	25	Replacement structural parts, e.g. gantry girders, bearings
3	50	Buildings and other common structures, other than those listed below
4	100 or more	Monumental buildings and other special or important structures. Large bridges

Table 2.4. Target β –values (Adapted from Table E-.2 of ISO 2394-1998)

Relative costs of safety measures	Consequences of failure			
	Small	Some	Moderate	Great
High	0	1.5(a)	2.3	3.1 (b)
Moderate	1.3	2.3	3.1	3.8 (c)
Low	2.3	3.1	3.8	4.3

(a) For serviceability limit states, use $\beta = 0$ for reversible and $\beta = 1.5$ for irreversible limit states.

(b) For fatigue limit states, use $\beta = 2.3$ to $b = 3.1$, depending on the possibility of inspection.

(c) For ultimate limit states design, use the safety classes $\beta = 3.1$, 3.8 and 4.3.

In addition, the table that shows the relationship between reliability index (β) and probability of failure (Pf) as shown in Table 2.5 was included in the document.

Table 2.5. Relationship between β and Pf (Adapted from Table E.1 of ISO 2394-1998)

Pf	10-1	10-2	10-3	10-4	10-5	10-6	10-7
β	1.3	2.3	3.1	3.7	4.2	4.7	5.2

2.2 Serviceability Limit States

The limit state can be defined as a boundary between desired and undesired performance (Nowak, 2000). If the limit state has been satisfied, the structure is safe. On the other hand, if the limit state has been exceeded, the structure is “failed”. Considering the corresponding consequences of the “failure”, the limit states can be categorized as ultimate or strength limit state and serviceability limit state. The violation of ultimate limit state causes the collapse of the structural member. Unlike the strength limit states, the violation of service limit will affect the service life and the maintenance costs of the structure.

In AASHTO LRFD Bridge Design Specifications, the service limit states refer to the limit states that control the stress, deformation, and crack width under regular service conditions (AASHTO (2010)). Similar to AASHTO, the cracking, deformation, stress, and vibration serviceability limit states are considered in the Canadian Highway Bridge Design Code (CAN/CSA-S6-06).

In European code, EN1990, and ISO 2394-1998, the serviceability limit state is classified into two categories, irreversible and reversible serviceability limit states. In the

“designers’ handbook to Eurocode 1: basis of design” by Gulvanessian and Holicky, 1996. They defined reversible and irreversible service limit states as following:

- a) Irreversible serviceability limit states (Figure 2.1-a), i.e. limit states that remain permanently exceeded even when the actions that caused the infringement are removed (e.g. a permanent local damage, permanent unacceptable deformations)
- b) Reversible serviceability limit states (Figure 2.1-b), i.e. limit states that will not be exceeded when the actions that caused the infringement are removed (e.g. cracks of prestressed components, temporary deflections, excessive vibration).

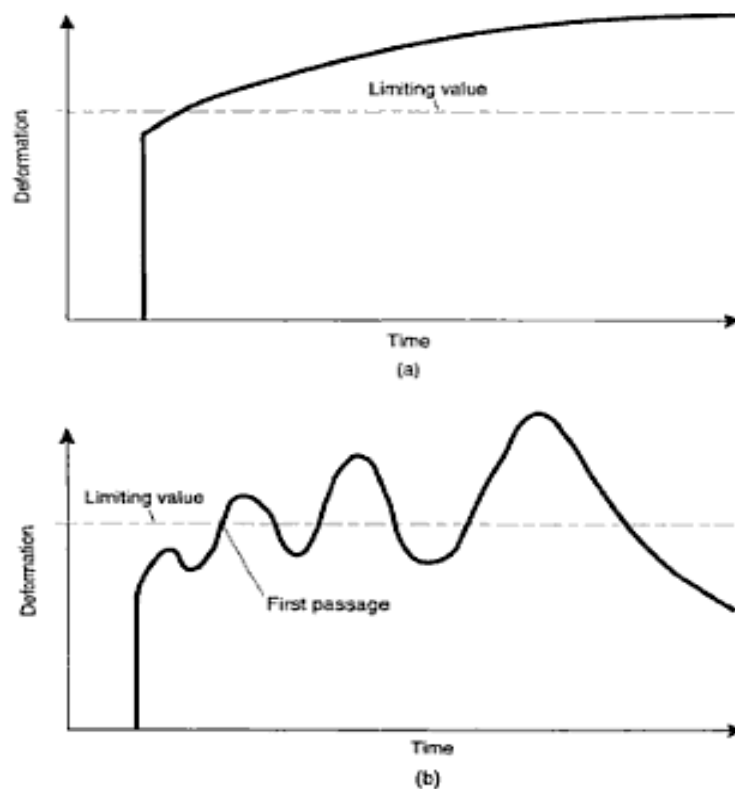


Figure 2.1 irreversible (a) and reversible (b) limit states (Gulvanessian and Holicky, 1996)

2.3 Structural Reliability Analysis

The structural reliability analysis begins from establishing the limit state function, which can be expressed as following:

$$g(R, Q) = R - Q \quad \text{Eq. 2.2}$$

Where the R is the capacity and Q is the load effects.

For each limit state, the probability of failure can be expressed as:

$$P_f = P(R - Q < 0) = P(g < 0) \quad \text{Eq. 2.3}$$

Figure 2.2 presents the probability density function (PDF) of load and resistance and probability of failure is corresponding to the shaded area in Figure 2.3.

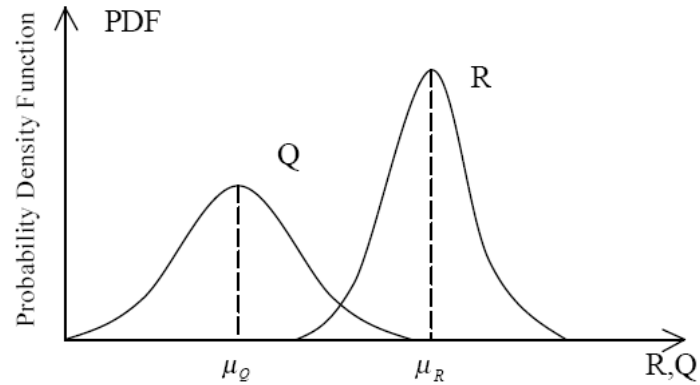


Figure 2.2 PDF of Load and Resistance

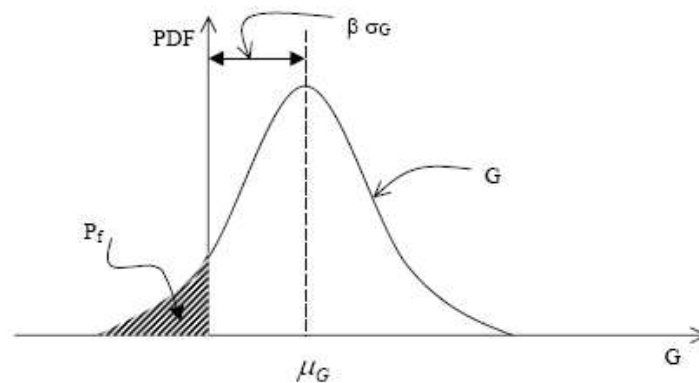


Figure 2.3 Illustration of Probability of Failure

Once the statistical information such as mean and standard deviation of R and Q has been obtained from the experimental or simulation techniques, the safety level of the structural member can be evaluated using reliability index β :

$$\beta = \frac{\mu_R - \mu_Q}{\sqrt{\sigma_R^2 + \sigma_Q^2}} \quad \text{Eq. 2.4}$$

where,

β = reliability Index.

μ_R = mean value of resistance moment.

μ_Q = mean value of the moment due to applied loads.

σ_R = standard deviation of the resistance moment.

σ_Q = standard deviation of the moment due to applied loads.

The reliability index β is correlated with the probability of failure and can be converted to it by looking up the tabulated values for normal probability distribution.

2.4 Target Reliability Index

Table 2.6 and Table 2.7 summarize the target reliability indices of serviceability limit states from various codes. The European Code selected the target reliability index for irreversible service limit state as 2.9 for a 1-year period, whereas the ISO 2394-1998 specified the target reliability index for reversible and irreversible limit state as 0 and 1.5, respectively. This is a large variance in the selection of the target reliability index between different codes.

In this study, the preliminary target reliability indices were selected based on the current practice and previous experiences from other Codes (European Code and ISO 2394 Document).

Table 2.6 Irreversible Service Limit States Reliability Indices (Adapted from Table (C2)-EN1990)

Reliability Class	Reference Period (years)	
	1	50
RC2	2.9	1.5

Table 2.7 Target Reliability Indices (Adapted from Table E-2 of ISO 2394-1998)

Relative Costs of Safety Measures	Consequences of Failure			
	Small	Some	Moderate	Great
High	0	1.5(a)	2.3	3.1 (b)
Moderate	1.3	2.3	3.1	3.8 (c)
Low	2.3	3.1	3.8	4.3

(a) For serviceability limit states, use $\beta = 0$ for reversible and $\beta = 1.5$ for irreversible limit states.

(b) For fatigue limit states, use $\beta = 2.3$ to $b = 3.1$, depending on the possibility of inspection.

(c) For ultimate limit states design, use the safety classes $\beta = 3.1, 3.8$ and 4.3 .

2.5 Random Variables

In order to perform the reliability analysis for the serviceability limit states, the probabilistic distribution and statistical parameters (μ and σ) of various random variables needed to be collected or estimated. Table 2.8 shows a summary of the information based on previous research studies by Siriaksorn and Naaman (1980) and Nowak (2008).

Table 2.8 Summary of typical statistical information for various variables from previous research

Variables	Distribution	Mean, m	COV., Ω	Remarks
b, b_1, b_w	normal	b_n	0	
h, h_{f1}, h_{f2}	normal	h_n	$1/6.4 \mu$	
d_p, d_s, e_1	normal	d_{pn}, d_{sn}, e_{1n}	$0.04-0.68/h_n$	
l, a	normal	l_n, a_n	$11/(32 \mu)$	
C_{E_c}	normal	33.6	0.1217	nominal=33 $E_c = C_{E_c} \cdot \gamma_c^{1.5} \cdot \sqrt{f'_c}$
C_{f_r}	normal	9.374	0.0938	nominal=7.5 & $f_r = C_{f_r} \sqrt{f'_c}$
f'_c	lognormal	$1.11 f'_{cn}$	0.11	
γ_c	normal	$\gamma_{cn} = 150$	0.03	
$C_{f_{ci}}$	normal	0.6445	0.073	nominal=0.8 & $f_{ci} = C_{f_{ci}} \cdot f'_c$
f_y	lognormal	$1.13 f_{yn}$	0.03	
A_s	normal	$0.9 A_{sn}$	0.015	
E_s	normal	E_{sn}	0.024	
A_{ps}	normal	$1.01176 A_{psn}$	0.0125	$A_{psn} = 0.153 \text{ in}^2$
f_{pu}	lognormal	$1.03 f_{pun}$	0.015	$f_{pun} = 270 \text{ ksi}$
f_{py}	lognormal	$1.027 f_{pyn}$	0.022	$f_{pyn} = 240 \text{ ksi}$
E_{ps}	normal	$1.011 E_{psn}$	0.01	$E_{psn} = 29000 \text{ ksi}$
$C_{f_{si}}$	normal	$C_{f_{sin}}$	0.08	$C_{f_{sin}} = 0.7$ $f_{si} = C_{f_{sin}} \cdot f_{pu}$
$C_{f_{se}}$	normal	$C_{f_{sen}}$	0.08	$C_{f_{sen}} = 0.83$ $f_{se} = C_{f_{se}} \cdot f_{si}$
$\Sigma 0$	normal	$\Sigma 0_n$	0.03	

2.6 Crack Control Reinforcement

This section is a review of previous research studies, which focused on crack control as well as predicting crack width in concrete members. Significant research has been conducted to control cracks in concrete members resulting in the development of numerous equations to predict the crack width at the bottom tension surface and the side faces at the level of reinforcement. Equations available to predict crack width were developed for concrete members with cover less than 2.5 in., but are not applicable for beams with larger concrete covers. Various equations have been adopted by different codes. However, for calibration purposes, there is a need to evaluate these equations with regard to accuracy and applicability. The results from various equations will be compared and validated using data collected from available literature.

2.6.1 Bottom Face of Concrete Member

One of the early studies by Clark (1956) included testing 58 specimens and collecting over 105 crack width readings. Clark concluded that the average crack width is closely related to the following parameters: 1) the diameter of the reinforcing bar, 2) reinforcing bar area, 3) area of the beam section, and 4) the distance from the bottom reinforcement to the beam bottom surface. Moreover, Clark stated that the average width was also proportional to the stresses in the reinforcing bars beyond the cracking stress. He suggested that the width of the cracks can be reduced by using a large number of small diameter bars and by increasing the ratio of the steel reinforcement. Based on these results, Equation 4 was developed to predict the average crack width of the concrete beams. The maximum crack width was estimated by multiplying the average crack width by 1.64 (Clark 1956).

$$w_{ave} = C_1 \frac{D}{p} \left[f_s - C_2 \left(\frac{1}{p} + n \right) \right] \quad \text{Eq. 2.5}$$

where,

w_{ave} = average width of cracks, in.

C_1, C_2 = coefficients that depend on distribution of bond stress, bond strength, and tensile strength of concrete, for Clark's study;
 $C_1 = 2.27 \times 10^{-8} (h - d) / d$, $C_2 = 56.6$.

D = diameter of reinforcing bar, in.

p = A_s / A_e = cross-sectional area of reinforcement / cross-sectional area of concrete.

A_e = bd , in. ²

f_s = computed stress in reinforcement, psi.

n = ratio of modulus of elasticity of steel to concrete (assumed to be 8 in Clark's study)

h = overall depth of beam/slab, in.

d = distance from compressive face of beam/slab to centroid of longitudinal tensile reinforcement.

Kaar and Mattock (1963) also developed a well-known crack width equation for bottom face cracking:

$$w_b = 0.115 \beta f_s \sqrt[4]{A} \quad \text{Eq. 2.6}$$

where,

w_b = maximum crack width, 0.001 in.

- β = ratio of distances to neutral axis from extreme tension fiber and from centroid of reinforcement.
- f_s = steel stress calculated by elastic crack section theory, ksi.
- d_c = bottom cover measured from center of lowest bar, in.
- A = average effective concrete area around reinforcing bar, having same centroid as reinforcement, in. ²

Broms (1965) conducted tests on 37 tension and 10 flexural members to analyze crack width and crack spacing. Broms observed that the crack spacing decreased rapidly with increasing load and that a number of primary tensile cracks formed on the surface of flexural and tension members. Secondary tensile cracks were confined to the surrounding area of reinforcement. The study concluded that the absolute minimum visible crack spacing is the same along the distance from the surface to the center of the reinforcing bar located nearest to the surface of the member. Thus, the theoretical minimum crack spacing is equal to the thickness of the concrete cover (Broms, 1965).

Gergely and Lutz (1968) developed an equation to predict the crack width based on a detailed statistical assessment of experimental data available in the literature at the time. Gergely and Lutz identified various parameters, such as reinforcing bar locations, stresses in the reinforcement, concrete cover depth, and spacing of the reinforcement as the controlling factors affecting the crack width. The Gergely and Lutz (1968) equation is presented as follows:

$$w_b = 0.076\beta f_s \sqrt[3]{Ad_c} \quad \text{Eq. 2.7}$$

where,

w_b = maximum crack width, 0.001 in.

β = ratio of distances to neutral axis from extreme tension fiber and from centroid of reinforcement.

f_s = steel stress calculated by elastic crack section theory, ksi.

d_c = bottom cover measured from center of lowest bar, in.

A = average effective concrete area around reinforcing bar, having same centroid as reinforcement, in. ²

The maximum concrete cover tested in this study was 3.31 inches. However, only three test specimens with cover greater than 2.5 in. were tested in the study.

In the study by Frosch (1999), the crack widths were determined from an equation developed based on a physical model. Results were compared with the test data used in Kaar and Mattock (1963) and Gergely and Lutz (1968). The crack width model developed in this study showed that the crack spacing and width are functions of the distance between the reinforcing steel. Crack control can be achieved by limiting the spacing of these reinforcing bars. Based on the research findings, Frosch suggested that limiting the maximum bar spacing would prevent large cracks in the concrete beams. Based on the physical model, the equation to calculate the maximum crack width for uncoated reinforcement was developed as shown below (Frosch 1999):

$$w_c = \frac{2f_s}{E_s} \beta \sqrt{\left(d_c^2 + \left(\frac{s}{2}\right)^2\right)} \quad \text{Eq. 2.8}$$

where,

s = maximum permissible bar spacing, in.

w_c = limiting crack width, in. (0.016 in, based on ACI 318-95).

E_s = elastic modulus of steel reinforcement (can be taken as 29000 ksi.)

β = $1.0 + 0.08 d_c$

d_c = bottom cover measured from center of lowest bar, in.

f_s = stress in steel reinforcement.

Frosch (1999) suggested that for epoxy-coated reinforcement, the above equation should be multiplied by a factor of 2. The equation above is rearranged to solve for the allowable bar spacing:

$$s = 2 \sqrt{\left(\left(\frac{w_c E_s}{2 f_s \beta} \right)^2 - d_c^2 \right)} \quad \text{Eq. 2.9}$$

Based on the physical model, the following design recommendation was presented that addressed the use of both the uncoated and coated reinforcement. The equation to calculate the maximum spacing of reinforcement was given as follows (Frosch 1999) :

$$s = 12 \alpha_s \left[2 - \frac{d_c}{3 \alpha_s} \right] \leq 12 \alpha_s \quad \text{Eq. 2.10}$$

where,

$$\alpha_s = \frac{36}{f_s} \gamma_c$$

d_c = thickness of concrete cover measured from extreme tension fiber to center of bar or wire located closest thereto, in.

s = maximum spacing of reinforcement, in.

α_s = reinforcement factor

γ_c = reinforcement coating factor: 1.0 for uncoated reinforcement; 0.5 for epoxy-coated reinforcement, unless test data can justify a higher value.

f_s = calculated stress in reinforcement at service load, ksi. It shall be computed as the moment divided by the product of steel area and internal moment arm. It shall be permitted to take f_s as 60 percent of the specified yield strength f_y .

Frosch (2001) summarized the physical model for cracking and illustrated the development and limitations of the proposed design method. Based on the physical model, he recommended formulas for calculating the maximum crack width for uncoated and epoxy-coated reinforcement, as well as the design recommendation for their use similar to those presented in Frosch (1999).

Epoxy-coated reinforcement is widely used to increase the durability of structures. The epoxy-coated reinforcement has been shown to lessen bond strength that can decrease crack spacing and bigger crack widths compared to uncoated reinforcement (Blackmand and Frosch 2005). Blackman and Frosch investigated crack width of concrete beams with epoxy-coated reinforcement. The primary variables used in the study include epoxy coating thickness and reinforcing bar spacing. Blackman and Frosch designed ten slab specimens in order to examine the effect of epoxy coating on cracks. It was concluded that the epoxy coating thickness does not affect the concrete crack significantly. Frosch (1999), Frosch (2001), Frosch (2002), and Blackman and Frosch (2005) presented an equation to compare the average-measured crack spacing for the uncoated and epoxy coated bars with the calculated values:

$$S_c = \Psi_s d^* \quad \text{Eq. 2.11}$$

where,

S_c = crack spacing

d^* = controlling cover distance

Ψ_s = crack spacing factor: 1.0 for minimum crack spacing; 1.5 for average crack spacing; 2.0 for maximum crack spacing

Choi and Oh (2009) studied the crack width for transversely post-tensioned concrete deck slabs in box girder bridges. They tested four full-scale concrete box girder segments and then derived the maximum crack width equation from the testing data:

$$w_{\max} = 3 \times 10^{-6} (f_s - f_0) \phi_s \left(\frac{A_{t,eff}}{A_{st} + \xi A_{pt}} \right) 0.75 \frac{h-x}{d-x} \quad \text{Eq. 2.12}$$

$$\xi = \sqrt{\frac{\tau_{ap}}{\tau_{as}} \frac{\pi + (n-1) \phi_s}{n\pi \phi_p}} \quad \text{Eq. 2.13}$$

where,

w_{\max} = predicted maximum crack width in mm

A_{st} = total area of reinforcing bars

A_{pt} = total area of prestressing tendons

x = depth of neutral axis in mm

h = height of cross section

d = effective depth in mm

f_s = increment of reinforcing bar stress after decompression

f_0 = steel stress at the initial occurrence of crack

ϕ_s = diameter of reinforcing bar in mm

ϕ_p = diameter of prestressing tendons

$\frac{\tau_{ap}}{\tau_{as}}$ = 0.465 for grouted post-tensioned tendons

Cracking of structures is rather common and is not always damaging to the structure. However, when considering a bridge deck, moderately sized cracking can be detrimental to the longevity of the structure due to the exposure to harsh environments. Recently, thicker concrete covers, coupled with the use of high-performance concrete, are becoming increasingly popular because of their durability. This often results in unrealistic bar spacing and prevents the use of contemporary crack control practices that are based on statistical studies. Therefore, it is desirable to develop methods to predict average and maximum crack widths of reinforced concrete members with thicker concrete covers at various locations.

2.6.2 Side Face of Concrete Member

In general, large cracks are expected only at the extreme tensile face of the beam. However, Beeby (1979) conducted studies that showed the largest crack widths occurring in the web along the beam side face with the maximum widths occurring at about mid-height.

Frantz and Breen (1980a) observed very wide cracks near mid-depth on the side faces of several 8-ft deep inverted T beams. Although the crack width at the flexural

reinforcement level was acceptable, the maximum crack width on the side face were up to three times as wide as the crack width at the flexural reinforcement level. The authors tested 44 laboratory size specimens to investigate the factors affects side face cracking: skin reinforcement cover, web width, area and distribution of skin reinforcement, and depth of beam. They concluded the following based on the testing results:

1. Since the skin reinforcement is only effective in a narrow strip of concrete along each side face, the web width has no significant effect on the web crack width.
2. The skin reinforcement cover did not affect the web crack width. However, the effectiveness of the skin reinforcement in controlling the web crack widths decreased as the skin reinforcement cover increased.
3. The skin reinforcement should be located within $5/8$ of the tension zone closest to the main reinforcement.
4. The effectiveness of skin reinforcement can be related to the skin reinforcement ratio, which is the area of skin reinforcement divided by the area of concrete strips along the side faces affected by the reinforcement.
5. The side face crack width increased as the beam tension depth increased.

Frantz and Breen (1980b) proposed the following design recommendations of skin reinforcement for large reinforced concrete beams:

1. For more than 36 in. deep concrete member, the longitudinal skin reinforcement shall be distributed uniformly over $1/2$ of the depth nearest the main reinforcement along the side faces.

2. The skin reinforcement ratio Q , which is the ratio of total area of skin reinforcement to the total area of strips along each side face, should be designed according to the following provisions:

- a. If $36 \text{ in.} \leq d \leq 100 \text{ in.}$, $Q \geq 0.00024(d - 30)$

- b. If $d \geq 100 \text{ in.}$, $Q \geq 0.011 + 0.00058d$

3. The maximum spacing of skin reinforcement shall be limited to smaller of $d/10$ or 12 in.

Adebar and Leeuwen (1999) conducted an experimental study to investigate the appropriate amount of distribution of the skin reinforcement in controlling flexural and diagonal cracking. The authors tested 21 large concrete beams having web depth equal to 47 inch. The area of skin reinforcement was varied from 50 to 300 percent of the ACI Code and AASHTO Specification requirements. Based on the testing results, they reached the following conclusions:

1. The web crack width decreased as the amount of well-distributed skin reinforcement increased.
2. The application of welded wire fabric reduced the crack width due to the smaller diameter and more closely spacing.
3. The maximum diagonal crack width in the webs of large beams depends on the following parameters:
 - a. The magnitude of shear stress
 - b. The longitudinal strain of the longitudinal reinforcement on the flexural tension side
 - c. The amount and arrangement of transverse reinforcement

- d. The amount and arrangement of skin reinforcement
- e. The cover of reinforcement

They also proposed the following new design equation to control flexural and diagonal cracking, wherein the SI unit mm and MPa was used:

$$s_b = \frac{5}{1 + \frac{b_w d_b}{8A_b}} \left(\frac{w_{\max}}{\varepsilon_x + \frac{v}{\rho_v E_s}} - 2c \right) \quad \text{Eq. 2.14}$$

where,

- A_b = the area of cross-section, mm^2
- d_b = diameter of side face reinforcing bars, mm
- b_w = width of web, mm
- c = clear cover of skin reinforcement, mm
- ε_x = strain of the longitudinal reinforcement on the flexural tension side at the service load level
- w_{\max} = maximum crack width, mm
- v = shear stress, MPa
- ρ_v = transverse reinforcement ratio
- E_s = modulus of elasticity of steel, MPa

Adebar (2001) studied diagonal cracking and diagonal crack control in structural concrete. The author reviewed fundamental concepts and mechanisms of diagonal

cracking. Additionally, the author proposed the same equation as Eq. (3.2-10) for diagonal cracking control.

Frosch (2002) conducted research on the modeling and control of cracking in side face of the concrete beams. The study showed that the maximum skin reinforcement spacing is a function of the concrete cover from the skin reinforcement. It was also shown that a maximum bar spacing of 12 in. provides reasonable crack control up to 3 in. of concrete cover. The crack model developed by Frosch allows for the calculation of the crack width at any point along the cross section. A profile of the crack width through the depth of the section is more easily created, allowing for information regarding optimum locations for placing skin reinforcement for the purpose of controlling side face cracks. Frosch (2002) showed that the crack spacing and crack width along the side face are functions of the distance from the reinforcement, so the crack can be controlled by adding skin reinforcement and limiting the reinforcement spacing. Since the maximum crack width was observed at halfway between the reinforcement and neutral axis, the following equation can be used to solve for the crack width at $x = (d - c) / 2$:

$$w_c = \varepsilon_s \sqrt{d_s^2 + \left(\frac{1}{2}(d - c) \right)^2} \quad \text{Eq. 2.15}$$

where,

ε_s = reinforcing strain = f_s / E_s

d_s = skin reinforcement cover, in.

d = effective depth, in.

c = depth of neutral axis, in.

The study of the physical model showed that sections with effective depth of 36 in. and covers up to 3 in. can be designed without skin reinforcement. For thicker covers, the maximum effective depth not requiring skin reinforcement should be decreased. Moreover, there is a reduction in the maximum effective depth for covers thicker than 3 in. for Grade 60 reinforcement resulting in a maximum depth, $d = 36$ inches. In order to prevent excessive cracks throughout the depth of the section, maximum spacing of the reinforcement should be determined. According to Frosch (2002), the placement of the first bar is the most critical for the spacing of the skin reinforcement. The maximum crack width was calculated halfway between the primary reinforcement and the first skin reinforcement at a distance $x = s/2$, yielding the following equation:

$$w_s = 2 \frac{f_s}{E_s} \sqrt{d_s^2 + \left(\frac{s}{2}\right)^2} \quad \text{Eq. 2.16}$$

For sections where skin reinforcement exists, it is necessary to determine the location in the section where the reinforcement can be discontinued. Since crack widths are controlled by skin reinforcement below its end point, it is required to calculate the maximum distance s_{na} where the skin reinforcement can be eliminated. The maximum crack width will occur approximately halfway between the neutral axis and the location of the first layer of skin reinforcement at a distance $x = s_{na} / 2$ from the neutral axis. The maximum crack width can be calculated with the following equation based on the physical model developed by Frosch (2002):

$$w_s = s_{na} \left(\frac{\epsilon_s}{d - c} \right) \sqrt{d_s^2 + \left(\frac{s_{na}}{2}\right)^2} \quad \text{Eq. 2.17}$$

where,

s_{na} = maximum distance where the skin reinforcement can be eliminated.

Frosch recommended that the design formula should be based on a physical model to address the control of cracking in reinforced concrete structures and to unify the design criteria for controlling cracking in side and bottom faces. Frosch (2002) recommended the maximum spacing of flexural tension reinforcement as follows:

$$s = 12\alpha_s \left[2 - \frac{d_c}{3\alpha_s} \right] \leq 12\alpha_s \quad \text{Eq. 2.18}$$

where,

$$\alpha_s = \frac{36}{f_s}$$

d_c = thickness of concrete cover, in., for bottom-face reinforcement,

measured from extreme tension fiber to center of bar, and for skin reinforcement, measured from side face to center of bar

S = maximum spacing of reinforcement, in.

α_s = reinforcement factor

f_s = Calculated stress in reinforcement at service load, ksi. It shall be computed as the moment divided by the product of steel area and internal moment arm. It shall be permitted to take f_s as 60 percent of the specified yield strength f_y

Skin reinforcement shall be required along both side faces of a member for a distance $d/2$ from the nearest flexural tension reinforcement if the effective depth exceeds the depth calculated by equation shown below:

$$d = 42\alpha_s - 2d_c \leq 36\alpha_s \quad \text{Eq. 2.19}$$

2.6.3 Summary

Section 3.2 presented a review of previous research work related to crack control of the bottom face and side face of concrete members. Researchers attempted to develop more accurate equations to predict the maximum crack width, and then control the crack width by distributing the reinforcement in an appropriate way.

Furthermore, various crack width prediction equations were validated with test data collected from literature. Frosch (1999) equation will be checked further since it provided good correlation with test data, and is considered the basis of the AASHTO LRFD (2008) provisions. Moreover, Response 2000 computer program and Frosch (1999) were validated and calibrated using the test data from previous studies. The results indicated that the calibrated Response 2000 provided good correlation with test data. Therefore, the research team will validate the calibrated Response 2000 further with data from various beam sections including deep members.

2.7 Control of Cracks in Current AASHTO LRFD Specifications Provisions

Section 2.6 presented a summary of the research on the maximum crack width and crack control. This section provides a review of code provisions related to the distribution of crack control reinforcement.

Crack control in concrete structures has been debated with regard to crack width and its effect on durability and aesthetics. Cracking is primarily caused by flexural and tensile stresses, but may also result from temperature, shrinkage, shear, and torsion. Although researchers do not agree on any one specific crack width equation, the most significant parameters to control cracking have been widely agreed upon. The most sensitive factor is the reinforcing steel stress, followed by concrete cover, bar spacing, and the area of concrete surrounding each bar. For engineering practice, equations in the ACI 318-08 Code and AASHTO LRFD (2008) Specifications are used to control cracking. The corresponding provisions are discussed below.

The ACI requirements for flexural crack control in beams and one-way slabs are based on the statistical analysis of maximum crack width data from several sources (Gergely and Lutz 1968). ACI maintains that crack control is particularly important when reinforcement with yield strength over 40,000 psi is used. Good detailing practices such as concrete cover and spacing of reinforcement should lead to adequate crack control, even when reinforcement strength of 60,000 psi is used. ACI 318-08 Section 10.6 does not make a distinction between interior and exterior exposure, since corrosion is not clearly correlated with surface crack widths in the range normally found with reinforcement stresses at service load levels. ACI 318-08 only requires that the spacing of reinforcement closest to a surface in tension, s , shall not exceed, as given by:

$$s = 15\left(\frac{40,000}{f_s}\right) - 2.5c_c \quad \text{Eq. 2.20}$$

but not greater than $12\left(\frac{40,000}{f_s}\right)$, where c_c is the least distance from surface of

reinforcement or prestressing steel to the tension face. If there is only one bar or wire

nearest to the extreme tension face s used in Eq. (3.3-1) becomes the width of the extreme tension face. These provisions are not sufficient for structures subject to very aggressive exposure or designed to be watertight. Special investigation is required for structures subject to very aggressive exposure or designed to be watertight. ACI 318-08 recommends the use of several bars at moderate spacing rather than fewer bars at larger spacing to control cracking. These provisions were updated recently to reflect the higher service stresses that occur in flexural reinforcement with the use of the load combinations introduced in ACI 318-02. The maximum bar spacing is specified to directly control cracking. Similar recommendations have been stated for deep beams with the requirement of skin reinforcement.

AASHTO LRFD (2008) also provides provisions for reinforcement spacing to control flexural cracking. Similar to the equation adopted in ACI, AASHTO emphasizes the importance of reinforcement detailing and the notion that smaller bars at moderate spacing are more effective than larger bars of equivalent area. AASHTO also agrees with ACI 318-08 on most of the important parameters affecting crack width and specifies a formula for distribution of reinforcement to control cracking. The equation in AASHTO LRFD (2008) is based on the physical crack model of Frosch (2001) rather than on the statistically-based model used in previous editions. The equation limits bar spacing rather than crack width as follows:

$$s \leq \frac{700\gamma_e}{\beta_s f_{ss}} - 2d_c \quad \text{Eq. 2.21}$$

where,

$$\beta_s = 1 + \frac{d_c}{0.7(h-d_c)} \text{ (geometric relationship between crack width at tension}$$

face versus crack width at reinforcement level)

γ_e = exposure factor = 1.00 for Class I exposure, 0.75 for Class II exposure

d_c = thickness of concrete cover measured from extreme tension fiber to center of the flexural reinforcement located closest thereto (in.)

f_{ss} = tensile stress in steel reinforcement at the service limit state (ksi)

h = overall thickness of depth of the component (in.)

Unlike ACI, AASHTO specifies exposure conditions to meet the needs of the authority having jurisdiction. Class I exposure condition is based on a crack width of 0.017 in. and applies when cracks can be tolerated due to reduced concerns of appearance and/or corrosion. This exposure class can be thought of as an upper bound in regards to crack width for appearance and corrosion. Class II exposure condition applies to transverse design of segmental concrete box girders for any loads applied prior to attaining full nominal concrete strength. This is used when there is an increased concern of appearance and/or corrosion such as in substructures exposed to water and decks. AASHTO LRFD also specifies requirements for skin reinforcement based on ACI 318-02. The AASHTO Equation (or Eq. 20 shown above) also applies to both reinforced and prestressed concrete with specifications on the steel stresses used. In general, if AASHTO Class II exposure condition is used, all AASHTO spacings were less than those derived by the ACI equation. However, if Class I exposure condition is used, ACI spacing becomes more conservative.

2.8 Concrete Tension Stresses

The overall objective of this literature review is to look into the origins of the allowable tensile stress limits in the current design provisions. The review traces back to the original and the subsequent changes and the research of the tensile strength limit conducted by various researchers.

This literature review is organized in three sections. The first section is the historical development of tensile strength limit provisions in the design specifications. The second section discusses the previous research of tensile strength limit, while the last section presents the summary of the previous research especially concerning the variation of the tensile stress limit.

2.8.1 Historical Development of Tensile Strength Limit Provisions

The early discussion of cracking control is diverse. At the First United States Conference on Prestressed Concrete in 1951, some experts believed the completely crackless concrete member is only better for a specific purpose, but other experts thought the cracking of prestressed concrete beam is of the same importance as the yielding. In 1958, the “Tentative Recommendations for Prestressed Concrete” proposed by ACI-ASCE Committee 323 (ACI-ASCE 323) suggested that the prestressed concrete stresses before losses due to creep and shrinkage should adhere to the following limits (please note the unit in the following provisions is psi for the allowable tensile stress):

1. $3\sqrt{f'_{ci}}$ for members without non-prestressed reinforcement;
2. $6\sqrt{f'_{ci}}$ for members with non-prestressed reinforcement provided to resist the tensile force in concrete; computed on the basis of an uncracked section.

The Building Code Requirements for Reinforced Concrete (ACI 318-63) included the recommendation for the tensile stress limits as proposed by joint committee ACI-ASCE 323, with some modifications, as follows:

1. $3\sqrt{f'_{ci}}$ for members without auxiliary reinforcement in the tension zone;
2. When the calculated tension stress exceeds $3\sqrt{f'_{ci}}$, reinforcement shall be provided to resist the total tension force in the concrete computed on the assumption of uncracked section.

The Building Code Requirements for Reinforced Concrete (ACI 318-77) modified the allowable tensile stress limit as follows:

1. $6\sqrt{f'_{ci}}$ for the extreme fiber stress in tension at ends of simply supported members;
2. $3\sqrt{f'_{ci}}$ for the extreme fiber stress in tension at other locations.

ACI 318-08, Section 18.4.1 specifies the allowable tensile in concrete immediately after prestress transfer (before time-dependent prestress losses) as follows:

1. Where computed concrete tensile strength, f_t , exceeds $6\sqrt{f'_{ci}}$ at ends of simply supported members, or $3\sqrt{f'_{ci}}$ at other locations, additional bonded reinforcement shall be provided in the tensile zone to resist the total tensile force in concrete computed with the assumption of an uncracked section.

Table 2.9- Tensile Stress Limits in Prestressed Concrete at Service Limit State After Losses, Fully Prestressed Components (AASHTO 2008 Table 5.9.4.2.2-1)

Bridge Type	Location	Stress Limit
Other Than Segmentally Constructed Bridges	Tension in the precompressed Tensile Zone Bridges, Assuming Uncracked Sections	
	For components with bonded prestressing tendons or reinforcement that are subjected to not worse than moderate corrosion condition.	$0.19\sqrt{f'_c}(ksi)$
	For components with bonded prestressing tendons or reinforcement that are subjected to severe corrosive conditions	$0.0948\sqrt{f'_c}(ksi)$
	For components with unbounded prestressing tendons	No tension
Segmentally Constructed Bridges	Longitudinal Stresses Through Joints in the Precompressed Tensile Zone	
	Joints with minimum bonded auxiliary reinforcement through the joints sufficient to carry the calculated longitudinal tensile force at a stress of 0.5 fy; internal tendons or external tendons	$0.0948\sqrt{f'_c}(ksi)$
	Joints without the minimum bonded auxiliary reinforcement through joints	No tension
	Transverse Stress Through Joints Tension in the transverse direction in precompressed tensile zone	$0.0948\sqrt{f'_c}(ksi)$
	Principal Tensile Stress at Neutral Axis in Web All types of segmental concrete bridges with internal and/or external tendons, unless the Owner imposes other criteria for critical structures.	$0.110\sqrt{f'_c}(ksi)$

The AASHTO Standard Specifications for Highway Bridges (AASHTO 1992) specified the allowable tensile stresses, before losses due to creep and shrinkage, as follows:

1. 200 psi or $3\sqrt{f'_{ci}}$ for members in tension areas with no bonded reinforcement;

2. Where the calculated tensile exceeds this value, reinforcement shall be provided to resist the total tension force in the concrete computed on the assumption of uncracked section. The maximum tensile stress shall not exceed $7.5\sqrt{f'_{ci}}$.

Table 2.9 shows the tensile stress limits and provisions by the AASHTO LRFD (2008) Specification. It is noted that the only change from the AASHTO LRFD (2004) Specifications is the principal tensile stress at Neutral Axis in Web.

2.8.2 Research Related to the Tensile Stress Limits

The majority of the research performed on tensile strength of concrete attempted to develop more precise prediction equations for the tensile strength. However, with the introduction of HPC and other pozzolanic material such as silica fume, fly ash, and slag, and based on their limited test results, few researchers aimed to revise the allowable tensile stress limits. Literature was reviewed to include the background work in this area that would either support such revisions or retain the current limits in the AASHTO LRFD (2008) provisions during the code calibration process.

McNeely and Lash (1963) performed tests on 35 cylinders to evaluate the compressive and tensile strengths and to evaluate the effect of pre-compression, loading rate, and cold temperature on the modulus of rupture. The results indicated that pre-compression had no significant effect on the tensile strength, and that the tensile strength is greater at zero °F than at room temperature. Based on their test data, they also concluded that the average tensile strength was 455 psi with a standard deviation of 30 psi.

Carrasquillo et al. (1981) performed uniaxial compressive tests on 4×8 in. and 6×12 in. concrete cylinders and modulus of rupture tests on $4 \times 4 \times 14$ in. beams. They used Type I Portland cement with water-cement ratio between 0.32 and 0.70. The uniaxial compressive testing results ranged from 3000 to 11,000 psi. Based on their test results, they recommended $11.7\sqrt{f'_c}$ psi for the modulus of rupture and $6.8\sqrt{f'_c}$ psi for the splitting tensile strength. They also reported that drying has more effect on the high strength concrete than normal strength concrete.

Carino and Lew (1982) derived an expression for the tensile splitting strength as a function of the compressive strength of normal weight concrete. They analyzed data from the published literature as well as the data acquired from the National Bureau of Standards (NBS) to formulate a more appropriate equation. They compared various forms of equations based on regression analysis of the NBS data, and concluded that an equation with a power function provides the best correlation with experimental data as follows:

$$f_{ct} = 0.80(f'_c)^{0.73}, \text{ psi} \quad \text{Eq. 2.22}$$

Raphael (1984) studied the relationship between the tensile and the compressive strength based on 12,000 tests compiled from Gonnerman and Shuman (1928), Walker and Bloem (1960), Grieb and Werner (1962), and Houk (1965). Figure 2.4 illustrates the compiled data with best-fit equations. They suggested that the modulus of rupture can be predicted using $2.3f_c^{2/3}$ (in psi) and is more suitable for concrete compressive strengths of up to 9,000 psi (Figure 2.4).

Oluokun et. al (1991) carried out tests on specimens from different mixes to establish a relationship between splitting tensile and compressive strengths at early ages. The tests were performed at the ages of 6 and 12 hr and 1, 2, 3, 7, and 28 days. They performed regression analysis and validated the results with the testing data from several different references. They proposed two equations for $f'_c > 1000\text{ psi}$ and $f'_c < 1000\text{ psi}$, respectively.

$$f_{ct} = 0.584(f'_c)^{0.79}, \text{ psi, for } f'_c > 1000\text{ psi} \quad \text{Eq. 2.23}$$

$$f_{ct} = 0.928(f'_c)^{0.6}, \text{ psi, for } f'_c < 1000\text{ psi} \quad \text{Eq. 2.24}$$

Huo and Tadros (2000) studied the allowable tensile stress of high performance concrete (HPC) bridge beams. The authors recommended that, if high performance concrete is used in bridge beams, the allowable tensile stress should be increased from $7.5\sqrt{f'_c}$ to $10\sqrt{f'_c}$, in psi, ($0.62\sqrt{f'_c}$ to $0.83\sqrt{f'_c}$ MPa) at release and from $6.0\sqrt{f'_c}$ to $7.9\sqrt{f'_c}$, in psi, ($0.50\sqrt{f'_c}$ to $0.66\sqrt{f'_c}$ (in MPa)) at service. The actual test results of the Texas HPC mixes showed that the new allowable stress limits were adequate and reasonable.

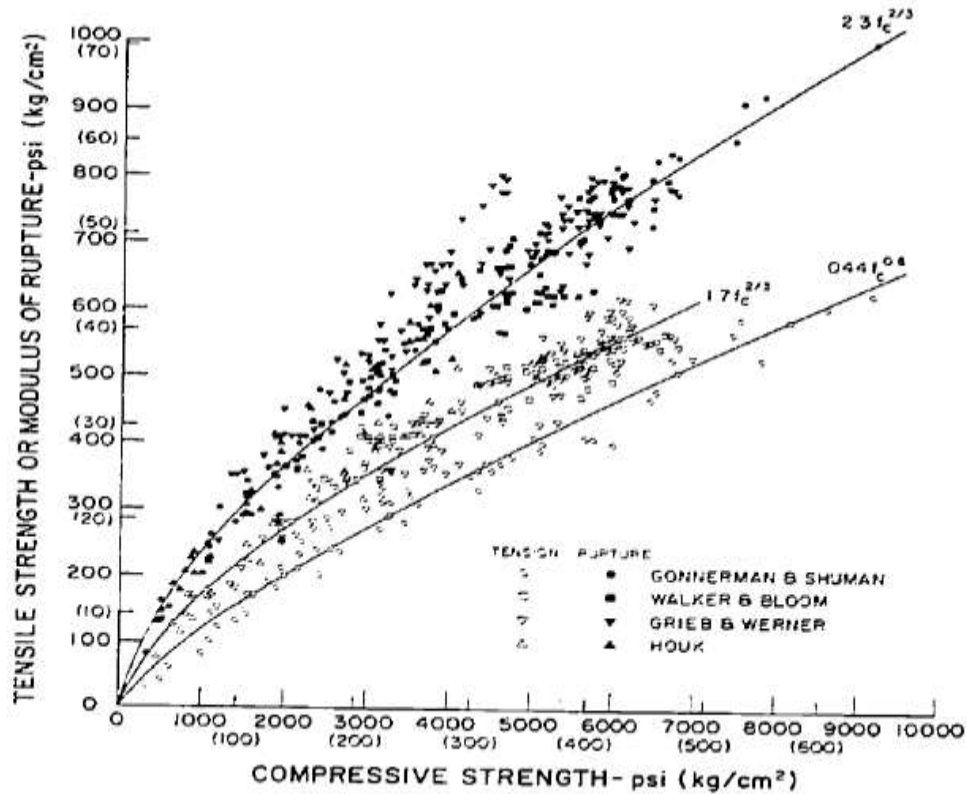


Figure 2.4 Flexural tensile strength vs. compressive strength (Raphael, 1984)

Hueste et al. (2004) performed a study to evaluate the mechanical properties of high-strength concrete for prestressed members, whereas high-strength concrete (HSC) is widely used in structures such as bridges. The study was initiated since the design provisions provided by AASHTO standard specification (1999) and AASHTO LRFD specifications (2000) were based on the mechanical properties attained from the testing of normal strength concrete (NSC).

The HSC samples used in this study were collected from three precasters in Texas. The selected precasters represent different geographical locations, coarse aggregate types, and production capacities. The testing parameters included compressive

strength, modulus of rupture, splitting tensile strength, and modulus of elasticity. Based on the test data, prediction equations were recommended as follows:

$$E_c = 63,000\sqrt{f'_c} \text{ psi} \quad \text{Eq. 2.25}$$

$$f_t = 6.6\sqrt{f'_c} \text{ psi} \quad \text{Eq. 2.26}$$

$$f_r = 10\sqrt{f'_c} \text{ psi} \quad \text{Eq. 2.27}$$

Table 2.10 shows the statistical parameters (i.e., bias factors) for each material properties of HSC.

In general, the authors recommended an increase in the resistance factor for HSC members because of the larger bias factor and smaller coefficient of variation. They also concluded that the allowable tensile stress specified in AASHTO LRFD specifications may be too conservative.

Table 2.10 Summary of 28-day bias factors (Hueste et. al, 2004)

Specified f'_c (psi)	Bias factor (Mean-to-Nominal Ratio)			
	Compressive Strength, f'_c	Modulus of Elasticity	Splitting Strength, f_t	Modulus of Rupture (MOR)
6000±1000	1.59	1.31	1.14	1.77
8000±1000	1.24	1.13	1.00	1.54
10,000±1000	1.10	1.09	0.98	1.54

Okeil (2006) studied the allowable tensile stress for webs of (PS) concrete bridges using a reliability-based approach.

Tuchscherer and Bayrak (2009) studied the tensile stress limit for prestressed concrete at release. The authors reviewed the background of the ACI 318 provisions

about the allowable tensile stress limit for prestressed concrete. The allowable tensile stress for prestressed concrete was $3\sqrt{f'_c}$, in psi, until 1977. After 1977, the ACI Code changed the limit to $6\sqrt{f'_c}$, in psi. For the tensile stress at the ends of simply supported members, the author questioned this change of the allowable tensile stress and performed the experimental work for seven 54 in. deep bridge beam. The results suggest that for some deep girders, the current ACI provisions about the allowable tensile stress limit is not adequate to prevent cracking at prestress release, so the author recommended the allowable tensile stress should be changed from $6\sqrt{f'_c}$ psi to $4\sqrt{f'_c}$, in psi.

Various authors studied the effects of various types of aggregates and other materials on the tensile strength of concrete. Lam et al. (1998) studied the effect of fly ash and silica fume on the compressive and tensile strength of concrete. They have tested 24 mixes with various water-cementitious material ratios, and various percentages of fly ash and Silica fume. Results show that the splitting tensile strength increased 13% when adding 5% silica fume.

Haque and Kayali (1998) studied the properties of high-strength concrete using fine fly ash. They concluded that the indirect tensile strength was about 5 and 6% of their respective compressive strength.

Zain et. al (2002) attempted to find a new expression for the tensile strength of HPC arguing that the current ACI prediction equation is too simple to cover HPC at different ages. Their new equation was related to the compressive strength of concrete, W/B ratio, and concrete age. The equation was based on experimental data and linear regression technique, as follows:

$$f_{ct} = \frac{f'_c}{0.10f'_c + 7.11}, \text{ MPa} \quad \text{Eq. 2.28}$$

Similar analysis was performed with regard to the relationship between the tensile strength and the W/B ratio and concrete age, as shown in Eq. (3.7.2-8) and (3.7.2-9), respectively.

$$f_{ct} = 0.54\sqrt{f'_c}(W/B)^{-0.07}, \text{ MPa} \quad \text{Eq. 2.29}$$

$$f_{ct,t} = 0.59\sqrt{f'_{c,t}}\left(\frac{t}{t_{28}}\right)^{0.04}, \text{ MPa} \quad \text{Eq. 2.30}$$

where $f_{ct,t}$ = the splitting tensile strength (MPa), at age t = in days, $f'_{c,t}$ = the compressive strength (in MPa) at age t = days, and t is age of concrete in days.

Choi and Yuan (2005) studied the relationship between the splitting tensile strength and compressive strength of Glass Fiber Reinforced Concrete (GFRC) and Polypropylene Fiber Reinforced Concrete (PFRC) using experimental data. They performed 5 mixes: 1) no fiber, 2) 1.0%, 3) 1.5% of glass fiber, 4) 1.0%, and 5) 1.5% of polypropylene fiber. They have developed equations similar to the format used in the ACI-318-08 Code in the SI system of units:

$$f_{ct} = 0.60\sqrt{f'_c}, \text{ For GFRC, MPa} \quad \text{Eq. 2.31}$$

$$f_{ct} = 0.55\sqrt{f'_c}, \text{ For PFRC, MPa} \quad \text{Eq. 2.32}$$

Bhanja and Sengupta (2005) studied the influence of silica fume on the tensile strength by testing 30 mixes. The mixes have different W/B ratio and percentage of Silica Fume. The compressive strength of concrete was measured, however, the splitting tensile strength was estimated from the compressive strength by using empirical correlation equations. They used regression analysis to obtain the relationship between

the 28-day splitting tensile strength and compressive strength, as shown in Equation below

$$f_{ct} = 0.284 \times (f_c)^{0.717}, \text{ MPa} \quad \text{Eq. 2.33}$$

The authors also obtained the relationship between the 28-day flexural tensile strength and compressive strength as shown in Equation below:

$$f_{ctf} = 0.275 \times (f_c)^{0.81}, \text{ MPa} \quad \text{Eq. 2.34}$$

2.8.3 Summary

Most researchers attempted to develop more precise prediction equations for the allowable tensile stress using the relationship between the tensile stress and compressive strength. However, few researchers attempted to find the variation of allowable tensile stress because of the application of new types of concrete such as High-Performance concrete (HPC) and High-Strength Concrete (HSC). For example, as stated earlier, Huo and Tadros (2000) studied the allowable tensile stress of HPC bridge girders and advocated an increase in the allowable tensile stress from $7.5 \sqrt{f'_c}$ to $10 \sqrt{f'_c}$ psi ($0.62 \sqrt{f'_c}$ (to $0.83 \sqrt{f'_c}$ MPa) at release and from $6.0 \sqrt{f'_c}$ to $7.9 \sqrt{f'_c}$ psi ($0.50 \sqrt{f'_c}$ to $0.66 \sqrt{f'_c}$ MPa) at service. In support of their recommendation, the authors show that the actual test results from the Texas HPC mixes showed that the proposed new allowable stress limits were adequate and reasonable. On the other hand, Tuchscherer and Bayrak (2009) found out that the ACI allowable tensile stress limit of $6 \sqrt{f'_c}$ psi at the end of prestressed concrete beam is not adequate to prevent cracking and recommended that the allowable

tensile stress should be changed from $6\sqrt{f'_c}$ to $4\sqrt{f'_c}$, in psi. This confirms the limit set by AASHTO LRFD (2008) provisions at $3\sqrt{f'_c}$, in psi.

2.9 Deflection of Concrete Members

The American Association of State Highway Transportation Officials (AASHTO) Load and Resistance Factor Design (LRFD) Bridge Specification (2008) establishes the use of a deflection design as optional criteria. Certain State Highway Agencies specify their own deflection limits as a mandatory requirement. The deflection criteria in AASHTO LRFD (2008) are shown as follows:

1. For the bridge designed for general vehicular load, the deflection limitation is $L/800$;
2. For the bridge designed for vehicular and/or pedestrian loads, the deflection limitation is $L/1000$;
3. For the bridge designed for vehicular load on cantilever arms, the deflection limitation is $L/300$;
4. For the bridge designed for vehicular and/or pedestrian loads on cantilever arms, the deflection limitation is $L/375$.

It is perceived that these deflection limits are usually based on a rather arbitrary and sometimes conservative approach in designing bridges (Demitz et. al, 2003). This raises questions on the rationality of these deflection limits in that pursuing a conservative design approach does not take advantage of today's bridge construction technologies. In principle, the deflection limits were established to eliminate damage to

any structural and non-structural components due to excessive deformations as well as to avoid loss of aesthetic appearance and interruption of its functionality. For highway bridges, vehicle rideability and human responses to bridge vibration under normal traffic conditions play an important role in determining the deflection limits. Moreover, if it is believed that deflection limits should be specified as a design parameter, there is a need for a rational approach to establish a limit state design philosophy that all designers can justifiably use. If the deformation (deflection) requirements in AASHTO LRFD Bridge Design Specifications, Subsection 2.5.2.6 become the controlling design issue, the most economical bridge designs, based on ultimate strength criteria, cannot be achieved. Table 2.5.2.6.3-1 Traditional Minimum Depths for Constant Depth Superstructures in AASHTO LRFD Bridge Design Specifications (2008) (shown in Table 2.11) will need to be modified to reflect current bridge design use of high strength concrete (HSC). This will enhance the use of HSC and address the bridge component property aspect. This will offset the use of a deflection limitation; such as, $L/800$.

It is generally agreed that the deformation requirements (*i.e.* deflection limits and corresponding span-to-depth ratio limits) were established to (a) prevent structural damage due to excessive deflections, and (b) control of bridge vibrations to offset human perceptions. The research team will provide a calibration procedure for deflection limit state based on the currently specified AASHTO's deflection limit at $L/800$. The procedure will establish the calibrated live load factors for the Service I limit State. However, it should be emphasized herein that the specifying deflection limits may provide enough stiffness of bridge superstructure, but dynamic characteristics of a bridge are determined by both mass and stiffness distributions of a bridge system. It is the

“resonances” due to the close frequencies of the bridge and truck loading system that generate undesirable bridge vibration. For example, if the truck frequency is normally between 2 and 5 Hz and if the bridge has a natural frequency around 2 Hz, there can be excessive deflection and vibrations. In other words, the deflection limits by themselves cannot provide an effective control of bridge vibration under normal traffic conditions.

A preliminary literature search indicated that the origin of the deformation requirements in bridge designs may be traced back to 1871 with a set of specifications established by the Phoenix Bridge Company (PBC). The ASCE report on deflection limits of bridges (ASCE, 1958) has been widely cited for the evolution of these requirements, (summarized in Table 2.12 below). The following conclusions may be drawn from the ASCE report:

1. The deflection limits were established before the span-to-depth ratio limits; that is, the span-to-depth ratio limits were used as indirect measures of the deflection limits.
2. Both deflection and span-to-depth ratio limits were empirically derived, mainly for the early bridge structures, such as wood plank decks, pony trusses, simple rolled beams, and pin-connected through-trusses (Wu, 2003).
3. The specified span-to-depth ratio limits for highway bridges (by AASHTO) followed what was established for railroad bridges (by AREA).
4. The deflection limit of $L/800$ was established in the 1930's, primarily for the vibration control of steel highway bridges.

Table 2.11 AASHTO LRFD Table 2.5.2.6.3-1 Traditional Minimum Depths for Constant Depth Superstructures (AASHTO LRFD (2008)).

Superstructure		Minimum Depth (Including Deck)	
		When variable depth members are used, values may be adjusted to account for changes in relative stiffness of positive and negative moment sections	
Material	Type	Simple Spans	Continuous Spans
Reinforced Concrete	Slabs with main reinforcement parallel to traffic	$\frac{1.2(S+10)}{30}$	$\frac{S+10}{30} \geq 0.54 \text{ ft.}$
	T-Beams	$0.070L$	$0.065L$
	Box Beams	$0.060L$	$0.055L$
	Pedestrian Structure Beams	$0.035L$	$0.033L$
Prestressed Concrete	Slabs	$0.030L \geq 6.5 \text{ in.}$	$0.027L \geq 6.5 \text{ in.}$
	CIP Box Beams	$0.045L$	$0.040L$
	Precast I-Beams	$0.045L$	$0.040L$
	Pedestrian Structure Beams	$0.033L$	$0.030L$
	Adjacent Box Beams	$0.030L$	$0.025L$
Steel	Overall Depth of Composite I-Beam	$0.040L$	$0.032L$
	Depth of I-Beam Portion of Composite I-Beam	$0.033L$	$0.027L$
	Trusses	$0.100L$	$0.100L$

It is generally agreed that the deformation requirements are intended to play an important role in bridge vibration controls and that the bridge-vehicle-road roughness interactions should be included in evaluating the rationality of the deformation requirements in current bridge design specifications. To address these requirements, Wright and Walker (1971), based on human responses to harmonic vertical vibrations (see Table 2.13) proposed a vibration-related static deflection limit. The limit is a

computed transient peak acceleration of a bridge, α , it should not exceed 100 in/sec^2 , where the static deflection, δ_s , is linked to α in such a way as:

$$\delta_s = 0.05 \times L \times \frac{\alpha}{(\text{speed} + 0.3 \times f_s \times L) \times f_s} \quad \text{Eq. 2.35}$$

where, L = span length; speed = vehicle speed; and f_s = natural frequency of a simple span bridge, which may be estimated as:

$$f_s = \frac{\pi}{2L^2} \sqrt{\frac{E_b I_b}{m}} \quad \text{Eq. 2.36}$$

where, $E_b I_b$ = flexural rigidity of a girder section; m = unit mass of a girder section. It should be noted that δ_s needs to be calculated for a live load with a girder distribution factor of 0.7.

Nowak and Grouni (1988) also stated that the deflection and vibration criteria should be derived by considering human reactions rather than structural performance. In addition, similar efforts that relate static deflection limits to the natural frequency of a bridge are shown in Canadian and Australian bridge design specifications (Ministry, 1991; CSA International, 2000; AUSTROADS, 1992, AUSTRALIAN, 1996). Figure 2.5 shows the relationship between the first flexural frequency (in Hz) and static deflections limits (in mm) at the edge of a bridge from the Ontario Highway Bridge Design Code (OHBD). This was developed from extensive field data collection and analytical models (Wright and Green, 1964). Figure 2.6 shows a similar relationship that is adopted in the Australian Bridge Design Codes. It is worthy of pointing out that the static deflection limits are usually absent in European bridge design specifications, and the

New Zealand Bridge Manual in 1994 limits the maximum vertical velocity to 2.2 *in*/sec instead of using the maximum acceleration. Figure 2.7 shows the human perception to particle velocities due to vibration (Oriard, 1972).

Debates on the necessity of deformation requirements in current bridge design specifications focus on two aspects: (1) whether excessive deflections cause structural damage; and (2) whether deflection limits provide effective controls of bridge vibrations under normal traffic. Based on the limited survey in the ASCE report (1958), no evidence of serious structural damage due to excessive vertical deflections was revealed. However, unfavorable psychological reactions to bridge vibrations caused more concerns on the subject of perceived bridge safety. Burke (2001) argued that if deflection limits were not mandated, the effective service life of reinforced concrete deck slabs could become considerably less than their normal replacement interval of 30 years. Moreover, the report on NCHRP project 20-7 (Roeder *et al.*, 2002) revealed that steel bridges clearly suffered severe structural damage due to excessive deformation, but provided little support for the idea that deflection limits should be used as a method of controlling these structural damages. In addition, deflection limits were not considered as the “good” method of controlling bridge vibrations (Azizinamini *et al.*, 2004).

Table 2.12 Evolution of Deformation Requirements in Bridge Design

Year	Agency	Deflection Limits	Span-to-Depth Ratio Limits
1871	PBC	1/1,200 of span length (at train speed: 30 mph)	
1905	AREA		10 for trusses 10 for plate girders 12 for rolled beams and channels
1907	AREA		10 for trusses 12 for plate girders 12 for rolled beams
1913	Bureau of Public Roads		10 for trusses 12 for plate girders 20 for rolled beams
1919	AREA		10 for trusses 12 for plate girders 15 for rolled beams
1924	AASHO		10 for trusses 12 for plate girders 20 for rolled beams
1931	AASHO		10 for trusses 15 for plate girders 20 for rolled beams
1935	AASHO		10 for trusses 25 for plate girders 25 for rolled beams
1936	Bureau of Public Roads	1/800 of span length (for vibration controls)	
1938	AASHO	1/800 of span length	
1960	AASHTO	1/1000 of span length (for pedestrian bridges)	

Table 2.13 Peak Acceleration for Human Response to Harmonic Vertical Vibration
(Wright and Walker, 1971)

Human Response	Transient Peak Acceleration, in./sec ²	Sustained Peak Acceleration, in./sec ²
Imperceptible	5	0.5
Perceptible to Some	10	1
Perceptible to Most	20	2
Perceptible	50	5
Unpleasant to Few	100	10
Unpleasant to Some	200	20
Unpleasant to Most	500	50
Intolerable to Some	1000	100
Intolerable to Most	2000	200

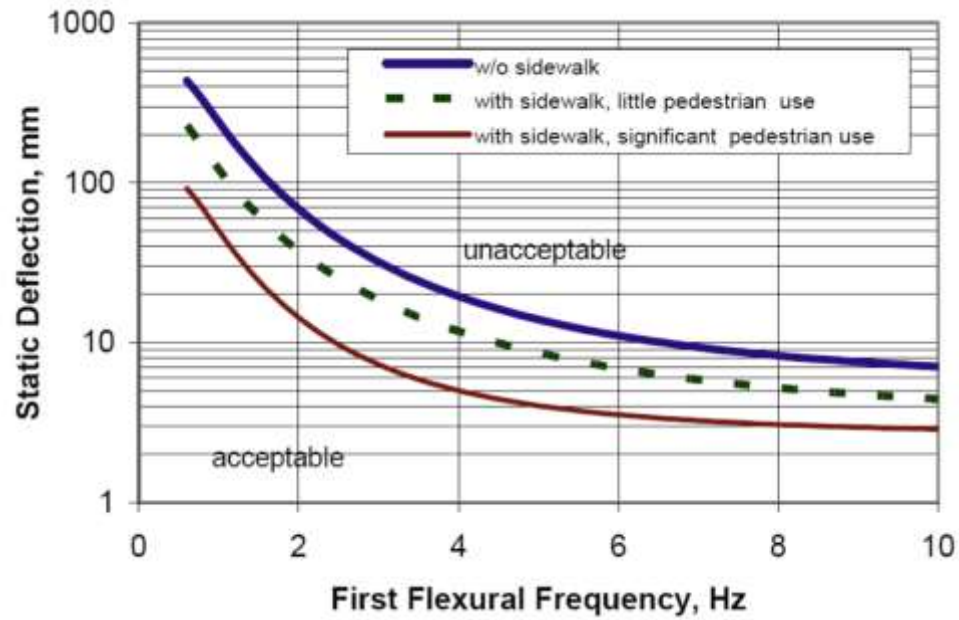


Figure 2.5 Static Deflection vs. First Flexural Frequency (Ministry, 1991; CSA International, 2000)

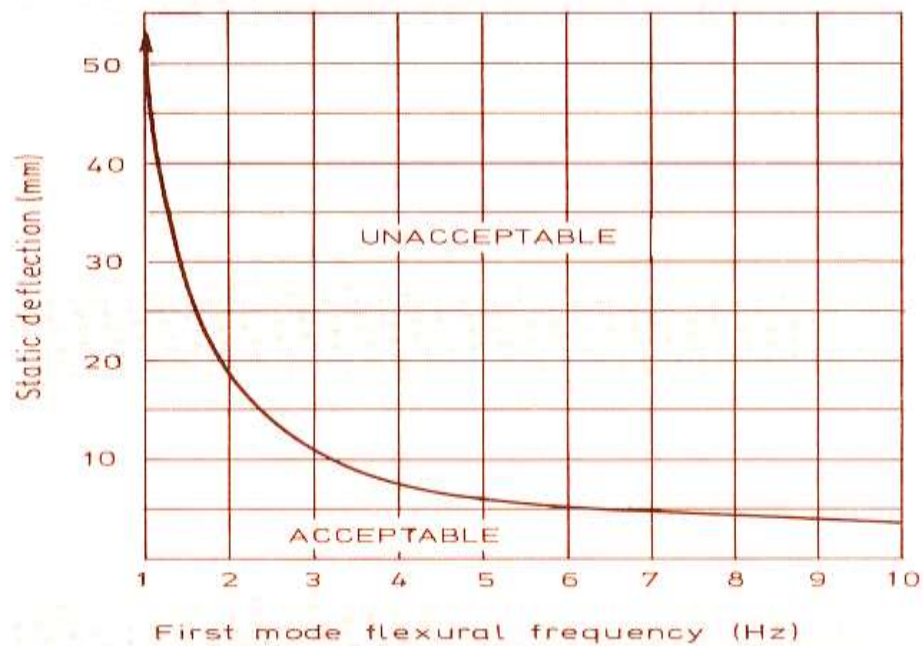


Figure 2.6 Static Deflection vs. First Mode Flexural Frequency (AUSTROADS, 1992; AUSTRALIAN, 1996)

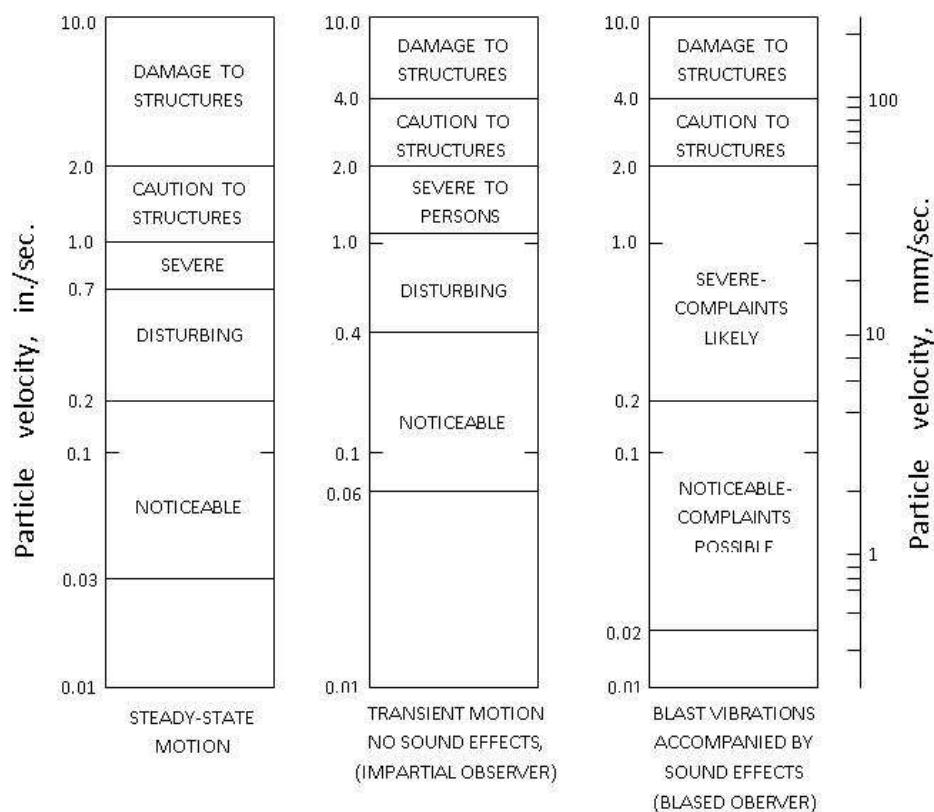


Figure 2.7 Human Response to Particle Velocity (Oriard, 1972)

Debates on the necessity of deformation requirements in current bridge design specifications focuses on two aspects: (1) whether excessive deflections cause structural damage, and (2) whether the deflection limits provide effective controls of bridge vibrations under normal traffic. Based on the limited survey in the ASCE report (1958), no evidence of serious structural damage due to excessive vertical deflections was revealed. However, unfavorable psychological reactions to bridge vibrations caused more concerns on the subject of perceived bridge safety.

A comprehensive research was conducted by Wright and Walker (1971) to study the factors regarding human perceptions and responses to bridge vibrations. The study concluded that peak accelerations were preferable to peak velocities when evaluating human perceptions to bridge vibrations that typically ranged from 1 to 10 Hz. Thus, a

peak acceleration is used as a guide to determine acceptable bridge vibrations (as opposed to a peak velocity), and the acceptable frequency range for these vibrations is between 1 and 10 Hz. Thus, peak acceleration, velocity, and frequency of bridge vertical vibrations will be considered to be the most important parameters in this research proposal. Figure 2.8 illustrates the human tolerance criteria to bridge vibrations in terms of vertical accelerations (Ministry, 1995).

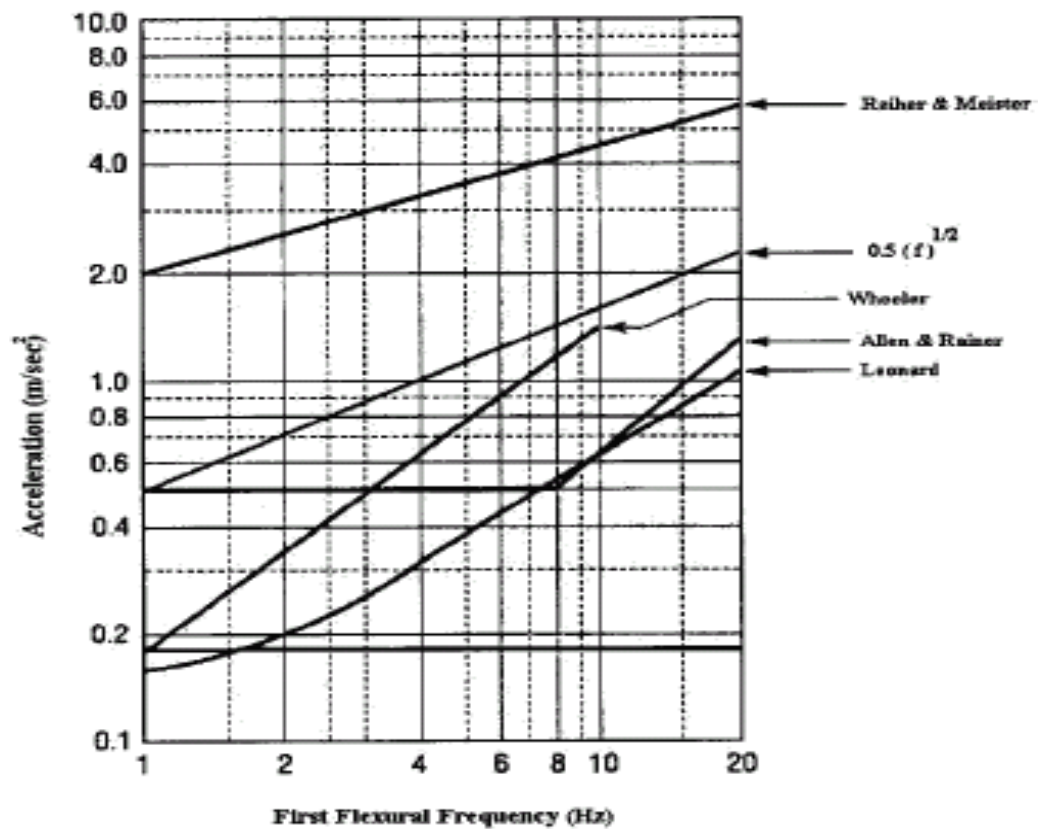


Figure 2.8 Criterion for Human Response to Acceleration (Ministry, 1995)

It is also important to emphasize that the factors relating to live loading conditions include truck weight, speed, tire properties, axle spacing, road roughness as well as the presence of multiple truck configurations on a bridge at the same time. The methods of computing deflections and girder distribution factors also greatly varied among State

Departments of Transportation (DOTs). For example, Wisconsin has a relatively low legal load limit, 80 kips (356 kN), wherein it enforces the most strict deflection limit, $L/1600$. The State of Michigan uses the standard $L/800$ limit with the highest legal loads in the United States, 164 kips (730 kN). In addition, impact and load factors were applied in some States and not in others. These variations coupled with variable state legal load limits resulted in an unknown, non-uniform level of safety for live-load deflection serviceability criteria. Therefore, addressing live loading condition factors to control deflection varies and becomes subjective.

In summary, it is clear that deformation requirements are necessary for both prevention of structural damage and control of bridge vibrations. Furthermore, it is believed that deformation requirements for bridge vibration control will be more restrictive than those for prevention of structural damage. Therefore, there is a need to focus future efforts of research on the establishment of the relationships between the deformation requirements of deflection limits and corresponding span-to-depth ratio limits and bridge vibration control.

CHAPTER 3

MODELS FOR STRUCTURAL RESISTANCE AND DEAD LOAD

Due to the fact that the section properties of structures, material properties and even construction procedures are subject to a great extent of uncertainty, a well-established statistical model for structural resistance and dead load is critical for structural analysis. Two steps should be taken for development of successful statistical models for structural resistance. The first step is deriving a precise equation or numerical model that could provide accurate estimation of structural resistance for various serviceability limit states. Since each serviceability limit state represents different design criteria or “failure mode”, the prediction equation or numerical model might be varied for each serviceability limit state or performance levels, even for the same structure. Second step is to appropriately extract the statistical information of structural resistance. This step involves selection of appropriate reliability analysis techniques and estimation of statistical information for each random variable involved. Utilizing appropriate reliability analysis technique, the statistical model of resistance would be developed and can be used to predict the reliability level of the structure.

3.1 Service I Limit State (Traditional)

As specified in the AASHTO LRFD Bridge Design Specifications (2012), the service I limit state mainly relates to the tension in reinforced concrete structures with the objective of crack control. Due to the fact that in most of the cases, the service limit state does not control the design of other Reinforced Concrete components such as pier cap, pier columns, the work of calibration for Service I limit state concentrated on reinforced concrete decks.

3.1.1 Derivation of Resistance Prediction Equation

As shown in Section 2.6, the maximum crack width of reinforced concrete member can be expressed as a function of stress in steel reinforcement, elastic modulus of steel and geometrical parameters such as reinforcement spacing, and concrete cover. Among these variables, stress in steel reinforcement is the only load-driven variable that indicates the relationship between the crack width and the applied live load. Therefore, the structural resistance is expressed as the stress in the steel reinforcement. After a comprehensive literature review and comparison with experimental data, the equation of maximum crack width as shown below, developed by Frosch (1999) is selected to be used in this study. The detailed comparison can be found in Section 3.1.2.

$$w_c = \frac{2f_s}{E_s} \beta \sqrt{\left(d_c^2 + \left(\frac{s}{2}\right)^2\right)} \quad \text{Eq. 3.1}$$

where:

s = maximum permissible bar spacing, in

w_c = limiting crack width, in (0.016 in, based on ACI 318-95)

E_s = Modulus of Elasticity of Steel, ksi

f_s = Stress in Steel Reinforcement

β = $1.0 + 0.08 d_c$

d_c = bottom cover measured from center of lowest bar, in

Rearranging terms in Eq. 3.1 to solve for f_s as the resistance yields the following:

$$f_s = \frac{w_c E_s}{2\beta \sqrt{\left(d_c^2 + \left(\frac{s}{2}\right)^2\right)}} \quad \text{Eq. 3.2}$$

The variables E_s , β , and d_c are random variables with statistical parameters. The values w_c and s are deterministic parameters based on ACI318-08 regulations of 0.016in for w_c and $S_{\max} = 12(40000 / f_s)$.

3.1.2 Comparison of Predication Equation for Maximum Crack Width of Reinforced Concrete Members

As indicated in Section 3.1.1, an appropriate crack width prediction equation is important for the accuracy of structural resistance. In this section, extensive literature review of the research done on crack control from the 1950s to present is undertaken. The purpose of the literature review is to understand the prior work (including code provisions) and assess the influence of various parameters on crack control. It has been found that the most contributing parameters are the steel stress, thickness of the concrete cover, and the cross sectional area of concrete surrounding each bar. Moreover, the crack width on the tension face is affected by the strain gradient from the level of steel to the tension face, and that the bar diameter is not a major variable. Various code provisions and crack

width equations have been reviewed. Table 3.1 lists the equations that were reviewed and discussed earlier. Each equation is examined for accuracy and applicability using test data from Clark (1956).

Table 3.1 Equations of Maximum Crack Width

Author	Maximum Crack Width Equation	Year
Clark	$w_{ave} = C_1 \frac{D}{p} [f_s - C_2 (\frac{1}{p} + n)]$	1956
Kaar-Mattock	$w_b = 0.115 \beta f_s \sqrt[4]{A}$	1963
Broms	$w_s = 4t_e \varepsilon_s = 0.133 t_e f_s$ $w_s = 4t_e \varepsilon_s = 0.133 t_e f_s$	1965
Gergely-Lutz	$w_b = 0.076 \beta f_s \sqrt[3]{A d_c}$	1968
Beeby	$w_m = (K_1 c + K_2 \frac{\phi}{\rho}) \varepsilon_m$	1979
CEB/FIP	$w_k = l_{s,max} (\varepsilon_{sm} - \varepsilon_{cm} - \varepsilon_{cs})$	1990
Eurocode	$w_k = (50 + 0.25 k_1 k_2 \frac{\phi}{\rho_{ef}}) (1 - \beta_1 \beta_2 (\frac{\sigma_{sr}}{\sigma_s})^2) \frac{\sigma_s}{E_s}$	1991
Frosch	$w_c = \frac{2f_s}{E_s} \beta \sqrt{(d_c^2 + (\frac{s}{2})^2)}$	1999

Figure 3.1 shows a comparison of the measured crack width and the predicted maximum crack width using Clark's equation. Similarly, Figure 3.2 shows a comparison of the measured crack width and the predicted maximum crack width using Clark's equation.

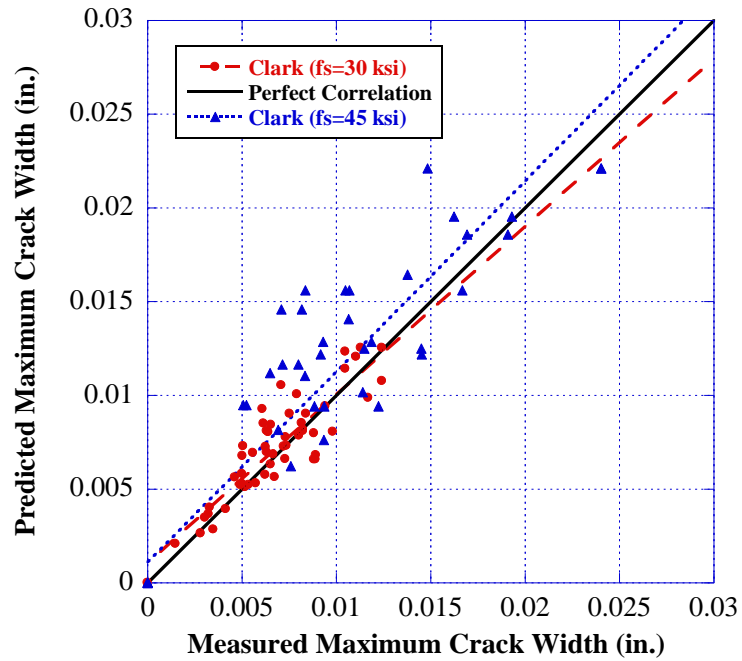


Figure 3.1 Comparison of the measured and predicted maximum crack width using equation developed by Clark (1956).

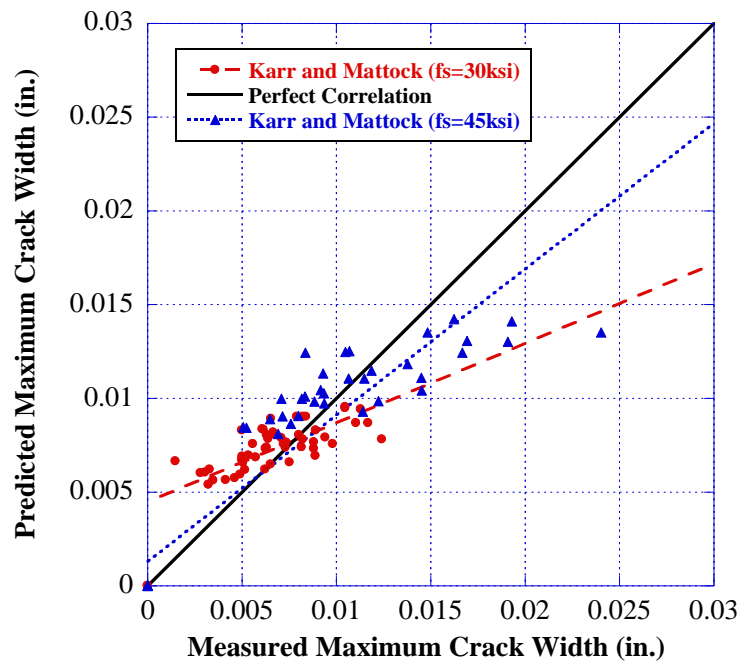


Figure 3.2 Comparison between the measured and predicted maximum crack width using equation developed by Karr and Mattock (1963).

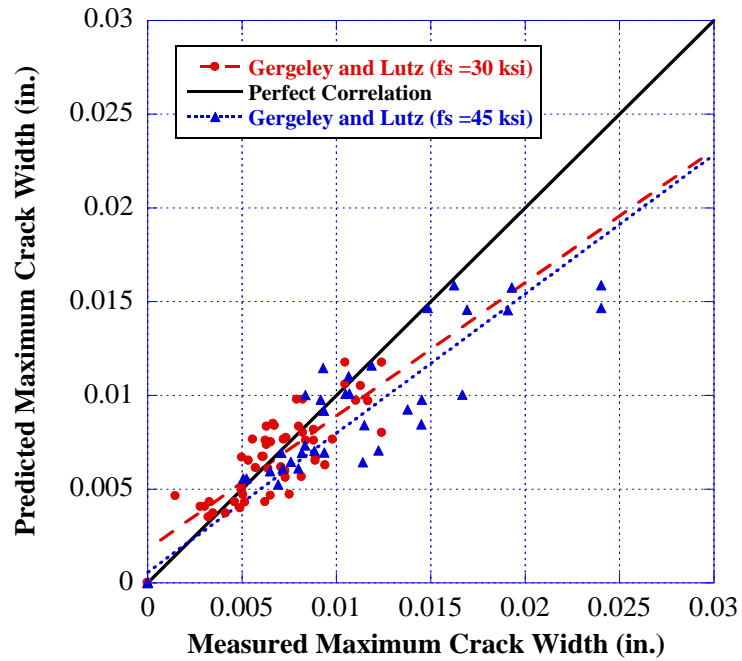


Figure 3.3 Comparison of the measured and predicted maximum crack widths using equation developed by Gergeley and Lutz (1968).

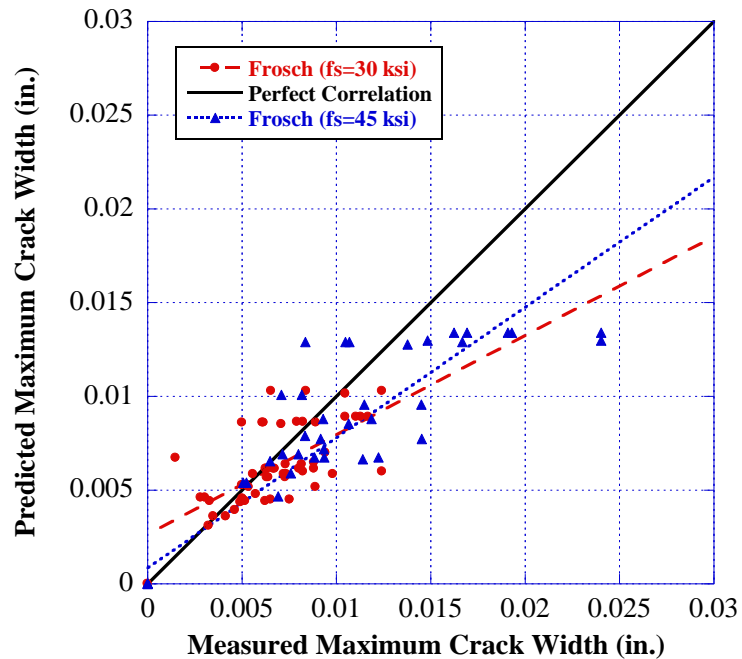


Figure 3.4 Comparison between the measured and predicted maximum crack width using equation developed by Frosch (1999).

Figure 3.3 presents a comparison between the measured and the predicted maximum crack widths using Eq. (3.4-3) by Gergely and Lutz (1968). Figure 3.4 presents a comparison between the measured and the predicted maximum crack widths using Eq. (3.4-3) by Frosch (1999).

In general, and based on the preliminary evaluation performed thus far using the limited test data from Clark (1956), the equation by Frosch (1999) will be used in the prediction of the Resistance model for f_s . The equation by Frosch (1999) is also applicable since it is the basis for the AASHTO LRFD (2008) provisions and has provided good correlation with the experimental data taken from Clark (1956). It is observed that all the equations used to predict the maximum crack width has exhibited similar margin of error between 20-30%.

3.1.3 Statistical Model for Structural Resistance

It is approved that if a random variable can be expressed as a function of other variables, the statistics such as mean and coefficient of variation (CoV) of this random variable can be estimated by first expanding the function in a Taylor series about the mean of the variables composed the function, then truncating higher order terms and calculating the expectations of that function. Therefore, the mean and CoV of a random variable can be expressed in terms of the mean and CoV of random variables that compose its function. However, due to the fact that the function of some random variables cannot be expressed in closed forms, it might be difficult to apply this method in this study. Moreover, since the distribution and statistical information of each basic random variable that composes the structural resistance function is known, the statistical

model of structural resistance can be developed using Monte Carlo Simulation by following the procedures below:

- (1) A set of random numbers that have the value of either 0 or 1 is generated to represent the probability of occurrence of the basic variables used in the resistance prediction functions. It is important to note that the distributions of all basic variables should be known.
- (2) The corresponding random values of each basic variable can be obtained by assigning the values generated in step 1 to its cumulative probability distribution. Note that all random variables were generated independently in accordance with their distribution.
- (3) Based on the resistance prediction equation developed in Section 3.1.1, calculate the structural resistance using the set of random values that generated in step 2 for each random variable.
- (4) Repeat step 1 to 3 to simulate a large sample database for the structural resistance. The statistical information such as mean and CoV can be estimated hereafter as the mean and CoV of the sample database.

It is important to point out that although the statistical model extracted from Monte-Carlo simulation was based on the distribution and statistical information of each random variable by its best estimation, due to the inherent randomness in each individual basic variables, certain prediction error is expected and should be taken into account as part of variability of structural resistance. Thus, the total CoV of structural resistance can be estimated using the equation below:

$$\Omega_R^2 = \delta_R^2 + \varepsilon_R^2 \quad \text{Eq. 3.3}$$

Where:

Ω_R = total coefficient of variation of structural resistance

δ_R = value of coefficient of variation of structural resistance obtained from Monte Carlo Simulation

ε_R = prediction error.

In this study, the prediction error of 0.1 is estimated from previous study performed by Siriaksorn and Naaman (1980) regarding the crack control of reinforced concrete members.

Table 3.2 Summary of Statistical Information for Random Variables for Service I Limit State

Variable	Distribution	Mean	CoV
A_s	normal	$0.9 A_{sn}$	0.015
b	normal	b_n	0.04
C_{E_c}	normal	33.6	0.1217
d	normal	d_n	0.06
d_c	normal	d_{cn}	0.06
E_s	normal	E_{sn}	0.024
f_c^c	lognormal $E_c = C_{E_c} \gamma_c^{1.5} \sqrt{f'_c}$	(psi) 3000: 1.31 f'_{cn} 3500: 1.27 f'_{cn} 4000: 1.24 f'_{cn} 4500: 1.21 f'_{cn} 5000: 1.19 f'_{cn}	3000: 0.17 3500: 0.16 4000: 0.15 4500: 0.14 5000: 0.135
f_y	lognormal	$1.13 f_{yn}$	0.03
h	normal	h_n	$1/(6.4\mu)$
g_c	normal	150 pcf	0.03

The statistical information of random variables that used in Service I limit state was summarized in Table 3.2.

3.2 Service I Limit State (Empirical)

Crack control of reinforcement concrete deck is an important issue for the serviceability and durability of concrete deck. The crack opening leads to the corrosion of reinforcement, and then further affects the rigidity and duration of the structure. Section 3.1 presents the statistical model for concrete deck design using traditional equivalent strip deck design method at Service I limit state. But besides the traditional equivalent strip deck design method, AASHTO LRFD Bridge Design Specification also provides empirical design method as specified in Article 9.7.2. The empirical method is mainly based on extensive lab tests showing that the arching or compressive membrane action of concrete deck could enhance the strength of concrete deck significantly (Figure 3.5). This method has been validated by extensive nonlinear FE analysis (Fang et al. 1986). The advantage of this design method is no analysis is needed during the design process. The designer could select the area of rebar directly as long as the design conditions specified in Article 9.7.2.4 are fulfilled.

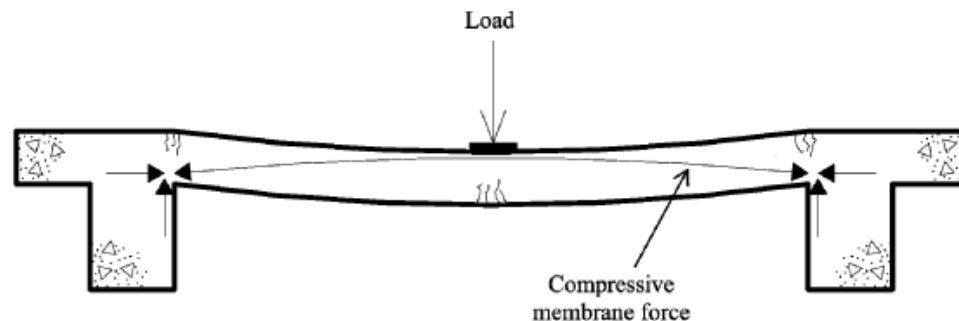


Figure 3.5 Compressive Membrane Action in Cross Section of Reinforced Concrete Beam-and-Slab Bridge Deck (Hon et al., 2005)

Unlike the reinforced concrete deck designed using traditional method, the moment resistance of reinforced concrete deck designed using empirical method contains two components: (1) resistance due to tension of the concrete and reinforcement at the bottom fiber of the concrete deck at positive moment region, and (2) resistance due to arching action at the positive moment region. It is noteworthy that the arching action only contributes to the resistance at positive moment area. In this section, sub-section 3.2.1 presents the comprehensive investigation of arching action mechanism has been conducted by the author. Sub-section 3.2.1 presents the resistance predication equation at both positive moment and negative moment region for concrete deck designed using empirical method. Sub-section 3.2.3 presents the statistical model of structural resistance for concrete deck designed using empirical method at Service I limit state.

3.2.1 Investigation of Arching Action of Concrete Deck

An early study regarding the ultimate strength and arching action effect of concrete was conducted by Park (1964). The author proposed a method to analyze the ultimate strength of rectangular concrete slabs based on plastic theory.

Tsui et al. (1986) studied the load capacity of the Ontario-type bridge deck on steel girders. A full-size composite bridge, in which half of it had a cast-in-place deck and another half had precast, prestressed panels, were tested with a series of static loads, 5 million cycles of fatigue loading, and concentrated load. Besides the experimental study, the finite element model was developed and the results were compared with the experimental results. The experimental results revealed that the precast, prestressed panel deck was stronger and provided better crack-resistant than the cast-in-place deck.

Guice and Rhomberg (1988) tested 16 one-way reinforced concrete slab strips to investigate the effects of the restraints. The author concluded that adequate lateral stiffness is required to develop both compressive and tensile membrane enhancements. The author also concluded that the small rotational freedoms do not significantly affect the compressive membrane capacity, but enhance the tensile membrane capacity.

Fang et al. (1990^a, 1990^b, 1990^c, 1994) conducted a series of study regarding the load capacity and fatigue behavior of Ontario-type reinforced concrete bridge decks. A full-scale Ontario-type bridge deck reinforced with about 60% of the reinforcement required by AASHTO Code was tested under service and overload conditions. The experimental results showed that the membrane action did not noticeably affect the performance of the deck prior to deck cracking but the flexural capacity of the deck was increased significantly due to the arching action of the bridge deck. The authors also concluded that both the ACI and AASHTO punching shear formulas were very conservative.

Rankin and Long (1997) performed a series of study regarding the compressive membrane action and strength enhancement of concrete slabs. They summarized the mechanism of arching action and proposed a method to calculate the strength enhancement. The steps for calculating the arching moment are summarized as follows:

(1) Horizontal translational restraint stiffness of concrete deck, K :

The horizontal translational restraint stiffness is an essential parameter to estimate the flexural capacity enhancement due to arching action. Rankin and Long (2003) proposed the following equation to compute the translational restraint stiffness of concrete deck:

$$K = \frac{EA_b}{L_e} \quad \text{Eq. 3.4}$$

Where,

E = The modulus of elasticity of the edge beams,

A_b = The equivalent area of the lateral stiffness,

L_e = half span of elastically-restrained strip, $L_e = L / 2$.

(2) Depth available for arching, d_1 :

$$d_1 = \frac{D - (p + p_c) \frac{f_{sy} d}{0.85 f_c'}}{2} \quad \text{Eq. 3.5}$$

Where,

D = The overall depth of the deck,

f_{sy} = The yield strength of reinforcement,

p = The positive reinforcement ratio,

p_c = The negative reinforcement ratio,

d = The effective depth of the deck,

f_c' = Compressive strength of the concrete,

(3) Equivalent length of rigidly restrained arch, L_r :

$$L_r = L_e \left[\left(\frac{E_c A}{K L_e} \right) + 1 \right]^{1/3} \quad \text{Eq. 3.6}$$

Where,

L_e = half span of elastically-restrained strip, $L_e = L / 2$,

E_c = The modulus of elasticity of concrete,

A = The effective area of arch leg, $A = d_1 \times b$.

(4) Plastic concrete strain, ε_c :

$$\varepsilon_c = (-400 + 60f'_c - 0.33f_c'^2) \times 10^{-6} \quad \text{Eq. 3.7}$$

(5) Geometric and material property parameter for arching, R :

$$R = \frac{\varepsilon_c L_r^2}{4d_1^2} \quad \text{Eq. 3.8}$$

(6) Arching moment ratio, M_r :

$$\text{If } R > 0.26, M_r = \frac{0.3615}{R}; \quad \text{Eq. 3.9}$$

$$\text{If } 0 < R < 0.26, M_r = 4.3 - 16.1\sqrt{3.3 \times 10^{-4} + 0.1243R}. \quad \text{Eq. 3.10}$$

(7) Arching moment, M_{ar} , and M_a

Arching moment (rigid restraint)

$$M_{ar} = \frac{M_r 0.85 f'_c d_1^2}{4} \quad \text{Eq. 3.11}$$

Arching moment (elastic restraint)

$$M_a = M_{ar} \frac{L_e}{L_r} \quad \text{Eq. 3.12}$$

Furthermore, the predicted ultimate strength was compared with the 80 experimental data tested by various researchers, the comparison show good correlation between the predicted and tested strength (Figure 3.6).

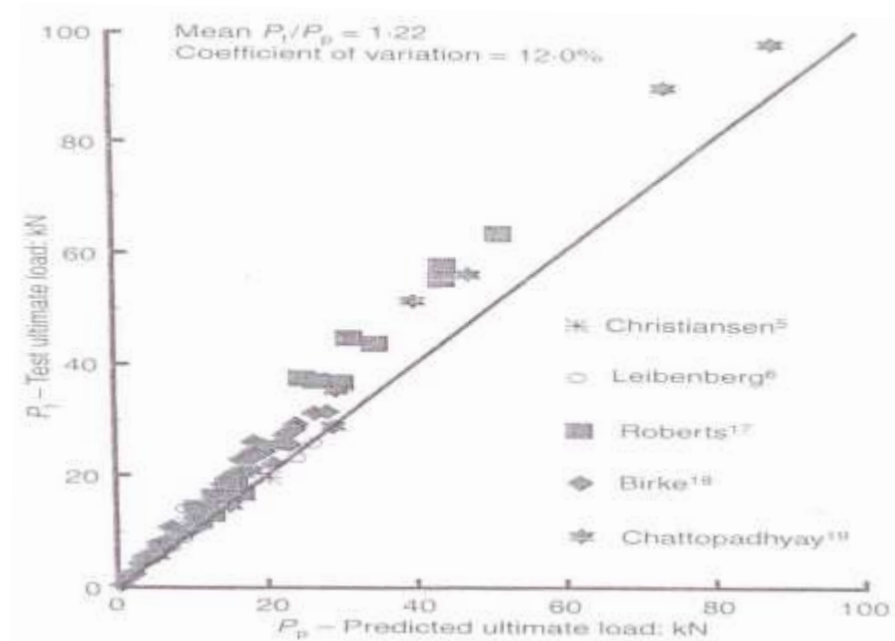


Figure 3.6 Correlation of Predictions with test results (Rankin and Long, 1997)

Bailey (2000) performed a study on the membrane action of unrestrained lightly reinforced concrete slabs at large displacement. The author conducted six compartment tests on a full-scale, eight story, steel frame building. The fire resistance and flexural behavior were investigated through the tests. The author decided to ignore any horizontal restraint to simplify the analysis. Based on the experimental results and analytical study, the author proposed a new theoretical approach to predict the load capacity of the slab at large displacement. Furthermore, the author compared the predicted results with published test data. The comparison indicates the prediction has excellent correlation with the test data.

Peel-Cross et al. (2000) conducted an experimental study of the ultimate load capacity of composite slabs. The experimental results demonstrated the compressive membrane effects significantly increase the load capacity of interior floor panels but with less contribution to the edge panels.

Taylor et al. (2001) tested 15 reinforced concrete slab strips constructed with high-strength concrete. The testing results indicated that the degree of external lateral restraint and the concrete compressive strength have significant effects on the strength of laterally restrained slabs.

Graddy et al. (2002) conducted a study regarding the punching-shear behavior of bridge decks under fatigue loading. Static and pulsating fatigue tests were performed on full-scale, cast-in-place and precast, prestressed panel specimens. The experimental data were compared with analytical predictions. The finite element models were also developed and the prediction was also compared with the experimental data. The authors concluded that the punching shear capacity predicted by AASHTO and ACI equation was conservative compared to the experimental data and arching action results in insignificant increase in flexural capacity of simply supported slabs.

Salim and Sebastian (2003) conducted an experimental study of the ultimate punching load capacity of reinforced concrete slabs. Four reinforced concrete slabs were tested in this study. Moreover, the authors proposed a theoretical method to predict the punching shear failure loads using plasticity theory. The predictions provided good agreement with the experimental data from the literature.

Hon et al. (2005) performed 8 punching shear failure tests and 15 flexural failure tests. They also adopted the method proposed by Rankin and Long (1997) in their study to predict the load capacity of the concrete slabs. The comparison between the experimental data and prediction shows both Rankin and Long (1997) and FE analysis shows good prediction (Figure 3.7).

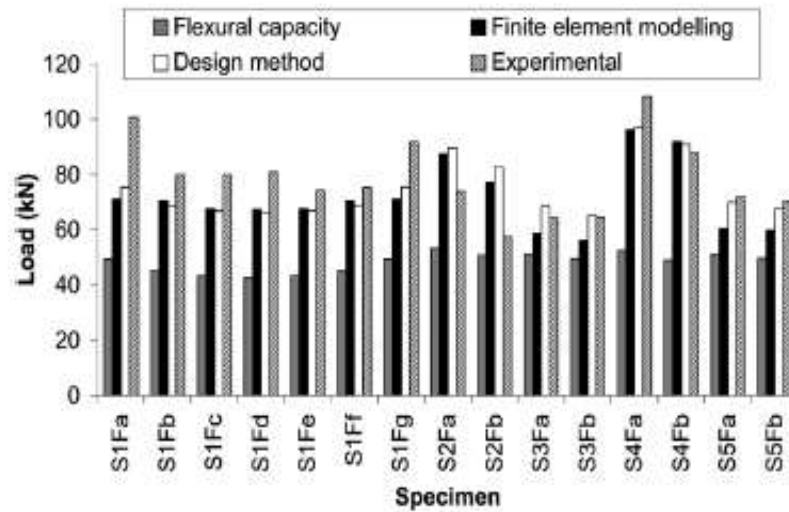


Figure 3.7 Comparison between peak loads for flexural failure tests (Hon et al., 2005)

Taylor et al. (2007) evaluated the serviceability of bridge deck slabs with arching action. The measured crack widths, deflections and the load capacity collected from the tests on a full scale bridge deck were compared with the current code requirements. The comparison indicates the UK code overestimated the crack widths in various loading level and ignored the beneficial effects of arching action. The comparison also shows both the ACI and BS codes give similar and conservative prediction for the strength of concrete slabs.

Bailey et al. (2008) tested 14 horizontally unrestrained concrete slabs with large vertical deflection. A simple approach was developed based on rigid-plastic behavior. The proposed approach provided good prediction of load-displacement response compared with the experimental results. Additionally, a finite element model (FEM) was developed and compared with the experimental data. The comparison indicated the FEM can be used to predict the load capacity of horizontally unrestrained concrete slabs.

Meadway (2008) conducted a comprehensive study to evaluate the current deck design practice. The author performed the laboratory test on four full scale models. A finite element model was developed and validated with the experimental data. A parametric study was performed using the validated finite element model. The author concluded that the strength of the concrete deck decrease by approximately 50 kips when the span length increased from 6 ft to 12 ft.

Schmeckpeper et al. (2010) investigated the effect of bridge deck design methodology on crack control. The authors reviewed the literature regarding the effect of bridge deck design methodology on deck cracking. They also surveyed all the states agencies regarding the bridge deck design methods. They believe the cracking problem can be better controlled by reducing the spacing and increasing the rebar size but further research needs to be conducted prior to providing detailed recommendations.

3.2.2 Derivation of Resistance Prediction Equation

Similar to the resistance prediction equation for concrete deck designed using traditional design method, the resistance due to the tension of reinforcement can be expressed as Eq. 3.2. At positive moment region, the resistance due to arching action can be expressed as:

$$f_s = \frac{3 \left(A_s E_s + 3 E_c b d + \sqrt{A_s^2 E_s^2 + 2 A_s E_s E_c b d} \right)}{d (4 A_s E_s + 9 E_c b d) A_s} \cdot \frac{M_r 0.85 f_c' d_1^2}{4} \quad \text{Eq. 3.13}$$

Therefore, total resistance at the positive moment region can be calculated using the equation below:

$$f_s = \frac{w_c E_s}{2\beta \sqrt{\left(d_c^2 + \left(\frac{s}{2}\right)^2\right)}} + \frac{3\left(A_s E_s + 3E_c b d + \sqrt{A_s^2 E_s^2 + 2A_s E_s E_c b d}\right)}{d(4A_s E_s + 9E_c b d)A_s} \cdot \frac{M, 0.85 f_c' d_1^2}{4} \quad \text{Eq. 3.14}$$

The resistance at negative moment region can be calculated using Eq. 3.2.

3.2.3 Statistical Model for Structural Resistance

Similar to the concrete deck designed by traditional method, the statistical model for structural resistance was developed using Monte-Carlo simulation. The statistical information of random variables that summarized in Table 3.2 was also used in Service I limit state for concrete deck designed by empirical method.

3.3 Service III Limit State

As specified in the AASHTO LRFD Bridge Design Specifications (2012), service limit state is the limit state to restrict stress, deformation, and crack width under regular service conditions. The service III limit state is mainly related to the tension in prestressed concrete superstructures with the objective of crack control and the principal tension in the webs of segmental concrete girders. There are three tension levels at the bottom of the prestressed concrete (P/C) girder that would need to be considered: (1) Decompression limit state, (2) Maximum allowable tensile stress limit state, and (3) Maximum allowable crack width limit state. For any given girder, regardless of the stress limit used in the design, the reliability index can be calculated for all three levels. As the live load increases, the girder reaches the state of decompression first, followed by the

tensile stress increasing until it reaches the prescribed cracking limit causing the concrete to crack. After cracking, the width of the crack increases until it reaches the prescribed crack width limit.

Similar to crack control of Service I limit state, the tension level at the bottom of concrete girder can be expressed by the tension in prestressing strands. Thus, the stresses in the prestressing strands were used as the resistances for Service III limit state for prestressed concrete girder in this study. In this section, sub-section 3.3.1 presents the derivation of the resistance prediction equation at three tension levels. Since the accuracy of the crack width prediction equation directly affects the accuracy of resistance estimation after the crack occurs at the bottom of prestressed concrete girder, sub-section 3.3.2 presents the comprehensive investigation and comparison of maximum crack width prediction equation at the bottom of prestressed concrete girder. Finally, Sub-section 3.2.3 presents the statistical model of structural resistance for prestressed concrete girders at Service III limit state.

3.3.1 Derivation of Resistance Prediction Equation

The derivation of the resistance prediction equation for a prestressed concrete girder subjected to flexural loading is shown in this section. Figure 3.8 shows the stress distribution diagram for a typical prestressed concrete bridge girder at various stages of loading.

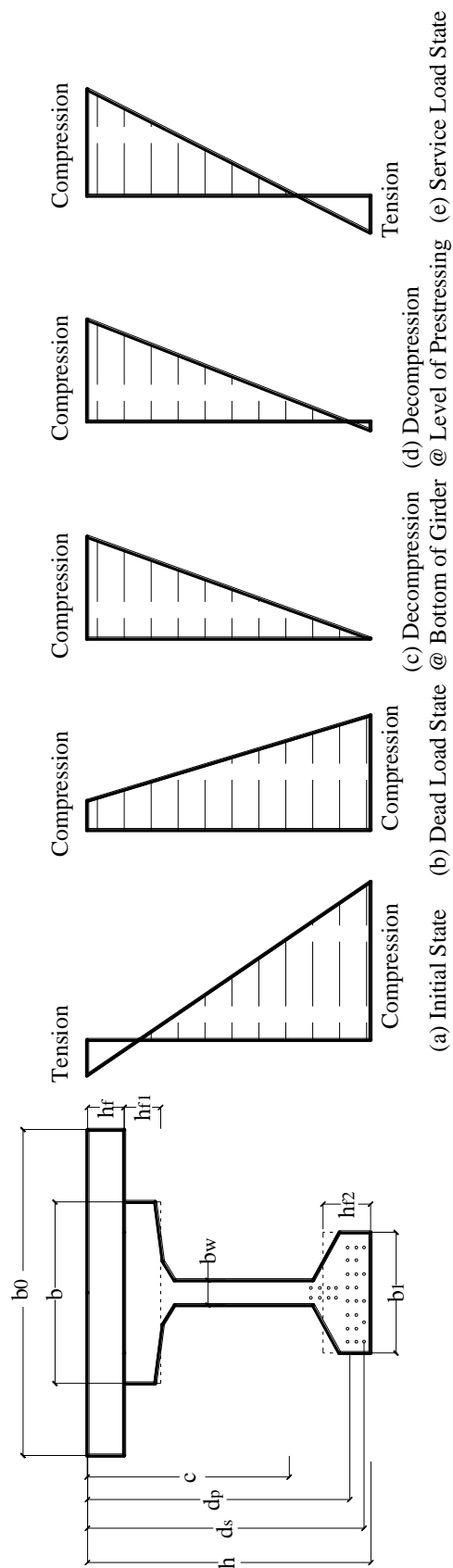


Figure 3.8 Stress Distribution Diagrams for a Typical Prestressed Concrete Bridge Girder at Various Stages of Loading

Using force equilibrium:

$$\begin{aligned}
 A_{ps}f_{ps} + A_sf_s &= \frac{f_{ct}}{2}b_0c - \frac{2}{c}(b_0 - b)(c - h_f)f_{ct} - \frac{2}{c}(b - b_w)(c - h_f - h_{f1})f_{ct} \\
 &= \frac{f_{ct}}{2c} \left[b_0c^2 - (c - h_f)^2(b_0 - b) - (c - h_f - h_{f1})^2(b - b_w) \right] \quad \text{Eq. 3.15}
 \end{aligned}$$

where,

- A_s = area of non-prestressing steel
- A_{ps} = area of prestressing steel in tension zone
- b = prestressed beam top flange width
- b_0 = effective deck width transformed to the beam material
- b_w = web thickness
- c = depth of neutral axis from the from extreme compression fiber
- f_{ct} = calculated stress in concrete at the top fiber.
- f_{ps} = calculated stress in prestressing steel.
- f_s = calculated stress in non-prestressing steel.
- h_f = deck thickness
- h_{f1} = top flange thickness

The stress in the prestressing steel can be calculated as follows:

$$f_{ps} = E_{ps}\epsilon_{ps} = E_{ps}(\epsilon_{se} + \epsilon_{ce}) + \frac{E_{ps}}{E_c}f_{ct}\left(\frac{d_p - c}{c}\right) \quad \text{Eq. 3.16}$$

By rearranging Eq. 3.16, the stress in the concrete at the top fiber can be calculated as follows:

$$f_{ct} = \frac{[f_{ps} - E_{ps}(\varepsilon_{se} + \varepsilon_{ce})] E_c c}{E_{ps}(d_p - c)} \quad \text{Eq. 3.17}$$

From strain compatibility,

$$f_s = E_s \varepsilon_s = \frac{E_s}{E_c} f_{ct} \left(\frac{d_s - c}{c} \right) \quad \text{Eq. 3.18}$$

where,

- c = depth of neutral axis from the extreme compression fiber
- d_p = the distance from extreme compression fiber to centroid of prestressing steel.
- d_s = the distance from extreme compression fiber to centroid of non-prestressing steel.
- E_c = modulus of elasticity of concrete
- E_{ps} = modulus of elasticity of prestressing steel
- E_s = modulus of elasticity of non-prestressing steel
- f_{ct} = stress in the concrete at the top of the beam after losses at service load
- ε_{ce} = strain in concrete at the level of prestressing steel after losses at dead load state
- ε_{ps} = strain in prestressing steel after losses at service load
- ε_s = strain in non-prestressing steel after losses at service load
- ε_{se} = strain in prestressing steel after losses at dead load state

Substitute Eq. 3.17 and Eq. 3.18 into Eq. 3.15:

$$A_{ps}f_{ps} = \frac{\left[f_{ps} - E_{ps}(\varepsilon_{se} + \varepsilon_{ce}) \right] E_c}{2E_{ps}(d_p - c)} \cdot \left[b_0c^2 - (c - h_f)^2(b_0 - b) - (c - h_f - h_{f1})^2(b - b_w) - \frac{2A_sE_s(d_s - c)}{E_c} \right] \quad \text{Eq. 3.19}$$

Eq. 3.19 can be simplified and rewritten as a quadratic equation with unknown c, neutral axis depth, as follows:

$$c^2 + \frac{2}{b_w} \left[\frac{A_{ps}f_{ps}E_{ps}}{\left[f_{ps} - E_{ps}(\varepsilon_{se} + \varepsilon_{ce}) \right] E_c} + b_0h_f + bh_{f1} - b_w h_f - b_w h_{f1} + \frac{A_sE_s}{E_c} \right] \cdot c - \frac{2}{b_w} \left[\frac{A_{ps}f_{ps}E_{ps}}{\left[f_{ps} - E_{ps}(\varepsilon_{se} + \varepsilon_{ce}) \right] E_c} - \frac{1}{2}(b - b_0)h_f^2 + \frac{1}{2}(b - b_w)(h_f + h_{f1})^2 + \frac{A_sE_s d_s}{E_c} \right] = 0 \quad \text{Eq. 3.20}$$

The moment resistance can be expressed as follows:

$$M_n = A_{ps}f_{ps}d_p + A_s f_s d_s - \frac{1}{6} f_{ct} b_0 c^2 + \frac{(c - h_f)^2 (b_0 - b)}{2c} f_{ct} \left(\frac{c + 2h_f}{3} \right) + \frac{(c - h_f - h_{f1})^2 (b - b_w)}{2c} f_{ct} \left(\frac{c + 2h_f + 2h_{f1}}{3} \right) \quad \text{Eq. 3.21}$$

where,

M_n = nominal moment resistance.

f_s is calculated using equation Eq. 3.18, and f_{ct} is calculated using equation Eq.

3.17.

The depth of neutral axis from the compression face, c, can be computed using Eq. 3.20.

Also, assuming linear elastic relationship in the behavior of the prestressing steel:

$$\varepsilon_{se} = \frac{f_{se}}{E_{ps}} \quad \text{Eq. 3.22}$$

Then,

$$\varepsilon_{ce} = \frac{A_{ps} f_{se}}{E_c} \left(\frac{1}{A_c} + \frac{e_0^2}{I} \right) - \frac{M_D e_0}{E_c I} \quad \text{Eq. 3.23}$$

where,

A_c = area of concrete at the cross-section considered.

e_0 = eccentricity of the prestressing force with respect to the centroid of the section at mid span.

E_c = modulus of elasticity of concrete.

E_{ps} = modulus of elasticity of prestressing steel.

f_{se} = effective stress in prestressing steel after losses.

I = moment of inertia.

M_D = dead load moment.

If we consider uncracked section behavior under service loads, and plane section remains plane, then the linear strain distribution diagram is as follows:

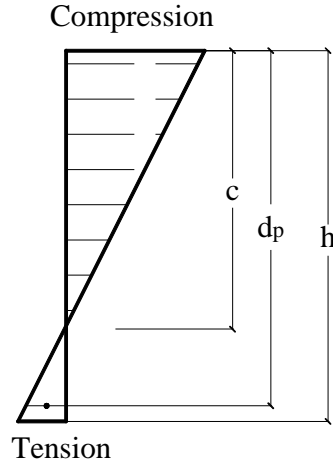


Figure 3.9 Strain distribution at service loads.

From Figure 3.9, the relationship between top and bottom strain as follows:

$$\frac{d_p - c}{h - c} \cdot \varepsilon_c = \varepsilon_{ps} \quad \text{Eq. 3.24}$$

$$\frac{d_p - c}{h - c} \cdot f_{cb} \frac{E_{ps}}{E_c} = \Delta f_{pt} \quad \text{Eq. 3.25}$$

where,

ε_c = strain in concrete at bottom fiber.

E_c = elastic modulus of concrete.

Δf_{pt} = change in prestressing tendons stress between decompression and the stress in concrete at the bottom of the girder reaching f_{ct} assuming uncracked section

f_{cb} = the concrete allowable tensile stress at the bottom of the girder.

According to the current AASHTO LRFD (2012) Specifications, $f_{cb}=0.19\sqrt{f'_c}$ or $f_{cb}=0.0948\sqrt{f'_c}$, which is depends on the exposure conditions.

Then f_{ps} for maximum tensile stress limit level (uncracked section) should be as follows:

$$f_{ps} = \Delta f_{pt} + f_{ps(M_{Dec})} \quad \text{Eq. 3.26}$$

For the section at the maximum crack width limit level (cracked section), the f_{ps} can be calculated by the following equation:

$$f_{ps} = \Delta f_{ps} + f_{ps(M_{Dec})} \quad \text{Eq. 3.27}$$

where

$f_{ps(M_{Dec})}$ = the stress in prestressing steel at decompression

Δf_{ps} = the increase in the prestressing steel stress beyond the decompression state for cracked members.

M_{Dec} = the decompression moment.

Δf_{pt} will vary according to the maximum allowable tensile stress at the bottom of the concrete girder.

Moreover, f_{ps} at decompression level, which expressed as $f_{ps(M_{Dec})}$ can be calculated using the following equation:

$$f_{ps(M_{Dec})} = f_{se} + \frac{E_{ps} [M_{Dec} - M_D]}{IE_c [1 + \frac{A_{ps} E_{ps}}{E_c} (\frac{1}{A_c} + \frac{e_0^2}{I})]} \quad \text{Eq. 3.28}$$

The decompression moment at level of prestressing strands, M_{Decp} , can be calculated using the following equation:

$$M_{Decp} = \frac{[f_{se} - \frac{M_D e_0 E_{ps}}{[I + \frac{A_{ps} E_{ps}}{E_c} (\frac{1}{A_c} + \frac{e_0^2}{I})] IE_c}]}{\frac{e_0}{I[\frac{1}{A_c} + \frac{e_0^2}{I}] A_{ps}} - \frac{e_0 E_{ps}}{[1 + \frac{A_{ps} E_{ps}}{E_c} (\frac{1}{A_c} + \frac{e_0^2}{I})] IE_c}} \quad \text{Eq. 3.29}$$

The decompression moment at bottom fiber of concrete girder, M_{Decb} , can be calculated using the following equation:

$$M_{Decb} = \frac{[f_{se} - \frac{M_D e_0 E_{ps}}{[I + \frac{A_{ps} E_{ps}}{E_c} (\frac{1}{A_c} + \frac{e_0^2}{I})] IE_c}]}{\frac{y_b}{I[\frac{1}{A_c} + \frac{e_0 y_b}{I}] A_{ps}} - \frac{e_0 E_{ps}}{[1 + \frac{A_{ps} E_{ps}}{E_c} (\frac{1}{A_c} + \frac{e_0^2}{I})] IE_c}} \quad \text{Eq. 3.30}$$

where,

A_c = area of concrete at the cross-section considered.

A_{ps} = the area of prestressing steel in tension zone.

e_0 = eccentricity of the prestressing force with respect to the centroid of the section at mid-span.

y_b = Distance from centroidal axis to extreme bottom fiber

E_c = modulus of elasticity of concrete.

E_{ps} = modulus of elasticity of prestressing steel.

f_{se} = effective stress in prestressing steel after losses.

I = moment of inertia.

M_D = dead load moment.

M_{Decb} = decompression moment at the bottom of the girder.

M_{Decp} = decompression moment at the level of the prestressing strands.

3.3.2 Comparison of Predication Equation for Maximum Crack Width at bottom fiber of Prestressed Concrete Girders

This section presents a review and a comparison of various prediction equations for the maximum crack width in prestressed concrete members. Test data from various sources were used in the comparisons. The equations below are listed in chronological order:

The 1970 CEB-FIP recommended adopting the following equation to predict the maximum crack width in partially prestressed beams:

$$w_{\max} = (\Delta f_s - 4000) \times 10^{-6} \quad \text{Eq. 3.31}$$

For static loads, the equation is:

$$w_{\max} = \Delta f_s \times 10^{-6} \quad \text{Eq. 3.32}$$

Please note that the Δf_s in the CEB-FIP equation is in N/cm^2 .

Nawy and Potyondy (1971) conducted a research program to study the flexural cracking behavior of pretensioned I and T beams. Table 3.3 shows the geometric and mechanical properties of the prestressed beam specimens. A_s represents the area of tension reinforcement comprising both prestressing and normal steel reinforcement and

A_s' represents the area of compression steel reinforcement. f'_c is the concrete cylinder compressive strength and f'_t is the concrete tensile splitting strength.

Table 3.3 Geometrical Properties of the Prestressed Beams (Nawy and Potyondy, 1971)

<i>Beam</i>	<i>Section</i>	<i>Width</i> <i>b, in.</i>	<i>Depth*</i> <i>d, in.</i>	<i>A_s</i> <i>sq in.</i>	$\rho = \frac{A_s}{bd}$ <i>Percent</i>	<i>A_s'</i> <i>sq in.</i>	$\rho' = \frac{A_s'}{bd}$ <i>Percent</i>	<i>f'_c</i> <i>psi</i>	<i>f'_t</i> <i>psi</i>	<i>Slump</i> <i>in.</i>
B1	T	8	8.75	0.271	0.389	-	-	4865	400	3
B2	I	6	8.90	0.271	0.518	-	-	4865	400	3
B3	T	8	8.75	0.271	0.389	-	-	4330	430	4
B4	I	6	8.90	0.271	0.518	-	-	4290	430	4
B5	I	6	8.90	0.271	0.518	-	-	4340	430	4
B6	T	8	8.75	0.271	0.389	-	-	4375	430	4
B7	T	8	8.75	0.271	0.389	-	-	4290	390	6
B8	I	6	8.90	0.271	0.518	-	-	4260	390	6
B9	I	6	8.90	0.271	0.518	-	-	4190	390	6
B10	T	8	8.75	0.271	0.389	-	-	4280	390	6
B11	T	8	8.75	0.271	0.389	-	-	4150	370	8
B12	I	6	8.90	0.271	0.518	-	-	3920	370	8
B13	I	6	8.90	0.281	0.518	-	-	3890	370	8
B14	T	8	8.75	0.271	0.389	-	-	4110	370	8
B15	T	8	8.75	0.271	0.389	0.93	1.332	3490	340	5 1/2
B16	I	6	8.90	0.271	0.518	0.33	0.631	3400	340	5 1/2
B17	I	6	8.90	0.271	0.518	0.93	1.776	3390	340	5 1/2
B18	T	8	8.75	0.271	0.389	0.33	0.473	3510	340	5 1/2
B19*	I	6	8.90	0.235	0.448	-	-	3610	385	6
B20*	I	6	8.90	0.235	0.448	-	-	3495	385	6
B21*	I	6	8.90	0.235	0.448	-	-	3430	355	6 1/2
B22*	I	6	8.90	0.235	0.448	-	-	3280	355	6 1/2
B23	I	6	8.90	0.271	0.518	-	-	4060	380	5
B24	I	6	8.90	0.271	0.518	-	-	4095	380	5
B25	I	6	8.90	0.271	0.518	-	-	3950	380	5
B26	I	6	8.90	0.271	0.518	-	-	4000	380	5

* Total depth h in each beam = 12 in.

+ A_s includes two 3/16 in. diameter normal high strength steel wire ($f_y = 96,000$ psi) cage bars in addition to prestressing tendons.

** Beams B19-B22 were continuous beams and were not included in the cracking analysis

Based on a regression analysis of the test data, the authors proposed the following prediction equation:

$$w_{\max} = 1.13 \times 10^{-6} \left(\frac{A_t}{A_s} \right)^{1/4} a_c \sqrt{\Delta f_{s1}^3} \quad \text{Eq. 3.33}$$

where,

$$\Delta f_{s1} = [f_s - f_d - 3.75], \text{ ksi}$$

$$a_c = \text{stabilized crack spacing, in.}$$

$$A_t = \text{area of concrete in tension, in}^2.$$

$$A_s = \text{total area of reinforcement, in}^2.$$

$$E = 27.5 \times 10^3 \text{ ksi was used.}$$

$$f_s = \text{stress in prestressing steel after cracking, ksi.}$$

$$f_d = \text{stress in the prestressing steel when the modulus of rupture of concrete at the extreme tensile fibers is reached, ksi.}$$

After further simplification of Eq. 3.31, Nawy and Potyondy (1971) recommended the following expression:

$$w_{\max} = 1.44 (\Delta f_s - 8.3) \quad \text{Eq. 3.34}$$

Please note the unit for Δf_s in Eq. 3.31 is in ksi and the unit for crack width is in inches.

Bennett and Veerasubramanian (1972) investigated the behavior of non-rectangular beams with limited prestress after flexural cracking. They tested 34 prestressed concrete beams with the cross-section and loading arrangement shown in Figure 3.10.

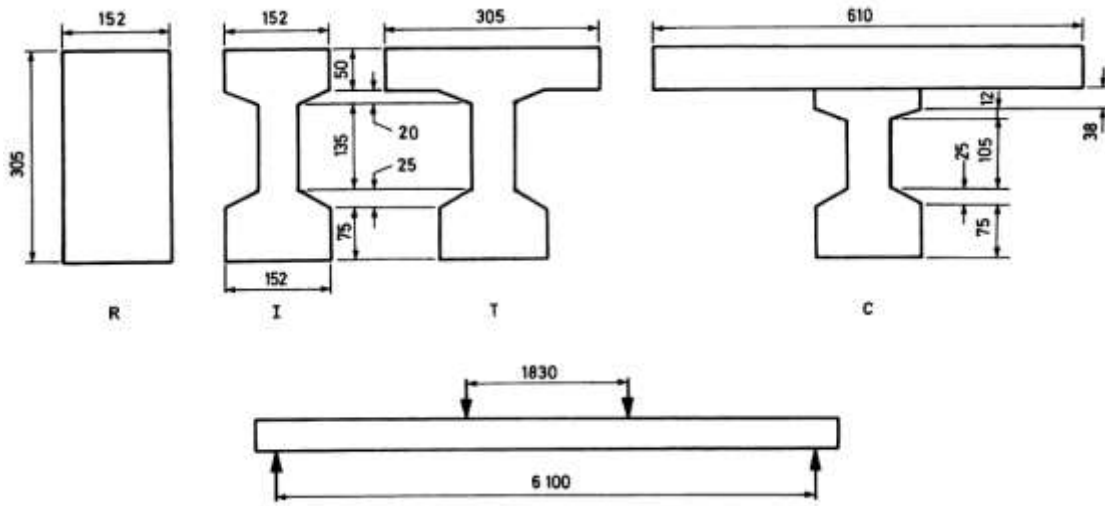


Figure 3.10 Cross section and loading arrangement of testing beams (Bennett and Veerasubramanian, 1972)

They recommended a prediction equation for the maximum crack width as follows:

$$w_{\max} = \beta_1 + \beta_2 \varepsilon_s d_c \quad \text{Eq. 3.35}$$

where,

β_1 = a constant representing the residual crack width measured after the first cycle of loading. The value suggested for deformed bars is 0.02 mm.

β_2 = a constant depending on bond characteristics of the nonprestressed steel.

The value recommended for deformed bars was 6.5.

ε_s = increase in strain in nonprestressed steel from stage of decompression of concrete at tensile face of beam, $\mu\varepsilon$.

d_c = clear cover over the nearest reinforcing bar to the tensile face, mm.

Please note that this equation uses the SI unit system.

Nawy and Huang (1977) studied crack and deflection control in pretensioned prestressed beams. They performed tests on twenty single-span and four continuous beams. Based on a detailed statistical analysis of the test data, they proposed the following equation:

$$w_{\max} = 5.85 \times 10^{-5} \frac{A_t}{\beta \sum 0} (\Delta f_{ps}) \quad \text{Eq. 3.36}$$

where,

A_t = area of concrete in tension, in².

β = ratio of distance from neutral axis of beam to concrete outside tension face to distance from neutral axis to steel reinforcement centroid.

Δf_{ps} = increase in stress in the prestressing steel beyond decompression state, ksi.

$\sum 0$ = sum of reinforcing element circumferences, in.

Table 3.4 presents a comparison of the crack widths measured from the beam tests performed by Nawy and Huang (1977) and the ones predicted using the equation developed by Nawy and Huang (1977). On average, Eq. (A-6) by Nawy and Huang (1977) provides prediction results that are within 20% of the measured maximum crack width of prestressed concrete beams.

Table 3.4 Observed vs. theoretical max. crack width at tensile face of beam (Nawy and Huang, 1977)

Net steel stress											
30 ksi			40 ksi			60 ksi			80 ksi		
W _{obs.}	W _{theory}	Error %	W _{obs.}	W _{theory}	Error %	W _{obs.}	W _{theory}	Error %	W _{obs.}	W _{theory}	Error %
0.0111	0.0131	-15.3	0.0151	0.0175	-13.7	0.0261	0.0262	-0.4	0.04	0.0349	14.6
0.0127	0.0118	7.6	0.0204	0.0157	29.9	0.0275	0.0236	16.5	0.0409	0.0313	30.7
0.0131	0.0128	2.3	0.0166	0.0172	-3.5	0.0304	0.0256	18.8	0.0382	0.0344	11.0
0.0097	0.013	-25.4	0.0158	0.0174	-9.2	0.0226	0.0259	-12.7	0.0304	0.0347	-12.4
0.0091	0.0147	-38.1	0.0117	0.0197	-40.6	0.0205	0.0294	-30.3	0.032	0.0393	-18.6
0.0124	0.0148	-16.2	0.0181	0.0199	-9.0	0.0213	0.0297	-28.3	0.0364	0.0397	-8.3
0.0052	0.0051	2.0	0.0068	0.0069	-1.4	0.0117	0.0103	13.6	0.0188	0.0137	37.2
0.0049	0.0051	-3.9	0.0061	0.0069	-11.6	0.0111	0.0103	7.8	0.0146	0.0137	6.6
0.0051	0.0045	13.3	0.0064	0.0061	4.9	0.0107	0.009	18.9	0.0165	0.0121	36.4
0.0058	0.0045	28.9	0.0082	0.0061	34.4	0.0134	0.009	48.9	0.0185	0.0121	52.9
0.0054	0.0059	-8.5	0.0069	0.0079	-12.7	0.0112	0.0119	-5.9	0.0172	0.0158	8.9
0.0048	0.0059	-18.6	0.0076	0.0079	-3.8	0.0134	0.0119	12.6	0.0192	0.0158	21.5
0.0043	0.0046	-6.5	0.0058	0.0062	-6.5	0.0105	0.0092	14.1	0.0138	0.0123	12.2
0.0052	0.0046	13.0	0.0059	0.0062	-4.8	0.0103	0.0092	12.0	0.0145	0.0123	17.9
0.0039	0.0057	-31.6	0.0061	0.0076	-19.7	0.0115	0.0114	0.9	0.0181	0.0153	18.3
0.0038	0.0057	-33.3	0.0057	0.0076	-25.0	0.0093	0.0114	-18.4	0.016	0.0153	4.6
0.0039	0.0056	-30.4	0.006	0.0074	-18.9	0.0098	0.0112	-12.5	0.0159	0.0148	7.4
0.003	0.0056	-46.4	0.0045	0.0074	-39.2	0.0086	0.0112	-23.2	0.0147	0.0148	-0.7
0.0057	0.0061	-6.6	0.0085	0.0081	4.9	0.0129	0.0121	6.6	0.0202	0.0163	23.9
0.0034	0.0045	-24.4	0.0045	0.0059	-23.7	0.0089	0.0089	0.0	0.0139	0.0119	16.8
Average		18.6	Average		15.9	Average		15.1	Average		18.0

Rao and Dilger (1992) developed a detailed crack control procedure for prestressed concrete members. The authors studied the prediction equation of maximum crack width developed by various previous researchers and proposed a new equation expressed as follows:

$$w_{\max} = k_1 f_s d_c \left(A_t / A_s \right)^{0.5} \quad \text{Eq. 3.37}$$

where,

k_1 = the bond coefficient defined for each combination of prestressed and nonprestressed reinforcement.

f_s = stress in steel after decompression, MPa.

d_c = concrete cover measured from surface to the center of nearest reinforcement bar, mm.

A_t = area of concrete in tension, mm^2 .

A_s = total area of reinforcement, mm^2 .

Eurocode 2 (2004) provides the following provisions to calculate the crack widths:

$$w_k = s_{r,\max} (\varepsilon_{sm} - \varepsilon_{cm}) \quad \text{Eq. 3.38}$$

where,

$s_{r,\max}$ = the maximum crack spacing;

w_k = the crack width;

ε_{sm} = the mean strain in the reinforcement under the relevant combination of loads, including the effect of imposed deformations and taking into account the effects of tension stiffening. Only the additional tensile strain beyond the state of zero strain of the concrete at the same level is considered;

ε_{cm} = the mean strain in the concrete between cracks.

In the above expression for Eq. 3.38 the crack $(\varepsilon_{sm} - \varepsilon_{cm})$ can be calculated from the following expression:

$$(\varepsilon_{sm} - \varepsilon_{cm}) = \frac{\sigma_s - k_t \frac{f_{ct,eff}}{\rho_{p,eff}} (1 + \alpha_e \rho_{p,eff})}{E_s} \geq 0.6 \frac{\sigma_s}{E_s} \quad \text{Eq. 3.39}$$

where,

A_p' = the area of pre or post-tensioned tendons within $A_{c,eff}$;

$A_{c,eff}$ = the effective area of concrete in tension surrounding the reinforcement

or pre-stressing tendons of depth, $h_{c,ef}$, where $h_{c,ef}$ is the lesser of

$2.5(h-d)$, $(h-x)/3$ or $h/2$, where h is the height of the beam, d is the effective depth of a cross section, and x is the neural axis depth;

k_t = a factor dependent on the duration of the load;

α_e = the ratio E_s / E_{cm} , where E_{cm} is the Secant modulus of elasticity of concrete and E_s is the Design value of modulus of elasticity of reinforcing steel;

$\rho_{p,eff} = (A_s + \xi_1^2 A_p') / A_{c,eff}$;

σ_s = the stress in the tension reinforcement assuming a cracked section. For pretensioned members, S_s may be replaced by DS_p the stress variation in prestressing tendons from the state of zero strain of the concrete at the same level;

ξ_1 = the adjusted ratio of bond strength taking into account the different diameters of pre-stressing and reinforcing steel, which would be calculated as

$$\sqrt{\xi \cdot \frac{\phi_s}{\phi_p}}, \text{ where } \xi \text{ is the ratio of bond strength of prestressing and}$$

reinforcing steel, ϕ_s is the largest bar diameter of reinforcing steel, and ϕ_p

is equivalent diameter of tendon;

$$s_{r,\max} = k_3 c + k_1 k_2 k_4 \phi / \rho_{p,\text{eff}} \quad \text{Eq. 3.40}$$

where,

ϕ = the bar diameter;

c = the cover to the longitudinal reinforcement;

k_1 = a coefficient that takes account of the bond properties of the bonded reinforcement;

k_2 = a coefficient that takes account of the distribution of strain;

k_3 = a coefficient can be found in National Annex according to different country, the recommended value is 3.4;

k_4 = a coefficient can be found in National Annex according to different country, the recommended value is 0.425.

Figure 3.11 through Figure 3.14 present a comparison of the equation developed by Nawy and Huang (1977) and four other prediction equations. The equations used in Eurocode were not compared with the testing data since there is insufficient information to apply this equation. Figure 3.11 indicates that the equation developed by Nawy and Potyondy (1971) did not provide good prediction results compared to the measured data

since it relates the maximum crack width with the Δf_{ps} only. The equation developed by Nawy and Huang (1977) exhibited excellent correlation at low values of crack width. The predicted values are slightly different from the measured data when the loading increases, but the results were still close to the measured data.

Figure 3.12 indicates the equation developed by Bennett and Veerasubramanian did not exhibit good correlation with measured results when the maximum crack width increases. Figure 3.13 indicates that the equation recommended by CEB-FIP overestimates the crack width prediction at small load. A number of beam specimens had fully prestressed tendons and the measured data did not compare well with the predicted value. Figure 3.14 indicates that the equation recommended by Rao and Dilger underestimates the crack width prediction, especially under heavy load.

In summary, based on the comparison, the equation developed by Nawy and Huang (1977) provides the best correlation with measured data. Furthermore, this equation took the effect of bar size into account in addition to the effect of the steel stress and can be easily incorporated into the calibration procedure. The equation by Nawy and Hwang (1977) was used in the calibration of the tension in prestressed concrete when the crack width was considered in the calibration.

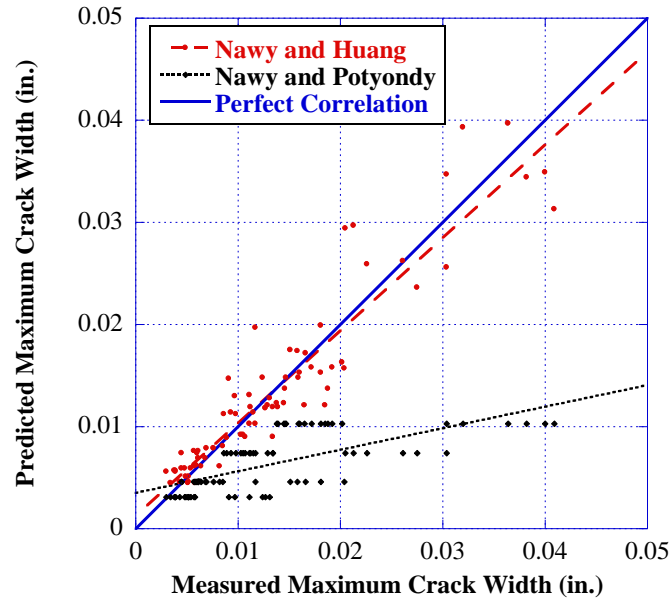


Figure 3.11 Comparison of the measured and predicted maximum crack widths using equations developed by Nawy and Huang (1977) and Nawy and Potyondy (1971).

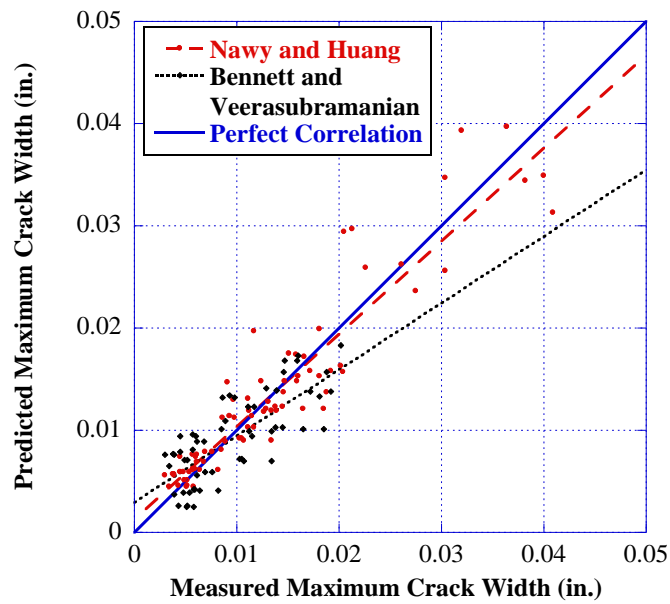


Figure 3.12 Comparison of the measured and predicted maximum crack widths using equations developed by Nawy and Huang (1977) and Bennett and Veerasubramanian (1972).

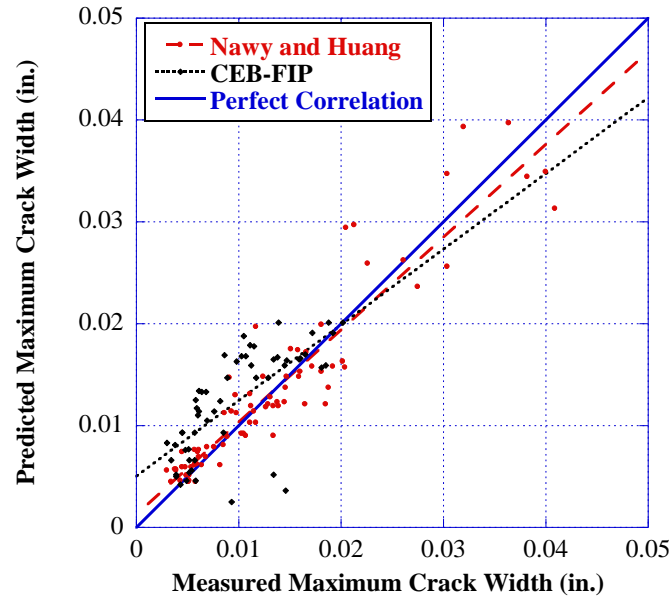


Figure 3.13 Comparison between the measured and predicted maximum crack widths using equations developed by Nawy and Huang (1977) and CEB-FIP (1970).

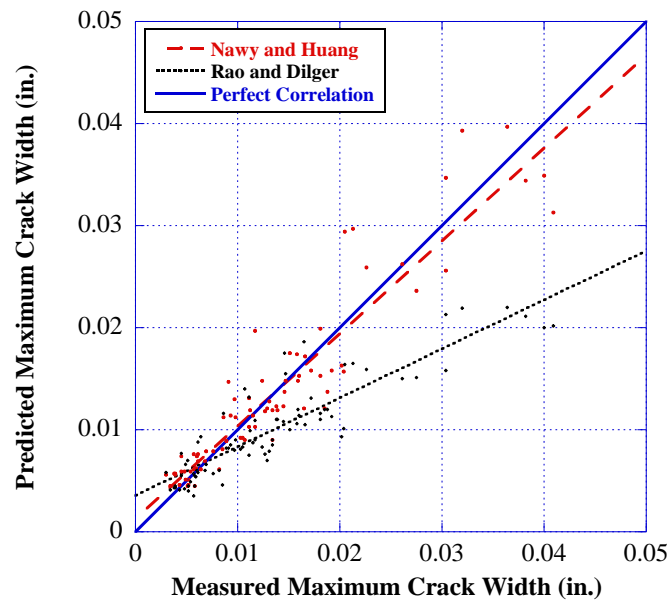


Figure 3.14 Comparison between the measured and predicted maximum crack widths using equations developed by Nawy and Huang (1977) and Rao and Dilger (1992).

3.3.3 Statistical Model for Structural Resistance

Similar to Service I limit state, the statistical model for structural resistance at Service III limit state was also developed using Monte-Carlo simulation. The statistical information of random variables as summarized in Table 3.5 was also used in Service III limit state.

Table 3.5 Random variables and the value their statistical parameters

Variables	Distribution	Mean, m	COV., Ω	Remarks
A_s	normal	$0.9A_{sn}^*$	0.015	
A_{ps}	normal	$1.01176A_{psn}$	0.0125	
b, b_0, b_1, b_w	normal	b_n	0.04	
C_{E_c}	normal	33.6	0.1217	nominal=33 $C_{E_c} = E_c / \left(\gamma_c^{1.5} \cdot \sqrt{f'_c} \right)$
$C_{f_{ci}}$	normal	0.6445	0.073	nominal=0.8 $C_{f_{ci}} = f_{ci} / f'_c$
d_p, d_s	normal	d_{pn}, d_{sn}	0.04	
e_1	normal	e_{0n}	0.04	
E_{ps}	normal	$1.011E_{psn}$	0.01	$E_{psn} = 29,000,000 \text{ psi}$
E_s	normal	E_{sn}	0.024	
f'_c	lognormal	$1.11f'_{cn}$	0.11	
f_{pu}	lognormal	$1.03f_{pun}$	0.015	$f_{pun} = 270,000 \text{ psi}$
f_{si}	normal	$0.97f_{sin}$	0.08	
f_y	lognormal	$1.13f_{yn}$	0.03	
h, h_f, h_{f1}, h_{f2}	normal	$h_n, h_{fn}, h_{f1n}, h_{f2n}$	0.025	
l	normal	l_n	$11/(32\mu)$	
γ_c	normal	$\gamma_{cn} = 150 \text{ pcf}$	0.03	
Δf_s	normal	$1.05 \Delta f_{sn}$	0.10	
$\Sigma 0$	normal	$\Sigma 0_n$	0.03	

* Subscript of “n” refers to nominal values

3.4 Deflection Limit State

Excessive deflection could result in severe structural damage and significantly shorten the service life of the bridge. However, there is no limit state specifically defined for the control of deflection in the current AASHTO LRFD Specification. Instead, the deflection limitation or depth to span ratio provision is used as an optional requirement during the girder design. Moreover, as described in section 2.9, these provisions are adopted from historic provisions in other specifications without rational verification. Thus, there is a need to develop and calibrate a deflection limit state based on using a reliability approach.

3.4.1 Derivation of Resistance Prediction Equation

For the deflection limit state, the moment resistance will be derived in accordance with the allowable deflection limit specified by the AASHTO LRFD (2008) Specifications. If the limit of the deflection due to live load is $\Delta_{LL} = L/800$, it can be expressed as follows:

$$\Delta_{LL} = \frac{CM_L}{E_C I} \leq \frac{L}{800} \quad \text{Eq. 3.41}$$

Where,

C = constant depends on the type of loading.

E_C = Elastic Modulus of Concrete

I = Gross moment of Inertia

M_L = Live Load Moment

So the moment resistance at the live load deflection limit would be:

$$M_L = \frac{L}{800} \cdot \frac{E_c I}{C} \quad \text{Eq. 3.42}$$

The total resistance moment at the limit state is given by,

$$M_{ALL} = M_D + M_L = M_D + \frac{L}{800} \cdot \frac{E_c I}{C} \quad \text{Eq. 3.43}$$

Eq. 3.43 is applicable if the total resistance moment is less than the cracking moment, M_{cr} . If the total resistance moment is larger than M_{cr} , Eq. 3.43 will need to be re-adjusted to account for the cracked section behavior. The bilinear model for the moment of inertia can be used and the resistance moment will be as follows:

$$M_{ALL} = M_D + M_L = \frac{L}{800} \cdot \frac{E_c I_e}{C} + (M_{cr} - M_D) \left[1 - \frac{I_e}{I_g} \right] + M_D \quad \text{Eq. 3.44}$$

Where, I_e is the effective moment of inertia that can be expressed in terms of the cracking moment, total moment, and cracking moment of Inertia, I_{cr} . The cracking moment of inertia, I_{cr} , is computed in terms of the depth of the neutral axis. The depth of the neutral axis can be determined from equilibrium equations and strain compatibility. Solving all equation simultaneously, the total resistance moment of the limit state of immediate deflection will be formulated.

3.4.2 Statistical Model for Structural Resistance

Similar to the Service III limit state, the statistical model for structural resistance was developed using Monte-Carlo simulation. The statistical information of random variables that summarized in Table 3.5 will be also used in Deflection limit state.

CHAPTER 4

MODELS FOR LIVE LOAD

Live load models and their statistical characteristics are essential parts of any structural reliability analysis. The prediction of the maximum load effect for various durations is one of the most important steps in developing and calibrating the serviceability limit states. During the calibration of strength limit states for AASHTO LRFD Bridge Design Specifications. A new live load model, HL-93 developed based on the Ontario truck survey data was adopted by AASHTO (Figure 4.1) (Nowak, 1999). In addition to HL-93 live load model, AASHTO also specified that owner-specified special design vehicles can be used in load combination for Strength II limit state, Figure 4.2 shows the permit vehicle specified in NJDOT Bridge Design Manual.

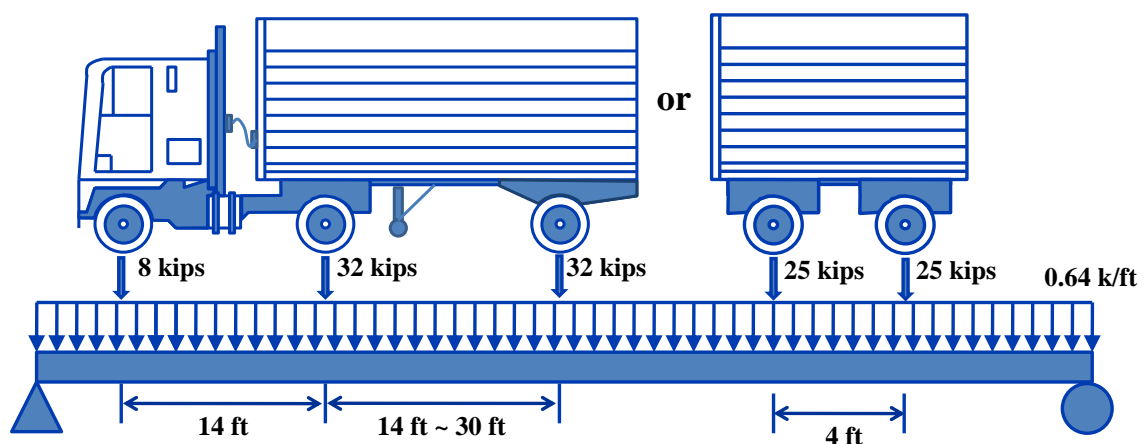


Figure 4.1 HL-93 Design Live Load Model (Nowak 1999)

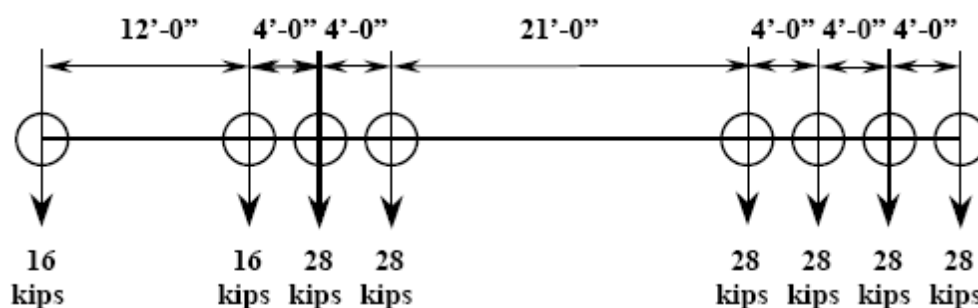


Figure 4.2 NJDOT Design Permit Vehicle (NJDOT, 2010)

The load effect in terms of moment and shear can be determined by running each truck over an influence line on various span lengths. The bias factor was calculated as a ratio between the load effect due to each truck and the effect due to design live load model. This factor was calculated for each Ontario truck and plotted on normal probability paper (NPP). Then the bias factors were extrapolated to various time periods at different span lengths. Table 4.1 presents the bias factors in terms of simple span moments calculated by Nowak during the LRFD calibration.

In this section, WIM data collected from various states will be processed using specially developed quality control and filtering routines to identify weighing errors, unusual truck configurations, and permit loads. Various refined prediction techniques will be used to extrapolate the load effects to various time periods. Moreover, live load models are proposed for various limit states.

Table 4.1 Mean Maximum Moments for Simple Spans Divided by Corresponding HL-93 Moments (Nowak 1999)

Span (ft)	M (HL-93) (k-ft)	Duration								
		1 day	2 weeks	1 month	2 months	6 months	1 year	5 years	50 years	75 years
10	88	0.88	1.02	1.07	1.12	1.18	1.25	1.33	1.5	1.5
20	232	0.9	0.98	1.02	1.06	1.1	1.14	1.21	1.3	1.3
30	397	0.95	1.04	1.08	1.12	1.15	1.19	1.26	1.35	1.35
40	578	1.02	1.11	1.14	1.17	1.21	1.23	1.28	1.35	1.35
50	826	1	1.08	1.12	1.15	1.18	1.22	1.25	1.33	1.33
60	1093	1.02	1.09	1.12	1.15	1.18	1.21	1.24	1.32	1.32
70	1376	1.02	1.08	1.12	1.15	1.18	1.21	1.25	1.31	1.31
80	1675	1.02	1.08	1.11	1.14	1.17	1.21	1.25	1.32	1.32
90	1990	1.02	1.08	1.11	1.14	1.16	1.2	1.24	1.31	1.31
100	2322	1.02	1.08	1.1	1.13	1.16	1.2	1.24	1.31	1.31
110	2670	1.02	1.07	1.1	1.12	1.15	1.19	1.24	1.31	1.31
120	3033	1.01	1.07	1.09	1.12	1.15	1.18	1.22	1.29	1.29
130	3413	1	1.06	1.09	1.11	1.13	1.16	1.2	1.27	1.27
140	3809	0.98	1.03	1.06	1.08	1.1	1.13	1.17	1.24	1.24
150	4220	0.98	1.03	1.06	1.07	1.09	1.12	1.16	1.23	1.23
160	4648	0.98	1.03	1.07	1.09	1.1	1.13	1.17	1.24	1.24
170	5092	0.99	1.03	1.07	1.09	1.11	1.13	1.18	1.24	1.24
180	5552	0.98	1.03	1.06	1.08	1.11	1.13	1.17	1.24	1.24
190	6028	0.97	1.02	1.06	1.08	1.1	1.13	1.17	1.24	1.24
200	6520	0.96	1.02	1.05	1.08	1.09	1.12	1.16	1.23	1.23

4.1 Analysis of Live Load Data

4.1.1 WIM Data Processing

Truck data from each WIM site was processed using the filtering criteria are listed below and Table 4.2 presents the number and percentage of trucks filtered by various filters. It is observed that the filter criteria 1 (minimum gross vehicle weight (GVW) of at least 15 kips) filters the most number of vehicles, ranging from 2.2% to 13.0%. This criterion removes any inconsequential truck records, passenger vehicles misclassified as

trucks, and sensor errors in measuring light axles. For the qualified trucks, the percentage range from 81.8% to 91.5%.

Filter Description

1. Gross Wt < 15k
2. Omit Class = 15
3. Tandems > 60k
4. Num of Axles=9 & Gross Wt>150k
5. Class = 9 & Wt1 > 15k
6. Class 8, if S3>5ft and GVW<20k
7. Num of Axles=10 & Gross Wt>200k
8. Any single axle over 40k
9. No axle spaces less than 2.5ft
10. 3 or more tandems = Permit
11. Permitted Cranes
12. Permitted Cranes with First Spacing<8.5ft, L<50ft, W>100k
13. Find and Reassign Fake CL13, split to CL9 + CL2
14. Find if L>50ft and GVW<20k, possible cars lumped together

Table 4.2 Percentage of Filtered Data for Various WIM Sites

WIM Site	Filtering Criteria and Percentage						
Site-0199	1	2	3	4	5	6	7
	4.74%	0.27%	0.40%	0.00%	2.07%	0.13%	0.00%
	8	9	10	11	12	13	14
	0.13%	0.00%	0.00%	0.00%	0.01%	0.00%	0.72%
Site-0580	1	2	3	4	5	6	7
	13.01%	0.42%	1.06%	0.00%	1.17%	0.28%	0.00%
	8	9	10	11	12	13	14
	0.75%	0.00%	0.01%	0.00%	0.01%	0.00%	1.32%
Site-2680	1	2	3	4	5	6	7
	8.75%	3.36%	0.43%	0.00%	1.17%	0.76%	0.00%
	8	9	10	11	12	13	14
	0.11%	0.00%	0.02%	0.00%	0.02%	0.00%	0.86%
Site-8280	1	2	3	4	5	6	7
	5.36%	0.40%	0.59%	0.00%	3.09%	0.43%	0.00%
	8	9	10	11	12	13	14
	0.07%	0.00%	0.00%	0.00%	0.00%	0.00%	1.83%
Site-8382	1	2	3	4	5	6	7
	2.17%	0.60%	2.67%	0.00%	2.04%	0.29%	0.00%
	8	9	10	11	12	13	14
	0.47%	0.00%	0.01%	0.00%	0.00%	0.00%	1.24%
Site-9121	1	2	3	4	5	6	7
	9.09%	0.15%	0.57%	0.00%	1.61%	0.27%	0.00%
	8	9	10	11	12	13	14
	0.06%	0.00%	0.01%	0.00%	0.00%	0.00%	0.79%
Site-9631	1	2	3	4	5	6	7
	4.06%	0.20%	0.58%	0.00%	1.38%	0.31%	0.00%
	8	9	10	11	12	13	14
	0.07%	0.00%	0.02%	0.00%	0.00%	0.00%	2.79%

After the study on the filtered and unfiltered data, we observed that filter 3, 5, and 8 filtered most of the above 200 kips trucks ,since some trucks fulfilled both the criteria 3 and 5, it was filtered by filter 3 because filter 3 runs first.

4.1.2 Statistics of WIM data

The following GVW study is based on the New York and Florida WIM data which was processed by the processing program shown in section 4.1.1. Figure 4.3 through Figure 4.11 present the histogram and statistics results of all the NY sites. Figure 4.12 and Figure 4.13 show the histogram and statistics of Florida sites.

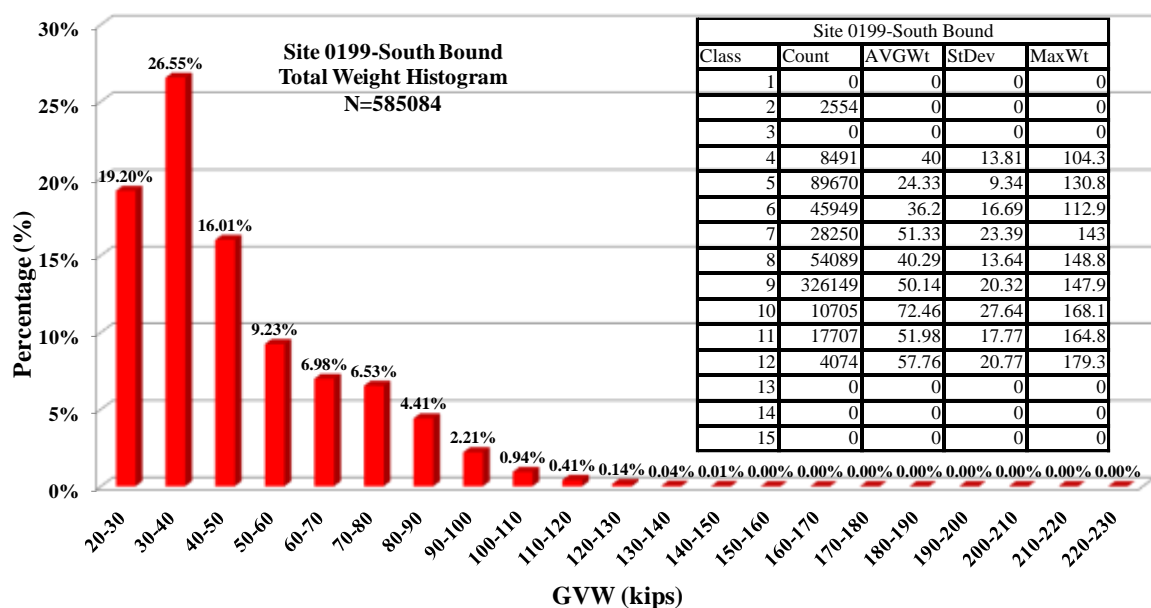


Figure 4.3 Histogram of Site 0199-South Bound

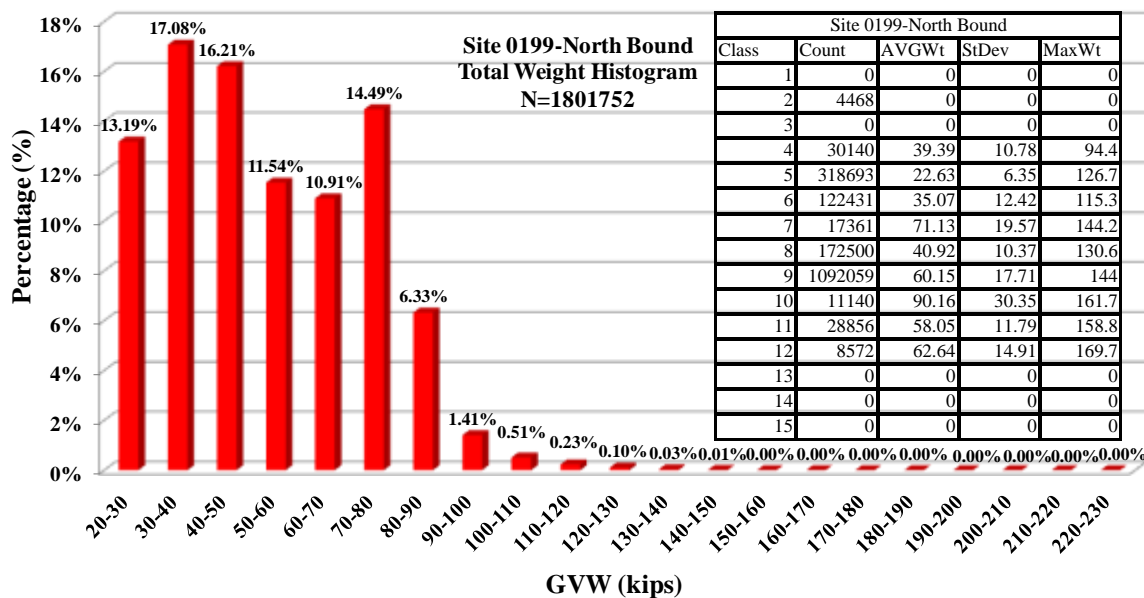


Figure 4.4 Histogram of Site 0199-North Bound

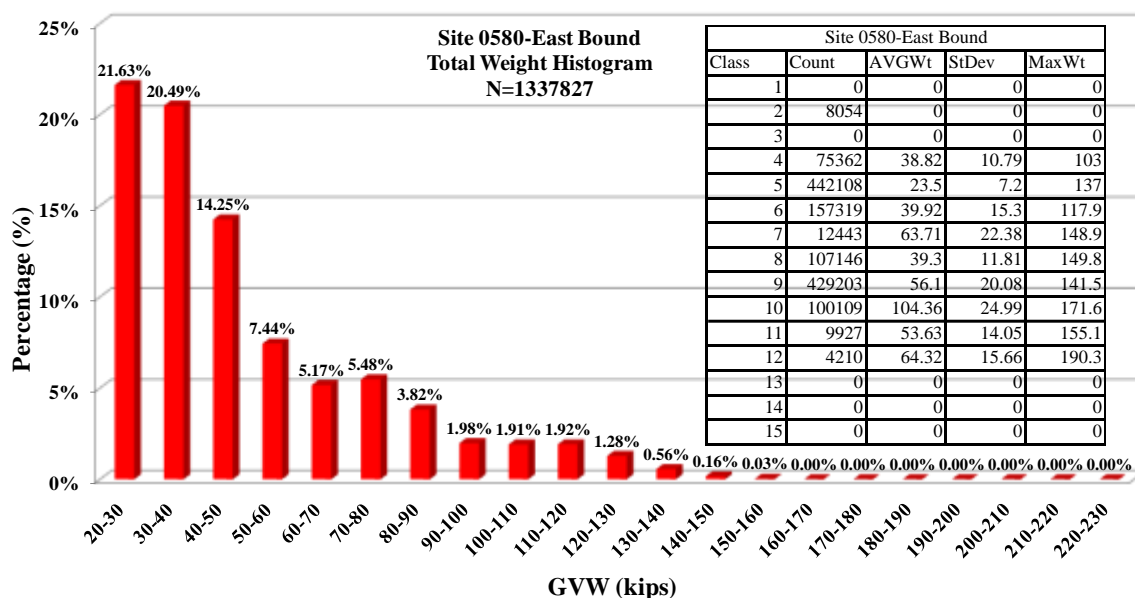


Figure 4.5 Histogram of Site 0580-East Bound

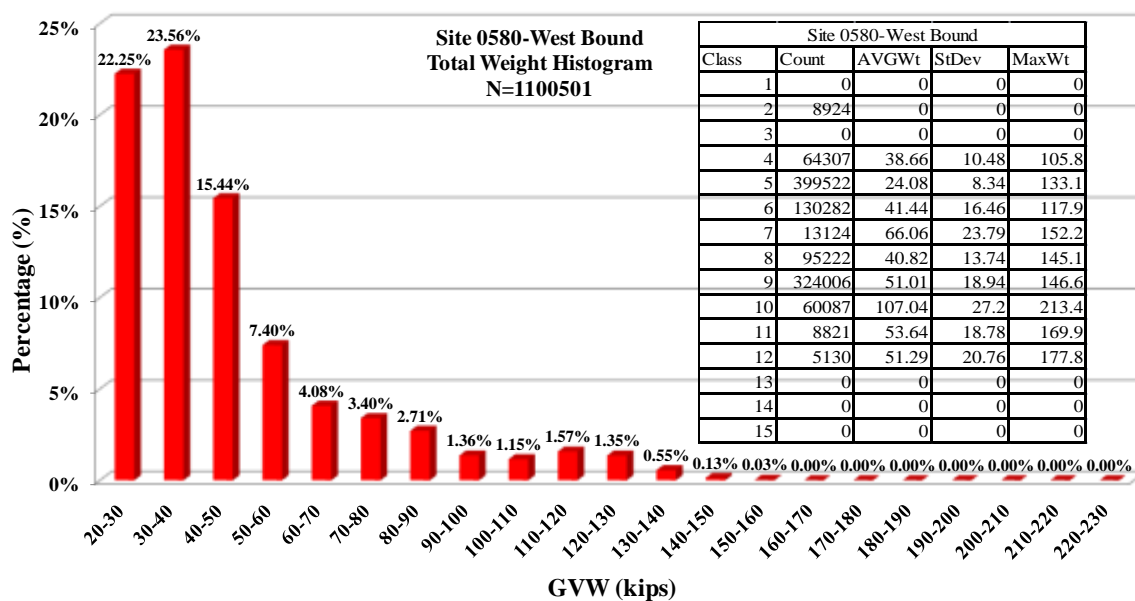


Figure 4.6 Histogram of Site 0580-West Bound

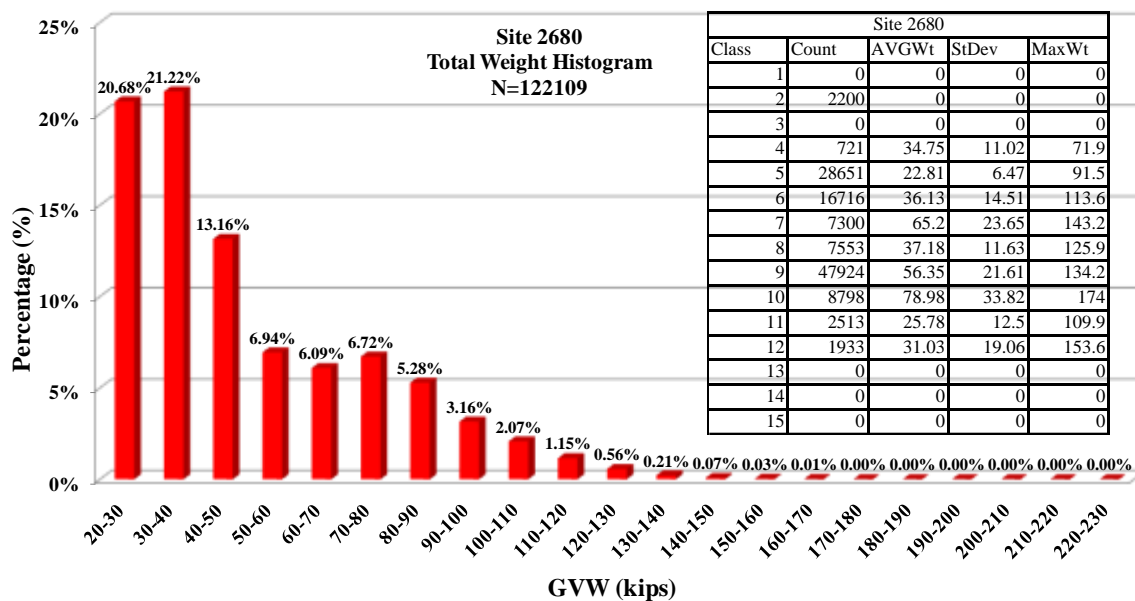


Figure 4.7 Histogram of Site 2680

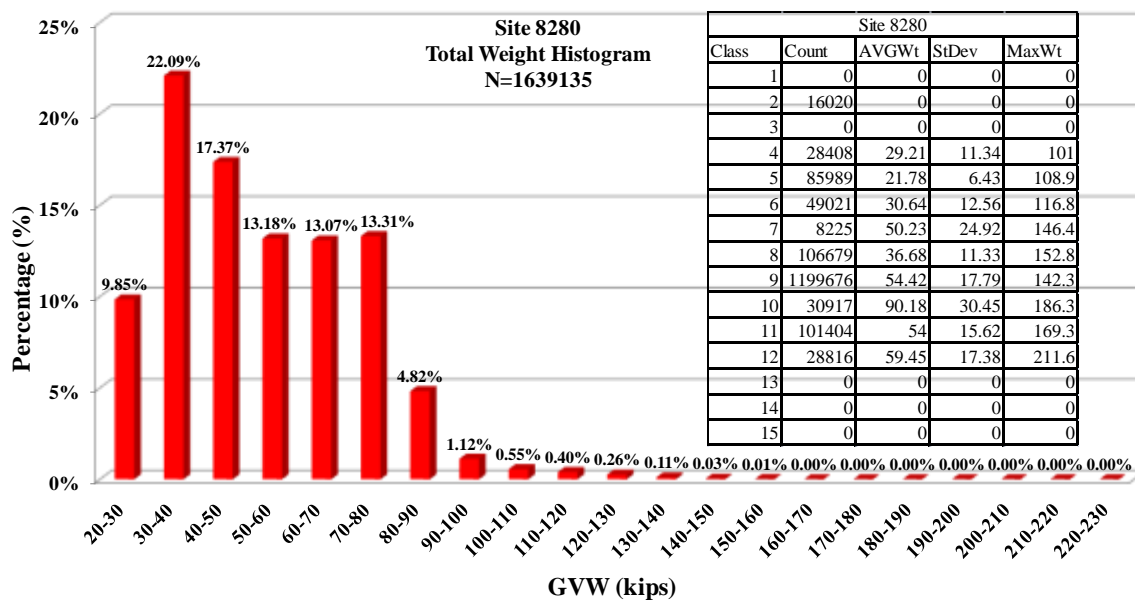


Figure 4.8 Histogram of Site 8280

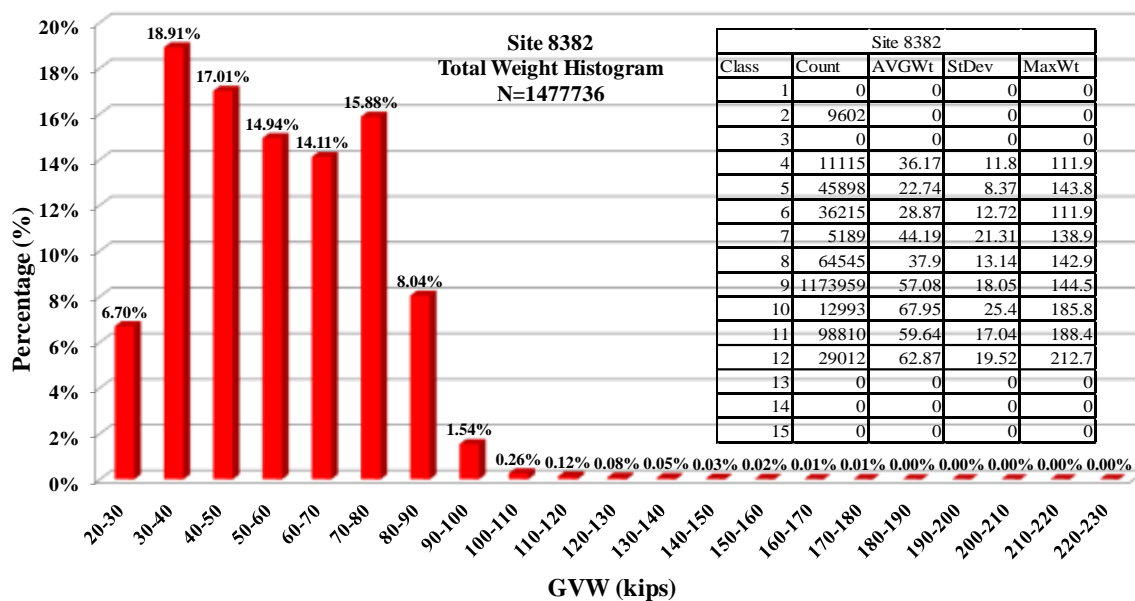


Figure 4.9 Histogram of Site 8382

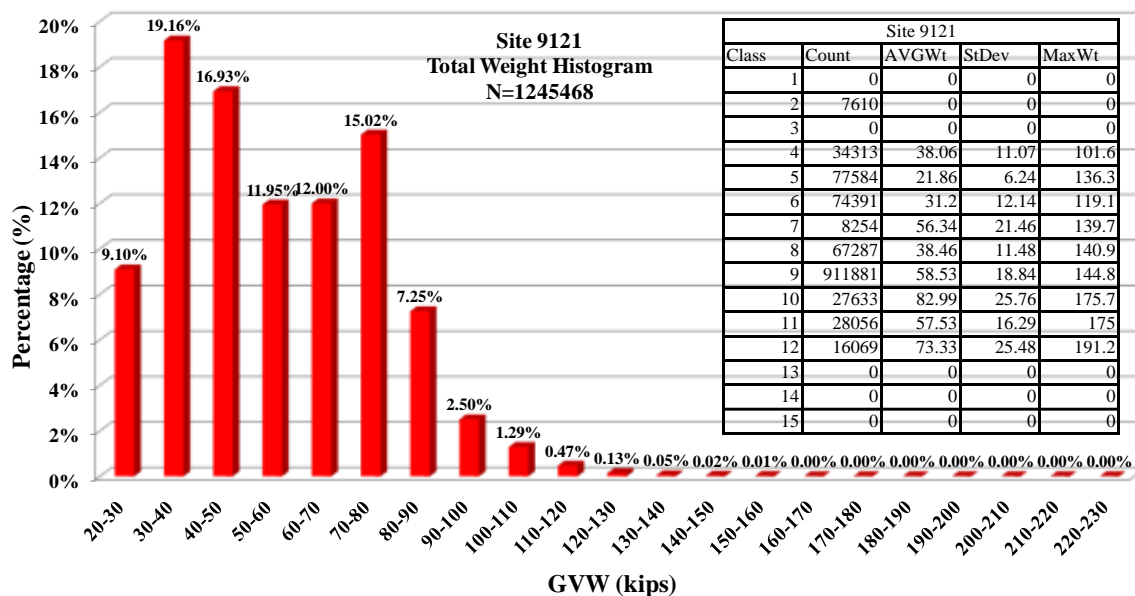


Figure 4.10 Histogram of Site 9121

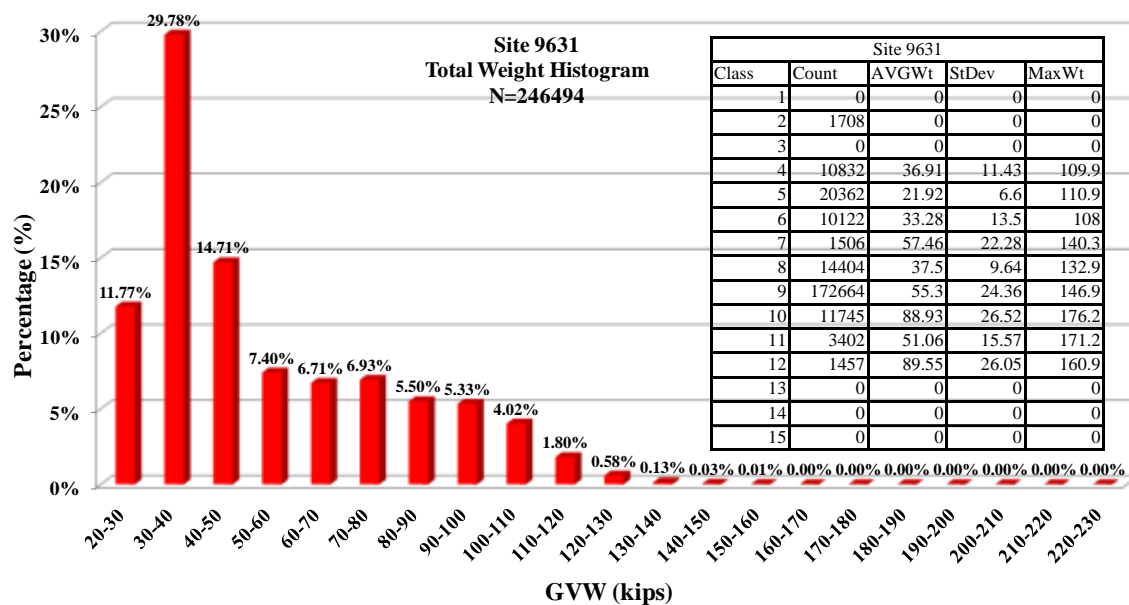


Figure 4.11 Histogram of Site 9631

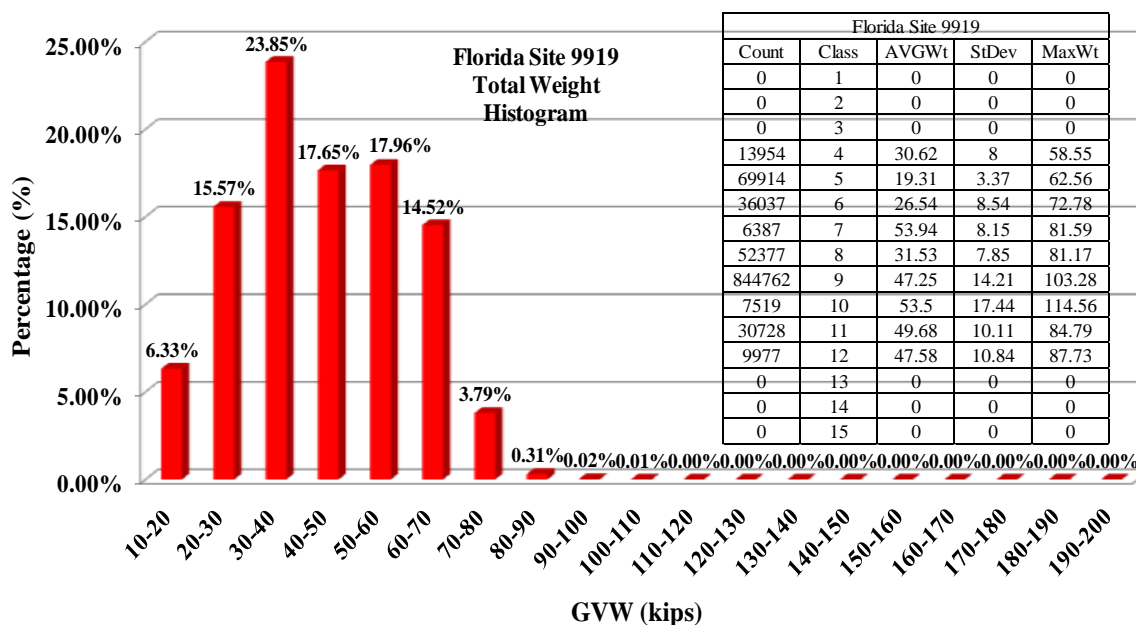


Figure 4.12 Histogram of Florida Site 9919

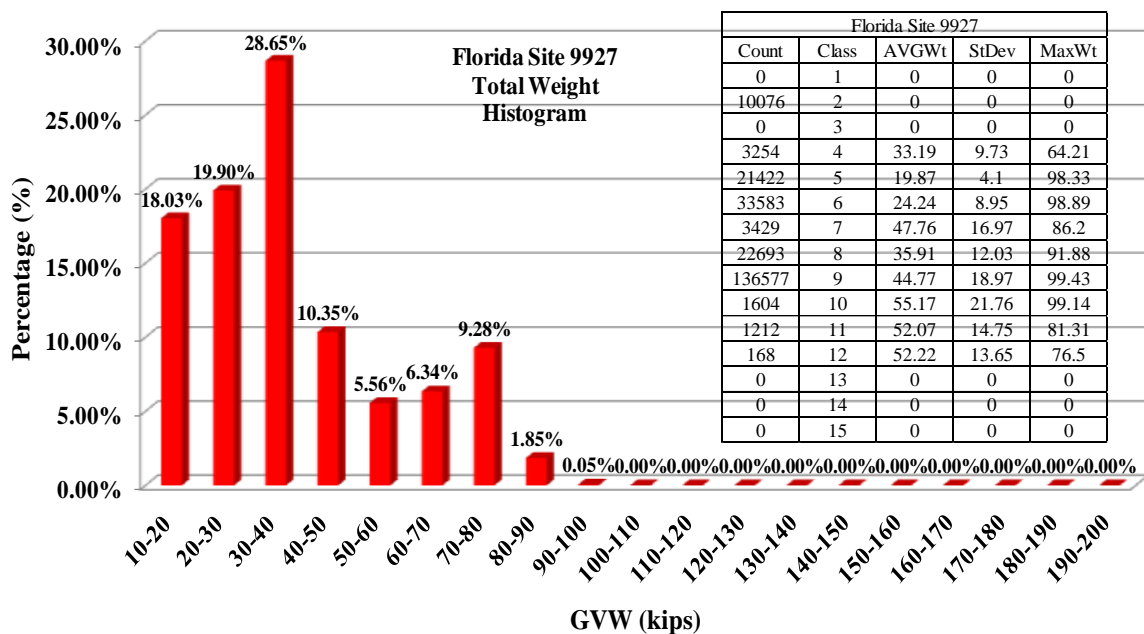


Figure 4.13 Histogram of Florida Site 9927

4.1.3 Multiple Presence Probabilities

Multiple presence statistics are needed to estimate the maximum moment caused by the presence of more than one truck on the bridge. Trucks may simultaneously occur on a bridge in many different arrangements. In general, four truck loading patterns are considered (see Figure 4.14):

(a) Single event; only one truck travels on the bridge span without any other trucks following or on other lanes.

(b) Following or in-lane; two trucks following each other with a varying headway distance measured from rear axle of one truck to front axle of the following truck

(c) Side-by-side in tandem; two trucks in adjacent lanes and overlapping by at least one-half the body length of the leading truck

(d) Side-by-side but staggered; two trucks in adjacent lanes and overlapping by less than at least one-half the body length of the leading truck

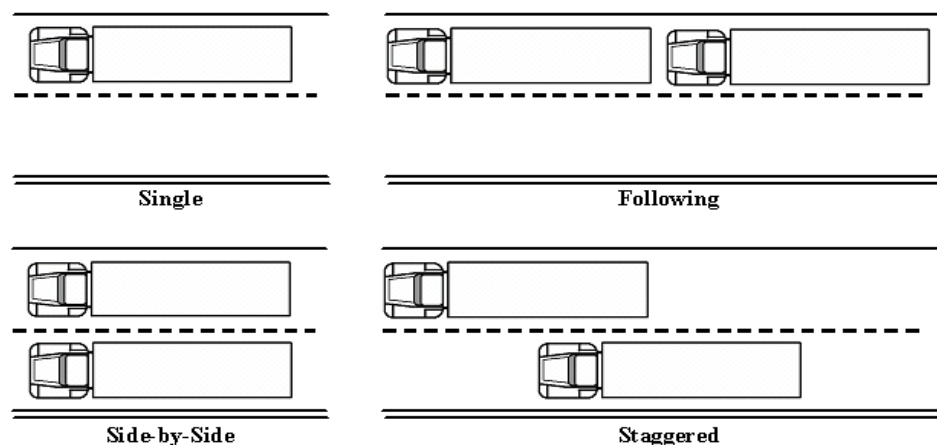


Figure 4.14 Multiple Presence Categories

Truck loading, including weight and loading patterns, is generally site-specific. Multiple presence statistics depend on factors such as truck volume, bridge span length, local industry, law enforcement, and traffic flow control. This has also been recognized by the AASHTO LRFD Specifications, which, despite having a calibrated live load model, highlights consideration to site-specific modifications to design live loads for cases in which the legal load is significantly greater than typical, there is an unusually high percentage of truck traffic, or there is truck pooling. Therefore, it is important to account for the uncertainty due to site variation in statistical modeling. Table 4.3 through Table 4.12 summarized the multiple presence statistics extracted from WIM data from various WIM sites. It shows that the percentage of following, side by side, and staggered events increased when the span length increased.

Table 4.3 Summary of Multiple Presence Statistics (Newark Bay Bridge WIM Site)

<i>Span</i>	<i>Following</i>	<i>Side by Side</i>	<i>Staggered</i>	<i>Single</i>	<i>Other</i>
40	0.01%	0.09%	0.00%	99.63%	0.27%
60	0.01%	0.43%	0.00%	99.29%	0.27%
80	0.01%	1.24%	0.03%	98.44%	0.28%
100	0.02%	2.42%	0.21%	97.06%	0.30%
120	0.04%	3.30%	1.02%	95.30%	0.34%
140	0.12%	3.70%	2.49%	93.27%	0.42%
160	0.43%	3.80%	4.28%	90.93%	0.56%
180	1.24%	3.77%	6.11%	88.04%	0.84%
200	2.75%	3.68%	7.70%	84.55%	1.33%

Table 4.4 Summary of Multiple Presence Statistics (NY WIM Site 2680)

<i>Span</i>	<i>Following</i>	<i>Side by Side</i>	<i>Staggered</i>	<i>Single</i>	<i>Other</i>
40	0.39%	0.06%	0.01%	95.44%	4.10%
60	0.39%	0.09%	0.03%	95.32%	4.17%
80	0.39%	0.16%	0.07%	95.11%	4.27%
100	0.41%	0.19%	0.14%	94.91%	4.35%
120	0.44%	0.19%	0.21%	94.72%	4.44%
140	0.51%	0.19%	0.28%	94.49%	4.53%
160	0.60%	0.19%	0.35%	94.21%	4.65%
180	0.73%	0.19%	0.43%	93.90%	4.75%
200	0.88%	0.18%	0.48%	93.60%	4.86%

Table 4.5 Summary of Multiple Presence Statistics (NY WIM Site 0199-I95)

<i>Span</i>	<i>Following</i>	<i>Side by Side</i>	<i>Staggered</i>	<i>Single</i>	<i>Other</i>
40	0.01%	0.12%	0.00%	99.63%	0.24%
60	0.01%	0.47%	0.00%	99.25%	0.27%
80	0.01%	1.21%	0.03%	98.41%	0.34%
100	0.01%	2.21%	0.27%	97.07%	0.44%
120	0.03%	2.86%	1.21%	95.36%	0.54%
140	0.14%	3.06%	2.65%	93.44%	0.71%
160	0.49%	3.04%	4.29%	91.30%	0.88%
180	1.54%	2.99%	5.92%	88.43%	1.12%
200	3.63%	2.90%	7.39%	84.55%	1.53%

Table 4.6 Summary of Multiple Presence Statistics (NY WIM Site 0199-Bronx)

<i>Span</i>	<i>Following</i>	<i>Side by Side</i>	<i>Staggered</i>	<i>Single</i>	<i>Other</i>
40	0.01%	0.09%	0.00%	99.61%	0.29%
60	0.01%	0.43%	0.00%	99.21%	0.35%
80	0.01%	1.23%	0.03%	98.23%	0.50%
100	0.02%	2.41%	0.21%	96.67%	0.69%
120	0.04%	3.28%	1.01%	94.70%	0.97%
140	0.12%	3.67%	2.47%	92.46%	1.28%
160	0.43%	3.76%	4.24%	89.93%	1.64%
180	1.23%	3.72%	6.03%	86.92%	2.10%
200	2.71%	3.62%	7.59%	83.34%	2.74%

Table 4.7 Summary of Multiple Presence Statistics (NY WIM Site 0580-EB)

<i>Span</i>	<i>Following</i>	<i>Side by Side</i>	<i>Staggered</i>	<i>Single</i>	<i>Other</i>
40	0.02%	0.07%	0.00%	99.31%	0.60%
60	0.02%	0.26%	0.00%	99.11%	0.61%
80	0.02%	0.69%	0.01%	98.67%	0.61%
100	0.02%	1.24%	0.16%	97.96%	0.62%
120	0.03%	1.64%	0.64%	97.05%	0.64%
140	0.12%	1.86%	1.43%	95.95%	0.64%
160	0.36%	1.96%	2.33%	94.68%	0.67%
180	0.85%	1.98%	3.27%	93.14%	0.76%
200	1.66%	1.99%	4.15%	91.32%	0.88%

Table 4.8 Summary of Multiple Presence Statistics (NY WIM Site 0580-WB)

<i>Span</i>	<i>Following</i>	<i>Side by Side</i>	<i>Staggered</i>	<i>Single</i>	<i>Other</i>
40	0.03%	0.08%	0.00%	99.10%	0.79%
60	0.03%	0.28%	0.00%	98.90%	0.79%
80	0.03%	0.64%	0.02%	98.51%	0.80%
100	0.03%	1.07%	0.19%	97.91%	0.80%
120	0.07%	1.34%	0.67%	97.13%	0.79%
140	0.23%	1.44%	1.32%	96.20%	0.81%
160	0.61%	1.45%	2.12%	94.96%	0.86%
180	1.37%	1.44%	2.86%	93.39%	0.94%
200	2.36%	1.42%	3.55%	91.60%	1.07%

Table 4.9 Summary of Multiple Presence Statistics (NY WIM Site 8280)

<i>Span</i>	<i>Following</i>	<i>Side by Side</i>	<i>Staggered</i>	<i>Single</i>	<i>Other</i>
40	0.03%	0.02%	0.00%	99.64%	0.31%
60	0.03%	0.04%	0.00%	99.58%	0.35%
80	0.03%	0.19%	0.00%	99.29%	0.49%
100	0.03%	0.56%	0.01%	98.54%	0.86%
120	0.03%	1.01%	0.15%	97.38%	1.43%
140	0.04%	1.28%	0.50%	96.14%	2.04%
160	0.04%	1.35%	1.04%	94.90%	2.67%
180	0.08%	1.36%	1.69%	93.57%	3.30%
200	0.23%	1.36%	2.36%	92.08%	3.97%

Table 4.10 Summary of Multiple Presence Statistics (NY WIM Site 8382)

<i>Span</i>	<i>Following</i>	<i>Side by Side</i>	<i>Staggered</i>	<i>Single</i>	<i>Other</i>
40	0.03%	0.01%	0.00%	99.60%	0.36%
60	0.03%	0.03%	0.00%	99.56%	0.38%
80	0.03%	0.14%	0.00%	99.32%	0.51%
100	0.03%	0.45%	0.00%	98.62%	0.90%
120	0.04%	0.81%	0.12%	97.60%	1.43%
140	0.04%	1.05%	0.39%	96.48%	2.04%
160	0.04%	1.09%	0.87%	95.41%	2.59%
180	0.07%	1.10%	1.42%	94.23%	3.18%
200	0.16%	1.10%	2.01%	92.91%	3.82%

Table 4.11 Summary of Multiple Presence Statistics (NY WIM Site 9291)

<i>Span</i>	<i>Following</i>	<i>Side by Side</i>	<i>Staggered</i>	<i>Single</i>	<i>Other</i>
40	0.05%	0.01%	0.00%	99.45%	0.49%
60	0.05%	0.04%	0.00%	99.39%	0.52%
80	0.05%	0.16%	0.00%	99.13%	0.66%
100	0.05%	0.43%	0.01%	98.53%	0.98%
120	0.07%	0.69%	0.12%	97.69%	1.43%
140	0.10%	0.80%	0.41%	96.78%	1.91%
160	0.13%	0.84%	0.77%	95.86%	2.40%
180	0.20%	0.84%	1.22%	94.81%	2.93%
200	0.37%	0.84%	1.64%	93.72%	3.43%

Table 4.12 Summary of Multiple Presence Statistics (NY WIM Site 9631)

<i>Span</i>	<i>Following</i>	<i>Side by Side</i>	<i>Staggered</i>	<i>Single</i>	<i>Other</i>
40	0.21%	0.02%	0.00%	97.90%	1.87%
60	0.21%	0.03%	0.00%	97.89%	1.87%
80	0.21%	0.08%	0.00%	97.80%	1.91%
100	0.21%	0.17%	0.00%	97.61%	2.01%
120	0.21%	0.23%	0.02%	97.40%	2.14%
140	0.21%	0.25%	0.08%	97.18%	2.28%
160	0.21%	0.26%	0.17%	96.96%	2.40%
180	0.23%	0.26%	0.25%	96.70%	2.56%
200	0.28%	0.26%	0.34%	96.40%	2.72%

4.2 Prediction of Long Term Live Load Effects

The prediction of the long term load effect is one of the most important steps in performing structural analysis. During the AASHTO LRFD calibration process, a 1975 truck weight survey from Ontario, Canada, performed by the Ontario Ministry of Transportation, was used (Agarwal and Wolkowicz, 1976). The survey included about 10,000 trucks that were randomly selected and stopped if they appeared to be heavy. If the weight of the truck was heavy in comparison to the average weight in its category, the truck record was retained; otherwise, the truck record was dismissed and not included in the dataset. Assuming this dataset to represent the upper 20% of 2 weeks of normal truck traffic in the United States (this corresponds to ADTT = 5000). In the original LRFD code calibration by Nowak (1994), extrapolation was done by simple linear extension of the upper tail to desired future level. In this section, various methods of predicting long term load effects were discussed including methods based on rate of increase in vehicle weight and probabilistic based extrapolation methods. The long term load effects from various sites predicted using various methods were also discussed in this section.

4.2.1 Rate of Increase in Vehicle Weight

Figure 4.15 shows the time variation of Gross Vehicle Weight (GVW) over years based on WIM data collected from New Jersey Site 195 from 1993 to 2009 without filtering permit vehicles. It is observed that the increase rate is 1.5% and 1.2% for mean maximum weight and 95th percentile, respectively. On the other hand, Figure 4.16 shows the time variation of weight statistics for 1993 to 2009 when permit vehicles were removed. It is observed that the rate of increase is only 0.06% and 0.15% for mean maximum weight and 95th percentile, respectively. When using an increase rate of 95th percentile truck weight to estimate the 75 years live load effect, the bias factor at 75 years is $1.3(1+(0.0015)*75)= 1.446$.

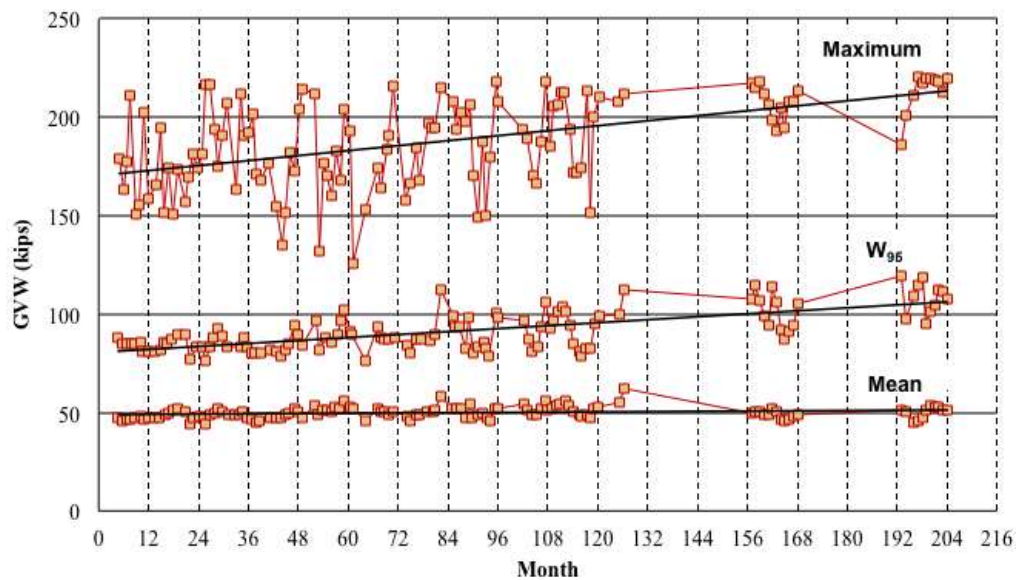


Figure 4.15 Time variation of total weight statistics for site 195, 1993-2009, (without filtering permits)

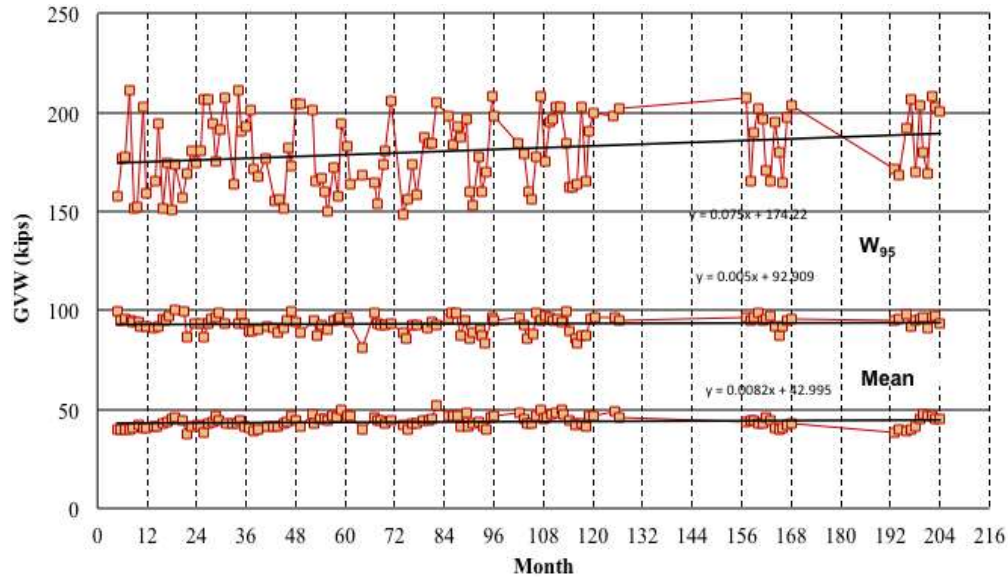


Figure 4.16 Time variation of total weight statistics for site 195, 1993-2009, (with filtering permits)

4.2.2 Probabilistic Based Extrapolation Methods

The prediction of the maximum 75-year load effect is one of the most important steps in calibrating the live load factors. During the AASHTO LRFD calibration process, a 1975 truck weight survey from Ontario, Canada, performed by the Ontario Ministry of Transportation, was used (Agarwal and Wolkowicz, 1976). The survey included about 10,000 trucks that were randomly selected and stopped if they appeared to be heavy. If the weight of the truck was heavy in comparison to the average weight in its category, the truck record was retained; otherwise, the truck record was dismissed and not included in the dataset. Assuming this dataset to represent the upper 20% of 2 weeks of normal truck traffic in the United States (this corresponds to ADTT = 5000). In the original LRFD code calibration by Nowak (1994), extrapolation was done by simple linear extension of the upper tail to desired future level. In this study, besides this approach, two other

approaches were also used in this study. Each approach is briefly discussed in the following section.

- a. Linear extension approach, the following steps were followed: (1) Calculate the moment ratio due to every truck from WIM data using the computer program developed by the authors; (2) Plot the calculation ratios on the Normal Probability Paper; (3) Extend the upper tail (20% of the total number of trucks by weight) as a straight-line to the desired future level. The x-coordinate of the intersection between the extension line and the 75-year level line is the bias factor representing the maximum 75-year load effects.
- b. Re-plotting the upper tail using normal approximation with mean and standard deviation of upper tail data, the following steps were used: (1) Calculate the moment ratio due to every truck from WIM data using the computer program developed by the authors; (2) Re-plot the upper tail points on the Normal Probability paper with the best-fit normal distribution; (3) Extrapolate the resulting normal distribution to the desired future level. The x-coordinate of the intersection between the extension line and 75-year level is the bias factor representing the maximum 75-year load effects.
- c. Re-plotting the upper tail using best-fit straight line in data points, the following steps were followed: (1) Calculate the moment ratio due to every truck from WIM data using the computer program developed by the authors; (2) Re-plot the upper tail points on the Normal Probability paper; (3) extrapolate the upper tail points as a best-fit straight line to the desired future level. The x-coordinate of the

intersection between the extension line and 75-year level is the bias factor representing the maximum 75-year load effects.

Figure 4.17 shows the extrapolation of 75-year moment ratio (moment demand divided by the moment demand of the standard HS20 design truck) for a 120-ft simply supported bridge span using the above three approaches. It is observed that all three methods provide similar results.

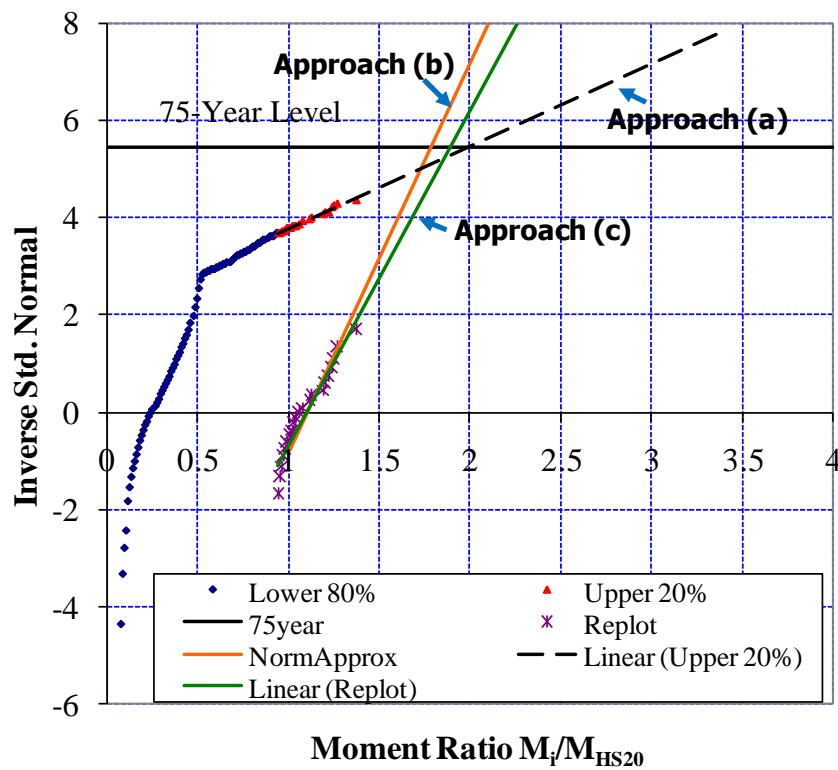


Figure 4.17 Typical Extrapolation of 75-Year Moment Ratio using Various Approaches

4.2.3 Long Term Load Effects from Various Sites

In this section, site-specific bias factors were extracted from WIM data from various sites. In addition, the outcome of long term load effects using different extrapolation methods were compared for four typical WIM sites. Moreover, the long term load effects for different sites were compared and discussed.

4.2.3.1 Site-Specific Bias Factors for Various WIM Sites

Table 4.13 through Table 4.20 present the bias factors for eight New York WIM sites that obtained using up 20% extrapolation. In addition, Table 4.21 presents the bias factors for New Jersey WIM site that also obtained using up 20% extrapolation. The NJ data was collected by Rutgers team at the Newark Bay Bridge site on NJ Turnpike. The Newark Bay Bridge connects the Newark and Bayonne with truck traffic between Newark and New York City. Since the NJ and NY are two neighboring states, the comparison of long term live load effect between NJ and NY could help to better understand the live load in this region and exam the consistency of the data. All the moment ratios in this section are shown in terms of HL-93 loading.

Table 4.13 Mean Maximum Moments for Simple Spans Divided by Corresponding HL-

93 Moment for site NY0199-NB

<i>Span (ft)</i>	<i>1 day</i>	<i>2 weeks</i>	<i>1 month</i>	<i>2 months</i>	<i>6 months</i>	<i>1 year</i>	<i>5 years</i>	<i>50 years</i>	<i>75 years</i>
20	1.343	1.525	1.572	1.615	1.679	1.719	1.807	1.925	1.944
40	1.334	1.511	1.558	1.599	1.662	1.701	1.787	1.902	1.921
60	1.236	1.379	1.417	1.451	1.501	1.533	1.602	1.694	1.710
80	1.187	1.312	1.344	1.374	1.417	1.445	1.505	1.585	1.599
100	1.143	1.260	1.291	1.319	1.361	1.386	1.443	1.519	1.532
120	1.097	1.209	1.238	1.264	1.304	1.329	1.382	1.454	1.467
140	1.054	1.160	1.188	1.212	1.250	1.273	1.324	1.392	1.404
160	1.011	1.112	1.139	1.163	1.199	1.221	1.270	1.336	1.348
180	0.969	1.067	1.093	1.116	1.151	1.172	1.219	1.283	1.294
200	0.931	1.024	1.050	1.071	1.104	1.125	1.170	1.230	1.240
220	0.894	0.986	1.011	1.033	1.065	1.086	1.131	1.191	1.201
240	0.862	0.949	0.973	0.993	1.025	1.044	1.087	1.143	1.153
260	0.830	0.915	0.938	0.958	0.989	1.007	1.048	1.103	1.113
280	0.801	0.883	0.905	0.924	0.954	0.972	1.012	1.066	1.075
300	0.774	0.854	0.875	0.893	0.922	0.940	0.978	1.029	1.038

Table 4.14 Mean Maximum Moments for Simple Spans Divided by Corresponding HL-93 Moment for Site NY0199-SB

<i>Span (ft)</i>	<i>1 day</i>	<i>2 weeks</i>	<i>1 month</i>	<i>2 months</i>	<i>6 months</i>	<i>1 year</i>	<i>5 years</i>	<i>50 years</i>	<i>75 years</i>
20	1.470	1.672	1.726	1.772	1.844	1.888	1.984	2.113	2.135
40	1.464	1.653	1.703	1.746	1.812	1.854	1.944	2.065	2.086
60	1.314	1.469	1.510	1.546	1.600	1.634	1.709	1.808	1.825
80	1.225	1.368	1.406	1.439	1.490	1.521	1.590	1.682	1.697
100	1.156	1.292	1.328	1.359	1.407	1.437	1.502	1.589	1.604
120	1.099	1.227	1.261	1.291	1.336	1.364	1.425	1.507	1.521
140	1.048	1.172	1.204	1.233	1.276	1.303	1.362	1.441	1.454
160	1.002	1.121	1.152	1.180	1.223	1.249	1.306	1.383	1.395
180	0.958	1.075	1.106	1.133	1.175	1.200	1.256	1.331	1.344
200	0.919	1.033	1.063	1.089	1.129	1.154	1.209	1.281	1.294
220	0.881	0.995	1.025	1.051	1.091	1.116	1.170	1.243	1.255
240	0.848	0.958	0.988	1.014	1.052	1.077	1.129	1.200	1.212
260	0.816	0.922	0.950	0.974	1.011	1.034	1.084	1.152	1.163
280	0.787	0.892	0.919	0.943	0.980	1.002	1.052	1.119	1.131
300	0.759	0.860	0.887	0.910	0.946	0.967	1.016	1.081	1.091

Table 4.15 Mean Maximum Moments for Simple Spans Divided by Corresponding HL-93 Moment for Site NY0580

<i>Span (ft)</i>	<i>1 day</i>	<i>2 weeks</i>	<i>1 month</i>	<i>2 months</i>	<i>6 months</i>	<i>1 year</i>	<i>5 years</i>	<i>50 years</i>	<i>75 years</i>
20	1.419	1.629	1.684	1.733	1.807	1.853	1.955	2.091	2.113
40	1.466	1.682	1.739	1.789	1.865	1.913	2.017	2.156	2.180
60	1.381	1.502	1.534	1.562	1.605	1.631	1.690	1.768	1.781
80	1.324	1.420	1.446	1.468	1.502	1.524	1.570	1.632	1.643
100	1.272	1.360	1.384	1.404	1.435	1.454	1.497	1.554	1.564
120	1.221	1.304	1.325	1.345	1.374	1.392	1.432	1.485	1.495
140	1.170	1.249	1.269	1.287	1.316	1.333	1.371	1.422	1.430
160	1.121	1.196	1.217	1.235	1.261	1.278	1.315	1.364	1.372
180	1.075	1.148	1.167	1.184	1.210	1.226	1.261	1.308	1.316
200	1.031	1.102	1.121	1.137	1.162	1.178	1.212	1.258	1.265
220	0.990	1.058	1.076	1.092	1.116	1.131	1.163	1.207	1.215
240	0.952	1.017	1.035	1.050	1.073	1.087	1.119	1.161	1.168
260	0.917	0.981	0.997	1.012	1.035	1.049	1.080	1.121	1.128
280	0.883	0.945	0.961	0.975	0.997	1.010	1.040	1.079	1.086
300	0.853	0.912	0.927	0.941	0.962	0.975	1.003	1.041	1.048

Table 4.16 Mean Maximum Moments for Simple Spans Divided by Corresponding HL-93 Moment for Site NY2680

<i>Span (ft)</i>	<i>1 day</i>	<i>2 weeks</i>	<i>1 month</i>	<i>2 months</i>	<i>6 months</i>	<i>1 year</i>	<i>5 years</i>	<i>50 years</i>	<i>75 years</i>
20	1.224	1.482	1.548	1.605	1.692	1.745	1.860	2.012	2.037
40	1.218	1.471	1.535	1.591	1.676	1.728	1.840	1.989	2.014
60	1.108	1.327	1.384	1.432	1.506	1.551	1.648	1.778	1.799
80	1.048	1.246	1.296	1.341	1.407	1.447	1.536	1.652	1.671
100	1.010	1.187	1.232	1.271	1.330	1.367	1.445	1.550	1.567
120	0.976	1.140	1.182	1.218	1.273	1.307	1.380	1.476	1.492
140	0.946	1.100	1.138	1.173	1.224	1.256	1.324	1.415	1.429
160	0.914	1.059	1.096	1.128	1.176	1.206	1.270	1.355	1.370
180	0.882	1.020	1.056	1.086	1.132	1.161	1.222	1.303	1.317
200	0.853	0.983	1.016	1.045	1.089	1.116	1.173	1.250	1.263
220	0.821	0.950	0.982	1.011	1.053	1.080	1.137	1.212	1.225
240	0.794	0.916	0.946	0.973	1.014	1.039	1.093	1.165	1.177
260	0.767	0.885	0.915	0.941	0.980	1.004	1.056	1.125	1.137
280	0.741	0.856	0.886	0.911	0.950	0.974	1.024	1.092	1.103
300	0.718	0.829	0.856	0.881	0.917	0.940	0.989	1.053	1.064

Table 4.17 Mean Maximum Moments for Simple Spans Divided by Corresponding HL-93 Moment for Site NY8280

<i>Span (ft)</i>	<i>1 day</i>	<i>2 weeks</i>	<i>1 month</i>	<i>2 months</i>	<i>6 months</i>	<i>1 year</i>	<i>5 years</i>	<i>50 years</i>	<i>75 years</i>
20	1.28	1.506	1.562	1.612	1.686	1.73	1.833	1.967	1.990
40	1.35	1.594	1.655	1.709	1.791	1.84	1.951	2.097	2.121
60	1.30	1.454	1.492	1.526	1.577	1.60	1.676	1.768	1.783
80	1.26	1.376	1.406	1.432	1.471	1.49	1.548	1.618	1.629
100	1.21	1.317	1.344	1.367	1.401	1.42	1.470	1.532	1.542
120	1.16	1.262	1.287	1.308	1.341	1.36	1.404	1.462	1.472
140	1.12	1.210	1.233	1.254	1.286	1.30	1.347	1.403	1.412
160	1.07	1.159	1.182	1.202	1.232	1.25	1.292	1.345	1.354
180	1.02	1.112	1.134	1.153	1.182	1.20	1.239	1.291	1.300
200	0.98	1.067	1.088	1.107	1.134	1.15	1.189	1.239	1.248
220	0.94	1.026	1.047	1.064	1.092	1.10	1.145	1.194	1.202
240	0.91	0.987	1.008	1.025	1.052	1.06	1.104	1.152	1.160
260	0.87	0.952	0.972	0.989	1.015	1.03	1.066	1.113	1.121
300	0.81	0.886	0.905	0.922	0.946	0.96	0.995	1.040	1.047

Table 4.18 Mean Maximum Moments for Simple Spans Divided by Corresponding HL-93 Moment for Site NY8382

<i>Span (ft)</i>	<i>1 day</i>	<i>2 weeks</i>	<i>1 month</i>	<i>2 months</i>	<i>6 months</i>	<i>1 year</i>	<i>5 years</i>	<i>50 years</i>	<i>75 years</i>
20	1.026	1.377	1.470	1.551	1.676	1.753	1.921	2.146	2.176
40	0.890	1.366	1.491	1.601	1.769	1.873	2.100	2.404	2.408
60	0.792	1.238	1.356	1.460	1.617	1.715	1.928	2.214	2.198
80	1.024	1.227	1.282	1.329	1.401	1.446	1.543	1.674	1.686
100	1.101	1.235	1.271	1.302	1.349	1.378	1.443	1.529	1.543
120	1.099	1.254	1.294	1.330	1.385	1.419	1.493	1.592	1.577
140	1.064	1.249	1.298	1.340	1.405	1.446	1.534	1.652	1.594
160	1.065	1.223	1.264	1.300	1.355	1.390	1.465	1.565	1.564
180	1.034	1.196	1.238	1.275	1.332	1.367	1.444	1.547	1.540
200	1.006	1.161	1.202	1.238	1.292	1.327	1.400	1.500	1.497
220	0.973	1.128	1.169	1.205	1.260	1.294	1.369	1.468	1.461
240	0.945	1.095	1.135	1.169	1.221	1.254	1.326	1.421	1.413
260	0.915	1.062	1.101	1.135	1.186	1.219	1.288	1.382	1.374
280	0.890	1.028	1.064	1.096	1.145	1.175	1.241	1.329	1.325
300	0.861	0.999	1.035	1.067	1.116	1.146	1.212	1.300	1.292

Table 4.19 Mean Maximum Moments for Simple Spans Divided by Corresponding HL-93 Moment for Site NY9121

<i>Span (ft)</i>	<i>1 day</i>	<i>2 weeks</i>	<i>1 month</i>	<i>2 months</i>	<i>6 months</i>	<i>1 year</i>	<i>5 years</i>	<i>50 years</i>	<i>75 years</i>
20	1.076	1.393	1.476	1.549	1.661	1.730	1.880	2.082	2.116
40	1.045	1.366	1.451	1.524	1.637	1.707	1.860	2.064	2.098
60	0.971	1.248	1.322	1.386	1.483	1.544	1.676	1.852	1.882
80	0.963	1.184	1.241	1.292	1.370	1.418	1.522	1.662	1.686
100	0.982	1.144	1.187	1.224	1.281	1.317	1.394	1.497	1.515
120	0.974	1.117	1.155	1.187	1.238	1.269	1.337	1.428	1.443
140	0.951	1.091	1.127	1.160	1.209	1.240	1.306	1.395	1.410
160	0.924	1.064	1.100	1.132	1.181	1.211	1.277	1.366	1.381
180	0.896	1.034	1.070	1.102	1.150	1.180	1.245	1.332	1.347
200	0.869	1.005	1.041	1.072	1.120	1.150	1.214	1.300	1.315
220	0.843	0.975	1.010	1.040	1.087	1.116	1.179	1.262	1.277
240	0.818	0.946	0.980	1.010	1.056	1.083	1.144	1.227	1.240
260	0.795	0.918	0.950	0.979	1.023	1.050	1.108	1.187	1.200
280	0.770	0.891	0.922	0.950	0.993	1.019	1.077	1.154	1.167
300	0.751	0.864	0.893	0.920	0.959	0.984	1.038	1.110	1.121

Table 4.20 Mean Maximum Moments for Simple Spans Divided by Corresponding HL-93 Moment for Site NY9631

<i>Span (ft)</i>	<i>1 day</i>	<i>2 weeks</i>	<i>1 month</i>	<i>2 months</i>	<i>6 months</i>	<i>1 year</i>	<i>5 years</i>	<i>50 years</i>	<i>75 years</i>
20	1.008	1.283	1.354	1.416	1.510	1.568	1.694	1.860	1.889
40	0.967	1.261	1.338	1.404	1.505	1.567	1.701	1.880	1.910
60	0.908	1.157	1.221	1.277	1.363	1.415	1.529	1.680	1.706
80	0.928	1.130	1.183	1.228	1.298	1.340	1.433	1.556	1.577
100	0.931	1.112	1.159	1.199	1.261	1.299	1.382	1.491	1.510
120	0.913	1.089	1.135	1.174	1.235	1.272	1.352	1.459	1.477
140	0.892	1.060	1.104	1.141	1.199	1.234	1.311	1.413	1.430
160	0.879	1.032	1.071	1.106	1.158	1.190	1.260	1.353	1.369
180	0.843	0.996	1.035	1.070	1.122	1.154	1.224	1.316	1.332
200	0.816	0.964	1.002	1.036	1.087	1.118	1.186	1.276	1.291
220	0.790	0.931	0.967	0.999	1.047	1.076	1.140	1.226	1.240
240	0.763	0.901	0.937	0.968	1.014	1.044	1.106	1.190	1.204
260	0.739	0.871	0.905	0.934	0.980	1.007	1.068	1.148	1.161
280	0.716	0.843	0.876	0.905	0.948	0.975	1.034	1.111	1.124
300	0.692	0.816	0.848	0.876	0.918	0.945	1.001	1.076	1.089

Table 4.21 Mean Maximum Moments for Simple Spans Divided by Corresponding HL-93 Moment Based on NJ data

<i>Span (ft)</i>	<i>1 day</i>	<i>2 weeks</i>	<i>1 month</i>	<i>2 months</i>	<i>6 months</i>	<i>1 year</i>	<i>5 years</i>	<i>50 years</i>	<i>75 years</i>
20	1.605	1.745	1.782	1.815	1.865	1.895	1.962	2.051	2.066
40	1.602	1.741	1.777	1.809	1.858	1.889	1.955	2.044	2.058
60	1.434	1.555	1.586	1.614	1.656	1.682	1.738	1.814	1.827
80	1.327	1.442	1.472	1.498	1.538	1.563	1.618	1.691	1.703
100	1.248	1.363	1.393	1.419	1.460	1.485	1.539	1.611	1.624
120	1.183	1.298	1.328	1.354	1.395	1.420	1.475	1.547	1.560
140	1.125	1.241	1.272	1.299	1.339	1.365	1.420	1.494	1.506
160	1.071	1.188	1.218	1.245	1.286	1.311	1.367	1.441	1.453
180	1.023	1.139	1.170	1.196	1.237	1.262	1.317	1.390	1.403
200	0.979	1.093	1.122	1.149	1.188	1.214	1.267	1.339	1.351
220	0.939	1.051	1.081	1.107	1.147	1.171	1.225	1.296	1.308
240	0.902	1.012	1.041	1.067	1.106	1.130	1.182	1.252	1.264
260	0.867	0.975	1.003	1.028	1.066	1.089	1.141	1.209	1.221
280	0.834	0.937	0.964	0.988	1.024	1.047	1.096	1.161	1.172
300	0.804	0.904	0.930	0.953	0.988	1.009	1.056	1.119	1.130

4.2.3.2 Comparison between Different WIM Sites

Figure 4.18 through Figure 4.35 show the comparison of load effects between various WIM sites at various return periods. It is observed that except site 8332, there is no significant difference between the long term load effects calculated from NJ data and NY data. The average difference ranges from 3.1% to 7.9%, 1.1% to 4.4%, and 1.3% to 4.5%, respectively, for upper 20% extension, re-plot extrapolation, and normal approximation method. It is also observed that the difference of the long term predication between NY site 8382 and other WIM sites is larger with an average difference of 8.7%, 11.3%, and 10.9% respectively for upper 20% extension; re-plot extrapolation, and normal approximation method. This phenomenon can be caused by large number of heavy vehicle that collected from NY 8382 site. There are 649 trucks above 150 kips while site 9021 only has 219 trucks above 150 kips.

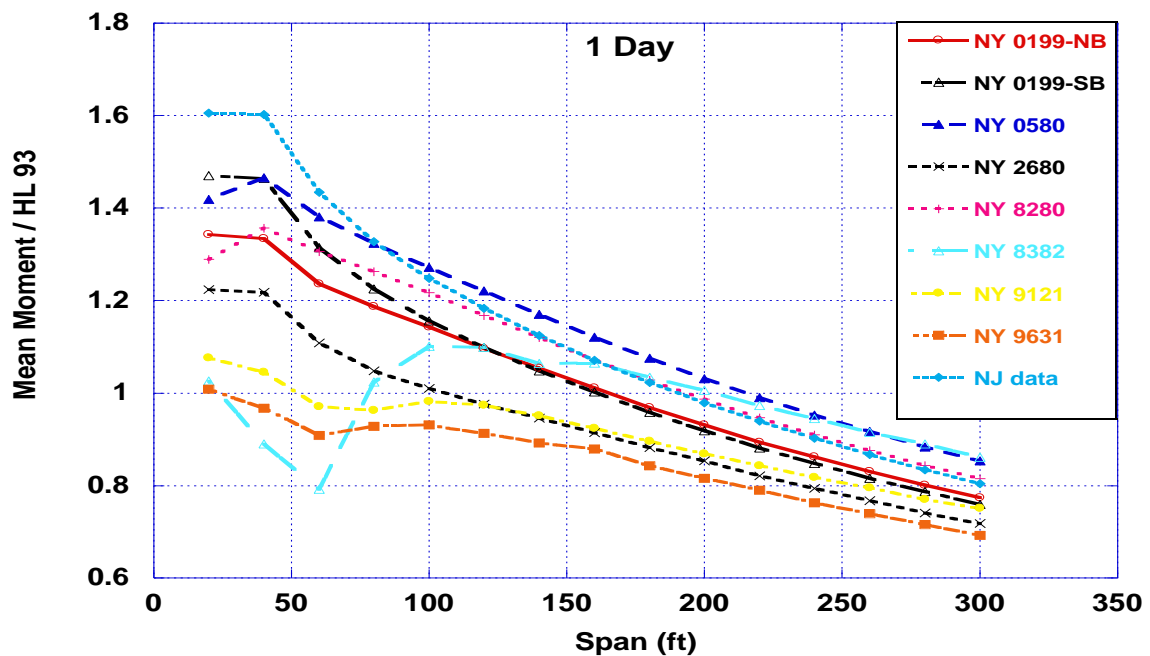


Figure 4.18 Comparison of Moment Ratio for Various WIM Sites (1 day period)

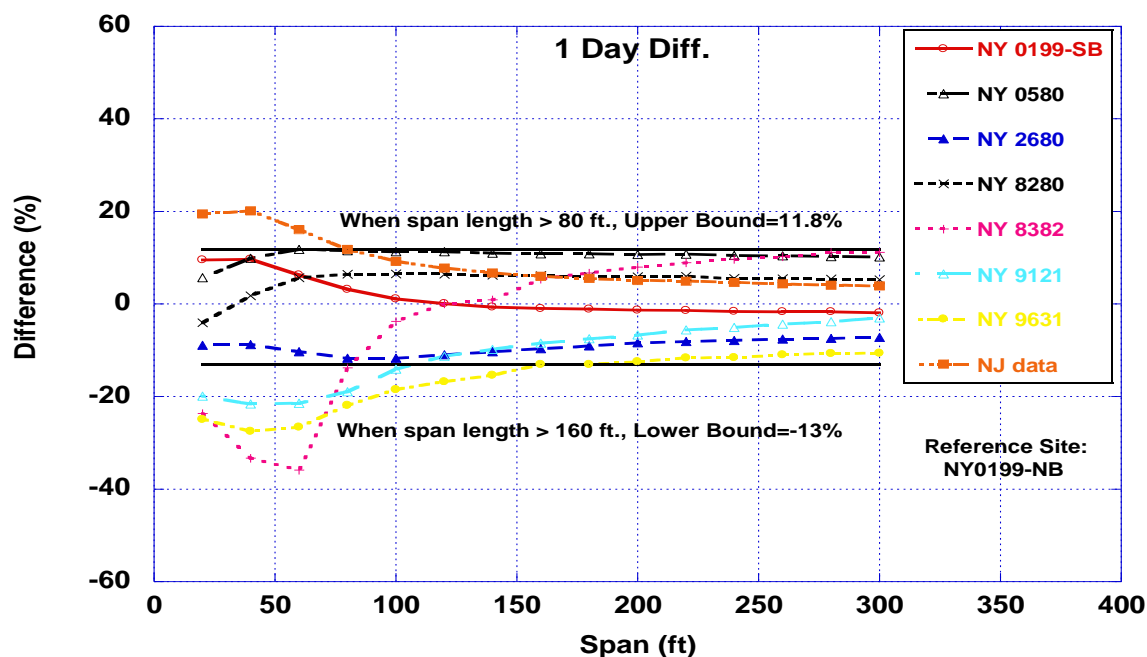


Figure 4.19 Comparison of Difference for Various WIM Sites (1 day period)

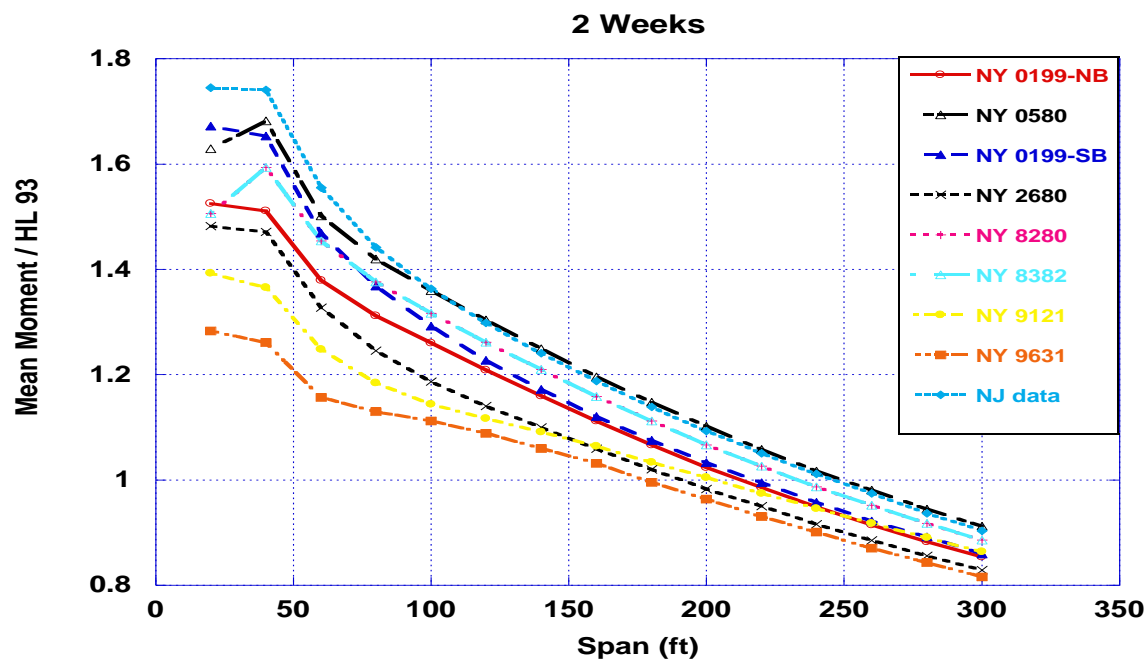


Figure 4.20 Comparison of Moment Ratio for Various WIM Sites (2 weeks period)

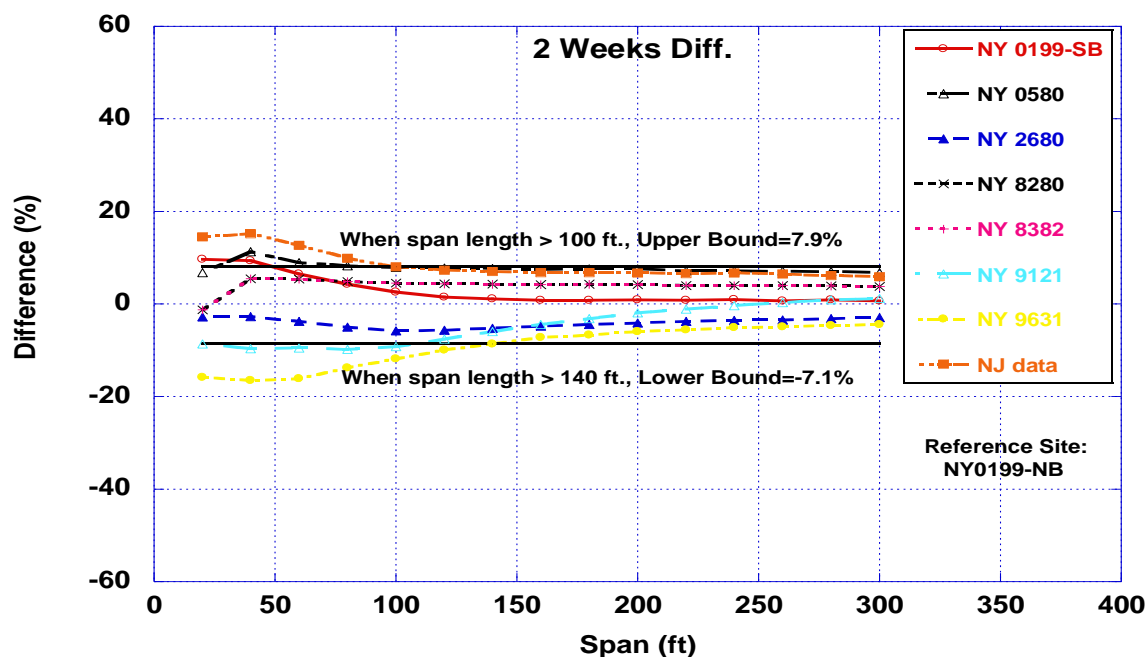


Figure 4.21 Comparison of Difference for Various WIM Sites (2 weeks period)

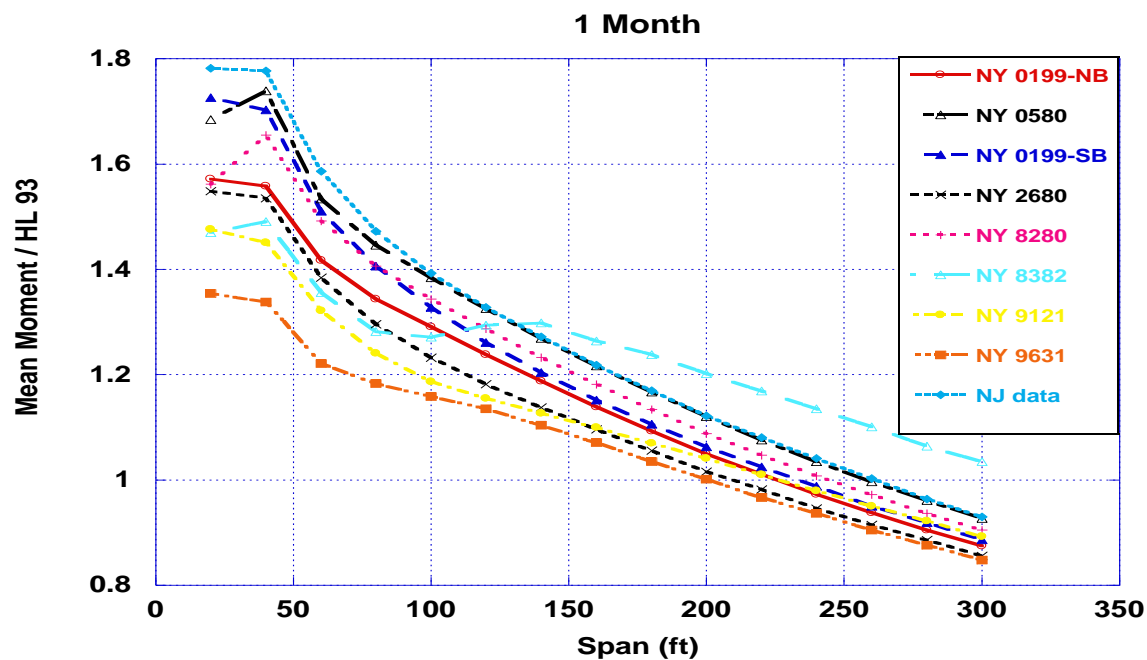


Figure 4.22 Comparison of Moment Ratio for Various WIM Sites (1 month period)

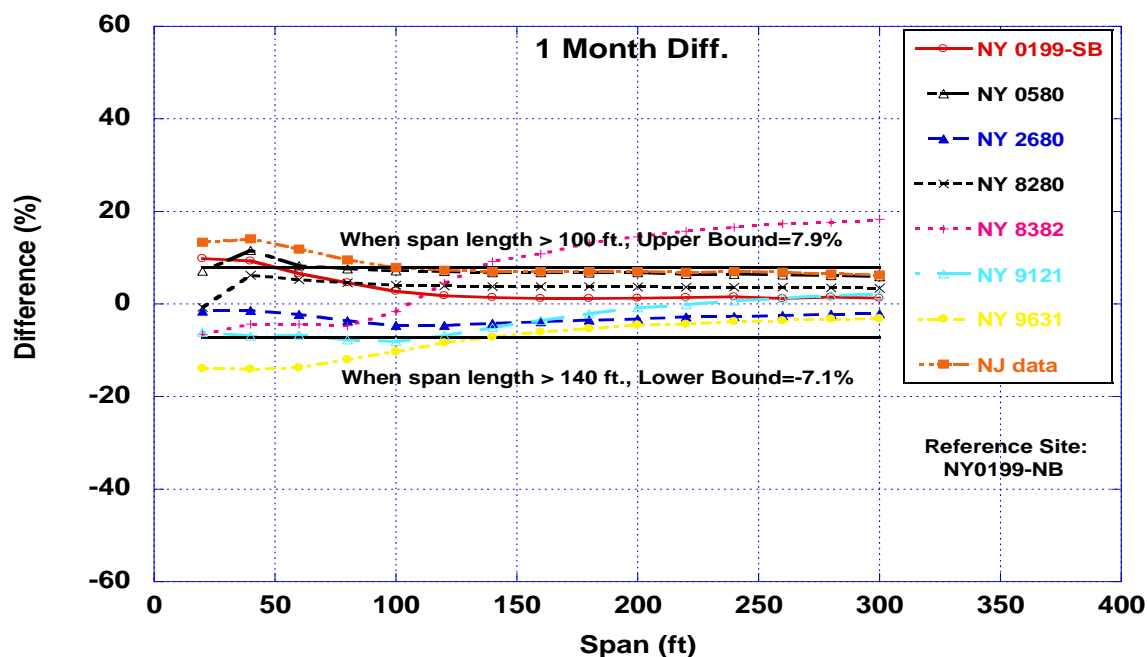


Figure 4.23 Comparison of Difference for Various WIM Sites (1 month period)

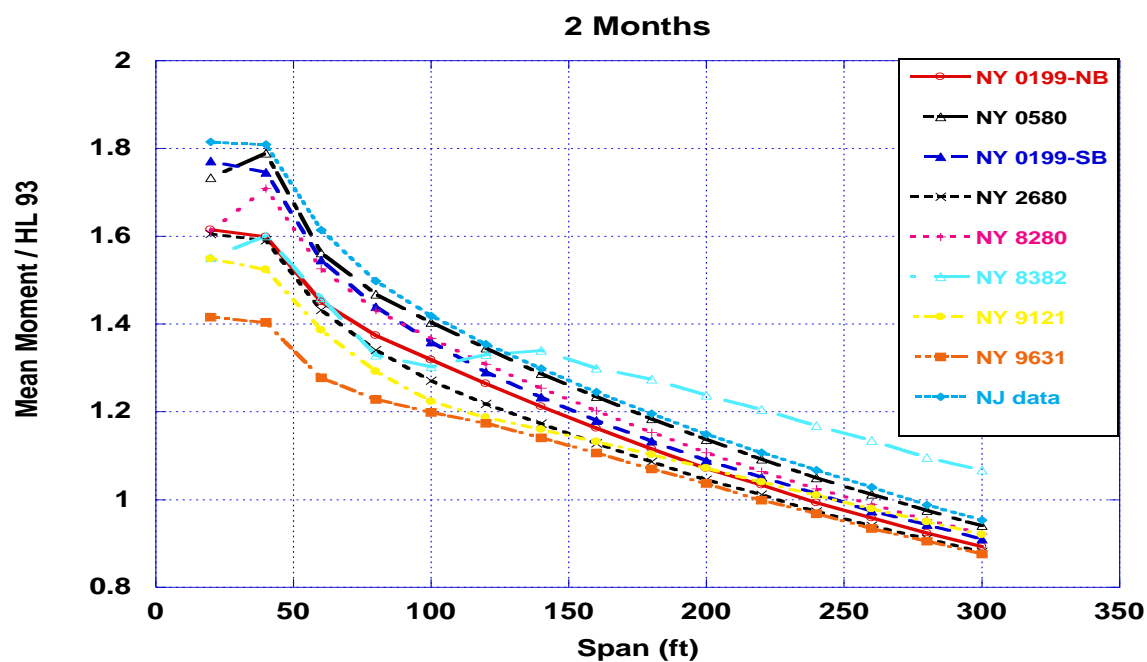


Figure 4.24 Comparison of Moment Ratio for Various WIM Sites (2 months period)

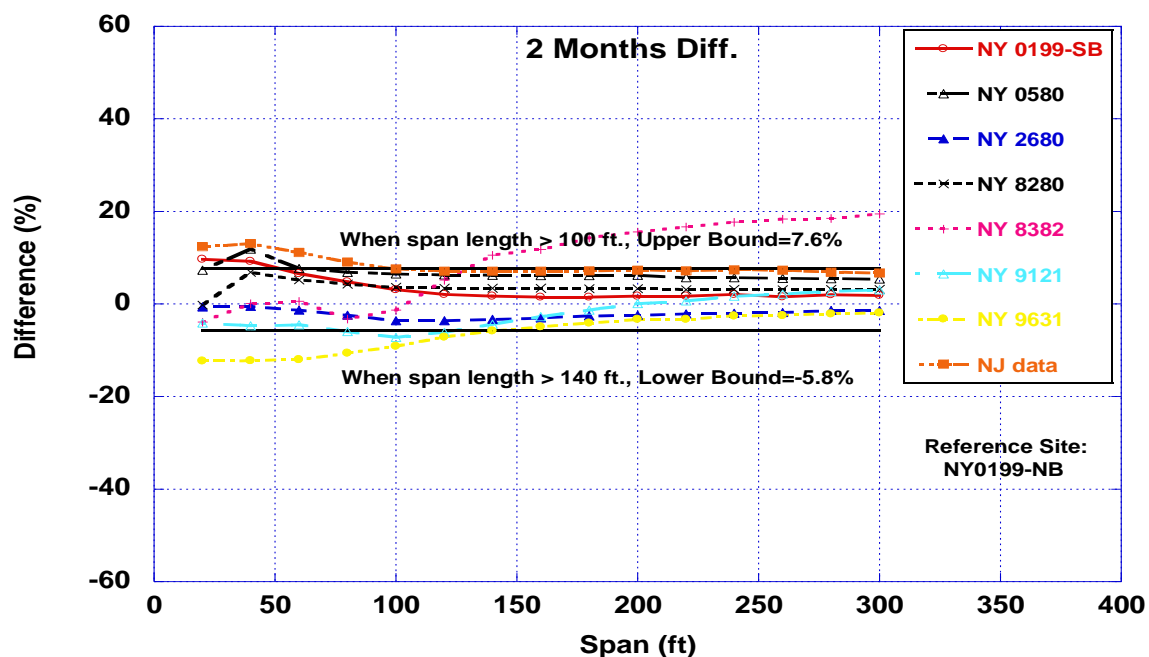


Figure 4.25 Comparison of Difference for Various WIM Sites (2 months period)

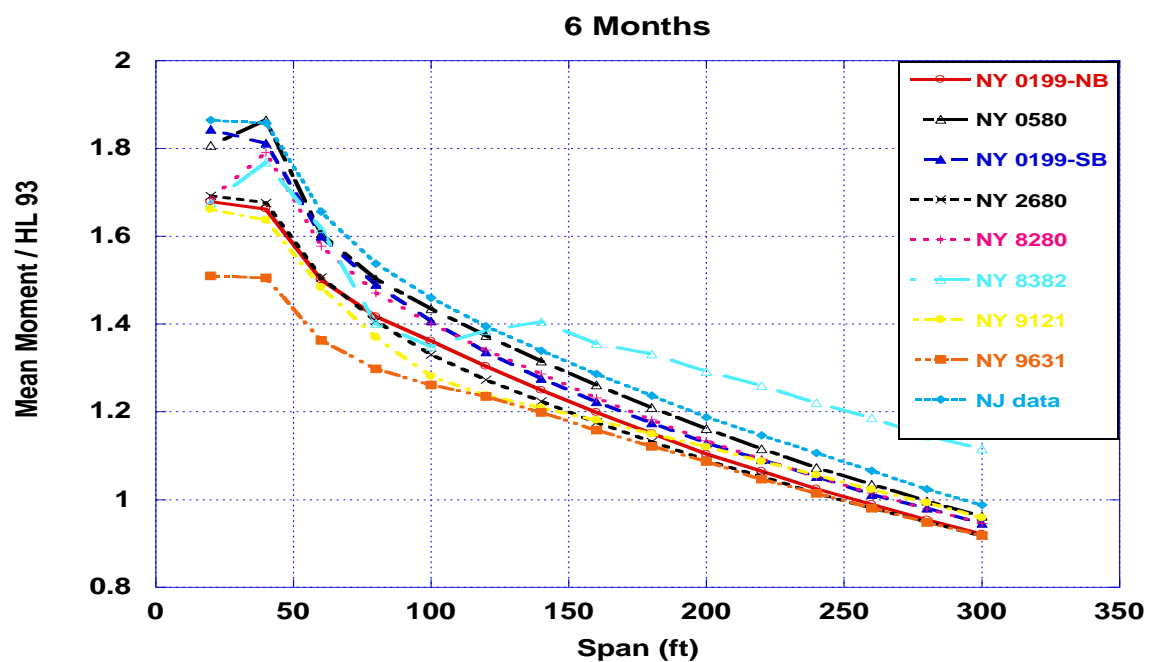


Figure 4.26 Comparison of Moment Ratio for Various WIM Sites (6 months period)

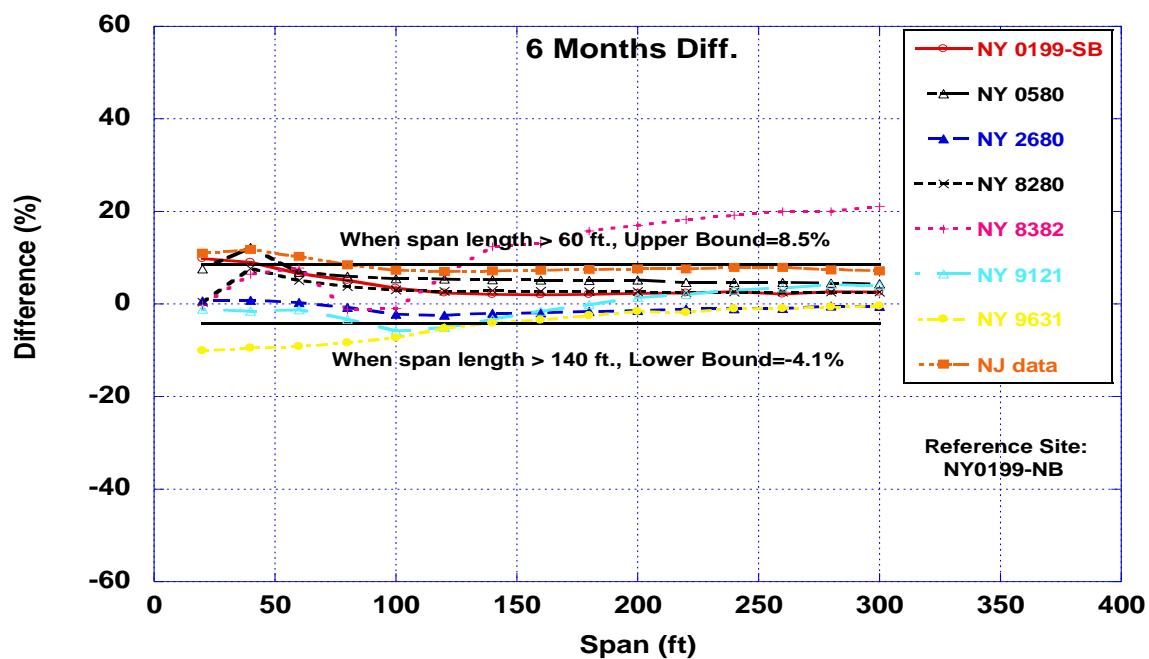


Figure 4.27 Comparison of Difference for Various WIM Sites (6 months period)

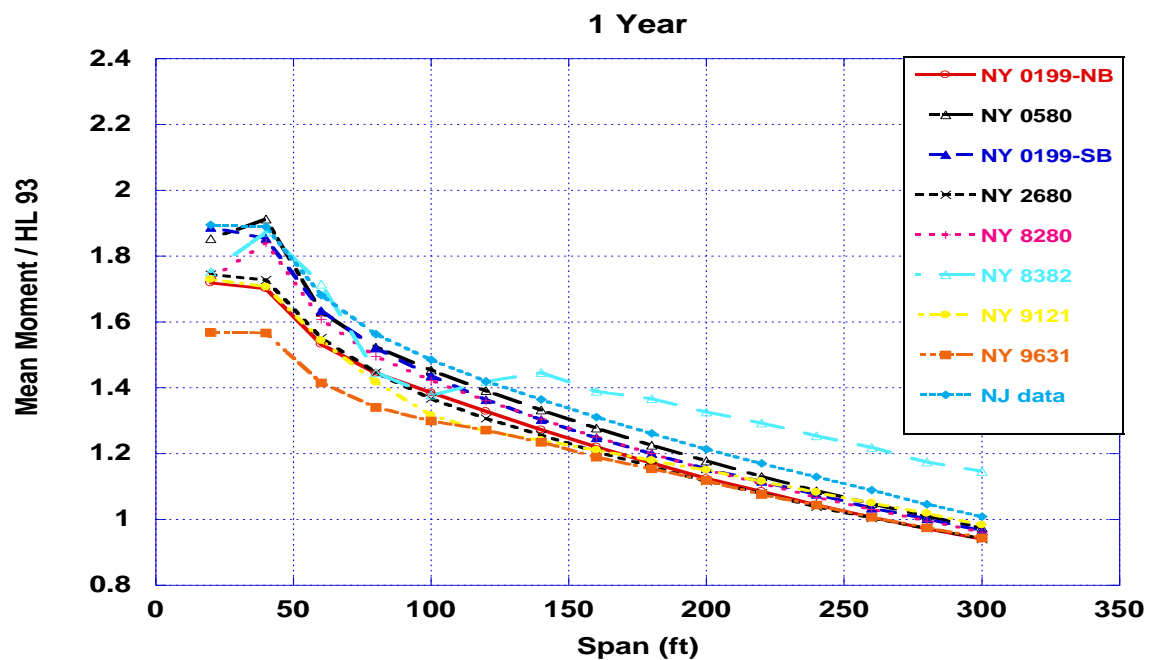


Figure 4.28 Comparison of Moment Ratio for Various WIM Sites (1 year period)

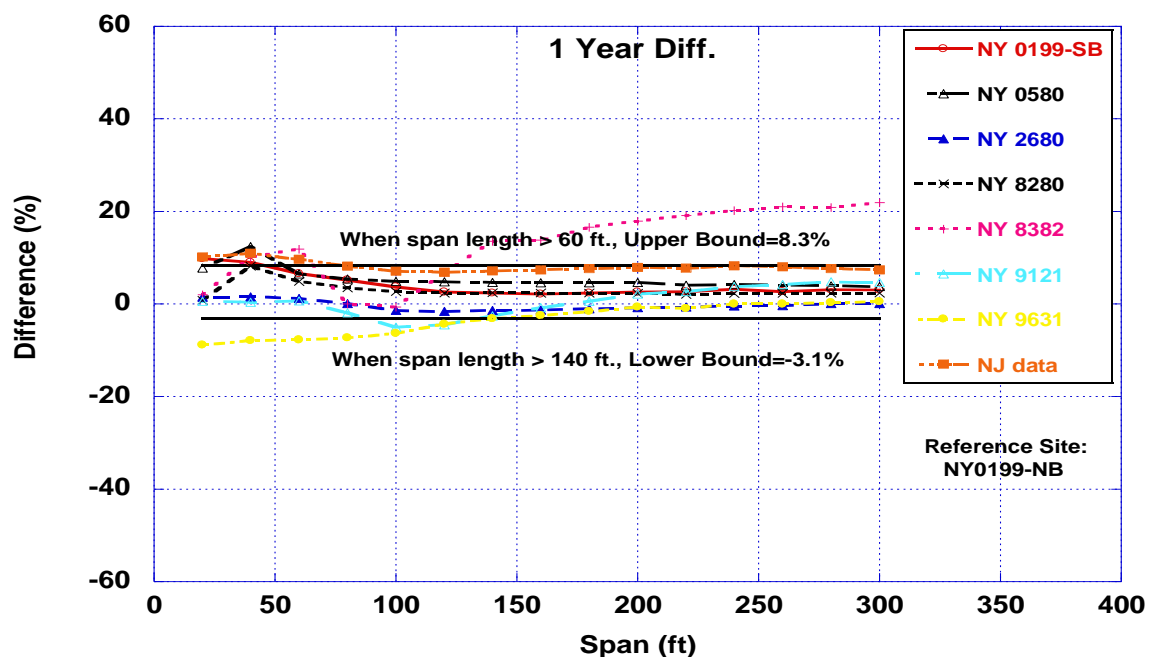


Figure 4.29 Comparison of Difference for Various WIM Sites (1 year period)

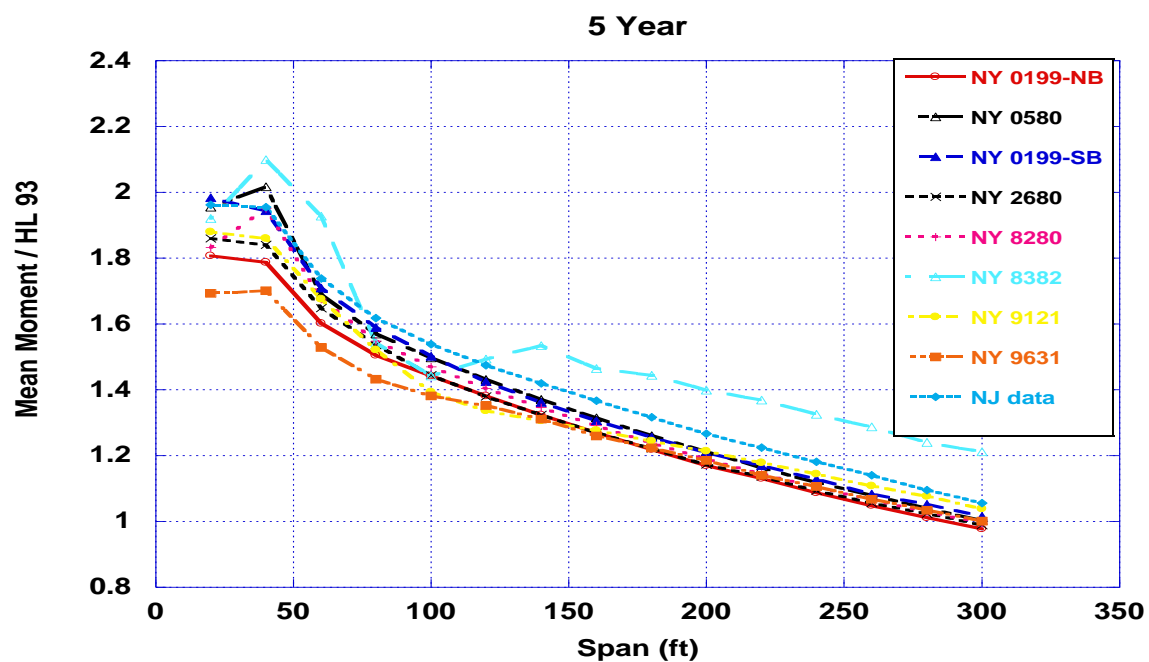


Figure 4.30 Comparison of Moment Ratio for Various WIM Sites (5 years period)

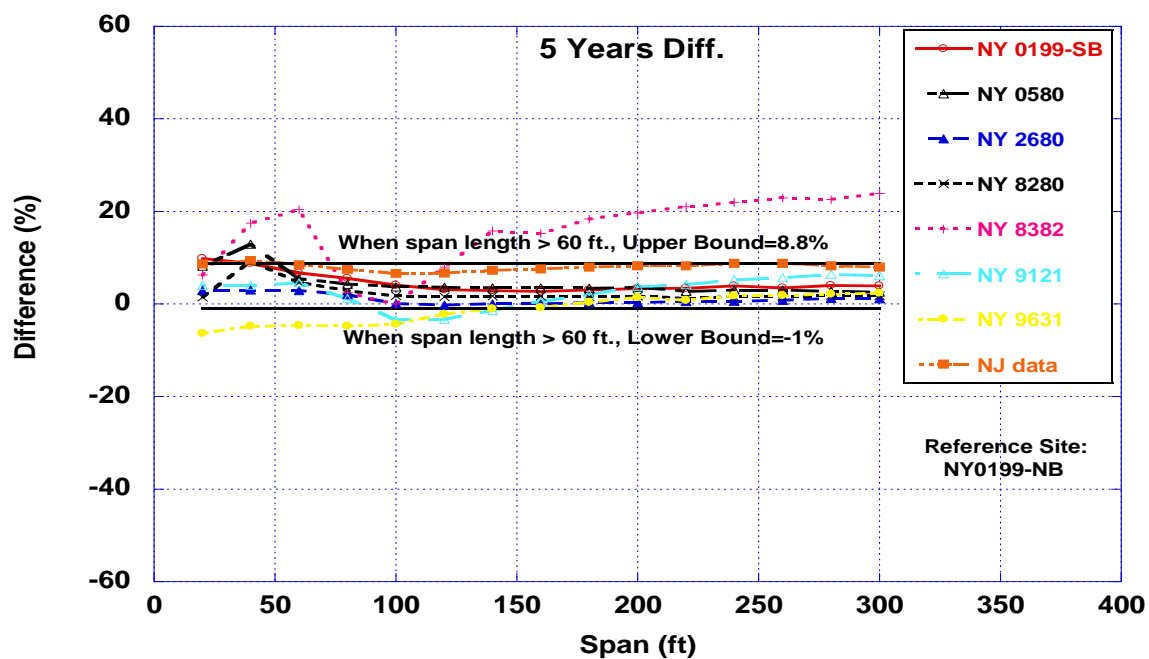


Figure 4.31 Comparison of Difference for Various WIM Sites (5 years period)

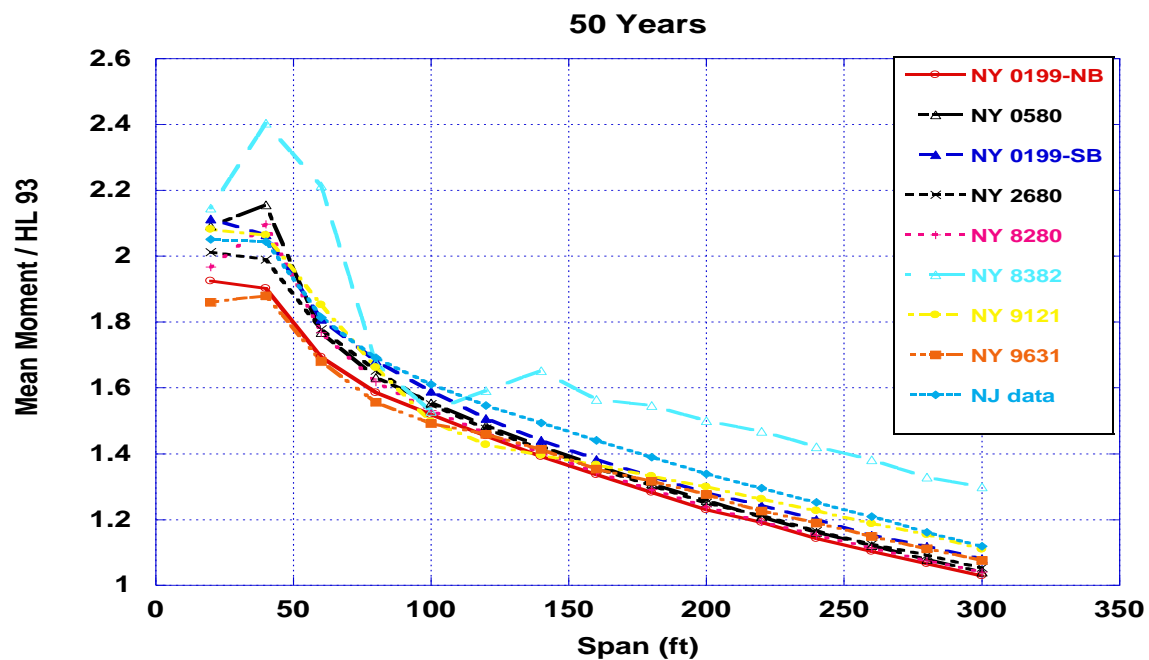


Figure 4.32 Comparison of Moment Ratio for Various WIM Sites (50 years period)

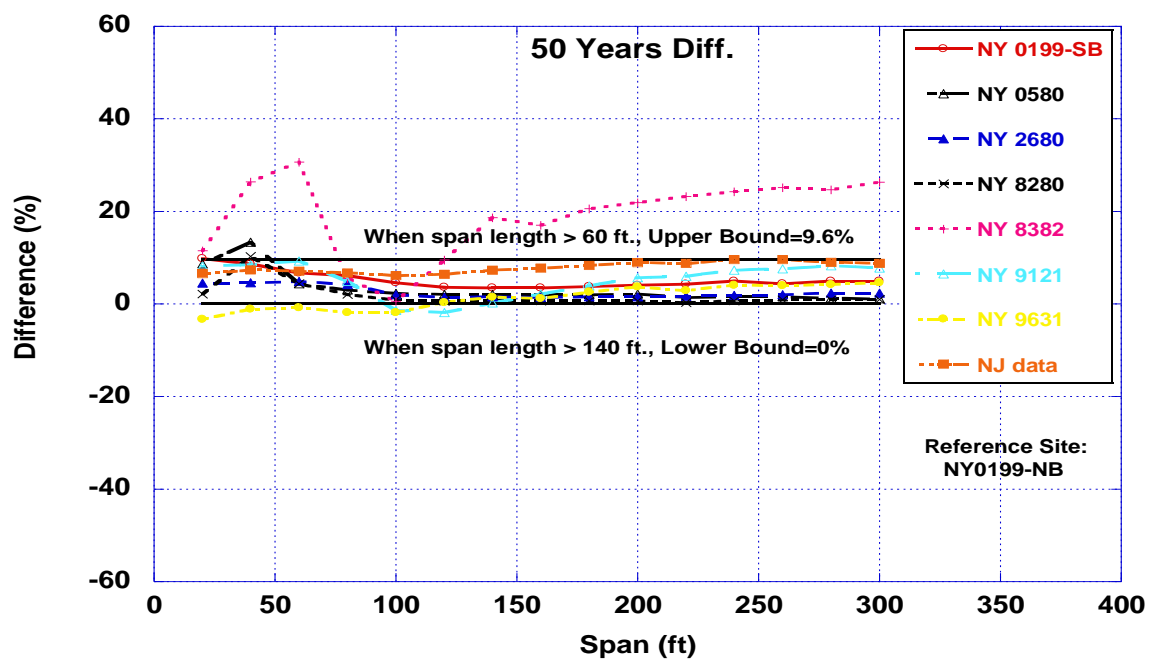


Figure 4.33 Comparison of Difference for Various WIM Sites (50 years period)

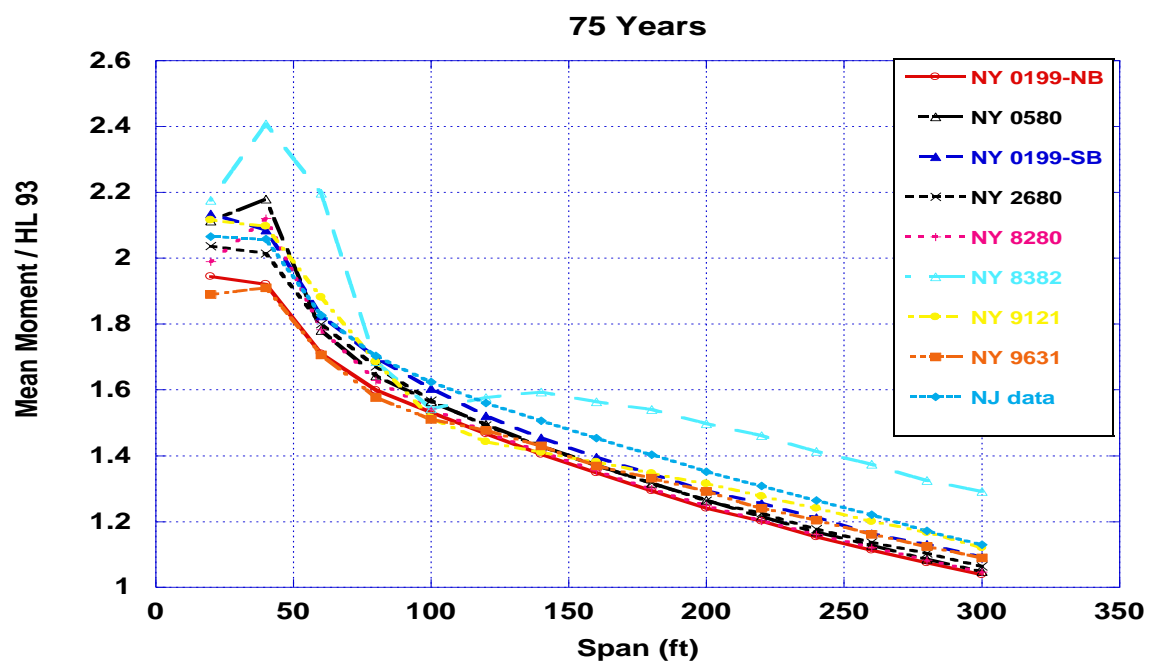


Figure 4.34 Comparison of Moment Ratio for Various WIM Sites (75 years period)

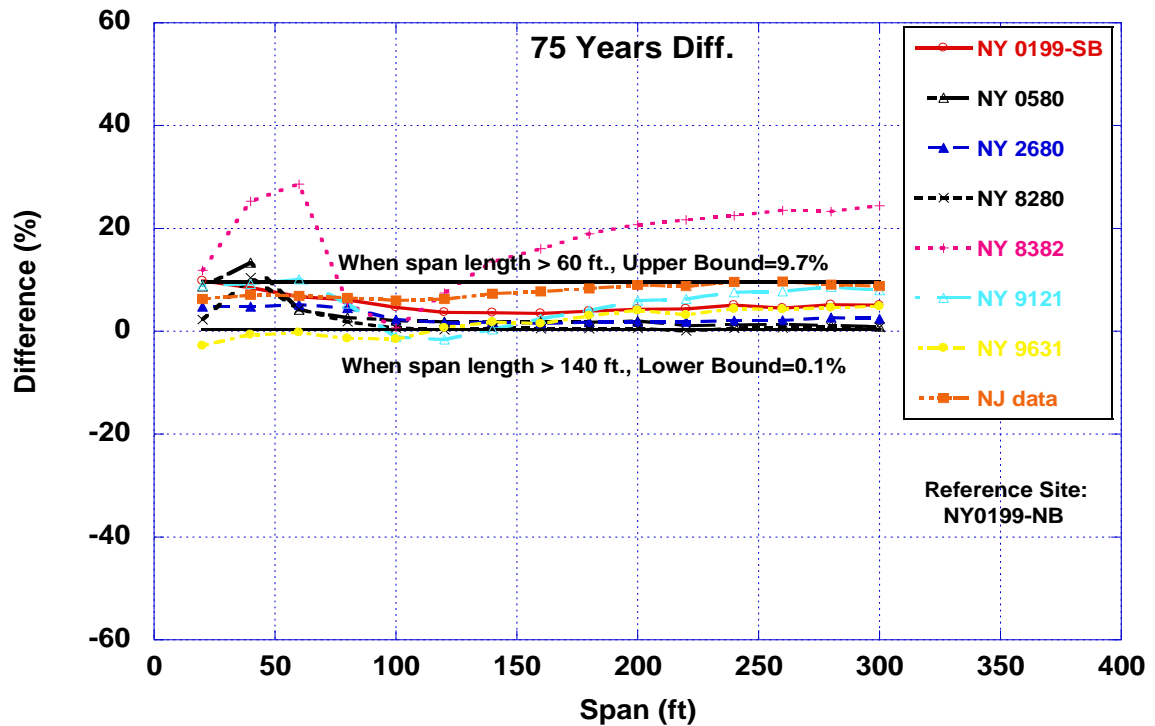


Figure 4.35 Comparison of Difference for Various WIM Sites (75 years period)

4.2.3.3 Effects of Extrapolation Methods

In section 4.2.2, various probabilistic extrapolation methods were discussed. In order to compare the outcome of each extrapolation methods, the bias factors that were calculated using different extrapolation methods including manual linear extension, up 20% extrapolation, re-plot of 20% extrapolation and normal approximation prediction were present for four typical New York WIM sites. Considerable difference is observed between manual linear extension and other methods.

4.2.3.3.1 NY Site 0580

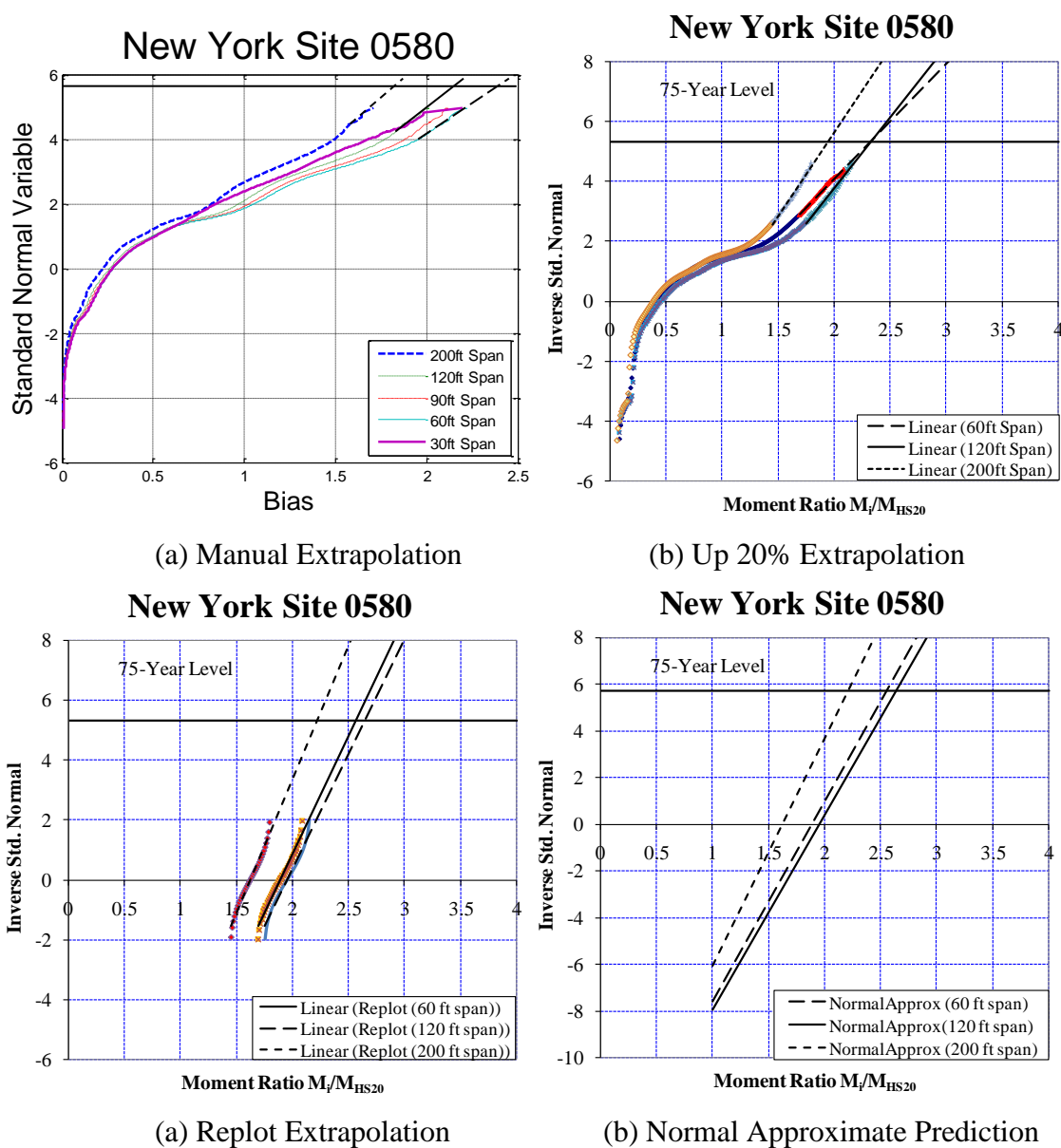


Figure 4.36 Extrapolation of Long Term Load Effects for Site 0580

Table 4.22 Extrapolation Summary for Site 0580 with respect to HL-93 Moment

Span Length	Lane 1		Lane 2		Lane 3		All Lanes Together		
	All trucks	Up 20%	All trucks	Up 20%	All trucks	Up 20%	U20 Extend	Replot	Normal Approx
60	1.792	1.846	1.655	1.686	1.747	1.727	1.781	1.927	1.885
120	1.473	1.475	1.449	1.453	1.602	1.564	1.495	1.672	1.636
200	1.248	1.232	1.222	1.218	1.317	1.244	1.265	1.421	1.387

4.2.3.3.2 NY Site 2680

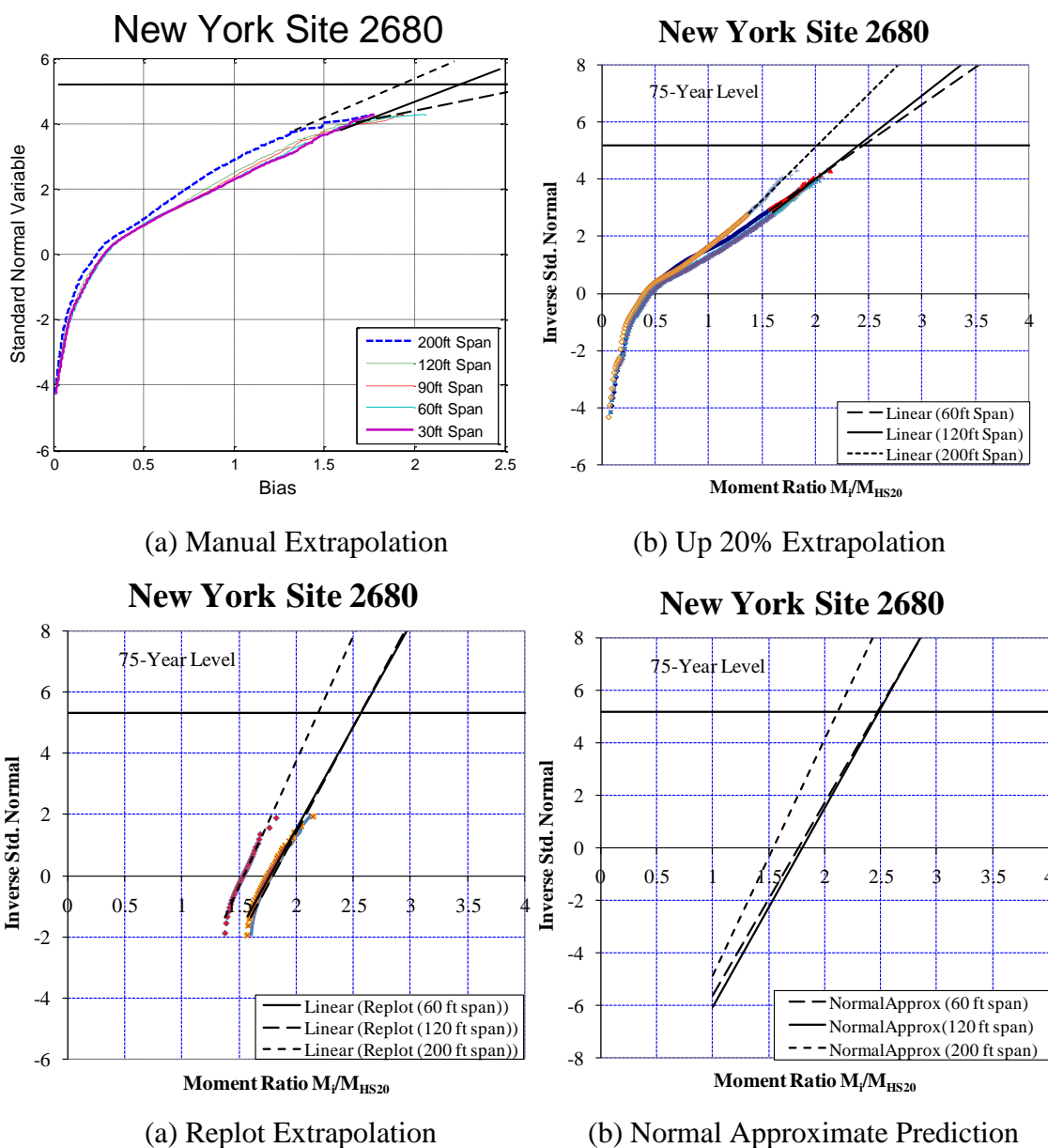


Figure 4.37 Extrapolation of Long Term Load Effects for Site 2680

Table 4.23 Extrapolation Summary for Site 2680 with respect to HL-93 Moment

Span Length	Lane 1		Lane 2		Lane 3		All Lanes Together		
	All trucks	Up 20%	All trucks	Up 20%	All trucks	Up 20%	U20 Extend	Replot	Normal Approx
60	1.774	1.844	1.500	1.572	1.497	1.503	1.823	1.887	1.799
120	1.393	1.402	1.214	1.221	1.440	1.388	1.514	1.544	1.492
200	1.218	1.189	1.051	0.961	1.241	1.168	1.280	1.229	1.263

4.2.3.3.3 NY Site 8382

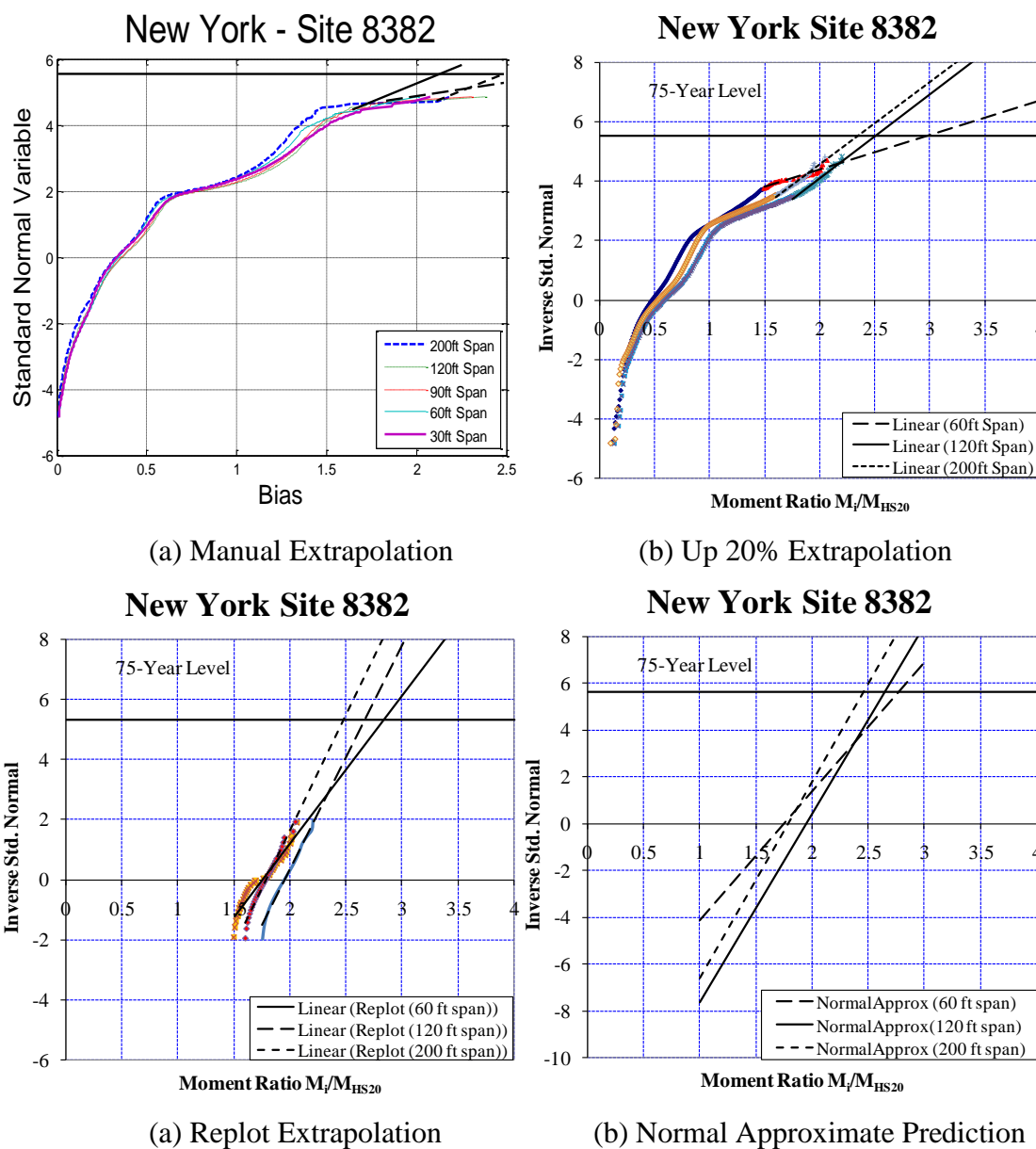


Figure 4.38 Extrapolation of Long Term Load Effects for Site 8382

Table 4.24 Extrapolation Summary for Site 8382 with respect to HL-93 Moment

Span Length	Lane 1		Lane 2		Lane 3		All Lanes Together		
	All trucks	Up 20%	All trucks	Up 20%	All trucks	Up 20%	U20 Extend	Replot	Normal Approx
60	2.217	2.379	1.461	1.447	1.242	1.265	1.478	1.569	2.198
120	1.573	1.547	1.182	1.189	1.101	1.117	1.279	1.289	1.577
200	1.493	1.456	1.141	1.072	1.021	0.977	1.237	1.173	1.497

4.2.3.3.4 NY Site 9631

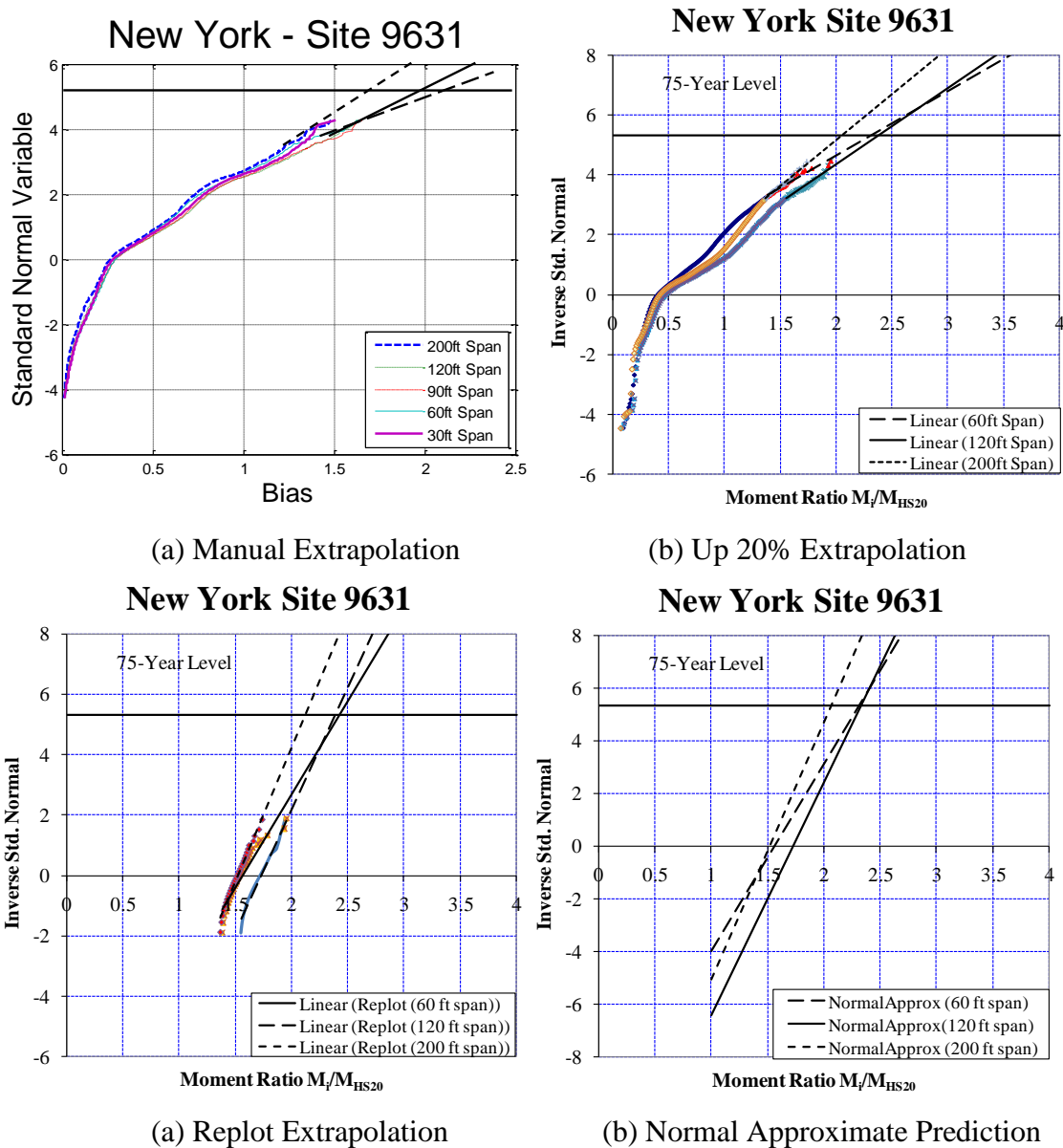


Figure 4.39 Extrapolation of Long Term Load Effects for Site 9631

Table 4.25 Extrapolation Summary for Site 9631 with respect to HL-93 Moment

Span Length	Lane 1		Lane 2		Lane 3		All Lanes Together		
	All trucks	Up 20%	All trucks	Up 20%	All trucks	Up 20%	U20 Extend	Replot	Normal Approx
60	1.418	1.559	1.375	1.283	1.516	1.465	1.724	1.869	1.706
120	1.251	1.139	1.336	1.180	1.551	1.475	1.449	1.487	1.477
200	1.150	0.982	1.180	1.006	1.358	1.273	1.236	1.253	1.291

4.3 Proposed Live Load Models

Although WIM data from many states have been investigated and their site specific live load effects were studied, the live load models that proposed to be used in this study were developed based on NCHRP and FHWA Weigh-in-Motion (WIM) database which contains 32 different WIM sites. For each site, approximately 1 year (12 months) of data was collected and the data was processed using a filtering program to remove the errors and permit vehicles.

A live load model for reliability analysis is defined with two parameters using HL-93 vehicle model as a reference. These two parameters are the bias factor and the coefficient of variation. The bias factor is a mean to nominal ratio between the mean maximum load effect (i.e. moment and shear) from WIM data and load effect from HL-93 Load. Moreover, due to the fact that the traffic volumes are different for different states and locations, the load models were developed for various traffic volume levels (i.e. Average Daily Truck Traffic (ADTT) of 1000, 2500, 5000, 10000). The following sections presents the live load models used in this study for various ADTT levels and various serviceability limit states.

4.3.1 Proposed Live Load Model for Service I Limit State

Since the reinforced concrete deck was designed for axle load, the axle load data including steering axle collected from 32 different WIM sites was processed using a quality control filtering routine. The cumulative distribution functions (CDF) of processed axle load data was plotted on a normal probability paper. The vertical coordinate of maximum axle weight, z_{\max} , is calculated using the equation below:

$$z_{\max} = \Phi^{-1}(1/N) \quad \text{Eq. 4.1}$$

where Φ^{-1} is the inverse standard normal distribution function and N is the total number of trucks.

Therefore, the total number of trucks for the same duration is different for different ADTT, which resulted in different probability as well as different inverse normal distribution value. For illustration purposes, the number of trucks N, probabilities, corresponding inverse normal distribution values z for corresponding return time period ranging from 1 day to 75 years for ADTT equals to 5000 are shown in Table 4.26. Figure 4.40 shows the extrapolation levels for different return period on Normal Probability Paper. The extrapolation level for different return period is the target line for extrapolation and the basis of finding the statistics for various parameters.

Table 4.27 shows the live load models for each ADTT at various return periods. However, to be consistent with previous WIM study, the live load models were converted to the format of ratio between the live load effect from WIM data and the one from HL-93 load. Table 4.28 and Table 4.29 show the bias factors and CoVs for various ADTT and various return periods.

Table 4.26 Time Period and Corresponding Inverse Normal Coordinate (ADTT= 5,000)

Time Period	Number of Trucks (N)	Probability (1/N)	Inverse Normal (z)
75 years	136,875,000	7.E-09	5.67
50 years	91,250,000	1.E-08	5.60
5 years	9,125,000	1.E-07	5.18
1 year	1,825,000	5.E-07	4.87
6 months	900,000	1.E-06	4.73
2 months	300,000	3.E-06	4.50
1 month	150,000	7.E-06	4.35
2 weeks	70,000	1.E-05	4.18
1 day	5,000	2.E-04	3.54

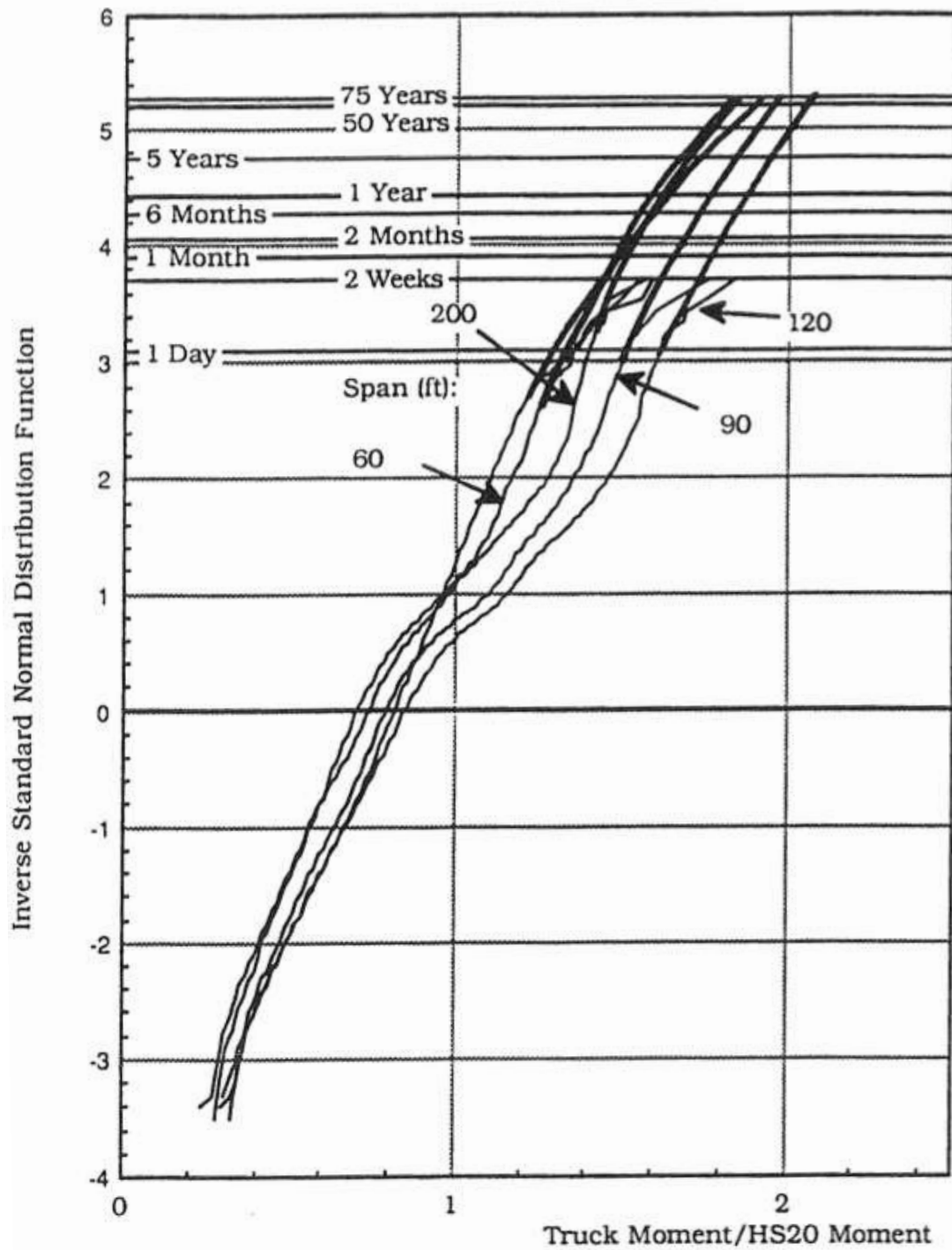


Figure 4.40 Extrapolation Levels for Different Return Periods (Nowak, 1999)

Table 4.27 Statistics for Various ADTTs at Various Return Periods

<i>Time period</i>	<i>ADTT=1000</i>		<i>ADTT=2500</i>		<i>ADTT=5000</i>		<i>ADTT=10000</i>	
	Mean* [kip]	CoV [%]	mean [kip]	CoV [%]	mean [kip]	CoV [%]	mean [kip]	CoV [%]
1 day	32.0	16.5	34.4	16.1	35.6	15.8	36.9	15.5
2 weeks	37.6	15.5	39.8	15.3	41.3	14.9	42.4	14.7
1 month	39.2	15.0	41.0	14.5	42.2	14.3	43.5	14.1
2 months	40.7	14.6	42.4	14.2	43.3	13.9	44.2	13.7
6 months	42.4	14.2	43.8	13.9	44.9	13.6	45.6	13.3
1 year	43.9	13.7	45.0	13.3	45.5	13.2	46.7	13.1
5 years	45.9	13.2	46.7	12.9	47.2	12.7	47.8	12.6
50 years	47.3	12.7	48.1	12.6	48.4	12.5	48.8	12.3
75 years	47.6	12.4	48.4	12.3	48.5	12.2	49.0	12.1
100 years	40.3	12.2	40.9	12.1	41.1	12.0	41.5	11.9

*Mean in this table is the actual mean plus 1.5 times of standard deviation.

Table 4.28 Live Load Bias Factors for Various ADTTs (Service I)

<i>ADTT</i>	<i>1 day</i>	<i>2 weeks</i>	<i>1 month</i>	<i>2 months</i>	<i>6 months</i>	<i>1 year</i>	<i>5 years</i>	<i>50 years</i>	<i>75 years</i>
1000	1.00	1.18	1.22	1.27	1.32	1.37	1.44	1.48	1.49
2500	1.08	1.24	1.28	1.32	1.37	1.41	1.46	1.50	1.51
5000	1.11	1.29	1.32	1.35	1.40	1.42	1.47	1.51	1.52
10000	1.15	1.32	1.36	1.38	1.43	1.46	1.49	1.53	1.53

Table 4.29 Coefficient of Variation (COV) for Various ADTTs (Service I)

<i>ADTT</i>	<i>1 day</i>	<i>2 weeks</i>	<i>1 month</i>	<i>2 months</i>	<i>6 months</i>	<i>1 year</i>	<i>5 years</i>	<i>50 years</i>	<i>75 years</i>
1000	0.17	0.16	0.15	0.15	0.14	0.14	0.13	0.13	0.12
2500	0.16	0.15	0.15	0.14	0.14	0.13	0.13	0.13	0.12
5000	0.16	0.15	0.14	0.14	0.14	0.13	0.13	0.13	0.12
10000	0.16	0.15	0.14	0.14	0.13	0.13	0.13	0.12	0.12

4.3.2 Proposed Live Load Model for Regular Truck Load for Service III Limit State

Similar to the live load model shown in Section 4.3.1 for Service I limit state, the same procedure was followed to develop the live load model for regular truck load for Service III limit state except the moment due to whole truck was considered instead of load effect due to axle load. The live load statistical information was derived from NCHRP and FHWA Weigh-in-Motion (WIM) database. The live load bias factors and coefficient of variation for various average daily truck traffic (ADTT) (1000, 2500, 5000, and 10000) are summarized in Table 4.38 through Table 4.41. Based on NCHRP 368 Report, The mean and standard deviation of dynamic load factor was taken as 0.09 and 0.05, respectively.

Table 4.30 Live Load Bias Factors for Various Span Lengths (ADTT=1000)

<i>Span (ft)</i>	<i>1 day</i>	<i>2 weeks</i>	<i>1 month</i>	<i>2 months</i>	<i>6 months</i>	<i>1 year</i>	<i>5 years</i>	<i>50 years</i>	<i>75 years</i>
30 ft	0.99	1.14	1.18	1.23	1.27	1.33	1.37	1.38	1.4
60 ft	0.89	1.13	1.19	1.26	1.31	1.34	1.37	1.42	1.42
90 ft	0.9	1.13	1.19	1.26	1.3	1.32	1.36	1.41	1.42
120 ft	0.89	1.14	1.19	1.23	1.27	1.31	1.35	1.41	1.41
200 ft	0.81	1.06	1.11	1.16	1.22	1.25	1.3	1.35	1.36
300 ft	0.71	0.97	1.01	1.07	1.15	1.18	1.24	1.28	1.29

Table 4.31 Coefficient of Variation (COV) for Various Span Lengths (ADTT=1000)

<i>Span (ft)</i>	<i>1 day</i>	<i>2 weeks</i>	<i>1 month</i>	<i>2 months</i>	<i>6 months</i>	<i>1 year</i>	<i>5 years</i>	<i>50 years</i>	<i>75 years</i>
30 ft	0.28	0.21	0.16	0.16	0.14	0.16	0.15	0.07	0.07
60 ft	0.2	0.16	0.16	0.18	0.16	0.16	0.13	0.12	0.11
90 ft	0.17	0.18	0.17	0.17	0.12	0.1	0.08	0.08	0.07
120 ft	0.17	0.16	0.16	0.13	0.11	0.1	0.1	0.11	0.1
200 ft	0.19	0.16	0.14	0.14	0.15	0.16	0.15	0.14	0.13
300 ft	0.19	0.16	0.14	0.14	0.15	0.16	0.15	0.14	0.13

Table 4.32 Live Load Bias Factors for Various Span Lengths (ADTT=2500)

<i>Span (ft)</i>	<i>1 day</i>	<i>2 weeks</i>	<i>1 month</i>	<i>2 months</i>	<i>6 months</i>	<i>1 year</i>	<i>5 years</i>	<i>50 years</i>	<i>75 years</i>
30 ft	1.03	1.2	1.23	1.28	1.31	1.34	1.36	1.4	1.4
60 ft	0.97	1.2	1.25	1.31	1.34	1.35	1.39	1.42	1.43
90 ft	0.97	1.2	1.26	1.29	1.32	1.36	1.39	1.43	1.43
120 ft	0.98	1.2	1.22	1.27	1.31	1.34	1.38	1.43	1.44
200 ft	0.9	1.12	1.16	1.21	1.25	1.28	1.33	1.37	1.37
300 ft	0.8	1.02	1.09	1.12	1.18	1.21	1.26	1.29	1.29

Table 4.33 Coefficient of Variation (COV) for Various Span Lengths (ADTT=2500)

<i>Span (ft)</i>	<i>1 day</i>	<i>2 weeks</i>	<i>1 month</i>	<i>2 months</i>	<i>6 months</i>	<i>1 year</i>	<i>5 years</i>	<i>50 years</i>	<i>75 years</i>
30 ft	0.19	0.19	0.16	0.15	0.15	0.14	0.12	0.08	0.07
60 ft	0.18	0.17	0.17	0.17	0.17	0.14	0.12	0.11	0.1
90 ft	0.17	0.17	0.17	0.11	0.1	0.09	0.08	0.07	0.07
120 ft	0.17	0.15	0.12	0.09	0.1	0.09	0.1	0.11	0.1
200 ft	0.19	0.14	0.15	0.15	0.16	0.15	0.16	0.15	0.14
300 ft	0.19	0.14	0.15	0.15	0.16	0.15	0.16	0.15	0.14

Table 4.34 Live Load Bias Factors for Various Span Lengths (ADTT=5000)

<i>Span (ft)</i>	<i>1 day</i>	<i>2 weeks</i>	<i>1 month</i>	<i>2 months</i>	<i>6 months</i>	<i>1 year</i>	<i>5 years</i>	<i>50 years</i>	<i>75 years</i>
30 ft	1.08	1.24	1.28	1.31	1.34	1.35	1.39	1.41	1.42
60 ft	1.02	1.26	1.32	1.34	1.35	1.38	1.4	1.44	1.45
90 ft	1.03	1.24	1.3	1.32	1.34	1.38	1.4	1.44	1.45
120 ft	1.03	1.24	1.26	1.31	1.32	1.36	1.41	1.46	1.46
200 ft	0.95	1.16	1.2	1.23	1.28	1.31	1.34	1.39	1.4
300 ft	0.84	1.06	1.13	1.16	1.23	1.25	1.28	1.3	1.31

Table 4.35 Coefficient of Variation (COV) for Various Span Lengths (ADTT=5000)

<i>Span (ft)</i>	<i>1 day</i>	<i>2 weeks</i>	<i>1 month</i>	<i>2 months</i>	<i>6 months</i>	<i>1 year</i>	<i>5 years</i>	<i>50 years</i>	<i>75 years</i>
30 ft	0.18	0.17	0.15	0.15	0.14	0.12	0.13	0.11	0.11
60 ft	0.17	0.17	0.18	0.17	0.14	0.14	0.12	0.1	0.1
90 ft	0.17	0.16	0.11	0.1	0.08	0.09	0.08	0.09	0.08
120 ft	0.17	0.13	0.09	0.1	0.09	0.09	0.11	0.12	0.11
200 ft	0.17	0.14	0.14	0.14	0.15	0.15	0.15	0.15	0.15
300 ft	0.17	0.14	0.14	0.14	0.15	0.15	0.15	0.15	0.15

Table 4.36 Live Load Bias Factors for Various Span Lengths (ADTT=10000)

<i>Span (ft)</i>	<i>1 day</i>	<i>2 weeks</i>	<i>1 month</i>	<i>2 months</i>	<i>6 months</i>	<i>1 year</i>	<i>5 years</i>	<i>50 years</i>	<i>75 years</i>
30 ft	1.17	1.29	1.32	1.35	1.35	1.37	1.39	1.4	1.41
60 ft	1.09	1.31	1.34	1.35	1.37	1.39	1.41	1.45	1.46
90 ft	1.11	1.29	1.32	1.35	1.37	1.39	1.42	1.45	1.47
120 ft	1.13	1.27	1.29	1.32	1.34	1.38	1.42	1.46	1.47
200 ft	1.02	1.22	1.25	1.28	1.3	1.32	1.37	1.4	1.4
300 ft	0.91	1.16	1.2	1.23	1.25	1.27	1.3	1.31	1.32

Table 4.37 Coefficient of Variation (COV) for Various Span Lengths (ADTT=10000)

<i>Span (ft)</i>	<i>1 day</i>	<i>2 weeks</i>	<i>1 month</i>	<i>2 months</i>	<i>6 months</i>	<i>1 year</i>	<i>5 years</i>	<i>50 years</i>	<i>75 years</i>
30 ft	0.22	0.18	0.16	0.16	0.13	0.11	0.08	0.06	0.06
60 ft	0.16	0.17	0.16	0.14	0.13	0.13	0.11	0.11	0.1
90 ft	0.18	0.11	0.1	0.09	0.09	0.08	0.08	0.08	0.08
120 ft	0.2	0.09	0.09	0.09	0.08	0.1	0.11	0.11	0.11
200 ft	0.17	0.16	0.16	0.15	0.15	0.15	0.15	0.15	0.14
300 ft	0.17	0.16	0.16	0.15	0.15	0.15	0.15	0.15	0.14

4.3.3 Proposed Live Load Model for Permit Vehicle Load for Service III Limit State

Permit trucks are an essential part of the truck population. Therefore, in addition to Service III limit state for regular trucks, Service III limit state for permit trucks is also investigated in this study.

The live load statistical information was derived based on Louisiana violation vehicle data and NJDOT issued permit vehicle data. As shown in Figure 4.41, the ratio of actual (i.e., weighed) GVW and allowable (i.e., permitted) GVW is taken as 1.0 and the coefficient of variation is 10%. Additionally, based on data from 47465 permit vehicle records issued by NJDOT, the live load bias factors and coefficient of variation for various average daily truck traffic (ADTT) (1000, 2500, 5000, and 10000) are summarized in Table 4.38 through Table 4.41. Based on NCHRP 368 Report, the mean and standard deviation of dynamic load factor for heavy trucks was taken as 0.09 and 0.05, respectively.

Table 4.38 Live Load Bias Factors for Various Span Lengths (ADTT=1000)

<i>Span (ft)</i>	<i>1 day</i>	<i>2 weeks</i>	<i>1 month</i>	<i>2 months</i>	<i>6 months</i>	<i>1 year</i>	<i>5 years</i>	<i>50 years</i>	<i>75 years</i>
30 ft	1.10	1.32	1.38	1.44	1.51	1.56	1.67	1.81	1.83
60 ft	1.00	1.32	1.40	1.48	1.59	1.65	1.80	1.99	2.03
90 ft	0.94	1.21	1.28	1.34	1.43	1.48	1.61	1.77	1.79
120 ft	0.94	1.15	1.20	1.25	1.32	1.36	1.46	1.59	1.61
200 ft	1.10	1.40	1.48	1.55	1.66	1.72	1.86	2.04	2.08
300 ft	1.30	1.60	1.68	1.75	1.86	1.92	2.06	2.24	2.28

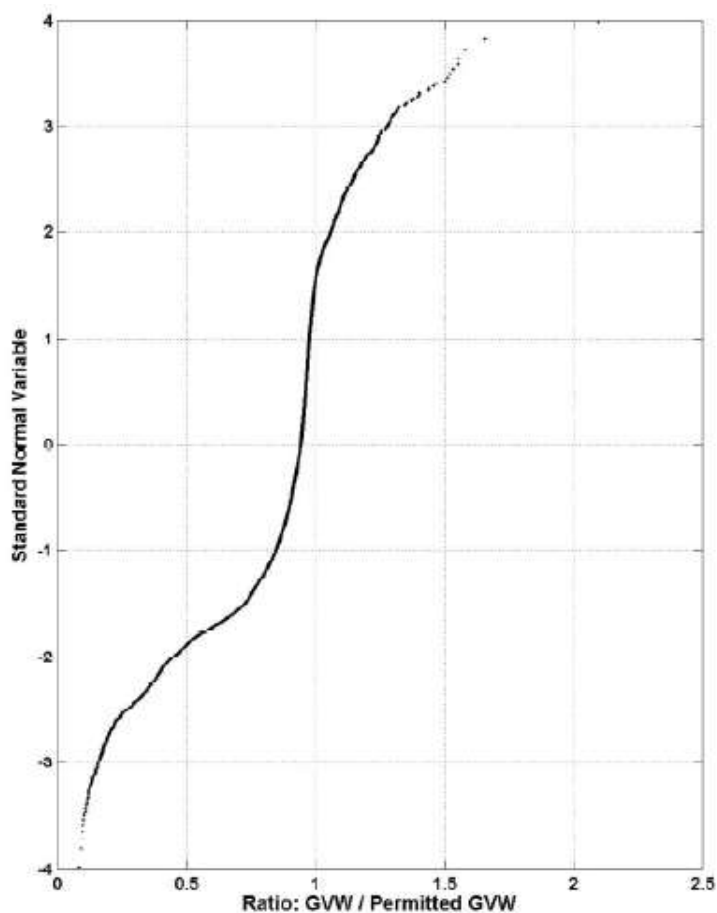


Figure 4.41 Ratio of GVW and Permitted GVW for Permit Vehicles

Table 4.39 Live Load Bias Factors for Various Span Lengths (ADTT=2500)

<i>Span (ft)</i>	<i>1 day</i>	<i>2 weeks</i>	<i>1 month</i>	<i>2 months</i>	<i>6 months</i>	<i>1 year</i>	<i>5 years</i>	<i>50 years</i>	<i>75 years</i>
30 ft	1.18	1.40	1.45	1.50	1.58	1.62	1.72	1.86	1.88
60 ft	1.12	1.42	1.50	1.57	1.67	1.74	1.88	2.07	2.10
90 ft	1.04	1.29	1.36	1.41	1.50	1.55	1.67	1.83	1.85
120 ft	1.01	1.21	1.26	1.31	1.38	1.42	1.51	1.64	1.66
200 ft	1.21	1.50	1.57	1.64	1.74	1.80	1.93	2.11	2.15
300 ft	1.41	1.70	1.77	1.84	1.94	2.00	2.13	2.31	2.35

Table 4.40 Live Load Bias Factors for Various Span Lengths (ADTT=5000)

<i>Span (ft)</i>	<i>1 day</i>	<i>2 weeks</i>	<i>1 month</i>	<i>2 months</i>	<i>6 months</i>	<i>1 year</i>	<i>5 years</i>	<i>50 years</i>	<i>75 years</i>
30 ft	1.24	1.45	1.50	1.55	1.62	1.67	1.77	1.90	1.92
60 ft	1.20	1.49	1.57	1.63	1.74	1.80	1.94	2.12	2.15
90 ft	1.11	1.35	1.41	1.47	1.55	1.61	1.72	1.87	1.90
120 ft	1.07	1.26	1.31	1.35	1.42	1.46	1.55	1.67	1.69
200 ft	1.29	1.57	1.64	1.70	1.80	1.86	1.99	2.17	2.20
300 ft	1.49	1.77	1.84	1.90	2.00	2.06	2.19	2.37	2.40

Table 4.41 Live Load Bias Factors for Various Span Lengths (ADTT=10000)

<i>Span (ft)</i>	<i>1 day</i>	<i>2 weeks</i>	<i>1 month</i>	<i>2 months</i>	<i>6 months</i>	<i>1 year</i>	<i>5 years</i>	<i>50 years</i>	<i>75 years</i>
30 ft	1.30	1.50	1.55	1.60	1.67	1.71	1.81	1.94	1.96
60 ft	1.28	1.56	1.63	1.70	1.80	1.86	1.99	2.17	2.20
90 ft	1.18	1.41	1.47	1.52	1.60	1.66	1.77	1.92	1.94
120 ft	1.12	1.30	1.35	1.39	1.46	1.50	1.59	1.71	1.73
200 ft	1.37	1.63	1.70	1.76	1.86	1.92	2.04	2.22	2.25
300 ft	1.57	1.83	1.90	1.96	2.06	2.12	2.24	2.42	2.45

Table 42 presents the summary of crack width information for various span lengths. The column of “ M_i/M_{HL-93} ” shows the ratio of applied moment to HL-93 moment when the crack width reaches 0.008 in or 0.016 in. It is observed that limited number of permit loads have caused extensive cracks. It is also observed that permit loads have more effect on the prestressed concrete girders with short span length. However, overall, only few (0.01% to 3.26%) permit trucks have caused cracks with width more than 0.016 in.

Table 42. Summary of Crack Width information for Various Span Lengths

Span Length	Crack Width of 0.008 in			Crack Width of 0.016 in		
	M_i/M_{HL-93}	Count	Percentage	M_i/M_{HL-93}	Count	Percentage
60 ft	0.818	14089	29.68%	1.048	1548	3.26%
80 ft	0.967	2181	4.59%	1.175	351	0.74%
100 ft	1.332	94	0.20%	1.766	4	0.01%
120 ft	1.575	8	0.02%	1.998	3	0.01%
140 ft	1.886	4	0.01%	2.305	3	0.01%

CHAPTER 5

DETERIORATION MODEL OF BRIDGE ELEMENTS

As more and more infrastructures are approaching the limit of their service life, the deterioration of structure gains more attention from the owner, user, as well as designers and engineers. However, current design specifications do not integrate the deterioration of structure into design process. During the calibration of AASHTO LRFD Design Specification for ultimate limit state, the long term effect of live load was considered by extrapolating to different return periods including 75 years. However, the deterioration of the resistance capacity was not included. Thus, it is needed to evaluate the structural deterioration on reliability of structures.

There are two most common causes of deterioration of concrete structures: Freezing-Thaw and corrosion of steel caused by chloride penetration. The deterioration of structure can be divided into two categories: deterioration of section and deterioration of strength. In this study, the time dependent properties of section and strength were investigated and discussed. Hereafter the deterioration models for structural resistance were developed for reinforced concrete decks at Service I limit state and prestressed concrete girders at Service III limit state. These deterioration models will be used in the reliability analysis in Chapter 6.

5.1 Deterioration Model for Prestressed Concrete Girders for Service III Limit State

Although overall prestressed concrete girder bridges have demonstrated good performance in adverse exposure conditions, due to extensive chlorides and moisture, tendon failures were found in several post-tensioned concrete girder bridges, such as Niles Channel, Mid-bay, and Bob Graham Sunshine Skyway bridges in Florida (FDOT, 1999, 2001^a, and 2001^b) and Varina-Enon Bridge in Virginia (Hansen 2007). Therefore, an appropriate deterioration model could help to better understand the effect of deterioration of reliability and serviceability of structure.

The deterioration of prestressed concrete girders contains three major components: time-variant of concrete strength, losses of concrete section, and strength losses in prestressing strands. Since the losses of concrete section has not been fully studied and minor loss of concrete section has no significant effect on the resistance of the structure, only time-variant property of concrete strength and strength losses in prestressing strands were considered in this study.

Due to the shrinkage and creep effects over time, the strength of concrete varies. The prediction equation developed by ACI Committee 209 is adopted in this study:

$$(f_c')_t = \frac{t}{a + \beta t} (f_c')_{28} \quad \text{Eq. 5.1}$$

where,

a = Empirical constant depends on the cement type and curing method

β = Empirical constant depends on the cement type and curing method

t = Age of concrete in days

$(f_c')_{28}$ = 28-day compressive strength of concrete

$(f_c')_t$ = Compressive strength of concrete at age of t.

The ultimate tensile strength of prestressing tendons for post-tensioned concrete girder at long term is predicted using the equation developed by Pillai, et. al (2010) as shown below:

$$(f_{pu})_t = f_{pu} \times \left[\theta_1 - \theta_3 h_{tWD} - \theta_4 \ln(h_{\%sCl^-}) h_{tWD} + \sigma \varepsilon \right] \quad \text{Eq. 5.2}$$

where,

θ_i = Model parameters, $\theta_1=0.9463$, $\theta_2=1.0333$, $\theta_3=0.3567$, and $\theta_4=0.0285$.

f_{pu} = Ultimate strength of prestressing tendon

$(f_{pu})_t$ = Ultimate strength of prestressing tendon in t years

$$h_{tWD} = \left(\frac{\text{Wet-time in a year}}{12(\text{months})} \right) \times \text{Total years}$$

$$h_{\%sCl^-} = \frac{\%Cl^- \text{ in the water inside the tendon}}{\text{Saturated Chloride Solution}}$$

σ = Standard deviation of model error, 0.0350

ε = Standard normal Variable~Normal (0,1)

The long term losses of prestressing strength ($\Delta f_{pSD} + \Delta f_{pCD} + \Delta f_{pR2} - \Delta f_{pSS}$) after deck placement are predicted using the provisions in AASHTO LRFD Bridge Design Specification 2012, as shown below:

Due to Shrinkage of Girder Concrete

$$\Delta f_{pSD} = \varepsilon_{bdf} E_p K_{df} \quad \text{Eq. 5.3}$$

for which:

$$K_{df} = \frac{1}{1 + \frac{E_p}{E_{ci}} \frac{A_{ps}}{A_c} \left(1 + \frac{A_c e_{pc}^2}{I_c} \right) (1 + 0.7\psi_{bif})} \quad \text{Eq. 5.4}$$

where:

Δf_{pSD} = prestress loss due to shrinkage of girder concrete between time of deck placement and final time

ϵ_{bdf} = shrinkage strain of girder between time of deck placement and final time

K_{df} = transformed section coefficient that accounts for time-dependent interaction between concrete and bonded steel in the section being considered for time period between deck placement and final time

e_{pc} = eccentricity of strands with respect to centroid of composite section

A_c = area of composite section calculated using the gross concrete section properties of the girder and the deck and the deck-to-girder modular ratio

I_c = moment of inertia of composite section calculated using the gross concrete section properties of the girder and the deck and the deck-to-girder modular ratio at service

Due to Creep of Girder Concrete:

$$\Delta f_{pCD} = \frac{E_p}{E_{ci}} f_{cgp} (\psi_{bif} - \psi_{bid}) K_{df} + \frac{E_p}{E_c} \Delta f_{cd} \psi_{bdf} K_{df} \geq 0.0 \quad \text{Eq. 5.5}$$

where:

Δf_{pCD} = prestress loss due to creep of girder concrete between time of deck placement and final time

Δf_{cd} = change in concrete stress at centroid of prestressing strands due to long-term losses between transfer and deck placement, combined with deck weight and superimposed loads

ψ_{bdf} = girder creep coefficient at final time for loading age at deck placement

Due to Relaxation of Prestressing Strands

$$\Delta f_{pR3} = \Delta f_{pR2} \quad \text{Eq. 5.6}$$

where:

Δf_{pR3} = prestress loss due to relaxation of prestressing strands in composite section between time of deck placement and final time

For low-relaxation strands, Δf_{pR2} may be assumed equal to 1.2 KSI

Due to Shrinkage of Deck Concrete

$$\Delta f_{pSS} = \frac{E_p}{E_c} \Delta f_{cdf} K_{df} (1 + 0.7 \psi_{bdf}) \quad \text{Eq. 5.7}$$

for which:

$$\Delta f_{cdf} = \frac{\epsilon_{ddf} A_d E_{cd}}{(1 + 0.7 \psi_{df})} \left(\frac{1}{A_c} + \frac{e_{pc} e_d}{I_c} \right) \quad \text{Eq. 5.8}$$

where:

- Δf_{pss} = prestress loss due to shrinkage of deck composite section
- Δf_{cdf} = change in concrete stress at centroid of prestressing strands due to shrinkage of deck concrete
- ϵ_{ddf} = shrinkage strain of deck concrete between placement and final time
- A_d = area of deck concrete
- E_{cd} = modulus of elasticity of deck concrete
- e_d = eccentricity of deck with respect to the transformed composite section, taken negative in common construction
- Ψ_{df} = creep coefficient of deck concrete at final time due to loading introduced shortly after deck placement.(i.e. overlays, barriers, etc.)

Therefore, the effective stress of prestressing tendon, $(f_{se})_t$, can be calculated using the following equation:

$$(f_{se})_t = f_{si} - (\Delta f_{si})_{st} - (\Delta f_{si})_{lt} \quad \text{Eq. 5.9}$$

where,

f_{si} = initial prestressing stress

$(\Delta f_{si})_{st}$ = short term prestressing losses

$(\Delta f_{si})_{lt}$ = long term prestressing losses, $(\Delta f_{si})_{lt} = \Delta f_{pSD} + \Delta f_{pCD} + \Delta f_{pR2} - \Delta f_{pss}$

The researchers have found that the corrosion of steel would affect the area of steel but not the local ultimate strength of steel (Hanjari (2010), Darmawan and Stewart (2007), and Almusallam (2001)). As shown in Figure 5.1, the degree of corrosion has little effect on ultimate strength of bar.

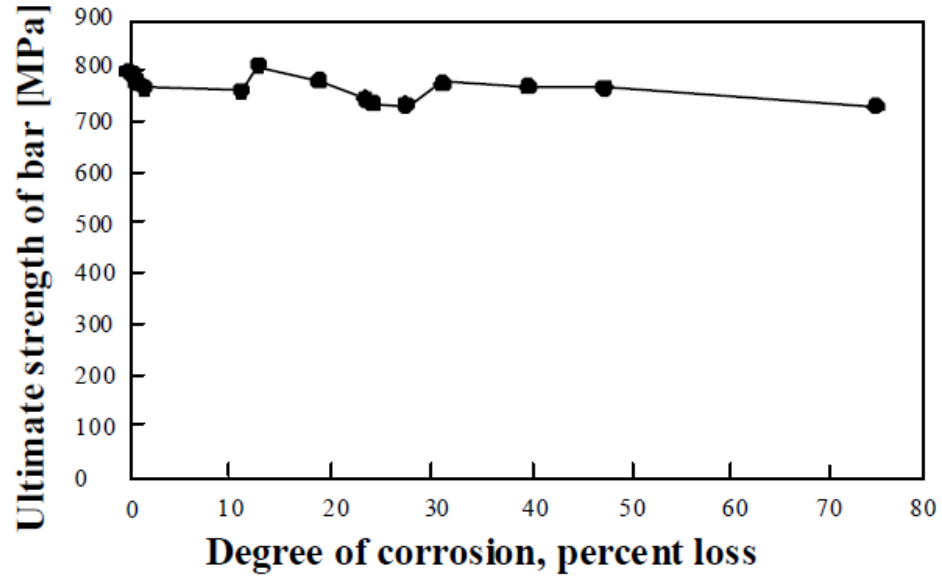


Figure 5.1 Variation of ultimate tensile strength for selected degrees of uniform corrosion of a 6 mm diameter steel bar, from Almusallam (2001)

The time variant area of non-prestressing steel is derived based on study conducted by Akgul and Frangopol (2004), as shown below:

$$(A_s)_t = A_{si} - 0.00497(t - t_{ci}) \quad \text{Eq. 5.10}$$

where,

$(A_s)_t$ = area of non-prestressing steel at t years.

A_{si} = original area of non-prestressing steel

t = year of structure in service in years.

t_{ci} = corrosion initiation time.

Therefore, applying all the time variant parameters, the deterioration model of resistance for prestressed concrete girders at Service III limit state can be expressed as formula below:

$$M_n = A_{ps} ((f_{pu})_t - (\Delta f_{ps1})_t - \Delta f_{ps2}) d_p + (A_s)_t f_s d_s - \frac{1}{6} f_{ct} b_0 c^2 + \frac{(c - h_f)^2 (b_0 - b)}{2c} f_{ct} \left(\frac{c + 2h_f}{3} \right) + \frac{(c - h_f - h_{f1})^2 (b - b_w)}{2c} f_{ct} \left(\frac{c + 2h_f + 2h_{f1}}{3} \right) \quad \text{Eq. 5.11}$$

where,

$(A_s)_t$ = area of non-prestressing steel at t years.

$(\Delta f_{ps1})_t$ = prestress losses at t years after prestressing.

Δf_{ps2} = change of stress in prestressing tendons after applying live load.

5.2 Deterioration Model for Reinforced Concrete Decks at Service I Limit State

Similar to deterioration model for prestressed concrete girders at Service III limit state, utilizing the time variant parameters listed in section 5.1, the deterioration model for resistance of reinforced concrete decks designed using empirical design method at Service I limit state can be expressed as:

$$f_s = \frac{w_c E_s}{2\beta \sqrt{d_c^2 + \left(\frac{s}{2}\right)^2}} + \frac{3 \left((A_s)_t E_s + 3E_c b d + \sqrt{(A_s)_t^2 E_s^2 + 2(A_s)_t E_s E_c b d} \right)}{d(4(A_s)_t E_s + 9E_c b d)(A_s)_t} \cdot \frac{M_r 0.85 (f'_c)_t d_1^2}{4}$$

Eq. 5.12

Although the resistance model for reinforced concrete decks designed using traditional design method does not involve any time variant parameters, the time variant parameters are included in the limit state function when calculating the stress due to the live load. Therefore, the deterioration of the concrete and steel will still be considered in the reliability analysis presented in section 6.1.5.

CHAPTER 6

STRUCTURAL RELIABILITY ANALYSIS

Structural reliability analysis method is a rational, probability based approach to identify the safety or probability of failure of a structure at various limit states. The term limit state is used to define the boundary between “success” and “failure” for various aspects of structural performance. The limit state is usually expressed as a function $g(X)$ with random variables $X = (X_1, X_2, \dots, X_N)$. Mathematically, if $g(X)$ is greater than 0, the structure is safe. If $g(X)$ is less than 0, the structure is failed for this limit state. The limit state can be used to represent various performance criteria in structural engineering. These performance criteria or limit state can be categorized into three main categories: ultimate, serviceability, and fatigue. Ultimate limit states are the limit states that represent the ultimate capacity of the structure in terms of flexure, shear, torsion, or buckling. The failure of ultimate limit state such as exceeding of the moment carrying capacity of the structure, crushing of concrete in compression, or buckling of the web is fatal to the structure and will result in unrecovered damage if the limit state is violated. In contrast, serviceability limit states are the limit states covers various aspects of serviceability of structure such as cracking, deflection, vibration, etc. Failure of serviceability limit states might not result in catastrophic consequences directly. However, Serviceability limit states related to stress, deformation, and crack under regular service conditions are essential to the performance, human experience, and

durability of structure. Finally, fatigue limit states are the limit states that related to the deterioration and damage of the structure under repeated loading. Failure of fatigue limit states can be occurrence of fatigue cracks, high stresses in secondary members, and damage to welded connections. The term “failure” is an expression of exceedance of limit state and the consequence of failure varies depending on the limit state.

Due to the nature of the limit state which always composes two basic variables, resistance and load, the limit state function is expressed as:

$$g(R, Q) = R - Q \quad \text{Eq. 6.1}$$

where R represents the resistance of the structure and Q represents the load effect that relates to the specific limit state. The limit state boundary is defined as a scenario whereby the resistance is numerically equal to the load effects, and is expressed by $g = 0$. When the resistance exceeds the load effect, $R > Q$, the structure is safe, otherwise the limit state is violated.

In previous sections, the resistance models and live load models were developed for various serviceability limit states. Moreover, the deterioration models were also developed for structural resistance in Chapter 5. In this Chapter, the limit state will be formulated and the structural reliability analysis procedure will be assembled for each serviceability limit state. Applying the resistance models, load models, and deterioration models developed in previous Chapters, structural reliability analysis will be performed and target reliability indices will be proposed hereafter for each serviceability limit state. Then various design provisions will be modified to improve the level and uniformity of reliability for each limit state. In addition, the effect of structural deterioration on reliability of structure will be evaluated.

6.1 Reinforced Concrete Decks Designed using Traditional Method (Service I Limit State)

In this section, utilizing the resistance model and load model developed in previous Chapters, the structural analysis will be performed for reinforced concrete decks designed using traditional method for Service I limit state. Section 6.1.1 shows the representative data base used in this study. Section 6.1.2 shows the assembled limit state function. Section 6.1.3 shows the reliability index of current practice and proposed target reliability index for this limit state. Section 6.1.4 shows reliability analysis results of various scenarios by changing design provisions. Finally, section 6.1.5 presents the effect of structural deterioration on reliability of reinforced concrete deck at Service I limit state.

6.1.1 Reinforced Concrete Deck Database

A set of reinforced concrete decks was designed using traditional equivalent strip method based on AASHTO LRFD Bridge Design Specification. These designed bridge decks covered various girder spacing and deck thickness. Table 6.1 presents the summary information of 15 designed bridge decks. This set of bridge decks will be used as a representative database in this study.

Table 6.1 Information of 15 Bridge Decks that Designed using AASHTO Traditional

Deck Design Method

Deck Group#	Girder Spacing (ft.)	Deck Thickness (in.)	Reinforcement	
			Positive	Negative
1	6	7	#5@11.5 in	#5@9 in
		7.5	#5@12.5 in	#5@9.5 in
		8	#5@13 in	#5@10.5 in
2	8	7.5	#5@11 in	#5@7.5 in
		8	#5@11.5 in	#5@8.5 in
		8.5	#5@12 in	#5@9 in
3	10	8	#5@10 in	#5@7 in
		8.5	#5@10.5 in	#5@7.5 in
		9	#5@11 in	#5@8 in
		9.5	#5@11.5 in	#5@8.5 in
4	12	8	#6@10.5 in	#6@7.5 in
		8.5	#6@11 in	#6@8 in
		9	#6@11.5 in	#6@8.5 in
		9.5	#6@12 in	#6@9 in
		10	#6@12.5 in	#6@9.5 in

6.1.2 Limit State Function for Reinforced Concrete Decks Designed using Traditional Method

The limit state function was formulate as $G = R - Q$, where G is the limit state function, R is the resistance, and Q is the load. For this study, the limit state of crack control in reinforced concrete members is formulated in terms of the stress in the reinforcing steel, f_s .

The reliability-based approach to analysis of crack width limit states is based on calculating a reliability index beta, β . Reliability is the probability that a structure will not fail to perform its intended function. The structural parameters are treated as random variables rather than deterministic values. This approach accounts for the many sources of uncertainty that are inherent in structural design. The Monte Carlo method is a technique used to generate some results numerically based on obtained statistical information without doing any physical testing.

The reliability index, β , is based on the mean and standard deviation of a limit state function, G , which is defined as $G = R - Q$. The Monte Carlo method, $\beta = \mu G / \sigma G$ where μG = mean of the function G and σG = standard deviation of the function G .

To approach crack width limit states using the reliability approach, the function G will be written in terms of the steel reinforcement stress, f_s , since research has shown this to be the most important parameter influencing crack widths. Moreover, the steel stress can be obtained directly from the applied load using equilibrium equation and strain compatibility. Thus, the limit state function would appear as such:

$$G = f_{s(\text{resistance})} - f_{s(\text{load})} \quad \text{Eq. 6.2}$$

The resistance R was derived as shown in section 3.1. The load, Q , in the reliability approach was derived based on principles of reinforced concrete analysis. Force and moment equilibrium were used to solve for two unknowns: 1) steel stress, f_s , and 2) depth of the neutral axis, C_{na} . The maximum moment is calculated based on HL-93 loading and the moment resistance is $A_s f_s (d - C_{na} / 3)$ where A_s is the area of steel reinforcement and f_y is the yield stress of the steel.

From force equilibrium and assuming linear concrete stress distribution, the compression force for a beam with rectangular section having a width b and depth d , is calculated as follows:

$$C_c = \frac{f_c C_{na} b}{2} = \frac{\epsilon_c E_c C_{na} b}{2} \quad \text{Eq. 6.3}$$

Moreover, assuming linear elastic behavior, the tension force carried by the steel reinforcement can be calculated as follows:

$$T = A_s f_s = A_s E_s \epsilon_s \quad \text{Eq. 6.4}$$

Using the force and moment equilibrium equations to solve for f_s the following equation is obtained:

$$f_s = \frac{3 \left(A_s E_s + 3 E_c b d + \sqrt{A_s^2 E_s^2 + 2 A_s E_s E_c b d} \right) M_{\max}}{d (4 A_s E_s + 9 E_c b d) A_s} \quad \text{Eq. 6.5}$$

where:

A_s = area of steel reinforcement, in²

E_s = elastic modulus of steel, psi

E_c = elastic modulus of concrete, psi

b = width of concrete section, in

d = effective depth of concrete section, in

P = applied load, lbs

L = span length, in

M_{\max} = The maximum live load moment due to HL-93 Loading.

Thus, the limit state function, $G = R - Q$, can be written as follows:

$$G = \frac{w_c E_s}{2\beta \sqrt{\left(d_c^2 + \left(\frac{s}{2} \right)^2 \right)}} - \frac{3 \left(A_s E_s + 3 E_c b d + \sqrt{A_s^2 E_s^2 + 2 A_s E_s E_c b d} \right) M_{\max}}{d (4 A_s E_s + 9 E_c b d) A_s} \quad \text{Eq. 6.6}$$

6.1.3 Target Reliability Index for Service I Limit State (Traditional Deck)

In this section, the reliability level of current practice was evaluated using the bridge database presented in section 6.1.1. In the design as well as the reliability analysis, the crack width is specified as 0.017 in and 0.01275 in for Class 1 and Class 2 exposure condition specified in AASHTO LRFD article 5.7.3.4, respectively. The reliability analysis was performed using the resistance and load model developed in Chapter 3 and Chapter 4. The reliability indices for various ADTT's and exposure conditions are summarized in Table 6.2.

Table 6.2 Summary of Reliability Indices for Concrete Decks Designed according to
AASHTO LRFD Design Specification 2012

ADTT	Positive Moment Region		Negative Moment Region	
	Reliability Index (Class I)	Reliability Index (Class II)	Reliability Index (Class I)	Reliability Index (Class II)
1000	2.44	1.54	2.37	1.77
2500	1.95	1.07	1.79	1.27
5000	1.66	0.85	1.61	1.05
10000	1.39	0.33	1.02	0.5
Avg.	1.86	0.95	1.70	1.15
Max.	2.44	1.54	2.37	1.77
Min.	1.39	0.33	1.02	0.50
Std Dev.	0.45	0.50	0.56	0.53
COV	24%	53%	33%	46%

It should be noted that even though the design for Class II resulted in more reinforcement than for the case in Class I Exposure, the reliability index for Class II is lower than that for Class I due to the more stringent limiting criteria (narrower crack width)

The target reliability indices for the serviceability limit states from various codes were discussed in previous sections. The European Code selected a target reliability

index for irreversible service limit state equal to 2.9 and 1.5 for 1-year and 50 years periods, respectively, whereas the ISO 2394-1998 specified target reliability indices for reversible and irreversible limit states as 0 and 1.5 for life time duration, respectively. These are general values that do not take into account the specific nature of the limit state being considered or the limiting criteria. For example, for reinforced concrete members, the limiting criteria is the width of the cracks. For the same component, the reliability index will depend on the prescribed crack width limit. Limited contacts with individuals, who contributed to the development of the European Code indicated that the reliability indices listed for service limit states were not supported by research, rather they were based on general consensus.

Current practices rarely result in the deck positive moment reinforcement being controlled by the Service I limit state due to the small bottom concrete cover. When Strength I limit state is considered, more positive moment reinforcement is typically required than by Service I. The additional reinforcement will result in actual reliability indices for positive moment region higher than those shown in Table 6.3.

For the negative moment region, the design is often controlled by the Service I limit state. Thus, the reliability indices shown for the negative moment region in Table 6.3 are considered representative of the actual reliability indices that would be calculated when all limit states, including Strength I, are considered in the analysis.

Therefore, it is recommended that the Target reliability index be based on the reliability index for the negative moment region. Since the Class II case is the more common case for decks, the reliability index for Class II will be used as the basis for selecting the target reliability index. The reliability index for Class I will be assumed to

represent relaxation of the base requirements. Table 6.3 shows the inherent and proposed target reliability indices for the negative moment region of decks designed for the current AASHTO LRFD Specifications.

Table 6.3 Reliability Indices of Existing Bridges based on 1-year return period

<i>ADTT</i>	<i>Reliability Index</i>			
	<i>Current Practice (Class I, Negative)</i>	<i>Current Practice (Class II, Negative)</i>	<i>Target β (Class I, Negative)</i>	<i>Target β (Class II, Negative)</i>
1000	2.37	1.77	1.6	1.0
2500	1.79	1.27		
5000	1.61	1.05		
10,000	1.02	0.50		

6.1.4 Reliability analysis results for Service I Limit State

6.1.4.1 Class 1 Exposure Condition (Maximum Crack Width of 0.017 in)

Figure 6.1 and Figure 6.2 present the reliability indices for various bridge decks designed using a live load factor of 1.0 over one year period, which reflected the reliability level of current design. It can be observed that the average reliability index is around 2.44 and 2.37 for positive and negative moment regions, respectively.



Figure 6.1 Reliability Indices of Various Bridge Decks Designed Using 1.0 Live Load Factor over 1 Year Returning Period (ADTT=1000), Positive Moment Region.



Figure 6.2 Reliability Indices of Various Bridge Decks Designed Using 1.0 Live Load Factor over 1 Year Returning Period (ADTT=1000), Negative Moment Region.

Figure 6.3 and Figure 6.4 present the reliability indices for an ADTT of 2500. It can be observed that the average reliability index is around 1.95 and 1.79 for positive and negative moment regions, respectively.

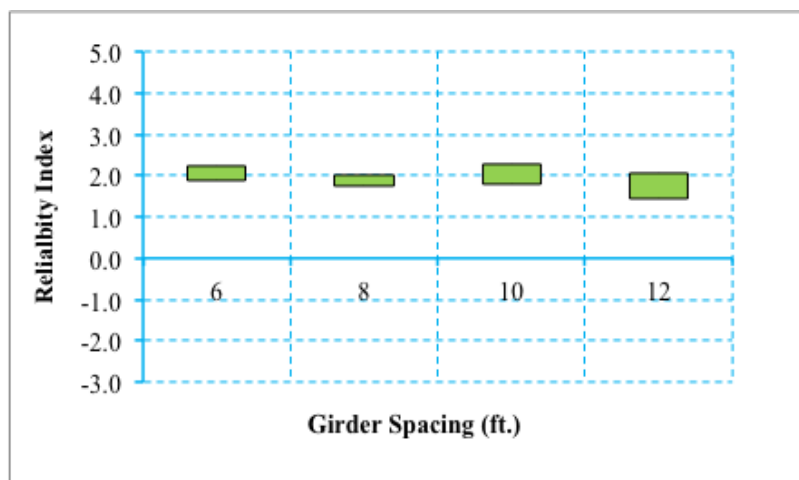


Figure 6.3 Reliability Indices of Various Bridge Decks Designed Using 1.0 Live Load Factor over 1 Year Returning Period (ADTT=2500), Positive Moment Region.

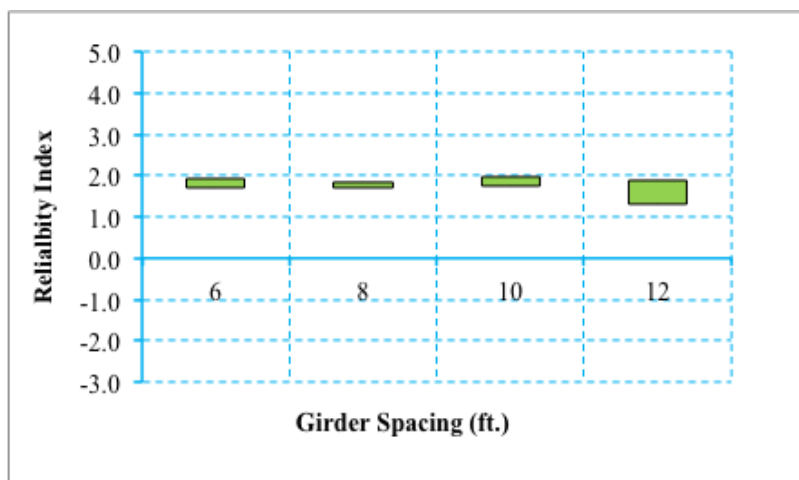


Figure 6.4 Reliability Indices of Various Bridge Decks Designed Using 1.0 Live Load Factor over 1 Year Returning Period (ADTT=2500), Negative Moment Region.

Figure 6.5 and Figure 6.6 present the reliability indices for various bridge decks designed using a live load factor of 1.0 over one year period for an ADTT of 5000. It can be observed that the average reliability index is around 1.66 and 1.61 for positive and negative moment region, respectively.



Figure 6.5 Reliability Indices of Various Bridge Decks Designed Using 1.0 Live Load Factor over 1 Year Returning Period (ADTT=5000), Positive Moment Region.



Figure 6.6 Reliability Indices of Various Bridge Decks Designed Using 1.0 Live Load Factor over 1 Year Returning Period (ADTT=5000), Negative Moment Region.

Figure 6.7 and Figure 6.8 presents the reliability indices for various bridge decks designed using a live load factor of 1.0 over one year period for an ADTT of 10000. It can be observed that the average reliability index is around 1.39 and 1.02 for positive and negative moment regions, respectively.



Figure 6.7 Reliability Indices of Various Bridge Decks Designed Using 1.0 Live Load Factor over 1 Year Returning Period (ADTT=10000), Positive Moment Region.



Figure 6.8 Reliability Indices of Various Bridge Decks Designed Using 1.0 Live Load Factor over 1 Year Returning Period (ADTT=10000), Negative Moment Region.

6.1.4.2 Class 2 Exposure Condition (Maximum Crack Width of 0.01275 in)

Figure 6.9 and Figure 6.10 present the reliability indices for various bridge decks designed using a live load factor of 1.0 over one year period, which corresponds to the

reliability level of current design. It can be observed that the average reliability index is around 1.54 and 1.77 for positive and negative moment regions, respectively.



Figure 6.9 Reliability Indices of Various Bridge Decks Designed Using 1.0 Live Load Factor over 1 Year Returning Period (ADTT=1000), Positive Moment Region

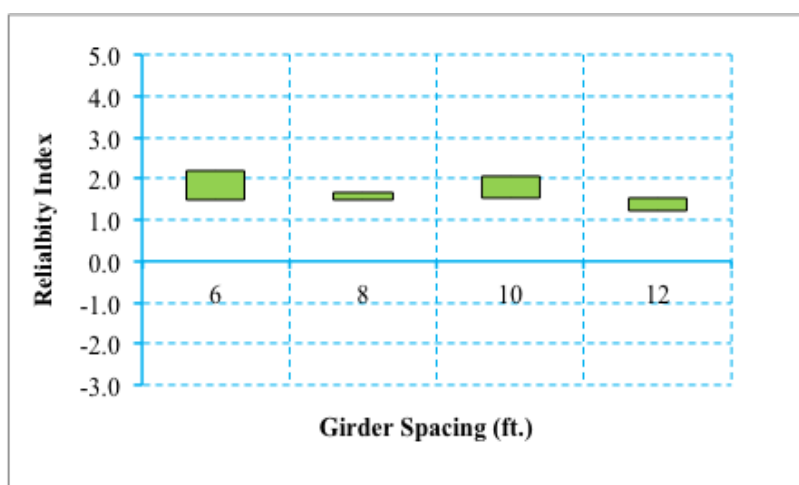


Figure 6.10 Reliability Indices of Various Bridge Decks Designed Using 1.0 Live Load Factor over 1 Year Returning Period (ADTT=1000), Negative Moment Region

Figure 6.11 and Figure 6.12 present the reliability indices for an ADTT of 2500. It can be observed that the average reliability index is around 1.07 and 1.27 for positive and negative moment region, respectively.

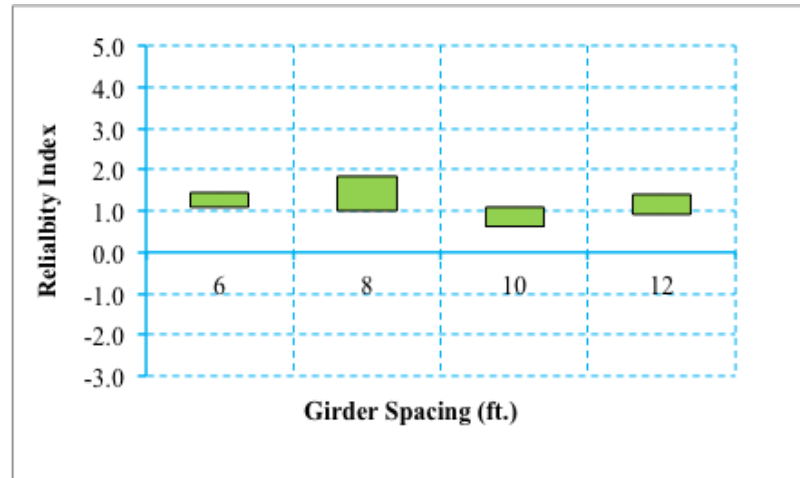


Figure 6.11 Reliability Indices of Various Bridge Decks Designed Using 1.0 Live Load Factor over 1 Year Returning Period (ADTT=2500), Positive Moment Region.

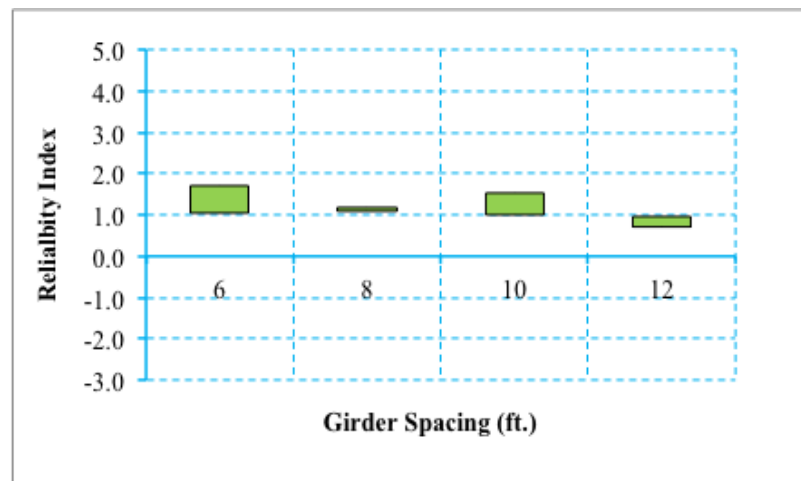


Figure 6.12 Reliability Indices of Various Bridge Decks Designed Using 1.0 Live Load Factor over 1 Year Returning Period (ADTT=2500), Negative Moment Region.

Figure 6.13 and Figure 6.14 present the reliability indices for various bridge decks designed using a live load factor of 1.0 over one year period for an ADTT of 5000. It can be observed that the average reliability index is around 0.85 and 1.05 for positive and negative moment region, respectively.

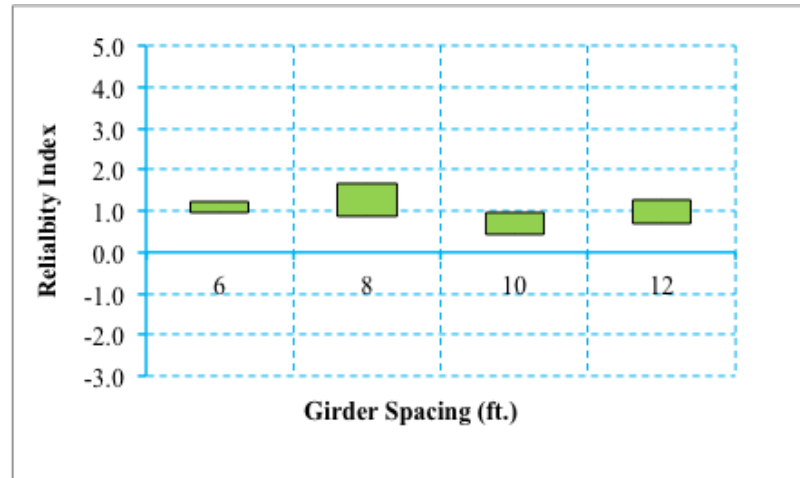


Figure 6.13 Reliability Indices of Various Bridge Decks Designed Using 1.0 Live Load Factor over 1 Year Returning Period (ADTT=5000), Positive Moment Region.

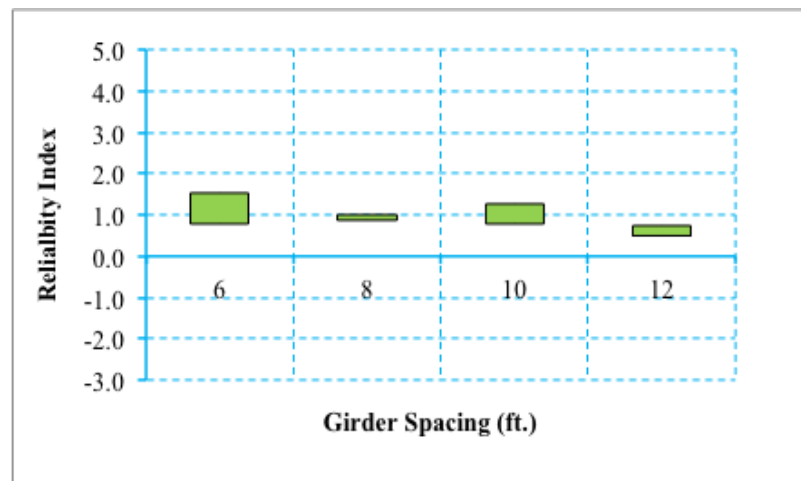


Figure 6.14 Reliability Indices of Various Bridge Decks Designed Using 1.0 Live Load Factor over 1 Year Returning Period (ADTT=5000), Negative Moment Region.

Figure 6.15 and Figure 6.16 present the reliability indices of various bridge decks designed using a 1.2 live load factor over one year period. It can be observed that the average reliability index is 1.61 and 2.2 for positive and negative moment regions for 1-year duration, respectively, which are higher than the target reliability index.

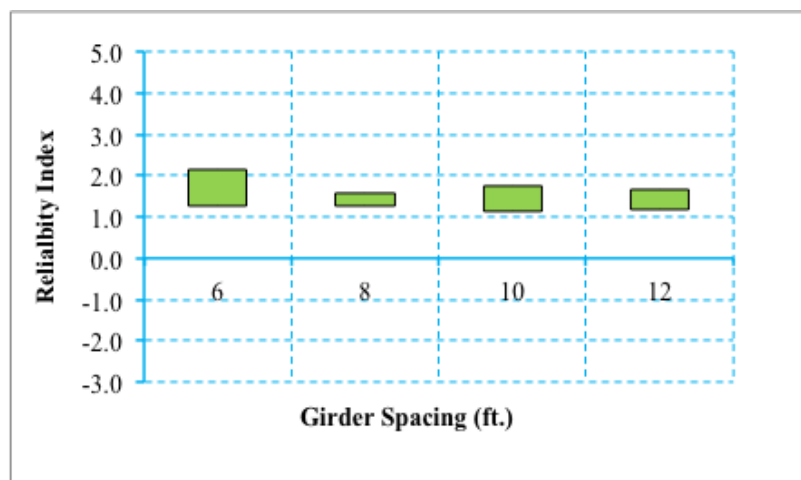


Figure 6.15 Reliability Indices of Various Bridge Decks Designed Using 1.2 Live Load Factor over 1 Year Return Period (ADTT=5000), Class II Exposure Condition, Positive Moment Region.



Figure 6.16 Reliability Indices of Various Bridge Decks Designed Using 1.2 Live Load Factor over 1 Year Return Period (ADTT=5000), Class II Exposure Condition, Negative Moment Region.

Figure 6.17 and Figure 6.18 presents the reliability indices for various bridge decks designed using a live load factor of 1.0 over one year period for an ADTT of 10000. It

can be observed that the average reliability index is around 0.33 and 0.5 for positive and negative moment region, respectively.

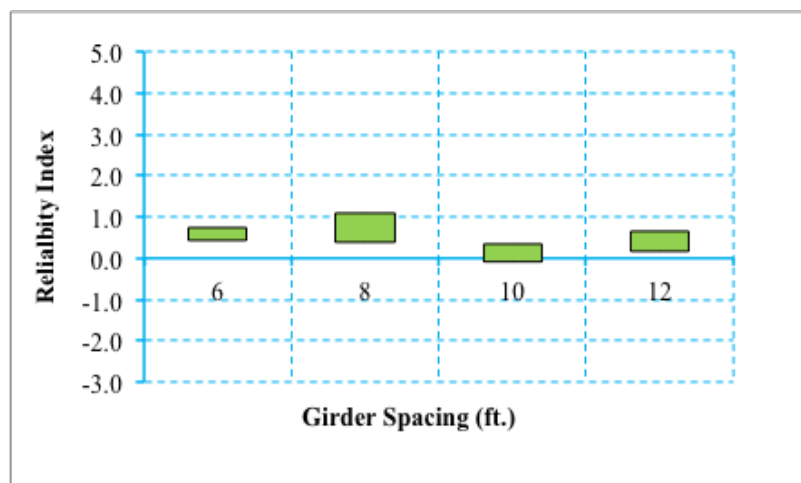


Figure 6.17 Reliability Indices of Various Bridge Decks Designed Using 1.0 Live Load Factor over 1 Year Returning Period (ADTT=10000), Positive Moment Region.

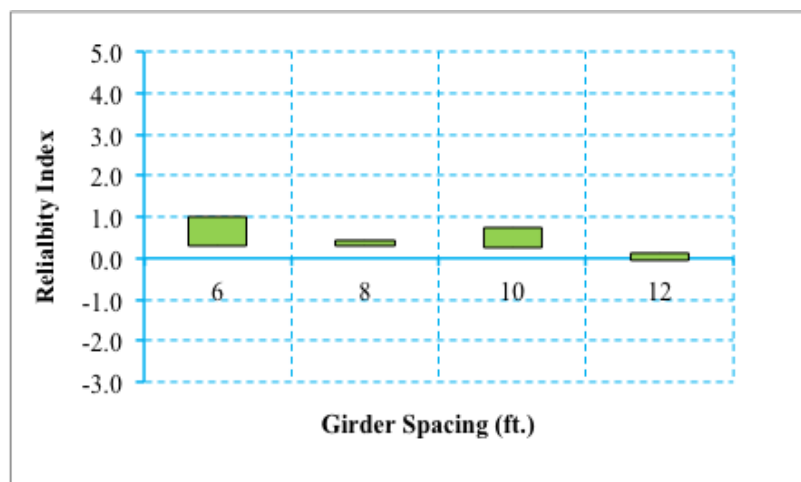


Figure 6.18 Reliability Indices of Various Bridge Decks Designed Using 1.0 Live Load Factor over 1 Year Returning Period (ADTT=10000), Negative Moment Region.

Table 6.4 shows the reliability indices for concrete deck designed with live load factor of 1.0 and 1.2. Although the reliability index of the scenario that ADTT equals to

10000 less than the target reliability indices, no revision in AASHTO Specification is recommended since the current practices satisfy the requirements of target reliability index for most of the scenarios (ADTT of 1000, 2500, and 5000). Therefore, live load factor of 1.0 is still being recommended to be used in AASHTO Specification.

Table 6.4 Summary of Reliability Indices for Concrete Decks Designed with Different Live Load Factors

ADTT	Positive Moment Region			Negative Moment Region		
	Class I	Class II		Class I	Class II	
	$\gamma_{LL}=1.0$	$\gamma_{LL}=1.0$	$\gamma_{LL}=1.2$	$\gamma_{LL}=1.0$	$\gamma_{LL}=1.0$	$\gamma_{LL}=1.2$
1000	2.44	1.54	2.24	2.37	1.77	2.56
2500	1.95	1.07	1.81	1.79	1.27	2.21
5000	1.66	0.85	1.6	1.61	1.05	2.2
10000	1.39	0.33	1.11	1.02	0.5	1.49

6.1.5 Effects of Structural Deterioration on Reliability of Service I Limit State (Traditional Deck)

Although the resistance model for reinforced concrete decks designed using traditional design method does not involve any time variant parameters, the time variant parameters are included in the limit state function when calculating the stress due to the live load. Applying the time variant parameters investigated in Chapter 5, the limit state function can be expressed as formula below:

$$G = \frac{w_c E_s}{2\beta \sqrt{\left(d_c^2 + \left(\frac{s}{2}\right)^2\right)}} - \frac{3\left((A_s)_t E_s + 3E_c bd + \sqrt{(A_s)_t^2 E_s^2 + 2(A_s)_t E_s (E_c)_t bd}\right) M_{\max}}{d(4(A_s)_t E_s + 9(E_c)_t bd)(A_s)_t}$$

Eq. 6.7

where,

$(A_s)_t$ = area of non-prestressing steel at t years.

$(E_c)_t$ = modulus of elasticity of concrete at t years.

In this section, the limit state function shown in Eq. 6.7 that incorporated with deterioration model for reinforced concrete deck at Service I limit state is applied in structural analysis and the effects of structural deterioration on reliability of Service I limit state is evaluated for a concrete deck.

A typical reinforced concrete deck that is designed using traditional design method specified by AASHTO LRFD Bridge Design Specification with thickness of 8 in, girder spacing of 6 ft and ADTT equals to 5000 is analyzed with and without deterioration model applied. As shown in Figure 6.19, it is observed that the deterioration of structure has significant effect on the reliability of structure, especially for long duration.

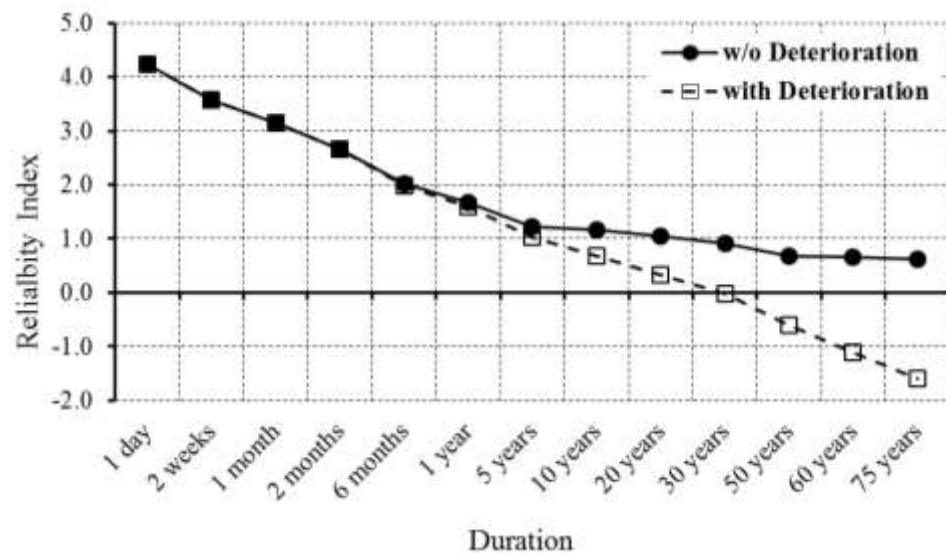


Figure 6.19 reliability index for reinforced concrete deck designed by traditional method
(with and w/o deterioration)

6.2 Reinforced Concrete Decks Designed using Empirical Method (Service I Limit State)

Similar to section 6.1, utilizing the resistance model and load model developed in previous Chapters, the structural analysis will be performed for reinforced concrete decks designed using empirical method for Service I limit state. Section 6.2.1 shows the representative data base used in this study. Section 6.2.2 shows the assembled limit state function. Section 6.2.3 shows the reliability index of current practice and proposed target reliability index for this limit state. Section 6.2.4 shows reliability analysis results of various scenarios by changing design provisions. Finally, section 6.2.5 presents the effect of structural deterioration on reliability of reinforced concrete deck at Service I limit state.

6.2.1 Reinforced Concrete Deck Database

A set of reinforced concrete decks was designed using empirical method based on AASHTO LRFD Bridge Design Specification. These designed bridge decks covered various girder spacing and deck thickness. Table 6.5 presents the summary information of 15 designed bridge decks. This set of bridge decks will be used as a representative database in this study.

Table 6.5 Information of 15 Bridge Decks that Designed using AASHTO Empirical Deck

Design Method

<i>Deck Group#</i>	<i>Girder Spacing (ft.)</i>	<i>Deck Thickness (in.)</i>
1	6	7
		7.5
		8
2	8	7.5
		8
		8.5
3	10	8
		8.5
		9
		9.5
4	12	8
		8.5
		9
		9.5
		10

6.2.2 Limit State Function for Reinforced Concrete Decks Designed using Empirical Method

The limit state function for reinforced concrete decks designed using Empirical Method is the same as the one for concrete deck designed using traditional method except that the resistance is different since arching action is considered for concrete decks designed using empirical method. Based on the resistance and load model developed from previous Chapters, the limit state function for reinforced concrete deck designed using empirical method can be expressed as:

$$G = \frac{w_c E_s}{2\beta \sqrt{\left(d_c^2 + \left(\frac{s}{2}\right)^2\right)}} + \frac{3\left(A_s E_s + 3E_c b d + \sqrt{A_s^2 E_s^2 + 2A_s E_s E_c b d}\right)}{d(4A_s E_s + 9E_c b d)A_s} \cdot \left(\frac{M_r 0.85 f'_c d_1^2}{4} - M_{\max}\right)$$

Eq. 6.8

6.2.3 Target Reliability Index for Service I Limit State (Empirical Deck)

Regardless of the design method that has been used during the design of reinforced concrete deck, the targeted reliability level should be the same for same exposure condition. For instance, when a concrete deck was designed in New Jersey, the same reliability level is expected regardless of design method. Thus, the target reliability indices proposed in section 6.1.3 are used also for the reliability analysis of concrete deck designed using empirical design method.

6.2.4 Reliability analysis results for Service I Limit State

6.2.4.1 Class 1 Exposure Condition (Maximum Crack Width of 0.017 in)

Figure 6.20 and Figure 6.21 present the reliability indices for various bridge decks designed using a live load factor of 1.0 over one year period, which reflected the reliability level of current design. It can be observed that the average reliability index is around 1.24 and 0.13 for positive and negative moment regions, respectively.

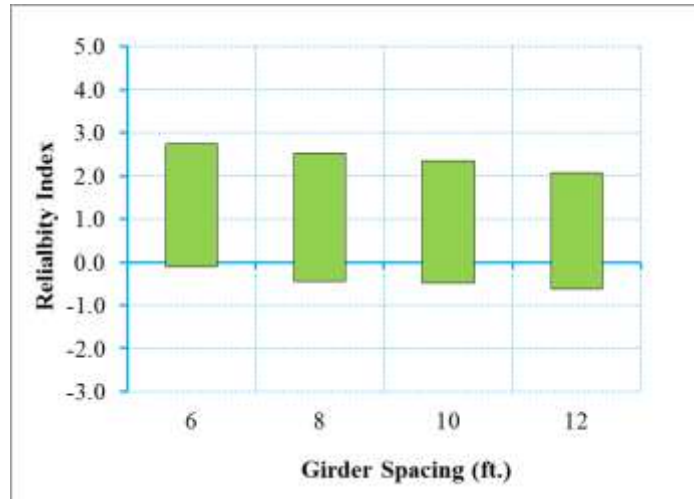


Figure 6.20 Reliability Indices of Various Bridge Decks Designed Using 1.0 Live Load Factor over 1 Year Returning Period (ADTT=1000), Positive Moment Region.

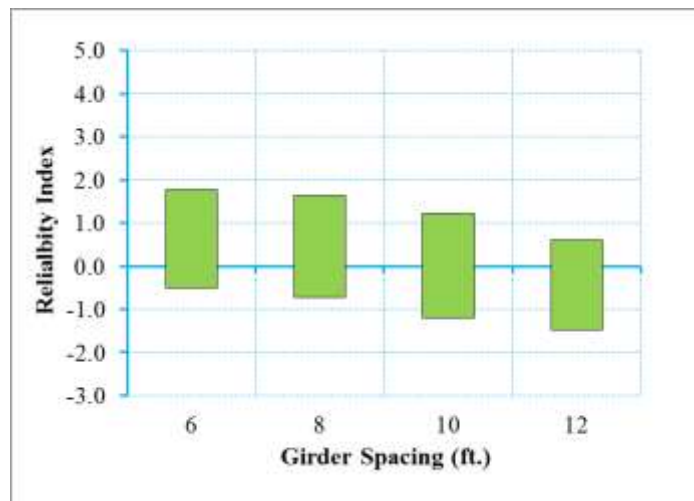


Figure 6.21 Reliability Indices of Various Bridge Decks Designed Using 1.0 Live Load Factor over 1 Year Returning Period (ADTT=1000), Negative Moment Region.

Figure 6.22 and Figure 6.23 present the reliability indices for an ADTT of 2500. It can be observed that the average reliability index is around 0.71 and -0.40 for positive and negative moment regions, respectively.

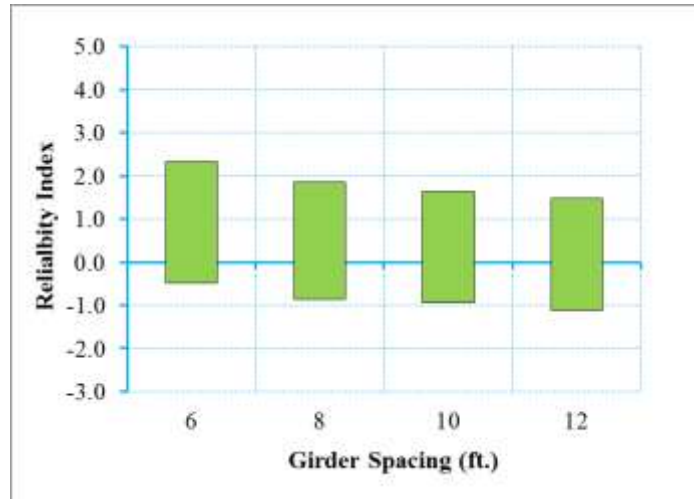


Figure 6.22 Reliability Indices of Various Bridge Decks Designed Using 1.0 Live Load Factor over 1 Year Returning Period (ADTT=2500), Positive Moment Region.

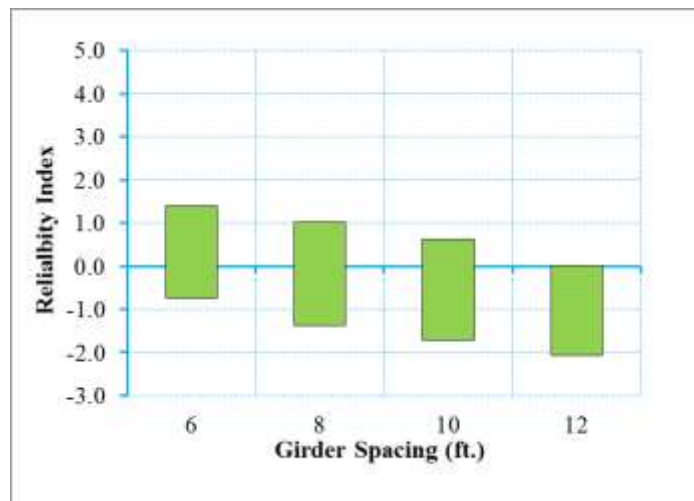


Figure 6.23 Reliability Indices of Various Bridge Decks Designed Using 1.0 Live Load Factor over 1 Year Returning Period (ADTT=2500), Negative Moment Region.

Figure 6.24 and Figure 6.25 present the reliability indices for various bridge decks designed using a live load factor of 1.0 over one year period for an ADTT of 5000. It can be observed that the average reliability index is around 0.57 and -0.51 for positive and negative moment region, respectively.

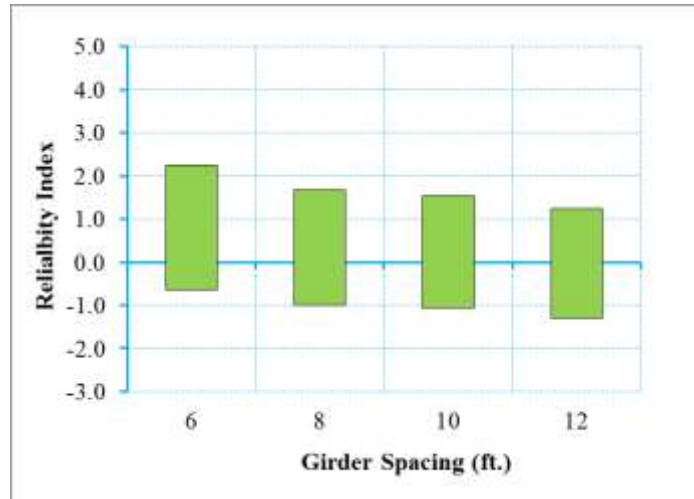


Figure 6.24 Reliability Indices of Various Bridge Decks Designed Using 1.0 Live Load Factor over 1 Year Returning Period (ADTT=5000), Positive Moment Region.

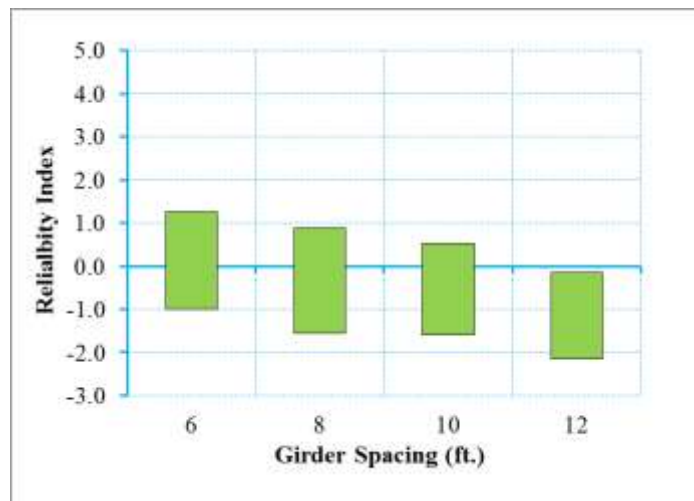


Figure 6.25 Reliability Indices of Various Bridge Decks Designed Using 1.0 Live Load Factor over 1 Year Returning Period (ADTT=5000), Negative Moment Region.

Figure 6.26 and Figure 6.27 presents the reliability indices for various bridge decks designed using a live load factor of 1.0 over one year period for an ADTT of 10000. It can be observed that the average reliability index is around 0.03 and -1.05 for positive and negative moment regions, respectively.

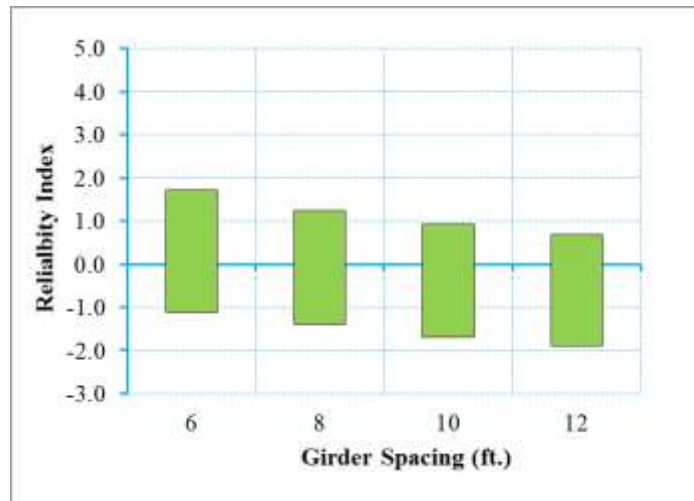


Figure 6.26 Reliability Indices of Various Bridge Decks Designed Using 1.0 Live Load Factor over 1 Year Returning Period (ADTT=10000), Positive Moment Region.

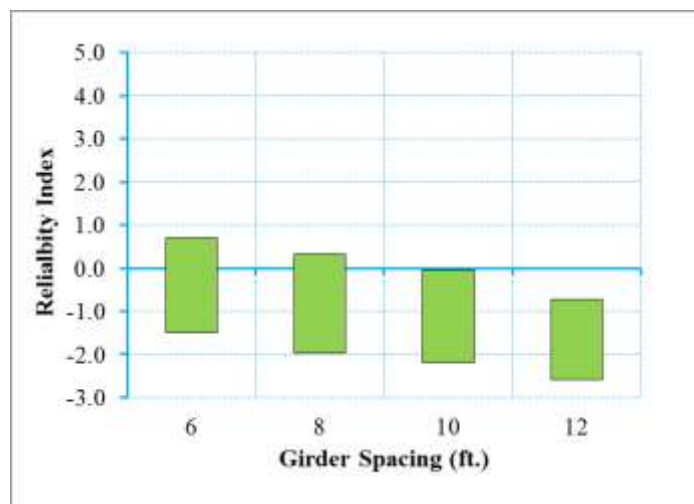


Figure 6.27 Reliability Indices of Various Bridge Decks Designed Using 1.0 Live Load Factor over 1 Year Returning Period (ADTT=10000), Negative Moment Region.

6.2.4.2 Class 2 Exposure Condition (Maximum Crack Width of 0.01275 in)

Figure 6.28 and Figure 6.29 present the reliability indices for various bridge decks designed using a live load factor of 1.0 over one year period, which corresponds to the reliability level of current design. It can be observed that the average reliability index is around 0.39 and -0.53 for positive and negative moment regions, respectively.

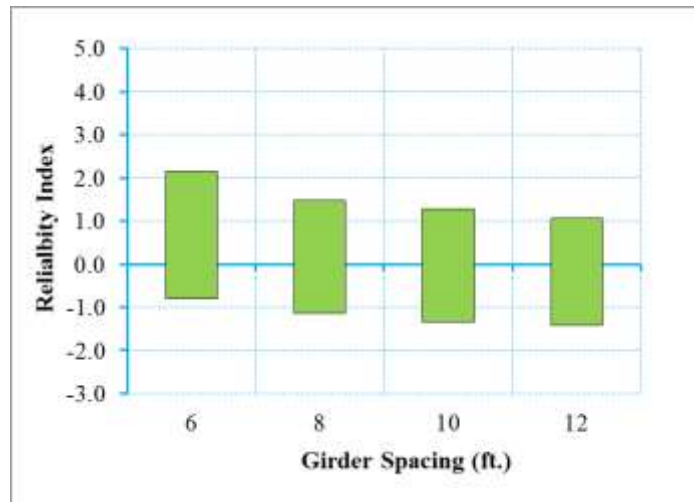


Figure 6.28 Reliability Indices of Various Bridge Decks Designed Using 1.0 Live Load Factor over 1 Year Returning Period (ADTT=1000), Positive Moment Region

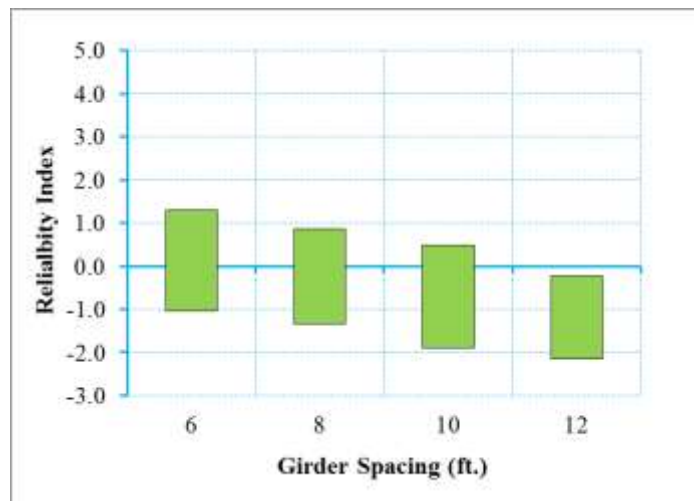


Figure 6.29 Reliability Indices of Various Bridge Decks Designed Using 1.0 Live Load Factor over 1 Year Returning Period (ADTT=1000), Negative Moment Region

Figure 6.30 and Figure 6.31 present the reliability indices for an ADTT of 2500. It can be observed that the average reliability index is around -0.17 and -0.98 for positive and negative moment region, respectively.

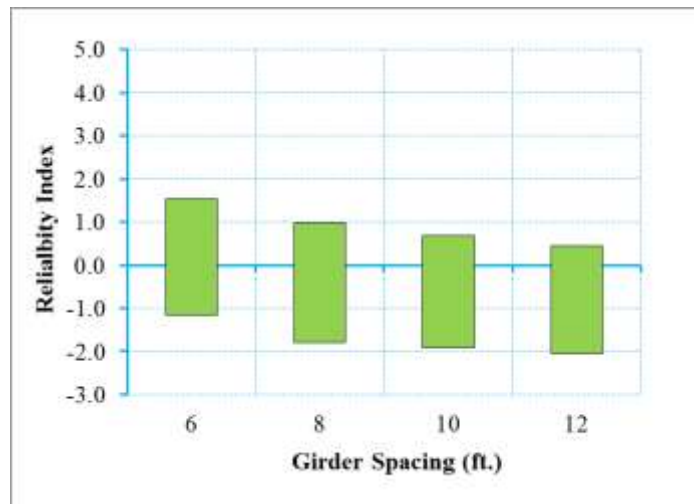


Figure 6.30 Reliability Indices of Various Bridge Decks Designed Using 1.0 Live Load Factor over 1 Year Returning Period (ADTT=2500), Positive Moment Region.

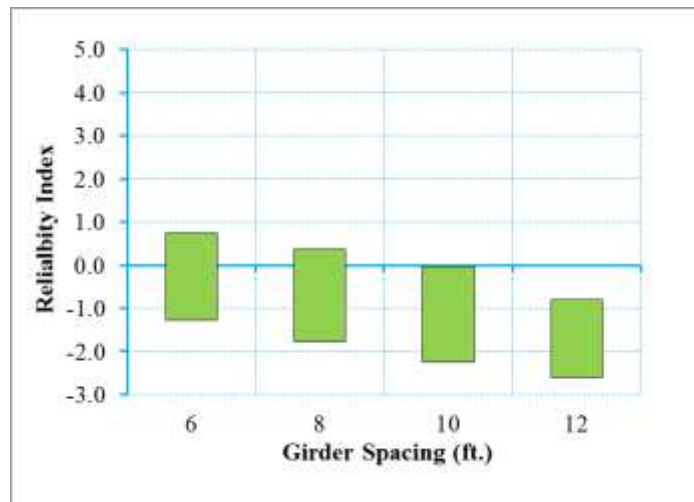


Figure 6.31 Reliability Indices of Various Bridge Decks Designed Using 1.0 Live Load Factor over 1 Year Returning Period (ADTT=2500), Negative Moment Region.

Figure 6.32 and Figure 6.33 present the reliability indices for various bridge decks designed using a live load factor of 1.0 over one year period for an ADTT of 5000. It can be observed that the average reliability index is around -0.29 and -1.15 for positive and negative moment region, respectively.

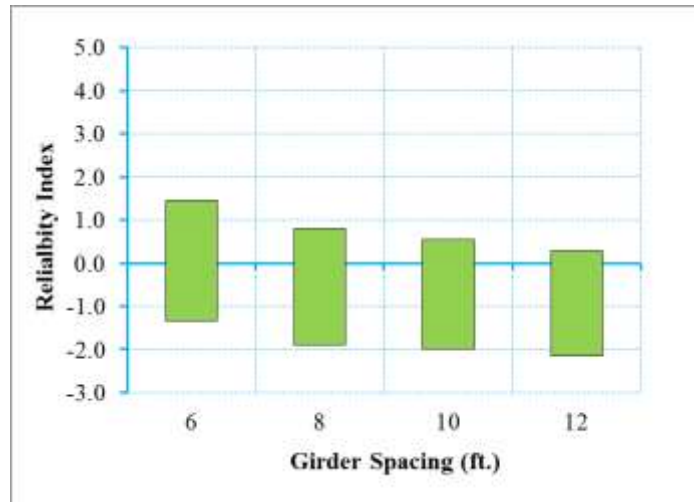


Figure 6.32 Reliability Indices of Various Bridge Decks Designed Using 1.0 Live Load Factor over 1 Year Returning Period (ADTT=5000), Positive Moment Region.

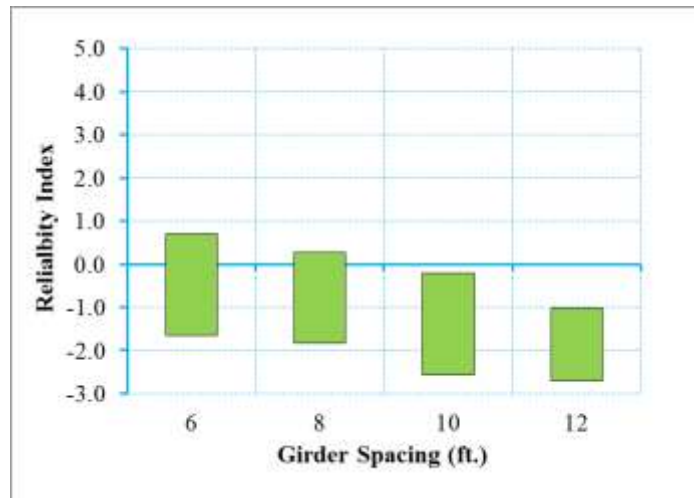


Figure 6.33 Reliability Indices of Various Bridge Decks Designed Using 1.0 Live Load Factor over 1 Year Returning Period (ADTT=5000), Negative Moment Region.

Figure 6.34 and Figure 6.35 presents the reliability indices for various bridge decks designed using a live load factor of 1.0 over one year period for an ADTT of 10000. It can be observed that the average reliability index is around -0.78 and -1.66 for positive and negative moment region, respectively.

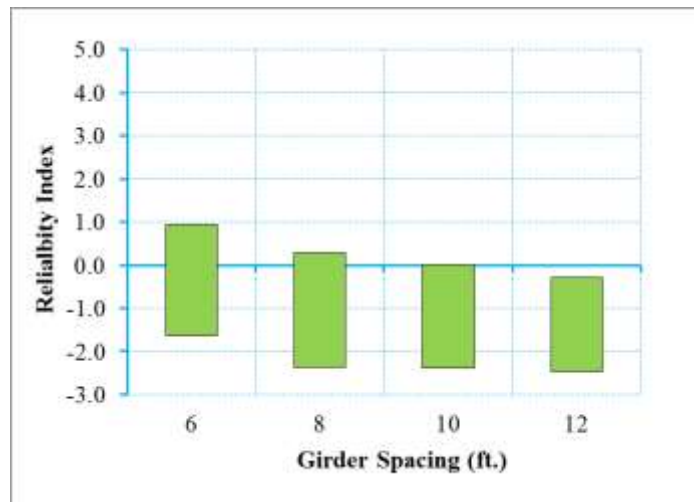


Figure 6.34 Reliability Indices of Various Bridge Decks Designed Using 1.0 Live Load Factor over 1 Year Returning Period (ADTT=10000), Positive Moment Region.

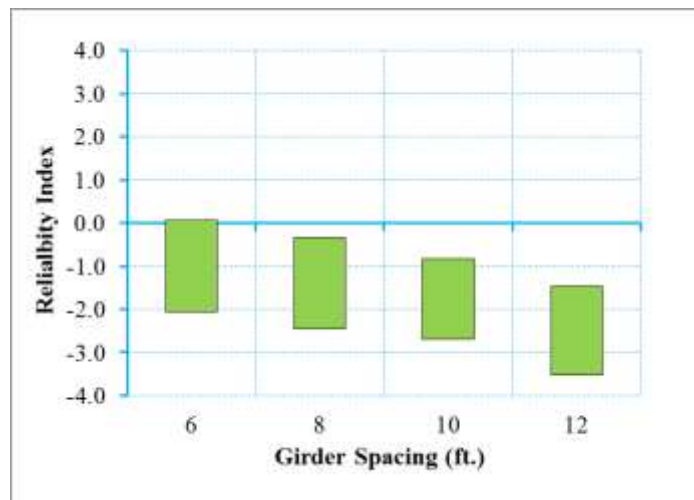


Figure 6.35 Reliability Indices of Various Bridge Decks Designed Using 1.0 Live Load Factor over 1 Year Returning Period (ADTT=10000), Negative Moment Region.

Based on the reliability analysis results, the reliability indices for various ADTTs and exposure conditions are summarized in Table 6.6.

Table 6.6 Summary of Reliability Indices for Concrete Decks Designed using Empirical Design Method

ADTT	<i>Positive Moment Region</i>		<i>Negative Moment Region</i>	
	<i>Reliability Index (Class I)</i>	<i>Reliability Index (Class II)</i>	<i>Reliability Index (Class I)</i>	<i>Reliability Index (Class II)</i>
1000	1.24	0.13	0.39	-0.53
2500	0.71	-0.40	-0.17	-0.98
5000	0.57	-0.51	-0.29	-1.15
10000	0.03	-1.05	-0.78	-1.66
Avg.	0.64	-0.46	-0.21	-1.08
Max.	1.24	0.13	0.39	-0.53
Min.	0.03	-1.05	-0.78	-1.66
Std Dev.	0.50	0.48	0.48	0.47

It is noted that the reliability level of concrete decks designed by empirical method are consistently lower than the decks designed by traditional method, which confirmed the recent study by Schmeckpeper (2009). Schmeckpeper (2009) concluded that the 0.3 percentage of required reinforcement ratio specified by AASHTO Bridge Design Specification is adequate to provide enough strength but much smaller than 0.6 ratio recommended by other researchers for crack control purpose. Therefore, the Empirical deck design method need to be calibrated to provide the same safety level at service I limit state (crack control). The same target reliability index should be applied to both empirical and traditional deck.

In Article C9.7.2.1, AASHTO LRFD Bridge Design Specification 2012, the required area of reinforcement is specified as 0.3% and 0.2% of gross area for positive

and negative moment region, respectively. In order to improve the reliability level of concrete deck designed by empirical method, the provisions are modified as 0.4% and 0.5% of gross area for positive and negative moment regions, respectively. The decks were redesigned using modified empirical design method and the reliability analysis results are presented in Table 6.7. It is observed that the reliability level of concrete deck at Service I limit state has improved to or close to the target level.

Table 6.7 Summary of Reliability Indices for Concrete Decks Designed using Modified Empirical Design Method

ADTT	<i>Positive Moment Region</i>		<i>Negative Moment Region</i>	
	<i>Reliability Index (Class I)</i>	<i>Reliability Index (Class II)</i>	<i>Reliability Index (Class I)</i>	<i>Reliability Index (Class II)</i>
1000	2.26	1.15	2.4	1.48
2500	1.74	0.63	1.86	1.05
5000	1.58	0.5	1.72	0.86
10000	1.05	-0.03	1.24	0.36

6.2.5 Effects of Structural Deterioration on Reliability of Service I Limit State (Empirical Deck)

Similar to section 6.1.5, in this section, the deterioration model for reinforced concrete deck at Service I limit state that developed in section 5.2 is applied in structural analysis and the effects of structural deterioration on reliability of Service I limit state is evaluated for a concrete deck designed using empirical design method.

A typical reinforced concrete deck that is designed using empirical design method specified by AASHTO LRFD Bridge Design Specification with thickness of 8 in, girder spacing of 6 ft and ADTT equals to 5000 is analyzed with and without deterioration

model applied. As shown in Figure 6.19, it is observed that the deterioration of structure has significant effect on the reliability of structure, especially for long duration.

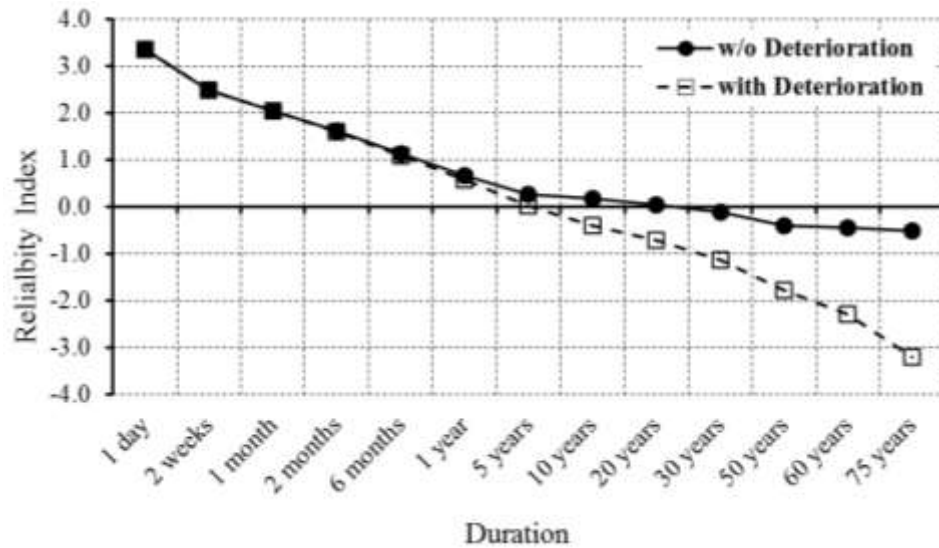


Figure 6.36 reliability index for reinforced concrete deck designed by empirical method
(with and w/o deterioration)

6.3 Prestressed Concrete Girders (Service III Limit State)

In this section, utilizing the resistance model and load model developed in previous Chapters, the reliability analysis will be performed for prestressed concrete girders at Service III limit state. Section 6.3.1 shows the representative data base used in this study. Section 6.3.2 shows the assembled limit state. Section 6.3.3 shows the reliability index of current practice and proposed target reliability index for this limit state. Section 6.3.4 shows reliability analysis results of various scenarios by changing design provisions. Finally, section 6.3.5 presents the effect of structural deterioration on reliability of prestressed concrete girder at Service III limit state.

6.3.1 Prestressed Concrete Girder Database

A database of existing prestressed concrete girder bridges was extracted from the database of bridges used in the NCHRP 12-78 project (Mlynarski, et. al. 2011) which were all taken from the NBI database. The database used in this study included 30 I- and bulb-T girder bridges, 31 adjacent box girder bridges and 36 spread box girder bridges. This database was used to evaluate the reliability level of existing prestressed concrete bridges. Besides database for existing bridges, a huge bridge database was developed to include major design parameters. These parameters include concrete strength, tensile stress limit, girder type, span length, design vehicle type, live load factor for Service III limit state. Figure 6.37 shows various parameters that varied to generate large amount of bridges. Table 6.8 shows how many cases that have been considered for each parameter. There are a total more than 400 bridges included in prestressed concrete girder database. More detailed information of bridge database can be found in Appendix A.

Table 6.8 Summary of Matrix of Designed Parameters

<i>Design Parameter</i>	<i>Number of Cases</i>	<i>Remarks</i>
Concrete Strength	3	6 ksi, 8 ksi, 10 ksi
Girder Type	4	AASHTO I, Spread Box, Adjacent Box, ASBI Box
Tensile Stress Limit	4	$0.0948\sqrt{f'_c}$, $0.158\sqrt{f'_c}$, $0.19\sqrt{f'_c}$, $0.253\sqrt{f'_c}$,
Live Load Factor	2	0.8, 1.0
Span Length	10	30 ft~220 ft
Design Vehicle	2	NJDOT Permit Vehicle, HL-93

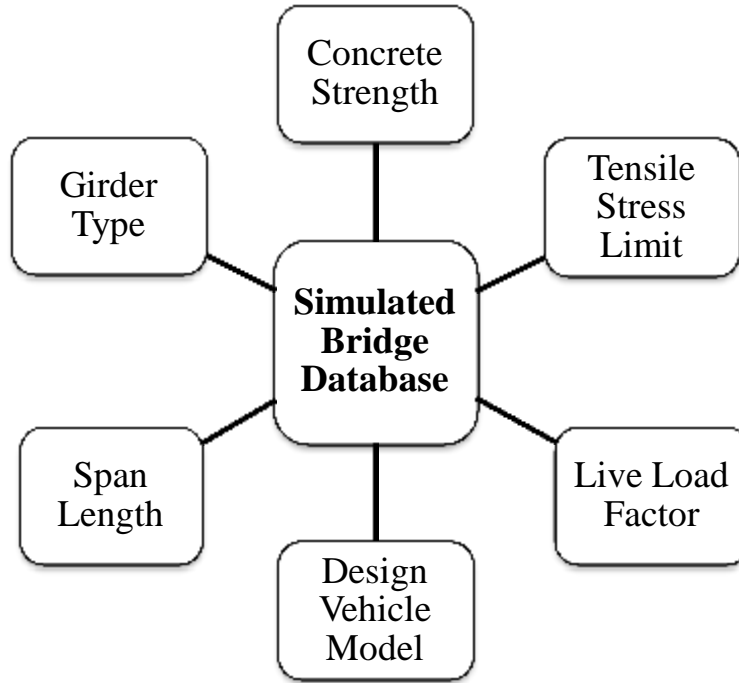


Figure 6.37 Composition of Simulated Bridge Database

6.3.2 Limit State Function for Service III Limit State

The limit state function of Service III limit state is expressed in terms of mid-span moment. It is formulated for three performance levels, decompression, maximum tensile stress limit, maximum crack width limit, as shown below:

$$\text{Decompression Level:} \quad G = M_{Dec} - M_Q \quad \text{Eq. 6.9}$$

$$\text{Maximum Tensile Stress Limit Level:} \quad G = M_T - M_Q \quad \text{Eq. 6.10}$$

$$\text{Maximum Crack Width Limit Level:} \quad G = M_{Cr} - M_Q \quad \text{Eq. 6.11}$$

As shown in Chapter 3, the resistance moment can be expressed in a uniform formula as:

$$\begin{aligned}
M_n = & A_{ps} f_{ps} d_p + A_s f_s d_s - \frac{1}{6} f_{ct} b_0 c^2 + \frac{(c - h_f)^2 (b_0 - b)}{2c} f_{ct} \left(\frac{c + 2h_f}{3} \right) \\
& + \frac{(c - h_f - h_{f1})^2 (b - b_w)}{2c} f_{ct} \left(\frac{c + 2h_f + 2h_{f1}}{3} \right)
\end{aligned} \tag{Eq. 6.12}$$

However, f_{ps} will be calculated by different equations for individual performance level:

$$\text{Decompression Level: } f_{ps(M_{Dec})} = f_{se} + \frac{E_{ps} [M_{Dec} - M_D]}{IE_c \left[1 + \frac{A_{ps} E_{ps}}{E_c} \left(\frac{1}{A_c} + \frac{e_0^2}{I} \right) \right]} \tag{Eq. 6.13}$$

$$\text{Maximum Tensile Stress Limit Level: } f_{ps} = \Delta f_{pt} + f_{ps(M_{Dec})} \tag{Eq. 6.14}$$

$$\text{Maximum Crack Width Limit Level: } f_{ps} = \Delta f_{ps} + f_{ps(M_{Dec})} \tag{Eq. 6.15}$$

where Δf_{ps} is calculated from crack width prediction equation developed by Nawy and Huang (1977) as shown in equation below:

$$\Delta f_{ps} = \frac{w_{\max} \cdot \beta \cdot \Sigma 0}{5.85 \times 10^{-5} \cdot A_t} \tag{Eq. 6.16}$$

On the other hand, the nominal moment due to load is calculated by influence line.

6.3.3 Target Reliability Index for Service III Limit State

In order to propose an appropriate target reliability index for Service III limit state, the reliability level of existing prestressed concrete girder bridges was investigated. Table 6.9 summarizes the average reliability indices for the existing prestressed concrete girder bridges database. For example, the average reliability indices at decompression

level, maximum allowable tensile stress limit under service loads of $f_t = 0.19\sqrt{f'_c}$, and maximum allowable crack width limit of 0.016 are 0.74, 1.05, and 2.69, respectively, for an ADTT of 5000 and a return period of one year.

Table 6.9 Summary of Reliability Indices for Existing Bridges with One Lane Loaded and Return Period of 1 Year

Performance Levels		ADTT			
		ADTT =1000	ADTT =2500	ADTT =5000	ADTT =10000
Decompression		0.95	0.85	0.74	0.61
Maximum Tensile Stress Limit	$f_t = 0.0948\sqrt{f'_c}$	1.15	1.01	0.94	0.82
	$f_t = 0.19\sqrt{f'_c}$	1.24	1.14	1.05	0.95
	$f_t = 0.25\sqrt{f'_c}$	1.40	1.27	1.19	1.07
Maximum Crack Width	0.008 in	2.29	2.21	1.99	1.85
	0.012 in	2.65	2.60	2.37	2.22
	0.016 in	3.06	2.89	2.69	2.56

A database of simulated simple span bridges was designed using AASHTO I-girder sections for four different cases. The simulated bridges have span of 30, 60, 80, 100 and 140 ft and girder spacing of 6, 8, 10 and 12 ft. This database was analyzed to determine the effect of the change in the method of estimating prestressing losses (pre-2004 and current methods) and the design environment (“severe corrosive conditions” and “normal” or “not worse than moderate corrosion conditions”). The two environmental conditions are signified by the maximum concrete tensile stress limit ($f_t = 0.0948\sqrt{f'_c}$ or $f_t = 0.19\sqrt{f'_c}$) used in the design. The four cases of design considered were:

Case 1: *AASHTO LRFD* with maximum concrete tensile stress of $f_t = 0.0948\sqrt{f'_c}$ and pre-2005 prestress loss method

Case 2: *AASHTO LRFD* with maximum concrete tensile stress of $f_t = 0.0948\sqrt{f'_c}$ and current (2012) prestress loss method

Case 3: *AASHTO LRFD* with maximum concrete tensile stress of $f_t = 0.19\sqrt{f'_c}$ and pre-2005 prestress loss method

Case 4: *AASHTO LRFD* with maximum concrete tensile stress of $f_t = 0.19\sqrt{f'_c}$ and current (2012) prestress loss method

Table 6.10 and Table 6.11 show the span length and girder spacing along with the calculated reliability indices for I-girder bridges designed for maximum concrete tensile stress $f_t = 0.0948\sqrt{f'_c}$ (Case 1 and Case 2) and $f_t = 0.19\sqrt{f'_c}$ (Case 3 and Case 4), respectively, for ADTT 5000.

In performing the design, the cases using current prestress loss method (Case 2 and Case 4) were designed using the smallest possible AASHTO girder size. To facilitate the comparisons, Case 1 and Case 3 were then designed using the same AASHTO section used for the same span and girder spacing for Case 2 and 4, respectively. In some cases, the section used for Case 2 or Case 4 was too small to be used for the corresponding Case 1 or Case 3. In such cases no design is shown in Table 6.10 and Table 6.11. For the 140 ft span bridges with 12 ft girder spacing, no AASHTO I-girder section was sufficient.

Bridges designed for Case 1 and Case 3 are also thought to be similar to those designed using AASHTO Standard specifications for the two environmental conditions. The reliability indices calculated for Case 1 and Case 3 represent the inherent reliability of bridges currently on the system as most of them were designed before 2005. Case 2 and Case 4 generally represent the inherent reliability of newer bridges designed using the 2005 and later versions of AASHTO LRFD for severe and normal environmental conditions, respectively.

Comparing Case 1 to Case 2 and Case 3 to Case 4 shows the effect of changing the prestressing loss method.

Using the current prestress loss method resulted in smaller number of strands than the old loss method. As shown in Table 6.10 and Table 6.11, the lower number of strands resulted in lower reliability index for bridges designed using the new (current) prestress loss method.

As shown in Table 6.10 and Table 6.11, regardless of the loss method and/or the limit state used, the reliability indices for each case varied significantly. This suggested the need to calibrate the limit state to develop a combination of load and resistance factors that produce a more uniform reliability index across different spans and girder spacings.

Table 6.10 Summary of the Reliability Indices of Bridges Designed Using AASHTO
Girders with ADTT 5000 and $f_t = 0.0948\sqrt{f'_c}$

Cases	Section Type	Span Length (ft)	Spac- ing (ft)	Case 1			Case 2		
				Designed Using Old Loss Method			Designed Using New Loss Method		
				Decomp .	Max. Tensil e	Max. Crack	Decomp .	Max. Tensil e	Max. Crack
1	AASHTO I	30	6	1.05	1.49	2.92	1.03	1.51	2.55
2	AASHTO I	30	8	0.9	0.94	2.41	0.93	1	2.32
3	AASHTO I	30	10	1.16	1.68	2.87	1.28	1.67	2.82
4	AASHTO I	30	12	1.28	1.67	2.91	0.63	0.97	2.29
Average for 30 ft Span				1.10	1.45	2.78	0.97	1.29	2.50
5	AASHTO II	60	6	0.66	1.01	3.35	0.23	0.61	2.47
6	AASHTO II	60	8	—	—	—	0.73	1.04	2.42
7	AASHTO III	60	10	1.22	1.62	3.01	0.43	0.76	1.97
8	AASHTO III	60	12	1.57	1.96	3.68	0.73	0.99	2.51
Average for 60 ft Span				1.15	1.53	3.35	0.53	0.85	2.34
9	AASHTO III	80	6	1.35	1.66	4.1	0.61	0.92	3.07
10	AASHTO III	80	8	1.8	2.14	5.23	0.82	1.13	3.64
11	AASHTO III	80	10	—	—	—	0.90	1.19	2.93
12	AASHTO IV	80	12	2.2	2.49	5.11	0.83	1.17	3.32
Average for 80 ft Span				1.78	2.10	4.81	0.79	1.10	3.24
13	AASHTO III	100	6	—	—	—	1.45	1.85	3.51
14	AASHTO IV	100	8	1.86	2	3.86	1.33	1.43	3.44
15	AASHTO IV	100	10	—	—	—	1.33	1.65	3.37
16	AASHTO V	100	12	1.68	1.99	4.08	0.93	1.24	3.33
Average for 100 ft Span				1.77	2.00	3.97	1.26	1.54	3.41
17	AASHTO IV	120	6	—	—	—	1.32	1.76	3.81
18	AASHTO V	120	8	1.54	2.05	3.65	0.92	1.4	3.14
19	AASHTO V	120	10	—	—	—	0.95	1.46	3.02
20	AASHTO VI	120	12	1.82	2.26	3.88	0.9	1.35	3.38
Average for 120 ft Span				1.68	2.16	3.77	1.02	1.49	3.34
21	AASHTO VI	140	6	1.48	1.99	3.91	0.86	1.36	2.32
22	AASHTO VI	140	8	—	—	—	0.99	1.47	2.79
23	AASHTO VI	140	10	—	—	—	1.05	1.53	3.22
24	—	140	12	—	—	—	—	—	—
Average for 140 ft Span				1.48	1.99	3.91	0.97	1.45	2.78
Average for All Spans				1.44	1.82	3.55	0.92	1.33	2.87

Table 6.11 Summary of the Reliability Indices of Bridges Designed Using AASHTO
Girders with ADTT 5000 and $f_t = 0.19\sqrt{f'_c}$

Cases	Section Type	Span Length (ft)	Spacing (ft)	Case 3			Case 4		
				Designed Using Old Loss Method			Designed Using New Loss Method		
				Decomp.	Max. Tensile	Max. Crack	Decomp.	Max. Tensile	Max. Crack
1	AASHTO I	30	6	1	1.55	2.39	0.97	1.55	2.46
2	AASHTO I	30	8	0.94	0.92	2.35	0.91	1.00	2.16
3	AASHTO I	30	10	1.29	1.66	2.91	1.18	1.66	2.79
4	AASHTO I	30	12	1.3	1.72	3.02	1.26	1.70	2.91
Average for 30 ft Span				1.13	1.46	2.67	1.08	1.48	2.58
5	AASHTO II	60	6	0.74	1.13	3.11	0.18	0.58	2.41
6	AASHTO II	60	8	1.04	1.39	2.82	0.28	0.66	1.91
7	AASHTO III	60	10	0.42	0.79	2.05	0.42	0.78	2.07
8	AASHTO III	60	12	0.66	1.00	2.5	0.68	0.96	2.53
Average for 60 ft Span				0.72	1.08	2.62	0.39	0.75	2.23
9	AASHTO III	80	6	0.56	0.97	3.13	0.13	0.51	2.53
10	AASHTO III	80	8	1.06	1.46	3.43	0.42	0.78	3.2
11	AASHTO III	80	10	1.58	1.84	3.65	0.37	0.65	2.72
12	AASHTO IV	80	12	0.83	1.15	3.72	0.51	0.87	3.11
Average for 80 ft Span				1.01	1.36	3.48	0.36	0.70	2.89
13	AASHTO III	100	6	—	—	—	0.82	1.23	3.44
14	AASHTO IV	100	8	1.31	1.42	3.6	0.69	0.76	2.76
15	AASHTO IV	100	10	1.8	1.98	3.67	0.75	1.04	3.12
16	AASHTO V	100	12	1.08	1.37	3.43	0.4	0.72	2.55
Average for 100 ft Span				1.40	1.59	3.57	0.67	0.94	2.97
17	AASHTO IV	120	6	1.53	1.98	3.71	0.7	1.28	3.1
18	AASHTO V	120	8	0.9	1.30	3.31	0.46	0.85	2.55
19	AASHTO V	120	10	1.25	1.65	3.35	0.26	0.78	2.68
20	AASHTO VI	120	12	1.19	1.66	3.37	0.47	0.91	2.69
Average for 120 ft Span				1.22	1.65	3.44	0.47	0.96	2.76
21	AASHTO VI	140	6	0.84	1.41	3.23	0.28	0.82	2.41
22	AASHTO VI	140	8	1.22	1.68	3.3	0.53	0.98	3.04
23	AASHTO VI	140	10	—	—	—	0.62	1.08	2.46
24	—	140	12	—	—	—	—	—	—
Average for 140 ft Span				1.03	1.55	3.27	0.48	0.96	2.64
Average for All Spans				1.07	1.43	3.15	0.58	0.96	2.68

The target reliability indices were selected based on the calculated average values of the reliability levels of existing bridges and previous practices with some consideration given to experiences from other Codes (*Eurocode* and ISO 2394 Document). As indicated earlier, a return period of 1 year was selected and an ADTT equal to 5000 was used.

Table 6.12 shows the target reliability indices selected in this study. Notice that the environmental condition for existing bridges was not known and that the two columns showing the reliability indices of the simulated bridges is for cases where the old prestressing loss method was used as these are thought to better represent the bridges currently on the system.

For example, the reliability index of existing bridges, simulated bridges designed for severe environments, and simulated bridges designed for normal environments, at the decompression performance level is around 0.74, 1.44 and 1.07, respectively (See Table 6.9 through Table 6.12). Therefore, a target reliability index of 1.2 and 1.0 was selected for the decompression performance level for bridges designed for severe environments and bridges designed for normal environments, respectively. The reliability index of 1.0 means that 15 out of 100 bridges will probably have the bottom of the girder decompress in any given year.

Table 6.12 Reliability Indices for Existing and Simulated Bridges (Return Period of 1 Year and ADTT 5000)

<i>Performance Level</i>	<i>Reliability Index</i>				
	Average β for Existing Bridges in the NCHRP 12-78	Average β for Simulated bridges designed for $f_t = 0.0948\sqrt{f'_c}$ and old loss method	Average β for Simulated bridges designed for $f_t = 0.19\sqrt{f'_c}$ and old loss method	Proposed Target β for bridges in severe environment	Proposed Target β for bridges in normal environment
Decompression	0.74	1.44	1.07	1.20	1.00
Maximum Allowable Tensile Stress of $f_t = 0.19\sqrt{f'_c}$	1.05	1.82	1.43	1.50	1.25
Maximum Allowable Crack Width of 0.016 in.	2.69	3.55	3.15	3.30	3.10

6.3.4 Reliability analysis results for Service III Limit State

In this section, the reliability analysis was performed for a selected bridge database (shown in Table 6.13) for illustration purpose. ADTT of 5000 is assumed in this example. Analysis for other bridge database is presented in Appendix B.

6.3.4.1 Maximum Allowable Tensile Stress Limit of $f_t = 0.0948\sqrt{f'_c}$

Figure 6.38 through Figure 6.40 show the reliability indices for the bridges designed using AASHTO type girders according to *AASHTO LRFD Specifications* (2012), including a load factor of 0.8 for Service III limit state, and assuming a maximum concrete tensile stress of $f_t = 0.0948\sqrt{f'_c}$. The geometric characteristics of the bridges

are shown in Table 6.13. It was observed that the average reliability index for the decompression limit state, maximum allowable tensile stress limit state, and maximum allowable crack width limit state is 0.97, 1.31, and 3.06, respectively. Since the reliability indices are lower than the target reliability indices and that the reliability indices are not uniform across different spans, modifications to the load factor will be conducted in an attempt to achieve higher, and more uniform, reliability indices.

As a second step, the bridges have been redesigned using a live load factor of 1.0 and the dead load and resistance factors were kept the same during the re-design. Table 6.14 shows the design geometric characteristics of the redesigned bridges.

Figure 6.41 through Figure 6.43 show the reliability indices for the re-designed bridges using a live load factor of 1.0. The average reliability index for the decompression limit state, the maximum allowable tensile stress limit state and the maximum allowable crack width limit state is 1.33, 1.70, and 3.32, respectively. It was observed that the reliability level of bridges became more uniform than for the case of using a live load factor of 0.8, particularly for the decompression and maximum tensile stress limit states. Therefore, a live load factor of 1.0 was proposed to be used if the tensile stress is limited to $f_t = 0.0948\sqrt{f'_c}$.

Table 6.13 Summary Information of Bridges Designed with $\gamma_{LL}=0.8$, ($f_t = 0.0948\sqrt{f'_c}$)

Cases	Section Type	Span Length (ft)	Girder Spacing (ft)	A_{ps} (in ²)	# of Strands
1	AASHTO I	30	6	1.224	8
2	AASHTO I	30	8	1.53	10
3	AASHTO I	30	10	1.836	12
4	AASHTO I	30	12	2.142	14
5	AASHTO II	60	6	2.448	16
6	AASHTO II	60	8	3.366	22
7	AASHTO III	60	10	3.06	20
8	AASHTO III	60	12	3.672	24
9	AASHTO III	80	6	3.672	24
10	AASHTO III	80	8	4.59	30
11	AASHTO III	80	10	5.508	36
12	AASHTO IV	80	12	5.202	34
13	AASHTO III	100	6	6.12	40
14	AASHTO IV	100	8	6.426	42
15	AASHTO IV	100	10	7.344	48
16	AASHTO V	100	12	7.038	46
17	AASHTO IV	120	6	7.956	52
18	AASHTO V	120	8	7.956	52
19	AASHTO V	120	10	9.18	60
20	AASHTO VI	120	12	8.874	58
21	AASHTO VI	140	6	8.262	54
22	AASHTO VI	140	8	9.792	64
23	AASHTO VI	140	10	11.322	74
24	AASHTO VI	140	12	-	-
25	FIB-96	160	6	5.508	36
26	FIB-96	160	8	6.426	42
27	FIB-96	160	10	7.344	48
28	FIB-96	160	12	-	-
29	FIB-96	180	6	7.344	48
30	Mod. BT-72	180	9	16.218	106
31	Mod. AASHTO VI	180	9	15.912	104
32	Mod. AASHTO VI	200	9	20.502	134
33	Mod. NEBT-2200	200	9	16.83	110
34	Mod. W95PTMG	200	9	16.83	110
35	Mod. NEBT-2200	220	9	20.808	136

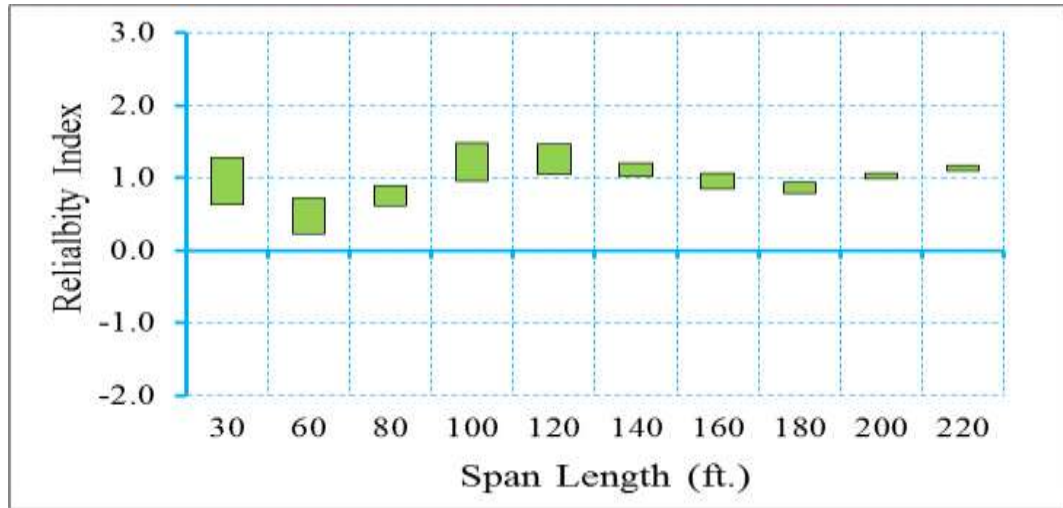


Figure 6.38 Reliability indices for bridges at decompression limit state (ADTT=5000), $\gamma_{LL}=0.8$, ($f_t = 0.0948\sqrt{f'_c}$).

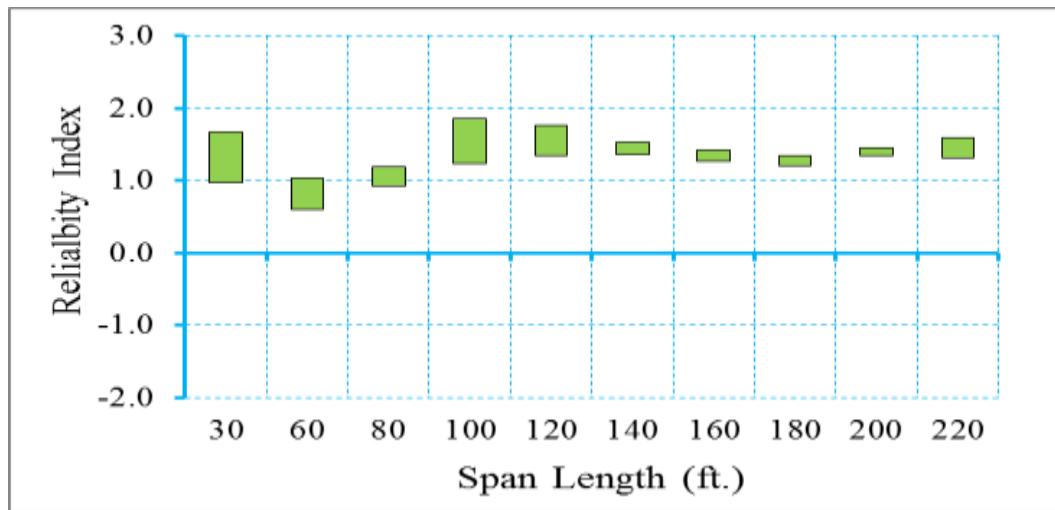


Figure 6.39 Reliability indices for bridges at maximum allowable tensile stress limit state (ADTT=5000), $\gamma_{LL}=0.8$, ($f_t = 0.0948\sqrt{f'_c}$).

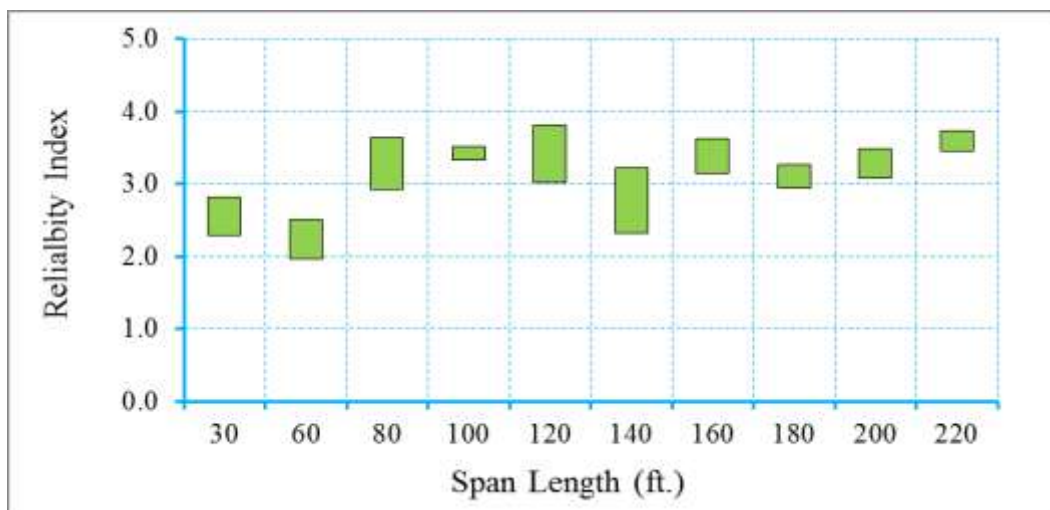


Figure 6.40 Reliability Indices for bridges at maximum allowable crack width limit state (ADTT=5000), $\gamma_{LL}=0.8$, ($f_t = 0.0948\sqrt{f'_c}$).

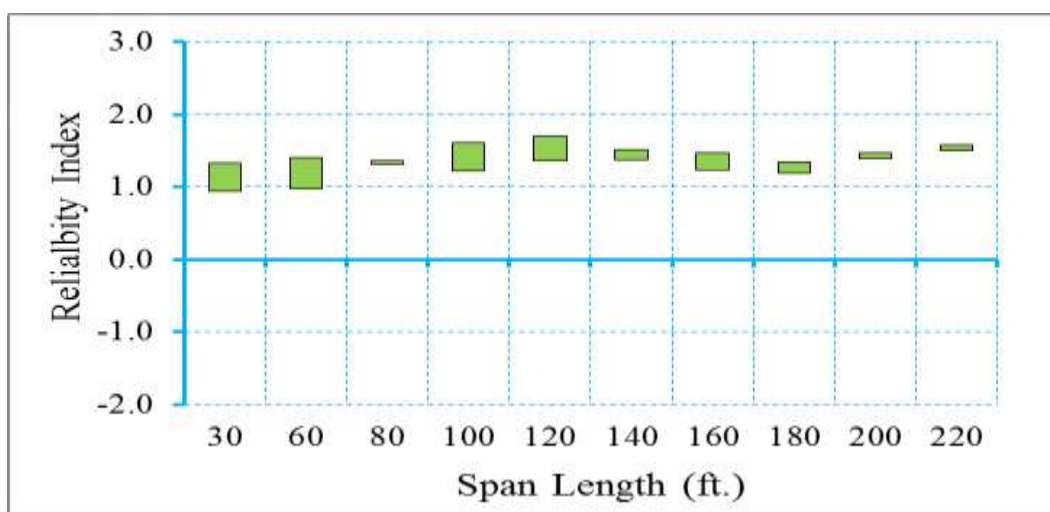


Figure 6.41 Reliability indices for bridges at decompression limit state (ADTT=5000), $\gamma_{LL}=1.0$ ($f_t = 0.0948\sqrt{f'_c}$).

Table 6.14 Summary Information of Bridges Designed with $\gamma_{LL}=1.0$, ($f_t = 0.0948\sqrt{f'_c}$)

	Section Type	Span Length (ft)	Girder Spacing (ft)	A_{ps} (in ²)	# of Strands
1	AASHTO I	30	6	1.224	8
2	AASHTO I	30	8	1.53	10
3	AASHTO I	30	10	1.836	12
4	AASHTO I	30	12	2.142	14
5	AASHTO II	60	6	3.06	20
6	AASHTO II	60	8	3.978	26
7	AASHTO III	60	10	3.366	22
8	AASHTO III	60	12	4.284	28
9	AASHTO III	80	6	4.284	28
10	AASHTO III	80	8	5.202	34
11	AASHTO III	80	10	6.12	40
12	AASHTO IV	80	12	5.814	38
13	AASHTO III	100	6	7.038	46
14	AASHTO IV	100	8	7.038	46
15	AASHTO IV	100	10	8.262	54
16	AASHTO V	100	12	7.65	50
17	AASHTO IV	120	6	8.874	58
18	AASHTO V	120	8	8.874	58
19	AASHTO V	120	10	10.404	68
20	AASHTO VI	120	12	9.792	64
21	AASHTO VI	140	6	8.874	58
22	AASHTO VI	140	8	10.71	70
23	AASHTO VI	140	10	-	-
24	AASHTO VI	140	12	-	-
25	FIB-96	160	6	5.814	38
26	FIB-96	160	8	7.344	48
27	FIB-96	160	10	7.956	52
28	FIB-96	160	12	-	-
29	FIB-96	180	6	7.956	52
30	Mod. BT-72	180	9	17.442	114
31	Mod. AASHTO VI	180	9	17.442	114
32	Mod. AASHTO VI	200	9	22.032	144
33	Mod. NEBT-2200	200	9	18.36	120
34	Mod. W95PTMG	200	9	18.36	120
35	Mod. NEBT-2200	220	9	22.338	146

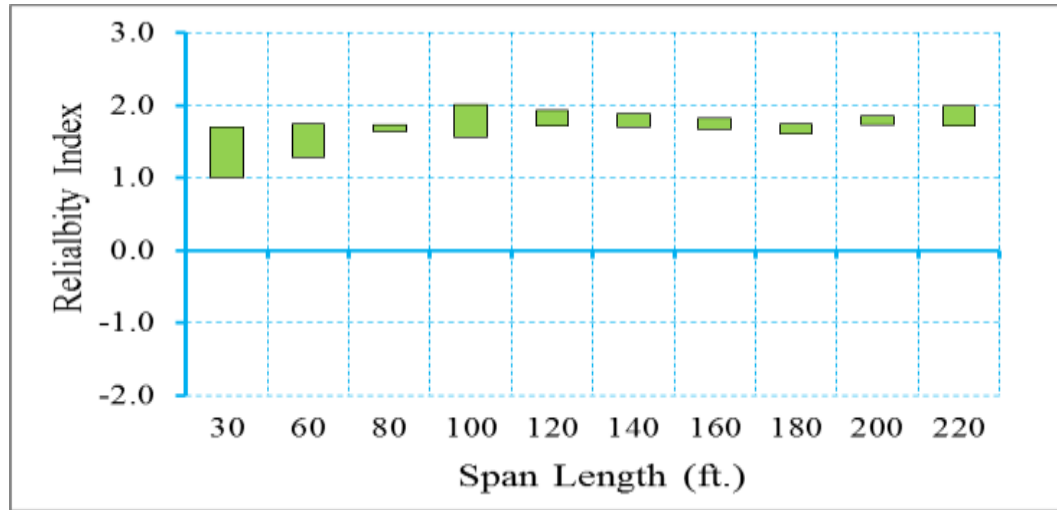


Figure 6.42 Reliability indices for bridges at maximum allowable tensile stress limit state (ADTT=5000), $\gamma_{LL}=1.0$ ($f_t = 0.0948\sqrt{f'_c}$).

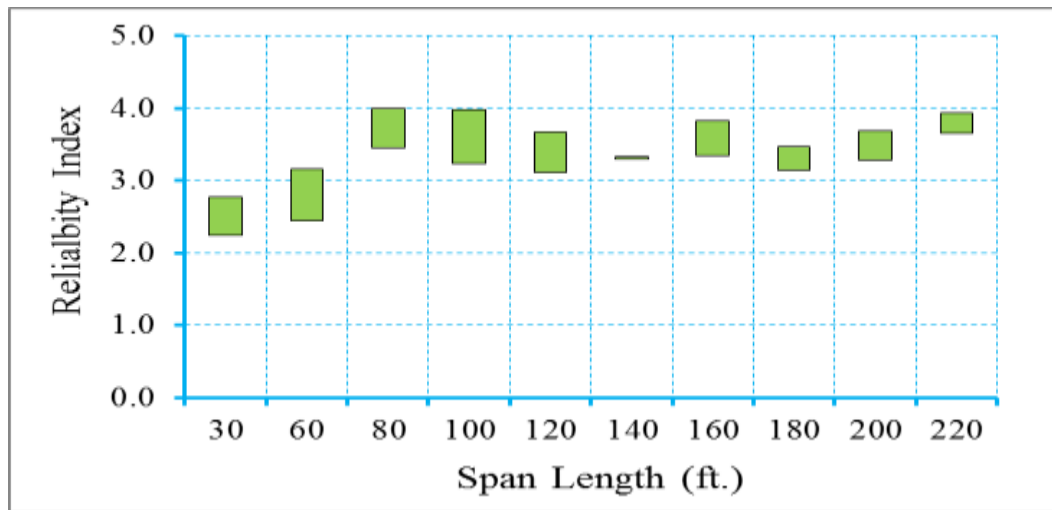


Figure 6.43 Reliability indices for bridges at maximum allowable crack width limit state (ADTT=1000), $\gamma_{LL}=1.0$ ($f_t = 0.0948\sqrt{f'_c}$).

6.3.4.2 Maximum Allowable Tensile Stress Limit of $f_t = 0.19\sqrt{f'_c}$

In this section, the work described under section 6.3.4.1 above was repeated except that the girders were redesigned assuming maximum concrete tensile stress of $f_t = 0.19\sqrt{f'_c}$. The detailed information of design can be found in Appendix A.

Figure 6.44 through Figure 6.46 show the reliability indices for the bridges designed using AASHTO type girders according to *AASHTO LRFD Specifications* (2012), including a load factor of 0.8 for Service III limit state, and assuming a maximum concrete tensile stress of $f_t = 0.19\sqrt{f'_c}$. It was observed that the average reliability index for the decompression limit state, maximum allowable tensile stress limit state, and maximum allowable crack width limit state is 0.68, 1.1, and 2.82, respectively. As a second step, the bridges have been redesigned using a live load factor of 1.0 and the dead load and resistance factors were kept the same during the re-design.

Figure 6.47 through Figure 6.49 show the reliability indices for the re-designed bridges using a live load factor of 1.0. The average reliability index for the decompression limit state, the maximum allowable tensile stress limit state and the maximum allowable crack width limit state is 1.00, 1.41, and 3.14, respectively. It was observed that the reliability level of bridges became more uniform than for the case of using a live load factor of 0.8, particularly for the decompression and maximum tensile stress limit states. Therefore, a live load factor of 1.0 was proposed to be used if the tensile stress is limited to $f_t = 0.19\sqrt{f'_c}$.

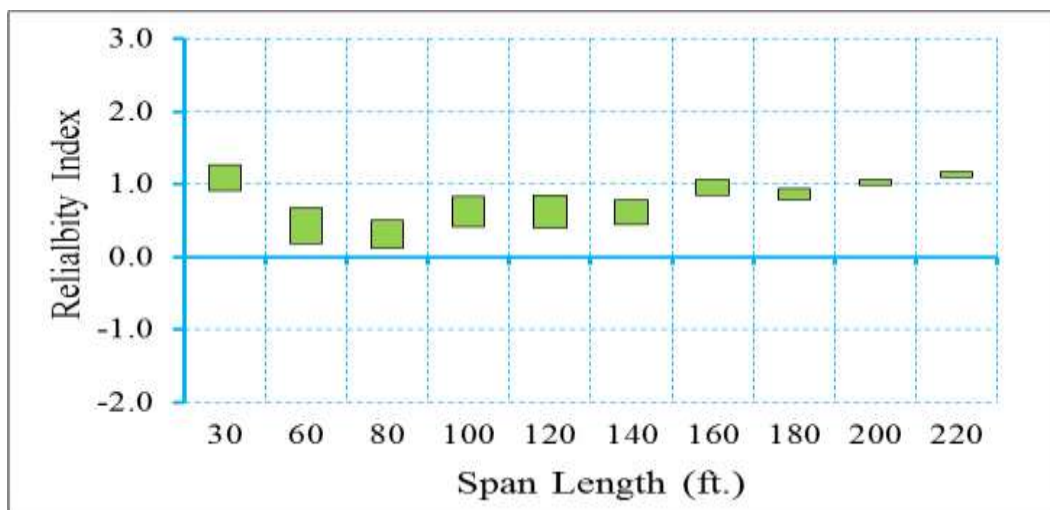


Figure 6.44 Reliability indices for bridges at decompression limit state (ADTT=5000), $\gamma_{LL}=0.8$ ($f_t = 0.19\sqrt{f'_c}$).

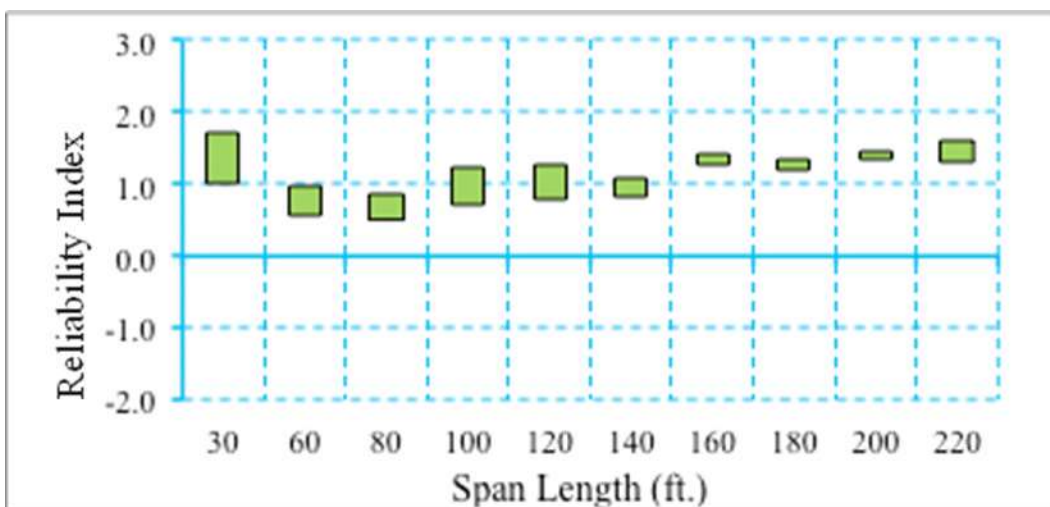


Figure 6.45 Reliability indices for bridges at maximum allowable tensile stress limit state (ADTT=5000), $\gamma_{LL}=0.8$ ($f_t = 0.19\sqrt{f'_c}$).

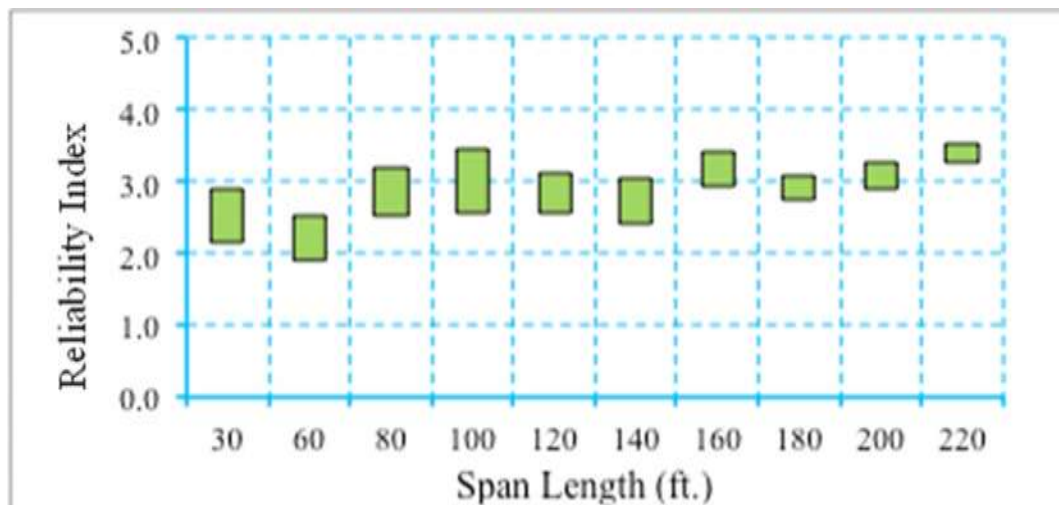


Figure 6.46 Reliability indices for bridges at maximum allowable crack width limit state (ADTT=5000), $\gamma_{LL}=0.8$ ($f_t = 0.19\sqrt{f'_c}$).

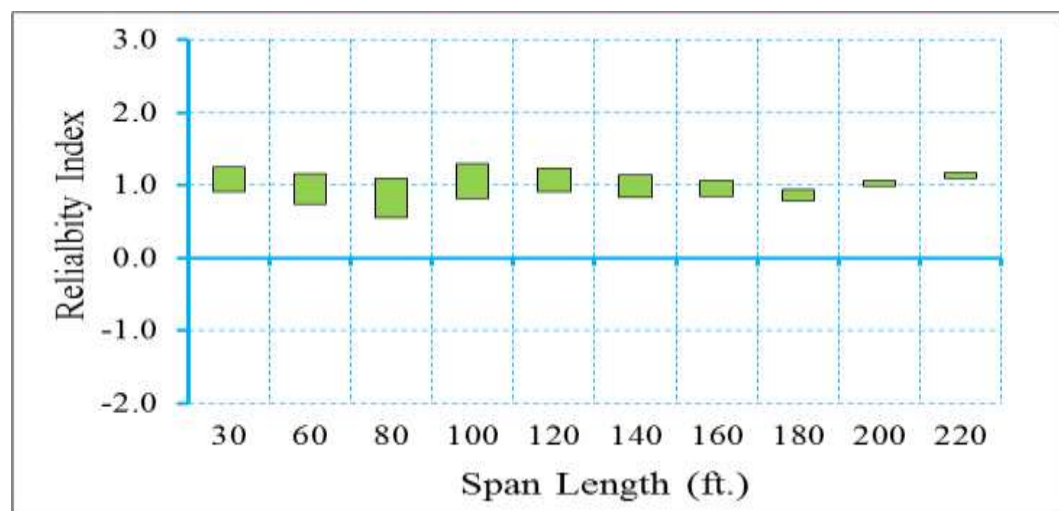


Figure 6.47 Reliability indices for bridges at decompression limit state (ADTT=5000), $\gamma_{LL}=1.0$ ($f_t = 0.19\sqrt{f'_c}$).

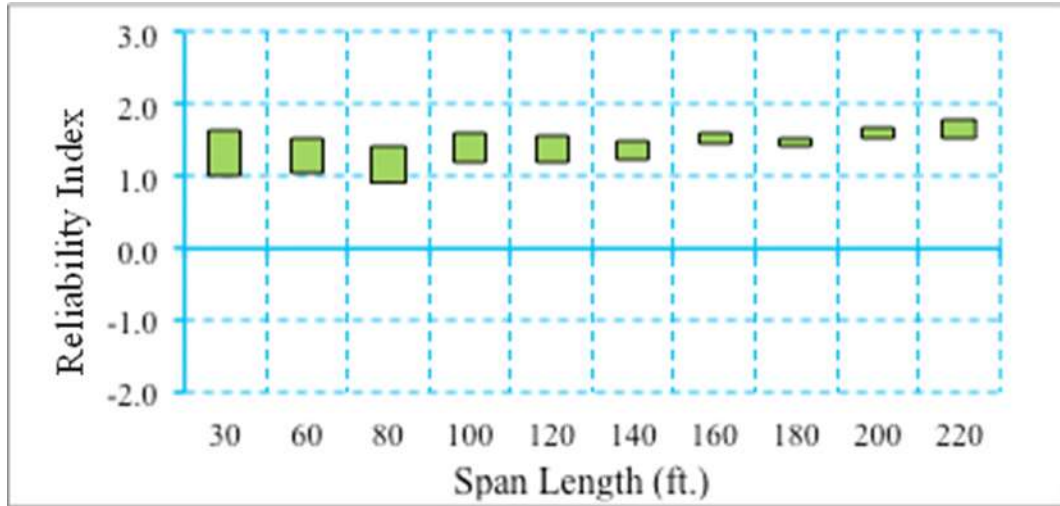


Figure 6.48 Reliability indices for bridges at maximum tensile stress limit state (ADTT=5000), $\gamma_{LL}=1.0$ ($f_t = 0.19\sqrt{f'_c}$).

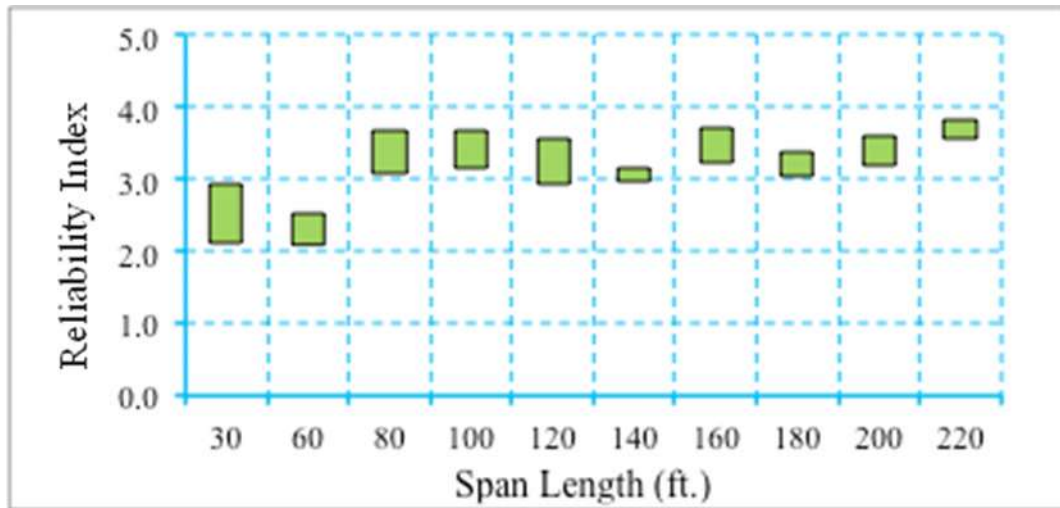


Figure 6.49 Reliability indices for bridges at maximum crack width limit state (ADTT=5000), $\gamma_{LL}=1.0$ ($f_t = 0.19\sqrt{f'_c}$).

6.3.4.3 Maximum Allowable Tensile Stress Limit of $f_t = 0.253\sqrt{f'_c}$

In this section, the work described under section 6.3.4.1 above was repeated except that the girders were redesigned assuming maximum concrete tensile stress of

$f_t = 0.253\sqrt{f'_c}$. The detailed information of design can be found in Appendix A.

Figure 6.50 through Figure 6.52 show the reliability indices for the bridges designed using AASHTO type girders according to *AASHTO LRFD Specifications* (2012), including a load factor of 0.8 for Service III limit state, and assuming a maximum concrete tensile stress of $f_t = 0.253\sqrt{f'_c}$. It was observed that the average reliability index for the decompression limit state, maximum allowable tensile stress limit state, and maximum allowable crack width limit state is 0.06, 0.41, and 2.66, respectively. As a second step, the bridges have been redesigned using a live load factor of 1.0 and the dead load and resistance factors were kept the same during the re-design.

Figure 6.53 through Figure 6.55 show the reliability indices for the re-designed bridges using a live load factor of 1.0. The average reliability index for the decompression limit state, the maximum allowable tensile stress limit state and the maximum allowable crack width limit state is 0.85, 1.23, and 2.92, respectively.

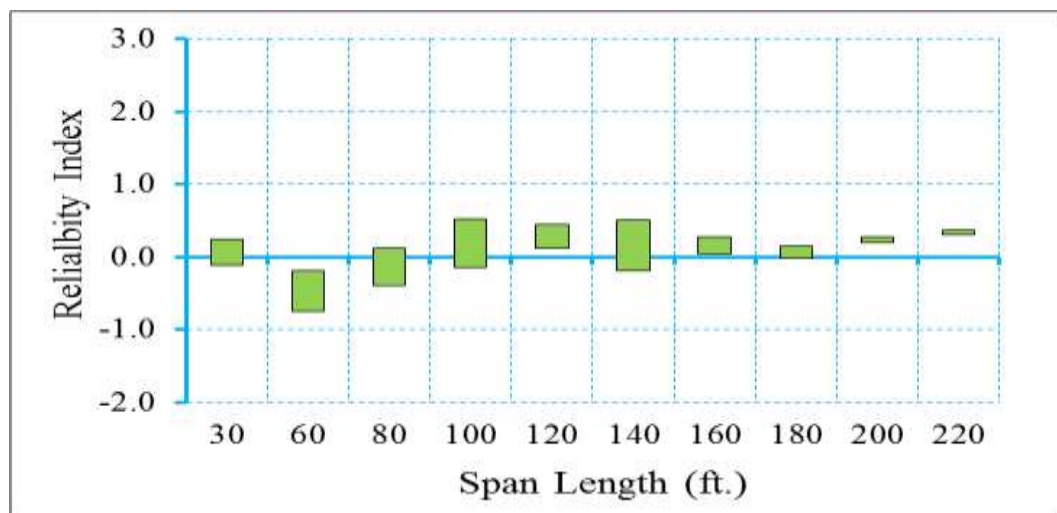


Figure 6.50 Reliability indices for bridges at decompression limit state (ADTT=5000), $\gamma_{LL}=0.8$ ($f_t = 0.25\sqrt{f'_c}$).

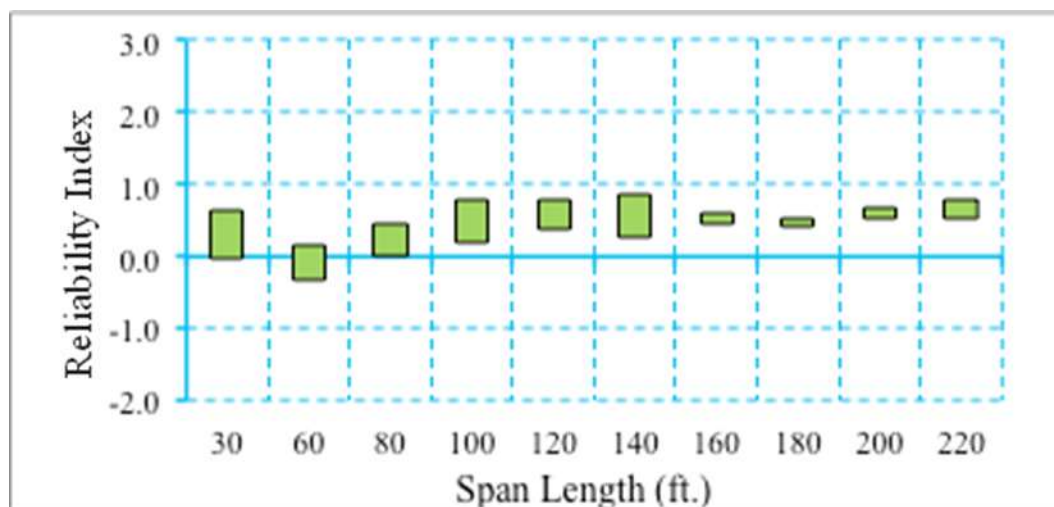


Figure 6.51 Reliability indices for bridges at maximum allowable tensile stress limit state (ADTT=5000), $\gamma_{LL}=0.8$ ($f_t = 0.25\sqrt{f'_c}$).

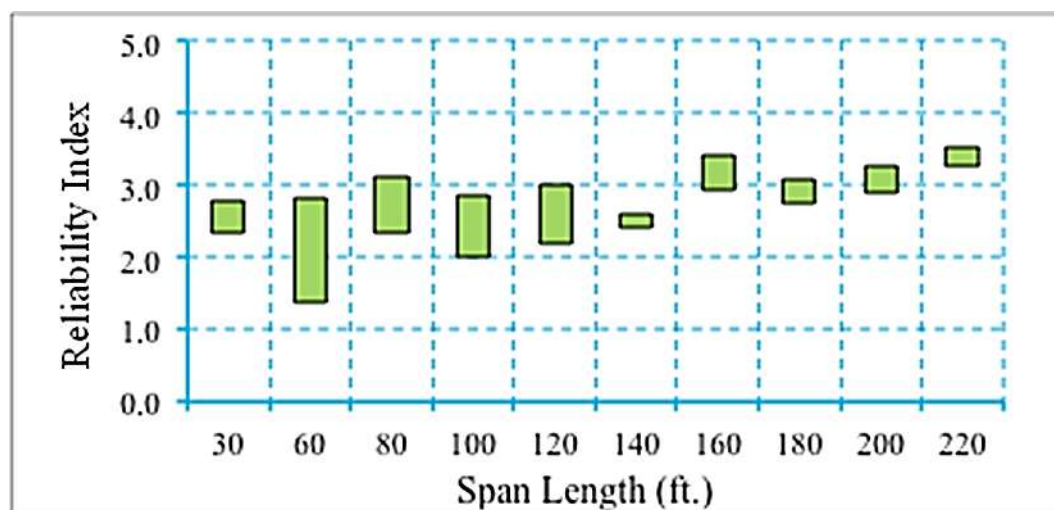


Figure 6.52 Reliability indices for bridges at maximum allowable crack width limit state (ADTT=5000), $\gamma_{LL}=0.8$ ($f_t = 0.25\sqrt{f'_c}$).

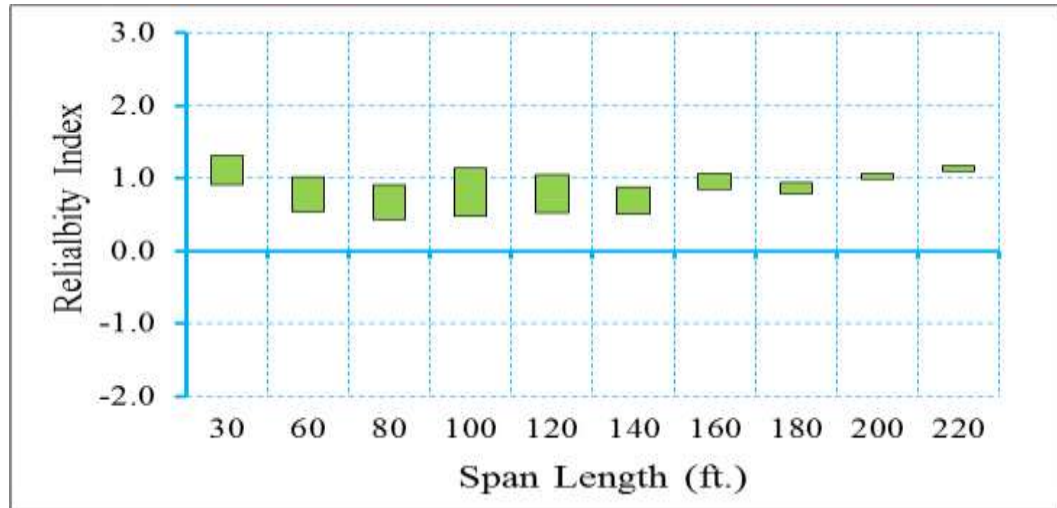


Figure 6.53 Reliability indices for bridges at decompression limit state (ADTT=5000), $\gamma_{LL}=1.0$ ($f_t = 0.25\sqrt{f'_c}$).

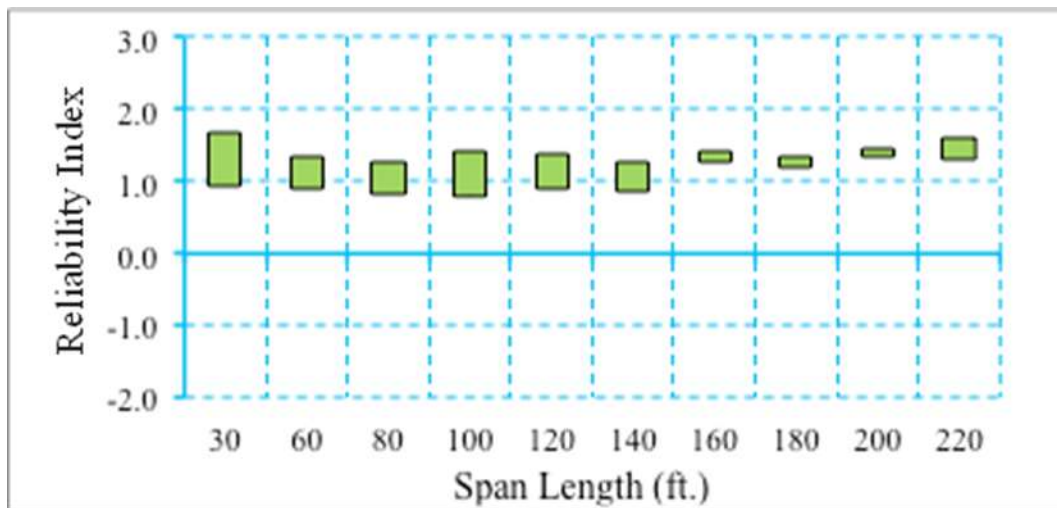


Figure 6.54 Reliability indices for bridges at maximum tensile stress limit state (ADTT=5000), $\gamma_{LL}=1.0$ ($f_t = 0.25\sqrt{f'_c}$).

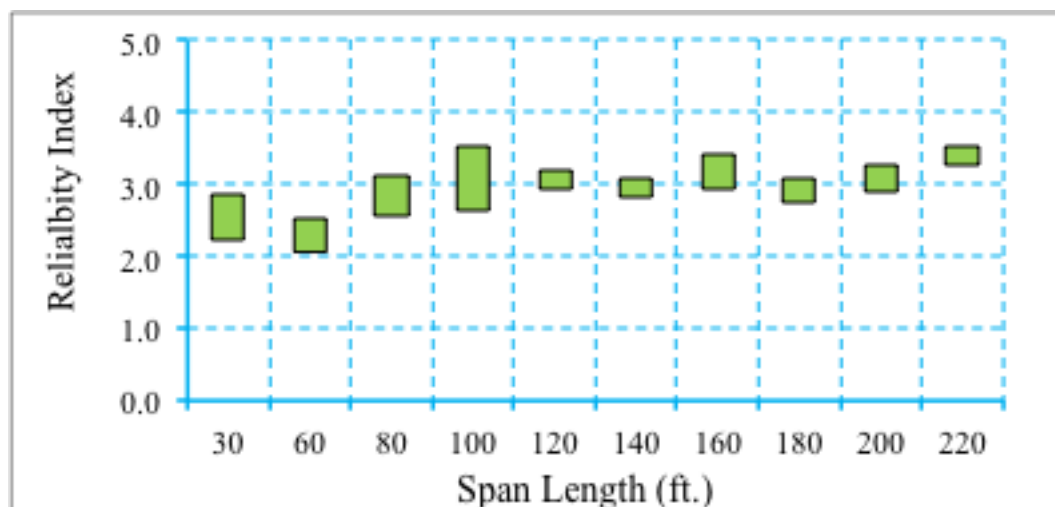


Figure 6.55 Reliability indices for bridges at maximum crack width limit state (ADTT=5000), $\gamma_{LL}=1.0$ ($f_t = 0.25\sqrt{f'_c}$).

The summary of the reliability index calculations is given in Table 6.15 through Table 6.18. Regardless of the maximum tensile stress limit used in the design, the limiting criterion for the limiting tensile stress when determining the reliability index was taken as $f_t = 0.19\sqrt{f'_c}$.

Table 6.15 Summary of Reliability Indices for Simulated Bridges Designed for $f_t = 0.0948\sqrt{f'_c}$

ADTT	Live Load Factor=0.8			Live Load Factor=1.0		
	De-compression	Stress Limit	Crack Width	De-compression	Stress Limit	Crack Width
1000	1.05	1.41	3.16	1.42	1.79	3.36
2500	1.01	1.35	3.11	1.38	1.75	3.33
5000	0.97	1.31	3.06	1.33	1.7	3.32
10000	0.94	1.30	3.00	1.32	1.66	3.28

Table 6.16 Summary of Reliability Indices for Simulated Bridges Designed for
 $f_t = 0.158\sqrt{f'_c}$

ADTT	Live Load Factor=0.8			Live Load Factor=1.0		
	De-compression	Stress Limit	Crack Width	De-compression	Stress Limit	Crack Width
1000	0.97	1.31	2.99	1.16	1.55	3.32
2500	0.83	1.19	2.96	1.12	1.50	3.29
5000	0.80	1.14	2.91	1.07	1.44	3.26
10000	0.76	1.11	2.85	1.04	1.40	3.22

Table 6.17 Summary of Reliability Indices for Simulated Bridges Designed for
 $f_t = 0.19\sqrt{f'_c}$

ADTT	Live Load Factor=0.8			Live Load Factor=1.0		
	De-compression	Stress Limit	Crack Width	De-compression	Stress Limit	Crack Width
1000	0.84	1.27	2.92	1.11	1.53	3.25
2500	0.7	1.15	2.87	1.04	1.46	3.17
5000	0.68	1.1	2.82	1.00	1.41	3.14
10000	0.64	1.07	2.78	0.98	1.34	3.11

Table 6.18 Summary of Reliability Indices for Simulated Bridges Designed for
 $f_t = 0.253\sqrt{f'_c}$

ADTT	Live Load Factor=0.8			Live Load Factor=1.0		
	De-compression	Stress Limit	Crack Width	De-compression	Stress Limit	Crack Width
1000	0.2	0.55	2.83	0.93	1.29	3.03
2500	0.08	0.49	2.77	0.89	1.27	2.95
5000	0.06	0.44	2.72	0.85	1.23	2.92
10000	0.02	0.41	2.66	0.82	1.2	2.88

6.3.5 Effects of Structural Deterioration on Reliability of Service III Limit State

In this section, the deterioration model for resistance of prestressed concrete girder at Service III limit state developed in Section 5.1 is applied in structural analysis and the effects of structural deterioration on reliability of Service III limit state is evaluated for typical bridges.

A typical prestressed concrete girder bridge (Bridge A) that designed using AASHTO LRFD Bridge Design Specification with span length of 80 ft, ASHTO III Girder, ADTT equals to 5000 and girder spacing of 8 ft is analyzed with and without deterioration model applied. As shown in Figure 6.56, it is observed that the deterioration of structure has significant effect on the reliability of structure, especially for long durations. In addition, similar analysis was also performed for another prestressed concrete girder bridge (Bridge B) with span length of 120 ft, ASHTO IV Girder, and girder spacing of 6 ft. The result as shown in Figure 6.57 demonstrates that the deterioration of structure has significant effect on long term reliability of structure.

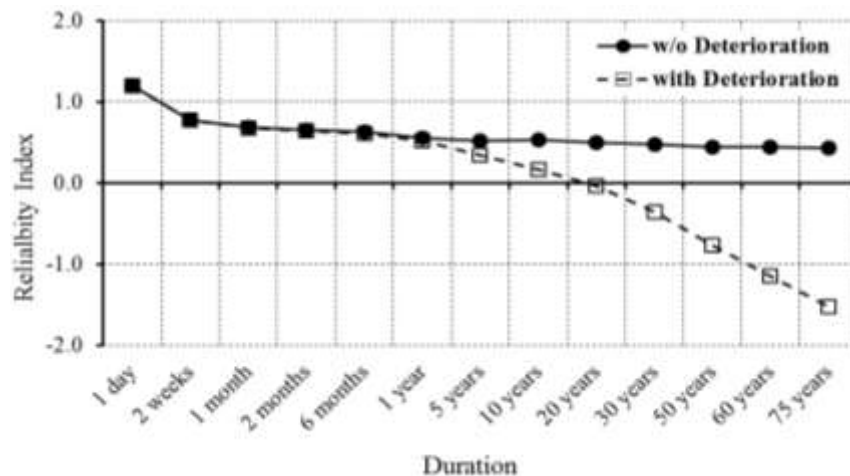


Figure 6.56 reliability index for prestressed concrete girder (Bridge A) at decompression level (with and w/o deterioration)

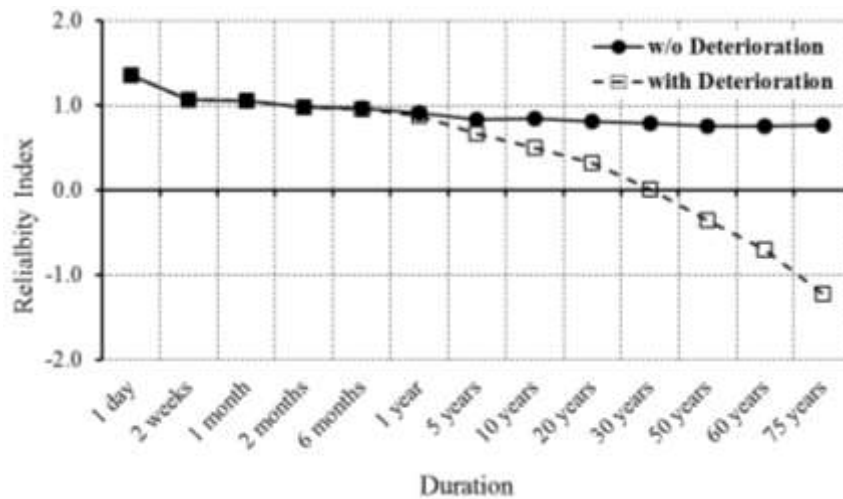


Figure 6.57 reliability index for prestressed concrete girder (Bridge B) at decompression level (with and w/o deterioration)

6.4 Prestressed Concrete Girders (Deflection Limit State)

In this section, utilizing the resistance model and load model developed in previous Chapters, the reliability analysis will be performed for prestressed concrete girders at Deflection limit state. Section 6.4.1 shows the representative data base used in this study. Section 6.4.2 shows the assembled limit state. Section 6.4.3 shows the reliability index of current practice and proposed target reliability index for this limit state. Finally, Section 6.4.4 shows reliability analysis results of various scenarios by changing design provisions.

6.4.1 Prestressed Concrete Girder Database

Similar to Service III limit state, a database of prestressed concrete girder bridges that covers various span lengths, section types, concrete strengths, etc. was developed and used in deflection limit state. There are total more than 400 bridges included in

prestressed concrete girder database. More detailed information of bridge database can be found in Appendix A.

6.4.2 Limit State Function for Deflection Limit State

The limit state function of Deflection limit state is expressed in terms of mid-span moment as shown below:

$$G = M_R - M_{LL} \quad \text{Eq.}$$

6.17

As shown in Chapter 3, for the uncracked section, the resistance moment can be expressed in a uniform formula as:

$$M_n = \frac{L}{800} \cdot \frac{E_c I}{C} \quad \text{Eq. 6.18}$$

For the cracked section, the resistance moment can be calculated using the equation below:

$$M_n = \frac{L}{800} \cdot \frac{E_c I_e}{C} + (M_{cr} - M_D) \left[1 - \frac{I_e}{I_g} \right]$$

On the other hand, the nominal moment due to load is calculated by influence line.

6.4.3 Target Reliability Index for Deflection Limit State

In order to propose an appropriate target reliability index for Deflection limit state, the reliability level of existing prestressed concrete girder bridges was investigated. Table 6.19 summarizes the average reliability indices for the existing prestressed concrete girder bridges database. For example, the average reliability indices for uncracked

section and cracked section are 3.14 and 4.52, respectively, for an ADTT of 5000 and a return period of one year.

Table 6.19 Summary of Reliability Indices for Existing Bridges with One Lane Loaded and Return Period of 1 Year at Deflection Limit State

Performance Levels	ADTT			
	ADTT =1000	ADTT =2500	ADTT =5000	ADTT =10000
Uncracked	3.34	3.25	3.14	3.02
Cracked	4.73	4.61	4.52	4.40

The target reliability indices were selected based on the calculated average values of the reliability levels of existing bridges and previous practices with some consideration given to experiences from other Codes (*Eurocode* and ISO 2394 Document). As indicated earlier, a return period of 1 year was selected and an ADTT equal to 5000 was used.

Table 6.20 shows the target reliability indices selected in this study. The reliability index of existing bridges for uncracked section and cracked is 3.14 and 4.52, respectively. Therefore, a target reliability index of 3.2 and 4.5 was selected for uncracked and cracked section, respectively.

Table 6.20 Reliability Indices for Existing and Simulated Bridges at Deflection Limit State (Return Period of 1 Year and ADTT 5000)

<i>Performance Level</i>	<i>Reliability Index</i>	
	Average β for Existing Bridges in the NCHRP 12-78	Proposed Target β
Uncracked	3.14	3.20
Cracked	4.52	4.50

6.4.4 Reliability analysis results for Deflection Limit State

In this section, the reliability analysis was performed for a selected bridge database (shown in Table 6.13) for illustration purpose. ADTT of 5000 is assumed in this example. Analysis for other bridge database is presented in Appendix B.

6.4.4.1 Uncracked Section

Figure 6.58 through Figure 6.61 show the reliability indices for the bridges designed using AASHTO type girders according to *AASHTO LRFD Specifications* (2012) and assuming a maximum concrete tensile stress of $f_t = 0.19\sqrt{f'_c}$. The geometric characteristics of the bridges are shown in Table A.3. It was observed that the average reliability indices for the ADTT of 1000, 2500, 5000, and 10,000 are 3.34, 3.25, 3.14, and 3.02, respectively. Since the reliability indices are higher than the target reliability indices, no revision is needed.

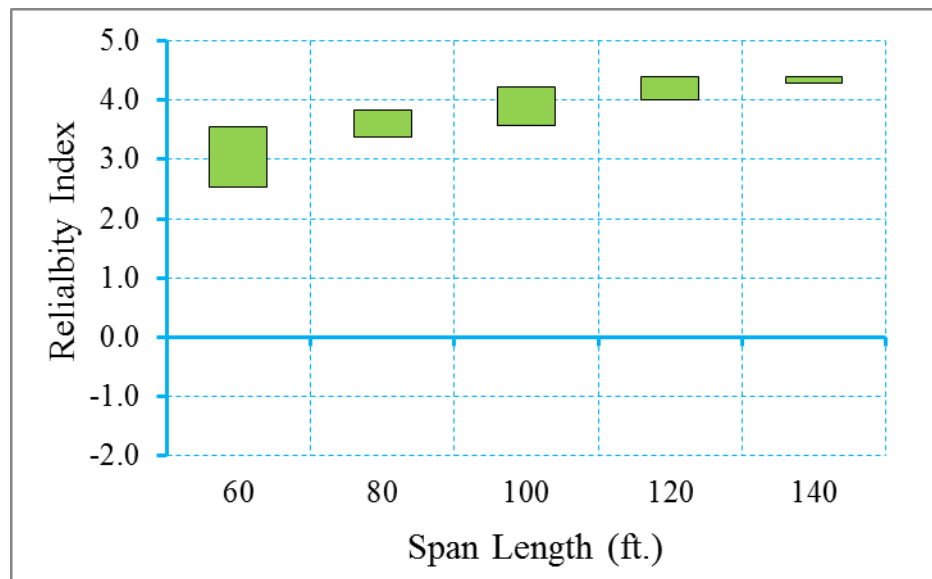


Figure 6.58 Reliability indices for Uncracked Section at Deflection Limit State (ADTT=1000), $\gamma_{LL}=0.8$, ($f_t = 0.19\sqrt{f'_c}$).

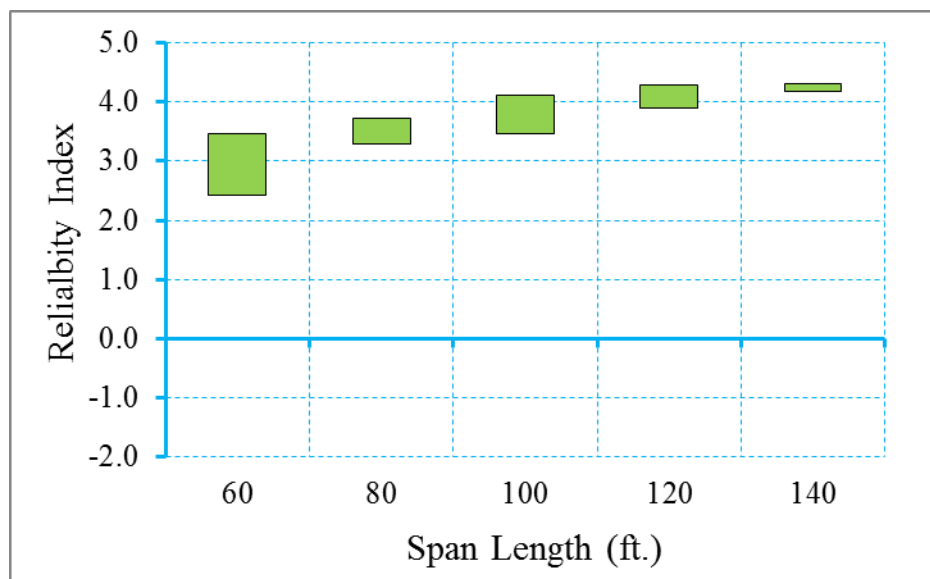


Figure 6.59 Reliability indices for Uncracked Section at Deflection Limit State (ADTT=2500), $\gamma_{LL}=0.8$, ($f_t = 0.19\sqrt{f'_c}$).

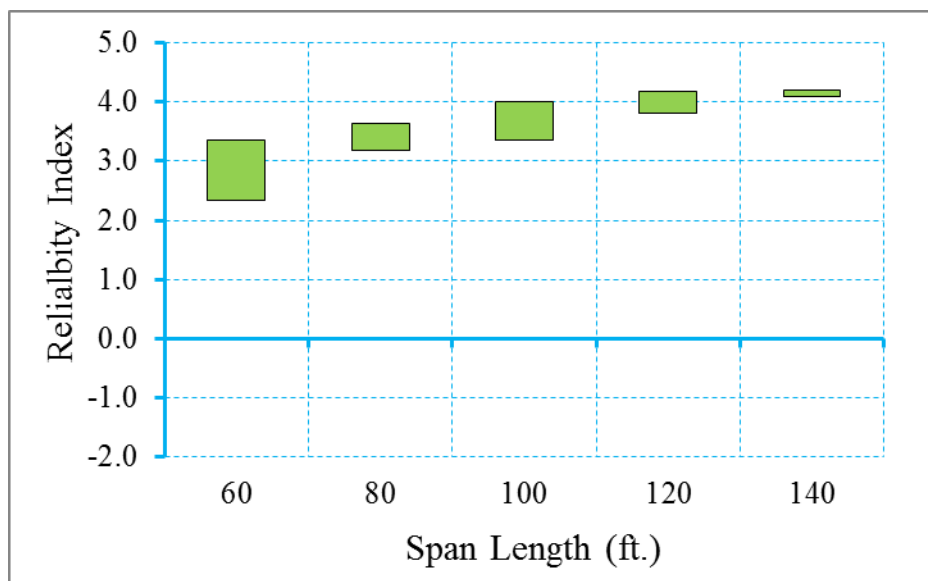


Figure 6.60 Reliability Indices for Uncracked Section at Deflection Limit State (ADTT=5000), $\gamma_{LL}=0.8$, ($f_t = 0.19\sqrt{f'_c}$).

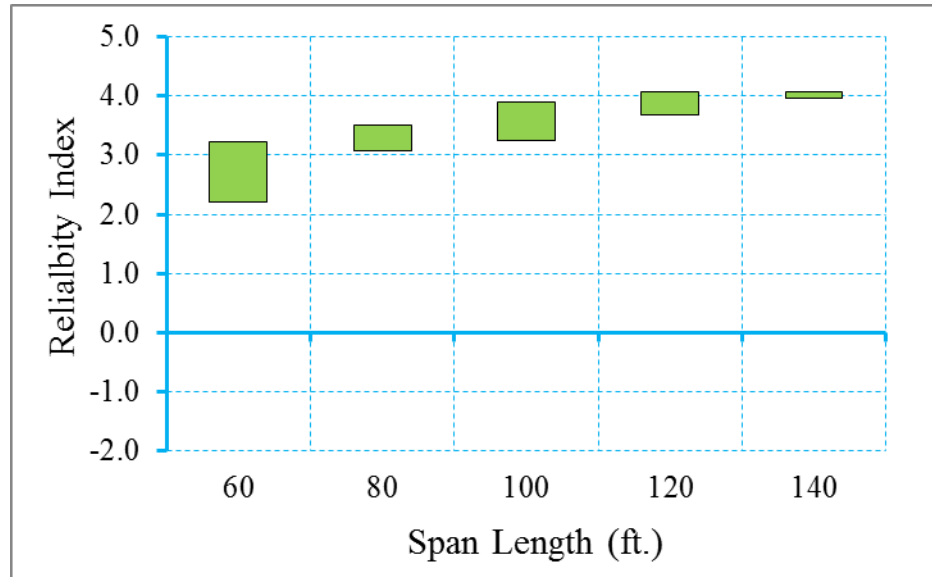


Figure 6.61 Reliability Indices for Uncracked Section at Deflection Limit State (ADTT=10,000), $\gamma_{LL}=0.8$, ($f_t = 0.19\sqrt{f'_c}$).

6.4.4.2 Cracked Section

In this section, the work described under section 6.4.4.1 above was repeated except that the girder sections were taken as cracked section.

Figure 6.62 through Figure 6.65 show the reliability indices for the bridges designed using AASHTO type girders according to *AASHTO LRFD Specifications* (2012) and assuming a maximum concrete tensile stress of $f_t = 0.19\sqrt{f'_c}$. It was observed that the average reliability indices for the ADTT of 1000, 2500, 5000, and 10,000 are 4.73, 4.61, 4.52, and 4.40, respectively. Since the reliability indices are higher than the target reliability indices, no revision is needed.

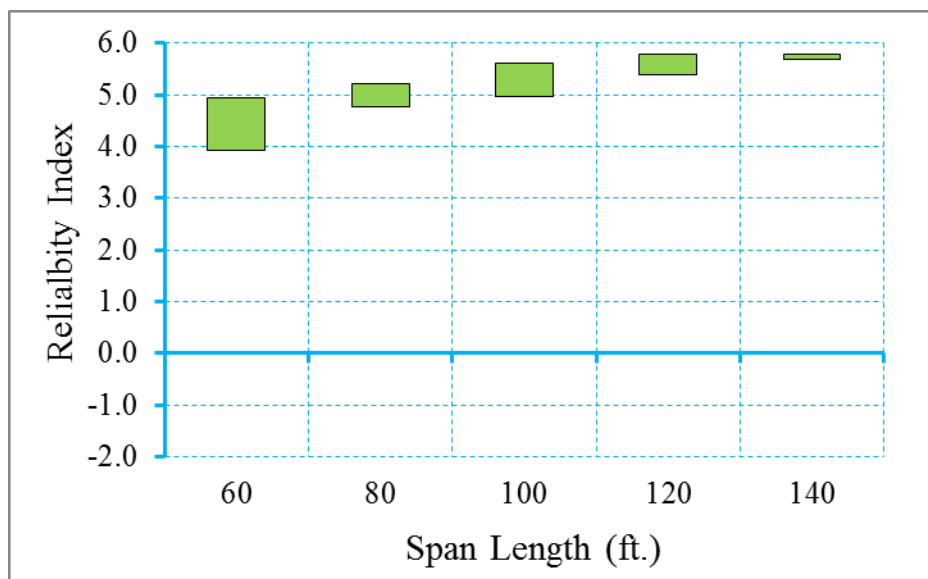


Figure 6.62 Reliability Indices for Cracked Section at Deflection Limit State (ADTT=1000), $\gamma_{LL}=0.8$, ($f_t = 0.19\sqrt{f'_c}$).

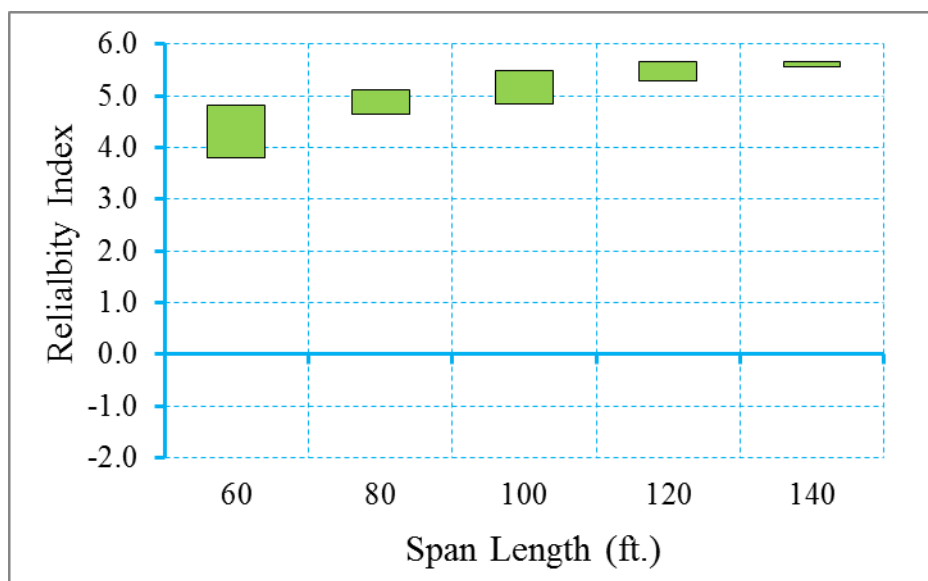


Figure 6.63 Reliability Indices for Cracked Section at Deflection Limit State (ADTT=2500), $\gamma_{LL}=0.8$, ($f_t = 0.19\sqrt{f'_c}$).

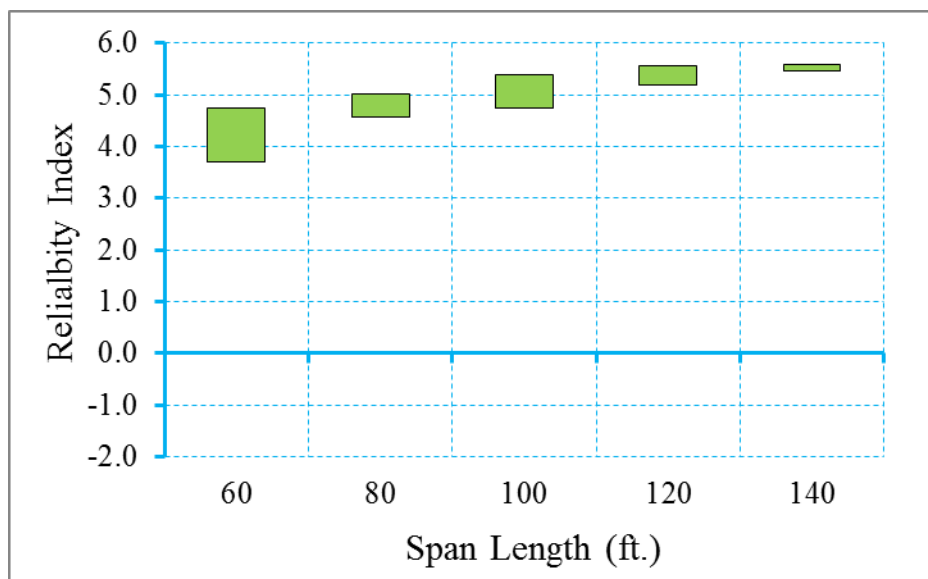


Figure 6.64 Reliability Indices for Cracked Section at Deflection Limit State
(ADTT=5000), $\gamma_{LL}=0.8$, ($f_t = 0.19\sqrt{f'_c}$).

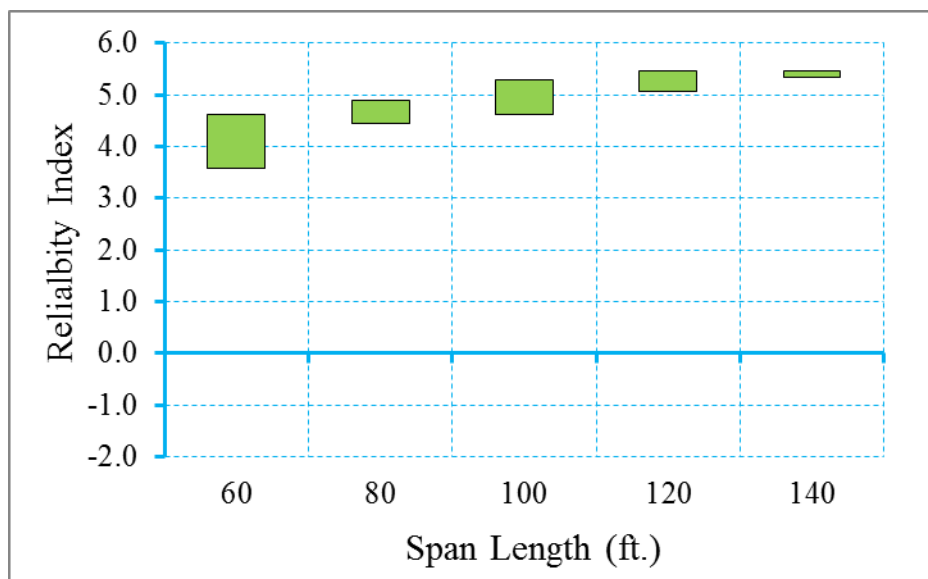


Figure 6.65 Reliability Indices for Cracked Section at Deflection Limit State
(ADTT=10,000), $\gamma_{LL}=0.8$, ($f_t = 0.19\sqrt{f'_c}$).

CHAPTER 7

SUMMARY AND CONCLUSIONS

7.1 SUMMARY

In this study, various serviceability limit states have been developed and investigated, including Service I limit state which is used for crack control of reinforced concrete and Service III limit state which is used for tension at the bottom of prestressed concrete girders. Extensive databases were developed for both Service I and Service III limit state. The databases included the existing structures as well as simulated structures with various design parameters been considered. These parameters include material properties, geometrical parameters, and design exposure conditions. Models for resistance and load were developed for both Service I and Service III limit state. Based on the developed resistance and load models, the limit states were formulated and reliability analysis was performed. Aiming at improving the level and uniformity of reliability for various serviceability limit state, the design provisions were revised and the effects of the changes was investigated. New design provisions are proposed to be included in AASHTO LRFD Design Specification and to be used in future practice. Furthermore, due to the fact the structural resistance would decrease because of deterioration of the material strength and structure section, the effect of resistance deterioration on reliability of structure at serviceability limit state was investigated.

7.2 PROPOSED REVISION IN AASHTO LRFD SPECIFICATION

As shown in previous Chapters, inconsistent reliability was observed for some scenarios if using the provisions in current AASHTO LRFD Bridge Design Specification (AASHTO, 2012). For instance, the bridge decks designed using the empirical method based on current AASHTO LRFD Bridge Design Specification demonstrates insufficient reliability level regarding the crack control limit state. Therefore, aiming at achieving uniform reliability over different designs, the following revisions are proposed to be included in AASHTO LRFD Bridge Design Specification.

7.2.1 Service I Limit State

The following revisions are proposed for Service I limit state regarding crack control of reinforced concrete members.

- (1) It is recommended that the ratio of the reinforcement area to section gross area be increased from 0.3% to 0.4% for bottom layer and 0.2% to 0.5% for top layer.
- (2) No revisions to the live load factor for Service I limit state.

7.2.2 Service III Limit State

The following revisions are proposed for Service III limit state regarding tension at tensile fibers of prestressed concrete members.

- (1) Live load factor of 1.0 for Service III limit state.

- (2) Maximum concrete tensile stress of $f_t = 0.0948\sqrt{f'_c}$ and $f_t = 0.19\sqrt{f'_c}$ for bridges in severe corrosion conditions and for bridges in no worse than moderate corrosion conditions, respectively.
- (3) Girders to be designed following conventional design methods and assuming the live loads exist in single lane or multiple lanes, whichever produces higher load effects. The appropriate multiple presence factor applies.

7.3 CONCLUSIONS

The following conclusions are based on the findings of this work:

- (1) The resistance of prestressed concrete girder at Service III limit state regarding the tension at tensile fibers could be derived using structural analysis for various performance levels named decompression, maximum allowable tensile stress limit, and maximum allowable crack width.
- (2) The statistical model for structural resistance and dead load can be obtained using derived prediction equation and Monte-Carlo simulation techniques.
- (3) A precise crack width prediction equation is important to provide an accurate estimation of structural resistance, for Service I limit state, as well as for Service III limit state at maximum allowable crack width level.
- (4) Utilizing appropriate deterioration model, the effects of deterioration on structural reliability can be evaluated. The deterioration of structure can be attributed to section losses due to corrosion, strength losses due to long term effects (shrinkage and creep of concrete).

- (5) Deterioration of structure has significant effects on structural reliability at both Service I and Service III limit state, especially for longer durations (e.g. 50 years, 75 years). Therefore, the deterioration of structure should be considered for structural reliability analysis, especially for evaluation of long term reliability of structure.
- (6) WIM data must be processed to remove erroneous data, light vehicles, and permit vehicles (if needed) before used for developing live load model.
- (7) The live load for permit vehicles can be developed based on issued permit data and statistics of actual permit vehicles.
- (8) No revision is needed to be added to AASHTO LRFD Bridge Design Specification for reinforced concrete deck designed using traditional design method.
- (9) No revision is needed to be added to AASHTO LRFD Bridge Design Specification for deflection limit state for prestressed concrete girder.
- (10) The reliability level of reinforced concrete deck designed using empirical deck is lower than target reliability index, for both positive moment and negative moment region. Therefore, the design provisions in current AASHTO LRFD Bridge Design Specifications need to be modified.
- (11) For a specific girder of known cross-section and specific number and arrangement of prestressing strands, the reliability index varies based on: (a) The design maximum concrete tensile stress (currently in the *AASHTO LRFD* maximum tensile stress of $f_t = 0.0948\sqrt{f'_c}$ and $f_t = 0.19\sqrt{f'_c}$), (b) The limit state function, i.e. decompression, tensile stress of a certain value (assumed to

be $f_t = 0.19\sqrt{f'_c}$ in the work shown above) or a crack width of a certain value (assumed to be 0.016) and (c)ADTT.

- (12) The target reliability index can be achieved uniformly across various span lengths using the load factor developed following the procedure developed in this study. The level of uniformity varies with the limiting criteria. The decompression limit state showed the highest level of uniformity and is recommended to be used as the basis for the reliability analysis, i.e. the determination of the load and resistance factors and associated design criteria.
- (13) It is recommended that the reliability indices corresponding to ADTT of 5000 be used as the basis for the calibration. The reliability index is not highly sensitive to changes in the ADTT so there is no need for using different load factor for ADTT's up to 10000.
- (14) With satisfactory past performance of prestressed beams, the target reliability index is selected to be similar to the average inherent reliability index of the bridges on the system. There is no scientific reason to substantiate targeting a different, higher or lower, reliability index.
- (15) The recommended target reliability index for the decompression limit state is 1.0 for bridges designed for no worse than moderate corrosion conditions and 1.2 for bridges designed for severe corrosion conditions. Based on the study of WIM data, the reliability index is determined assuming live load exists in single lane and without applying the multiple presence factor. This would appear on the "load side" of the limit state function.

REFERENCES

- AASHTO (2004). "LRFD bridge design specifications", American Society of State Highway and Transportation Officials (AASHTO), Washington, D.C.
- Agarwal, A. C. and Wolkowicz, M. (1976). "Interim Report on 1975 Commercial Vehicle Survey," Res. and Dev. Div., Ministry of Transportation, Downsview, Ontario, Canada.
- American Society for Testing and Materials, ASTM (1985). "E1049-85, Standard practices for cycle counting in fatigue analysis."
- American Society for Testing and Materials, ASTM (2002). "E1318-02, Standard Specification for Highway Weigh-in-Motion (WIM) Systems with User Requirements and Test Methods."
- Ang, A. H.-S., and Tang, W.H. (1975). *Probability Concepts in Engineering Planning and Design: Volume I. Basic Principles*. New York: Wiley.
- Ang, A. H.-S., and Tang, W.H. (1984). *Probability Concepts in Engineering Planning and Design: Volume II. Decision, Risk, and Reliability*. New York: Wiley.
- Atlantic Trailer Company (2004), website: <http://www.atlantictrailers.com>
- Bannantine, J.A., Comer, J.J., and Handrock, J.L. (1990). *Fundamentals of Metal Fatigue Analysis*. Prentice Hall, Englewood Cliffs, NJ.
- Bakht, B. and Jaeger, L. G. (1985). *Bridge Analysis Simplified*. McGraw-Hill:New York
- Barker, R. M., J. M. Duncan, K.B. Rojiani, P. S. K. Ooi, C. K. Tan, and S. G. Kim (1991). *Manual for the Design of Bridge Foundations, NCHRP Report 343*, Transportation Research Board, Washington, DC, 308 pp.
- Barker, R.M. and Puckett, J.A. (1997). *Design of highway bridges: based on AASHTO LRFD Bridge Design Specifications*. New York: Wiley.
- Brodtkorb, P.A., Johannesson, P., Lindgren, G., Rychlik, I., Ryden, J., and Sjo, E. (2000). "WAFO – A Matlab toolbox for analysis of random waves and loads." Norwegian University of Science and Technology, Lund Institute of Technology.
- Chen, Y. (1994). "Modeling Bridges Subjected to Moving Loads," *Mathematical Modeling and Scientific Computing*, Vol. 4, pp 567-572.

Coles, S. (2001). "An Introduction to Statistical Modeling of Extreme Values". Springer-Verlag, London.

Dressler, K., Hack, M., Krueger, W. (1997). "Stochastic reconstruction of loading histories from a rainflow matrix." *Zeit. F. ang. Math. U. Mech.* 77(3), pp 217-226.

Dressler, K., Gründer, B., Hack, M., and Köttgen, V.B. (1996). "Extrapolation of Rainflow Matrices." SAE Technical Paper 960569.

Downing, S.D. and Socie, D.F. (1982). "Simple rainflow counting algorithms." *International Journal of Fatigue*, 4(1), pp 31-40.

Federal Highway Administration, FHWA (2001). "FHWA Vehicle Types," USDOT online: <http://www.fhwa.dot.gov/policy/ohpi/vehclass.htm>

Federal Highway Administration, FHWA (2006). "Bridge Formula," USDOT online: <http://www.fhwa.dot.gov/policy/ohpi/vehclass.htm>

Fisher, J.W., Mertz, D.R., and Zhong, A. (1983) "Steel bridge members under variable amplitude long life fatigue loading." National Cooperative Highway Research Program Report 267.

Fisher, J.W., Jian, J., Wagner, D.C., and Yen, B.T. (1990). "Distortion-induced fatigue cracking in steel bridges." National Cooperative Highway Research Program Report 336.

Fisher, J.W., G.L Kulak, and I.F. Smith (1998) "A Fatigue Primer for Structural Engineers." National Steel Bridge Alliance, American Institute of Steel Construction.

Fu, G., Feng, J., Dekelbab, W., Moses, F., Cohen, H., Mertz, D., and Thompson, P. Effect of Truck Weight on Bridge Network Costs. NCHRP Report 495. Transportation Research Board. Washington D.C., 2003.

Hahin, C., South, J.M., Mohammadi, J., and Polpeddi, R.K. (1993). "Accurate and Rapid Determination of Fatigue Damage in Steel Bridges." *Journal of Structural Engineering*. ASCE, 119(1), 150-168.

International Road Dynamics Inc. (1999), "Software User's Manual: IRD Weigh-In-Motion Data Collection System," Version 7.5.0, December.

International Road Dynamics Inc. (2005), "Operator's Manual-TC/C 540," Revision C, Part No. 69004801, January.

Jaeger, L. G. and Bakht, B. (1982). "The Grillage Analogy in Bridge Analysis," *Canadian Journal of Civil Engineering*, Vol. 9, pp. 224-235.

Jaeger, L.G. and Bahkt, B. (1989). *Bridge Analysis by Microcomputer*. McGraw-Hill Co., New York.

Johannesson, P., Thomas, J-J. (2001). "Extrapolation of rainflow matrices." *Extremes*, 4(3), 241-262.

Khosrovaneh, A.K. and Dowling, N.E. (1990). "Fatigue loading history reconstruction based on the rainflow technique." *International Journal of Fatigue*, 12(2), pp 99-106.

Laman, J. and Nowak, A. (1996). "Fatigue-load model for girder bridges." *Journal of Structural Engineering*, ASCE, 122(7), pp726-733.

Liu, M. (1996). "A Three-Dimensional Dynamic Model for Bridge-Road-Vehicle System," Master's Thesis, Bradley University, Peoria, IL.

Manitowok Crane Group (2006). "Specifications for Grove portable cranes" online: <http://www.manitowokcranegroup.com>

MATLAB (2000), The Language of Technical Computing, Version 6.0, Release 12, The MathWorks, Inc., MA.

Matsuishi, M. and Endo, T. (1968). "Fatigue of metals subjected to varying stress-fatigue lives under random loading." *Preliminary Proceedings of the Kyushu District Meeting*, pages 37-40. The Japan Society of Mechanical Engineers. In Japanese, March 1968.

Microsoft Terraserver Aerial Photographs (2005), <http://terraserver.microsoft.com>

Microsoft Virtual Earth (2007). <http://live.local.com>

Mohammadi, J., Guralnick, S.A., and Polepeddi, R. (1998). "Bridge fatigue life estimation from field data." *Practice Periodical on Structural Design and Construction*, 3(3), 128-133.

Mohammadi, J., and Polepeddi, R. (2000). "Bridge rating with consideration for fatigue damage from overloads." *Journal of Bridge Engineering*, ASCE, 5(3), 259-265.

Moses, F. (2001) "Calibration of Load Factors for LRFR Bridge Evaluation," *NCHRP Report 454*, Transportation Research Board, National Research Council, Washington, D.C.

Moses, F., Schilling, C.G., and Raju, K.S. (1987) "Fatigue evaluation procedures for steel bridges." National Cooperative Highway Research Program Report 299.

Munse, W.H. (1990). "Fatigue, brittle fracture, and lamellar tearing." *Structural engineering handbook*, 3rd Ed. E.H. Gaylord Jr. and C.N. Gaylord, eds., McGraw-Hill Inc., N.Y., 4.1-4.24.

Nassif, H. H., Gindy, M. and Davis, J. (2005). "Monitoring of Bridge Girder Deflection Using Laser Doppler Vibrometer," *Journal of Non-Destructive Testing and Evaluation*, 38,

Nassif, H. H. and Liu, M. (2004). "Analytical Modeling of Bridge-Road-Vehicle Dynamic Interaction System," *Journal of Vibration and Control*, Vol. 10, pp. 215-241.

Nassif, H. H., Liu, M. and Ertekin, O. (2003). "Model Validation for Bridge-Road-Vehicle Dynamic Interaction System," *Journal of Bridge Engineering*, Vol. 8, No. 2, pp.112-120.

New Jersey Department of Transportation, NJDOT (2002), *Bridges and Structures Design Manual*, 2002 available online at <http://www.state.nj.us/transportation/>

New Jersey Department of Transportation, NJDOT (2005), email correspondence with Research Bureau, Dec 2005.

Nowak, A. S. and Lind, N. C. (1979). "Practical bridge code calibration." *Journal of the Structural Division*, ASCE, 105(12), 2497-2510, Dec.

Nowak, A.S., Nassif, H.N., and DeFrain, L. (1993). "Effect of truck loads on bridges." *Journal of Transportation Engineering*. 119(6), 853-867.

Nowak, A.S., Nassif, N., and Frank, K.H. (1993). "Fatigue Load Spectra for a Steel Girder Bridge." *Transportation Research Record 1393*, pp. 154-161.

Nowak, A.S., Nassif, H., and Frank, K.H. (1993). "Fatigue load spectra for a steel girder bridge." *Transportation Research Record 1393*, Transportation Research Board, Washington, D.C.

Nowak, A.S. (1995). "Calibration of the LRFD bridge code." *Journal of Structural Engineering*. ASCE, 121(8), 1245-1251

Nowak, A.S. (1999). "Calibration of the LRFD Bridge Design Code." *NCHRP Report 368*, Transportation Research Board, National Research Council, Washington, D.C.

Nowak, A. S. and Collins, K. R. (2000). "Reliability of Structures". McGraw Hill Companies, Inc.

Nowak, A. S. and Hong, Y. K. (1991). "Bridge Live-Load Models," *Journal of Structural Engineering*, ASCE, 117(9), pp. 2757-2767.

Phuvoravan, K., W. Chung, J. Liu, and E.D. Sotelino, (2004). "Simplified Live-Load Distribution Factor Equations for Steel Girder Bridges," *Transportation Research*

- Record: Journal of the Transportation Research Board*, No. 1892, National Research Council, Washington, D.C., pp. 88-97.
- Port Authority of New York and New Jersey, PANYNJ (2005). "Freight volumes study 2005" available online: <http://www.panynj.gov>
- Schilling, C.G., et al. (1978). "Fatigue of welded steel bridge members under variable-amplitude loadings." NCHRP Report 188.
- Socie, D. (2001). "Modeling expected service usage from short term loading measurements." *International Journal of Materials & Product Technology*, 16(4/5).
- Socie, D.F. and Pompetzki, M.A. (2004). "Modeling variability in service loading spectra." *Journal of ASTM International*, 1(2), Paper ID JAI11561, Feb. 2004.
- Southgate, H. (2000). "Quality Assurance of Weigh-in-motion Data" FHWA Contract No. DTFH61-P-00724. Federal Highway Administration USDOT, Washington D.C.
- Thoft-Christensen, P. and Baker, M. J., *Structural Reliability Theory and Its Applications*. Springer-Verlag, 1982.
- West, R. (1973). "Recommendations on the Use of Grillage Analysis for Slab and Pseudo-slab Bridge Decks," Cement and Concrete Association and Construction Industry Research and Information Association, London, UK.
- Zokaie, T., T.A. Osterkamp, and R.A. Imbsen (1991). *Distribution of Wheel Loads on Highway Bridges*, Final Report Project 12-26/1, National Cooperative Highway Research Program, Transportation Research Board, National Research Council, Washington, DC.
- Park R., (1964) "Ultimate Strength of Rectangular Concrete Slabs under Short-term Uniform Loading with Edges Restrained against Lateral Movement," *Proceedings of the Institution of Civil Engineers, Structures and Buildings*, V. 28, pp. 125-150.
- Fang, I.-K., Worley, J., Klingner, R. E., and Burns, N. H., (1986) "Behavior of Ontario-Type Bridge Decks on Steel Girders," Research Report 350-1, Center for Transportation Research, University of Texas at Austin, Austin, TX.
- Tsui, C. K., Burns, N. H., and Klingner, R. E., (1986) "Behavior of Ontario-Type Bridge Decks on Steel Girders: Negative Moment Region and Load Capacity," Research Report 350-3, Center for Transportation Research, University of Texas at Austin, Austin, TX.
- Guice, L. K. and Rhombery, E. J., (1988) "Membrane Action in Partially Restrained Slabs," *ACI Structural Journal*, Vol. 85, No. 4, p. 365-373.

Fang, I.-K., Worley, J., Burns, N. H., and Klingner, R. E., (1990^a) "Behavior of Isotropic R/C Bridge Decks on Steel Girders," ,” *ASCE, Journal of Structural Engineering*. Vol. 116, No. 3, pp 659-678.

Fang, I.-K., Tsui, C. K., Burns, N. H., and Klingner, R. E., (1990^b) "Fatigue Behavior of Cast-in-Place and Precast Panel Bridge Decks with Isotropic Reinforcement," *PCI Journal*. May-June, pp 28-39.

Fang, I.-K., Tsui, C. K., Burns, N. H., and Klingner, R. E., (1990^c) "Load Capacity of Isotropically Reinforced, Cast-in-Place and Precast Panel Bridge Decks," *PCI Journal*. July-August, pp 104--113.

Fang, I.-K., Lee, J.-H., and Chen, C.-R., (1994) "Behavior of Partially Restrained Slabs under Concentrated Load," *ACI Structural Journal*. Vol. 91, No. 2, pp 133--139.

Rankin, G. I. B., and Long, A. E., (1997) "Arching Action Strength Enhancement in Laterally- Restrained Slab Strips," *Proceedings of the Institution of Civil Engineers, Structures and Buildings*, V. 122, pp. 461-467.

Frosch, Robert J., (1999) "Another Look at Cracking and Crack Control in Reinforced Concrete" *ACI Structural Journal*, Vol. 96, No. 3, p. 437.

Siriaksorn, A. and Naaman, A. E., *Reliability of partially prestressed beams at serviceability limit states*, University of Illinois at Chicago Circle, Dept. of Materials Engineering. Research Report, June 1980. 126 pp.

Peel-Cross, J., Rankin, G. I. B., Gilbert, S. G., and Long, A. E. (2000) "Compressive Membrane Action in Composite Floor Slabs in the Cardington LBTF," *Proceedings of the Institution of Civil Engineers, Structures and Buildings*, V. 146, pp. 217-226.

Bailey, C. G., (2001) "Membrane Action of Unrestrained Lightly Reinforced Concrete Slabs at Large Displacements," *Engineering Structures*, V. 23, pp 470-483.

Graddy, J. C., Kim, J., Whitt, J. H., Burns, N. H., and Klingner, R. E. (2002), "Punching-Shear Behavior of Bridge Decks under Fatigue Loading", *ACI Structural Journal*, Vol. 99, pp 257-266.

Salim, W. and Sebastian, W. M. (2003) "Punching Shear Failure in Reinforced Concrete Slabs with Compressive Membrane Action," *ACI Structural Journal*, Vol. 100, pp 39-48.

Taylor, S. E., Rankin, B., and Cleland, D. J. (2003) "Real Strength of High-performance Concrete Bridge Deck Slabs" *Proceedings of the Institution of Civil Engineers*. Issue BE2 pp 81-90.

Taylor, S. E., Rankin, B., Cleland, D. J. and Kirkpatrick, J. (2007) "Serviceability of Bridge Deck Slabs with Arching Action," *ACI Structural Journal*, Vol. 104, pp 471-479.

Bailey, C. G., Toh, W. S., and Chan, B. K. (2008) "Simplified and Advanced Analysis of Membrane Action of Concrete Slabs," *ACI Structural Journal*, Vol. 105, pp 30-40.

Nowak, A. S., Szerszen, M. M., Szeliga, E. K., Szwed, A., and Podhorecki, P. J. (2008), "Reliability-Based Calibration for Structural Concrete, Phase 3" Portland Cement Association and Precast/Prestressed Concrete Institute. PCA R&D Serial No.2849, 110 pp.

Meadway, J. M. (2008) "Evaluation of Current Deck Design Practices," Master Thesis, West Virginia University.

Taylor, S.E., Rankin, G. I. B., and Cleland, D. J. (2003), "Real Strength of High-performance Concrete Bridge Deck Slabs," *Proceedings of the Institution of Civil Engineers, Bridge Engineering*, V. 156, pp. 81-90.

Mufti, A. and Hassan, T. (2005), "Finite Element Analysis and Theoretical Study of Punching Shear Strength of Concrete Bridge Decks," *Canadian Journal of Civil Engineering*, V32, pp 449-453.

Hon, A., Taplin, G., Al-Mahaidi, R. S. (2005), "Strength of Reinforced Concrete Bridge Decks under Compressive Membrane Action," *ACI Structural Journal*, V102, pp 393-401.

Schmeckpeper, E. R., Nielsen, R., Shiner, C., and Blandford, M. (2009), "the effect of bridge deck design methodology on crack control," Research Report N09-08.

FDOT. (1999). "Corrosion evaluation of post-tensioned tendons on the Niles Channel Bridge". Florida Department of Transportation (FDOT), Tallahassee, Florida.

FDOT. (2001^a). "Mid-Bay bridge post-tensioning evaluation", final report. Washington (DC): Corven Engineering, Inc., Florida Department of Transportation (FDOT), Tallahassee, Florida.

FDOT. (2001^b). "Sunshine skyway bridge post-tensioned tendons investigation". Parsons Brinckerhoff Quade and Douglas, Inc., Florida Department of Transportation (FDOT), Tallahassee, Florida.

Hansen B. (2007). "Forensic engineering: tendon failure raises questions about grout in post-tensioned bridges". *Civil Eng News*; November: 17-8.

Pillai, R. G., Hueste, M. D., Gardoni, P., Trejo, D., & Reinschmidt, K. F. (2010). Time-variant service reliability of post-tensioned, segmental, concrete bridges exposed to corrosive environments. *Engineering Structures*, 32(9), 2596-2605.

ACI Committee 209, (1997). Prediction of creep, shrinkage and temperature effects in concrete structures, ACI Manual of concrete practice, Part I, 209R 1-92.

Darmawan, M. S. and Stewart, M. G. (2007). Effect of pitting corrosion on capacity of prestressing wires. *Magazine of Concrete Research*, Vol. 59, No. 2, pp. 131–139.

Zandi Hanjari, K. (2010). Structural behaviour of deteriorated concrete structures. Chalmers University of Technology.

Akgül, F., & Frangopol, D. M. (2004). Time-dependent interaction between load rating and reliability of deteriorating bridges. *Engineering structures*, 26(12), 1751-1765.

APPENDIX A

BRIDGE DATABASES

In order to develop a comprehensive limit state, a broad bridge database that covers various design criteria and various design conditions is required. Therefore, bridge databases were developed for various girder types that used in current practice, includes AASHTO I Girders, AASHTO Adjacent Box Girders, AASHTO Spread Box Girders, and AASHTO ASBI Large Box Girders. For each girder type, a set of bridges were designed for span lengths ranging from 30 ft to 160 ft, except for AASHTO ASBI Large Box Girders, which were designed for span lengths ranging from 100 ft to 200 ft. Various design criteria such as live load factor, prestress losses calculation method, and maximum allowable tensile stress were also considered for each girder type. Furthermore, databases of existing bridges from NCHRP Project 12-78 were also included in this study for the investigation of reliability level of existing bridges. The databases for existing bridges contains I girders, spread box girders and adjacent box girders.

A.1 I Girder Bridges

Table A.1- Design Outcomes of I Girder Bridges Designed with Compressive Strength of 6ksi, Live Load Factor of 0.8 and Tensile Stress Limit of $0.0948\sqrt{f'_c}$.

Cases	Section Type	Span Length (ft)	Spacing (ft)	Aps (in ²)	# of Tendons
1	AASHTO I	30	6	1.224	8
2	AASHTO I	30	8	1.53	10
3	AASHTO I	30	10	1.836	12
4	AASHTO I	30	12	2.142	14
5	AASHTO II	60	6	2.754	18
6	AASHTO III	60	8	2.754	18
7	AASHTO III	60	10	3.366	22
8	AASHTO III	60	12	3.672	24
9	AASHTO III	80	6	3.978	26
10	AASHTO III	80	8	4.896	32
11	AASHTO IV	80	10	4.59	30
12	AASHTO IV	80	12	5.508	36
13	AASHTO IV	100	6	5.508	36
14	AASHTO IV	100	8	6.426	42
15	AASHTO V	100	10	6.426	42
16	AASHTO V	100	12	7.344	48
17	AASHTO V	120	6	7.038	46
18	AASHTO V	120	8	8.262	54
19	AASHTO VI	120	10	8.262	54
20	AASHTO VI	120	12	9.486	62
21	AASHTO VI	140	6	8.568	56
22	AASHTO VI	140	8	10.098	66
23	AASHTO VI	140	10	-	-
24	F.I.B.-96	160	6	8.246	38
25	F.I.B.-96	160	8	9.548	44
26	F.I.B.-96	160	10	10.85	50

Table A.2- Design Outcomes of I Girder Bridges Designed with Compressive Strength of 6ksi, Live Load Factor of 0.8 and Tensile Stress Limit of $0.158\sqrt{f'_c}$.

Cases	Section Type	Span Length (ft)	Spacing (ft)	Aps (in ²)	# of Tendons
1	AASHTO I	30	6	1.224	8
2	AASHTO I	30	8	1.53	10
3	AASHTO I	30	10	1.53	10
4	AASHTO I	30	12	1.836	12
5	AASHTO II	60	6	2.448	16
6	AASHTO III	60	8	2.448	16
7	AASHTO III	60	10	3.06	20
8	AASHTO III	60	12	3.366	22
9	AASHTO III	80	6	3.672	24
10	AASHTO IV	80	8	3.978	26
11	AASHTO IV	80	10	4.284	28
12	AASHTO IV	80	12	4.896	32
13	AASHTO IV	100	6	5.202	34
14	AASHTO IV	100	8	6.12	40
15	AASHTO V	100	10	5.814	38
16	AASHTO V	100	12	6.732	44
17	AASHTO V	120	6	6.426	42
18	AASHTO V	120	8	7.65	50
19	AASHTO VI	120	10	7.65	50
20	AASHTO VI	120	12	8.874	58
21	AASHTO VI	140	6	7.956	52
22	AASHTO VI	140	8	9.792	64
23	AASHTO VI	140	10	-	-
24	F.I.B.-96	160	6	7.378	34
25	F.I.B.-96	160	8	8.68	40
26	F.I.B.-96	160	10	10.416	48

Table A.3- Design Outcomes of I Girder Bridges Designed with Compressive Strength of 6ksi, Live Load Factor of 0.8 and Tensile Stress Limit of $0.19\sqrt{f'_c}$.

Cases	Section Type	Span Length (ft)	Spacing (ft)	Aps (in ²)	# of Tendons
1	AASHTO I	30	6	1.224	8
2	AASHTO I	30	8	1.53	10
3	AASHTO I	30	10	1.836	12
4	AASHTO I	30	12	2.142	14
5	AASHTO II	60	6	2.448	16
6	AASHTO III	60	8	2.142	14
7	AASHTO III	60	10	2.754	18
8	AASHTO III	60	12	3.366	22
9	AASHTO III	80	6	3.366	22
10	AASHTO III	80	8	4.59	30
11	AASHTO IV	80	10	4.284	28
12	AASHTO IV	80	12	4.896	32
13	AASHTO IV	100	6	4.896	32
14	AASHTO IV	100	8	6.12	40
15	AASHTO V	100	10	5.814	38
16	AASHTO V	100	12	6.732	44
17	AASHTO V	120	6	6.12	40
18	AASHTO V	120	8	7.65	50
19	AASHTO VI	120	10	7.344	48
20	AASHTO VI	120	12	8.568	56
21	AASHTO VI	140	6	7.65	50
22	AASHTO VI	140	8	9.18	60
23	AASHTO VI	140	10	-	-
24	F.I.B.-96	160	6	7.378	34
25	F.I.B.-96	160	8	8.68	40
26	F.I.B.-96	160	10	9.982	46

Table A.4- Design Outcomes of I Girder Bridges Designed with Compressive Strength of 6ksi, Live Load Factor of 0.8 and Tensile Stress Limit of $0.253\sqrt{f'_c}$.

Cases	Section Type	Span Length (ft)	Spacing (ft)	Aps (in ²)	# of Tendons
1	AASHTO I	30	6	1.224	8
2	AASHTO I	30	8	1.224	8
3	AASHTO I	30	10	1.53	10
4	AASHTO I	30	12	1.836	12
5	AASHTO II	60	6	2.142	14
6	AASHTO III	60	8	2.142	14
7	AASHTO III	60	10	2.448	16
8	AASHTO III	60	12	3.06	20
9	AASHTO III	80	6	3.366	22
10	AASHTO IV	80	8	3.366	22
11	AASHTO IV	80	10	3.978	26
12	AASHTO IV	80	12	4.59	30
13	AASHTO IV	100	6	4.59	30
14	AASHTO IV	100	8	5.814	38
15	AASHTO V	100	10	5.202	34
16	AASHTO V	100	12	6.12	40
17	AASHTO V	120	6	5.814	38
18	AASHTO V	120	8	7.038	46
19	AASHTO VI	120	10	7.038	46
20	AASHTO VI	120	12	7.956	52
21	AASHTO VI	140	6	7.344	48
22	AASHTO VI	140	8	8.874	58
23	AASHTO VI	140	10	10.404	68
24	F.I.B.-96	160	6	6.944	32
25	F.I.B.-96	160	8	7.812	36
26	F.I.B.-96	160	10	9.114	42

Table A.5- Design Outcomes of I Girder Bridges Designed with Compressive Strength of 6ksi, Live Load Factor of 1.0 and Tensile Stress Limit of $0.0948\sqrt{f'_c}$.

Cases	Section Type	Span Length (ft)	Spacing (ft)	Aps (in ²)	# of Tendons
1	AASHTO I	30	6	1.224	8
2	AASHTO I	30	8	1.53	10
3	AASHTO I	30	10	1.836	12
4	AASHTO I	30	12	2.142	14
5	AASHTO II	60	6	3.06	20
6	AASHTO III	60	8	3.06	20
7	AASHTO III	60	10	3.672	24
8	AASHTO III	60	12	4.284	28
9	AASHTO III	80	6	4.284	28
10	AASHTO IV	80	8	4.59	30
11	AASHTO IV	80	10	5.202	34
12	AASHTO IV	80	12	6.12	40
13	AASHTO IV	100	6	6.12	40
14	AASHTO V	100	8	6.12	40
15	AASHTO V	100	10	7.038	46
16	AASHTO V	100	12	7.956	52
17	AASHTO V	120	6	7.65	50
18	AASHTO VI	120	8	7.65	50
19	AASHTO VI	120	10	8.874	58
20	AASHTO VI	120	12	-	-
21	AASHTO VI	140	6	9.18	60
22	AASHTO VI	140	8	-	-
23	AASHTO VI	140	10	-	-
24	F.I.B.-96	160	6	8.68	40
25	F.I.B.-96	160	8	10.416	48
26	F.I.B.-96	160	10	11.718	54

Table A.6- Design Outcomes of I Girder Bridges Designed with Compressive Strength of 6ksi, Live Load Factor of 1.0 and Tensile Stress Limit of $0.158\sqrt{f'_c}$.

Cases	Section Type	Span Length (ft)	Spacing (ft)	Aps (in ²)	# of Tendons
1	AASHTO I	30	6	1.224	8
2	AASHTO I	30	8	1.53	10
3	AASHTO I	30	10	1.836	12
4	AASHTO I	30	12	2.448	16
5	AASHTO II	60	6	2.754	18
6	AASHTO III	60	8	2.754	18
7	AASHTO III	60	10	3.366	22
8	AASHTO III	60	12	3.978	26
9	AASHTO III	80	6	3.978	26
10	AASHTO IV	80	8	4.284	28
11	AASHTO IV	80	10	4.896	32
12	AASHTO IV	80	12	5.814	38
13	AASHTO IV	100	6	5.508	36
14	AASHTO IV	100	8	7.038	46
15	AASHTO V	100	10	6.732	44
16	AASHTO V	100	12	7.65	50
17	AASHTO V	120	6	7.038	46
18	AASHTO V	120	8	8.568	56
19	AASHTO VI	120	10	8.568	56
20	AASHTO VI	120	12	-	-
21	AASHTO VI	140	6	8.874	58
22	AASHTO VI	140	8	-	-
23	AASHTO VI	140	10	-	-
24	F.I.B.-96	160	6	8.246	38
25	F.I.B.-96	160	8	9.548	44
26	F.I.B.-96	160	10	11.284	52

Table A.7- Design Outcomes of I Girder Bridges Designed with Compressive Strength of 6ksi, Live Load Factor of 1.0 and Tensile Stress Limit of $0.19\sqrt{f'_c}$.

Cases	Section Type	Span Length (ft)	Spacing (ft)	Aps (in ²)	# of Tendons
1	AASHTO I	30	6	1.224	8
2	AASHTO I	30	8	1.53	10
3	AASHTO I	30	10	1.836	12
4	AASHTO I	30	12	2.448	16
5	AASHTO II	60	6	2.754	18
6	AASHTO III	60	8	2.448	16
7	AASHTO III	60	10	3.366	22
8	AASHTO III	60	12	3.978	26
9	AASHTO III	80	6	3.978	26
10	AASHTO IV	80	8	3.978	26
11	AASHTO IV	80	10	4.59	30
12	AASHTO IV	80	12	5.508	36
13	AASHTO IV	100	6	5.508	36
14	AASHTO IV	100	8	6.732	44
15	AASHTO V	100	10	6.426	42
16	AASHTO V	100	12	7.344	48
17	AASHTO V	120	6	6.732	44
18	AASHTO V	120	8	8.262	54
19	AASHTO VI	120	10	8.262	54
20	AASHTO VI	120	12	9.486	62
21	AASHTO VI	140	6	8.568	56
22	AASHTO VI	140	8	10.404	68
23	AASHTO VI	140	10	-	-
24	F.I.B.-96	160	6	7.812	36
25	F.I.B.-96	160	8	9.548	44
26	F.I.B.-96	160	10	10.85	50

Table A.8- Design Outcomes of I Girder Bridges Designed with Compressive Strength of 6ksi, Live Load Factor of 1.0 and Tensile Stress Limit of $0.253\sqrt{f'_c}$.

Cases	Section Type	Span Length (ft)	Spacing (ft)	Aps (in ²)	# of Tendons
1	AASHTO I	30	6	1.224	8
2	AASHTO I	30	8	1.224	8
3	AASHTO I	30	10	1.53	10
4	AASHTO I	30	12	1.836	12
5	AASHTO II	60	6	2.448	16
6	AASHTO III	60	8	2.448	16
7	AASHTO III	60	10	3.06	20
8	AASHTO III	60	12	3.672	24
9	AASHTO III	80	6	3.672	24
10	AASHTO IV	80	8	3.672	24
11	AASHTO IV	80	10	4.284	28
12	AASHTO IV	80	12	5.202	34
13	AASHTO IV	100	6	5.202	34
14	AASHTO IV	100	8	6.426	42
15	AASHTO V	100	10	5.814	38
16	AASHTO V	100	12	7.038	46
17	AASHTO V	120	6	6.426	42
18	AASHTO V	120	8	7.956	52
19	AASHTO VI	120	10	7.65	50
20	AASHTO VI	120	12	8.874	58
21	AASHTO VI	140	6	7.956	52
22	AASHTO VI	140	8	9.792	64
23	AASHTO VI	140	10	-	-
24	F.I.B.-96	160	6	7.378	34
25	F.I.B.-96	160	8	8.68	40
26	F.I.B.-96	160	10	10.416	48

Table A.9- Design Outcomes of I Girder Bridges Designed with Compressive Strength of 8ksi, Live Load Factor of 0.8 and Tensile Stress Limit of $0.0948\sqrt{f'_c}$.

Cases	Section Type	Span Length (ft)	Spacing (ft)	Aps (in ²)	# of Tendons
1	AASHTO I	30	6	1.224	8
2	AASHTO I	30	8	1.53	10
3	AASHTO I	30	10	1.836	12
4	AASHTO I	30	12	1.836	12
5	AASHTO II	60	6	2.448	16
6	AASHTO II	60	8	3.366	22
7	AASHTO III	60	10	3.06	20
8	AASHTO III	60	12	3.672	24
9	AASHTO III	80	6	3.672	24
10	AASHTO III	80	8	4.59	30
11	AASHTO III	80	10	5.508	36
12	AASHTO IV	80	12	5.202	34
13	AASHTO III	100	6	6.12	40
14	AASHTO IV	100	8	6.426	42
15	AASHTO IV	100	10	7.344	48
16	AASHTO V	100	12	7.038	46
17	AASHTO IV	120	6	7.956	52
18	AASHTO V	120	8	7.956	52
19	AASHTO V	120	10	9.18	60
20	AASHTO VI	120	12	8.874	58
21	AASHTO VI	140	6	8.262	54
22	AASHTO VI	140	8	9.792	64
23	AASHTO VI	140	10	11.322	74
24	F.I.B.-96	160	6	7.812	36
25	F.I.B.-96	160	8	9.114	42
26	F.I.B.-96	160	10	10.416	48

Table A.10- Design Outcomes of I Girder Bridges Designed with Compressive Strength of 8ksi, Live Load Factor of 0.8 and Tensile Stress Limit of $0.158\sqrt{f'_c}$.

Cases	Section Type	Span Length (ft)	Spacing (ft)	Aps (in ²)	# of Tendons
1	AASHTO I	30	6	1.224	8
2	AASHTO I	30	8	1.53	10
3	AASHTO I	30	10	1.836	12
4	AASHTO I	30	12	2.295	15
5	AASHTO II	60	6	2.448	16
6	AASHTO II	60	8	3.672	24
7	AASHTO III	60	10	3.06	20
8	AASHTO III	60	12	3.672	24
9	AASHTO III	80	6	3.366	22
10	AASHTO III	80	8	4.284	28
11	AASHTO III	80	10	5.202	34
12	AASHTO IV	80	12	4.896	32
13	AASHTO III	100	6	5.814	38
14	AASHTO IV	100	8	5.814	38
15	AASHTO IV	100	10	7.038	46
16	AASHTO V	100	12	6.426	42
17	AASHTO IV	120	6	7.344	48
18	AASHTO V	120	8	7.344	48
19	AASHTO V	120	10	8.568	56
20	AASHTO VI	120	12	8.262	54
21	AASHTO VI	140	6	7.65	50
22	AASHTO VI	140	8	9.18	60
23	AASHTO VI	140	10	10.71	70
24	F.I.B.-96	160	6	7.378	34
25	F.I.B.-96	160	8	8.68	40
26	F.I.B.-96	160	10	9.548	44

Table A.11- Design Outcomes of I Girder Bridges Designed with Compressive Strength of 8ksi, Live Load Factor of 0.8 and Tensile Stress Limit of $0.19\sqrt{f'_c}$.

Cases	Section Type	Span Length (ft)	Spacing (ft)	Aps (in ²)	# of Tendons
1	AASHTO I	30	6	1.224	8
2	AASHTO I	30	8	1.53	10
3	AASHTO I	30	10	1.836	12
4	AASHTO I	30	12	2.295	15
5	AASHTO II	60	6	2.448	16
6	AASHTO II	60	8	3.06	20
7	AASHTO III	60	10	3.06	20
8	AASHTO III	60	12	3.672	24
9	AASHTO III	80	6	3.366	22
10	AASHTO III	80	8	4.284	28
11	AASHTO III	80	10	4.896	32
12	AASHTO IV	80	12	4.896	32
13	AASHTO III	100	6	5.814	38
14	AASHTO IV	100	8	5.814	38
15	AASHTO IV	100	10	6.732	44
16	AASHTO V	100	12	6.426	42
17	AASHTO IV	120	6	7.344	48
18	AASHTO V	120	8	7.344	48
19	AASHTO V	120	10	8.262	54
20	AASHTO VI	120	12	8.262	54
21	AASHTO VI	140	6	7.344	48
22	AASHTO VI	140	8	8.874	58
23	AASHTO VI	140	10	10.404	68
24	F.I.B.-96	160	6	6.944	32
25	F.I.B.-96	160	8	8.246	38
26	F.I.B.-96	160	10	9.548	44

Table A.12- Design Outcomes of I Girder Bridges Designed with Compressive Strength of 8ksi, Live Load Factor of 0.8 and Tensile Stress Limit of $0.253\sqrt{f'_c}$.

Cases	Section Type	Span Length (ft)	Spacing (ft)	Aps (in ²)	# of Tendons
1	AASHTO I	30	6	1.224	8
2	AASHTO I	30	8	1.53	10
3	AASHTO I	30	10	1.836	12
4	AASHTO I	30	12	2.142	14
5	AASHTO II	60	6	2.142	14
6	AASHTO II	60	8	2.754	18
7	AASHTO III	60	10	2.448	16
8	AASHTO III	60	12	3.06	20
9	AASHTO III	80	6	3.06	20
10	AASHTO III	80	8	3.978	26
11	AASHTO III	80	10	4.59	30
12	AASHTO IV	80	12	4.284	28
13	AASHTO III	100	6	5.202	34
14	AASHTO IV	100	8	5.202	34
15	AASHTO IV	100	10	6.426	42
16	AASHTO V	100	12	5.814	38
17	AASHTO IV	120	6	6.732	44
18	AASHTO V	120	8	6.732	44
19	AASHTO V	120	10	7.956	52
20	AASHTO VI	120	12	7.65	50
21	AASHTO VI	140	6	6.732	44
22	AASHTO VI	140	8	8.262	54
23	AASHTO VI	140	10	9.792	64
24	F.I.B.-96	160	6	6.51	30
25	F.I.B.-96	160	8	7.378	34
26	F.I.B.-96	160	10	8.68	40

Table A.13- Design Outcomes of I Girder Bridges Designed with Compressive Strength of 8ksi, Live Load Factor of 1.0 and Tensile Stress Limit of $0.0948\sqrt{f'_c}$.

Cases	Section Type	Span Length (ft)	Spacing (ft)	Aps (in ²)	# of Tendons
1	AASHTO I	30	6	1.224	8
2	AASHTO I	30	8	1.53	10
3	AASHTO I	30	10	1.836	12
4	AASHTO I	30	12	2.295	15
5	AASHTO II	60	6	3.06	20
6	AASHTO II	60	8	3.978	26
7	AASHTO III	60	10	3.366	22
8	AASHTO III	60	12	4.284	28
9	AASHTO III	80	6	4.284	28
10	AASHTO III	80	8	5.202	34
11	AASHTO III	80	10	6.12	40
12	AASHTO IV	80	12	5.814	38
13	AASHTO III	100	6	7.038	46
14	AASHTO IV	100	8	7.038	46
15	AASHTO IV	100	10	8.262	54
16	AASHTO V	100	12	7.65	50
17	AASHTO IV	120	6	8.874	58
18	AASHTO V	120	8	8.874	58
19	AASHTO V	120	10	10.404	68
20	AASHTO VI	120	12	9.792	64
21	AASHTO VI	140	6	8.874	58
22	AASHTO VI	140	8	10.71	70
23	AASHTO VI	140	10	12.852	84
24	F.I.B.-96	160	6	8.246	38
25	F.I.B.-96	160	8	10.199	47
26	F.I.B.-96	160	10	11.284	52

Table A.14- Design Outcomes of I Girder Bridges Designed with Compressive Strength of 8ksi, Live Load Factor of 1.0 and Tensile Stress Limit of $0.158\sqrt{f'_c}$.

Cases	Section Type	Span Length (ft)	Spacing (ft)	Aps (in ²)	# of Tendons
1	AASHTO I	30	6	1.224	8
2	AASHTO I	30	8	1.53	10
3	AASHTO I	30	10	1.836	12
4	AASHTO I	30	12	2.295	15
5	AASHTO II	60	6	2.754	18
6	AASHTO II	60	8	3.672	24
7	AASHTO III	60	10	3.06	20
8	AASHTO III	60	12	3.672	24
9	AASHTO III	80	6	3.978	26
10	AASHTO III	80	8	4.896	32
11	AASHTO III	80	10	5.814	38
12	AASHTO IV	80	12	5.508	36
13	AASHTO III	100	6	6.732	44
14	AASHTO IV	100	8	6.426	42
15	AASHTO IV	100	10	7.65	50
16	AASHTO V	100	12	7.344	48
17	AASHTO IV	120	6	8.262	54
18	AASHTO V	120	8	8.262	54
19	AASHTO V	120	10	9.486	62
20	AASHTO VI	120	12	9.18	60
21	AASHTO VI	140	6	8.262	54
22	AASHTO VI	140	8	10.098	66
23	AASHTO VI	140	10	11.628	76
24	F.I.B.-96	160	6	7.812	36
25	F.I.B.-96	160	8	9.114	42
26	F.I.B.-96	160	10	10.416	48

Table A.15- Design Outcomes of I Girder Bridges Designed with Compressive Strength of 8ksi, Live Load Factor of 1.0 and Tensile Stress Limit of $0.19\sqrt{f'_c}$.

Cases	Section Type	Span Length (ft)	Spacing (ft)	Aps (in ²)	# of Tendons
1	AASHTO I	30	6	1.224	8
2	AASHTO I	30	8	1.53	10
3	AASHTO I	30	10	1.836	12
4	AASHTO I	30	12	2.295	15
5	AASHTO II	60	6	2.448	16
6	AASHTO II	60	8	3.366	22
7	AASHTO III	60	10	3.06	20
8	AASHTO III	60	12	3.672	24
9	AASHTO III	80	6	3.672	24
10	AASHTO III	80	8	4.59	30
11	AASHTO III	80	10	5.814	38
12	AASHTO IV	80	12	5.202	34
13	AASHTO III	100	6	6.426	42
14	AASHTO IV	100	8	6.426	42
15	AASHTO IV	100	10	7.65	50
16	AASHTO V	100	12	7.038	46
17	AASHTO IV	120	6	7.956	52
18	AASHTO V	120	8	7.956	52
19	AASHTO V	120	10	9.18	60
20	AASHTO VI	120	12	8.874	58
21	AASHTO VI	140	6	7.956	52
22	AASHTO VI	140	8	9.792	64
23	AASHTO VI	140	10	11.322	74
24	F.I.B.-96	160	6	7.378	34
25	F.I.B.-96	160	8	8.68	40
26	F.I.B.-96	160	10	10.416	48

Table A.16- Design Outcomes of I Girder Bridges Designed with Compressive Strength of 8ksi, Live Load Factor of 1.0 and Tensile Stress Limit of $0.253\sqrt{f'_c}$.

Cases	Section Type	Span Length (ft)	Spacing (ft)	Aps (in ²)	# of Tendons
1	AASHTO I	30	6	1.224	8
2	AASHTO I	30	8	1.53	10
3	AASHTO I	30	10	1.836	12
4	AASHTO I	30	12	2.295	15
5	AASHTO II	60	6	2.448	16
6	AASHTO II	60	8	3.366	22
7	AASHTO III	60	10	3.06	20
8	AASHTO III	60	12	3.672	24
9	AASHTO III	80	6	3.366	22
10	AASHTO III	80	8	4.284	28
11	AASHTO III	80	10	5.202	34
12	AASHTO IV	80	12	4.896	32
13	AASHTO III	100	6	6.12	40
14	AASHTO IV	100	8	5.814	38
15	AASHTO IV	100	10	7.038	46
16	AASHTO V	100	12	6.426	42
17	AASHTO IV	120	6	7.65	50
18	AASHTO V	120	8	7.344	48
19	AASHTO V	120	10	8.874	58
20	AASHTO VI	120	12	8.568	56
21	AASHTO VI	140	6	7.344	48
22	AASHTO VI	140	8	9.18	60
23	AASHTO VI	140	10	10.71	70
24	F.I.B.-96	160	6	6.944	32
25	F.I.B.-96	160	8	8.246	38
26	F.I.B.-96	160	10	9.548	44

Table A.17- Design Outcomes of I Girder Bridges Designed with Compressive Strength of 10 ksi, Live Load Factor of 0.8 and Tensile Stress Limit of $0.0948\sqrt{f'_c}$.

Cases	Section Type	Span Length (ft)	Spacing (ft)	Aps (in ²)	# of Tendons
1	AASHTO I	30	6	1.224	8
2	AASHTO I	30	8	1.53	10
3	AASHTO I	30	10	1.53	10
4	AASHTO I	30	12	1.836	12
5	AASHTO II	60	6	2.448	16
6	AASHTO II	60	8	3.366	22
7	AASHTO III	60	10	3.06	20
8	AASHTO III	60	12	3.672	24
9	AASHTO III	80	6	3.672	24
10	AASHTO III	80	8	4.59	30
11	AASHTO III	80	10	5.202	34
12	AASHTO IV	80	12	5.202	34
13	AASHTO III	100	6	6.12	40
14	AASHTO IV	100	8	6.12	40
15	AASHTO IV	100	10	7.038	46
16	AASHTO V	100	12	6.732	44
17	AASHTO IV	120	6	7.65	50
18	AASHTO V	120	8	7.65	50
19	AASHTO V	120	10	8.874	58
20	AASHTO VI	120	12	8.568	56
21	AASHTO VI	140	6	7.956	52
22	AASHTO VI	140	8	9.486	62
23	AASHTO VI	140	10	11.016	72
24	F.I.B.-96	160	6	7.812	36
25	F.I.B.-96	160	8	8.68	40
26	F.I.B.-96	160	10	9.982	46

Table A.18- Design Outcomes of I Girder Bridges Designed with Compressive Strength of 10 ksi, Live Load Factor of 0.8 and Tensile Stress Limit of $0.158\sqrt{f'_c}$.

Cases	Section Type	Span Length (ft)	Spacing (ft)	Aps (in ²)	# of Tendons
1	AASHTO I	30	6	0.918	6
2	AASHTO I	30	8	1.224	8
3	AASHTO I	30	10	1.224	8
4	AASHTO I	30	12	1.53	10
5	AASHTO II	60	6	2.142	14
6	AASHTO II	60	8	3.06	20
7	AASHTO III	60	10	2.754	18
8	AASHTO III	60	12	3.366	22
9	AASHTO III	80	6	3.366	22
10	AASHTO III	80	8	4.284	28
11	AASHTO III	80	10	4.896	32
12	AASHTO IV	80	12	4.59	30
13	AASHTO III	100	6	5.508	36
14	AASHTO IV	100	8	5.814	38
15	AASHTO IV	100	10	6.732	44
16	AASHTO V	100	12	6.426	42
17	AASHTO IV	120	6	7.344	48
18	AASHTO V	120	8	7.038	46
19	AASHTO V	120	10	8.262	54
20	AASHTO VI	120	12	8.262	54
21	AASHTO VI	140	6	7.344	48
22	AASHTO VI	140	8	8.874	58
23	AASHTO VI	140	10	10.098	66
24	F.I.B.-96	160	6	6.944	32
25	F.I.B.-96	160	8	8.246	38
26	F.I.B.-96	160	10	9.548	44

Table A.19- Design Outcomes of I Girder Bridges Designed with Compressive Strength of 10 ksi, Live Load Factor of 0.8 and Tensile Stress Limit of $0.19\sqrt{f'_c}$.

Cases	Section Type	Span Length (ft)	Spacing (ft)	Aps (in ²)	# of Tendons
1	AASHTO I	30	6	1.224	8
2	AASHTO I	30	8	1.53	10
3	AASHTO I	30	10	1.836	12
4	AASHTO I	30	12	2.142	14
5	AASHTO II	60	6	2.142	14
6	AASHTO II	60	8	2.754	18
7	AASHTO III	60	10	2.448	16
8	AASHTO III	60	12	3.06	20
9	AASHTO III	80	6	3.366	22
10	AASHTO III	80	8	3.978	26
11	AASHTO III	80	10	4.896	32
12	AASHTO IV	80	12	4.59	30
13	AASHTO III	100	6	5.508	36
14	AASHTO IV	100	8	5.508	36
15	AASHTO IV	100	10	6.426	42
16	AASHTO V	100	12	6.12	40
17	AASHTO IV	120	6	7.038	46
18	AASHTO V	120	8	7.038	46
19	AASHTO V	120	10	7.956	52
20	AASHTO VI	120	12	7.956	52
21	AASHTO VI	140	6	7.038	46
22	AASHTO VI	140	8	8.568	56
23	AASHTO VI	140	10	9.792	64
24	F.I.B.-96	160	6	6.944	32
25	F.I.B.-96	160	8	8.246	38
26	F.I.B.-96	160	10	9.114	42

Table A.20- Design Outcomes of I Girder Bridges Designed with Compressive Strength of 10 ksi, Live Load Factor of 0.8 and Tensile Stress Limit of $0.253\sqrt{f'_c}$.

Cases	Section Type	Span Length (ft)	Spacing (ft)	Aps (in ²)	# of Tendons
1	AASHTO I	30	6	0.918	6
2	AASHTO I	30	8	1.224	8
3	AASHTO I	30	10	1.224	8
4	AASHTO I	30	12	1.836	12
5	AASHTO II	60	6	2.142	14
6	AASHTO II	60	8	2.754	18
7	AASHTO III	60	10	2.142	14
8	AASHTO III	60	12	2.754	18
9	AASHTO III	80	6	3.06	20
10	AASHTO III	80	8	3.672	24
11	AASHTO III	80	10	4.59	30
12	AASHTO IV	80	12	3.978	26
13	AASHTO III	100	6	5.202	34
14	AASHTO IV	100	8	5.202	34
15	AASHTO IV	100	10	6.12	40
16	AASHTO V	100	12	5.508	36
17	AASHTO IV	120	6	6.426	42
18	AASHTO V	120	8	6.426	42
19	AASHTO V	120	10	7.65	50
20	AASHTO VI	120	12	7.344	48
21	AASHTO VI	140	6	6.426	42
22	AASHTO VI	140	8	7.956	52
23	AASHTO VI	140	10	9.18	60
24	F.I.B.-96	160	6	6.076	28
25	F.I.B.-96	160	8	7.378	34
26	F.I.B.-96	160	10	8.246	38

Table A.21- Design Outcomes of I Girder Bridges Designed with Compressive Strength of 10 ksi, Live Load Factor of 1.0 and Tensile Stress Limit of $0.0948\sqrt{f'_c}$.

Cases	Section Type	Span Length (ft)	Spacing (ft)	Aps (in ²)	# of Tendons
1	AASHTO I	30	6	1.224	8
2	AASHTO I	30	8	1.53	10
3	AASHTO I	30	10	1.836	12
4	AASHTO I	30	12	2.142	14
5	AASHTO II	60	6	3.06	20
6	AASHTO II	60	8	3.978	26
7	AASHTO III	60	10	3.366	22
8	AASHTO III	60	12	3.978	26
9	AASHTO III	80	6	3.978	26
10	AASHTO III	80	8	4.896	32
11	AASHTO III	80	10	6.12	40
12	AASHTO IV	80	12	5.814	38
13	AASHTO III	100	6	6.732	44
14	AASHTO IV	100	8	6.732	44
15	AASHTO IV	100	10	7.956	52
16	AASHTO V	100	12	7.65	50
17	AASHTO IV	120	6	8.568	56
18	AASHTO V	120	8	8.568	56
19	AASHTO V	120	10	10.098	66
20	AASHTO VI	120	12	9.486	62
21	AASHTO VI	140	6	8.568	56
22	AASHTO VI	140	8	10.404	68
23	AASHTO VI	140	10	11.934	78
24	F.I.B.-96	160	6	8.246	38
25	F.I.B.-96	160	8	9.548	44
26	F.I.B.-96	160	10	10.85	50

Table A.22- Design Outcomes of I Girder Bridges Designed with Compressive Strength of 10 ksi, Live Load Factor of 1.0 and Tensile Stress Limit of $0.158\sqrt{f'_c}$.

Cases	Section Type	Span Length (ft)	Spacing (ft)	Aps (in ²)	# of Tendons
1	AASHTO I	30	6	1.224	8
2	AASHTO I	30	8	1.53	10
3	AASHTO I	30	10	1.53	10
4	AASHTO I	30	12	2.142	14
5	AASHTO II	60	6	2.754	18
6	AASHTO II	60	8	3.672	24
7	AASHTO III	60	10	3.06	20
8	AASHTO III	60	12	3.672	24
9	AASHTO III	80	6	3.672	24
10	AASHTO III	80	8	4.59	30
11	AASHTO III	80	10	5.508	36
12	AASHTO IV	80	12	5.202	34
13	AASHTO III	100	6	6.426	42
14	AASHTO IV	100	8	6.426	42
15	AASHTO IV	100	10	7.65	50
16	AASHTO V	100	12	7.038	46
17	AASHTO IV	120	6	7.956	52
18	AASHTO V	120	8	7.956	52
19	AASHTO V	120	10	9.18	60
20	AASHTO VI	120	12	8.874	58
21	AASHTO VI	140	6	7.956	52
22	AASHTO VI	140	8	9.486	62
23	AASHTO VI	140	10	11.322	74
24	F.I.B.-96	160	6	7.812	36
25	F.I.B.-96	160	8	9.114	42
26	F.I.B.-96	160	10	10.416	48

Table A.23- Design Outcomes of I Girder Bridges Designed with Compressive Strength of 10 ksi, Live Load Factor of 1.0 and Tensile Stress Limit of $0.19\sqrt{f'_c}$.

Cases	Section Type	Span Length (ft)	Spacing (ft)	Aps (in ²)	# of Tendons
1	AASHTO I	30	6	1.224	8
2	AASHTO I	30	8	1.53	10
3	AASHTO I	30	10	1.53	10
4	AASHTO I	30	12	1.836	12
5	AASHTO II	60	6	2.448	16
6	AASHTO II	60	8	3.366	22
7	AASHTO III	60	10	2.754	18
8	AASHTO III	60	12	3.672	24
9	AASHTO III	80	6	3.672	24
10	AASHTO III	80	8	4.59	30
11	AASHTO III	80	10	5.508	36
12	AASHTO IV	80	12	5.202	34
13	AASHTO III	100	6	6.12	40
14	AASHTO IV	100	8	6.12	40
15	AASHTO IV	100	10	7.344	48
16	AASHTO V	100	12	6.732	44
17	AASHTO IV	120	6	7.65	50
18	AASHTO V	120	8	7.65	50
19	AASHTO V	120	10	8.874	58
20	AASHTO VI	120	12	8.568	56
21	AASHTO VI	140	6	7.65	50
22	AASHTO VI	140	8	9.18	60
23	AASHTO VI	140	10	11.016	72
24	F.I.B.-96	160	6	7.378	34
25	F.I.B.-96	160	8	8.68	40
26	F.I.B.-96	160	10	9.982	46

Table A.24- Design Outcomes of I Girder Bridges Designed with Compressive Strength of 10 ksi, Live Load Factor of 1.0 and Tensile Stress Limit of $0.253\sqrt{f'_c}$.

Cases	Section Type	Span Length (ft)	Spacing (ft)	Aps (in ²)	# of Tendons
1	AASHTO I	30	6	1.224	8
2	AASHTO I	30	8	1.53	10
3	AASHTO I	30	10	1.53	10
4	AASHTO I	30	12	1.836	12
5	AASHTO II	60	6	2.448	16
6	AASHTO II	60	8	3.06	20
7	AASHTO III	60	10	2.754	18
8	AASHTO III	60	12	3.366	22
9	AASHTO III	80	6	3.366	22
10	AASHTO III	80	8	4.284	28
11	AASHTO III	80	10	5.202	34
12	AASHTO IV	80	12	4.59	30
13	AASHTO III	100	6	5.814	38
14	AASHTO IV	100	8	5.814	38
15	AASHTO IV	100	10	6.732	44
16	AASHTO V	100	12	6.426	42
17	AASHTO IV	120	6	7.344	48
18	AASHTO V	120	8	7.038	46
19	AASHTO V	120	10	8.262	54
20	AASHTO VI	120	12	8.262	54
21	AASHTO VI	140	6	7.038	46
22	AASHTO VI	140	8	8.874	58
23	AASHTO VI	140	10	10.404	68
24	F.I.B.-96	160	6	6.51	30
25	F.I.B.-96	160	8	8.246	38
26	F.I.B.-96	160	10	9.114	42

A.2 Adjacent Box Girder Bridges

Table A.25- Design Outcomes of Adjacent Box Girder Bridges Designed with Compressive Strength of 6 ksi, Live Load Factor of 0.8 and Tensile Stress Limit of $0.0948\sqrt{f'_c}$.

Cases	Section Type	Span Length (ft)	Spacing (ft)	Aps (in ²)	# of Tendons
1	BI-36	30	3	1.224	8
2	BI-48	30	4	1.224	8
3	BI-36	60	3	2.754	18
4	BI-48	60	4	3.366	22
5	BII-36	80	3	3.672	24
6	BI-48	80	4	5.508	36
7	BIII-36	100	3	4.896	32
8	BII-48	100	4	7.038	46
9	BIV-36	120	3	6.732	44
10	BIII-48	120	4	8.874	58

Table A.26- Design Outcomes of Adjacent Box Girder Bridges Designed with Compressive Strength of 6 ksi, Live Load Factor of 0.8 and Tensile Stress Limit of $0.158\sqrt{f'_c}$.

Cases	Section Type	Span Length (ft)	Spacing (ft)	Aps (in ²)	# of Tendons
1	BI-36	30	3	0.918	6
2	BI-48	30	4	0.918	6
3	BI-36	60	3	2.448	16
4	BI-48	60	4	3.06	20
5	BII-36	80	3	3.366	22
6	BI-48	80	4	5.202	34
7	BIII-36	100	3	4.59	30
8	BII-48	100	4	6.426	42
9	BIV-36	120	3	6.12	40
10	BIII-48	120	4	8.262	54

Table A.27- Design Outcomes of Adjacent Box Girder Bridges Designed with Compressive Strength of 6 ksi, Live Load Factor of 0.8 and Tensile Stress Limit of $0.19\sqrt{f'_c}$.

Cases	Section Type	Span Length (ft)	Spacing (ft)	Aps (in ²)	# of Tendons
1	BI-36	30	3	0.918	6
2	BI-48	30	4	0.918	6
3	BI-36	60	3	2.448	16
4	BI-48	60	4	2.754	18
5	BII-36	80	3	3.366	22
6	BI-48	80	4	5.508	36
7	BIII-36	100	3	4.284	28
8	BII-48	100	4	6.426	42
9	BIV-36	120	3	6.12	40
10	BIII-48	120	4	7.956	52

Table A.28- Design Outcomes of Adjacent Box Girder Bridges Designed with Compressive Strength of 6 ksi, Live Load Factor of 0.8 and Tensile Stress Limit of $0.253\sqrt{f'_c}$.

Cases	Section Type	Span Length (ft)	Spacing (ft)	Aps (in ²)	# of Tendons
1	BI-36	30	3	0.612	4
2	BI-48	30	4	0.612	4
3	BI-36	60	3	2.142	14
4	BI-48	60	4	2.754	18
5	BII-36	80	3	3.06	20
6	BI-48	80	4	4.896	32
7	BIII-36	100	3	3.978	26
8	BII-48	100	4	6.12	40
9	BIV-36	120	3	5.814	38
10	BIII-48	120	4	7.344	48

Table A.29- Design Outcomes of Adjacent Box Girder Bridges Designed with Compressive Strength of 6 ksi, Live Load Factor of 1.0 and Tensile Stress Limit of $0.0948\sqrt{f'_c}$.

Cases	Section Type	Span Length (ft)	Spacing (ft)	Aps (in ²)	# of Tendons
1	BI-36	30	3	1.224	8
2	BI-48	30	4	1.224	8
3	BI-36	60	3	2.754	18
4	BI-48	60	4	3.366	22
5	BII-36	80	3	3.978	26
6	BI-48	80	4	5.814	38
7	BIII-36	100	3	4.896	32
8	BII-48	100	4	7.344	48
9	BIV-36	120	3	7.344	48
10	BIII-48	120	4	-	-

Table A.30- Design Outcomes of Adjacent Box Girder Bridges Designed with Compressive Strength of 6 ksi, Live Load Factor of 1.0 and Tensile Stress Limit of $0.158\sqrt{f'_c}$.

Cases	Section Type	Span Length (ft)	Spacing (ft)	Aps (in ²)	# of Tendons
1	BI-36	30	3	0.918	6
2	BI-48	30	4	1.224	8
3	BI-36	60	3	2.754	18
4	BI-48	60	4	3.06	20
5	BII-36	80	3	3.672	24
6	BI-48	80	4	5.508	36
7	BIII-36	100	3	4.896	32
8	BII-48	100	4	7.038	46
9	BIV-36	120	3	6.732	44
10	BIII-48	120	4	8.874	58

Table A.31- Design Outcomes of Adjacent Box Girder Bridges Designed with Compressive Strength of 6 ksi, Live Load Factor of 1.0 and Tensile Stress Limit of $0.19\sqrt{f'_c}$.

Cases	Section Type	Span Length (ft)	Spacing (ft)	Aps (in ²)	# of Tendons
1	BI-36	30	3	0.918	6
2	BI-48	30	4	0.918	6
3	BI-36	60	3	2.448	16
4	BI-48	60	4	3.06	20
5	BII-36	80	3	3.366	22
6	BI-48	80	4	5.508	36
7	BIII-36	100	3	4.59	30
8	BII-48	100	4	6.732	44
9	BIV-36	120	3	6.426	42
10	BIII-48	120	4	8.568	56

Table A.32- Design Outcomes of Adjacent Box Girder Bridges Designed with Compressive Strength of 6 ksi, Live Load Factor of 1.0 and Tensile Stress Limit of $0.253\sqrt{f'_c}$.

Cases	Section Type	Span Length (ft)	Spacing (ft)	Aps (in ²)	# of Tendons
1	BI-36	30	3	0.918	6
2	BI-48	30	4	0.612	4
3	BI-36	60	3	2.448	16
4	BI-48	60	4	2.754	18
5	BII-36	80	3	3.366	22
6	BI-48	80	4	5.202	34
7	BIII-36	100	3	4.284	28
8	BII-48	100	4	6.426	42
9	BIV-36	120	3	6.12	40
10	BIII-48	120	4	7.956	52

Table A.33- Design Outcomes of Adjacent Box Girder Bridges Designed with Compressive Strength of 8 ksi, Live Load Factor of 0.8 and Tensile Stress Limit of $0.0948\sqrt{f'_c}$.

Cases	Section Type	Span Length (ft)	Spacing (ft)	Aps (in ²)	# of Tendons
1	BI-36	30	3	1.224	8
2	BI-48	30	4	1.224	8
3	BI-36	60	3	2.754	18
4	BI-48	60	4	3.06	20
5	BII-36	80	3	3.672	24
6	BI-48	80	4	5.202	34
7	BIII-36	100	3	4.59	30
8	BII-48	100	4	6.732	44
9	BIV-36	120	3	6.426	42
10	BIII-48	120	4	8.262	54

Table A.34- Design Outcomes of Adjacent Box Girder Bridges Designed with Compressive Strength of 8 ksi, Live Load Factor of 0.8 and Tensile Stress Limit of $0.158\sqrt{f'_c}$.

Cases	Section Type	Span Length (ft)	Spacing (ft)	Aps (in ²)	# of Tendons
1	BI-36	30	3	0.918	6
2	BI-48	30	4	0.918	6
3	BI-36	60	3	2.448	16
4	BI-48	60	4	2.754	18
5	BII-36	80	3	3.366	22
6	BI-48	80	4	4.896	32
7	BIII-36	100	3	4.284	28
8	BII-48	100	4	6.12	40
9	BIV-36	120	3	5.814	38
10	BIII-48	120	4	7.65	50

Table A.35- Design Outcomes of Adjacent Box Girder Bridges Designed with Compressive Strength of 8 ksi, Live Load Factor of 0.8 and Tensile Stress Limit of $0.19\sqrt{f'_c}$.

Cases	Section Type	Span Length (ft)	Spacing (ft)	Aps (in ²)	# of Tendons
1	BI-36	30	3	0.918	6
2	BI-48	30	4	0.918	6
3	BI-36	60	3	2.448	16
4	BI-48	60	4	2.754	18
5	BII-36	80	3	3.06	20
6	BI-48	80	4	4.896	32
7	BIII-36	100	3	4.284	28
8	BII-48	100	4	6.12	40
9	BIV-36	120	3	5.814	38
10	BIII-48	120	4	7.344	48

Table A.36- Design Outcomes of Adjacent Box Girder Bridges Designed with Compressive Strength of 8 ksi, Live Load Factor of 0.8 and Tensile Stress Limit of $0.253\sqrt{f'_c}$.

Cases	Section Type	Span Length (ft)	Spacing (ft)	Aps (in ²)	# of Tendons
1	BI-36	30	3	0.612	4
2	BI-48	30	4	0.612	4
3	BI-36	60	3	2.142	14
4	BI-48	60	4	2.448	16
5	BII-36	80	3	3.06	20
6	BI-48	80	4	4.59	30
7	BIII-36	100	3	3.978	26
8	BII-48	100	4	5.814	38
9	BIV-36	120	3	5.508	36
10	BIII-48	120	4	7.038	46

Table A.37- Design Outcomes of Adjacent Box Girder Bridges Designed with Compressive Strength of 8 ksi, Live Load Factor of 1.0 and Tensile Stress Limit of $0.0948\sqrt{f'_c}$.

Cases	Section Type	Span Length (ft)	Spacing (ft)	Aps (in ²)	# of Tendons
1	BI-36	30	3	1.224	8
2	BI-48	30	4	1.53	10
3	BI-36	60	3	2.754	18
4	BI-48	60	4	3.366	22
5	BII-36	80	3	3.672	24
6	BI-48	80	4	5.814	38
7	BIII-36	100	3	4.896	32
8	BII-48	100	4	7.038	46
9	BIV-36	120	3	6.732	44
10	BIII-48	120	4	8.874	58

Table A.38- Design Outcomes of Adjacent Box Girder Bridges Designed with Compressive Strength of 8 ksi, Live Load Factor of 1.0 and Tensile Stress Limit of $0.158\sqrt{f'_c}$.

Cases	Section Type	Span Length (ft)	Spacing (ft)	Aps (in ²)	# of Tendons
1	BI-36	30	3	0.918	6
2	BI-48	30	4	0.918	6
3	BI-36	60	3	2.448	16
4	BI-48	60	4	3.06	20
5	BII-36	80	3	3.366	22
6	BI-48	80	4	5.508	36
7	BIII-36	100	3	4.59	30
8	BII-48	100	4	6.732	44
9	BIV-36	120	3	6.12	40
10	BIII-48	120	4	8.262	54

Table A.39- Design Outcomes of Adjacent Box Girder Bridges Designed with Compressive Strength of 8 ksi, Live Load Factor of 1.0 and Tensile Stress Limit of $0.19\sqrt{f'_c}$.

Cases	Section Type	Span Length (ft)	Spacing (ft)	Aps (in ²)	# of Tendons
1	BI-36	30	3	0.918	6
2	BI-48	30	4	0.918	6
3	BI-36	60	3	2.448	16
4	BI-48	60	4	3.06	20
5	BII-36	80	3	3.366	22
6	BI-48	80	4	5.202	34
7	BIII-36	100	3	4.284	28
8	BII-48	100	4	6.426	42
9	BIV-36	120	3	6.12	40
10	BIII-48	120	4	7.956	52

Table A.40- Design Outcomes of Adjacent Box Girder Bridges Designed with Compressive Strength of 8 ksi, Live Load Factor of 1.0 and Tensile Stress Limit of $0.253\sqrt{f'_c}$.

Cases	Section Type	Span Length (ft)	Spacing (ft)	Aps (in ²)	# of Tendons
1	BI-36	30	3	0.612	4
2	BI-48	30	4	0.612	4
3	BI-36	60	3	2.142	14
4	BI-48	60	4	2.754	18
5	BII-36	80	3	3.06	20
6	BI-48	80	4	4.896	32
7	BIII-36	100	3	3.978	26
8	BII-48	100	4	6.12	40
9	BIV-36	120	3	5.814	38
10	BIII-48	120	4	7.344	48

A.3 Spread Box Girder Bridges

Table A.41- Design Outcomes of Spread Box Girder Bridges Designed with Compressive Strength of 6ksi, Live Load Factor of 0.8 and Tensile Stress Limit of $0.0948\sqrt{f'_c}$.

Cases	Section Type	Span Length (ft)	Spacing (ft)	Aps (in ²)	# of Tendons
1	BI-36	30	6	1.53	10
2	BI-36	30	8	1.836	12
3	BI-36	30	10	1.836	12
4	BI-36	30	12	2.142	14
5	BI-36	60	6	4.284	28
6	BI-36	60	8	4.896	32
7	BI-36	60	10	4.59	30
8	BI-48	60	12	5.202	34
9	BI-48	80	6	5.814	38
10	BII-48	80	8	5.814	38
11	BII-48	80	10	6.426	42
12	BIII-48	80	12	7.038	46
13	BIII-48	100	6	7.344	48
14	BIII-48	100	8	-	-
15	BIV-48	100	10	-	-

Table A.42- Design Outcomes of Spread Box Girder Bridges Designed with Compressive Strength of 6ksi, Live Load Factor of 0.8 and Tensile Stress Limit of $0.158\sqrt{f'_c}$.

Cases	Section Type	Span Length (ft)	Spacing (ft)	Aps (in ²)	# of Tendons
1	BI-36	30	6	1.224	8
2	BI-36	30	8	1.53	10
3	BI-36	30	10	1.836	12
4	BI-36	30	12	1.836	12
5	BI-36	60	6	3.978	26
6	BI-36	60	8	4.896	32
7	BI-36	60	10	4.284	28
8	BI-48	60	12	4.896	32
9	BI-48	80	6	5.508	36
10	BII-48	80	8	5.508	36
11	BII-48	80	10	6.12	40
12	BIII-48	80	12	6.426	42
13	BIII-48	100	6	7.038	46
14	BIII-48	100	8	-	-
15	BIV-48	100	10	-	-

Table A.43- Design Outcomes of Spread Box Girder Bridges Designed with Compressive Strength of 6ksi, Live Load Factor of 0.8 and Tensile Stress Limit of $0.19\sqrt{f'_c}$.

Cases	Section Type	Span Length (ft)	Spacing (ft)	Aps (in ²)	# of Tendons
1	BI-36	30	6	1.224	8
2	BI-36	30	8	1.53	10
3	BI-36	30	10	1.53	10
4	BI-36	30	12	1.836	12
5	BI-36	60	6	3.672	24
6	BI-36	60	8	4.59	30
7	BI-36	60	10	3.978	26
8	BI-48	60	12	4.59	30
9	BI-48	80	6	5.202	34
10	BII-48	80	8	5.202	34
11	BII-48	80	10	6.12	40
12	BIII-48	80	12	6.426	42
13	BIII-48	100	6	7.038	46
14	BIII-48	100	8	-	-
15	BIV-48	100	10	-	-

Table A.44- Design Outcomes of Spread Box Girder Bridges Designed with Compressive Strength of 6ksi, Live Load Factor of 0.8 and Tensile Stress Limit of $0.253\sqrt{f'_c}$.

Cases	Section Type	Span Length (ft)	Spacing (ft)	Aps (in ²)	# of Tendons
1	BI-36	30	6	1.224	8
2	BI-36	30	8	1.224	8
3	BI-36	30	10	1.53	10
4	BI-36	30	12	1.53	10
5	BI-36	60	6	3.672	24
6	BI-36	60	8	4.284	28
7	BII-36	60	10	3.978	26
8	BII-48	60	12	4.284	28
9	BII-48	80	6	4.896	32
10	BIII-48	80	8	4.896	32
11	BIII-48	80	10	5.814	38
12	BIV-48	80	12	5.814	38
13	BIII-48	100	6	6.426	42
14	BIII-48	100	8	-	-
15	BIV-48	100	10	-	-

Table A.45- Design Outcomes of Spread Box Girder Bridges Designed with Compressive Strength of 6ksi, Live Load Factor of 1.0 and Tensile Stress Limit of $0.0948\sqrt{f'_c}$.

Cases	Section Type	Span Length (ft)	Spacing (ft)	Aps (in ²)	# of Tendons
1	BI-36	30	6	1.53	10
2	BI-36	30	8	1.836	12
3	BI-36	30	10	2.142	14
4	BI-36	30	12	2.448	16
5	BI-36	60	6	4.59	30
6	BII-36	60	8	4.284	28
7	BII-36	60	10	4.896	32
8	BII-48	60	12	5.814	38
9	BII-48	80	6	6.12	40
10	BIII-48	80	8	6.12	40
11	BIV-48	80	10	6.732	44
12	BIV-48	80	12	7.65	50
13	BIV-48	100	6	7.344	48
14	BIII-48	100	8	-	-
15	BIV-48	100	10	-	-

Table A.46- Design Outcomes of Spread Box Girder Bridges Designed with Compressive Strength of 6ksi, Live Load Factor of 1.0 and Tensile Stress Limit of $0.158\sqrt{f'_c}$.

Cases	Section Type	Span Length (ft)	Spacing (ft)	Aps (in ²)	# of Tendons
1	BI-36	30	6	1.53	10
2	BI-36	30	8	1.836	12
3	BI-36	30	10	1.836	12
4	BI-36	30	12	2.142	14
5	BI-36	60	6	4.284	28
6	BII-36	60	8	3.978	26
7	BII-36	60	10	4.59	30
8	BII-48	60	12	5.508	36
9	BII-48	80	6	5.814	38
10	BIII-48	80	8	5.814	38
11	BIII-48	80	10	6.732	44
12	BIV-48	80	12	7.038	46
13	BIII-48	100	6	7.65	50
14	BIII-48	100	8	-	-
15	BIV-48	100	10	-	-

Table A.47- Design Outcomes of Spread Box Girder Bridges Designed with Compressive Strength of 6ksi, Live Load Factor of 1.0 and Tensile Stress Limit of $0.19\sqrt{f'_c}$.

Cases	Section Type	Span Length (ft)	Spacing (ft)	Aps (in ²)	# of Tendons
1	BI-36	30	6	1.53	10
2	BI-36	30	8	1.53	10
3	BI-36	30	10	1.836	12
4	BI-36	30	12	2.142	14
5	BI-36	60	6	4.284	28
6	BI-36	60	8	5.202	34
7	BII-36	60	10	4.59	30
8	BII-48	60	12	5.202	34
9	BII-48	80	6	5.814	38
10	BIII-48	80	8	5.814	38
11	BIII-48	80	10	6.732	44
12	BIV-48	80	12	7.038	46
13	BIII-48	100	6	7.65	50
14	BIII-48	100	8	-	-
15	BIV-48	100	10	-	-

Table A.48- Design Outcomes of Spread Box Girder Bridges Designed with Compressive Strength of 6ksi, Live Load Factor of 1.0 and Tensile Stress Limit of $0.253\sqrt{f'_c}$.

Cases	Section Type	Span Length (ft)	Spacing (ft)	Aps (in ²)	# of Tendons
1	BI-36	30	6	1.224	8
2	BI-36	30	8	1.53	10
3	BI-36	30	10	1.53	10
4	BI-36	30	12	1.836	12
5	BI-36	60	6	3.978	26
6	BI-36	60	8	4.896	32
7	BII-36	60	10	4.284	28
8	BII-48	60	12	4.896	32
9	BII-48	80	6	5.508	36
10	BIII-48	80	8	5.508	36
11	BIII-48	80	10	6.426	42
12	BIV-48	80	12	7.038	46
13	BIII-48	100	6	7.038	46
14	BIII-48	100	8	-	-
15	BIV-48	100	10	-	-

Table A.49- Design Outcomes of Spread Box Girder Bridges Designed with Compressive Strength of 8ksi, Live Load Factor of 0.8 and Tensile Stress Limit of $0.0948\sqrt{f'_c}$.

Cases	Section Type	Span Length (ft)	Spacing (ft)	Aps (in ²)	# of Tendons
1	BI-36	30	6	1.53	10
2	BI-36	30	8	1.836	12
3	BI-36	30	10	1.836	12
4	BI-36	30	12	2.142	14
5	BI-36	60	6	3.978	26
6	BI-36	60	8	4.896	32
7	BI-36	60	10	5.508	36
8	BI-48	60	12	6.426	42
9	BI-48	80	6	7.038	46
10	BII-48	80	8	6.732	44
11	BII-48	80	10	7.65	50
12	BIII-48	80	12	7.038	46
13	BIII-48	100	6	7.344	48
14	BIII-48	100	8	9.18	60
15	BIV-48	100	10	10.404	68

Table A.50- Design Outcomes of Spread Box Girder Bridges Designed with Compressive Strength of 8ksi, Live Load Factor of 0.8 and Tensile Stress Limit of $0.158\sqrt{f'_c}$.

Cases	Section Type	Span Length (ft)	Spacing (ft)	Aps (in ²)	# of Tendons
1	BI-36	30	6	1.224	8
2	BI-36	30	8	1.53	10
3	BI-36	30	10	1.836	12
4	BI-36	30	12	1.836	12
5	BI-36	60	6	3.672	24
6	BI-36	60	8	4.59	30
7	BI-36	60	10	5.202	34
8	BI-48	60	12	5.814	38
9	BI-48	80	6	6.732	44
10	BII-48	80	8	6.12	40
11	BII-48	80	10	7.344	48
12	BIII-48	80	12	6.732	44
13	BIII-48	100	6	7.038	46
14	BIII-48	100	8	8.262	54
15	BIV-48	100	10	9.18	60

Table A.51- Design Outcomes of Spread Box Girder Bridges Designed with Compressive Strength of 8ksi, Live Load Factor of 0.8 and Tensile Stress Limit of $0.19\sqrt{f'_c}$.

Cases	Section Type	Span Length (ft)	Spacing (ft)	Aps (in ²)	# of Tendons
1	BI-36	30	6	1.224	8
2	BI-36	30	8	1.53	10
3	BI-36	30	10	1.53	10
4	BI-36	30	12	1.836	12
5	BI-36	60	6	3.672	24
6	BI-36	60	8	4.284	28
7	BI-36	60	10	5.202	34
8	BI-48	60	12	5.814	38
9	BI-48	80	6	6.426	42
10	BII-48	80	8	6.12	40
11	BII-48	80	10	7.038	46
12	BIII-48	80	12	6.732	44
13	BIII-48	100	6	6.732	44
14	BIII-48	100	8	7.956	52
15	BIV-48	100	10	8.568	56

Table A.52- Design Outcomes of Spread Box Girder Bridges Designed with Compressive Strength of 8ksi, Live Load Factor of 0.8 and Tensile Stress Limit of $0.253\sqrt{f'_c}$.

Cases	Section Type	Span Length (ft)	Spacing (ft)	Aps (in ²)	# of Tendons
1	BI-36	30	6	0.918	6
2	BI-36	30	8	1.224	8
3	BI-36	30	10	1.53	10
4	BI-36	30	12	1.53	10
5	BI-36	60	6	3.366	22
6	BI-36	60	8	4.284	28
7	BI-36	60	10	4.896	32
8	BI-48	60	12	5.508	36
9	BI-48	80	6	6.12	40
10	BII-48	80	8	5.814	38
11	BII-48	80	10	6.732	44
12	BIII-48	80	12	6.12	40
13	BIII-48	100	6	6.426	42
14	BIII-48	100	8	7.65	50
15	BIV-48	100	10	7.956	52

Table A.53- Design Outcomes of Spread Box Girder Bridges Designed with Compressive Strength of 8ksi, Live Load Factor of 1.0 and Tensile Stress Limit of $0.0948\sqrt{f'_c}$.

Cases	Section Type	Span Length (ft)	Spacing (ft)	Aps (in ²)	# of Tendons
1	BI-36	30	6	1.53	10
2	BI-36	30	8	1.836	12
3	BI-36	30	10	2.142	14
4	BI-36	30	12	2.142	14
5	BI-36	60	6	4.284	28
6	BI-36	60	8	5.202	34
7	BI-36	60	10	6.426	42
8	BI-48	60	12	7.038	46
9	BI-48	80	6	7.65	50
10	BII-48	80	8	7.344	48
11	BII-48	80	10	8.874	58
12	BIII-48	80	12	7.956	52
13	BIII-48	100	6	7.956	52
14	BIII-48	100	8	-	-
15	BIV-48	100	10	-	-

Table A.54- Design Outcomes of Spread Box Girder Bridges Designed with Compressive Strength of 8ksi, Live Load Factor of 1.0 and Tensile Stress Limit of $0.158\sqrt{f'_c}$.

Cases	Section Type	Span Length (ft)	Spacing (ft)	Aps (in ²)	# of Tendons
1	BI-36	30	6	1.53	10
2	BI-36	30	8	1.53	10
3	BI-36	30	10	1.836	12
4	BI-36	30	12	2.142	14
5	BI-36	60	6	4.284	28
6	BI-36	60	8	4.896	32
7	BI-36	60	10	5.814	38
8	BI-48	60	12	6.732	44
9	BI-48	80	6	7.344	48
10	BII-48	80	8	6.732	44
11	BII-48	80	10	7.956	52
12	BIII-48	80	12	7.344	48
13	BIII-48	100	6	7.344	48
14	BIII-48	100	8	9.792	64
15	BIV-48	100	10	-	-

Table A.55- Design Outcomes of Spread Box Girder Bridges Designed with Compressive Strength of 8ksi, Live Load Factor of 1.0 and Tensile Stress Limit of $0.19\sqrt{f'_c}$.

Cases	Section Type	Span Length (ft)	Spacing (ft)	Aps (in ²)	# of Tendons
1	BI-36	30	6	1.224	8
2	BI-36	30	8	1.53	10
3	BI-36	30	10	1.836	12
4	BI-36	30	12	1.836	12
5	BI-36	60	6	3.978	26
6	BI-36	60	8	4.896	32
7	BI-36	60	10	5.814	38
8	BI-48	60	12	6.426	42
9	BI-48	80	6	7.038	46
10	BII-48	80	8	6.732	44
11	BII-48	80	10	7.956	52
12	BIII-48	80	12	7.344	48
13	BIII-48	100	6	7.038	46
14	BIII-48	100	8	9.18	60
15	BIV-48	100	10	-	-

Table A.56- Design Outcomes of Spread Box Girder Bridges Designed with Compressive Strength of 8ksi, Live Load Factor of 1.0 and Tensile Stress Limit of $0.253\sqrt{f'_c}$.

Cases	Section Type	Span Length (ft)	Spacing (ft)	Aps (in ²)	# of Tendons
1	BI-36	30	6	1.224	8
2	BI-36	30	8	1.224	8
3	BI-36	30	10	1.53	10
4	BI-36	30	12	1.836	12
5	BI-36	60	6	3.672	24
6	BI-36	60	8	4.59	30
7	BI-36	60	10	5.508	36
8	BI-48	60	12	6.12	40
9	BI-48	80	6	6.732	44
10	BII-48	80	8	6.426	42
11	BII-48	80	10	7.344	48
12	BIII-48	80	12	6.732	44
13	BIII-48	100	6	6.732	44
14	BIII-48	100	8	8.568	56
15	BIV-48	100	10	8.874	58

Table A.57- Design Outcomes of Spread Box Girder Bridges Designed with Compressive Strength of 10ksi, Live Load Factor of 0.8 and Tensile Stress Limit of $0.0948\sqrt{f'_c}$.

Cases	Section Type	Span Length (ft)	Spacing (ft)	Aps (in ²)	# of Tendons
1	BI-36	30	6	1.53	10
2	BI-36	30	8	1.53	10
3	BI-36	30	10	1.836	12
4	BI-36	30	12	2.142	14
5	BI-36	60	6	3.978	26
6	BI-36	60	8	4.59	30
7	BI-36	60	10	5.508	36
8	BI-48	60	12	6.12	40
9	BI-48	80	6	6.732	44
10	BII-48	80	8	6.426	42
11	BII-48	80	10	7.344	48
12	BIII-48	80	12	7.038	46
13	BIII-48	100	6	7.038	46
14	BIII-48	100	8	8.568	56
15	BIV-48	100	10	9.486	62

Table A.58- Design Outcomes of Spread Box Girder Bridges Designed with Compressive Strength of 10ksi, Live Load Factor of 0.8 and Tensile Stress Limit of $0.158\sqrt{f'_c}$.

Cases	Section Type	Span Length (ft)	Spacing (ft)	Aps (in ²)	# of Tendons
1	BI-36	30	6	1.224	8
2	BI-36	30	8	1.53	10
3	BI-36	30	10	1.53	10
4	BI-36	30	12	1.836	12
5	BI-36	60	6	3.672	24
6	BI-36	60	8	4.284	28
7	BI-36	60	10	5.202	34
8	BI-48	60	12	5.814	38
9	BI-48	80	6	6.426	42
10	BII-48	80	8	6.12	40
11	BII-48	80	10	7.038	46
12	BIII-48	80	12	6.426	42
13	BIII-48	100	6	6.732	44
14	BIII-48	100	8	7.956	52
15	BIV-48	100	10	8.568	56

Table A.59- Design Outcomes of Spread Box Girder Bridges Designed with Compressive Strength of 10ksi, Live Load Factor of 0.8 and Tensile Stress Limit of $0.19\sqrt{f'_c}$.

Cases	Section Type	Span Length (ft)	Spacing (ft)	Aps (in ²)	# of Tendons
1	BI-36	30	6	1.224	8
2	BI-36	30	8	1.224	8
3	BI-36	30	10	1.53	10
4	BI-36	30	12	1.836	12
5	BI-36	60	6	3.672	24
6	BI-36	60	8	4.284	28
7	BI-36	60	10	4.896	32
8	BI-48	60	12	5.508	36
9	BI-48	80	6	6.426	42
10	BII-48	80	8	5.814	38
11	BII-48	80	10	6.732	44
12	BIII-48	80	12	6.426	42
13	BIII-48	100	6	6.732	44
14	BIII-48	100	8	7.65	50
15	BIV-48	100	10	8.262	54

Table A.60- Design Outcomes of Spread Box Girder Bridges Designed with Compressive Strength of 10ksi, Live Load Factor of 0.8 and Tensile Stress Limit of $0.253\sqrt{f'_c}$.

Cases	Section Type	Span Length (ft)	Spacing (ft)	Aps (in ²)	# of Tendons
1	BI-36	30	6	0.918	6
2	BI-36	30	8	1.224	8
3	BI-36	30	10	1.224	8
4	BI-36	30	12	1.53	10
5	BI-36	60	6	3.366	22
6	BI-36	60	8	3.978	26
7	BI-36	60	10	4.59	30
8	BI-48	60	12	5.202	34
9	BI-48	80	6	5.814	38
10	BII-48	80	8	5.508	36
11	BII-48	80	10	6.426	42
12	BIII-48	80	12	5.814	38
13	BIII-48	100	6	6.12	40
14	BIII-48	100	8	7.344	48
15	BIV-48	100	10	7.65	50

Table A.61- Design Outcomes of Spread Box Girder Bridges Designed with Compressive Strength of 10ksi, Live Load Factor of 1.0 and Tensile Stress Limit of $0.0948\sqrt{f'_c}$.

Cases	Section Type	Span Length (ft)	Spacing (ft)	Aps (in ²)	# of Tendons
1	BI-36	30	6	1.53	10
2	BI-36	30	8	1.836	12
3	BI-36	30	10	2.142	14
4	BI-36	30	12	2.142	14
5	BI-36	60	6	4.284	28
6	BI-36	60	8	5.202	34
7	BI-36	60	10	6.12	40
8	BI-48	60	12	6.732	44
9	BI-48	80	6	7.344	48
10	BII-48	80	8	7.038	46
11	BII-48	80	10	8.262	54
12	BIII-48	80	12	7.65	50
13	BIII-48	100	6	7.65	50
14	BIII-48	100	8	-	-
15	BIV-48	100	10	-	-

Table A.62- Design Outcomes of Spread Box Girder Bridges Designed with Compressive Strength of 10ksi, Live Load Factor of 1.0 and Tensile Stress Limit of $0.158\sqrt{f'_c}$.

Cases	Section Type	Span Length (ft)	Spacing (ft)	Aps (in ²)	# of Tendons
1	BI-36	30	6	1.53	10
2	BI-36	30	8	1.53	10
3	BI-36	30	10	1.836	12
4	BI-36	30	12	2.142	14
5	BI-36	60	6	3.978	26
6	BI-36	60	8	4.896	32
7	BI-36	60	10	5.814	38
8	BI-48	60	12	6.426	42
9	BI-48	80	6	7.038	46
10	BII-48	80	8	6.732	44
11	BII-48	80	10	7.65	50
12	BIII-48	80	12	7.344	48
13	BIII-48	100	6	7.344	48
14	BIII-48	100	8	8.874	58
15	BIV-48	100	10	10.098	66

Table A.63- Design Outcomes of Spread Box Girder Bridges Designed with Compressive Strength of 10ksi, Live Load Factor of 1.0 and Tensile Stress Limit of $0.19\sqrt{f'_c}$.

Cases	Section Type	Span Length (ft)	Spacing (ft)	Aps (in ²)	# of Tendons
1	BI-36	30	6	1.224	8
2	BI-36	30	8	1.53	10
3	BI-36	30	10	1.836	12
4	BI-36	30	12	1.836	12
5	BI-36	60	6	3.978	26
6	BI-36	60	8	4.59	30
7	BI-36	60	10	5.508	36
8	BI-48	60	12	6.12	40
9	BI-48	80	6	6.732	44
10	BII-48	80	8	6.426	42
11	BII-48	80	10	7.65	50
12	BIII-48	80	12	7.038	46
13	BIII-48	100	6	7.038	46
14	BIII-48	100	8	8.568	56
15	BIV-48	100	10	9.486	62

Table A.64- Design Outcomes of Spread Box Girder Bridges Designed with Compressive Strength of 10ksi, Live Load Factor of 1.0 and Tensile Stress Limit of $0.253\sqrt{f'_c}$.

Cases	Section Type	Span Length (ft)	Spacing (ft)	Aps (in ²)	# of Tendons
1	BI-36	30	6	0.918	6
2	BI-36	30	8	1.224	8
3	BI-36	30	10	1.53	10
4	BI-36	30	12	1.53	10
5	BI-36	60	6	3.672	24
6	BI-36	60	8	4.59	30
7	BI-36	60	10	5.202	34
8	BI-48	60	12	5.814	38
9	BI-48	80	6	6.426	42
10	BII-48	80	8	6.12	40
11	BII-48	80	10	7.038	46
12	BIII-48	80	12	6.426	42
13	BIII-48	100	6	6.732	44
14	BIII-48	100	8	7.956	52
15	BIV-48	100	10	8.568	56

A.4 PCI ASBI Box Girder Bridge

Table A.65- Design Outcomes of Spread Box Girder Bridges Designed with Compressive Strength of 8ksi, Live Load Factor of 0.8 and Tensile Stress Limit of $0.0948\sqrt{f'_c}$.

Cases	Section Type	Span Length (ft)	Aps (in ²)	# of Tendons
1	1800-2	100	7.344	48
2	1800-2	120	10.71	70
3	1800-2	140	14.076	92
4	2100-2	160	21.266	98
5	2400-2	180	22.568	104
6	2400-2	200	27.342	126

Table A.66- Design Outcomes of Spread Box Girder Bridges Designed with Compressive Strength of 8ksi, Live Load Factor of 0.8 and Tensile Stress Limit of $0.158\sqrt{f'_c}$.

Cases	Section Type	Span Length (ft)	Aps (in ²)	# of Tendons
1	1800-2	100	5.814	38
2	1800-2	120	9.18	60
3	1800-2	140	12.546	82
4	2100-2	160	19.096	88
5	2400-2	180	20.398	94
6	2400-2	200	25.172	116

Table A.67- Design Outcomes of Spread Box Girder Bridges Designed with Compressive Strength of 8ksi, Live Load Factor of 0.8 and Tensile Stress Limit of $0.19\sqrt{f'_c}$.

Cases	Section Type	Span Length (ft)	Aps (in ²)	# of Tendons
1	1800-2	100	5.202	34
2	1800-2	120	8.568	56
3	1800-2	140	11.934	78
4	2100-2	160	17.794	82
5	2400-2	180	19.096	88
6	2400-2	200	24.304	112

Table A.68- Design Outcomes of Spread Box Girder Bridges Designed with Compressive Strength of 8ksi, Live Load Factor of 0.8 and Tensile Stress Limit of $0.253\sqrt{f'_c}$.

Cases	Section Type	Span Length (ft)	Aps (in ²)	# of Tendons
1	1800-2	100	3.978	26
2	1800-2	120	7.344	48
3	1800-2	140	10.404	68
4	2100-2	160	16.058	74
5	2400-2	180	16.926	78
6	2400-2	200	22.134	102

A.5 Existing Bridges from NCHRP 12-78

Table A.69- Summary of NCHRP 12-78 I-Girder Bridge

Bridge Name	Section Type	Girder Spacing (ft.)	Span Length (ft.)	Aps (in ²)	# of Tendons
82	MN type 63	10.33	82.75	5.20	34
3107	36" I BEAM	5.77	49.54	1.84	12
4794	BEAM Type 4	9.33	66.67	5.05	33
4827	BEAM Type 2	7.17	50.58	2.75	18
5624	BEAM Type 4	7.25	59.37	3.06	20
5794	BEAM Type 3	5.83	72.00	4.34	20
5840	BEAM Type 6	9.00	85.00	4.59	30
5884	BEAM Type 6	8.17	90.01	5.81	38
8330	BEAM Type 6	8.67	76.38	4.28	28
8783	AASHTO VI	7.75	143.15	9.98	46
8832	36" I BEAM	10.00	43.26	3.06	20
8885	BT-63	10.58	90.01	5.51	36
8889	BT-63	10.58	90.85	5.51	36
8890	AASHTO VI	8.00	143.50	10.42	48
8891	BEAM Type 6	9.25	47.17	2.14	14
8957	BEAM Type 6	8.67	98.00	5.64	26
9378	Wisconsin Girder	10.42	101.83	6.12	40
10269	AASHTO III	6.67	78.00	4.28	28
10599	AASHTO II	6.75	62.83	4.28	28
10740	AASHTO III	7.00	78.55	4.90	32
10755	AASHTO II	7.00	52.50	3.67	24
10803	BT-72	6.00	138.25	7.68	46
11030	BT-72	6.38	136.00	7.65	50
11938	BT-63	7.31	116.52	7.68	46
12589	AASHTO IV	8.75	73.21	4.59	30
12596	AASHTO IV	11.15	96.79	10.85	50
12603	AASHTO II	11.48	37.73	3.04	14
12610	AASHTO IV	7.13	108.53	7.96	52
15620	Bulb-Tee	5.35	119.82	10.42	48
18067	AL BT-54 Mod.	5.29	131.02	10.85	50

Table A.70- Summary of NCHRP 12-78 Spread Box Girder Bridge

Bridge Name	Section Type	Girder Spacing (ft.)	Span Length (ft.)	Aps (in ²)	# of Tendons
1150	33" x 36" Box	8.50	70.58	5.97	39
3577	27"x36" IDOT	6.70	38.58	2.92	27
3754	33"x36" IDOT	6.36	53.61	3.24	30
8875	27"x48" P/S Box	11.25	38.00	3.52	23
9090	MDOT 33" Box	7.08	66.04	4.34	20
9091	MDOT 33" Box	7.08	66.20	4.34	20
9128	1525 Box	7.49	33.69	0.87	4
9192	21" x 36" Box	9.83	38.67	2.75	18
9217	17" Box	6.21	42.30	3.47	16
9219	MDOT 21" Box	5.25	53.17	3.47	16
9243	33in x 36in Box	6.17	73.33	4.56	21
9248	21 in Box Beam	8.00	37.75	3.91	18
9282	17" x 36" Box	7.83	36.30	2.45	16
9284	17" x 36" Box	6.66	31.56	1.95	9
9286	27" x 36" Box	8.04	50.67	4.34	20
9310	21" x 36" Box	5.97	51.97	4.34	20
9324	27" x 36" Box	10.50	42.33	3.06	20
9328	27" x 36" Box	6.92	57.27	3.98	26
9349	21" x 36" Box	7.00	48.67	3.37	22
9355	39" x 36" Box	7.92	75.20	5.64	26
9356	39" x 36" Box	7.92	75.20	5.64	26
9361	27" x 36" Box	6.00	65.79	4.59	30
9368	33" x 36" Box	7.38	71.25	4.59	30
9369	27" x 36" Box	6.50	51.32	3.04	14
9370	27" x 36" Box	6.42	51.32	3.04	14
9376	27" x 36" Box	7.38	53.35	3.26	15
9380	21" x 36" Box	9.10	32.09	1.84	12
9383	27" x 36" Box	10.58	46.82	3.47	16
9384	21" x 36" Box	6.60	44.13	3.04	14
9394	27x 48 in Box	7.50	66.91	5.20	34
12870	36" x 48"	6.50	77.50	4.59	30
14969	BIV-48	7.88	78.74	7.34	48
16293	1220 x 1220 box	8.86	57.27	5.64	26
16366	Beams B1-B6	6.58	60.38	5.81	38
17240	BII-48	8.00	51.50	3.67	24
17338	BII-48	8.00	49.00	2.75	18

Table A.71- Summary of NCHRP 12-78 Adjacent Box Girder Bridge

Bridge Name	Section Type	Girder Spacing (ft.)	Span Length (ft.)	Aps (in ²)	# of Tendons
3805	27"x36" IDOT	3.00	59.04	2.30	15
3819	33"x36" IDOT	3.00	74.88	2.60	17
5125	48"x33" P/S Box	4.00	66.00	3.98	26
5911	36"x27"P/S Box	3.00	59.42	2.14	14
9071	MDOT 840 x 915 Box	3.12	83.64	3.47	16
9103	MDOT 1220 x 1220 Box	4.13	111.21	5.43	25
9167	685mm x 1220mm Box	4.13	75.56	4.77	22
9180	MDOT 535 x 915 Box	3.13	44.70	2.82	13
9181	MDOT 535 x 915 Box	3.13	60.37	3.21	21
9191	27" x 36" Box	3.14	72.50	3.06	20
9228	1220mm x 1220 mm Box	4.23	110.44	5.21	24
9240	33in x 36in Box	3.13	97.92	4.28	28
9314	27" x 36" Box	3.13	83.67	4.77	22
12807	BII-48	4.04	84.00	5.20	34
12809	BII-48	4.04	82.00	5.20	34
12952	BIV-48 modified	3.79	79.96	6.43	42
13118- interior 915	AASHTO BI-915	3.35	69.23	3.87	18
13118-Interior 1220	AASHTO BI-1220	3.85	69.23	4.09	19
13788	BIV-48	4.04	83.00	4.90	32
13805	BI-48	4.06	52.50	3.67	24
14070	B 3' 45"	3.10	115.00	6.43	42
14246	BI-48	4.04	52.00	3.67	24
14987	BIV-48	4.06	73.00	5.20	34
15238	BII-48, 1.220 m Wide	4.04	73.82	5.20	34
16538	PS box	4.06	101.71	5.81	38
16799	PS Shape 1-Interior	4.00	84.00	5.85	38
17008	AASHTO BII-1220	4.00	82.51	5.81	38
17042	4' PS Box	3.75	50.03	3.67	24
17075	BIV-48Modified	4.00	107.00	6.73	44
17143	BIII-48	3.75	70.00	4.59	30
17175	BII-48	3.75	88.75	6.73	44

APPENDIX B

RELIABILITY ANALYSIS RESULTS

This appendix contains reliability analysis results for prestressed concrete girders designed using various girder types for various design criteria considering different traffic volume.

B.1 I Girder Bridges

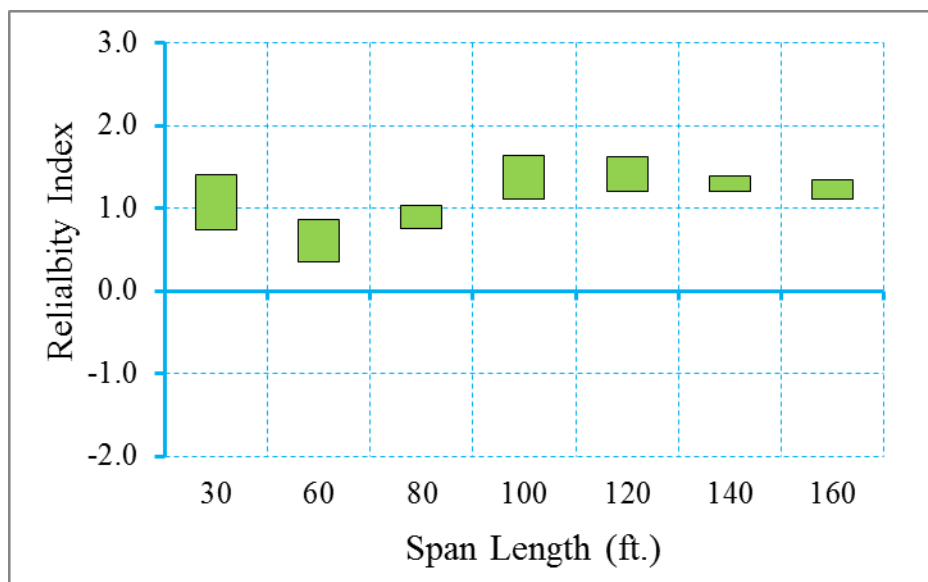


Figure B.1 Reliability Indices for AASHTO I Girder Bridges at Decompression Limit State (ADTT=1000), $\gamma_{LL}=0.8$ ($f_t = 0.0948\sqrt{f'_c}$)

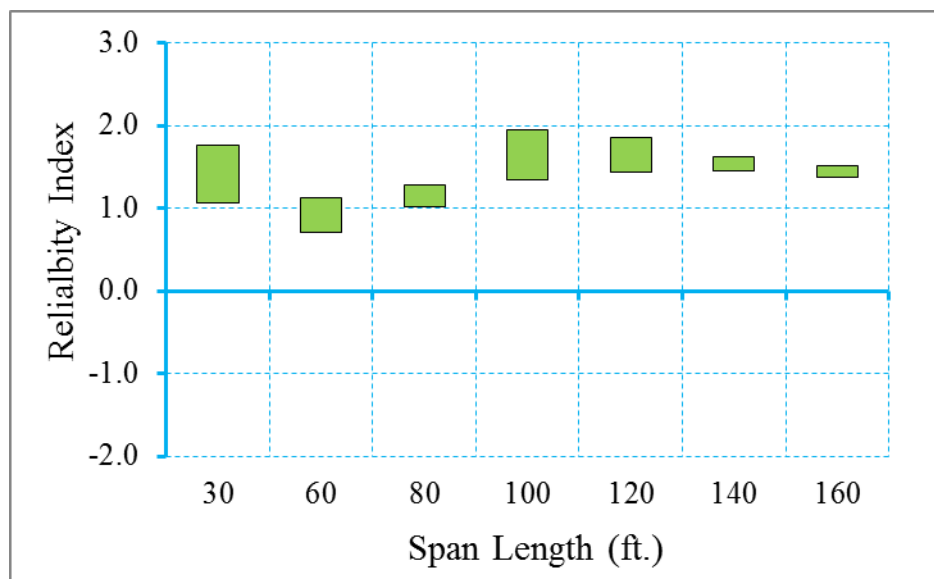


Figure B.2 Reliability Indices for AASHTO I Girder Bridges at Maximum Allowable Tensile Stress Limit State (ADTT=1000), $\gamma_{LL}=0.8$ ($f_t = 0.0948\sqrt{f'_c}$)

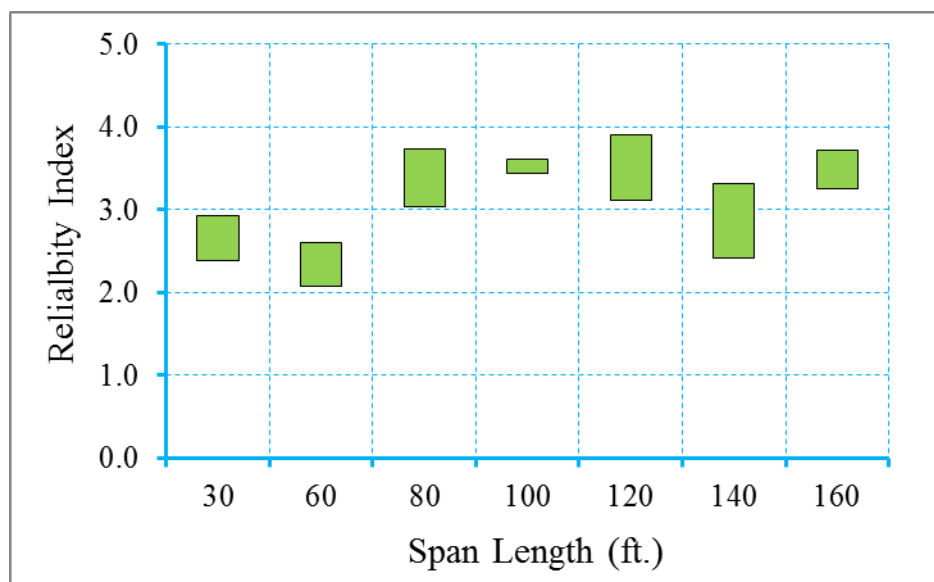


Figure B.3 Reliability Indices for AASHTO I Girder Bridges at Maximum Allowable Crack Width Limit State (ADTT=1000), $\gamma_{LL}=0.8$ ($f_t = 0.0948\sqrt{f'_c}$)

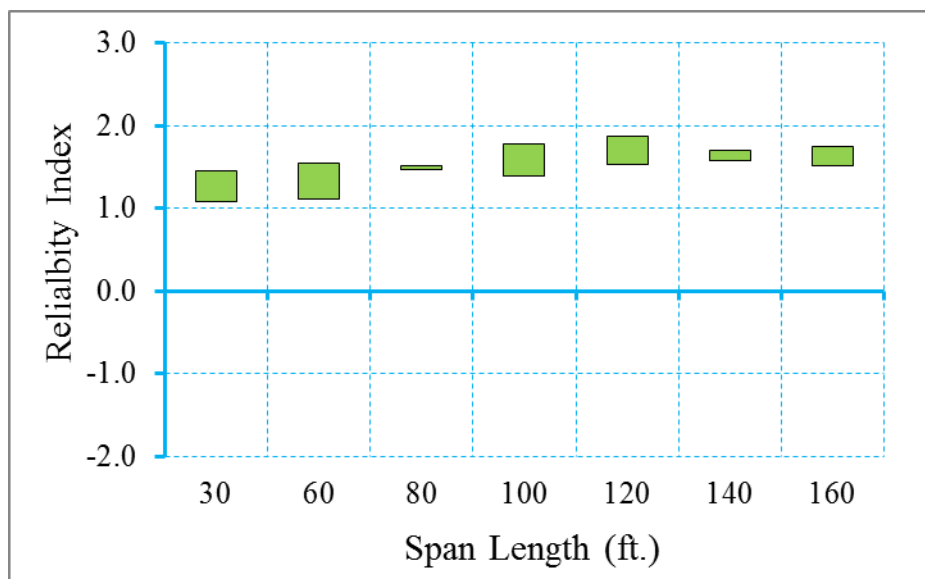


Figure B.4 Reliability Indices for AASHTO I Girder Bridges at Decompression Limit State (ADTT=1000), $\gamma_{LL}=1.0$ ($f_t = 0.0948\sqrt{f'_c}$)

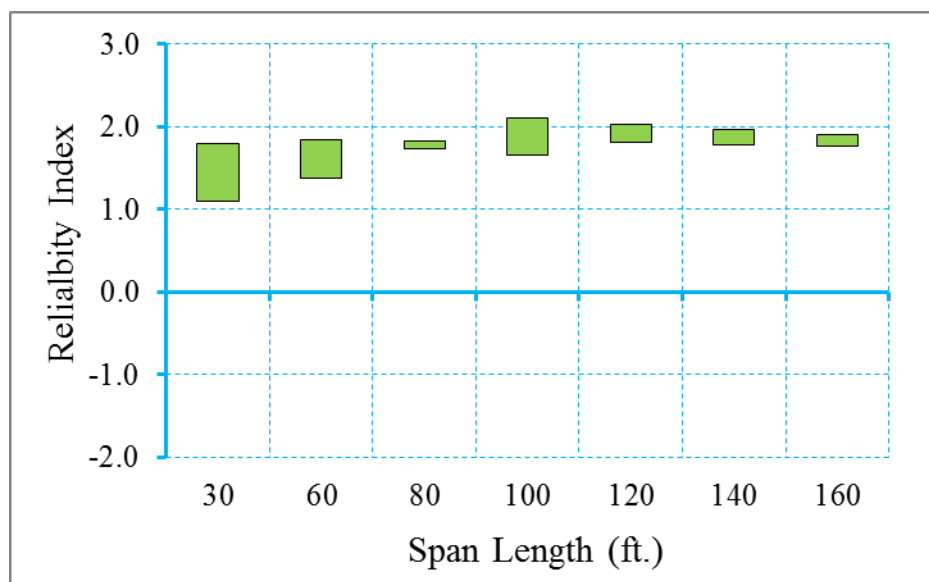


Figure B.5 Reliability Indices for AASHTO I Girder Bridges at Maximum Tensile Stress Limit State (ADTT=1000), $\gamma_{LL}=1.0$ ($f_t = 0.0948\sqrt{f'_c}$)

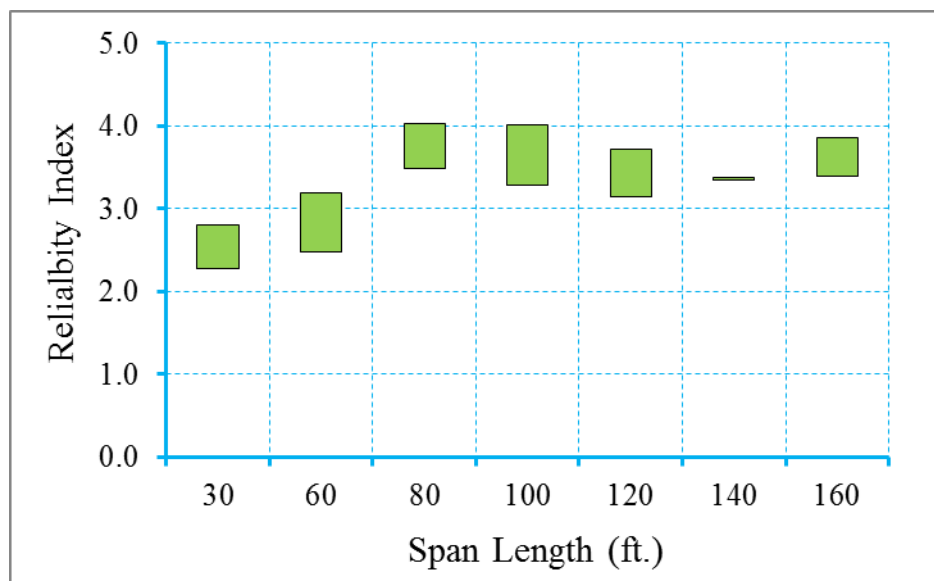


Figure B.6 Reliability Indices for AASHTO I Girder Bridges at Maximum Crack Width Limit State (ADTT=1000), $\gamma_{LL}=1.0$ ($f_t = 0.0948\sqrt{f'_c}$)

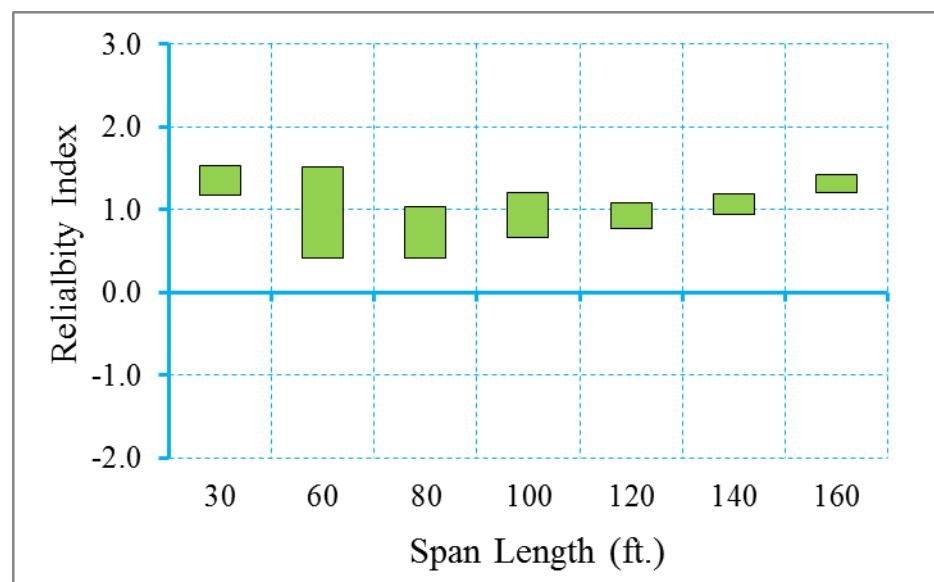


Figure B.7 Reliability Indices for AASHTO I Girder Bridges at Decompression Limit State (ADTT=1000), $\gamma_{LL}=0.8$ ($f_t = 0.158\sqrt{f'_c}$)

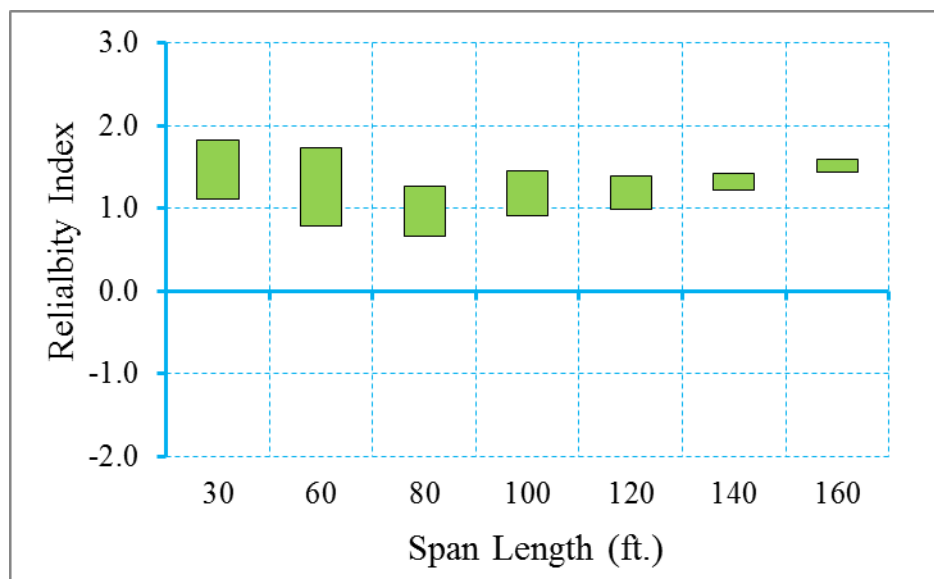


Figure B.8 Reliability Indices for AASHTO I Girder Bridges at Maximum Allowable Tensile Stress Limit State (ADTT=1000), $\gamma_{LL}=0.8$ ($f_t = 0.158\sqrt{f'_c}$)

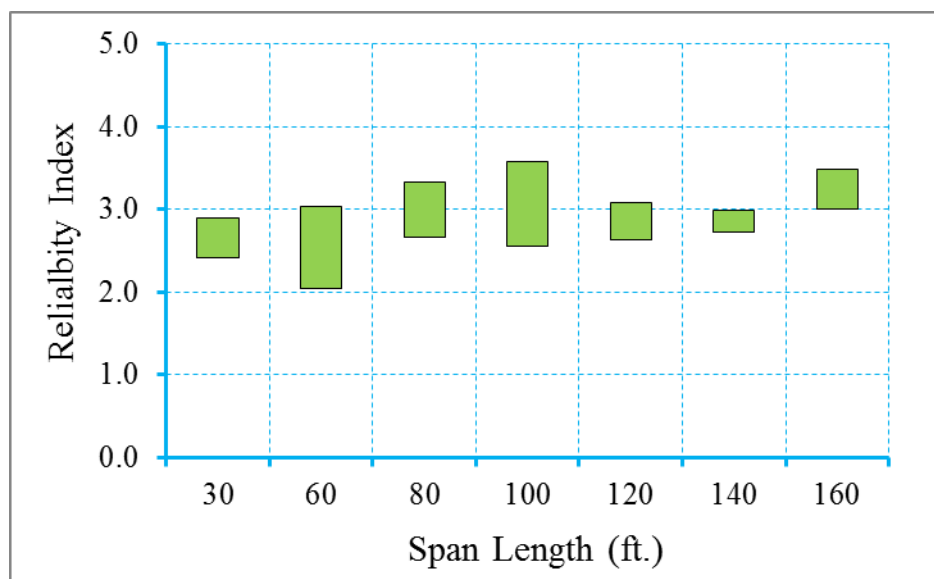


Figure B.9 Reliability Indices for AASHTO I Girder Bridges at Maximum Allowable Crack Width Limit State (ADTT=1000), $\gamma_{LL}=0.8$ ($f_t = 0.158\sqrt{f'_c}$)

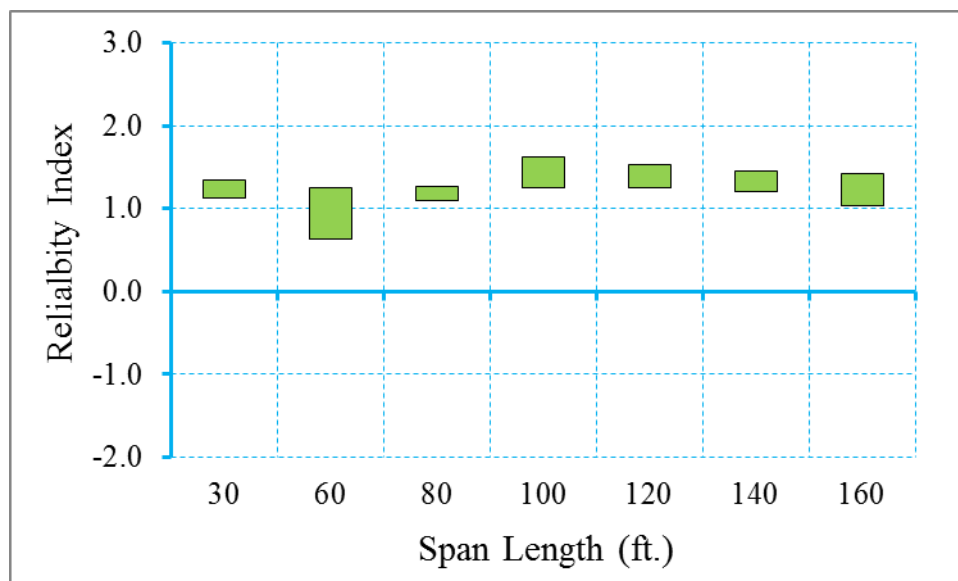


Figure B.10 Reliability Indices for AASHTO I Girder Bridges at Decompression Limit State (ADTT=1000), $\gamma_{LL}=1.0$ ($f_t = 0.158\sqrt{f'_c}$)

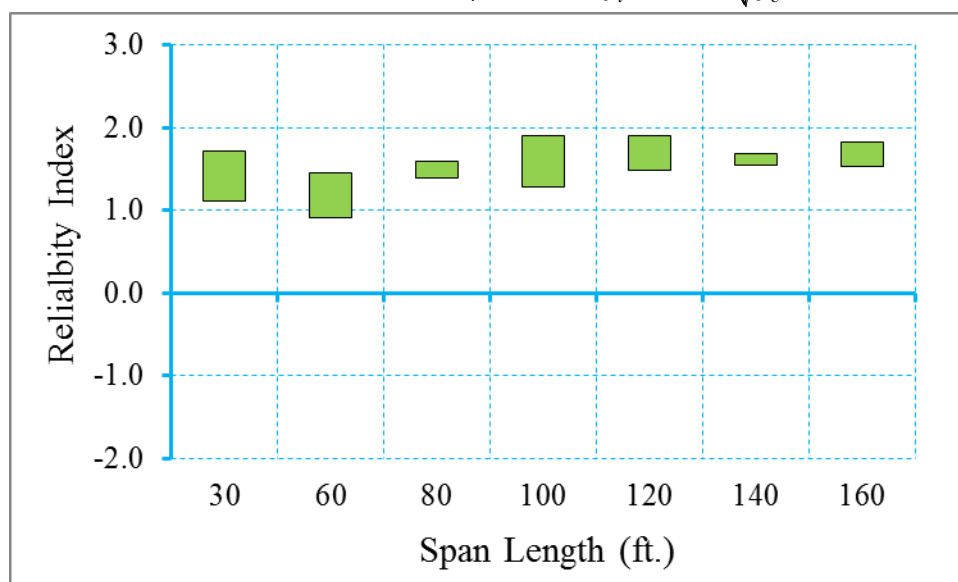


Figure B.11 Reliability Indices for AASHTO I Girder Bridges at Maximum Tensile Stress Limit State (ADTT=1000), $\gamma_{LL}=1.0$ ($f_t = 0.158\sqrt{f'_c}$)

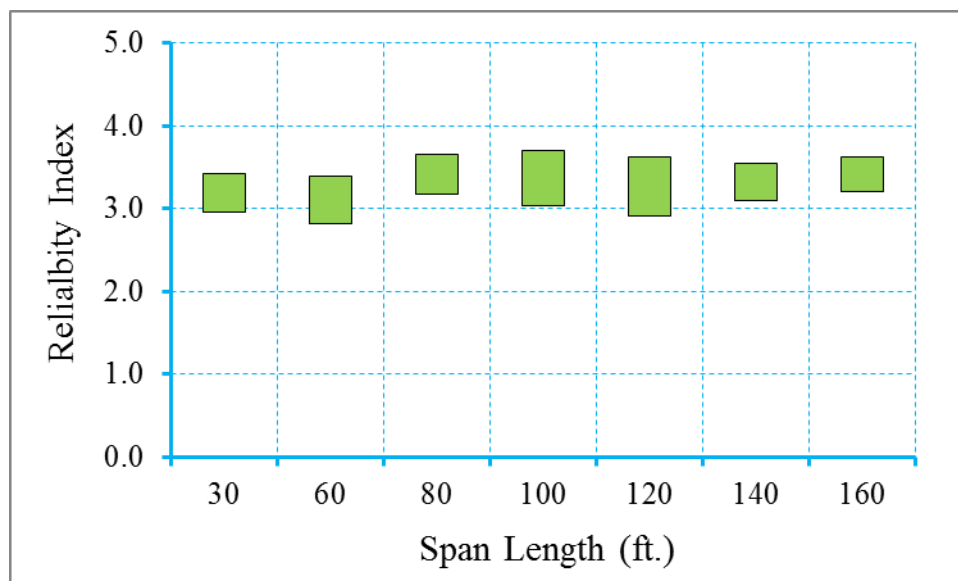


Figure B.12 Reliability Indices for AASHTO I Girder Bridges at Maximum Crack Width Limit State (ADTT=1000), $\gamma_{LL}=1.0$ ($f_t = 0.158\sqrt{f'_c}$)

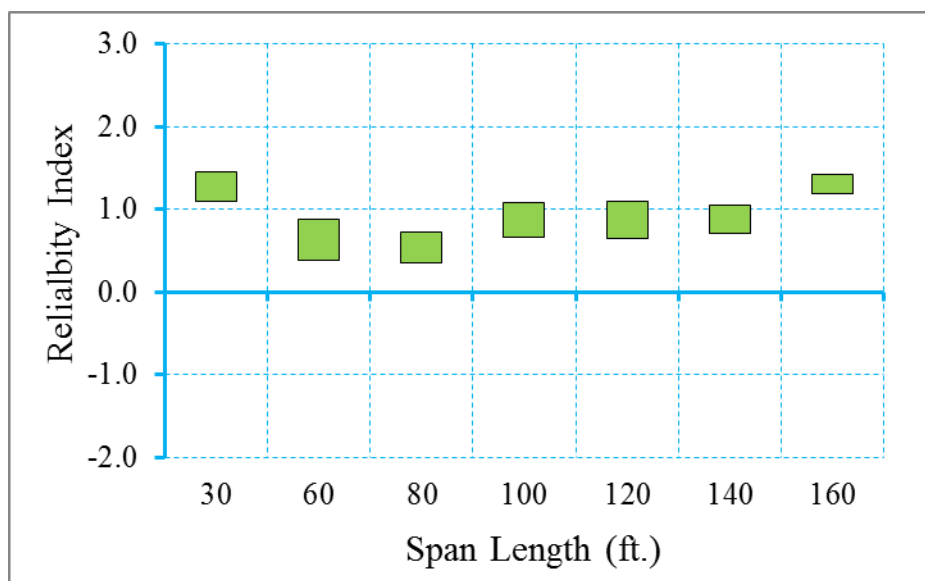


Figure B.13 Reliability Indices for AASHTO I Girder Bridges at Decompression Limit State (ADTT=1000), $\gamma_{LL}=0.8$ ($f_t = 0.19\sqrt{f'_c}$)

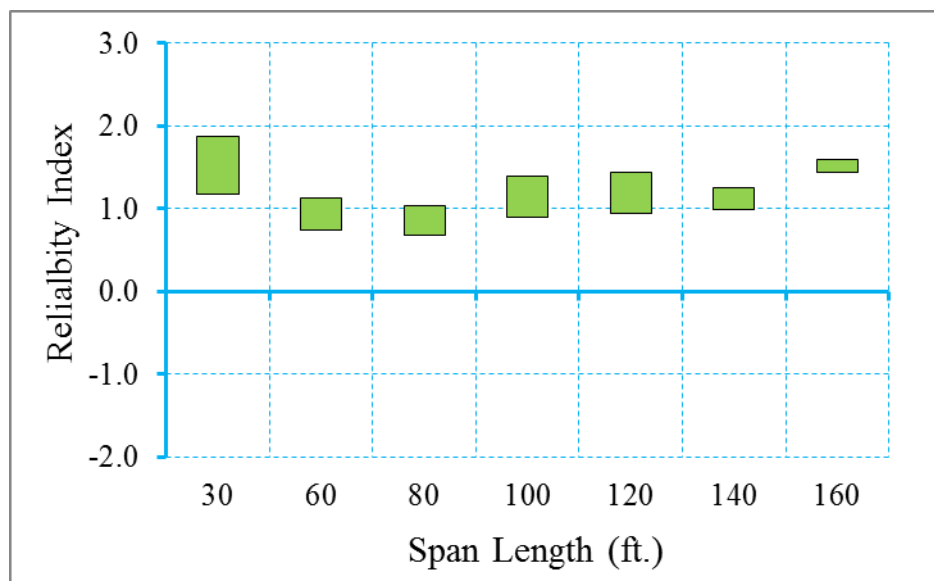


Figure B.14 Reliability Indices for AASHTO I Girder Bridges at Maximum Allowable Tensile Stress Limit State (ADTT=1000), $\gamma_{LL}=0.8$ ($f_t = 0.19\sqrt{f'_c}$)

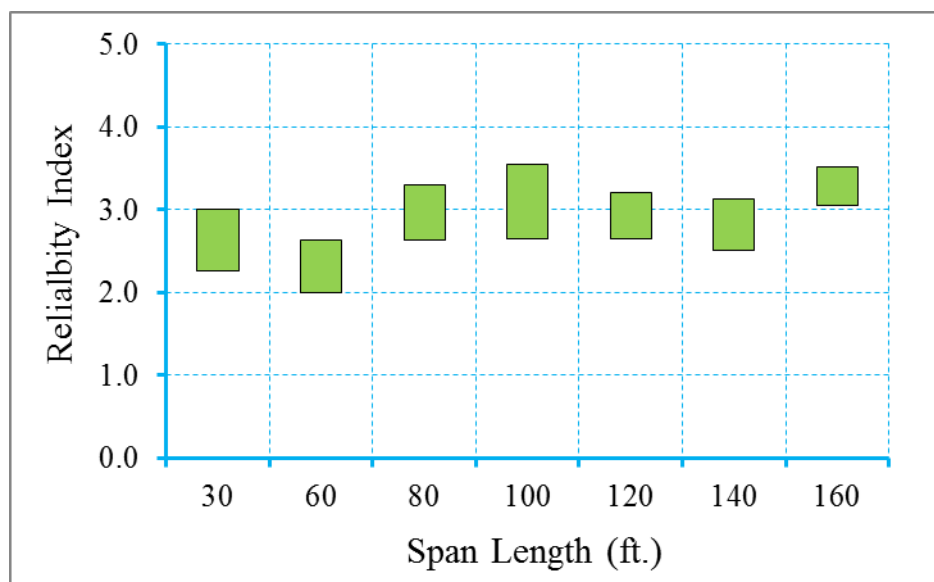


Figure B.15 Reliability Indices for AASHTO I Girder Bridges at Maximum Allowable Crack Width Limit State (ADTT=1000), $\gamma_{LL}=0.8$ ($f_t = 0.19\sqrt{f'_c}$)

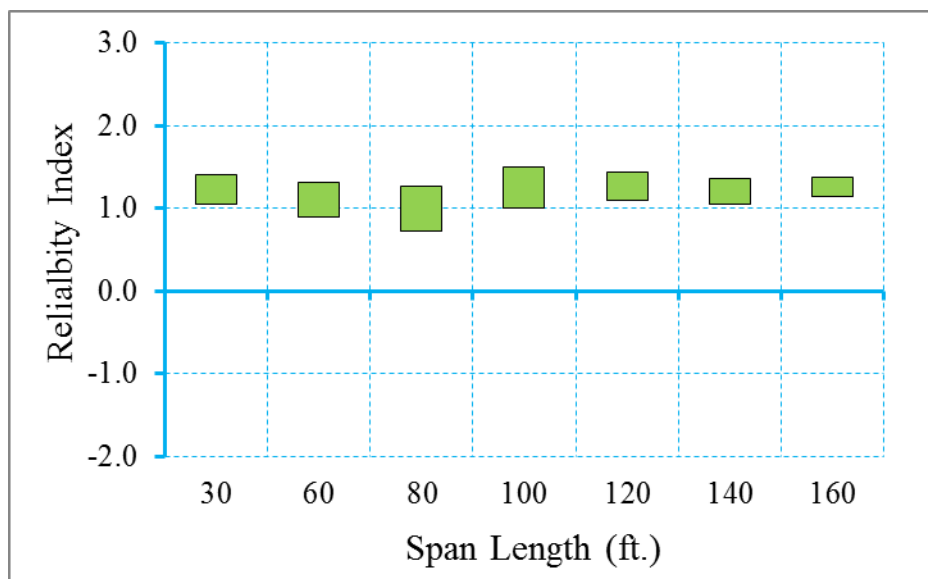


Figure B.16 Reliability Indices for AASHTO I Girder Bridges at Decompression Limit State (ADTT=1000), $\gamma_{LL}=1.0$ ($f_t = 0.19\sqrt{f'_c}$)

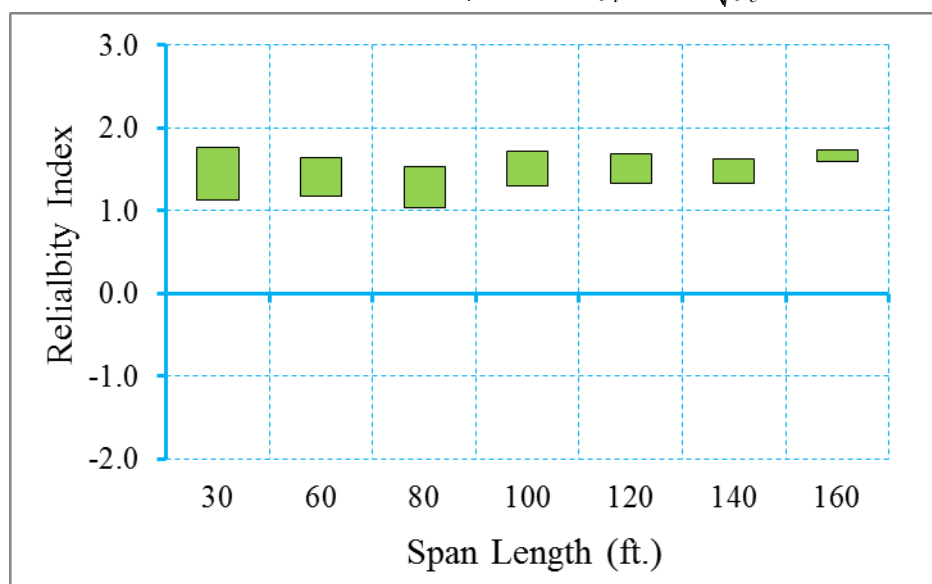


Figure B.17 Reliability Indices for AASHTO I Girder Bridges at Maximum Tensile Stress Limit State (ADTT=1000), $\gamma_{LL}=1.0$ ($f_t = 0.19\sqrt{f'_c}$)

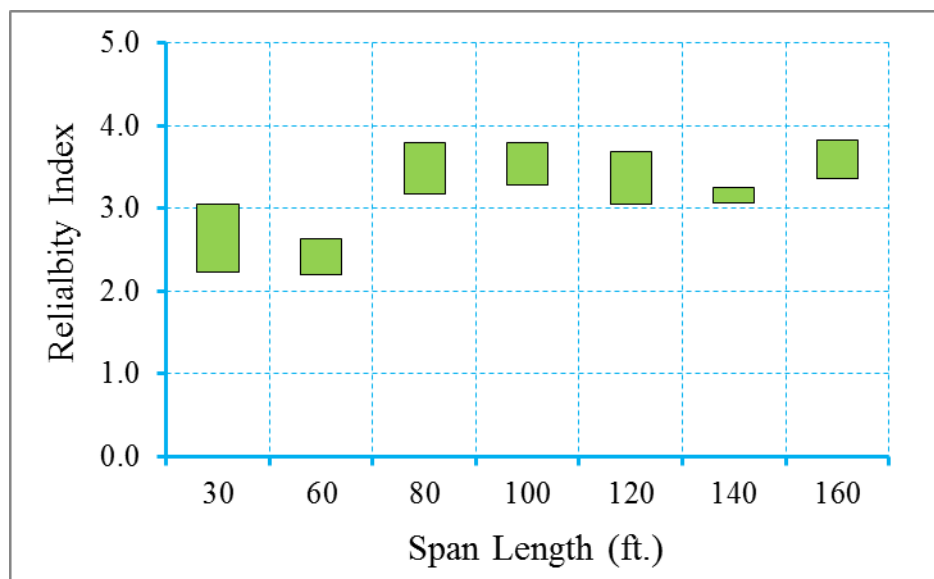


Figure B.18 Reliability Indices for AASHTO I Girder Bridges at Maximum Crack Width Limit State (ADTT=1000), $\gamma_{LL}=1.0$ ($f_t = 0.19\sqrt{f'_c}$)

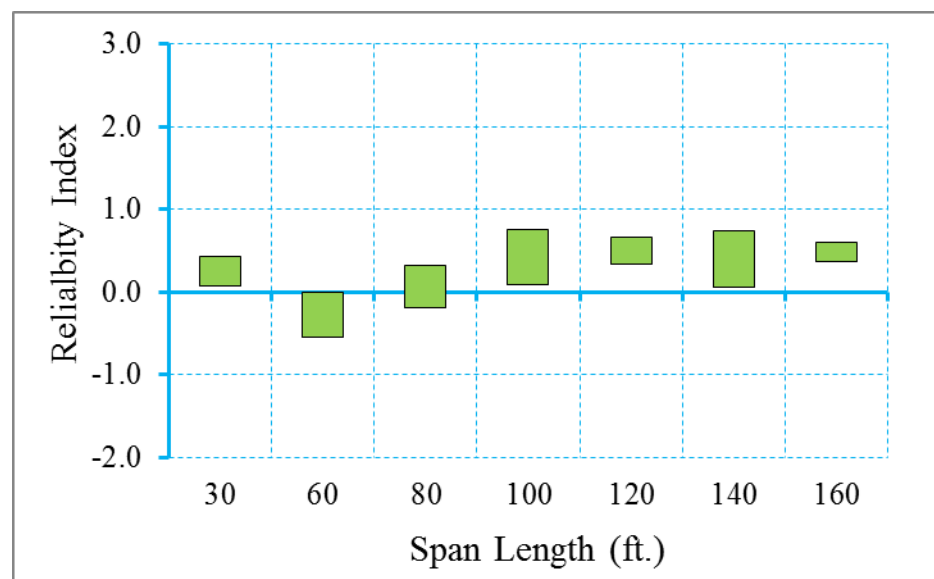


Figure B.19 Reliability Indices for AASHTO I Girder Bridges at Decompression Limit State (ADTT=1000), $\gamma_{LL}=0.8$ ($f_t = 0.253\sqrt{f'_c}$)

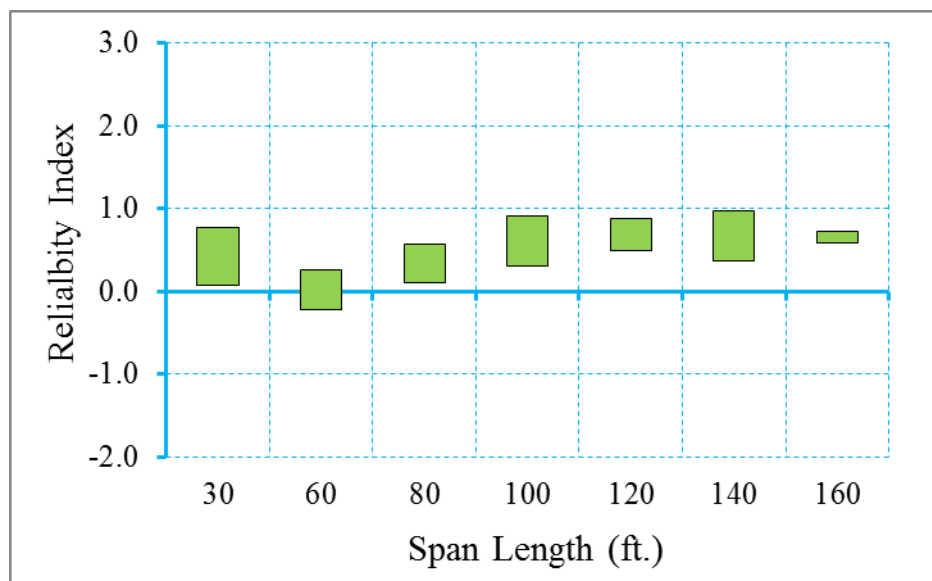


Figure B.20 Reliability Indices for AASHTO I Girder Bridges at Maximum Allowable Tensile Stress Limit State (ADTT=1000), $\gamma_{LL}=0.8$ ($f_t = 0.253\sqrt{f'_c}$)

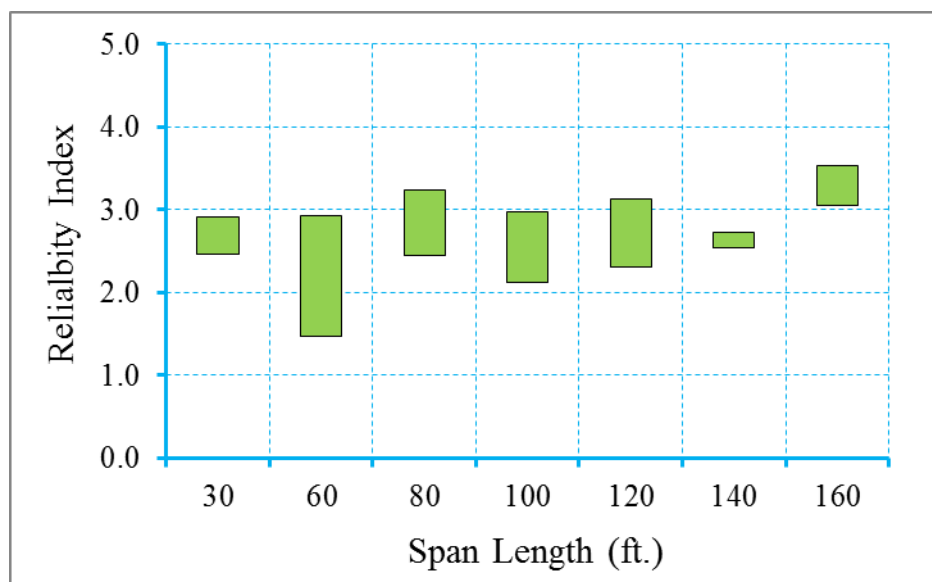


Figure B.21 Reliability Indices for AASHTO I Girder Bridges at Maximum Allowable Crack Width Limit State (ADTT=1000), $\gamma_{LL}=0.8$ ($f_t = 0.253\sqrt{f'_c}$)

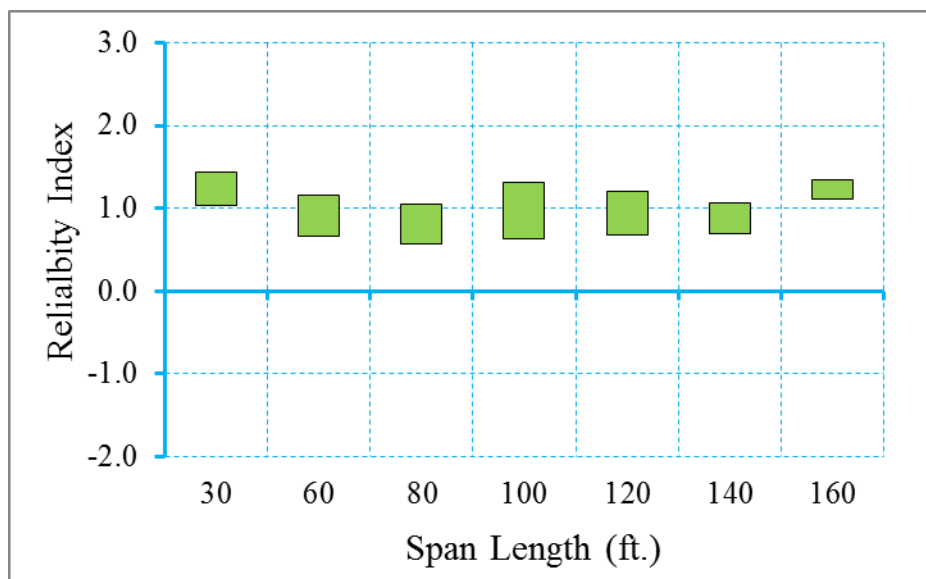


Figure B.22 Reliability Indices for AASHTO I Girder Bridges at Decompression Limit State (ADTT=1000), $\gamma_{LL}=1.0$ ($f_t = 0.253\sqrt{f'_c}$)

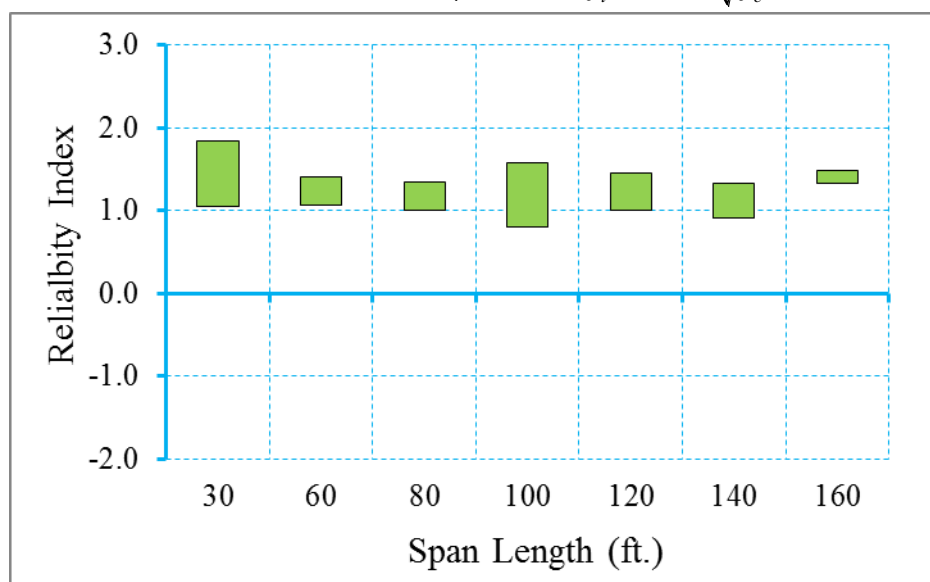


Figure B.23 Reliability Indices for AASHTO I Girder Bridges at Maximum Allowable Tensile Stress Limit State (ADTT=1000), $\gamma_{LL}=1.0$ ($f_t = 0.253\sqrt{f'_c}$)

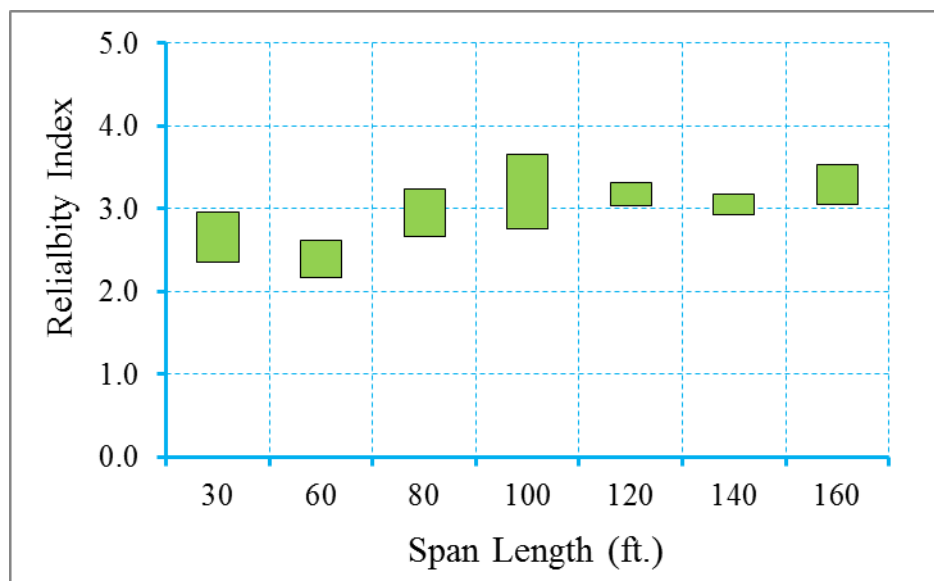


Figure B.24 Reliability Indices for AASHTO I Girder Bridges at Maximum Allowable Crack Width Limit State (ADTT=1000), $\gamma_{LL}=1.0$ ($f_t = 0.253\sqrt{f'_c}$)

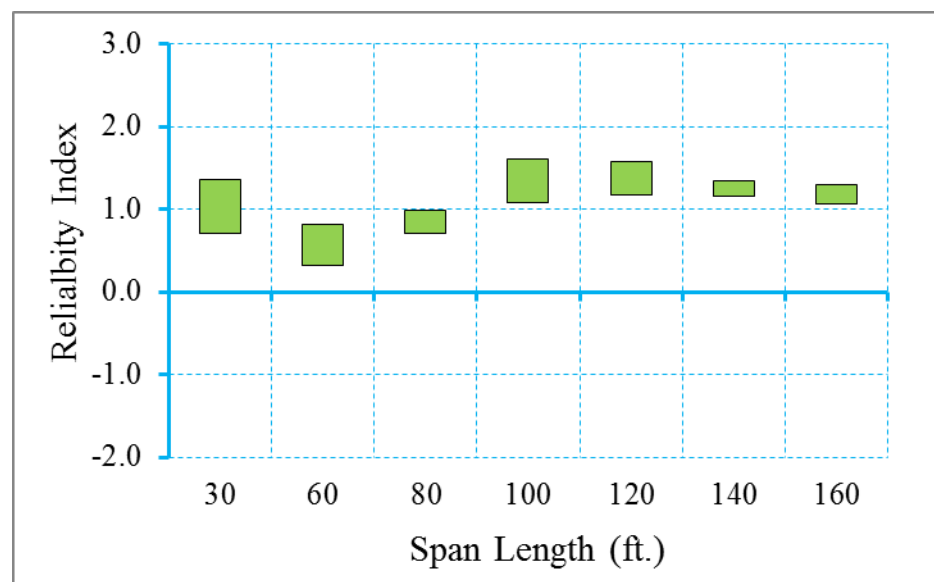


Figure B.25 Reliability Indices for AASHTO I Girder Bridges at Decompression Limit State (ADTT=2500), $\gamma_{LL}=0.8$ ($f_t = 0.0948\sqrt{f'_c}$)

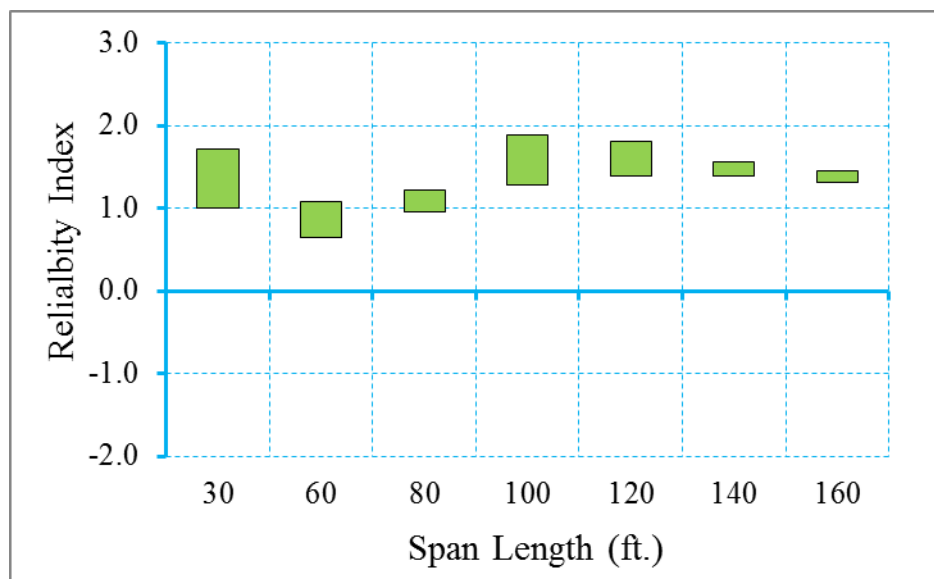


Figure B.26 Reliability Indices for AASHTO I Girder Bridges at Maximum Allowable Tensile Stress Limit State (ADTT=2500), $\gamma_{LL}=0.8$ ($f_t = 0.0948\sqrt{f'_c}$)

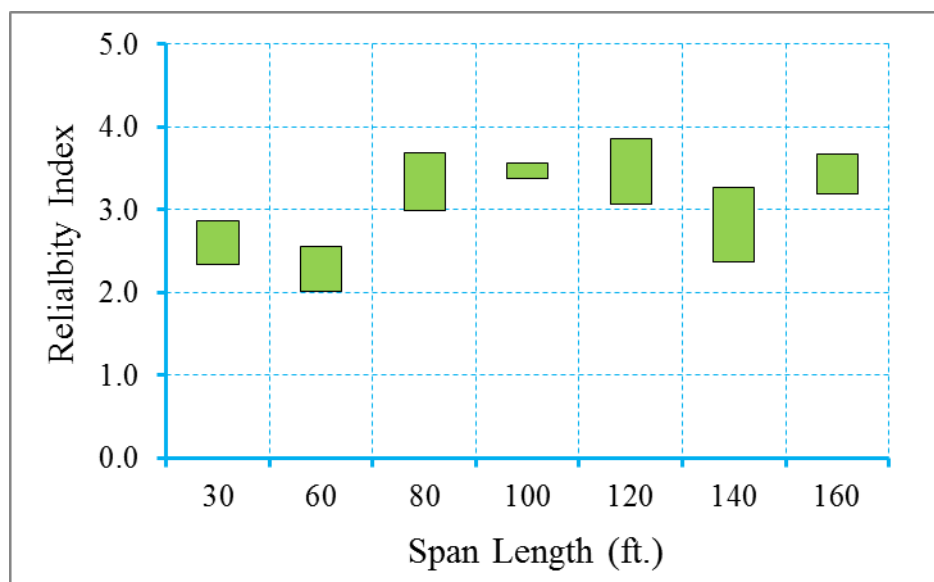


Figure B.27 Reliability Indices for AASHTO I Girder Bridges at Maximum Allowable Crack Width Limit State (ADTT=2500), $\gamma_{LL}=0.8$ ($f_t = 0.0948\sqrt{f'_c}$)

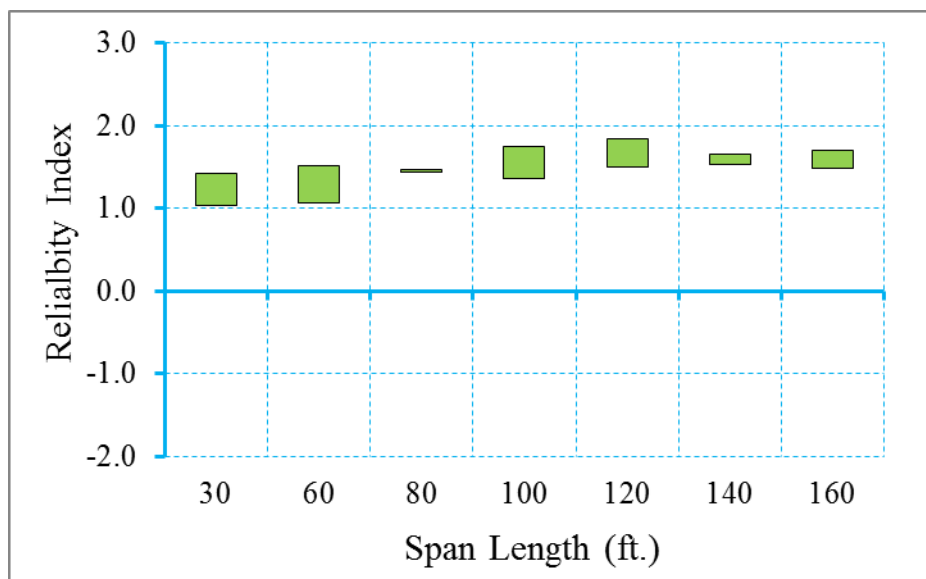


Figure B.28 Reliability Indices for AASHTO I Girder Bridges at Decompression Limit State (ADTT=2500), $\gamma_{LL}=1.0$ ($f_t = 0.0948\sqrt{f'_c}$)

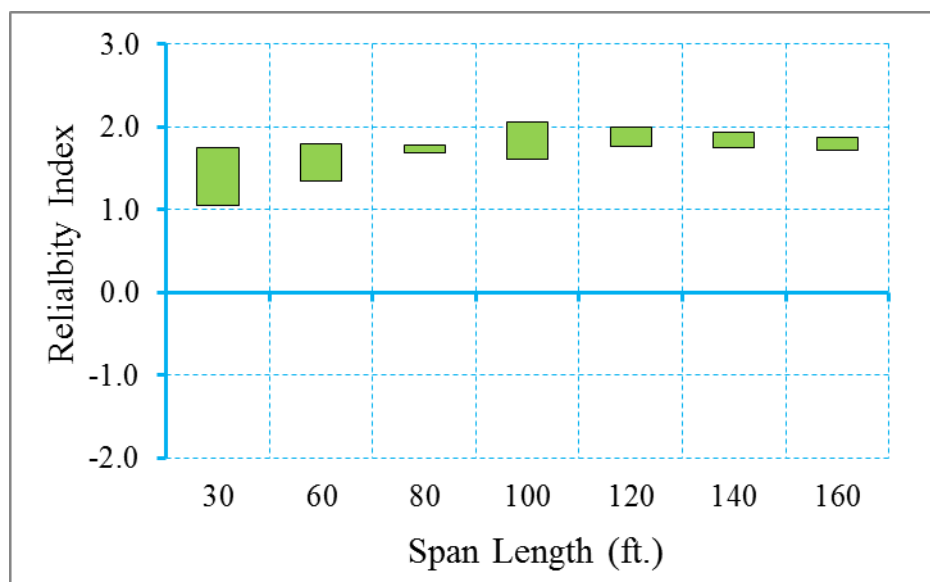


Figure B.29 Reliability Indices for AASHTO I Girder Bridges at Maximum Tensile Stress Limit State (ADTT=2500), $\gamma_{LL}=1.0$ ($f_t = 0.0948\sqrt{f'_c}$)

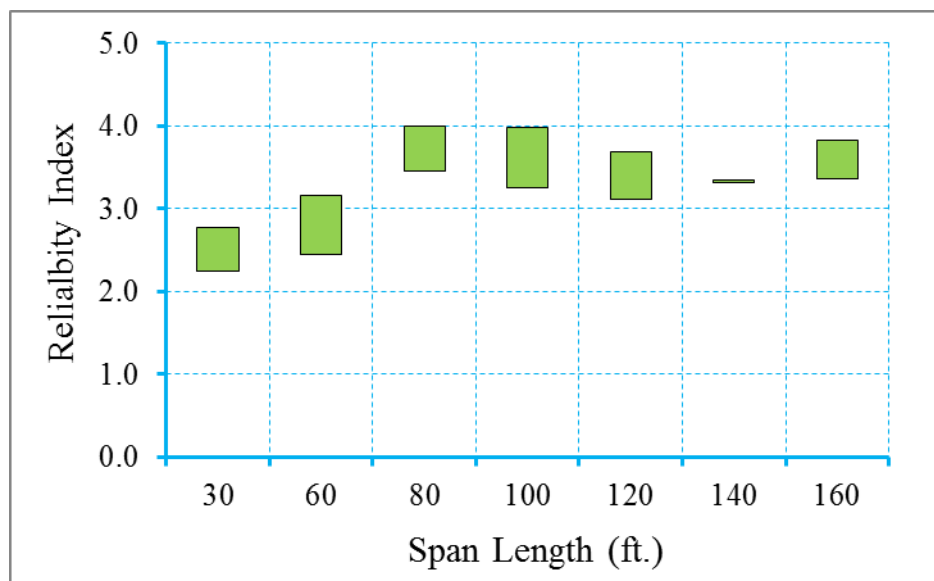


Figure B.30 Reliability Indices for AASHTO I Girder Bridges at Maximum Crack Width Limit State (ADTT=2500), $\gamma_{LL}=1.0$ ($f_t = 0.0948\sqrt{f'_c}$)

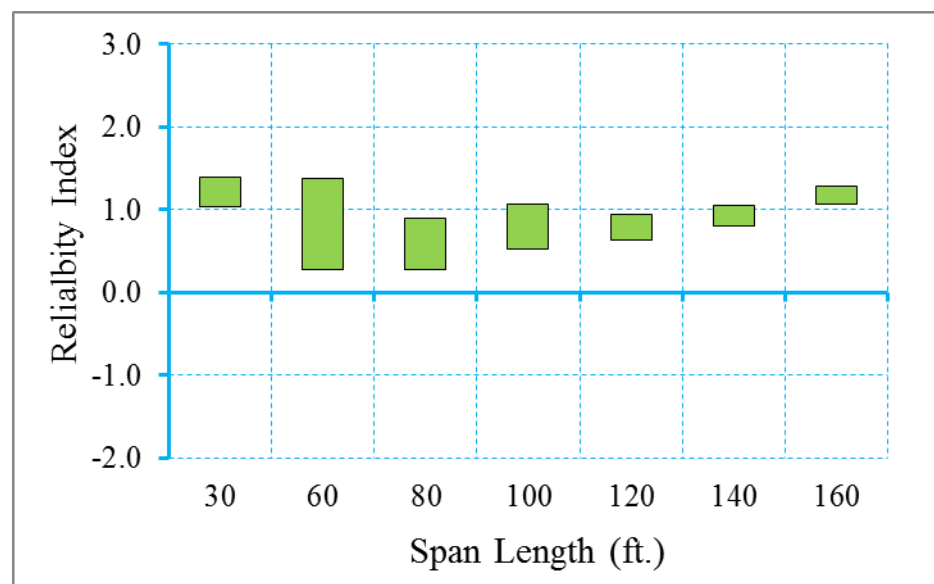


Figure B.31 Reliability Indices for AASHTO I Girder Bridges at Decompression Limit State (ADTT=2500), $\gamma_{LL}=0.8$ ($f_t = 0.158\sqrt{f'_c}$)

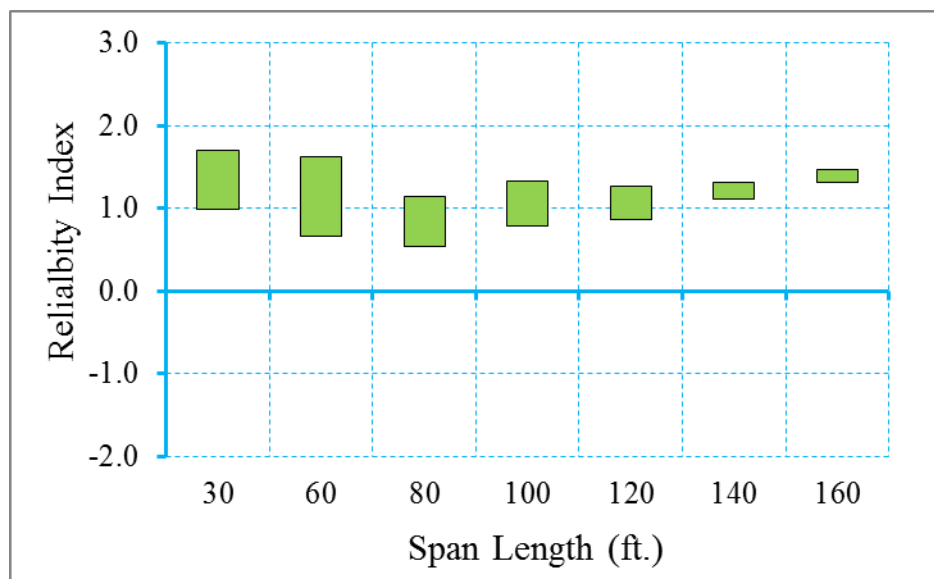


Figure B.32 Reliability Indices for AASHTO I Girder Bridges at Maximum Allowable Tensile Stress Limit State (ADTT=2500), $\gamma_{LL}=0.8$ ($f_t = 0.158\sqrt{f'_c}$)

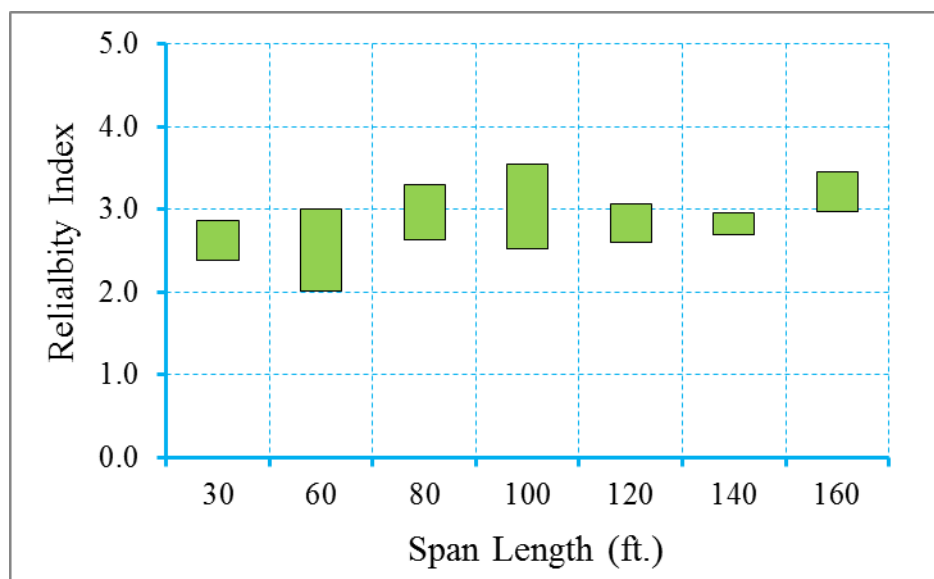


Figure B.33 Reliability Indices for AASHTO I Girder Bridges at Maximum Allowable Crack Width Limit State (ADTT=2500), $\gamma_{LL}=0.8$ ($f_t = 0.158\sqrt{f'_c}$)

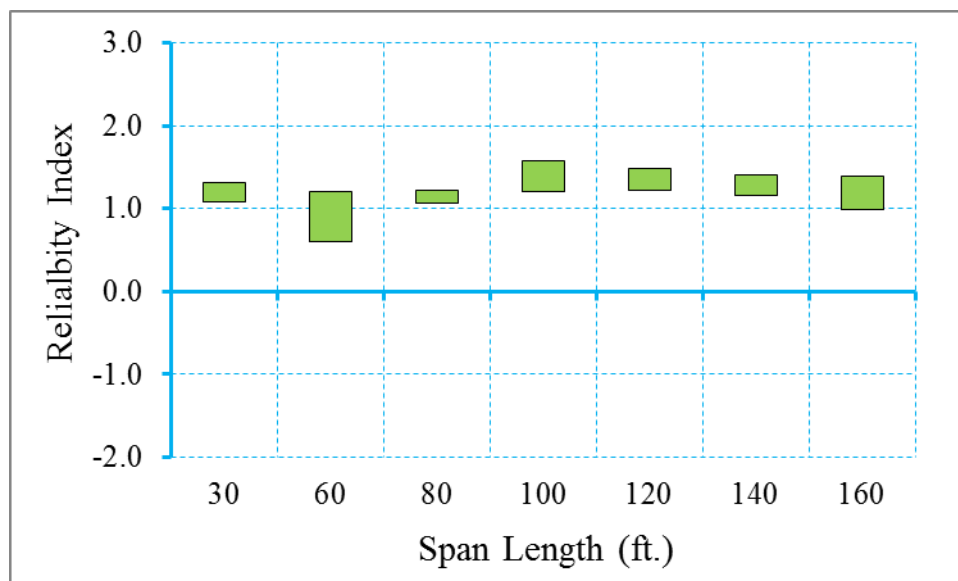


Figure B.34 Reliability Indices for AASHTO I Girder Bridges at Decompression Limit State (ADTT=2500), $\gamma_{LL}=1.0$ ($f_t = 0.158\sqrt{f'_c}$)

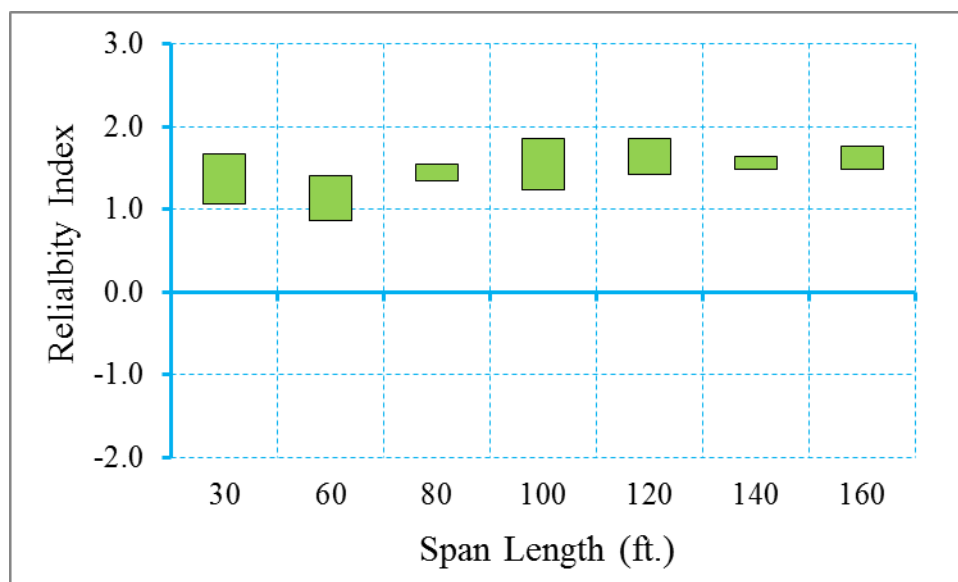


Figure B.35 Reliability Indices for AASHTO I Girder Bridges at Maximum Tensile Stress Limit State (ADTT=2500), $\gamma_{LL}=1.0$ ($f_t = 0.158\sqrt{f'_c}$)

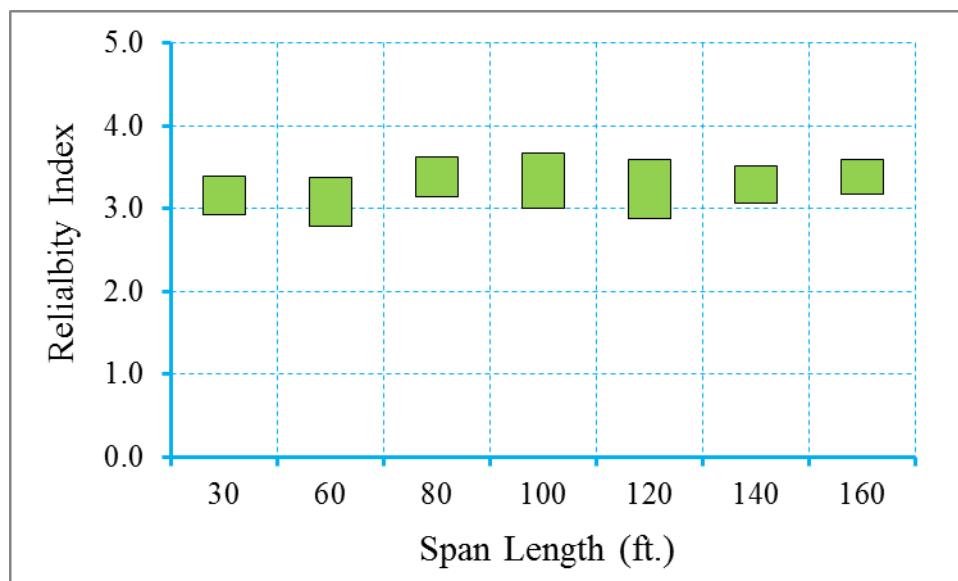


Figure B.36 Reliability Indices for AASHTO I Girder Bridges at Maximum Crack Width Limit State (ADTT=2500), $\gamma_{LL}=1.0$ ($f_t = 0.158\sqrt{f'_c}$)

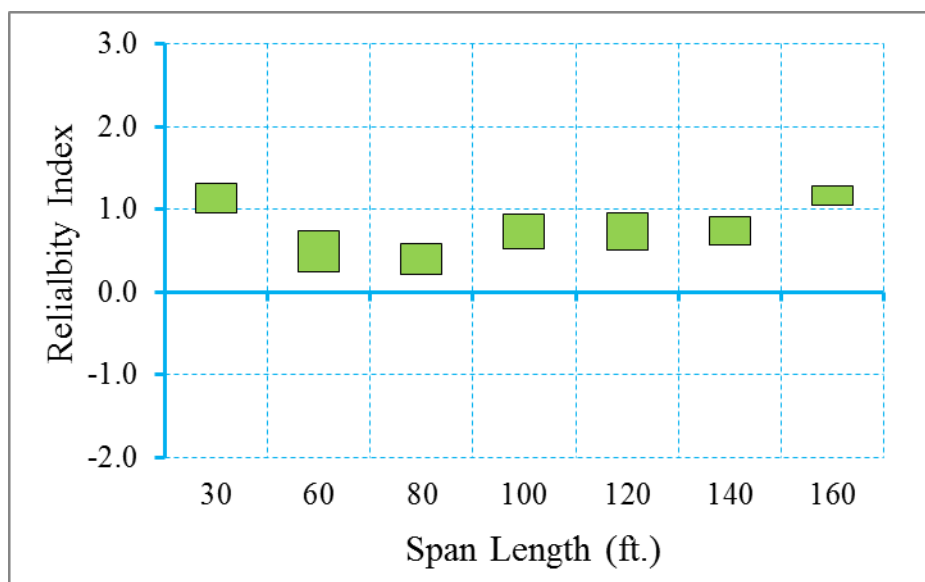


Figure B.37 Reliability Indices for AASHTO I Girder Bridges at Decompression Limit State (ADTT=2500), $\gamma_{LL}=0.8$ ($f_t = 0.19\sqrt{f'_c}$)

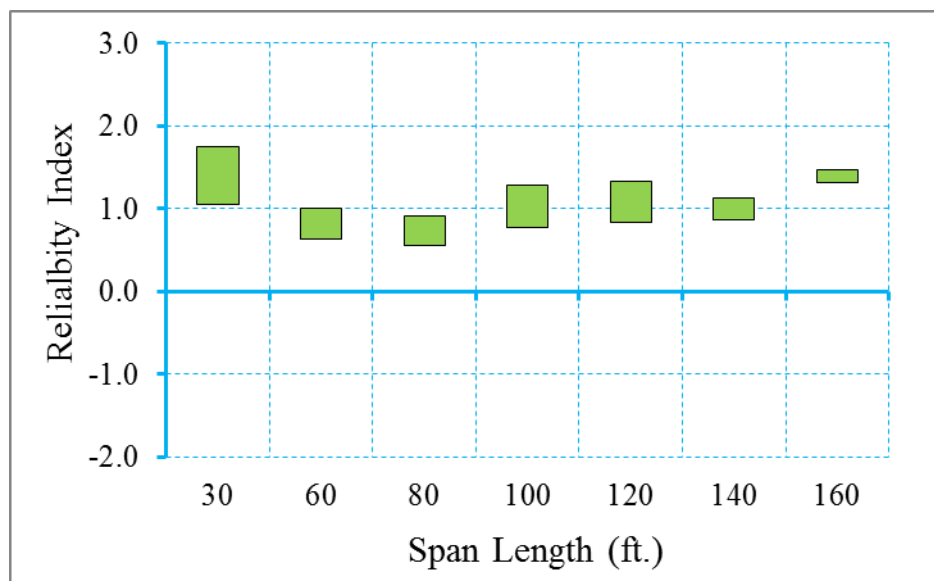


Figure B.38 Reliability Indices for AASHTO I Girder Bridges at Maximum Allowable Tensile Stress Limit State (ADTT=2500), $\gamma_{LL}=0.8$ ($f_t = 0.19\sqrt{f'_c}$)

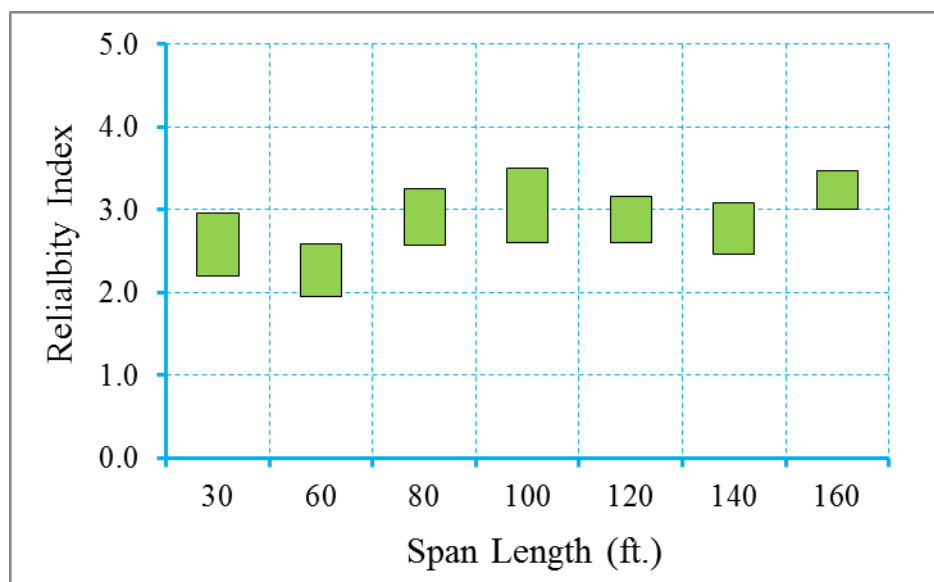


Figure B.39 Reliability Indices for AASHTO I Girder Bridges at Maximum Allowable Crack Width Limit State (ADTT=2500), $\gamma_{LL}=0.8$ ($f_t = 0.19\sqrt{f'_c}$)

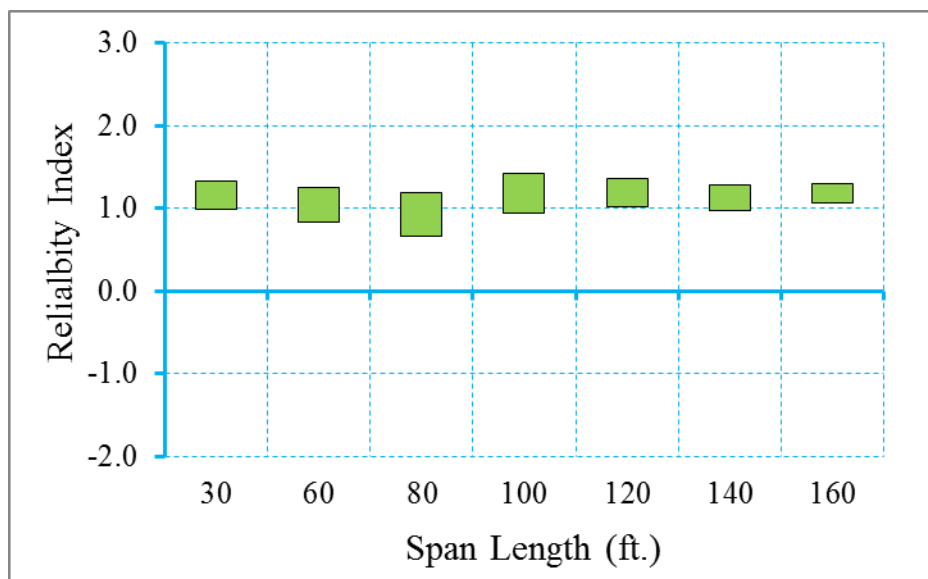


Figure B.40 Reliability Indices for AASHTO I Girder Bridges at Decompression Limit State (ADTT=2500), $\gamma_{LL}=1.0$ ($f_t = 0.19\sqrt{f'_c}$)

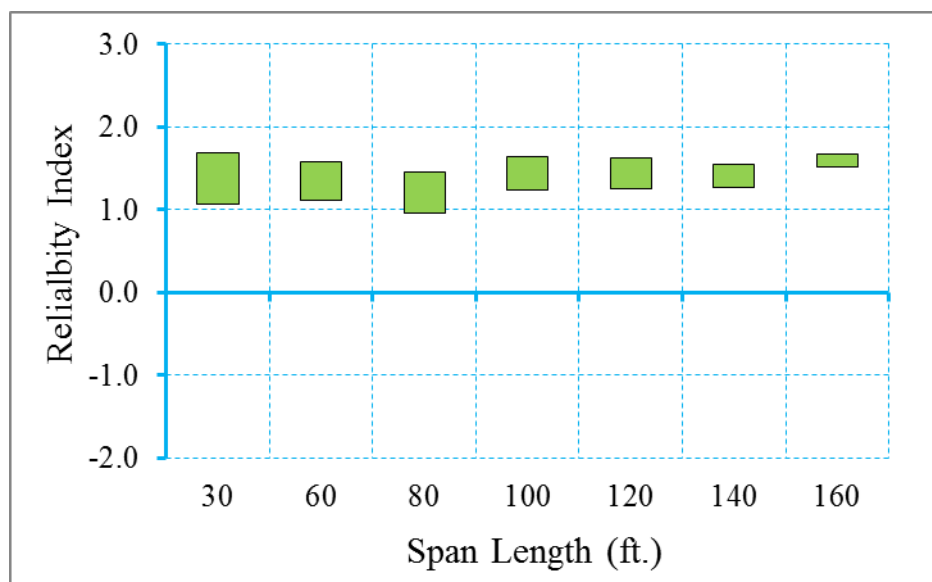


Figure B.41 Reliability Indices for AASHTO I Girder Bridges at Maximum Tensile Stress Limit State (ADTT=2500), $\gamma_{LL}=1.0$ ($f_t = 0.19\sqrt{f'_c}$)

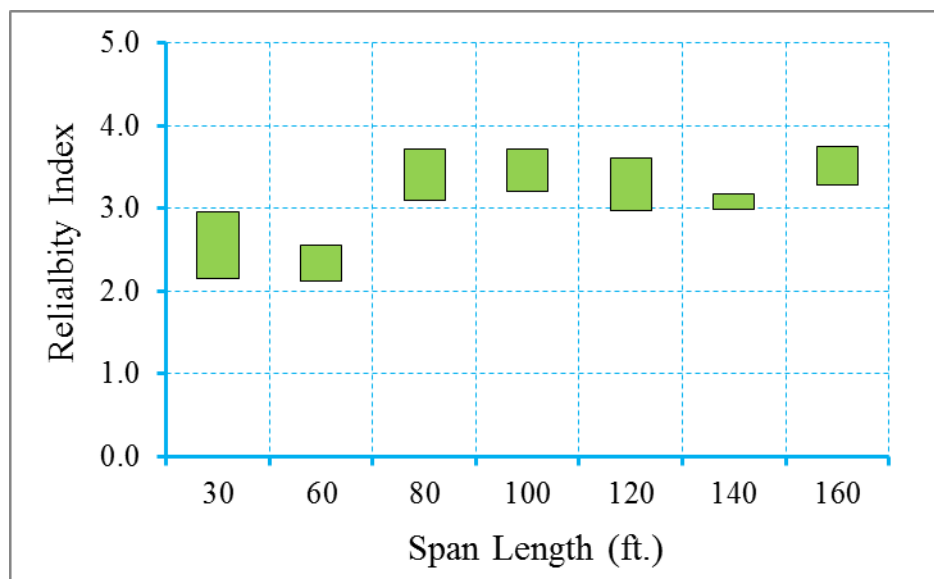


Figure B.42 Reliability Indices for AASHTO I Girder Bridges at Maximum Crack Width Limit State (ADTT=2500), $\gamma_{LL}=1.0$ ($f_t = 0.19\sqrt{f'_c}$)

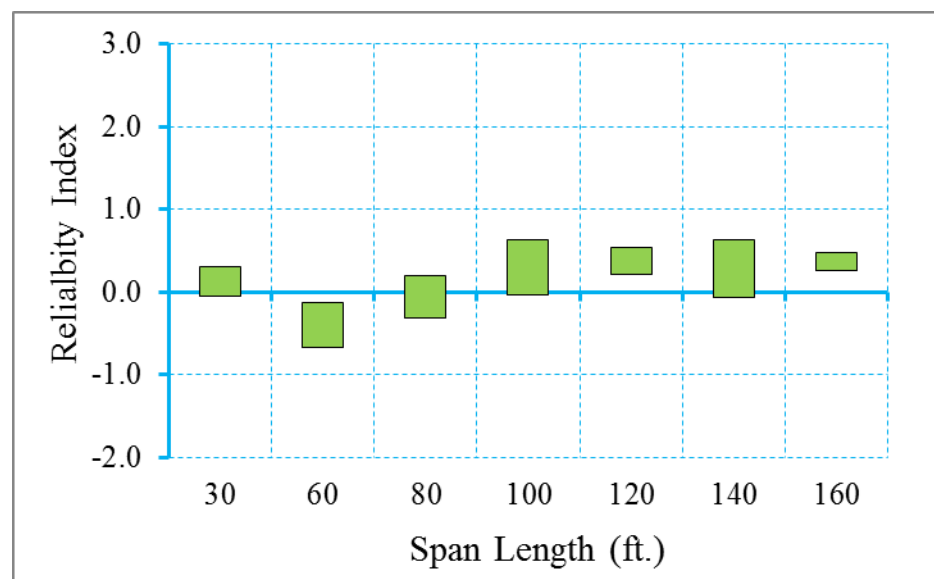


Figure B.43 Reliability Indices for AASHTO I Girder Bridges at Decompression Limit State (ADTT=2500), $\gamma_{LL}=0.8$ ($f_t = 0.253\sqrt{f'_c}$)

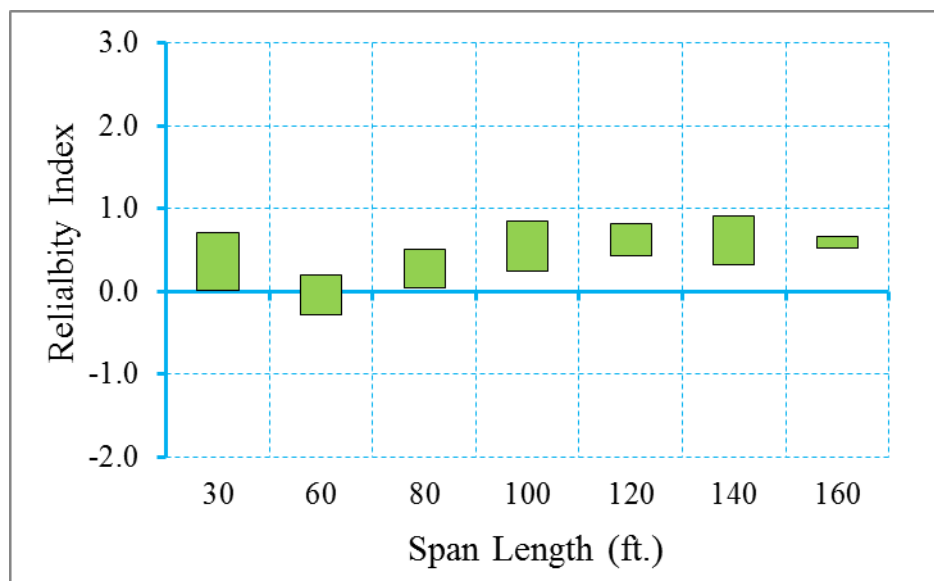


Figure B.44 Reliability Indices for AASHTO I Girder Bridges at Maximum Allowable Tensile Stress Limit State (ADTT=2500), $\gamma_{LL}=0.8$ ($f_t = 0.253\sqrt{f'_c}$)

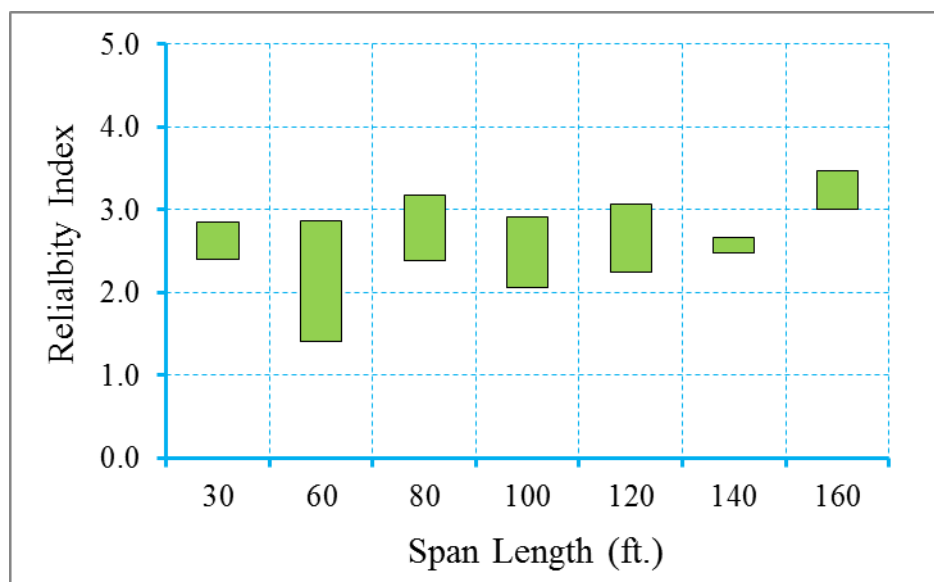


Figure B.45 Reliability Indices for AASHTO I Girder Bridges at Maximum Allowable Crack Width Limit State (ADTT=2500), $\gamma_{LL}=0.8$ ($f_t = 0.253\sqrt{f'_c}$)

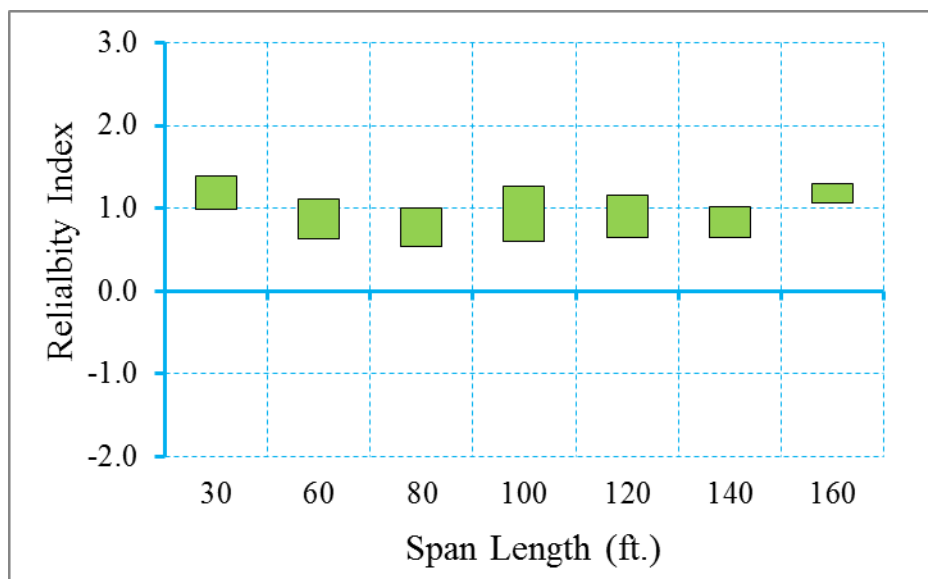


Figure B.46 Reliability Indices for AASHTO I Girder Bridges at Decompression Limit State (ADTT=2500), $\gamma_{LL}=1.0$ ($f_t = 0.253\sqrt{f'_c}$)

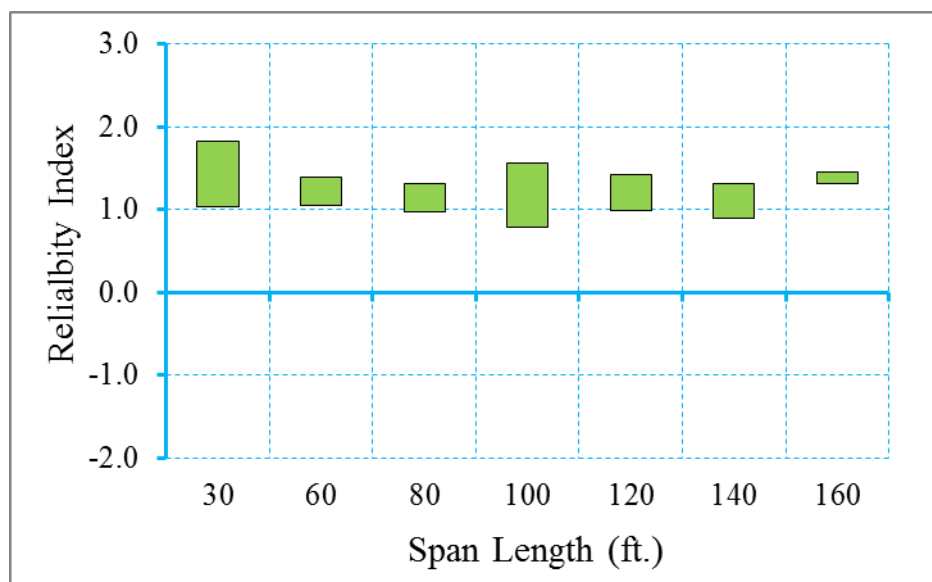


Figure B.47 Reliability Indices for AASHTO I Girder Bridges at Maximum Tensile Stress Limit State (ADTT=2500), $\gamma_{LL}=1.0$ ($f_t = 0.253\sqrt{f'_c}$)

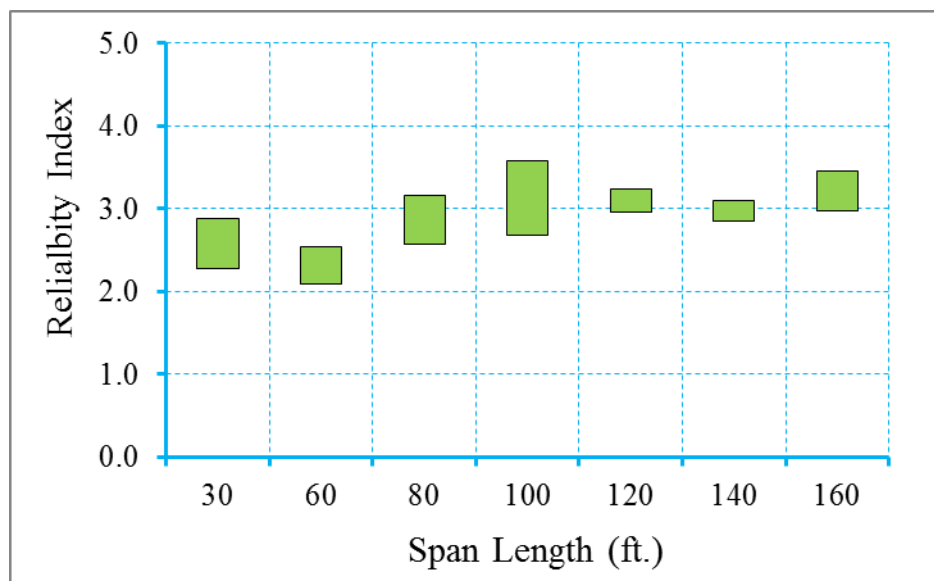


Figure B.48 Reliability Indices for AASHTO I Girder Bridges at Maximum Crack Width Limit State (ADTT=2500), $\gamma_{LL}=1.0$ ($f_t = 0.253\sqrt{f'_c}$)

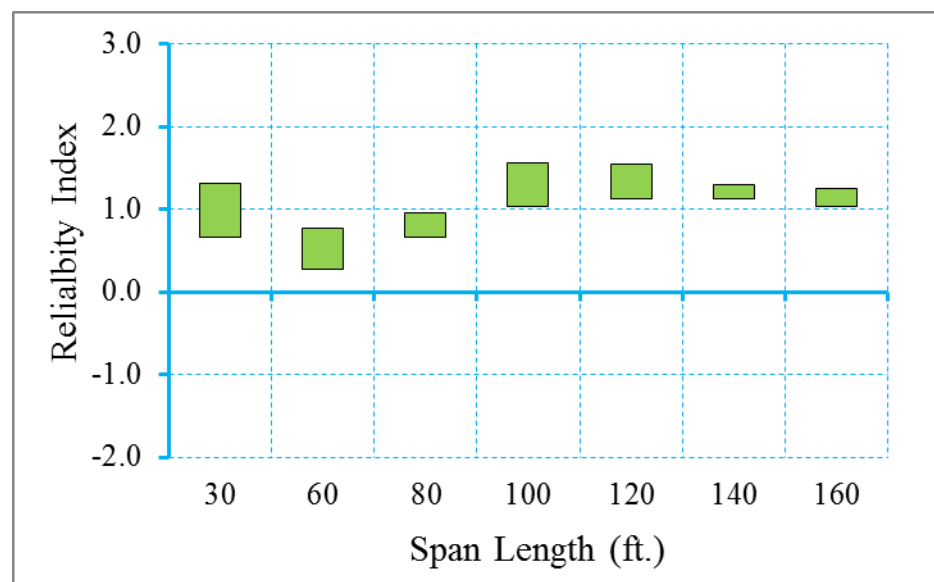


Figure B.49 Reliability Indices for AASHTO I Girder Bridges at Decompression Limit State (ADTT=5000), $\gamma_{LL}=0.8$ ($f_t = 0.0948\sqrt{f'_c}$)

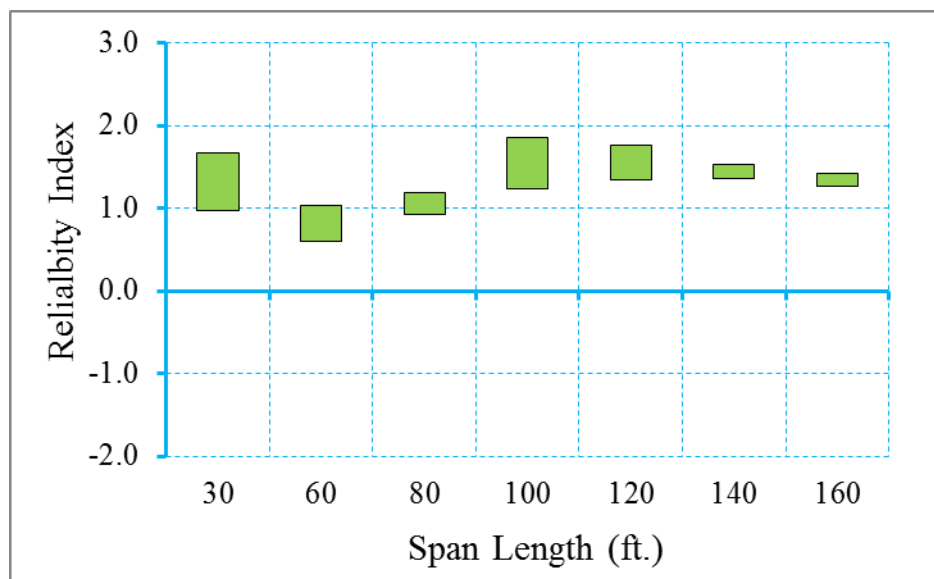


Figure B.50 Reliability Indices for AASHTO I Girder Bridges at Maximum Allowable Tensile Stress Limit State (ADTT=5000), $\gamma_{LL}=0.8$ ($f_t = 0.0948\sqrt{f'_c}$)

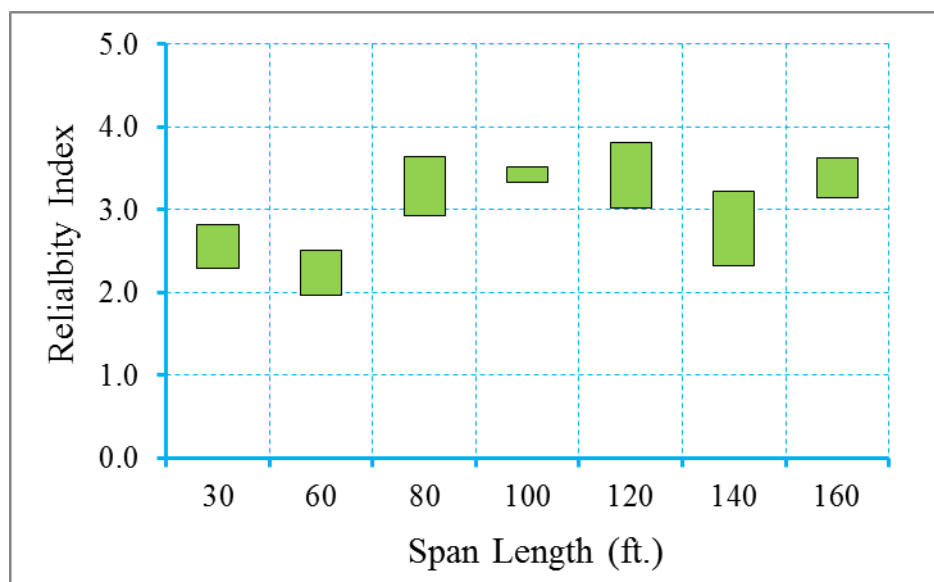


Figure B.51 Reliability Indices for AASHTO I Girder Bridges at Maximum Allowable Crack Width Limit State (ADTT=5000), $\gamma_{LL}=0.8$ ($f_t = 0.0948\sqrt{f'_c}$)

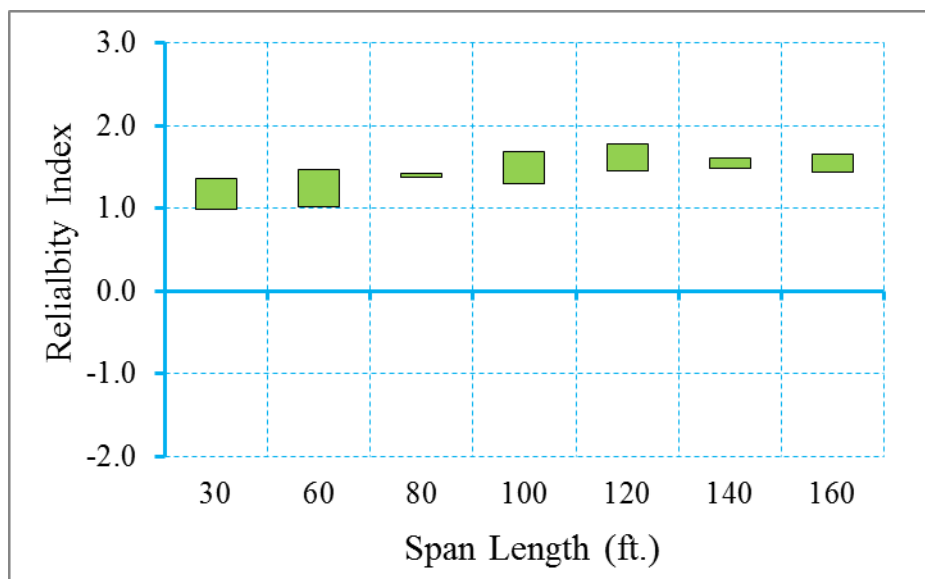


Figure B.52 Reliability Indices for AASHTO I Girder Bridges at Decompression Limit State (ADTT=5000), $\gamma_{LL}=1.0$ ($f_t = 0.0948\sqrt{f'_c}$)

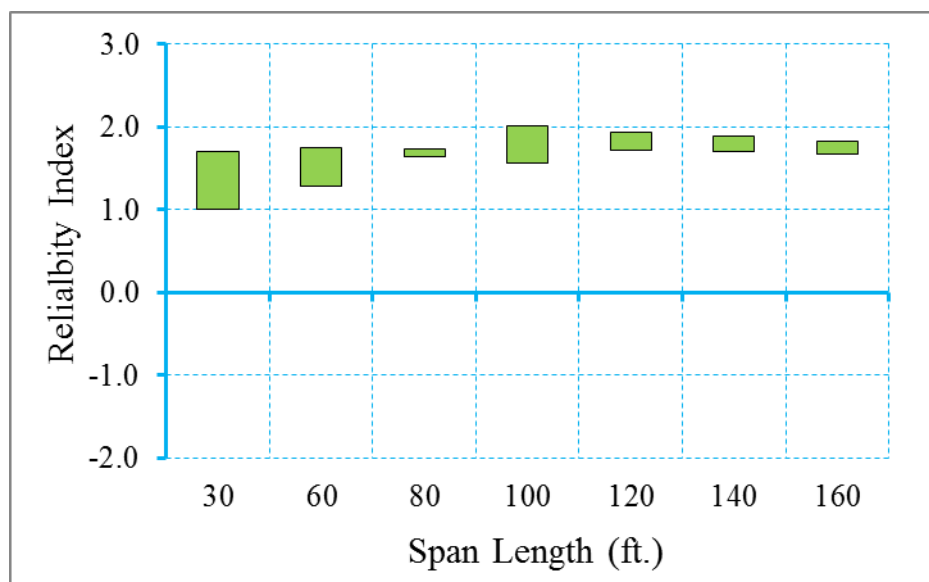


Figure B.53 Reliability Indices for AASHTO I Girder Bridges at Maximum Tensile Stress Limit State (ADTT=5000), $\gamma_{LL}=1.0$ ($f_t = 0.0948\sqrt{f'_c}$)

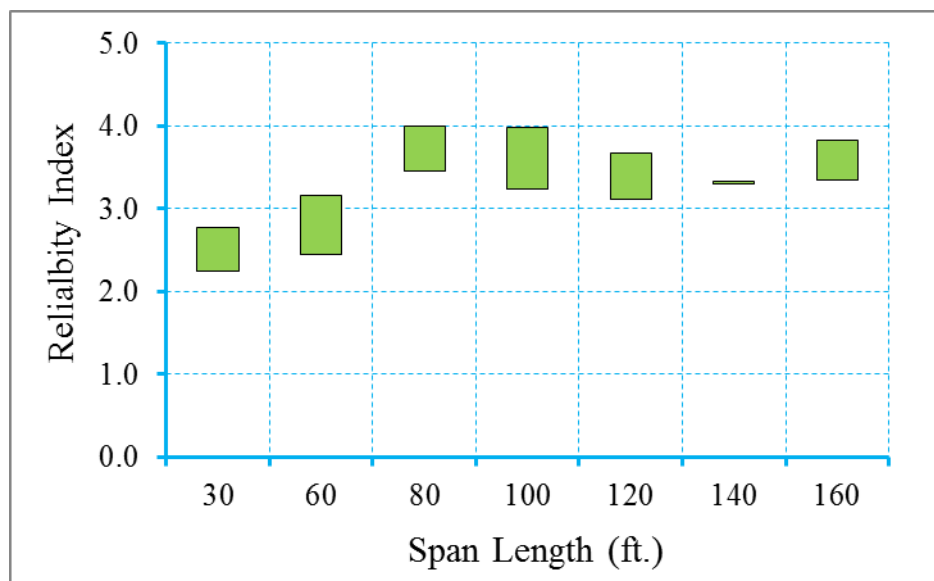


Figure B.54 Reliability Indices for AASHTO I Girder Bridges at Maximum Crack Width Limit State (ADTT=5000), $\gamma_{LL}=1.0$ ($f_t = 0.0948\sqrt{f'_c}$)

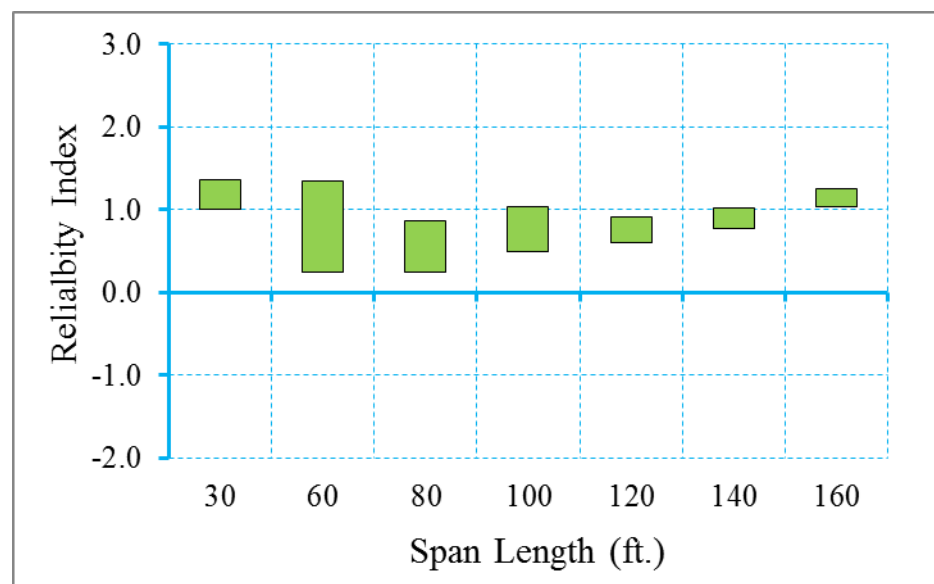


Figure B.55 Reliability Indices for AASHTO I Girder Bridges at Decompression Limit State (ADTT=5000), $\gamma_{LL}=0.8$ ($f_t = 0.158\sqrt{f'_c}$)

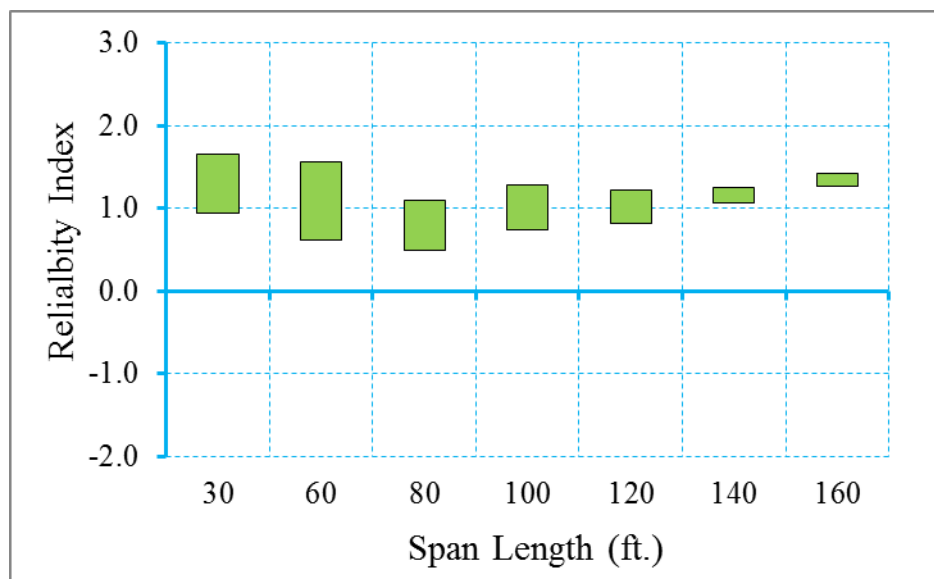


Figure B.56 Reliability Indices for AASHTO I Girder Bridges at Maximum Allowable Tensile Stress Limit State (ADTT=5000), $\gamma_{LL}=0.8$ ($f_t = 0.158\sqrt{f'_c}$)

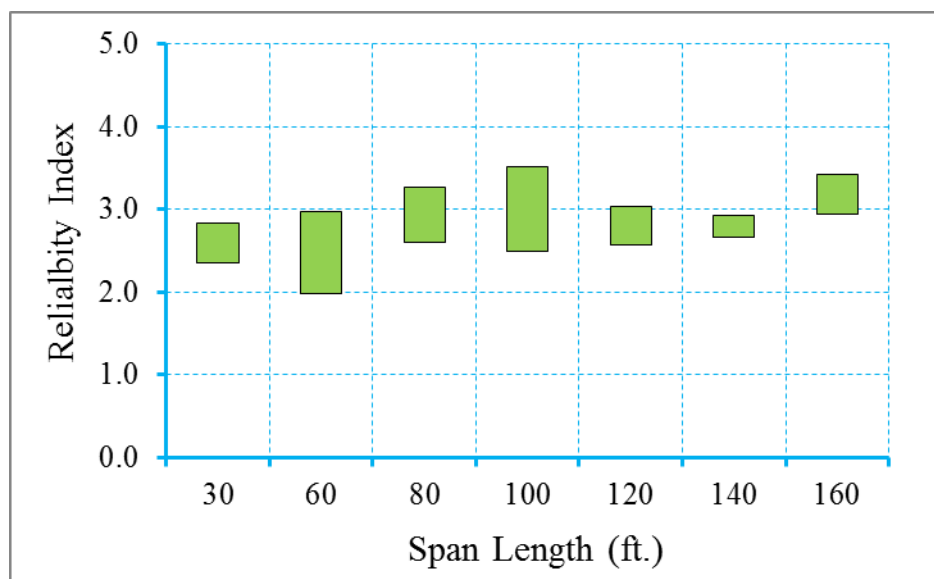


Figure B.57 Reliability Indices for AASHTO I Girder Bridges at Maximum Allowable Crack Width Limit State (ADTT=5000), $\gamma_{LL}=0.8$ ($f_t = 0.158\sqrt{f'_c}$)

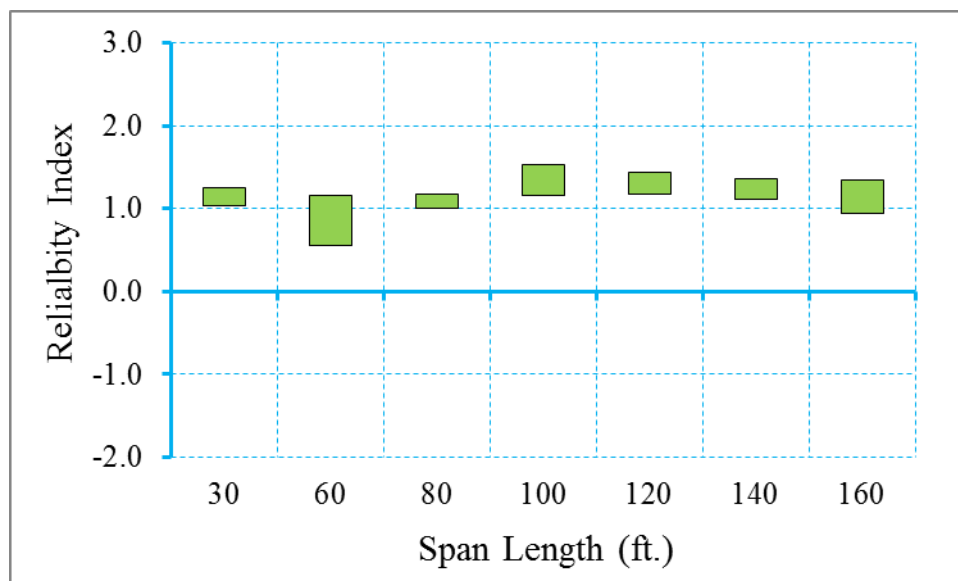


Figure B.58 Reliability Indices for AASHTO I Girder Bridges at Decompression Limit State (ADTT=5000), $\gamma_{LL}=1.0$ ($f_t = 0.158\sqrt{f'_c}$)

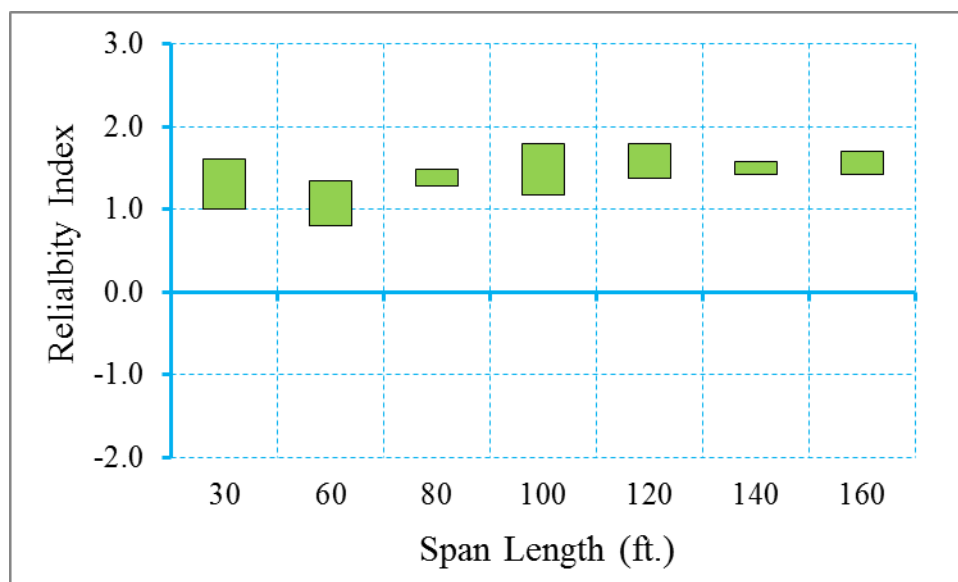


Figure B.59 Reliability Indices for AASHTO I Girder Bridges at Maximum Tensile Stress Limit State (ADTT=5000), $\gamma_{LL}=1.0$ ($f_t = 0.158\sqrt{f'_c}$)

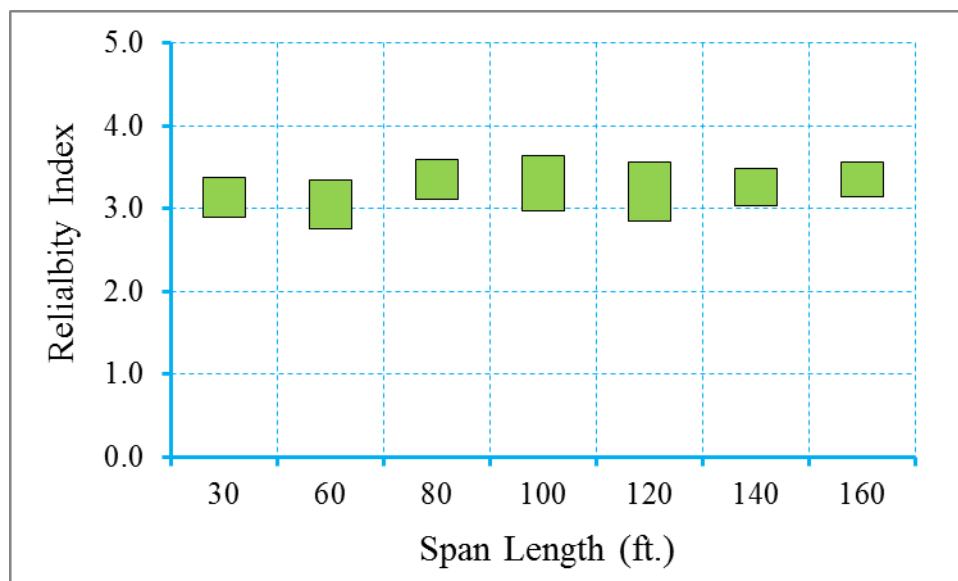


Figure B.60 Reliability Indices for AASHTO I Girder Bridges at Maximum Crack Width Limit State (ADTT=5000), $\gamma_{LL}=1.0$ ($f_t = 0.158\sqrt{f'_c}$)

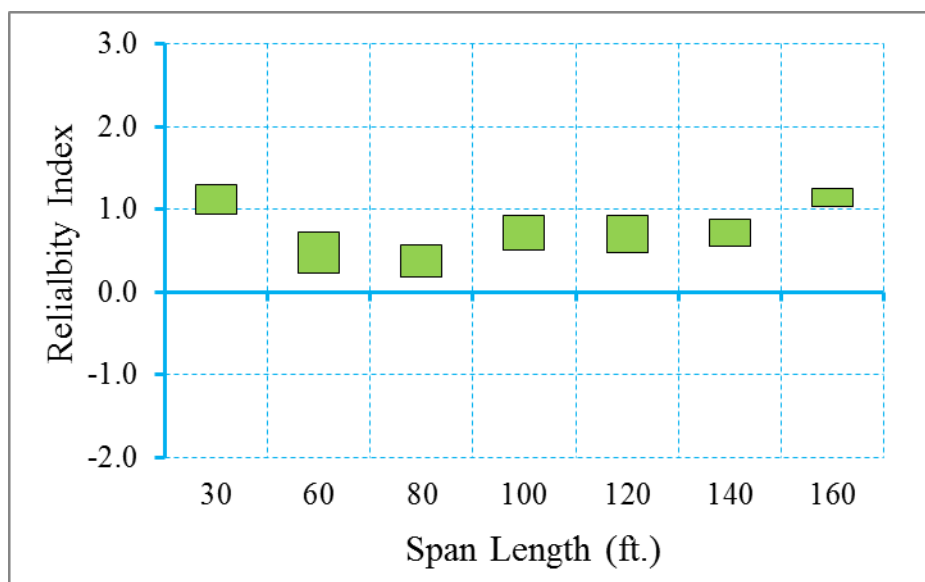


Figure B.61 Reliability Indices for AASHTO I Girder Bridges at Decompression Limit State (ADTT=5000), $\gamma_{LL}=0.8$ ($f_t = 0.19\sqrt{f'_c}$)

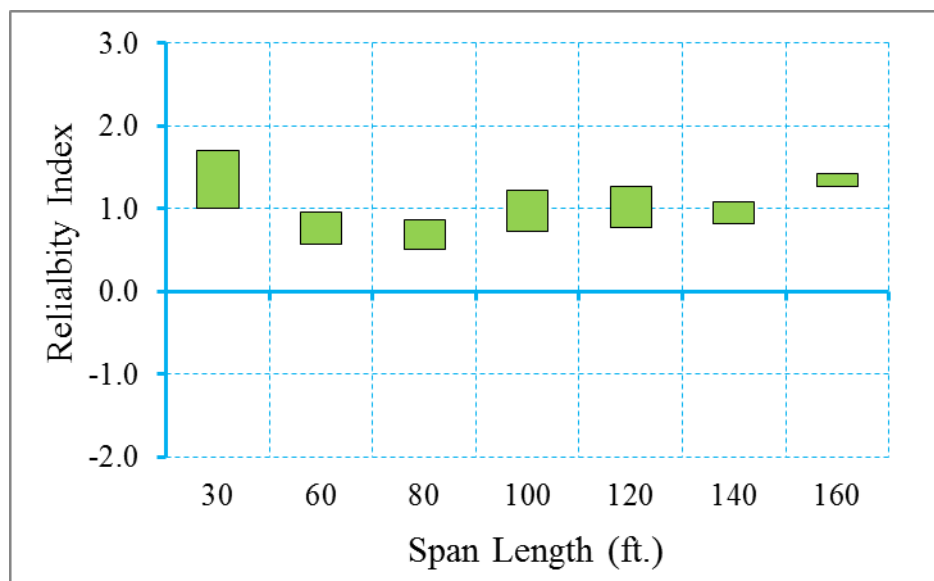


Figure B.62 Reliability Indices for AASHTO I Girder Bridges at Maximum Allowable Tensile Stress Limit State (ADTT=5000), $\gamma_{LL}=0.8$ ($f_t = 0.19\sqrt{f'_c}$)

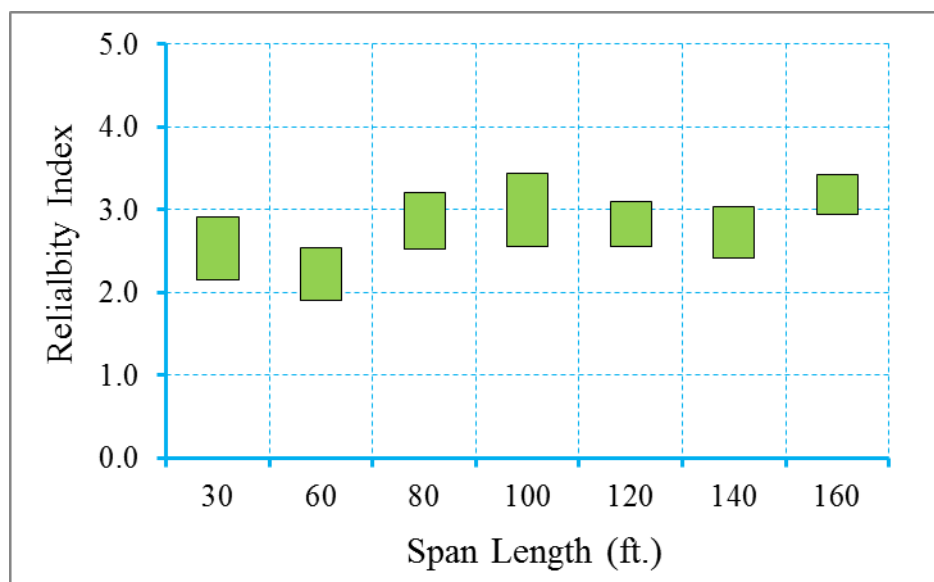


Figure B.63 Reliability Indices for AASHTO I Girder Bridges at Maximum Allowable Crack Width Limit State (ADTT=5000), $\gamma_{LL}=0.8$ ($f_t = 0.19\sqrt{f'_c}$)

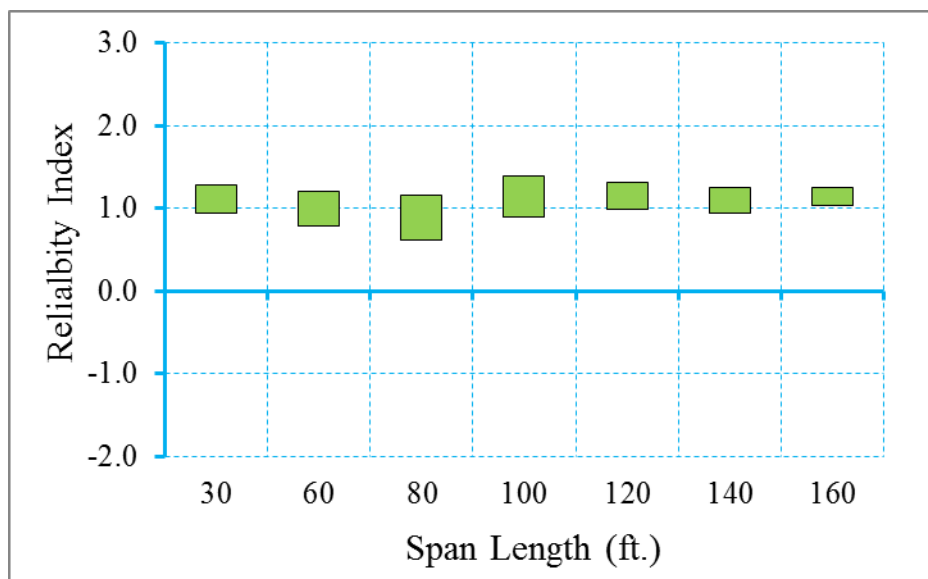


Figure B.64 Reliability Indices for AASHTO I Girder Bridges at Decompression Limit State (ADTT=5000), $\gamma_{LL}=1.0$ ($f_t = 0.19\sqrt{f'_c}$)

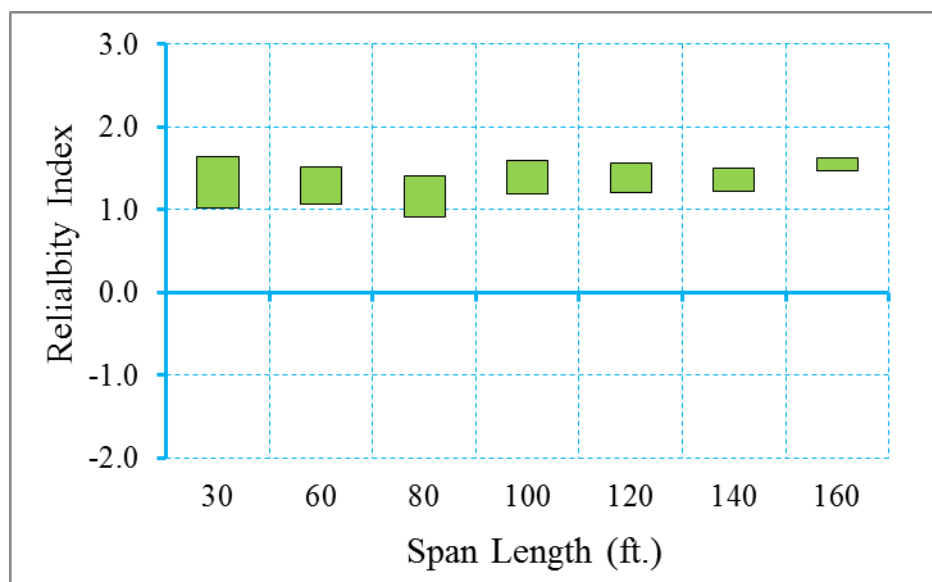


Figure B.65 Reliability Indices for AASHTO I Girder Bridges at Maximum Tensile Stress Limit State (ADTT=5000), $\gamma_{LL}=1.0$ ($f_t = 0.19\sqrt{f'_c}$)

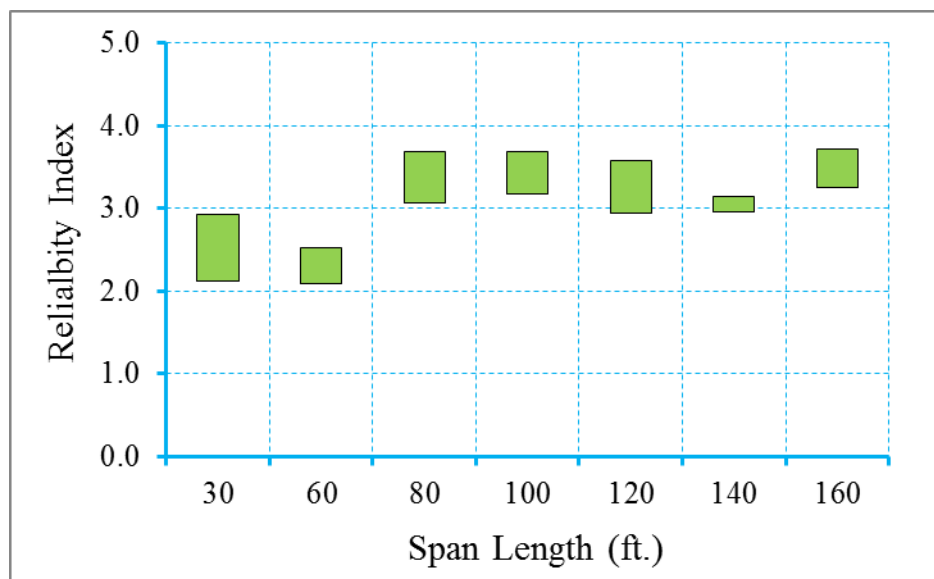


Figure B.66 Reliability Indices for AASHTO I Girder Bridges at Maximum Crack Width Limit State (ADTT=5000), $\gamma_{LL}=1.0$ ($f_t = 0.19\sqrt{f'_c}$)

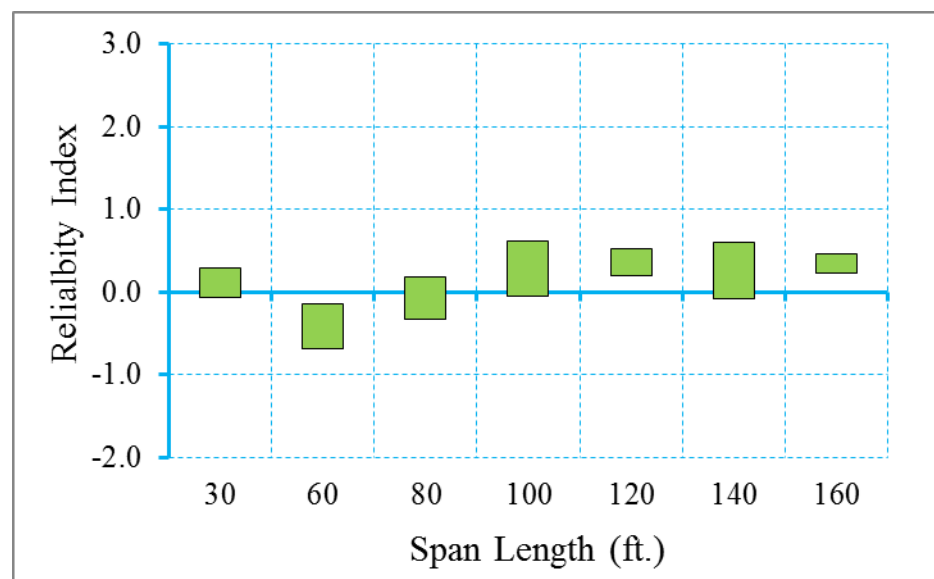


Figure B.67 Reliability Indices for AASHTO I Girder Bridges at Decompression Limit State (ADTT=5000), $\gamma_{LL}=0.8$ ($f_t = 0.253\sqrt{f'_c}$)

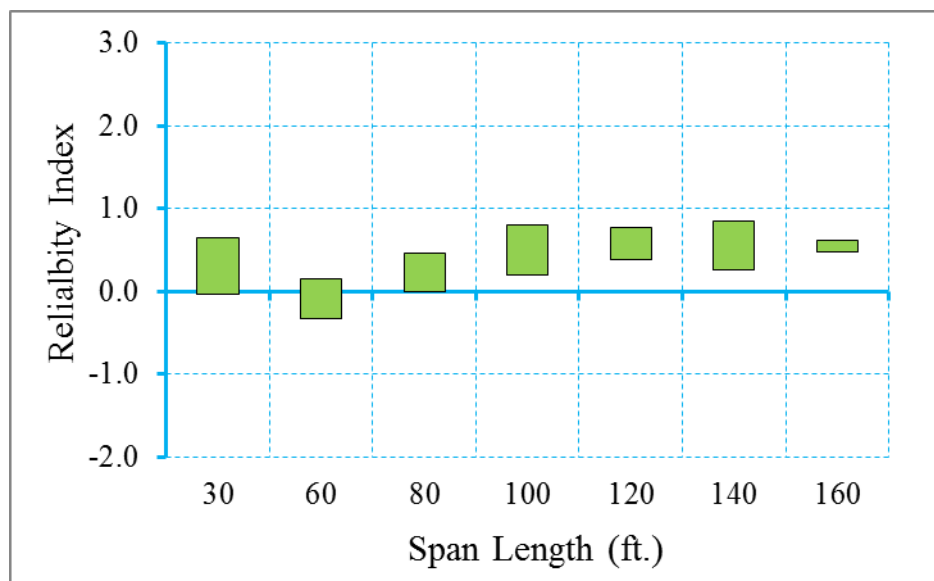


Figure B.68 Reliability Indices for AASHTO I Girder Bridges at Maximum Allowable Tensile Stress Limit State (ADTT=5000), $\gamma_{LL}=0.8$ ($f_t = 0.253\sqrt{f'_c}$)

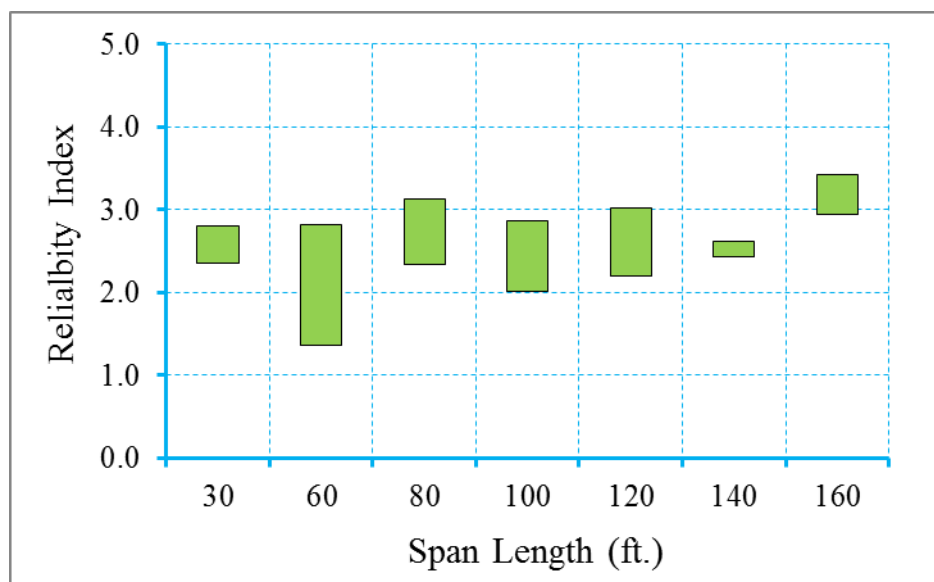


Figure B.69 Reliability Indices for AASHTO I Girder Bridges at Maximum Allowable Crack Width Limit State (ADTT=5000), $\gamma_{LL}=0.8$ ($f_t = 0.253\sqrt{f'_c}$)

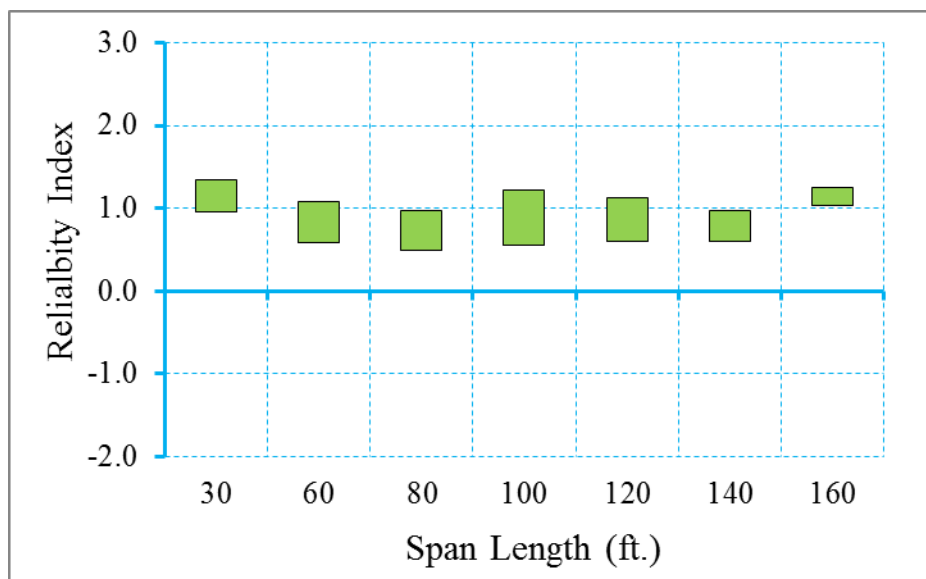


Figure B.70 Reliability Indices for AASHTO I Girder Bridges at Decompression Limit State (ADTT=5000), $\gamma_{LL}=1.0$ ($f_t = 0.253\sqrt{f'_c}$)

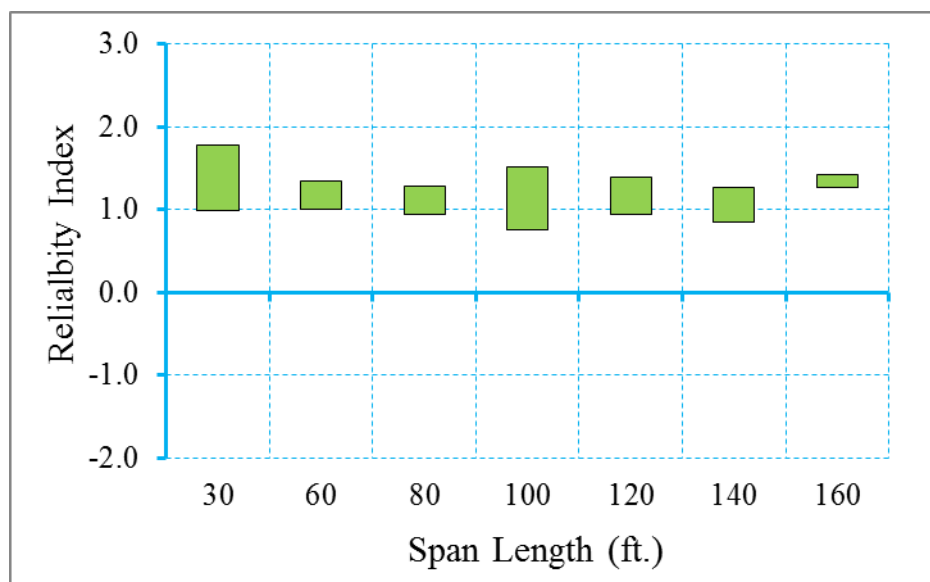


Figure B.71 Reliability Indices for AASHTO I Girder Bridges at Maximum Tensile Stress Limit State (ADTT=5000), $\gamma_{LL}=1.0$ ($f_t = 0.253\sqrt{f'_c}$)

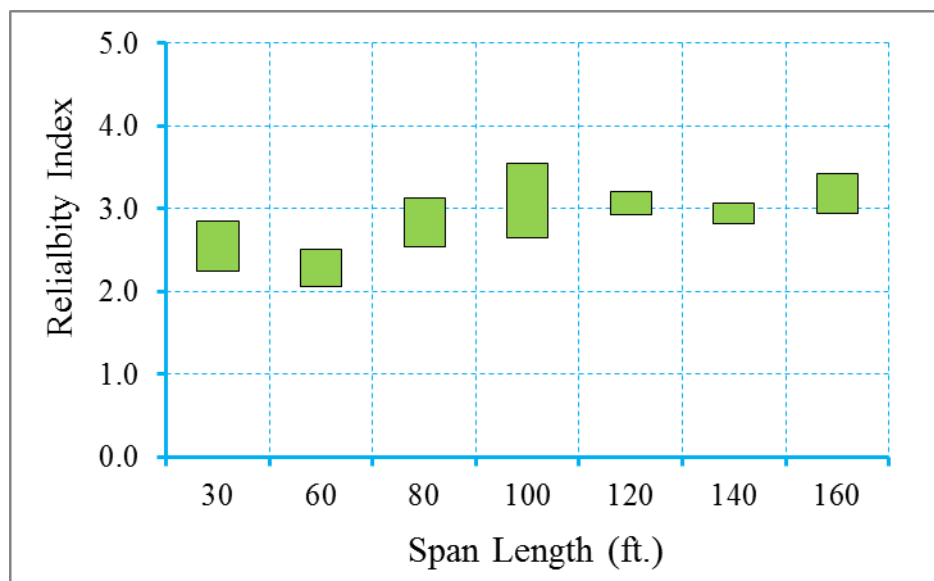


Figure B.72 Reliability Indices for AASHTO I Girder Bridges at Maximum Crack Width Limit State (ADTT=5000), $\gamma_{LL}=1.0$ ($f_t = 0.253\sqrt{f'_c}$)

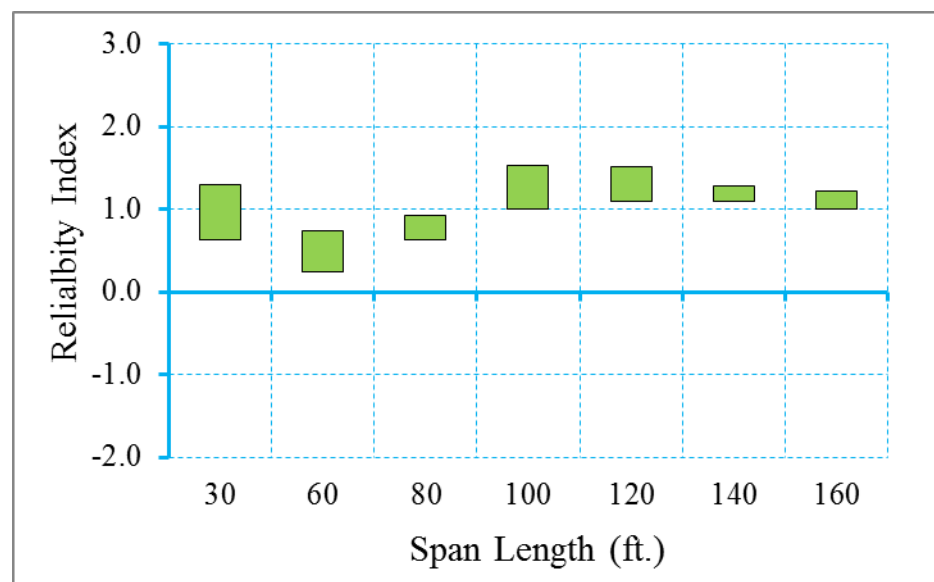


Figure B.73 Reliability Indices for AASHTO I Girder Bridges at Decompression Limit State (ADTT=10000), $\gamma_{LL}=0.8$ ($f_t = 0.0948\sqrt{f'_c}$)

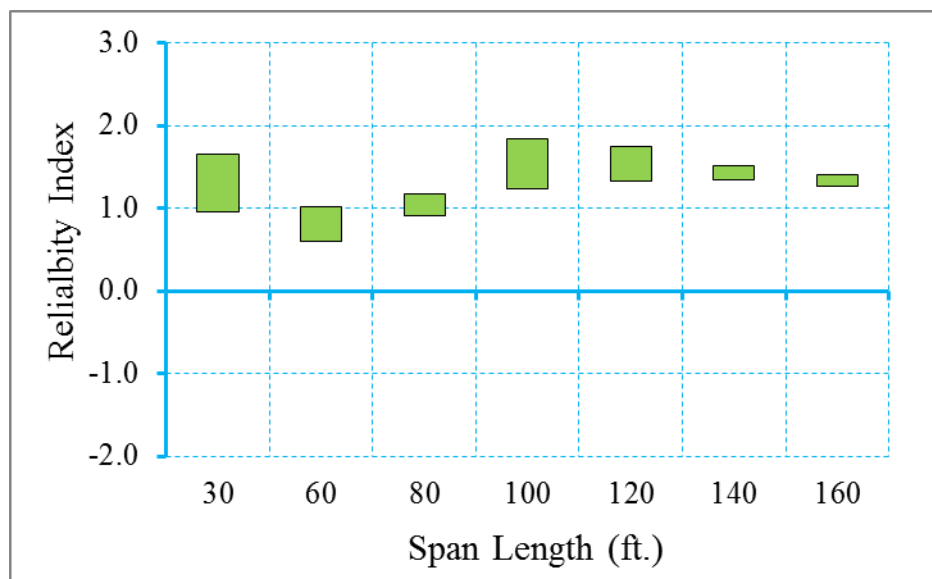


Figure B.74 Reliability Indices for AASHTO I Girder Bridges at Maximum Allowable Tensile Stress Limit State (ADTT=10000), $\gamma_{LL}=0.8$ ($f_t = 0.0948\sqrt{f'_c}$)

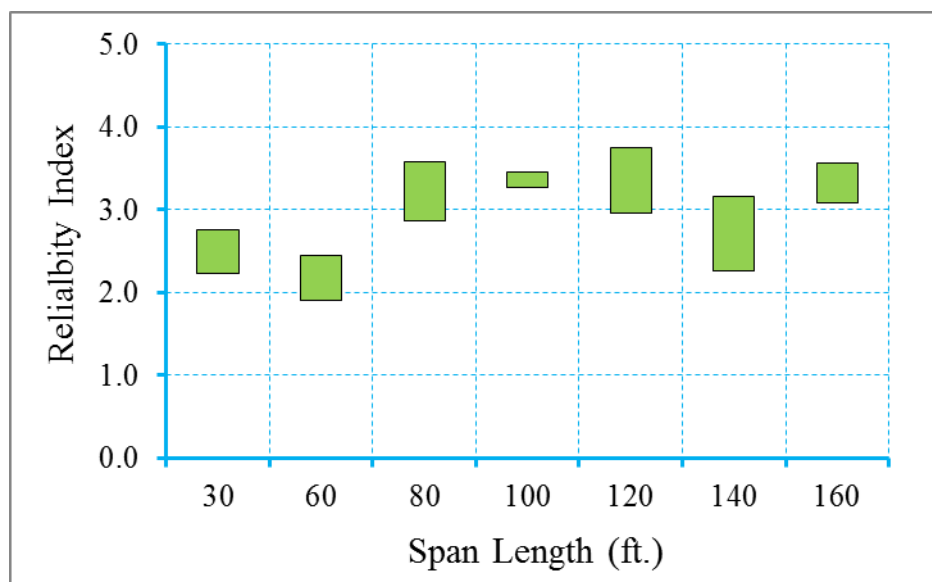


Figure B.75 Reliability Indices for AASHTO I Girder Bridges at Maximum Allowable Crack Width Limit State (ADTT=10000), $\gamma_{LL}=0.8$ ($f_t = 0.0948\sqrt{f'_c}$)

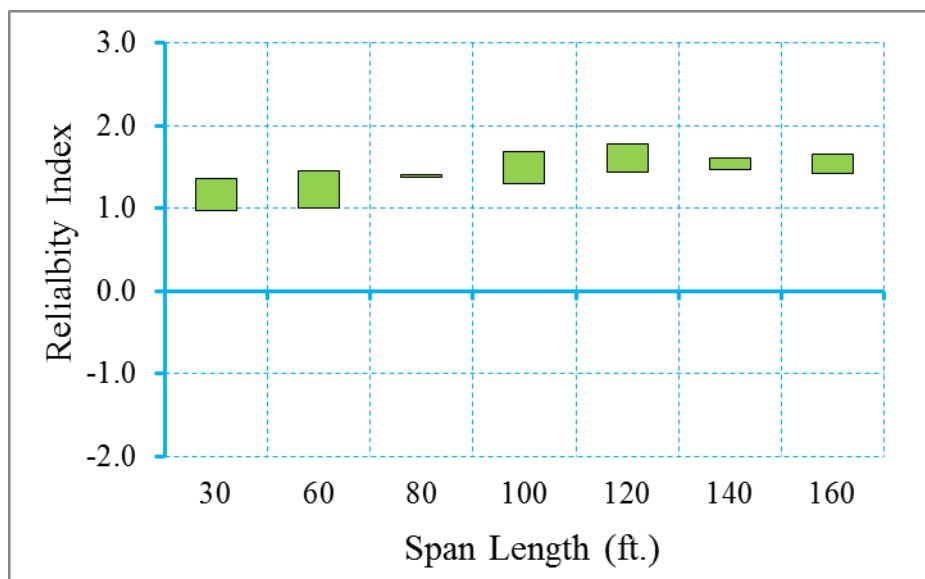


Figure B.76 Reliability Indices for AASHTO I Girder Bridges at Decompression Limit State (ADTT=10000), $\gamma_{LL}=1.0$ ($f_t = 0.0948\sqrt{f'_c}$)

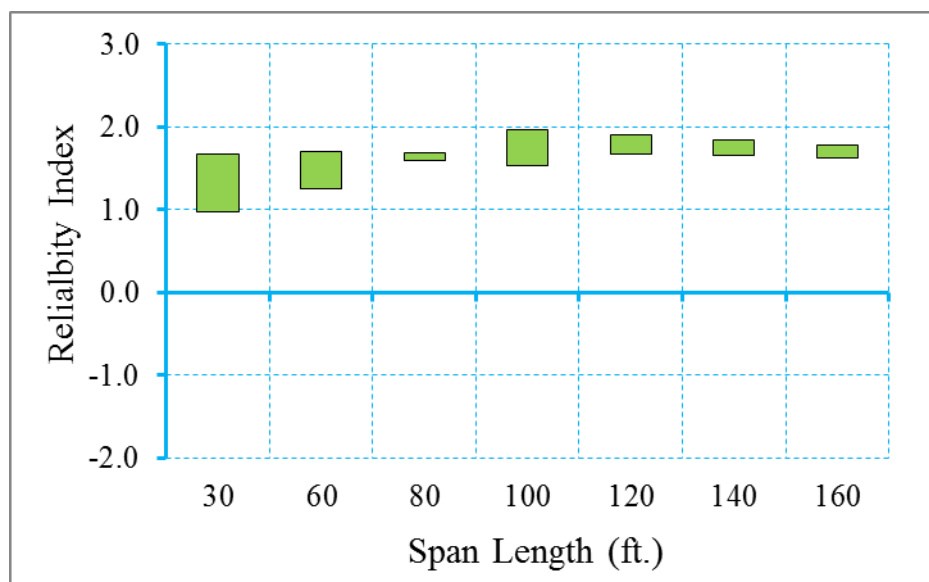


Figure B.77 Reliability Indices for AASHTO I Girder Bridges at Maximum Tensile Stress Limit State (ADTT=10000), $\gamma_{LL}=1.0$ ($f_t = 0.0948\sqrt{f'_c}$)

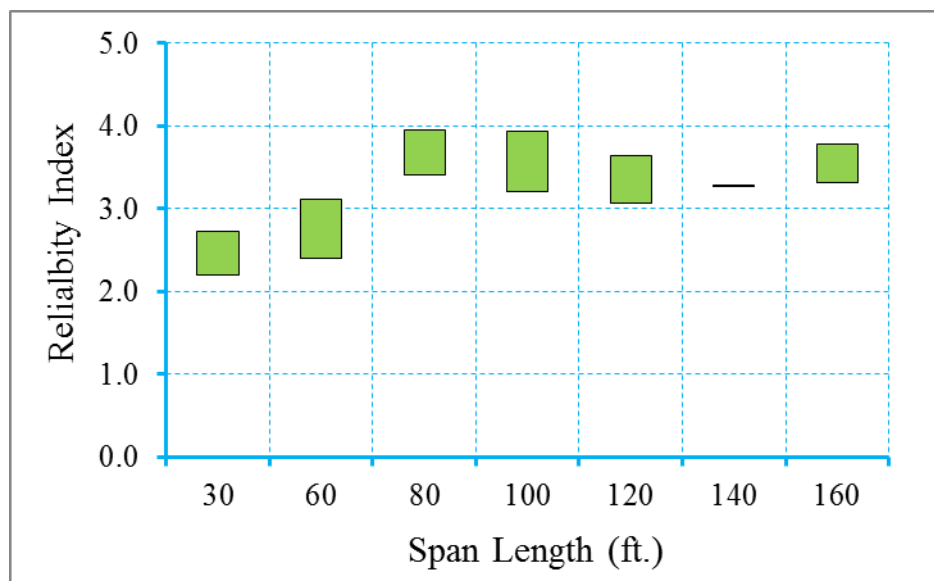


Figure B.78 Reliability Indices for AASHTO I Girder Bridges at Maximum Crack Width Limit State (ADTT=10000), $\gamma_{LL}=1.0$ ($f_t = 0.0948\sqrt{f'_c}$)

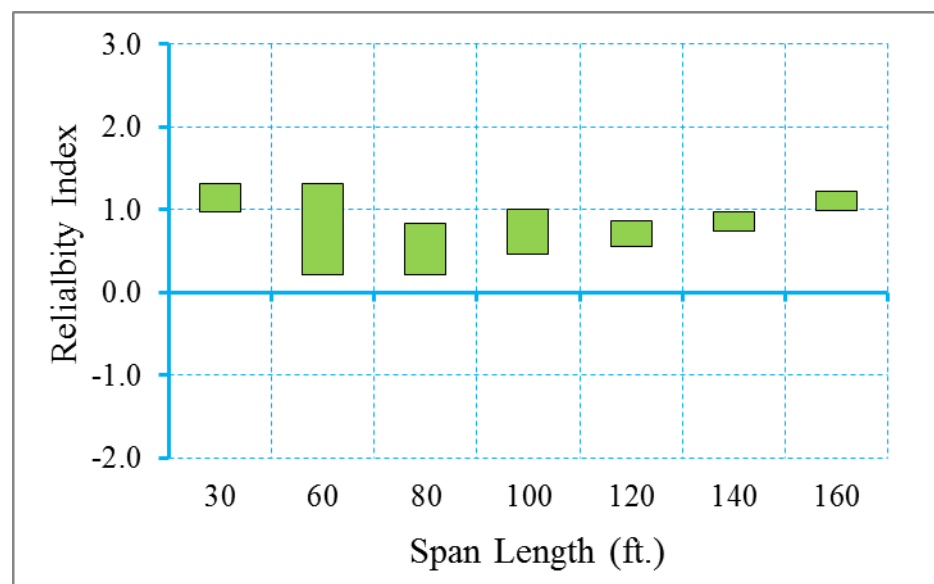


Figure B.79 Reliability Indices for AASHTO I Girder Bridges at Decompression Limit State (ADTT=10000), $\gamma_{LL}=0.8$ ($f_t = 0.158\sqrt{f'_c}$)

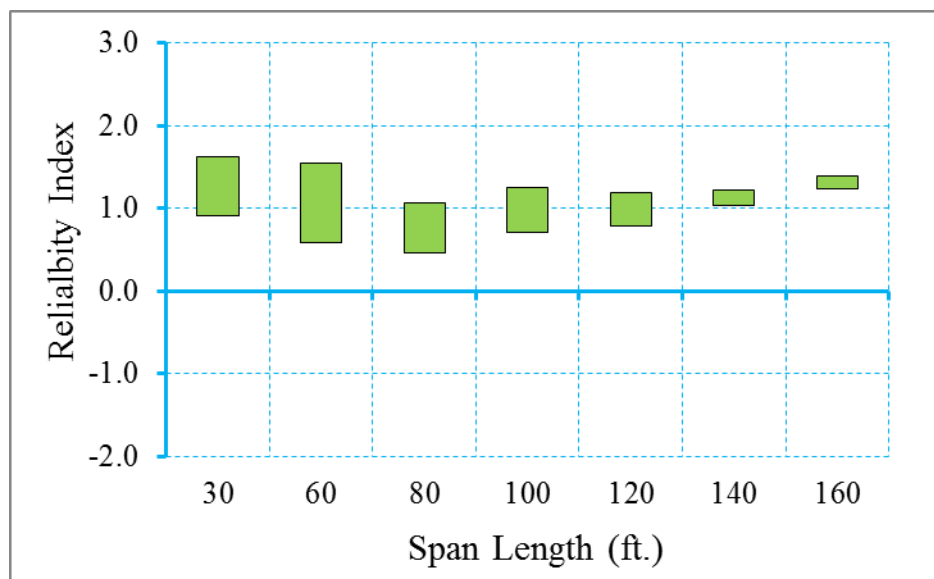


Figure B.80 Reliability Indices for AASHTO I Girder Bridges at Maximum Allowable Tensile Stress Limit State (ADTT=10000), $\gamma_{LL}=0.8$ ($f_t = 0.158\sqrt{f'_c}$)

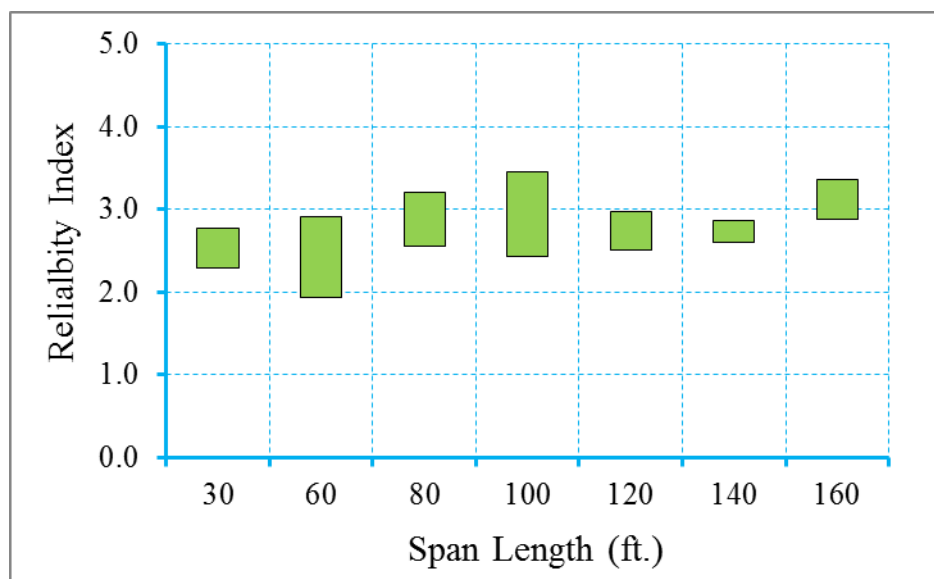


Figure B.81 Reliability Indices for AASHTO I Girder Bridges at Maximum Allowable Crack Width Limit State (ADTT=10000), $\gamma_{LL}=0.8$ ($f_t = 0.158\sqrt{f'_c}$)

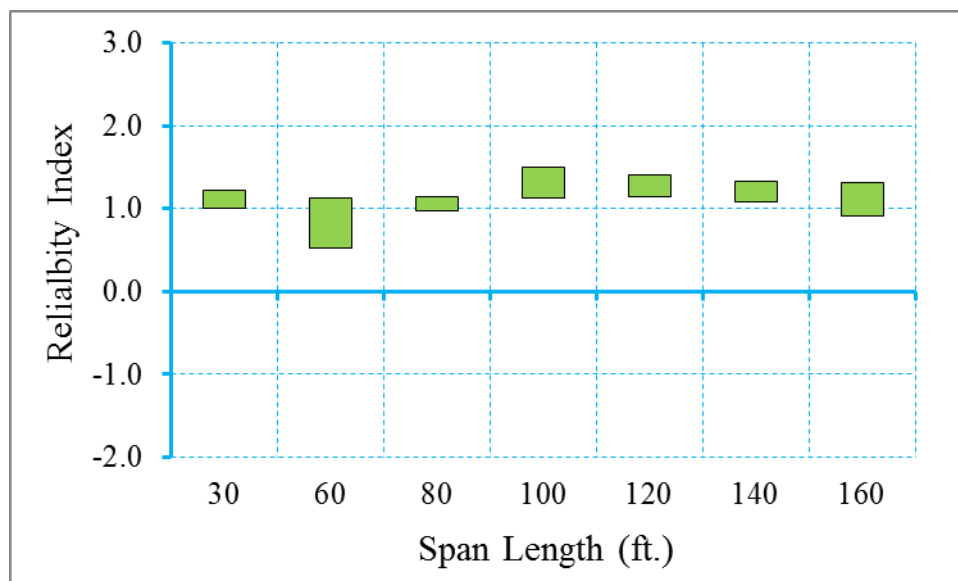


Figure B.82 Reliability Indices for AASHTO I Girder Bridges at Decompression Limit State (ADTT=10000), $\gamma_{LL}=1.0$ ($f_t = 0.158\sqrt{f'_c}$)

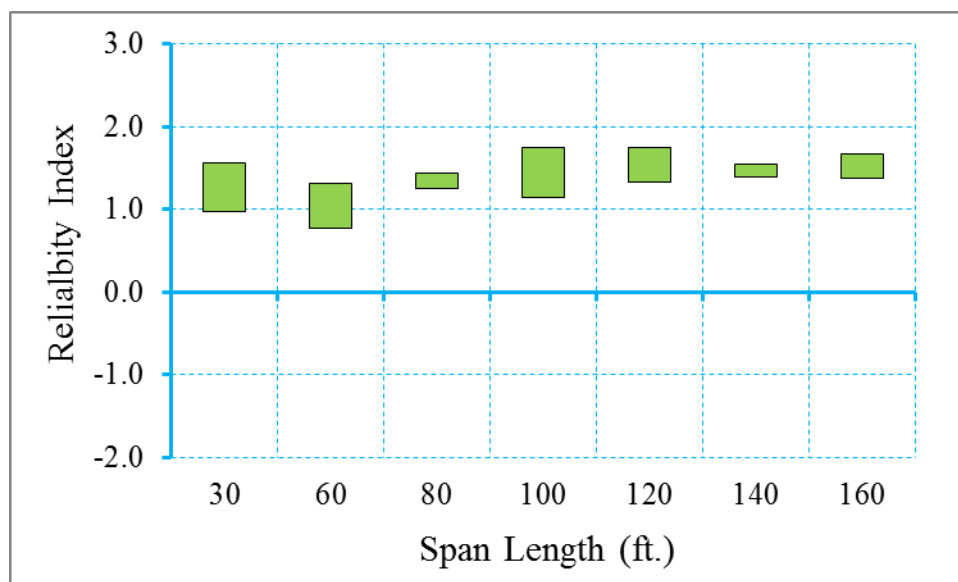


Figure B.83 Reliability Indices for AASHTO I Girder Bridges at Maximum Tensile Stress Limit State (ADTT=10000), $\gamma_{LL}=1.0$ ($f_t = 0.158\sqrt{f'_c}$)

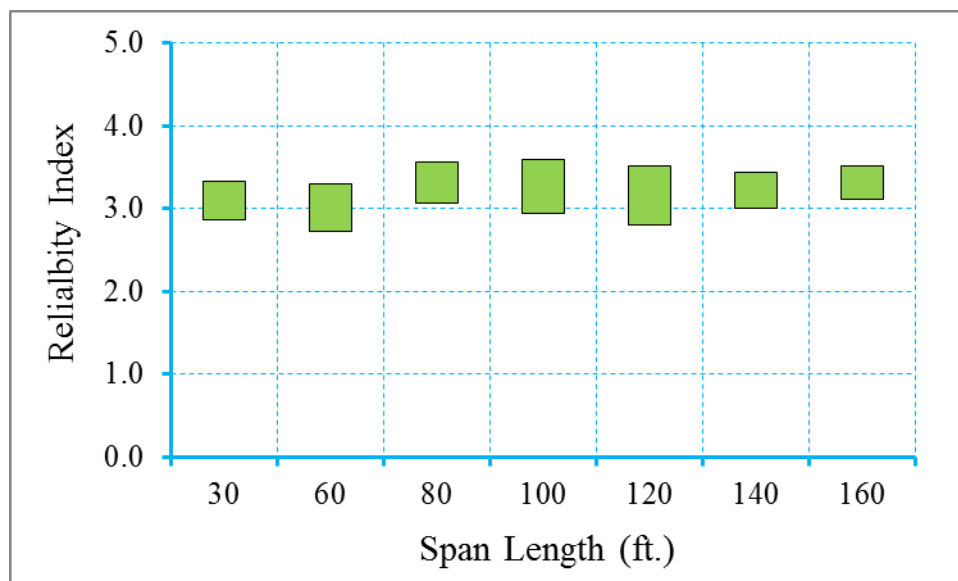


Figure B.84 Reliability Indices for AASHTO I Girder Bridges at Maximum Crack Width Limit State (ADTT=10000), $\gamma_{LL}=1.0$ ($f_t = 0.158\sqrt{f'_c}$)

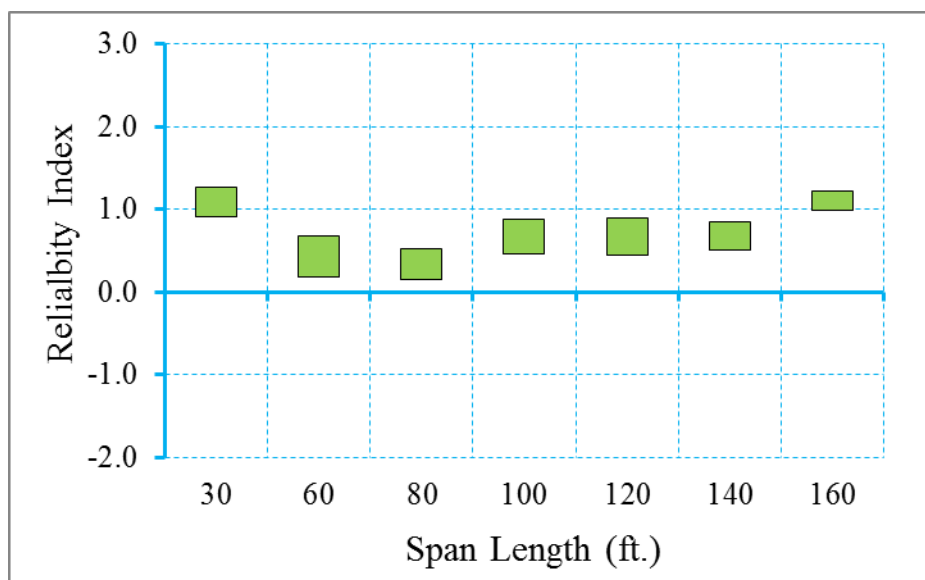


Figure B.85 Reliability Indices for AASHTO I Girder Bridges at Decompression Limit State (ADTT=10000), $\gamma_{LL}=0.8$ ($f_t = 0.19\sqrt{f'_c}$)

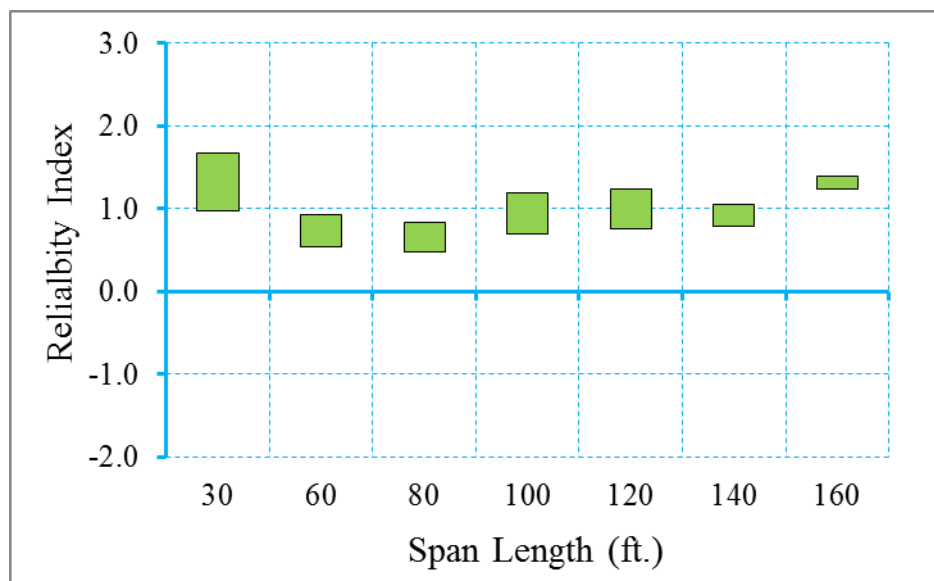


Figure B.86 Reliability Indices for AASHTO I Girder Bridges at Maximum Allowable Tensile Stress Limit State (ADTT=10000), $\gamma_{LL}=0.8$ ($f_t = 0.19\sqrt{f'_c}$)

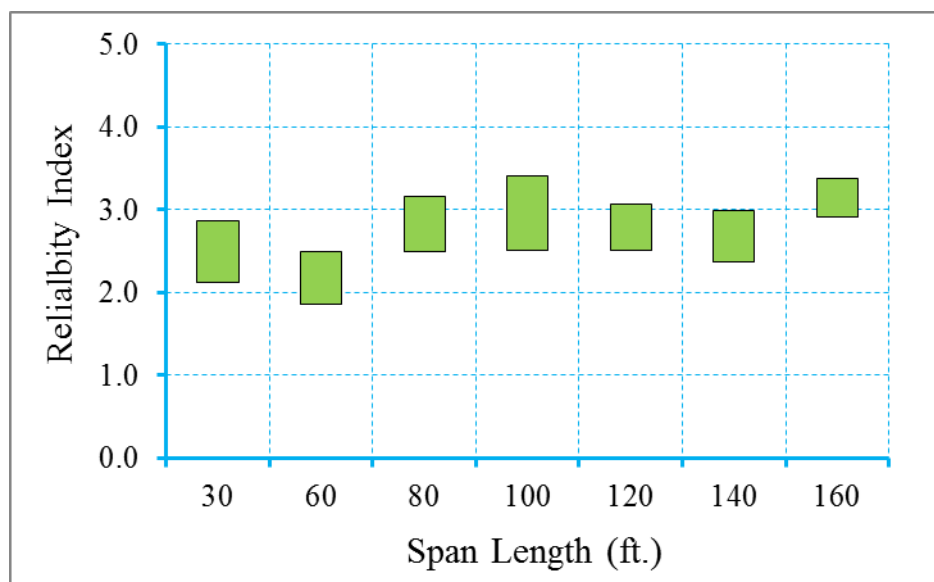


Figure B.87 Reliability Indices for AASHTO I Girder Bridges at Maximum Allowable Crack Width Limit State (ADTT=10000), $\gamma_{LL}=0.8$ ($f_t = 0.19\sqrt{f'_c}$)

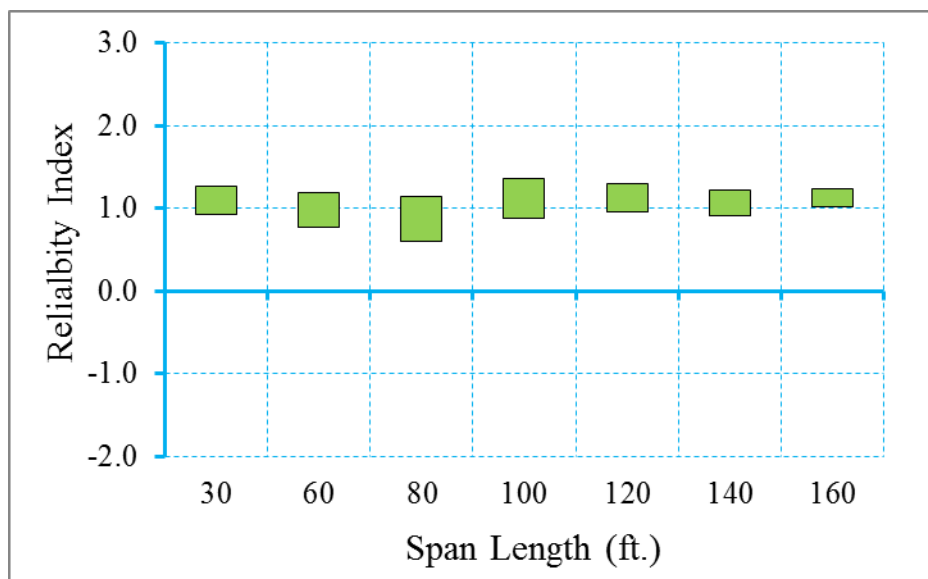


Figure B.88 Reliability Indices for AASHTO I Girder Bridges at Decompression Limit State (ADTT=10000), $\gamma_{LL}=1.0$ ($f_t = 0.19\sqrt{f'_c}$)

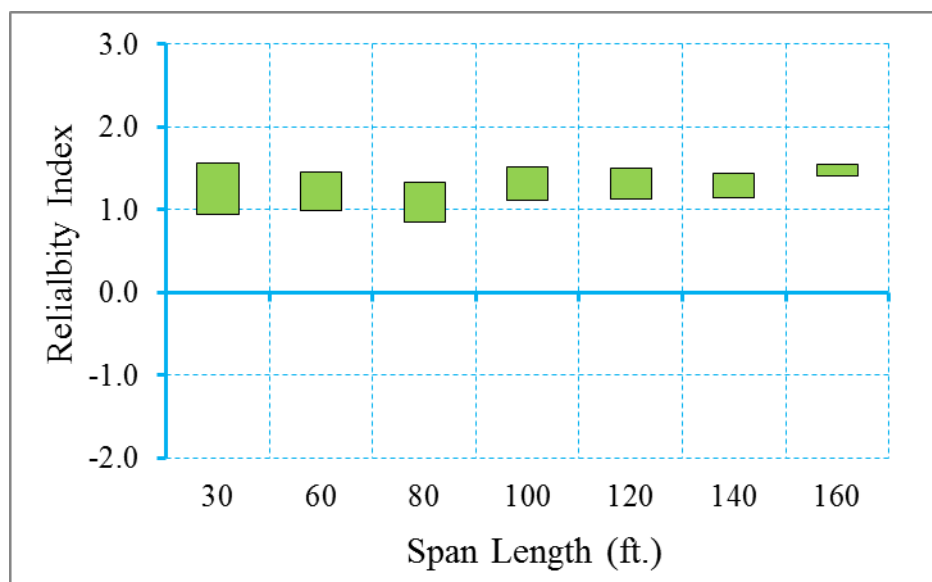


Figure B.89 Reliability Indices for AASHTO I Girder Bridges at Maximum Tensile Stress Limit State (ADTT=10000), $\gamma_{LL}=1.0$ ($f_t = 0.19\sqrt{f'_c}$)

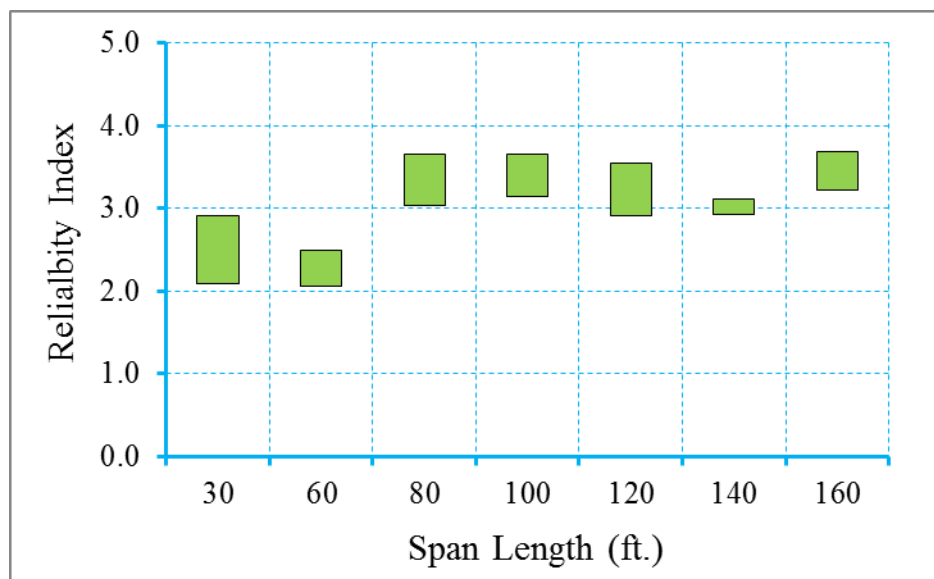


Figure B.90 Reliability Indices for AASHTO I Girder Bridges at Maximum Crack Width Limit State (ADTT=10000), $\gamma_{LL}=1.0$ ($f_t = 0.19\sqrt{f'_c}$)

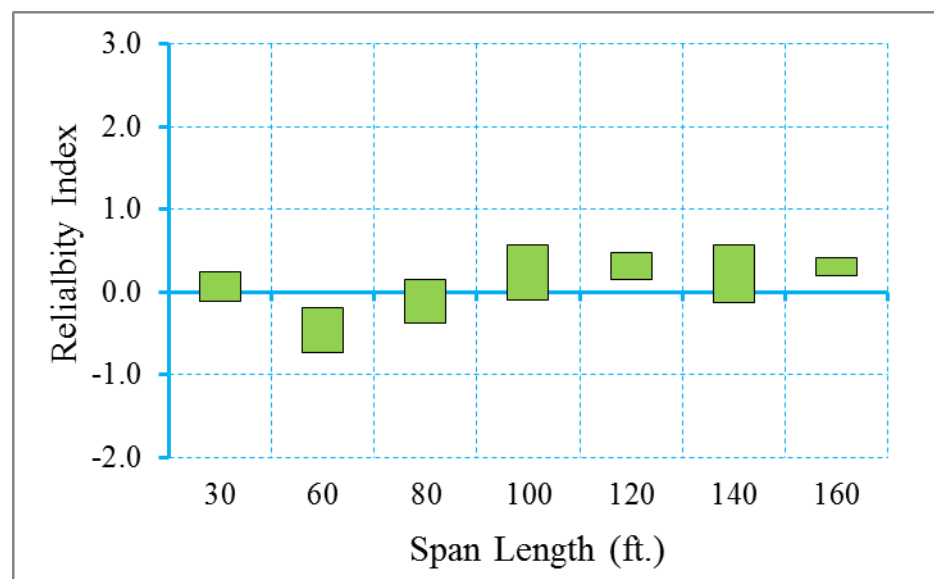


Figure B.91 Reliability Indices for AASHTO I Girder Bridges at Decompression Limit State (ADTT=10000), $\gamma_{LL}=0.8$ ($f_t = 0.253\sqrt{f'_c}$)

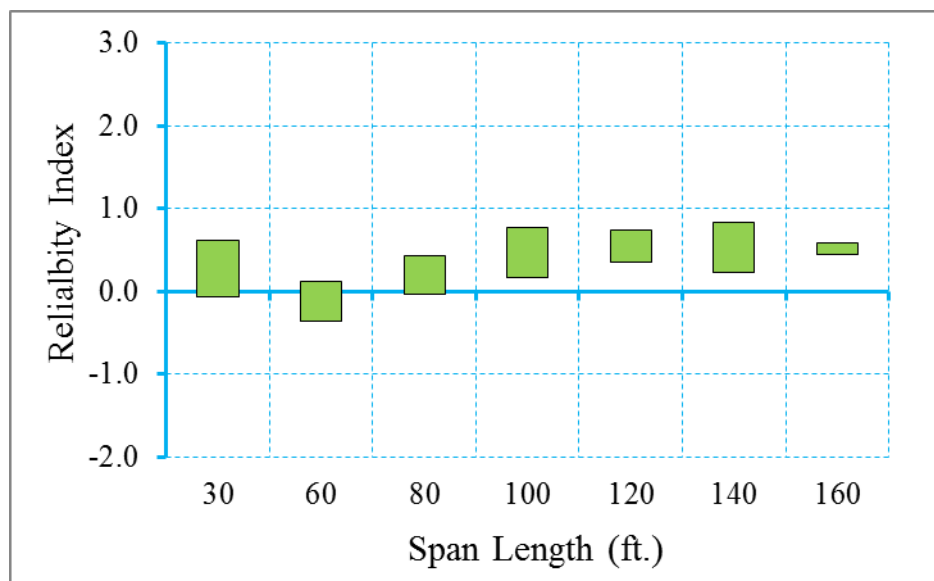


Figure B.92 Reliability Indices for AASHTO I Girder Bridges at Maximum Allowable Tensile Stress Limit State (ADTT=10000), $\gamma_{LL}=0.8$ ($f_t = 0.253\sqrt{f'_c}$)

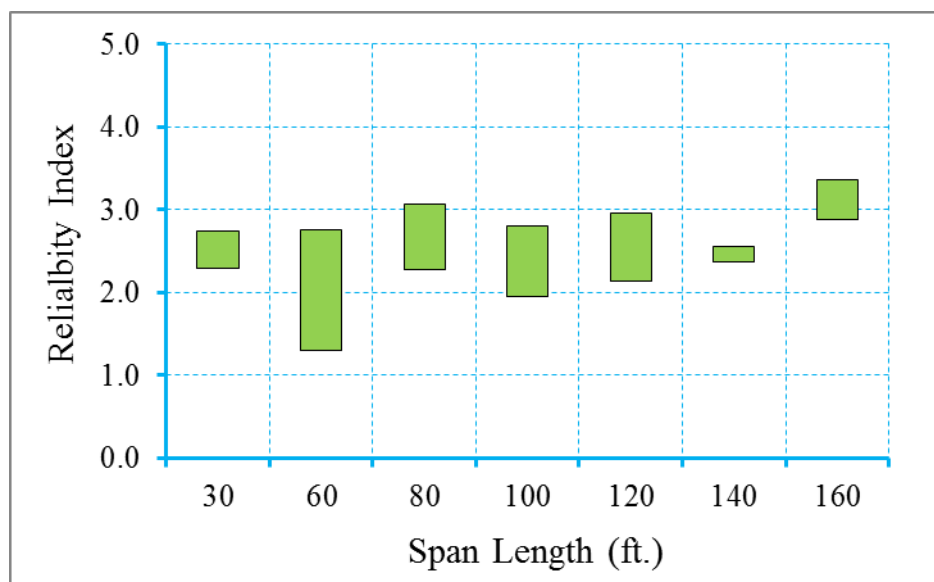


Figure B.93 Reliability Indices for AASHTO I Girder Bridges at Maximum Allowable Crack Width Limit State (ADTT=10000), $\gamma_{LL}=0.8$ ($f_t = 0.253\sqrt{f'_c}$)

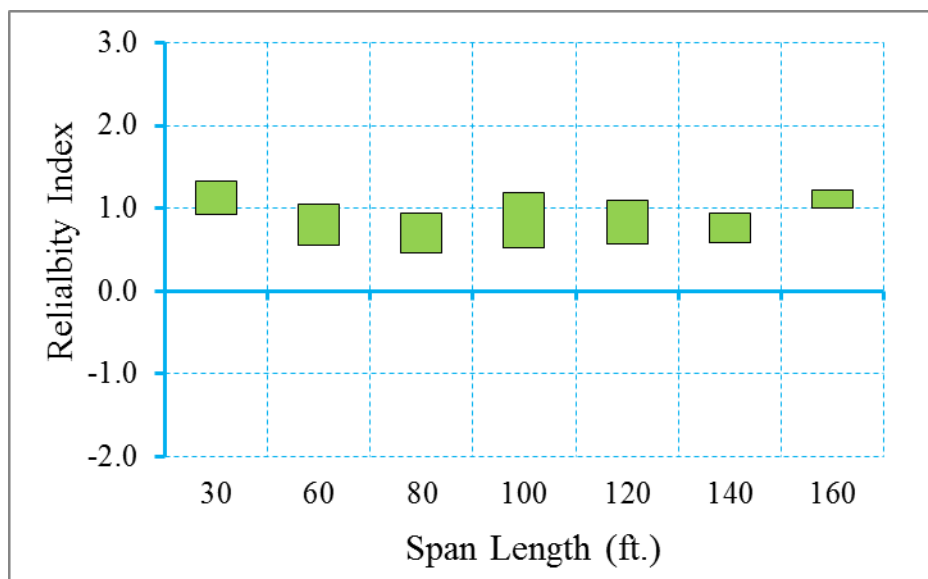


Figure B.94 Reliability Indices for AASHTO I Girder Bridges at Decompression Limit State (ADTT=10000), $\gamma_{LL}=1.0$ ($f_t = 0.253\sqrt{f'_c}$)

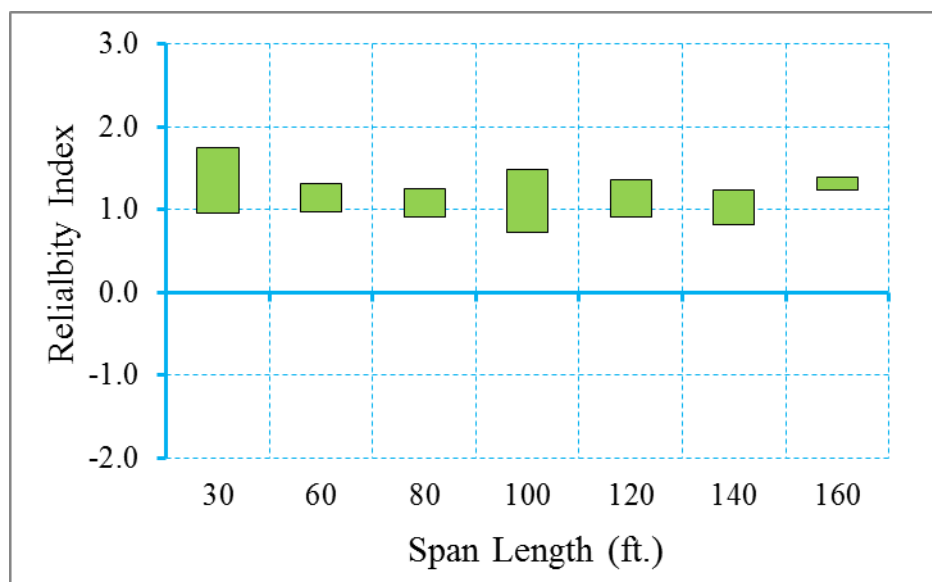


Figure B.95 Reliability Indices for AASHTO I Girder Bridges at Maximum Tensile Stress Limit State (ADTT=10000), $\gamma_{LL}=1.0$ ($f_t = 0.253\sqrt{f'_c}$)

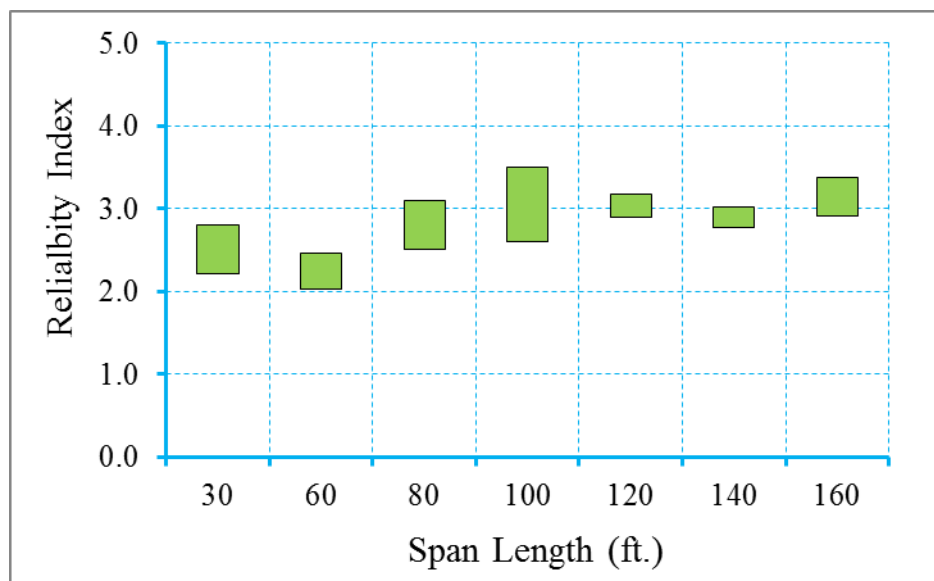


Figure B.96 Reliability Indices for AASHTO I Girder Bridges at Maximum Crack Width Limit State (ADTT=10000), $\gamma_{LL}=1.0$ ($f_t = 0.253\sqrt{f'_c}$)

B.2 Adjacent Box Girder Bridges

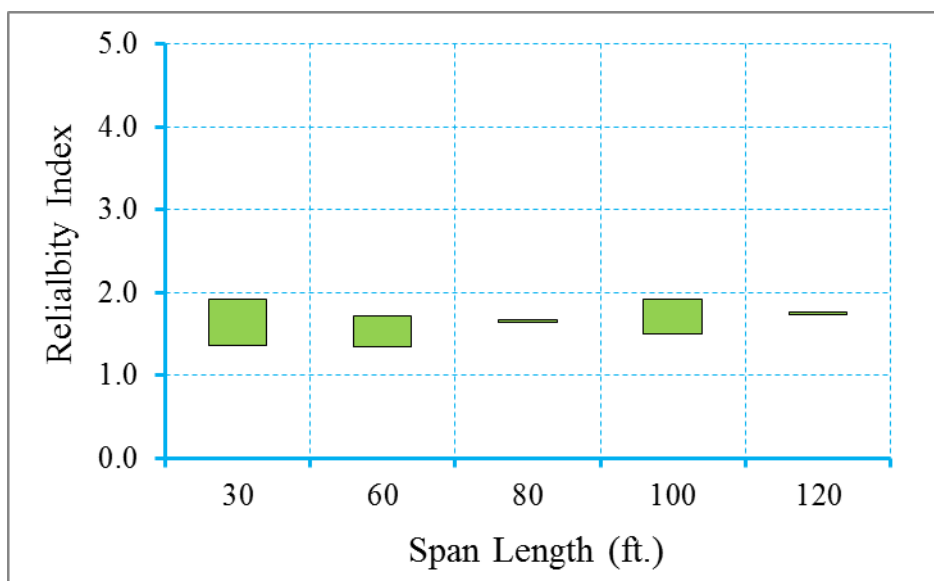


Figure B.97 Reliability Indices for AASHTO Adjacent Box Girder Bridges at Decompression Limit State (ADTT=5000), $\gamma_{LL}=0.8$ ($f_t = 0.0948\sqrt{f'_c}$)

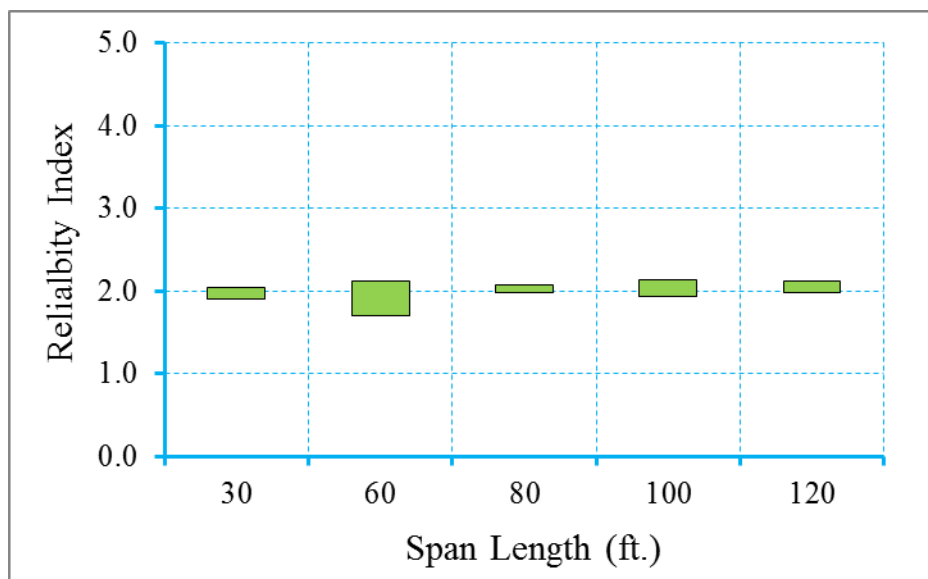


Figure B.98 Reliability Indices for AASHTO Adjacent Box Girder Bridges at Maximum Allowable Tensile Stress Limit State (ADTT=5000), $\gamma_{LL}=0.8$ ($f_t = 0.0948\sqrt{f'_c}$)

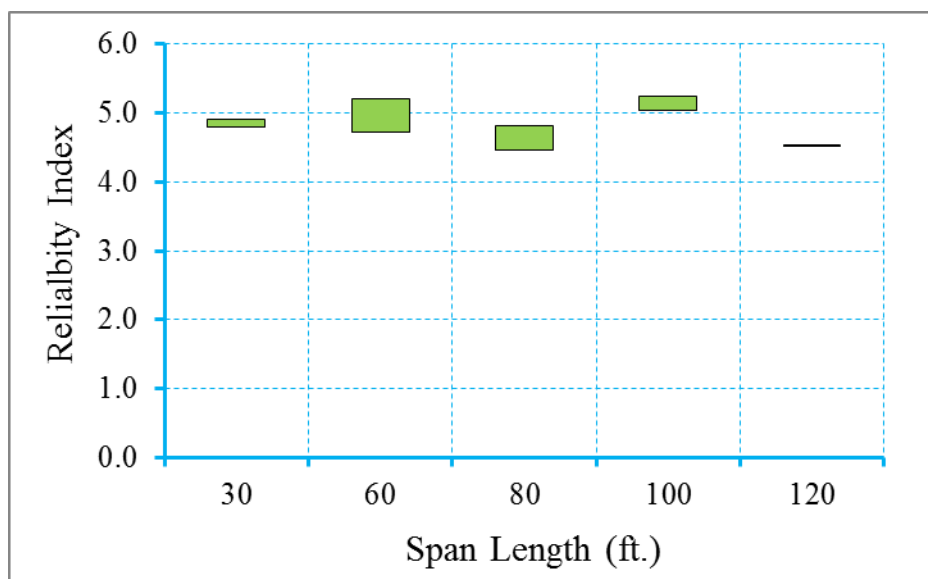


Figure B.99 Reliability Indices for AASHTO Adjacent Box Girder Bridges at Maximum Allowable Crack Width Limit State (ADTT=5000), $\gamma_{LL}=0.8$ ($f_t = 0.0948\sqrt{f'_c}$)

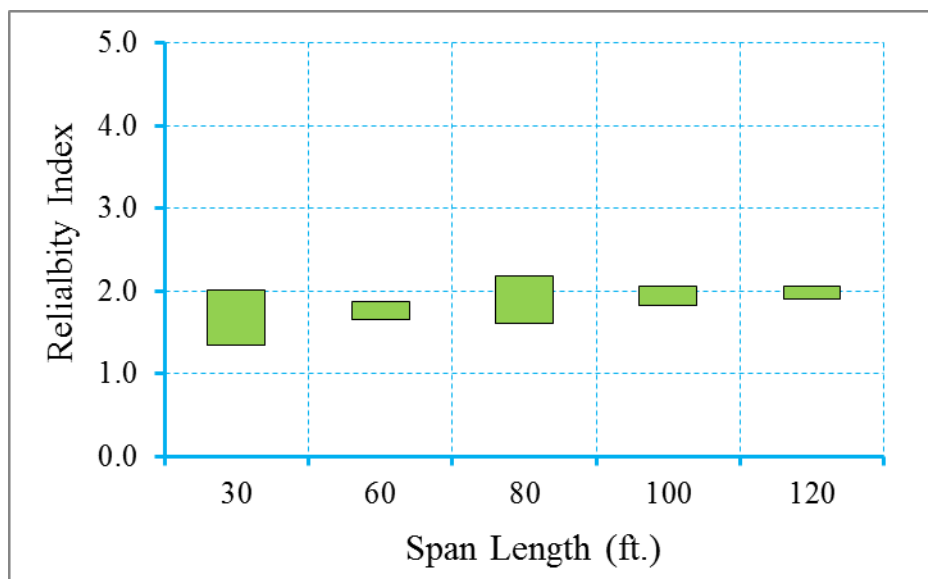


Figure B.100 Reliability Indices for AASHTO Adjacent Box Girder Bridges at Decompression Limit State (ADTT=5000), $\gamma_{LL}=1.0$ ($f_t = 0.0948\sqrt{f'_c}$)

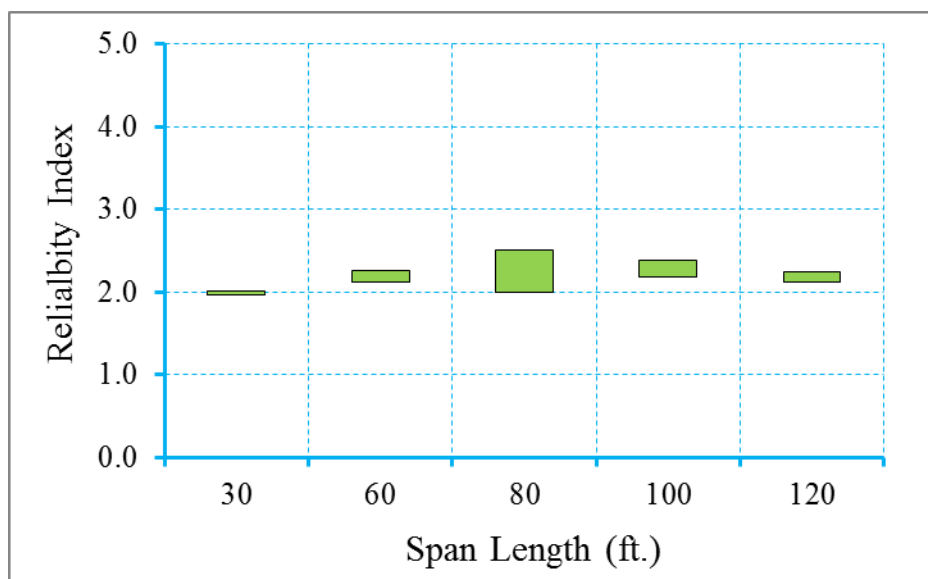


Figure B.101 Reliability Indices for AASHTO Adjacent Box Girder Bridges at Maximum Tensile Stress Limit State (ADTT=5000), $\gamma_{LL}=1.0$ ($f_t = 0.0948\sqrt{f'_c}$)

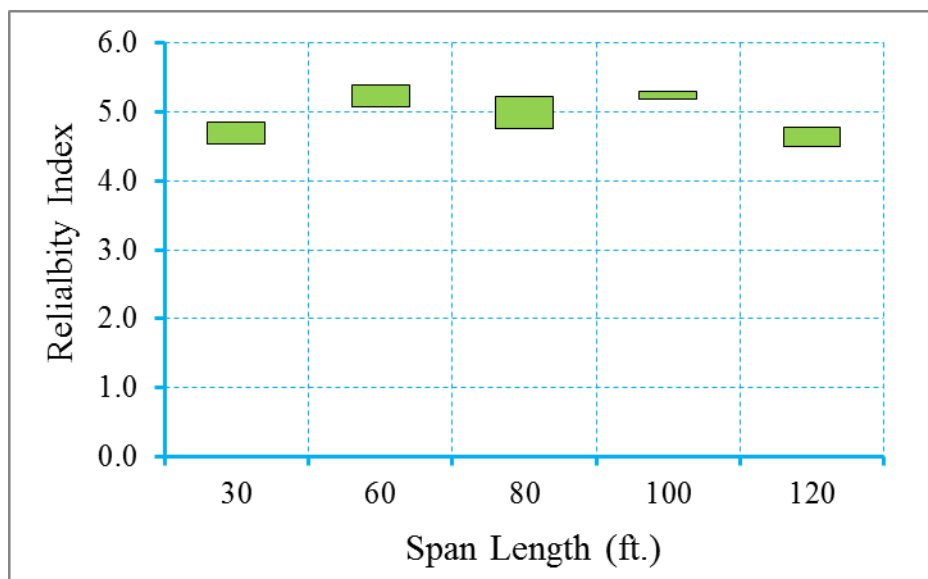


Figure B.102 Reliability Indices for AASHTO Adjacent Box Girder Bridges at Maximum Crack Width Limit State (ADTT=5000), $\gamma_{LL}=1.0$ ($f_t = 0.0948\sqrt{f'_c}$)

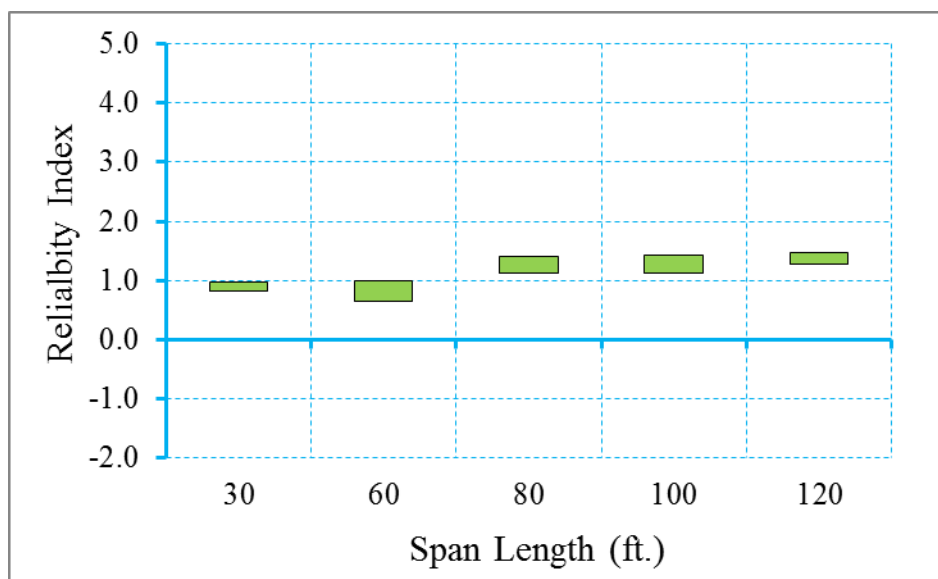


Figure B.103 Reliability Indices for AASHTO Adjacent Box Girder Bridges at Decompression Limit State (ADTT=5000), $\gamma_{LL}=0.8$ ($f_t = 0.158\sqrt{f'_c}$)

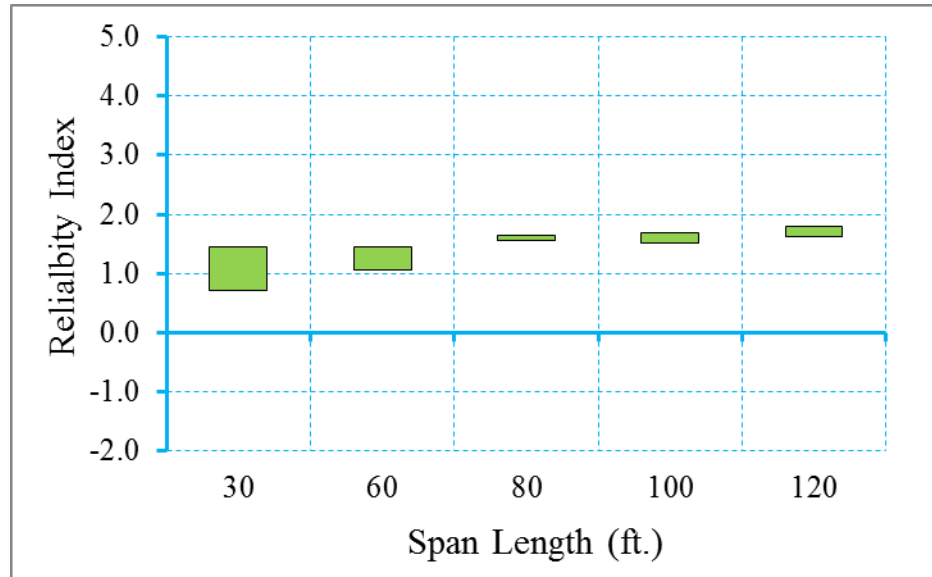


Figure B.104 Reliability Indices for AASHTO Adjacent Box Girder Bridges at Maximum Allowable Tensile Stress Limit State (ADTT=5000), $\gamma_{LL}=0.8$ ($f_t = 0.158\sqrt{f'_c}$)

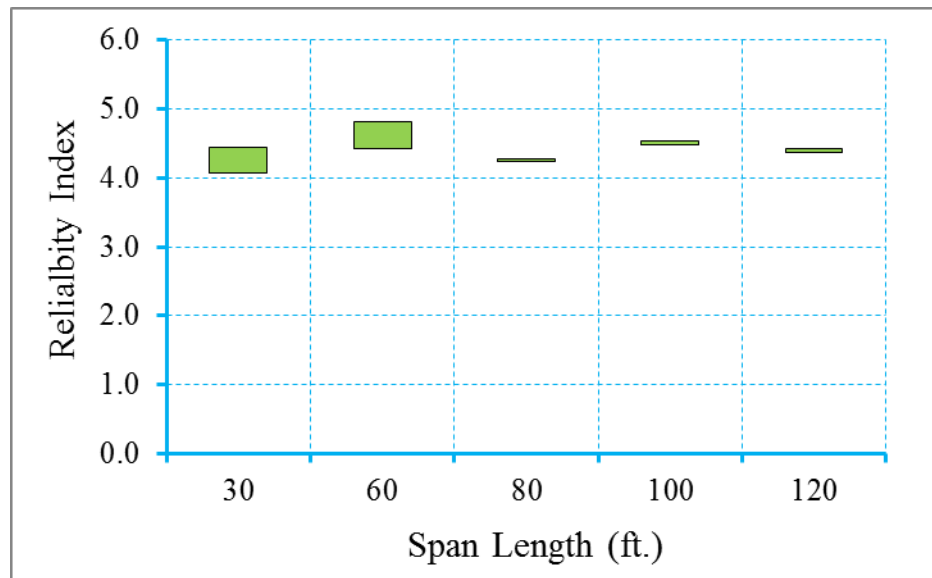


Figure B.105 Reliability Indices for AASHTO Adjacent Box Girder Bridges at Maximum Allowable Crack Width Limit State (ADTT=5000), $\gamma_{LL}=0.8$ ($f_t = 0.158\sqrt{f'_c}$)

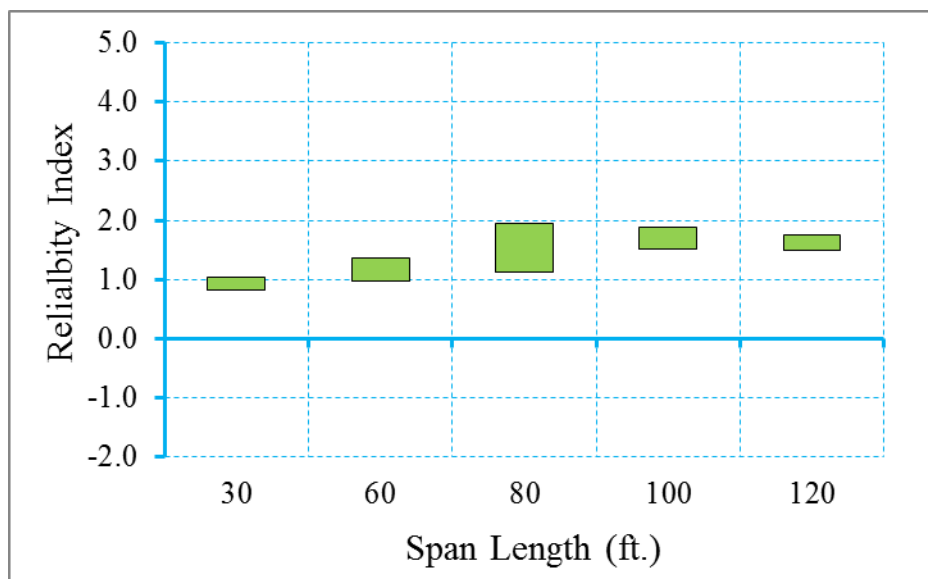


Figure B.106 Reliability Indices for AASHTO Adjacent Box Girder Bridges at Decompression Limit State (ADTT=5000), $\gamma_{LL}=1.0$ ($f_t = 0.158\sqrt{f'_c}$)

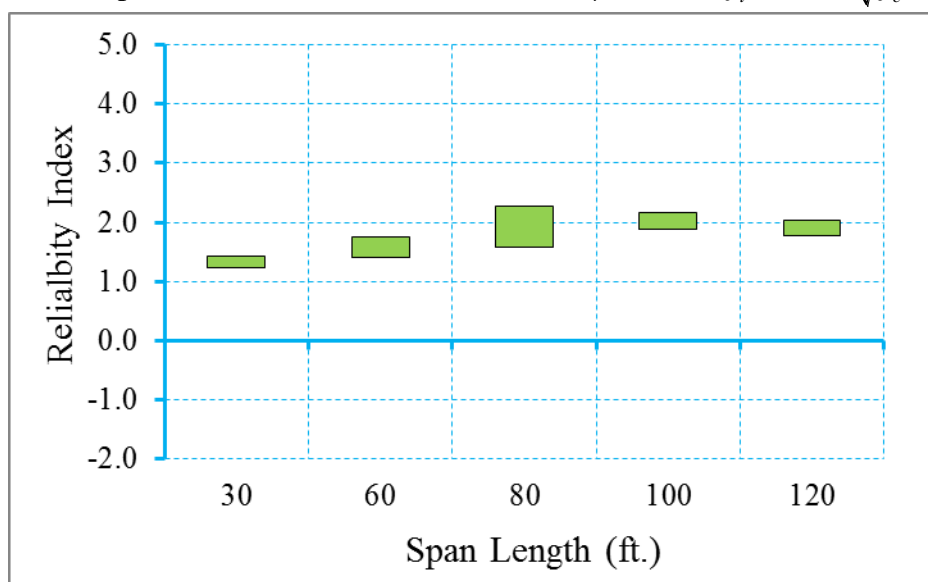


Figure B.107 Reliability Indices for AASHTO Adjacent Box Girder Bridges at Maximum Tensile Stress Limit State (ADTT=5000), $\gamma_{LL}=1.0$ ($f_t = 0.158\sqrt{f'_c}$)

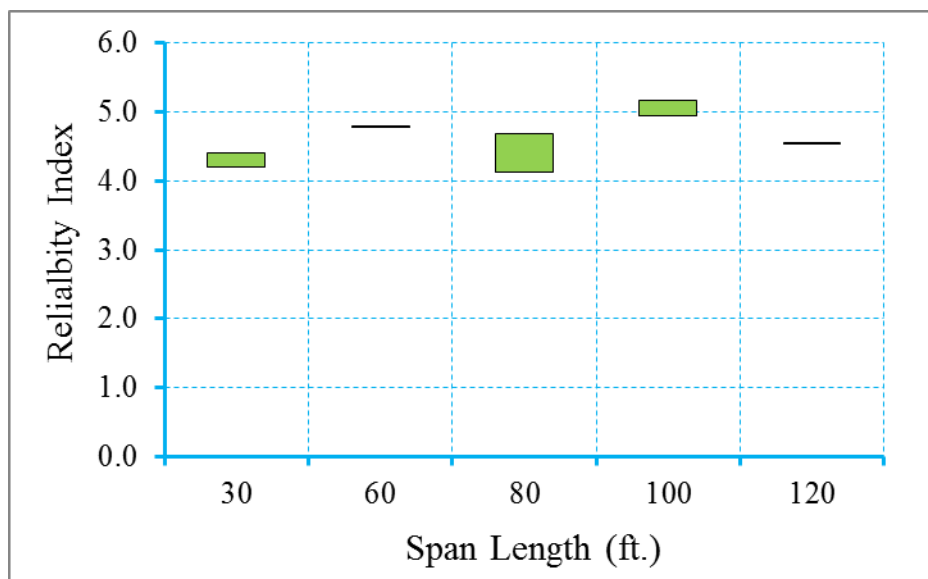


Figure B.108 Reliability Indices for AASHTO Adjacent Box Girder Bridges at Maximum Crack Width Limit State (ADTT=5000), $\gamma_{LL}=1.0$ ($f_t = 0.158\sqrt{f'_c}$)

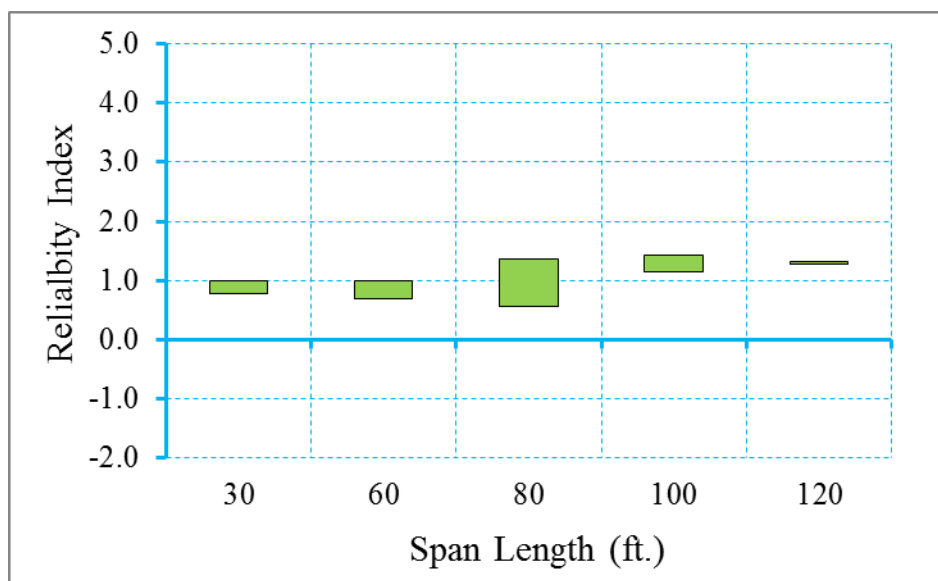


Figure B.109 Reliability Indices for AASHTO Adjacent Box Girder Bridges at Decompression Limit State (ADTT=5000), $\gamma_{LL}=0.8$ ($f_t = 0.19\sqrt{f'_c}$)

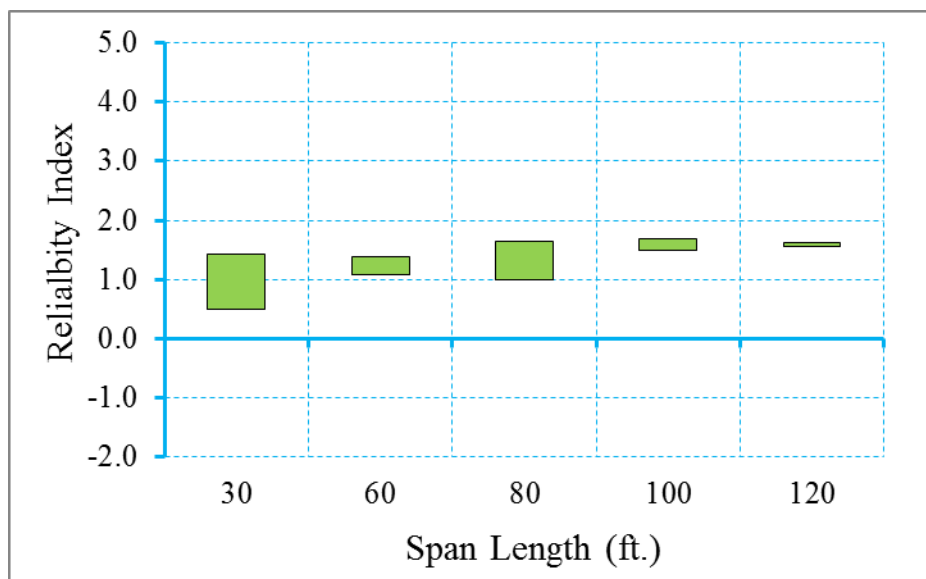


Figure B.110 Reliability Indices for AASHTO Adjacent Box Girder Bridges at Maximum Allowable Tensile Stress Limit State (ADTT=5000), $\gamma_{LL}=0.8$ ($f_t = 0.19\sqrt{f'_c}$)

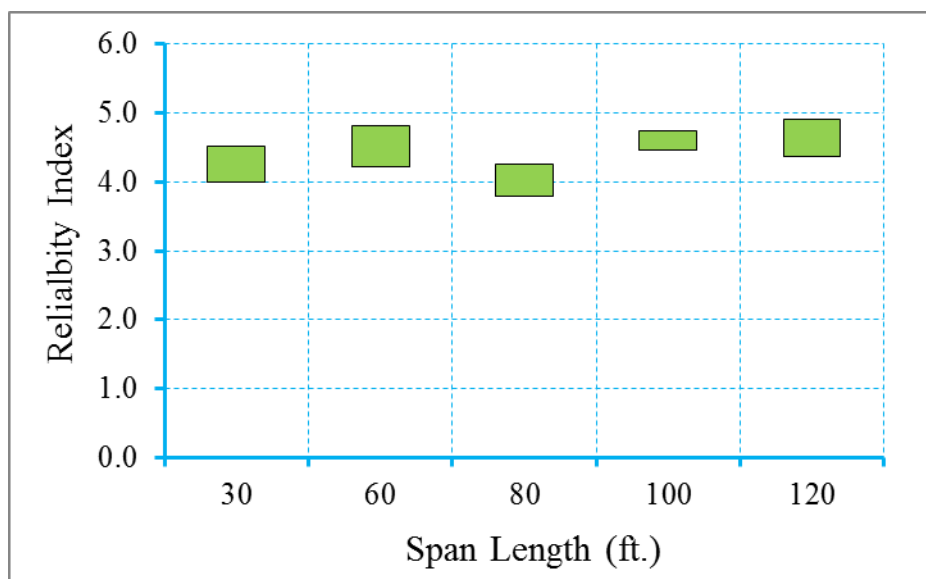


Figure B.111 Reliability Indices for AASHTO Adjacent Box Girder Bridges at Maximum Allowable Crack Width Limit State (ADTT=5000), $\gamma_{LL}=0.8$ ($f_t = 0.19\sqrt{f'_c}$)

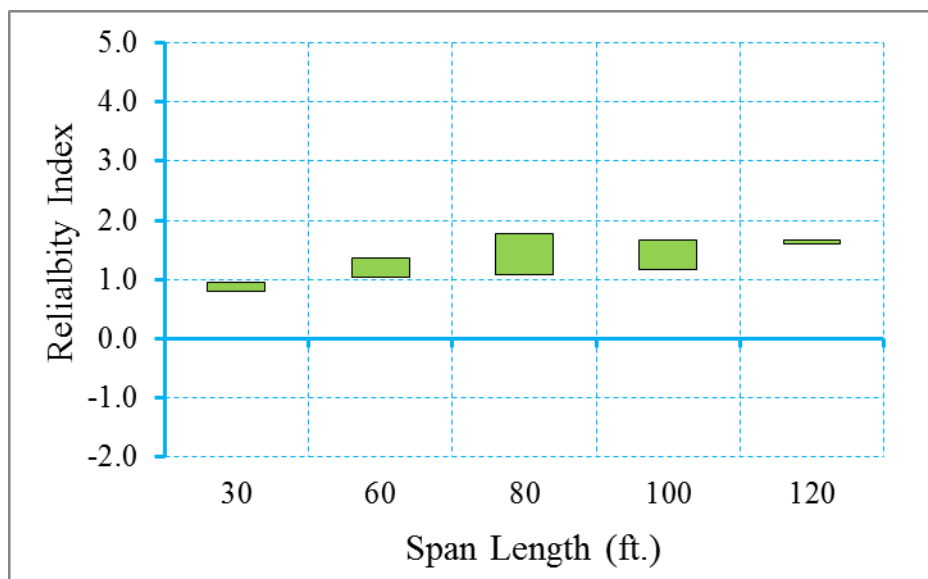


Figure B.112 Reliability Indices for AASHTO Adjacent Box Girder Bridges at Decompression Limit State (ADTT=5000), $\gamma_{LL}=1.0$ ($f_t = 0.19\sqrt{f'_c}$)

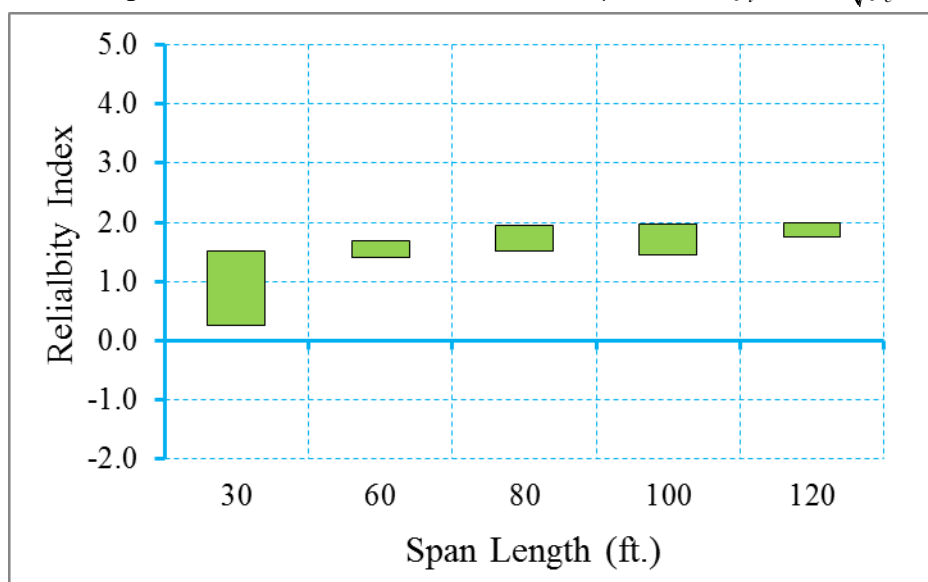


Figure B.113 Reliability Indices for AASHTO Adjacent Box Girder Bridges at Maximum Tensile Stress Limit State (ADTT=5000), $\gamma_{LL}=1.0$ ($f_t = 0.19\sqrt{f'_c}$)

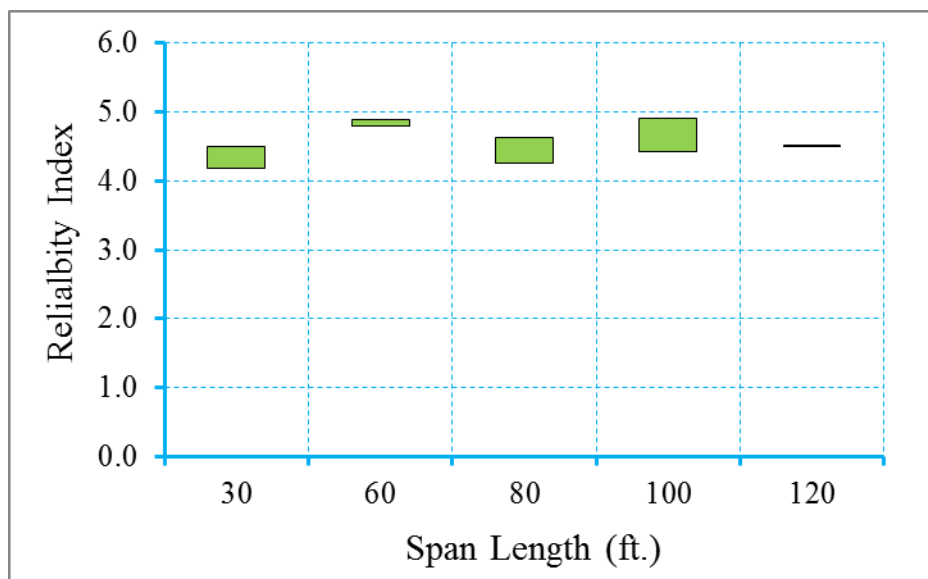


Figure B.114 Reliability Indices for AASHTO Adjacent Box Girder Bridges at Maximum Crack Width Limit State (ADTT=5000), $\gamma_{LL}=1.0$ ($f_t = 0.19\sqrt{f'_c}$)

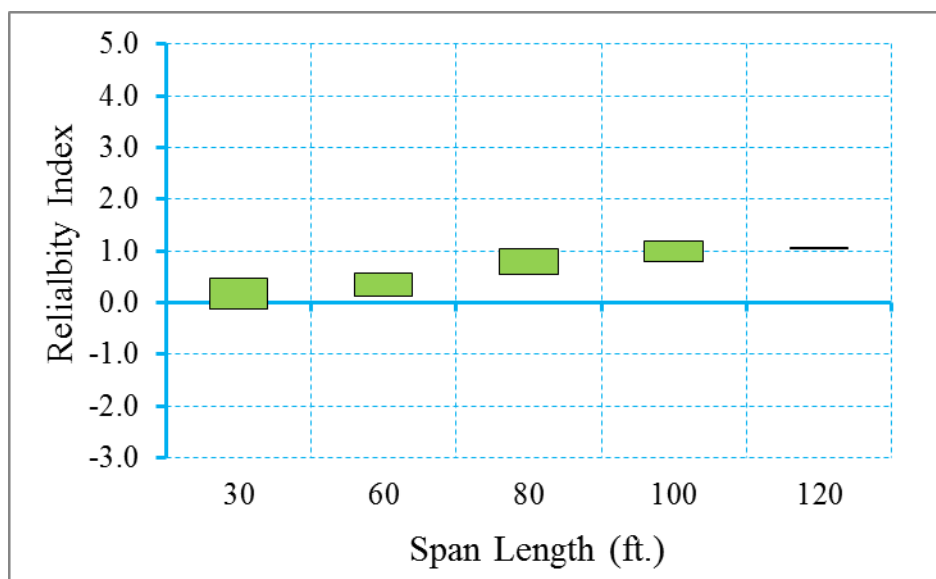


Figure B.115 Reliability Indices for AASHTO Adjacent Box Girder Bridges at Decompression Limit State (ADTT=5000), $\gamma_{LL}=0.8$ ($f_t = 0.253\sqrt{f'_c}$)

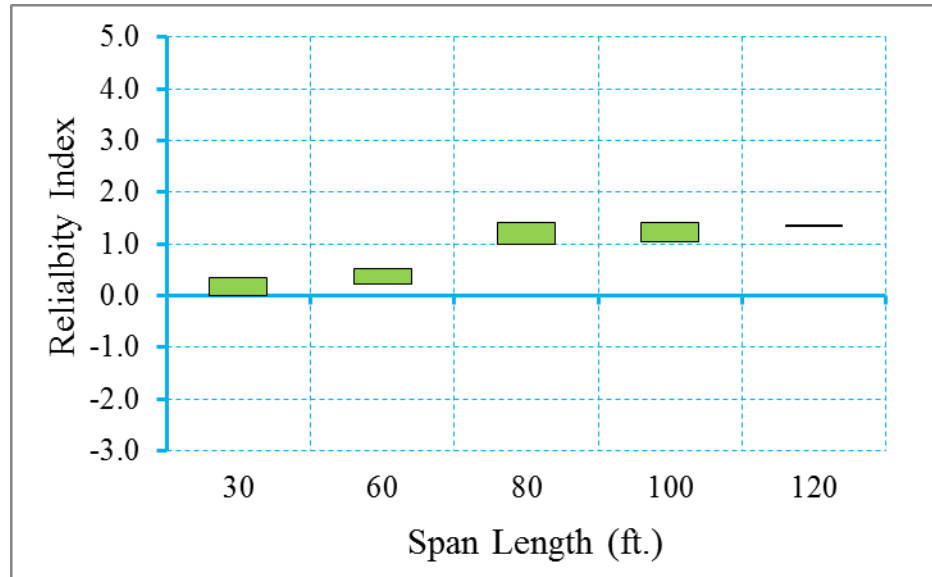


Figure B.116 Reliability Indices for AASHTO Adjacent Box Girder Bridges at Maximum Allowable Tensile Stress Limit State (ADTT=5000), $\gamma_{LL}=0.8$ ($f_t = 0.253\sqrt{f'_c}$)

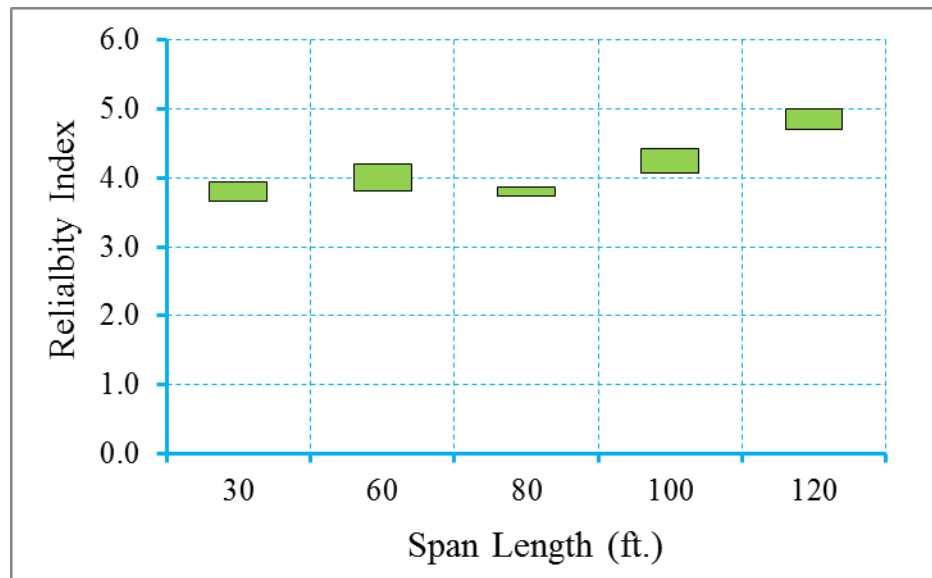


Figure B.117 Reliability Indices for AASHTO Adjacent Box Girder Bridges at Maximum Allowable Crack Width Limit State (ADTT=5000), $\gamma_{LL}=0.8$ ($f_t = 0.253\sqrt{f'_c}$)

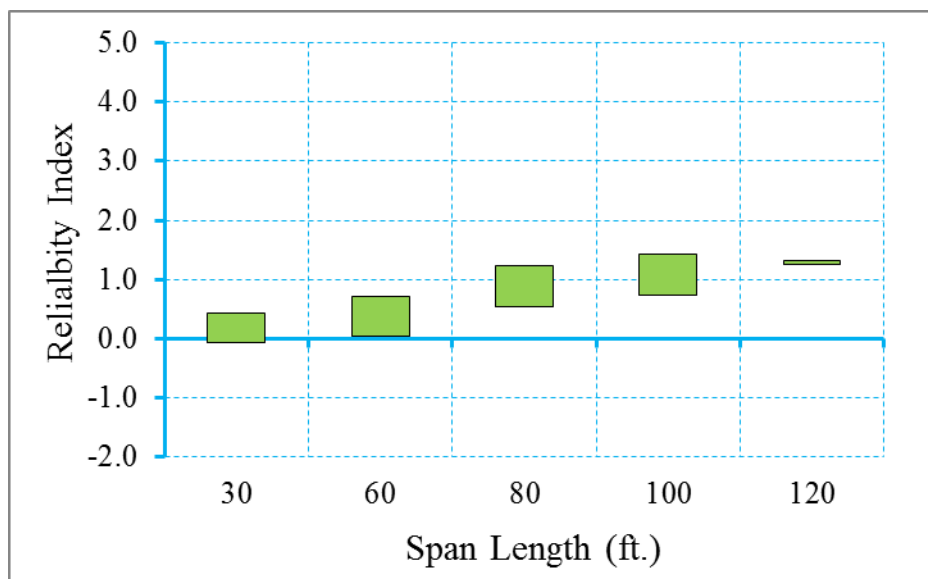


Figure B.118 Reliability Indices for AASHTO Adjacent Box Girder Bridges at Decompression Limit State (ADTT=5000), $\gamma_{LL}=1.0$ ($f_t = 0.253\sqrt{f'_c}$)

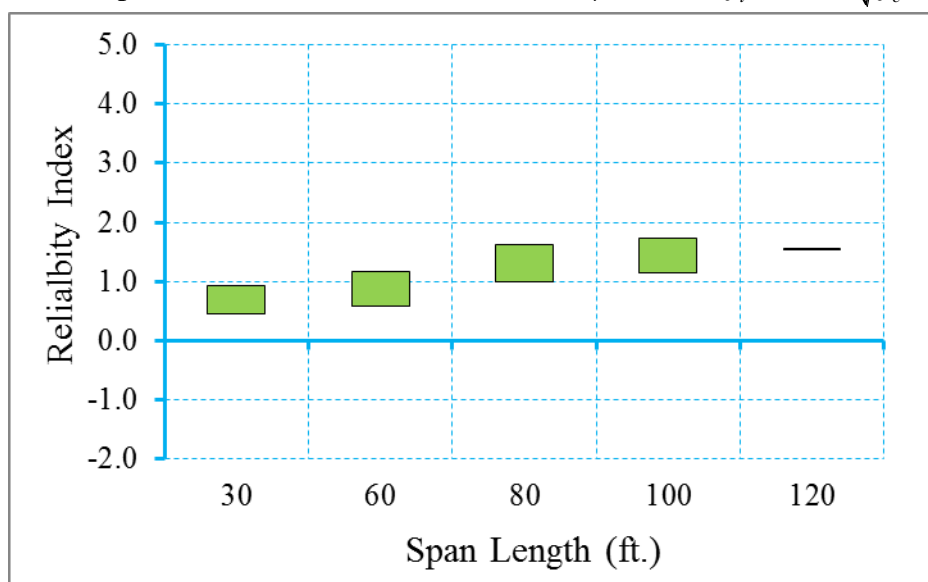


Figure B.119 Reliability Indices for AASHTO Adjacent Box Girder Bridges at Maximum Allowable Tensile Stress Limit State (ADTT=5000), $\gamma_{LL}=1.0$ ($f_t = 0.253\sqrt{f'_c}$)

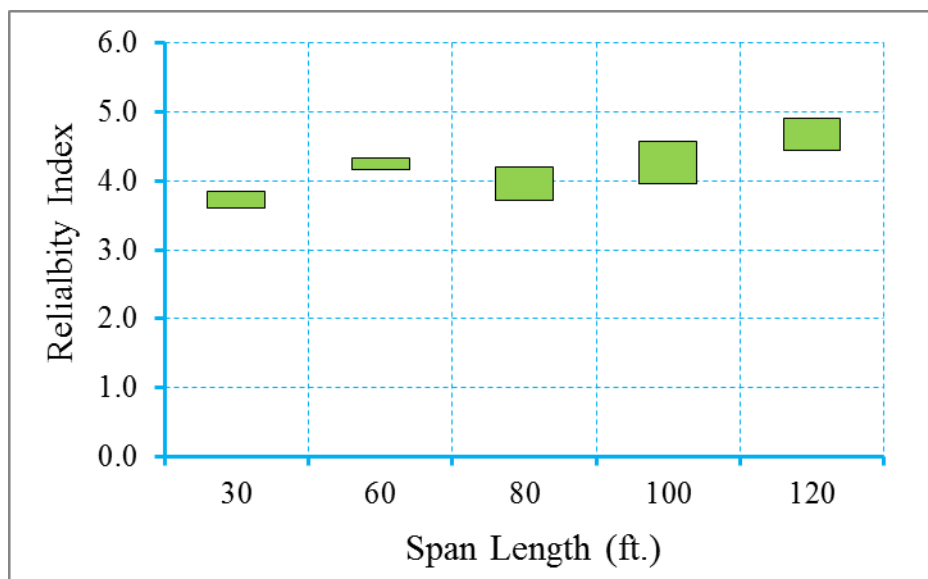


Figure B.120 Reliability Indices for AASHTO Adjacent Box Girder Bridges at Maximum Allowable Crack Width Limit State (ADTT=5000), $\gamma_{LL}=1.0$ ($f_t = 0.253\sqrt{f'_c}$)

B.3 Spread Box Girder Bridges

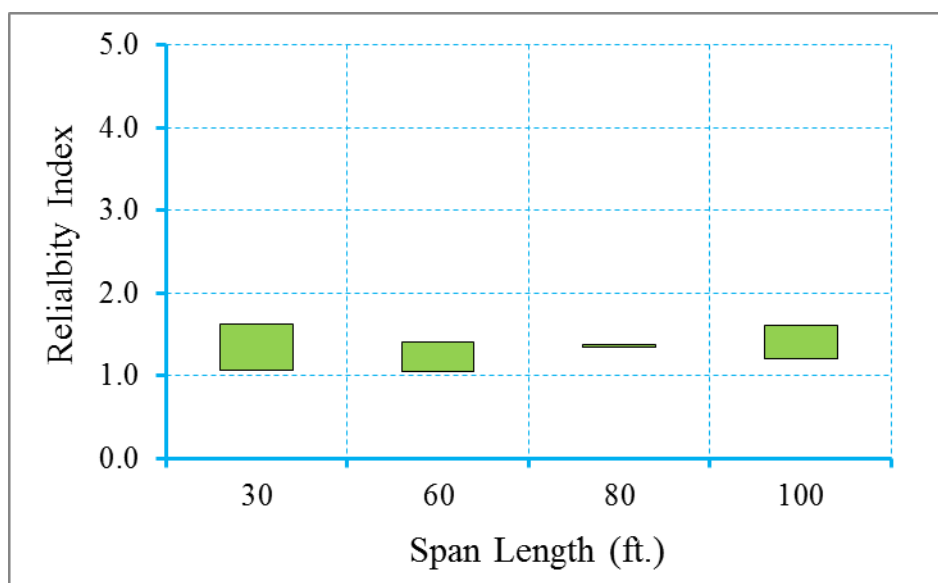


Figure B.121 Reliability Indices for AASHTO Spread Box Girder Bridges at Decompression Limit State (ADTT=5000), $\gamma_{LL}=0.8$ ($f_t = 0.0948\sqrt{f'_c}$)

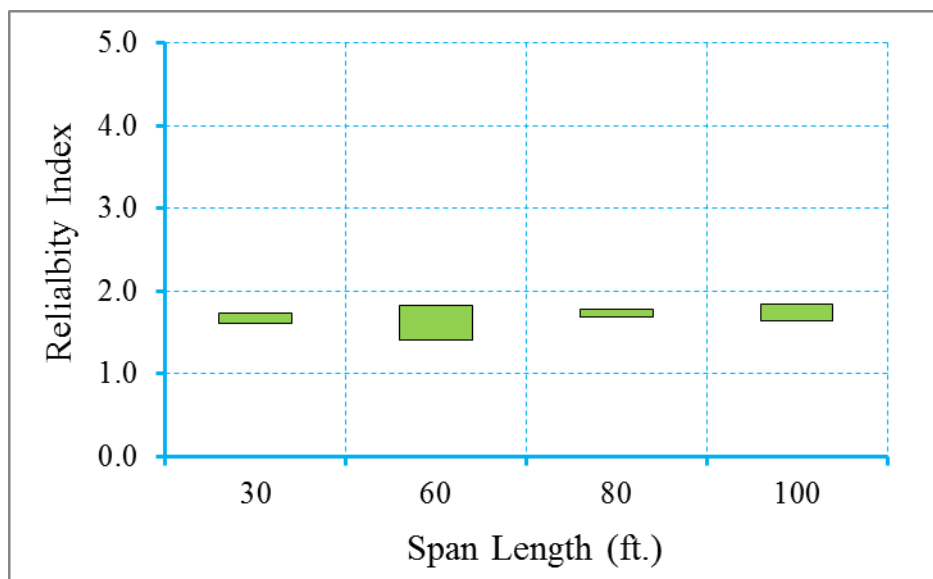


Figure B.122 Reliability Indices for AASHTO Spread Box Girder Bridges at Maximum Allowable Tensile Stress Limit State (ADTT=5000), $\gamma_{LL}=0.8$ ($f_t = 0.0948\sqrt{f'_c}$)

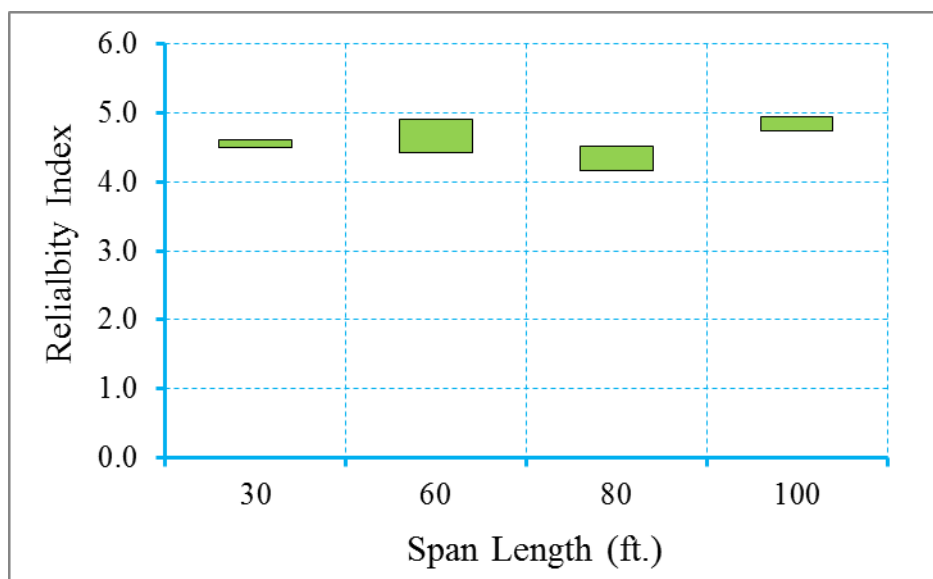


Figure B.123 Reliability Indices for AASHTO Spread Box Girder Bridges at Maximum Allowable Crack Width Limit State (ADTT=5000), $\gamma_{LL}=0.8$ ($f_t = 0.0948\sqrt{f'_c}$)

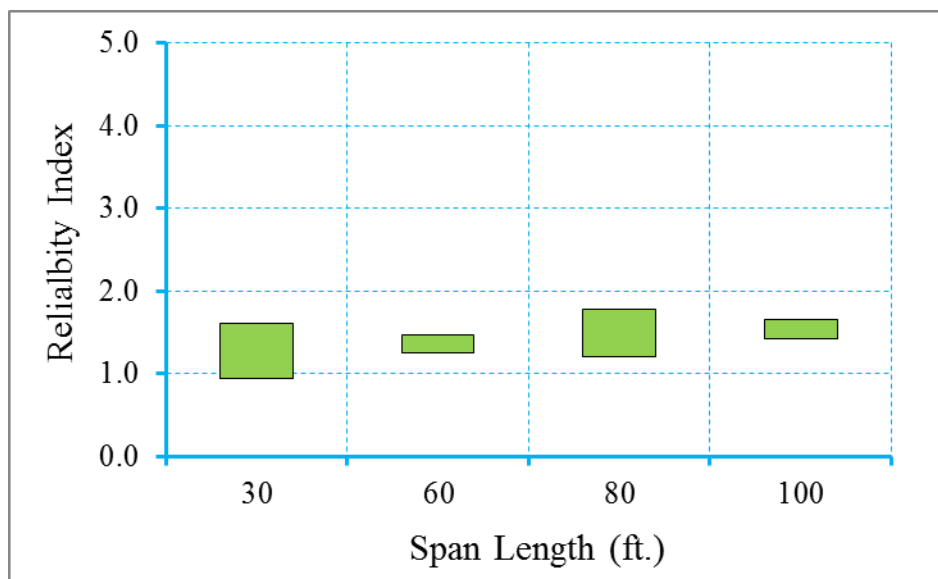


Figure B.124 Reliability Indices for AASHTO Spread Box Girder Bridges at Decompression Limit State (ADTT=5000), $\gamma_{LL}=1.0$ ($f_t = 0.0948\sqrt{f'_c}$)

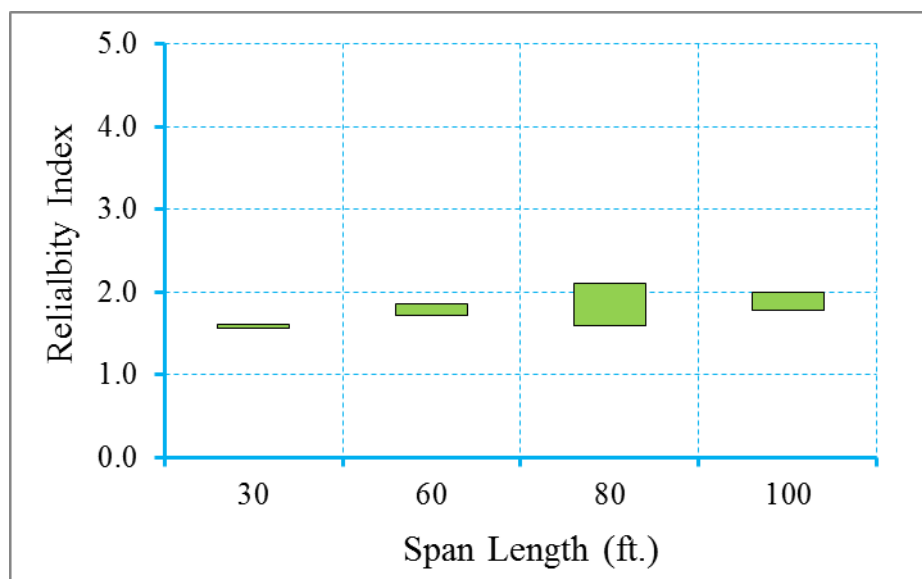


Figure B.125 Reliability Indices for AASHTO Spread Box Girder Bridges at Maximum Tensile Stress Limit State (ADTT=5000), $\gamma_{LL}=1.0$ ($f_t = 0.0948\sqrt{f'_c}$)

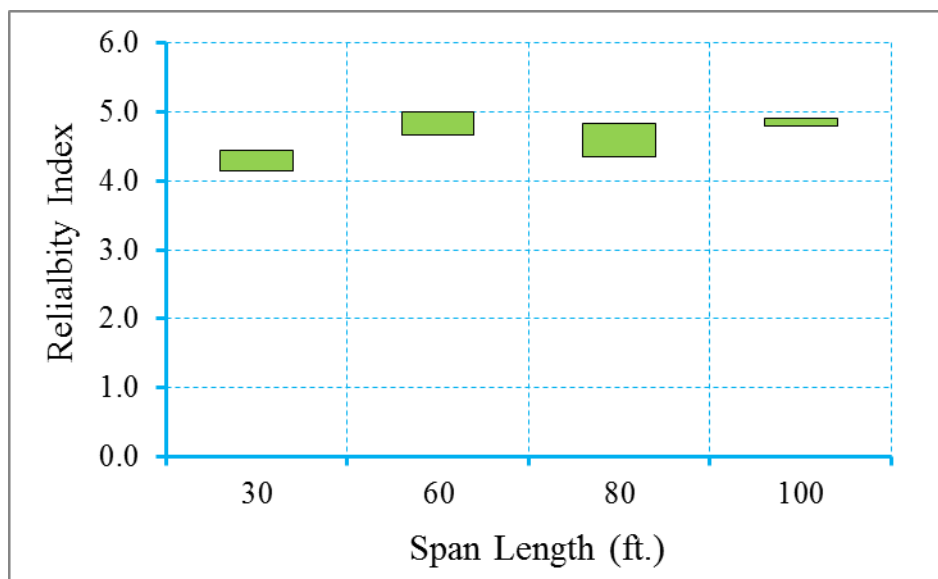


Figure B.126 Reliability Indices for AASHTO Spread Box Girder Bridges at Maximum Crack Width Limit State (ADTT=5000), $\gamma_{LL}=1.0$ ($f_t = 0.0948\sqrt{f'_c}$)

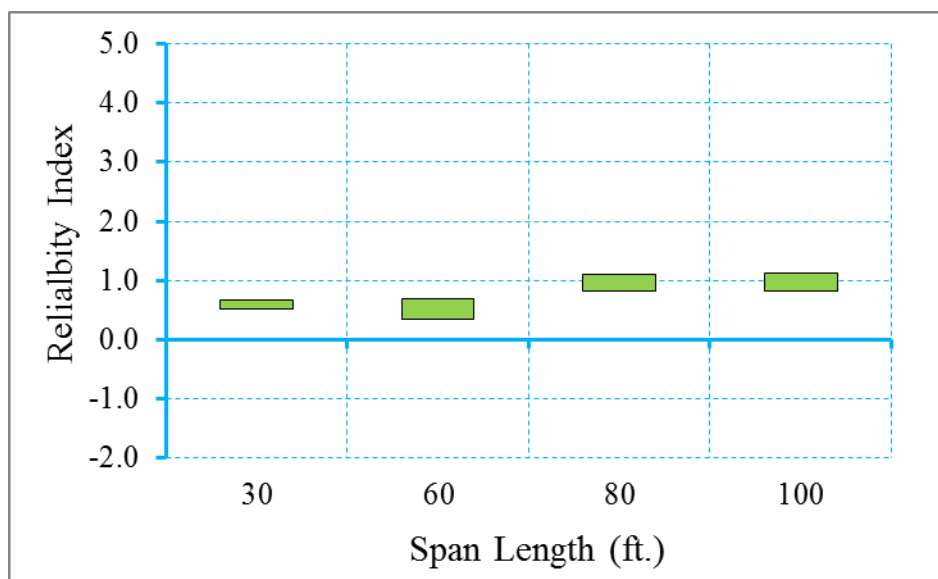


Figure B.127 Reliability Indices for AASHTO Spread Box Girder Bridges at Decompression Limit State (ADTT=5000), $\gamma_{LL}=0.8$ ($f_t = 0.158\sqrt{f'_c}$)

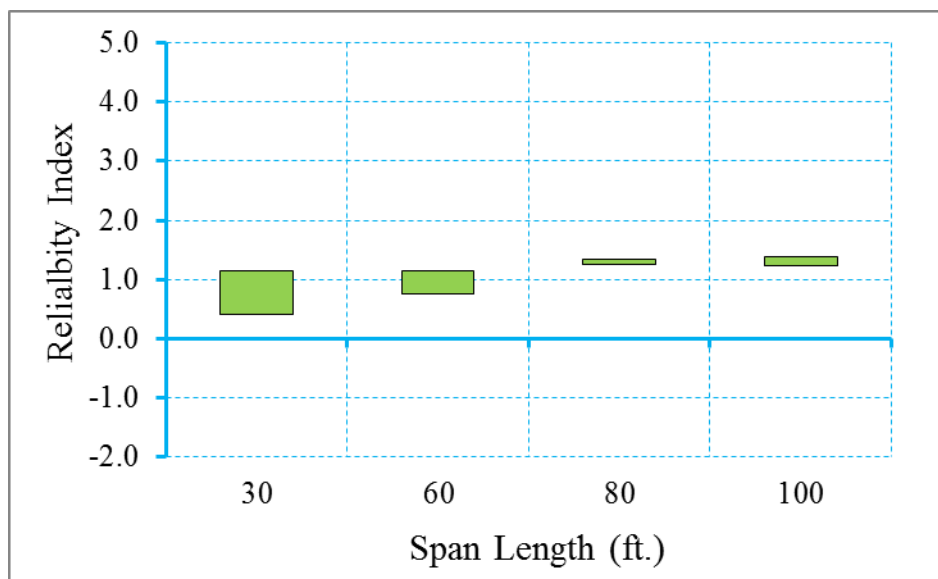


Figure B.128 Reliability Indices for AASHTO Spread Box Girder Bridges at Maximum Allowable Tensile Stress Limit State (ADTT=5000), $\gamma_{LL}=0.8$ ($f_t = 0.158\sqrt{f'_c}$)

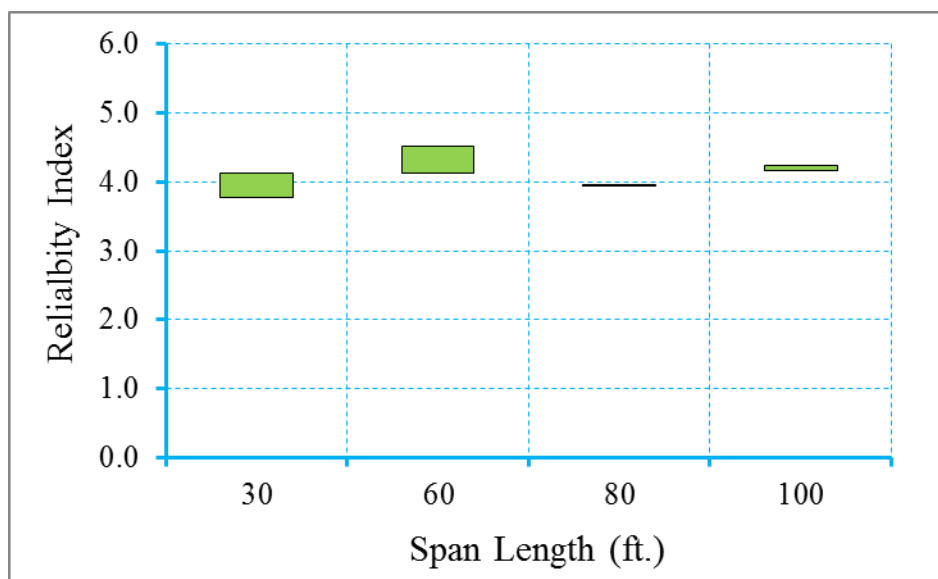


Figure B.129 Reliability Indices for AASHTO Spread Box Girder Bridges at Maximum Allowable Crack Width Limit State (ADTT=5000), $\gamma_{LL}=0.8$ ($f_t = 0.158\sqrt{f'_c}$)

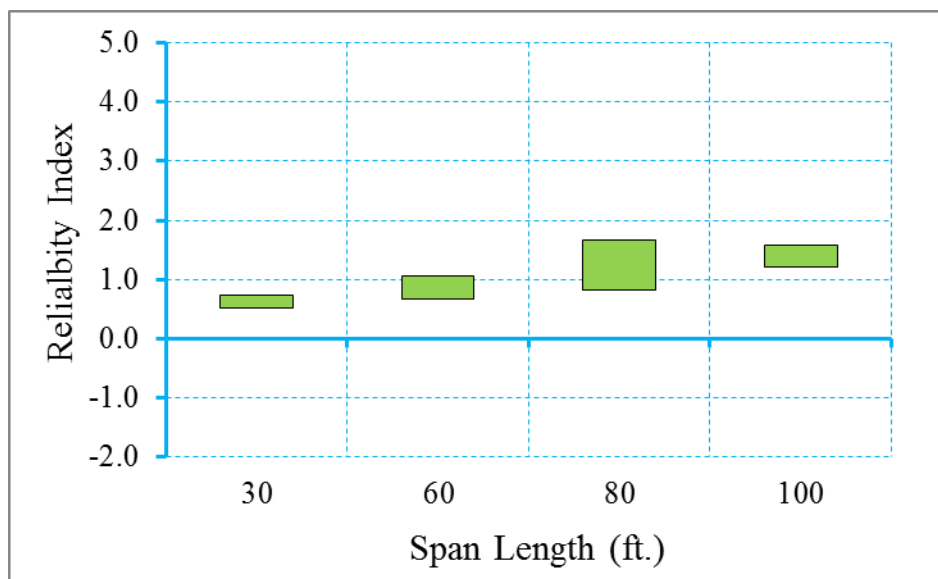


Figure B.130 Reliability Indices for AASHTO Spread Box Girder Bridges at Decompression Limit State (ADTT=5000), $\gamma_{LL}=1.0$ ($f_t = 0.158\sqrt{f'_c}$)

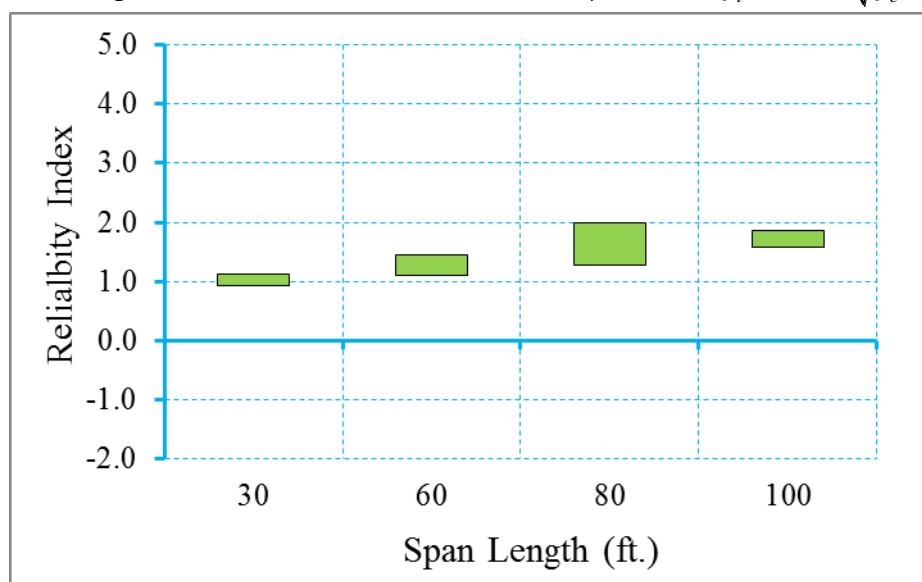


Figure B.131 Reliability Indices for AASHTO Spread Box Girder Bridges at Maximum Tensile Stress Limit State (ADTT=5000), $\gamma_{LL}=1.0$ ($f_t = 0.158\sqrt{f'_c}$)

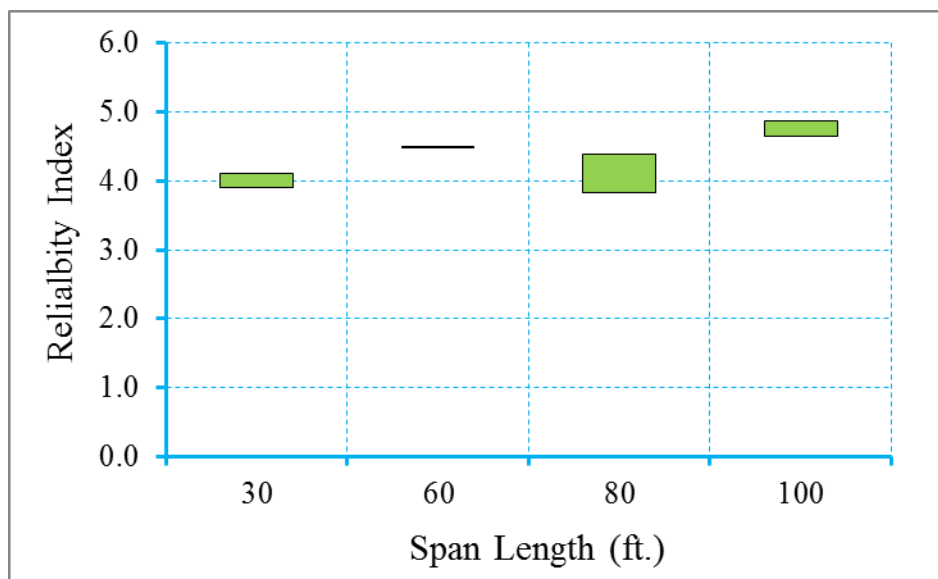


Figure B.132 Reliability Indices for AASHTO Spread Box Girder Bridges at Maximum Crack Width Limit State (ADTT=5000), $\gamma_{LL}=1.0$ ($f_t = 0.158\sqrt{f'_c}$)

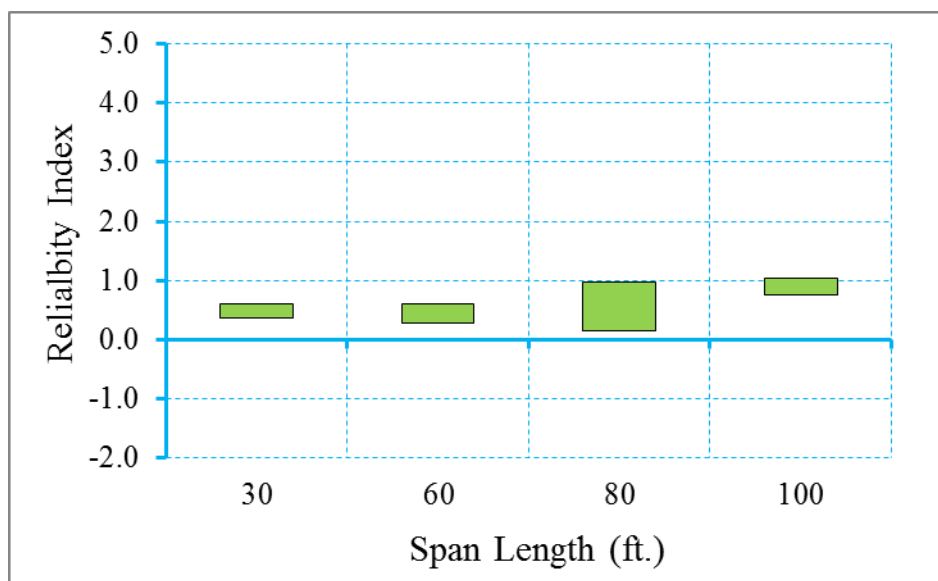


Figure B.133 Reliability Indices for AASHTO Spread Box Girder Bridges at Decompression Limit State (ADTT=5000), $\gamma_{LL}=0.8$ ($f_t = 0.19\sqrt{f'_c}$)

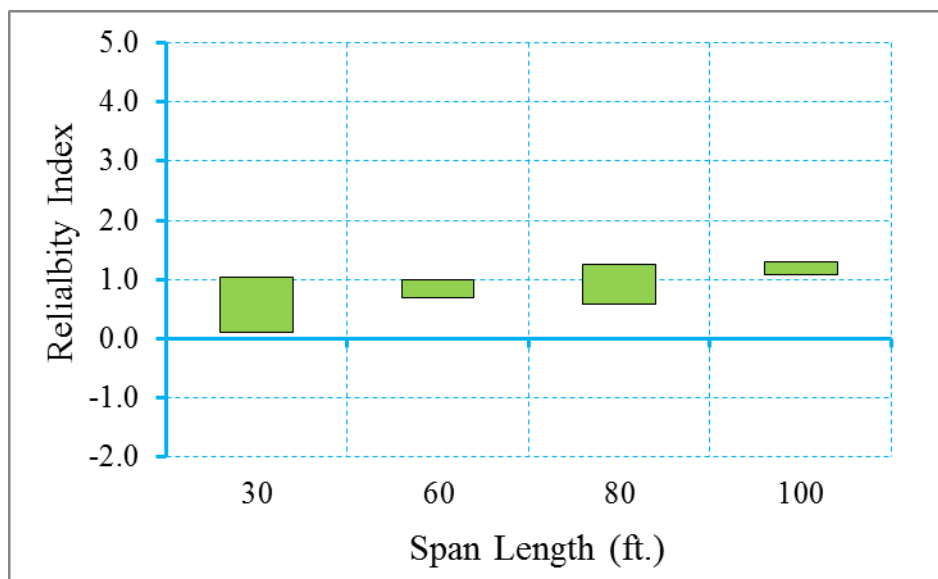


Figure B.134 Reliability Indices for AASHTO Spread Box Girder Bridges at Maximum Allowable Tensile Stress Limit State (ADTT=5000), $\gamma_{LL}=0.8$ ($f_t = 0.19\sqrt{f'_c}$)

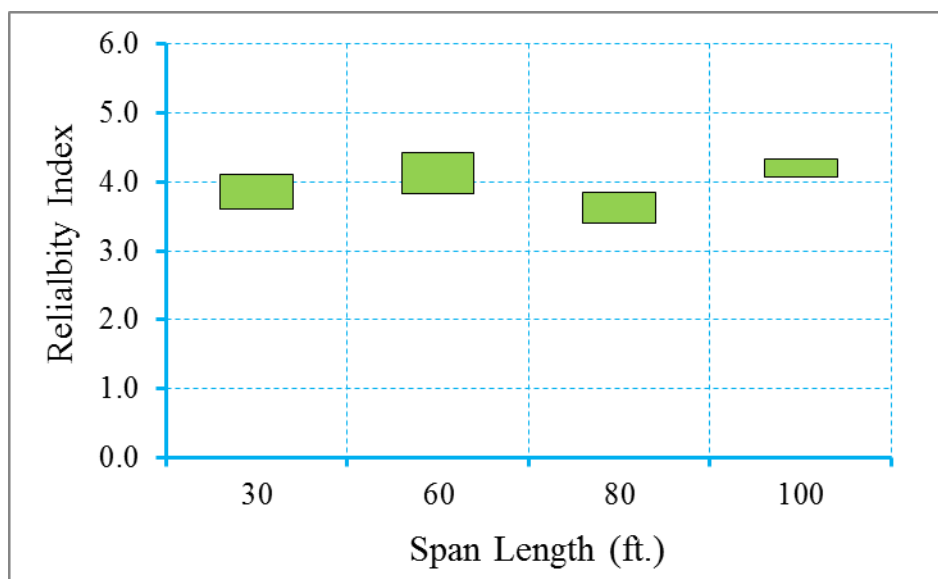


Figure B.135 Reliability Indices for AASHTO Spread Box Girder Bridges at Maximum Allowable Crack Width Limit State (ADTT=5000), $\gamma_{LL}=0.8$ ($f_t = 0.19\sqrt{f'_c}$)

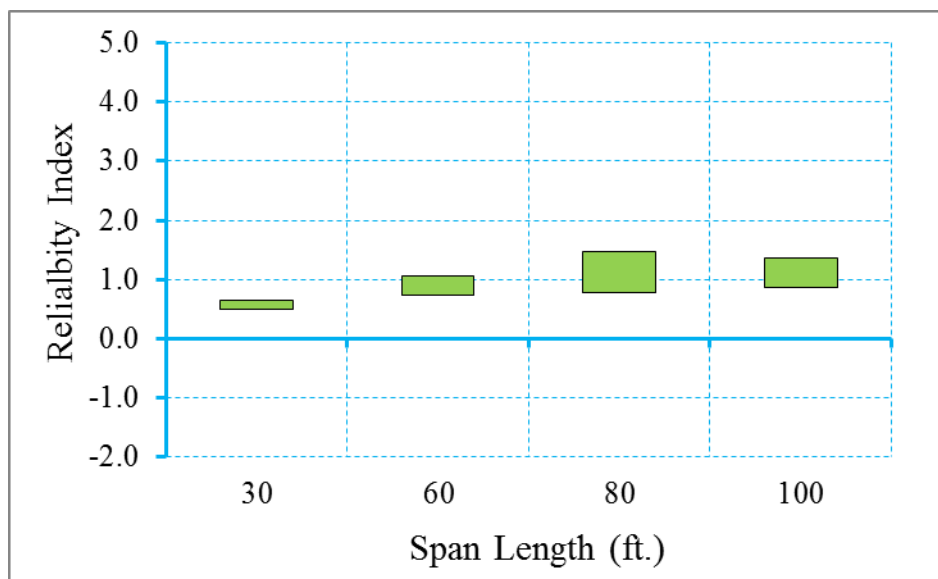


Figure B.136 Reliability Indices for AASHTO Spread Box Girder Bridges at Decompression Limit State (ADTT=5000) $\gamma_{LL}=1.0$ ($f_t = 0.19\sqrt{f'_c}$)

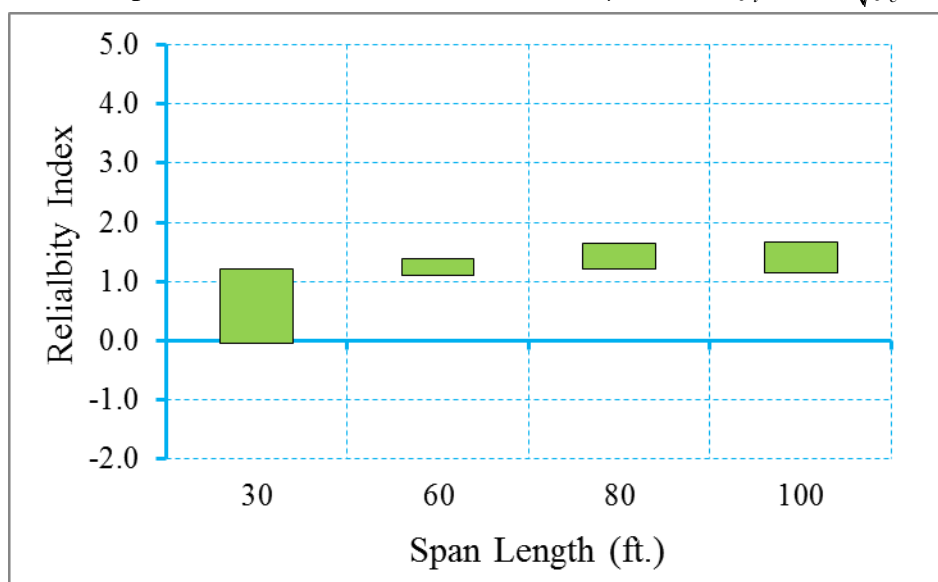


Figure B.137 Reliability Indices for AASHTO Spread Box Girder Bridges at Maximum Tensile Stress Limit State (ADTT=5000), $\gamma_{LL}=1.0$ ($f_t = 0.19\sqrt{f'_c}$)

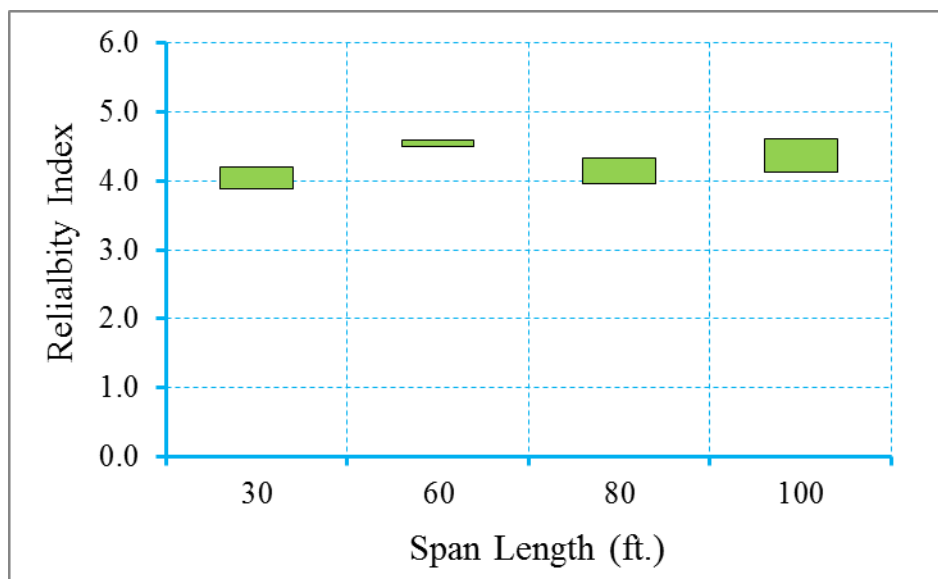


Figure B.138 Reliability Indices for AASHTO Spread Box Girder Bridges at Maximum Crack Width Limit State (ADTT=5000), $\gamma_{LL}=1.0$ ($f_t = 0.19\sqrt{f'_c}$)

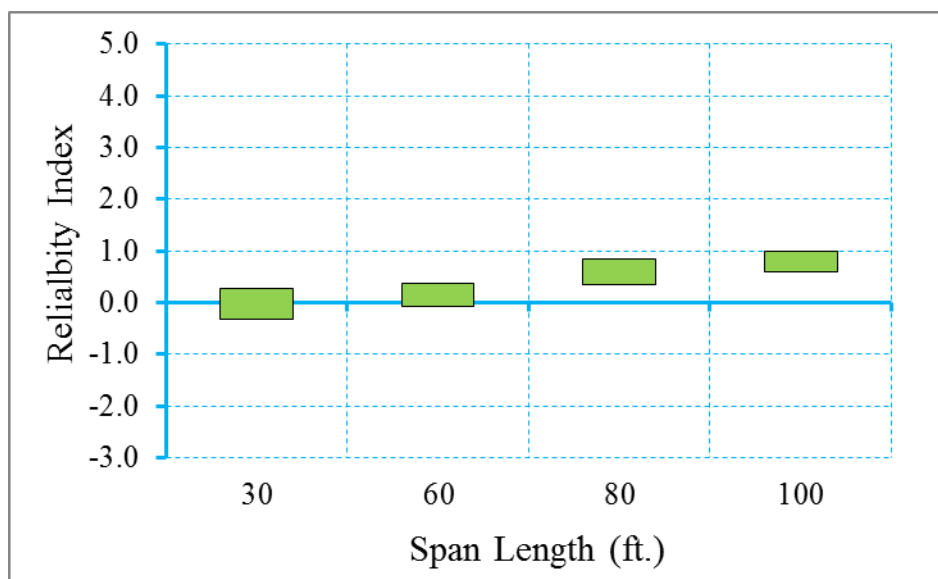


Figure B.139 Reliability Indices for AASHTO Spread Box Girder Bridges at Decompression Limit State (ADTT=5000), $\gamma_{LL}=0.8$ ($f_t = 0.253\sqrt{f'_c}$)

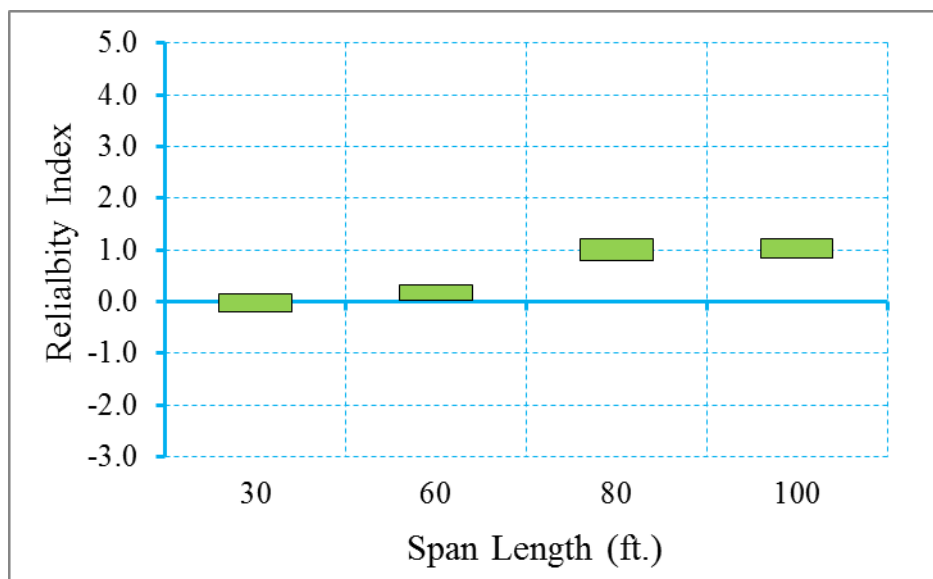


Figure B.140 Reliability Indices for AASHTO Spread Box Girder Bridges at Maximum Allowable Tensile Stress Limit State (ADTT=5000), $\gamma_{LL}=0.8$ ($f_t = 0.253\sqrt{f'_c}$)

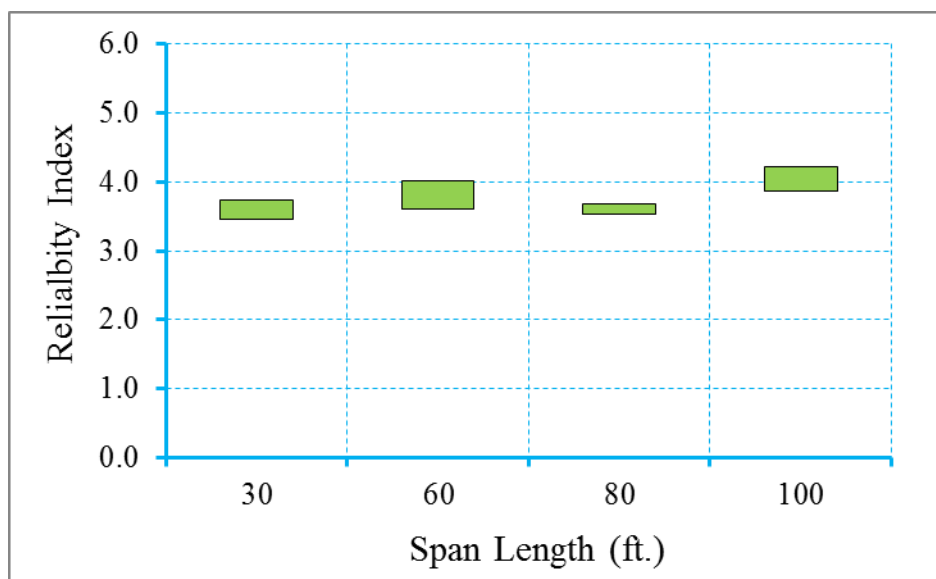


Figure B.141 Reliability Indices for AASHTO Spread Box Girder Bridges at Maximum Allowable Crack Width Limit State (ADTT=5000), $\gamma_{LL}=0.8$ ($f_t = 0.253\sqrt{f'_c}$)

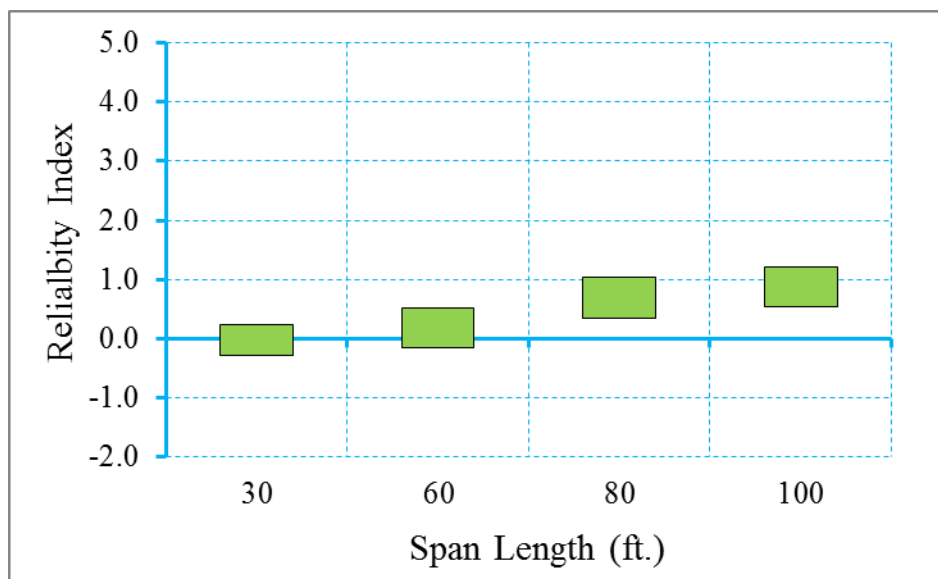


Figure B.142 Reliability Indices for AASHTO Spread Box Girder Bridges at Decompression Limit State (ADTT=5000), $\gamma_{LL}=1.0$ ($f_t = 0.253\sqrt{f'_c}$)

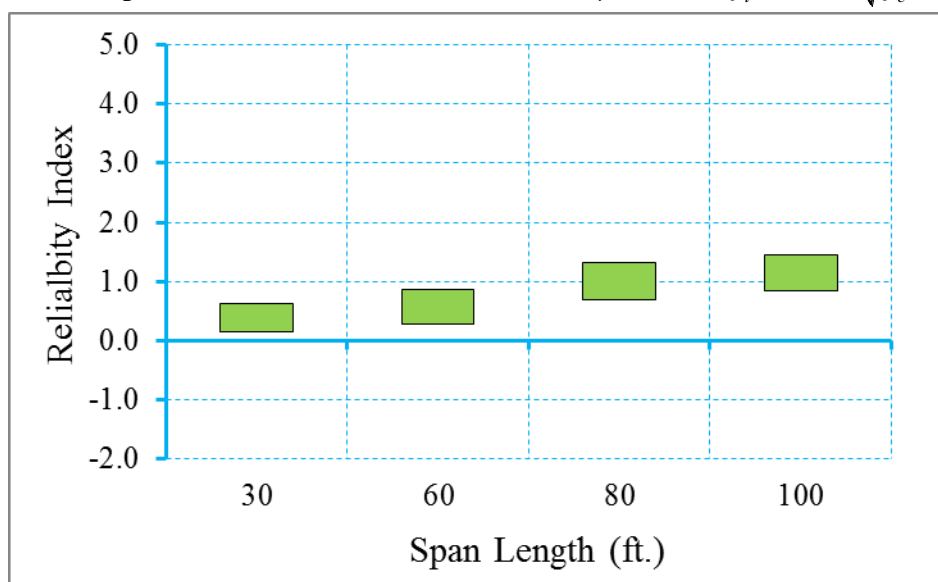


Figure B.143 Reliability Indices for AASHTO Spread Box Girder Bridges at Maximum Allowable Tensile Stress Limit State (ADTT=5000), $\gamma_{LL}=1.0$ ($f_t = 0.253\sqrt{f'_c}$)

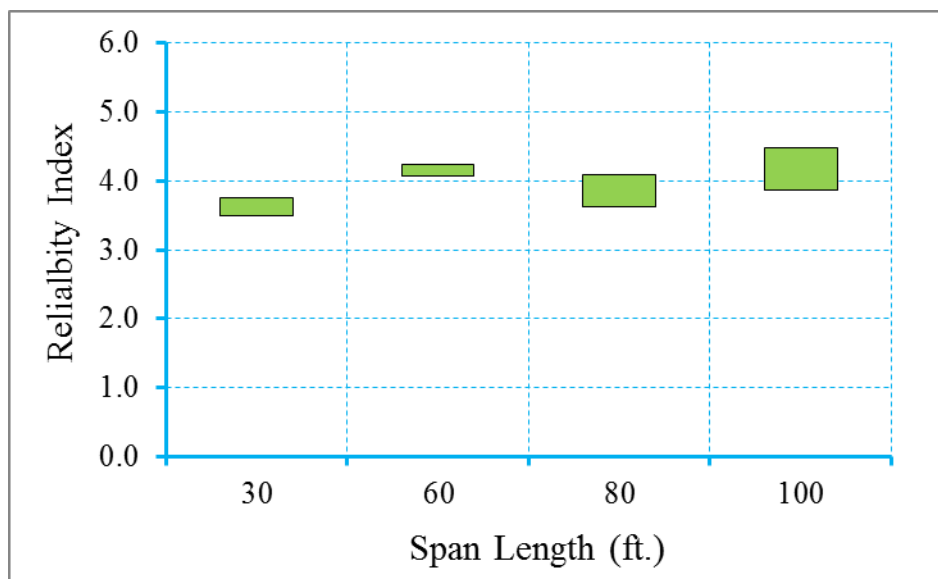


Figure B.144 Reliability Indices for AASHTO Spread Box Girder Bridges at Maximum Allowable Crack Width Limit State (ADTT=5000), $\gamma_{LL}=1.0$ ($f_t = 0.253\sqrt{f'_c}$)

B.3 ASBI Box Girder Bridges

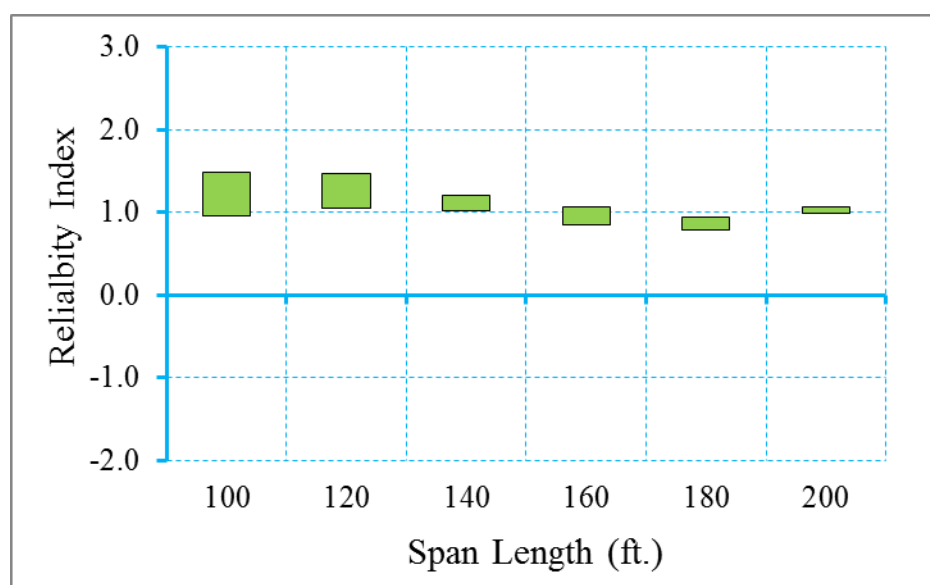


Figure B.145 Reliability Indices for ASBI Box Girder Bridges at Decompression Limit State (ADTT=5000), $\gamma_{LL}=0.8$ ($f_t = 0.0948\sqrt{f'_c}$)

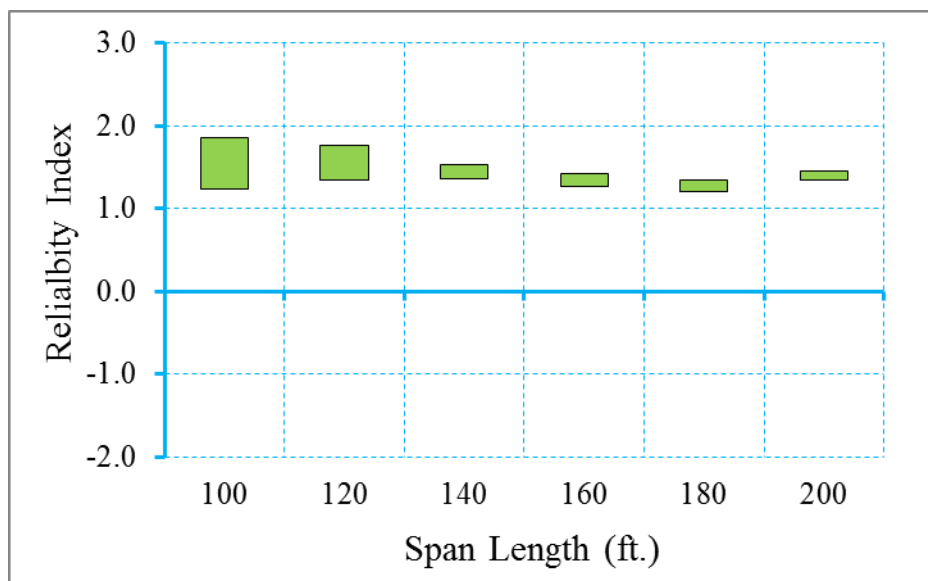


Figure B.146 Reliability Indices for ASBI Box Girder Bridges at Maximum Allowable Tensile Stress Limit State (ADTT=5000), $\gamma_{LL}=0.8$ ($f_t = 0.0948\sqrt{f'_c}$)

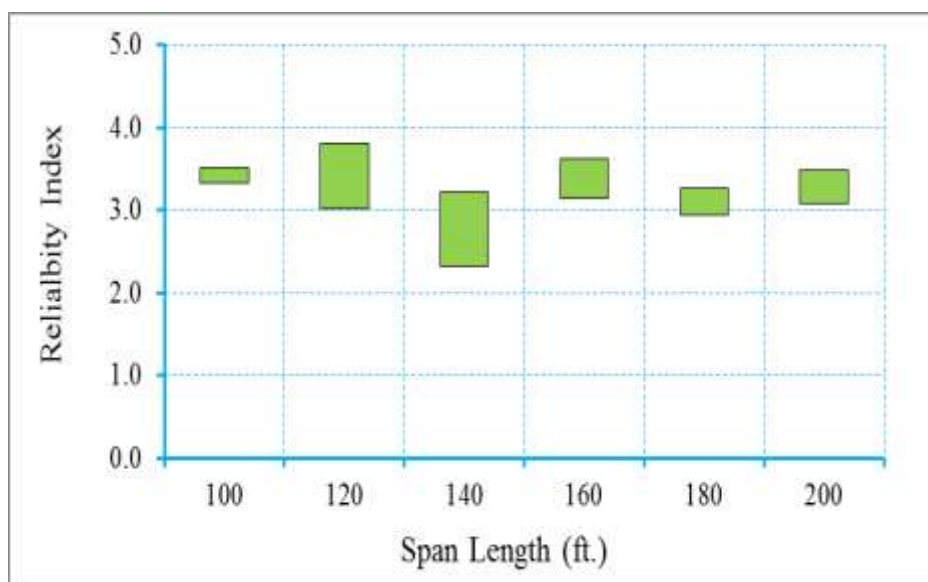


Figure B.147 Reliability Indices for ASBI Box Girder Bridges at Maximum Allowable Crack Width Limit State (ADTT=5000), $\gamma_{LL}=0.8$ ($f_t = 0.0948\sqrt{f'_c}$)

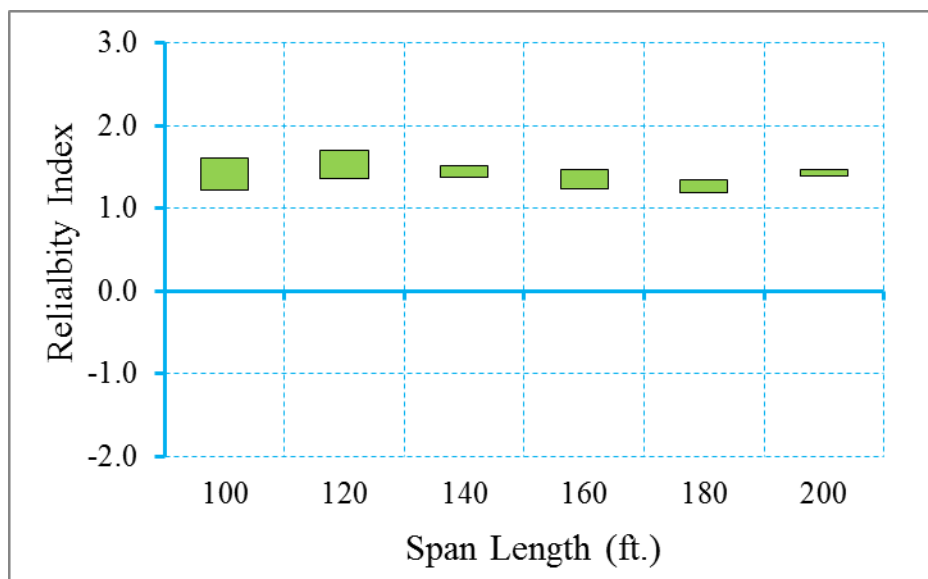


Figure B.148 Reliability Indices for ASBI Box Girder Bridges at Decompression Limit State (ADTT=5000), $\gamma_{LL}=1.0$ ($f_t = 0.0948\sqrt{f'_c}$)

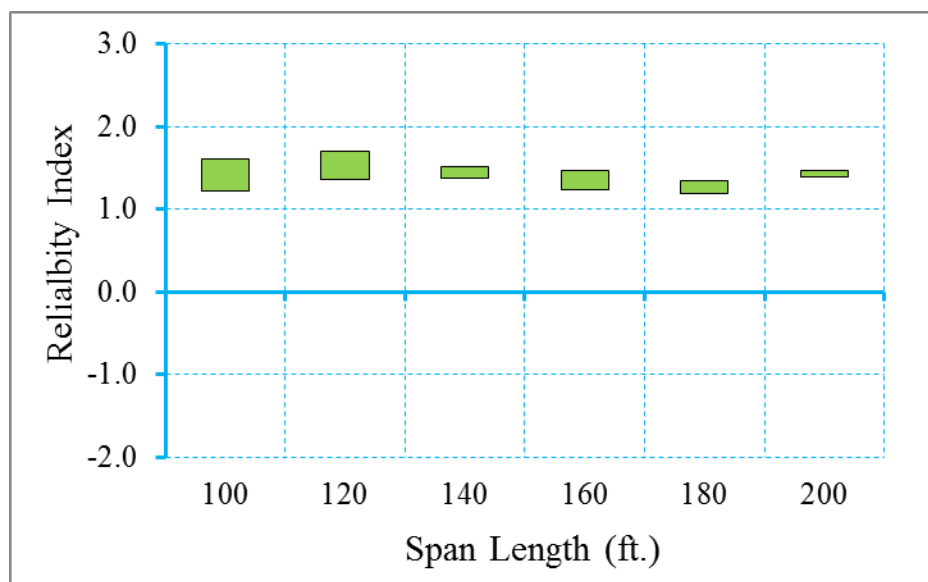


Figure B.149 Reliability Indices for ASBI Box Girder Bridges at Maximum Tensile Stress Limit State (ADTT=5000), $\gamma_{LL}=1.0$ ($f_t = 0.0948\sqrt{f'_c}$)

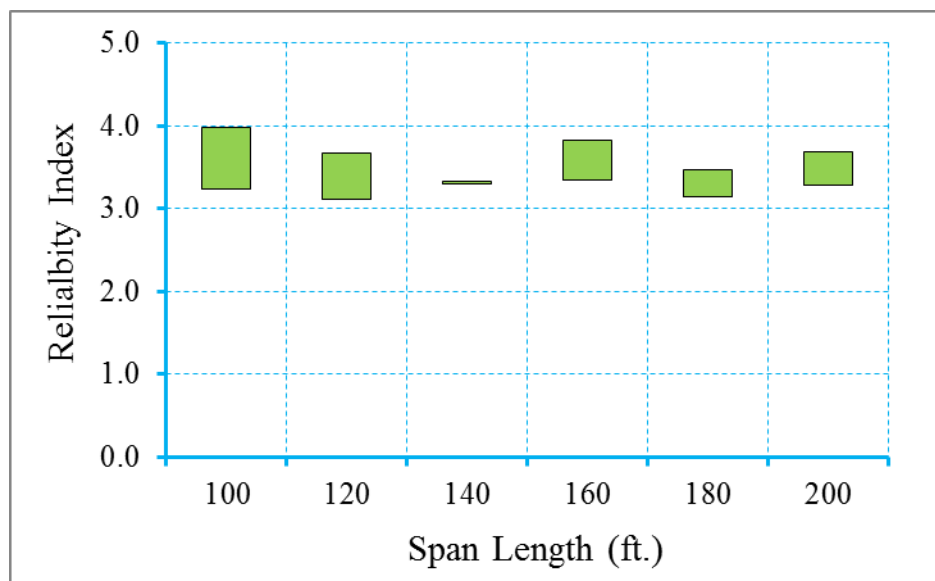


Figure B.150 Reliability Indices for ASBI Box Girder Bridges at Maximum Crack Width Limit State (ADTT=5000), $\gamma_{LL}=1.0$ ($f_t = 0.0948\sqrt{f'_c}$)

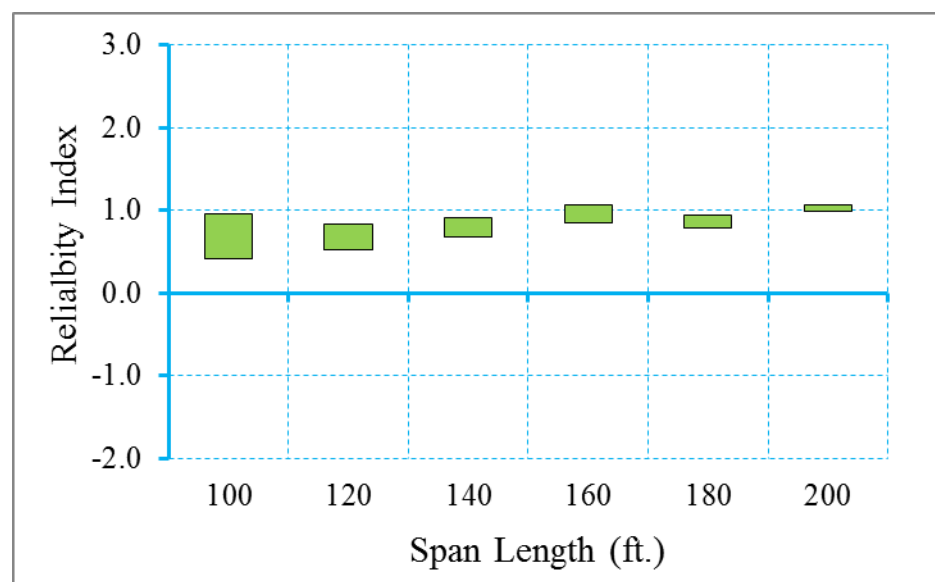


Figure B.151 Reliability Indices for ASBI Box Girder Bridges at Decompression Limit State (ADTT=5000), $\gamma_{LL}=0.8$ ($f_t = 0.158\sqrt{f'_c}$)

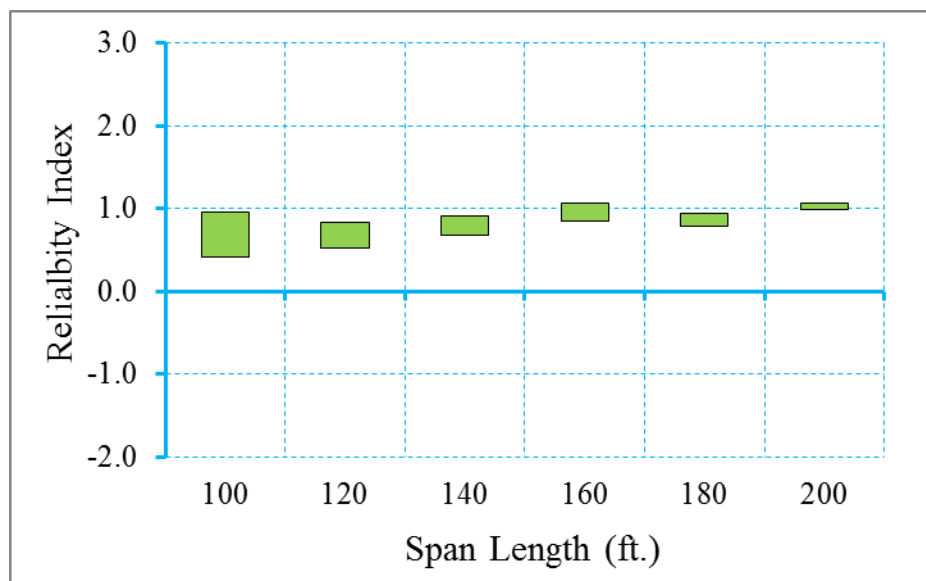


Figure B.152 Reliability Indices for ASBI Box Girder Bridges at Maximum Allowable Tensile Stress Limit State (ADTT=5000), $\gamma_{LL}=0.8$ ($f_t = 0.158\sqrt{f'_c}$)

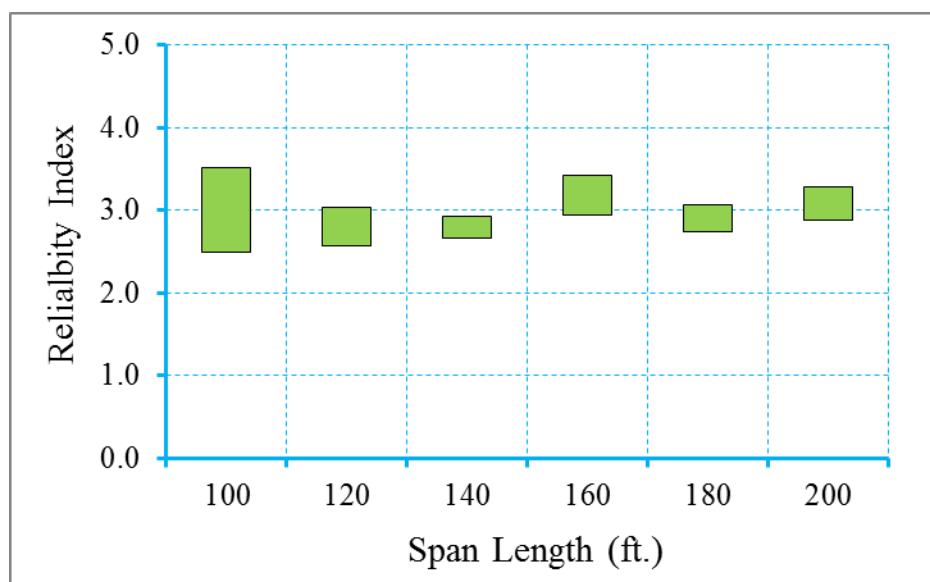


Figure B.153 Reliability Indices for ASBI Box Girder Bridges at Maximum Allowable Crack Width Limit State (ADTT=5000), $\gamma_{LL}=0.8$ ($f_t = 0.158\sqrt{f'_c}$)

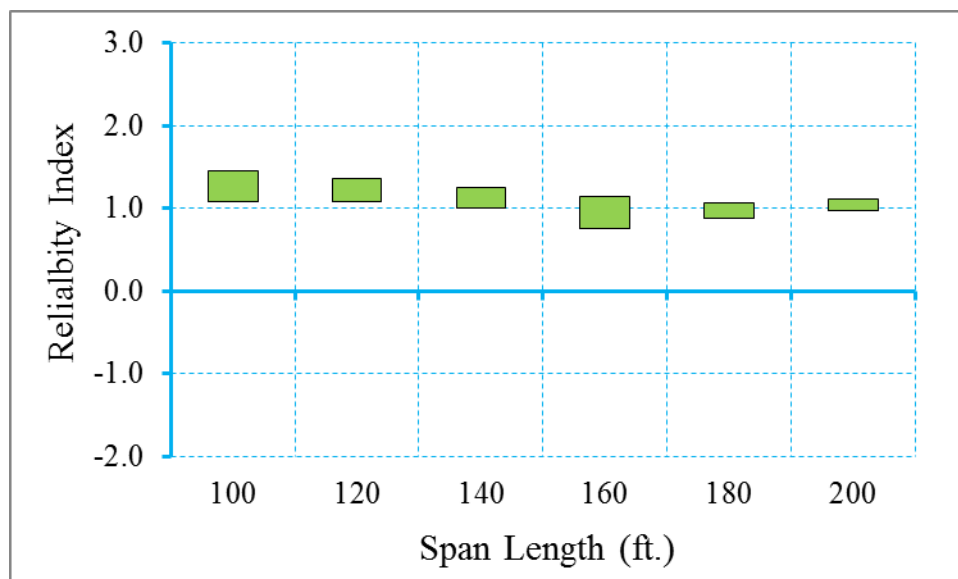


Figure B.154 Reliability Indices for ASBI Box Girder Bridges at Decompression Limit State (ADTT=5000), $\gamma_{LL}=1.0$ ($f_t = 0.158\sqrt{f'_c}$)

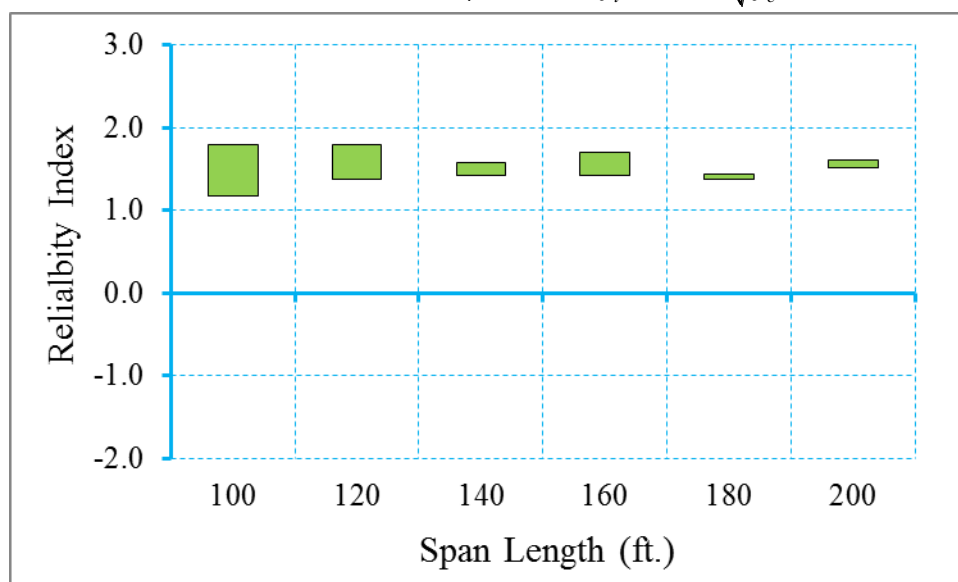


Figure B.155 Reliability Indices for ASBI Box Girder Bridges at Maximum Tensile Stress Limit State (ADTT=5000), $\gamma_{LL}=1.0$ ($f_t = 0.158\sqrt{f'_c}$)

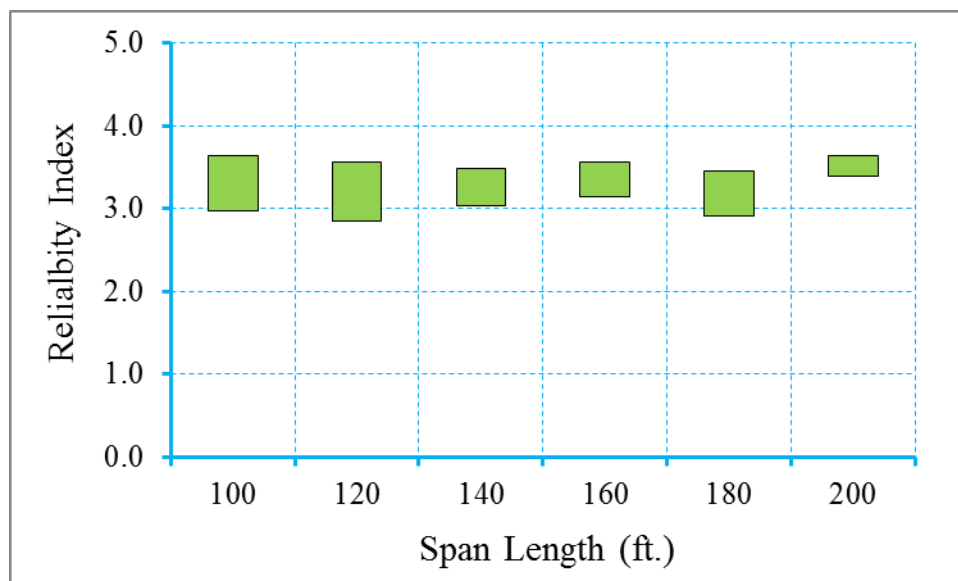


Figure B.156 Reliability Indices for ASBI Box Girder Bridges at Maximum Crack Width Limit State (ADTT=5000), $\gamma_{LL}=1.0$ ($f_t = 0.158\sqrt{f'_c}$)

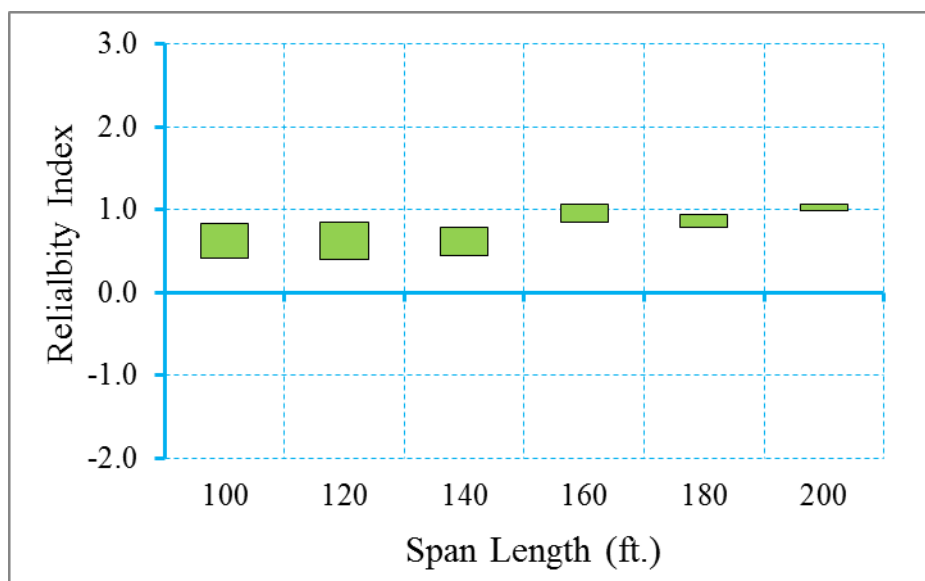


Figure B.157 Reliability Indices for ASBI Box Girder Bridges at Decompression Limit State (ADTT=5000), $\gamma_{LL}=0.8$ ($f_t = 0.19\sqrt{f'_c}$)

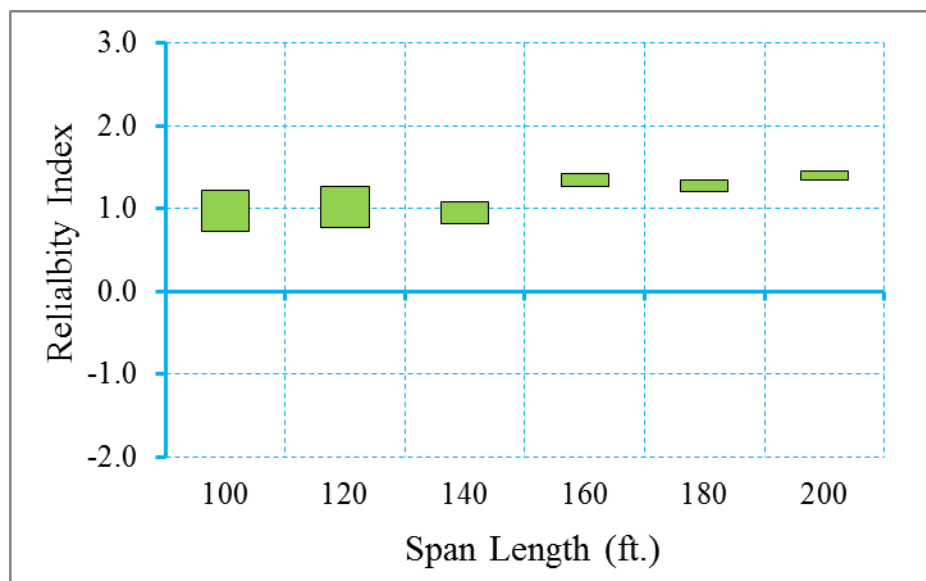


Figure B.158 Reliability Indices for ASBI Box Girder Bridges at Maximum Allowable Tensile Stress Limit State (ADTT=5000), $\gamma_{LL}=0.8$ ($f_t = 0.19\sqrt{f'_c}$)

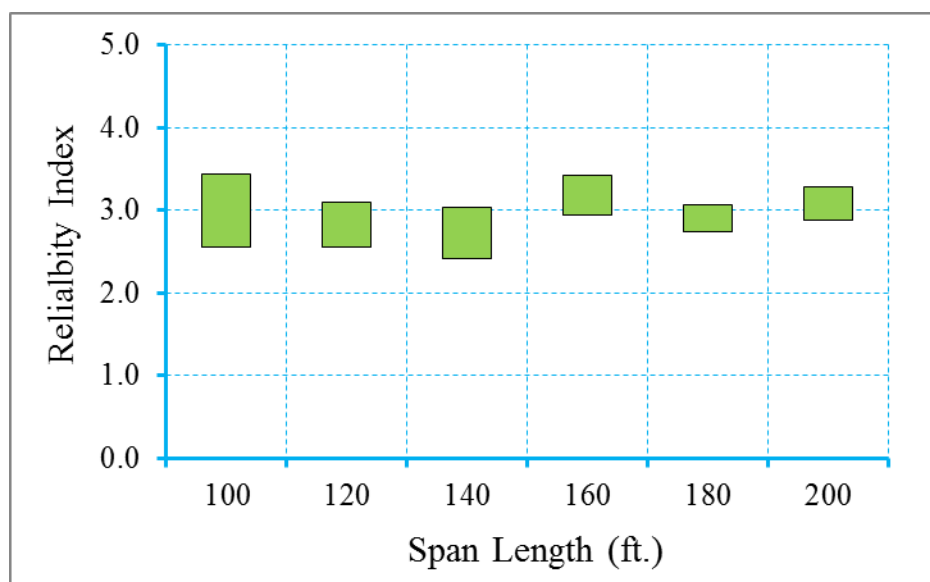


Figure B.159 Reliability Indices for ASBI Box Girder Bridges at Maximum Allowable Crack Width Limit State (ADTT=5000), $\gamma_{LL}=0.8$ ($f_t = 0.19\sqrt{f'_c}$)

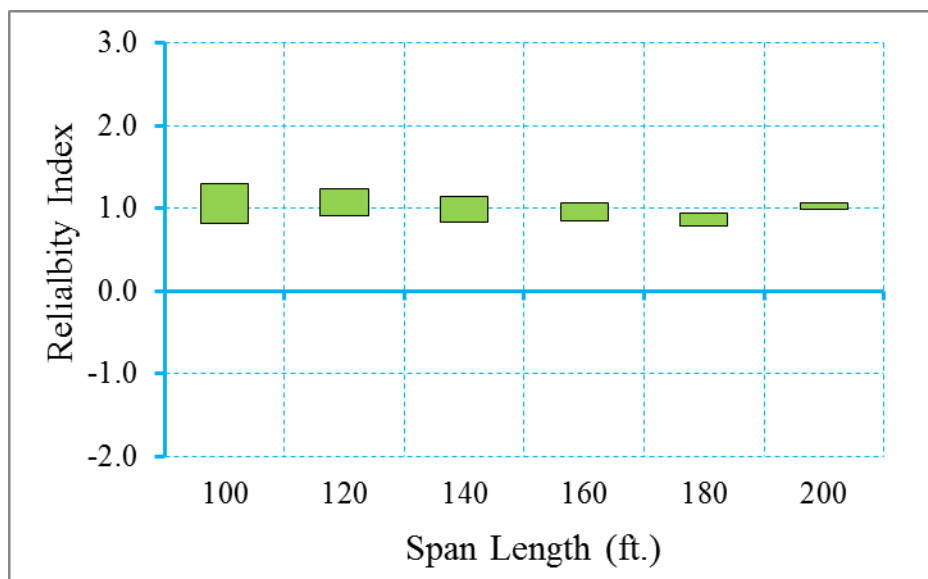


Figure B.160 Reliability Indices for ASBI Box Girder Bridges at Decompression Limit State (ADTT=5000), $\gamma_{LL}=1.0$ ($f_t = 0.19\sqrt{f'_c}$)

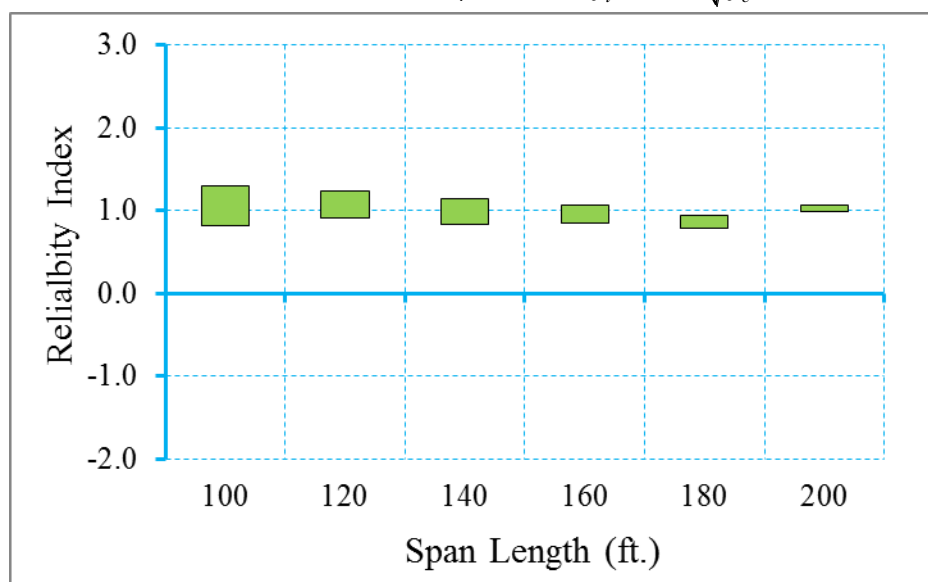


Figure B.161 Reliability Indices for ASBI Box Girder Bridges at Maximum Tensile Stress Limit State (ADTT=5000), $\gamma_{LL}=1.0$ ($f_t = 0.19\sqrt{f'_c}$)

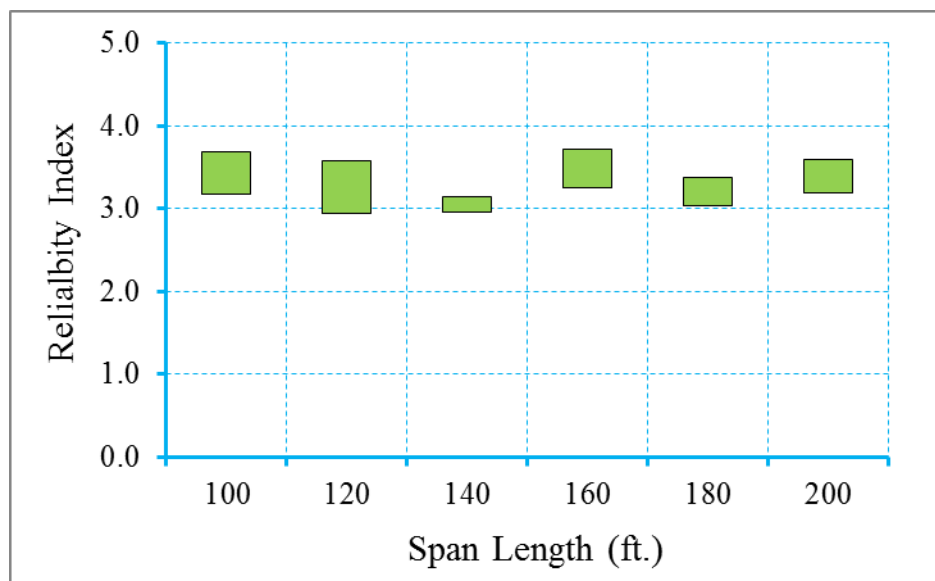


Figure B.162 Reliability Indices for ASBI Box Girder Bridges at Maximum Crack Width Limit State (ADTT=5000), $\gamma_{LL}=1.0$ ($f_t = 0.19\sqrt{f'_c}$)

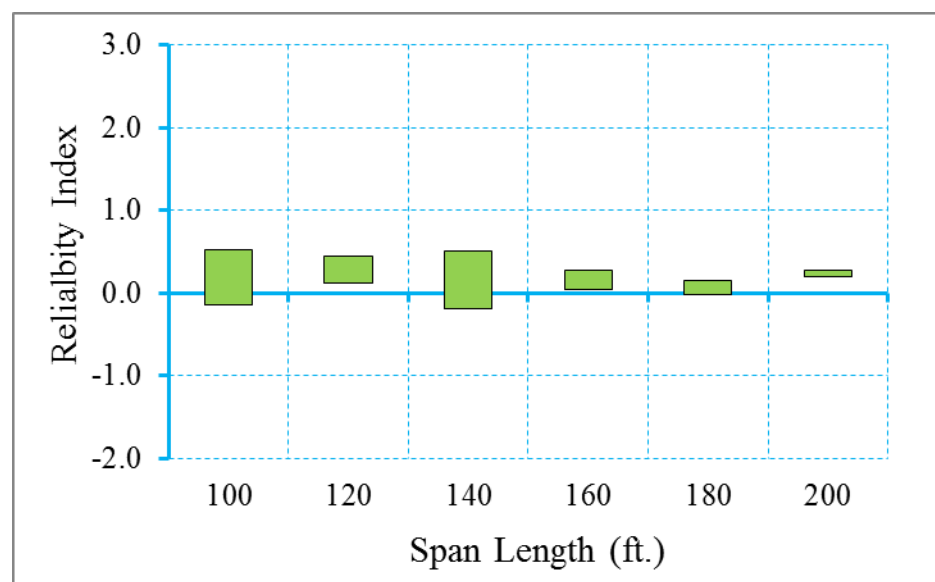


Figure B.163 Reliability Indices for ASBI Box Girder Bridges at Decompression Limit State (ADTT=5000), $\gamma_{LL}=0.8$ ($f_t = 0.253\sqrt{f'_c}$)

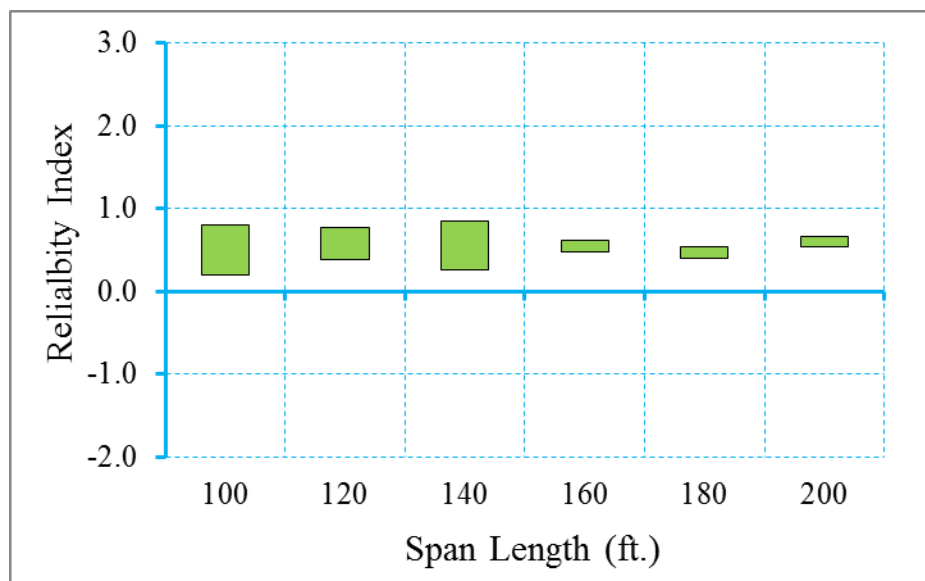


Figure B.164 Reliability Indices for ASBI Box Girder Bridges at Maximum Allowable Tensile Stress Limit State (ADTT=5000), $\gamma_{LL}=0.8$ ($f_t = 0.253\sqrt{f'_c}$)

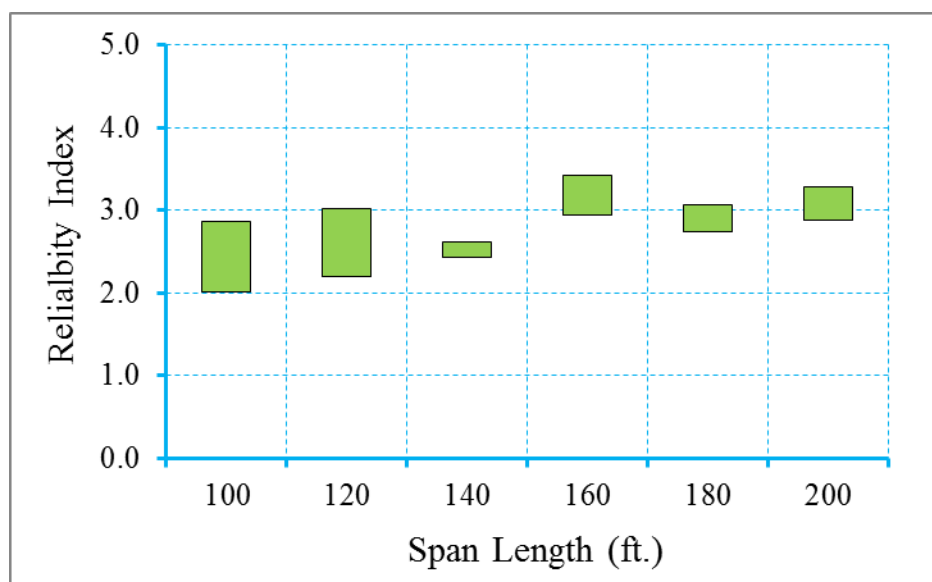


Figure B.165 Reliability Indices for ASBI Box Girder Bridges at Maximum Allowable Crack Width Limit State (ADTT=5000), $\gamma_{LL}=0.8$ ($f_t = 0.253\sqrt{f'_c}$)

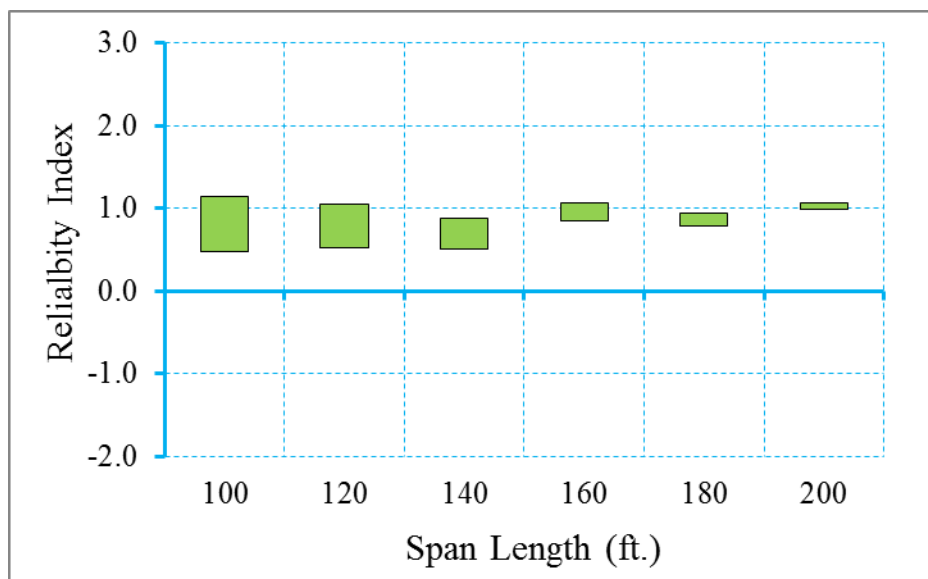


Figure B.166 Reliability Indices for ASBI Box Girder Bridges at Decompression Limit State (ADTT=5000), $\gamma_{LL}=1.0$ ($f_t = 0.253\sqrt{f'_c}$)

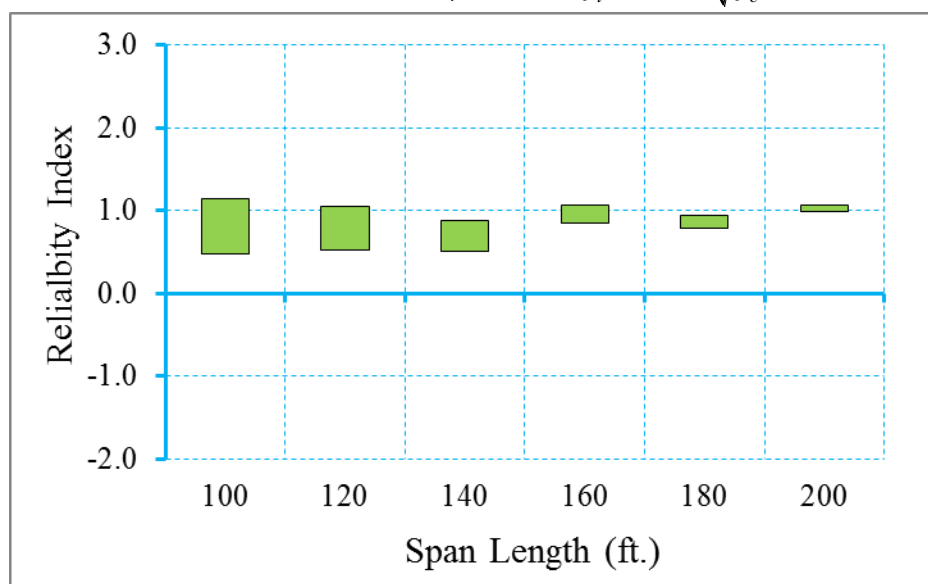


Figure B.167 Reliability Indices for ASBI Box Girder Bridges at Maximum Allowable Tensile Stress Limit State (ADTT=5000), $\gamma_{LL}=1.0$ ($f_t = 0.253\sqrt{f'_c}$)

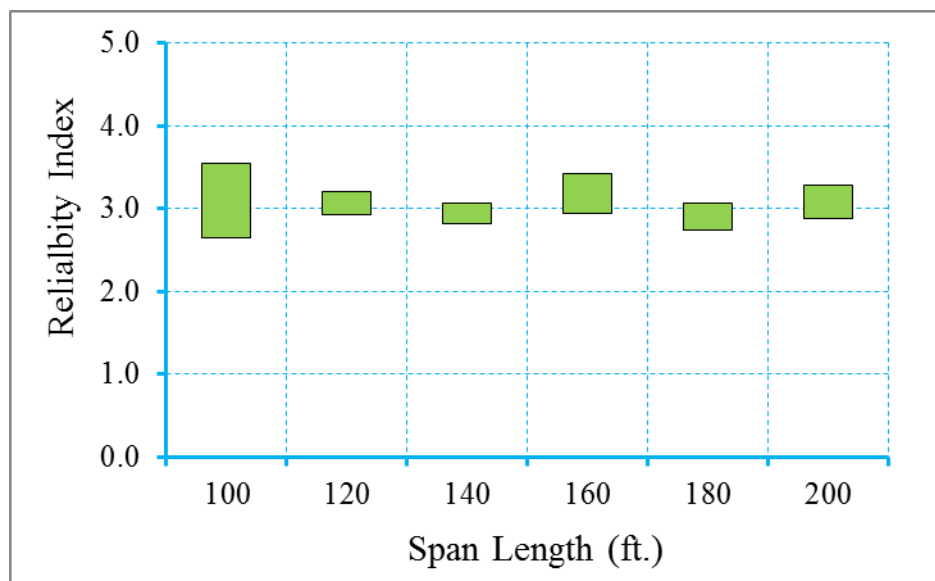


Figure B.168 Reliability Indices for ASBI Box Girder Bridges at Maximum Allowable Crack Width Limit State (ADTT=5000), $\gamma_{LL}=1.0$ ($f_t = 0.253\sqrt{f'_c}$)